

PRESSURE DROP AND FLOW CHARACTERISTICS FOR THE
PNEUMATIC TRANSPORT OF FINE PARTICLES THROUGH
CURVED AND STRAIGHT CIRCULAR PIPES

by

J. S. MASON

(Thesis submitted for the Degree of Doctor of
Philosophy under the conditions for the award
of higher degrees of the Council for National
Academic Awards.)

Department of Mechanical Marine
and Production Engineering,
Liverpool Polytechnic.

May 1972



Pressure drop and flow characteristics for the pneumatic transport of fine particles through curved and straight circular pipes

J.S. Mason

PhD Thesis, Liverpool John Moores University, 1972

Items to be redacted:

Conference paper C1: C1-1 – C1-16, bound between pages 152 and 168

**VOLUME CONTAINS
CLEAR OVERLAYS**

**OVERLAYS HAVE BEEN
SCANNED SEPERATELY
AND THEN AGAIN OVER
THE RELEVANT PAGE**

BEST COPY AVAILABLE.

**TEXT IN ORIGINAL IS
CLOSE TO THE EDGE OF
THE PAGE**

SYNOPSIS

The initial results of an investigation into the flow properties of a gaseous suspension of fine particles are reported. The objective of the work has been the acquisition of extensive experimental data, the analysis of which provides a better understanding of the pressure drop and flow characteristics of pneumatically transported solid particles. The versatility of the test rig is demonstrated by the diversity of the investigations performed during this study.

Quantitative results were acquired for the flow of different-sized alumina particles flowing through vertical and horizontal pipes of different diameters, and around six bends of varying geometry. Dimensional analysis is profitably applied to the correlation of the experimental data and the ensuing deductions examined critically. These conclusions were either substantiated or refuted by a visual appreciation of the nature of the flowing suspension.

Investigations into bend erosion have explained the mechanism of the erosion process, and the data analysis has produced an equation which defines the mean wear rate as a function of the mean air velocity and the solids-to-air mixture ratio.

This study has revealed the need for extensive study of topics not yet fully examined. Suggestions for further work are included at the end of Chapters 5, 6, 7 and 8.

ACKNOWLEDGEMENTS

The author would like to thank Dr. R. G. Boothroyd for his advice during the last three years.

Sincere gratitude is extended to Mr. W. Dean, Senior Technician, for his enthusiasm and dedication which have contributed greatly to the success of this investigation.

Much assistance was received from Mr. R. E. Venables in the preparation of computer programs, and from Mr. B. V. Smith in the work concerned with bend erosion.

The particle size analyses were carried out by Mr. J. F. Humphreys-Jones and Mrs. P. E. Jones of the School of Pharmacy, Liverpool Polytechnic.

The author is indebted to the Department for its facilities and to the support of Dr. M. D. Longfield.

AUTHOR'S NOTE

All the work in this thesis is the sole and original work of the author except where stated otherwise by acknowledgement or reference.

Attention is drawn to reference (3), which is part of the text. The graphs in this paper are not included elsewhere in the thesis and discussion of the results is not included in the typescript.

A large part of Chapter 8 has been accepted for publication by The International Journal of Powder Technology under the title, "The Erosion of Bends by Pneumatically-Conveyed Suspensions of Abrasive Particles".

CONTENTS

	<u>Page No.</u>
Synopsis	
Acknowledgements	
Author's Note	
Contents	
1. <u>OUTLINE OF THE STUDY</u>	
1.1 Introduction	1
1.2 Industrial Interests	2
1.2.1 Pneumatic Conveying Systems	2
1.2.2 Transport Chemical Reactors	4
1.2.3 Augmented Heat Transfer	4
1.2.4 Static Electrification	5
1.3 Outline of the Contents of the Thesis	6
1.4 Research Policy	7
1.5 Publication Policy	8
2. <u>FLOW THEORY</u>	
2.1 Introduction	9
2.2 Motion of the Solid Phase	10
2.2.1 Coarse Particle Suspensions	10
2.2.2 Fine Particle Suspensions	11
2.2.3 Agglomeration	12
2.2.4 Electrostatic Charging	13
2.3 Basic Flow Description	14
2.4 Dimensional Analysis	15
3. <u>EQUIPMENT DESIGN</u>	
3.1 Introduction	19
3.2 Flow System Specification	20

3.3	Outline Description of Equipment	22
3.3.1	Compressor	23
3.3.2	Air Flow Distribution	24
3.3.3	Gas-Solid Flow Circuit	25
3.3.4	Solids Circulation	27
3.3.5	Air Filtration Plant	28
3.4	Method of Plant Operation	31
3.5	Problems Associated with Plant Operation	33
3.6	Suggestions for Improvement to the Equipment	34

4. EXPERIMENTAL MEASUREMENTS

4.1	Introduction	38
4.2	Temperature Measurement of the Gaseous Phase	41
4.2.1	Introduction	41
4.2.2	Experimental Arrangement and Procedure	42
4.2.3	Density of the Gaseous Phase	48
4.2.4	Viscosity of the Gaseous Phase	48
4.3	Measurement of the Superficial Velocity of the Gaseous Phase	49
4.3.1	Introduction	49
4.3.2	Orifice Plate Calibration Procedure	49
4.3.3	Analysis and Results of Pitot-tube Traverse	49
4.3.4	Alternative Method of Ascertaining the Superficial Air Velocity	55
4.4	Pressure Drop Measurements	58
4.4.1	Introduction	58
4.4.2	Pressure Measurements in a Vertical Duct	58
4.4.2.1	Experimental Procedure	61
4.4.2.2	Blocked Manometer Tappings	62

4.4.3	Bend, Vertical and Horizontal Duct Circuit Pressure Measurements	63
4.4.3.1	Experimental Procedure	64
4.4.4	Pressure Drop due to Air Only Flowing	66
4.5	Measurement of Solids Mass Flow Rate	67
4.5.1	Introduction	67
4.5.2	Screw-feeder Arrangement and Calibration Procedure	68
4.5.3	Discussion and Results	71
4.6	Powder Property Determinations	73
4.6.1	Introduction	73
4.6.2	Routine Analysis of Powder Samples	73

5. GAS-SOLID FLOW THROUGH VERTICAL DUCTS

5.1	Introduction	103
5.2	Literature Survey	104
5.3	Experimental Procedure	116
5.4	Data Analysis	116
5.5	Results and Discussions	121
5.6	Conclusions	129
5.7	Suggestions for Further Work	130
5.8	Comparison of Friction Factors	132

6. GAS-SOLID FLOW THROUGH HORIZONTAL DUCTS

6.1	Introduction	169
6.2	Literature Survey	170
6.3	Experimental Procedure	177
6.4	Data Analysis	178
6.5	Results and Discussions	178
6.6	Conclusions	187
6.7	Suggestions for Further Work	189

7.	<u>GAS-SOLID FLOW THROUGH BENDS OF VARYING GEOMETRY</u>	
7.1	Introduction	217
7.2	Literature Survey	219
7.3	Experimental Procedure	225
7.4	Data Analysis	225
7.5	Results and Discussions	226
7.6	Conclusions	233
7.7	Suggestions for Further Work	234
8.	<u>BEND EROSION TESTS</u>	
8.1	Introduction	257
8.1.1	The Mechanism of Erosion	257
8.1.2	Physical Properties of the Abrasive	258
8.1.3	Results of Previous Researchers	258
8.2	Experimental	261
8.2.1	Apparatus	261
8.2.2	Experimental Procedure	262
8.3	Data Analysis	263
8.3.1	Erosion	263
8.3.2	Mass and Velocity of Impinging Particles	264
8.3.3	Angle of Impingement	264
8.3.4	Properties of the Particles and Eroded Surface	264
8.3.5	Bend Geometry and Orientation	265
8.3.6	Analysis of Experimental Results	265
8.3.7	Examination of the Mean Wear Rate Equation	267
8.4	Results and Discussions	268
8.4.1	Erosion History for Bend 1	268
8.4.1.1	Nature of the Flowing Suspension	268

8.4.1.2	Wear Development	268
8.4.1.3	Flow Pattern	270
8.4.2	Erosion History for Bend 2	270
8.4.2.1	Nature of the Flowing Suspension	270
8.4.2.2	Wear Development	271
8.4.3	Erosion History for Bend 3	271
8.4.3.1	Nature of the Flowing Suspension and Wear Development	271
8.4.4	Erosion History for Bend 4	272
8.4.4.1	Nature of the Flowing Suspension	272
8.4.4.2	Wear Development	272
8.4.4.3	Flow Pattern	273
8.4.4.4	Pressure Loss	273
8.4.5	Powder Property Determinations	274
8.4.6	Relevance to Industry	274
8.5	Conclusions	275
8.6	Suggestions for Further Work	279
9.	<u>CONCLUSIONS</u>	301

A.1.	Computer Programs	303
A.1.1.	Pitot-tube Traverse	304
A.1.2.	Basic Flow Parameters and Pressure Differentials	307
A.1.3.	Pre-data	322
A.2.	Screw-feeder Paper	323
A.3.	Apparatus : Additional Details	
A.3.1.	Perspex Hoppers	340
A.3.2.	Bearing and Seal Assembly	341
A.4.	China Clay Investigation	
A.4.1.	Introduction	344
A.4.2.	Experimental Procedure and Apparatus	344
A.4.3.	Powder Property Determinations	344
A.4.4.	Test Results Summary	346
A.4.5.	Scaling-Up	246
A.4.6.	Conveyability of China Clay	348
A.4.7.	Flowability of China Clay through Storage Hoppers	349
A.4.8.	Alternative Ways of Hopper Discharge	350
A.4.9.	Air Filtration	351
A.4.10.	Material Entrainment	351
A.4.11.	Conclusions	352
A.5.	Additional Graphical Results	353
A.6.	Nomenclature	365

A.7. References

368

A.8. Plate Captions and Keys

382

A.9. Supplementary List of Figure Captions

385

CHAPTER 1

OUTLINE OF THE STUDY

1.1 Introduction

This thesis reports part of the results of an extensive experimental investigation into the properties of a turbulently flowing suspension of fine alumina particles. The apparatus developed for this work has been solely designed by the author, whose intention has been to ensure maximum flexibility in order to allow a large number of system parameters to be examined.

The author's interest in the subject was initially evolved by the varied and seemingly under-exploited industrial potential of pneumatic transport. There are many specialised areas embraced by this field of investigation, such as transport chemical reactors, but even the relatively established design procedures for the pneumatic conveyance of particulate matter offers unbelievable scope for long term research projects. Apart from these commercially-orientated interests, the academic aspects, which demand a knowledge of several traditional disciplines in the pure and applied sciences, also offer an exciting challenge.

The primary purpose of the present study is to investigate the flow characteristics of gas-solid mixtures for fine particles having different particle size spectra. The ultimate objective is to acquire data which will facilitate the design of multiphase flow systems in which the problems of flow stability, pressure drop and bend erosion are resolved.

The design and operation of gas-solid transport systems necessitates quantitative information of such two phase flows in conveying lines. Recent work increasing the understanding

of the dynamics of two phase flow has generally been restricted to small bore conduits^{7,8,11} or concerned with idealised solid particles such as spherical glass beads^{4,13}. Even for these simplified studies the relationship between all pertinent variables has not been firmly established. Consequently, the universal prediction of solids flow rate from pressure drop measurements remains unsolved.

An analysis of the measurements of the pressure differentials encountered in a transport system consisting of vertical and horizontal sections connected by different geometry bends is a most complex problem. The nature of the pressure losses varies between these three components; the losses in the vertical duct may be largely due to inter-particulate collisions and wall-particle impacts, in the horizontal section particle deposition concentrates most of the material along the lower part of the pipe resulting in an entirely different transport mechanism, and finally the bend centrifugal force undoubtedly influences the extent of the pressure loss around this transition section. The many other considerations, such as the effect of changes in the potential and kinetic energy of the particles, combine to make the subject worthy of serious study.

1.2 Industrial Interests

1.2.1 Pneumatic Conveying Systems

It has been stated many times that pneumatic conveying is a rapidly growing part of the bulk materials handling field^{104,108} and yet design techniques in this industry have remained relatively unsophisticated^{105,106,107}. When designing a pneumatic transport system the first requirement is an understanding of the material to be handled; is it abrasive,

explosive, toxic, hygroscopic, cohesive, fine or granular, friable and so on? A small change in the material characteristics can result in catastrophic deviations from the anticipated product behaviour, a fact which has influenced designers to use largely empirical methods strengthened by "know-how". Consequently, manufacturers jealously guard the procedures and criteria which they use¹⁰⁹.

It is not intended here to classify the multiplicity of pneumatic conveying systems and the reader is referred to references 109 to 111.

Industrial applications of pneumatic conveyors are widespread and although power consumption is generally higher than for transportation by conventional methods there are many benefits inherent in pneumatic systems. The principal advantages are the relatively low capital cost, flexibility, ease of automation, accuracy of control, safety, cleanliness, self-cleaning ability, uniformity of processing, high standards of hygiene, and reduced maintenance and labour costs. Typical problems in pneumatic conveying are saltation in horizontal ducts, choking in vertical transport lines, attrition of the solid particles, erosion of ductwork and bends in particular with consequent contamination of the product, the explosion hazard, and the difficulty of filtering ultra-fine particles. Many of these problems can be avoided or at least minimised by good design procedure, but the corollary is the design which has interpreted the flexibility of a pneumatic system to be taken as a license to use meandering pipelines. For the designer a full knowledge of such parameters as pressure drop, relative slip between phases and electrostatic charging must be obtained before the plant can be optimised, assuming that

he has previously acquired a complete understanding of the characteristics of the material itself.

1.2.2 Transport Chemical Reactors

In many chemical processes there is a reaction between the solid and gaseous phases, the solids may simply act as catalysts between reacting gases or they may participate directly in the reactions. Until recently the fluidised bed reactor has been preferred to the transport reactor, however, the development of more complex processing techniques involving many materials has increased the popularity of the latter. A basic disadvantage of the transport reactor is that for a low rate of chemical reaction a long reactor is necessary to ensure completion of the reaction, necessitating long tubular coils giving rise to excessive power requirements for circulating the suspension. On the other hand the transport reactor has advantages such as more intimate contacting of the solid and gaseous phases, a more uniform reaction time, highly-automated continuous processing which is ideally suited to the delicate operations associated with finer chemicals, and the flexibility of being able to add or extract material at any position along the length of the duct. In addition, localised heat transfer at selected points throughout the transport line can be used to optimise the yield. It may be concluded that both transport and fluidised bed reactors enjoy the attributes of good mixing and uniform temperature of the reactants.

1.2.3 Augmented Heat Transfer

A suspension of fine particles in a flowing gas constitutes an effective heat transfer medium and becomes a possible coolant for nuclear reactors^{112,113}. The presence of the solid particles improves the thermal capacity and

convective heat transfer coefficient of a gas considerably, to a magnitude comparable with the values for liquids. The use of liquid coolants may involve corrosion problems and require pressurisation to avoid change of phase by boiling. Thus, a gas-solid suspension appears to exhibit the best features of both single phase gases and liquids. The author has no evidence of the use of such coolants in large systems, but the potential applications indicate that this would be a most rewarding area of investigation.

1.2.4 Static Electrification

The mechanism of electrification is complicated and barely understood despite scientists having been aware of this phenomenon for a considerable period of time. It is particularly important in pneumatic conveying from two view points. Firstly the electric charge on a particle caused by dissimilar surfaces interacting in the transport system may have a significant effect on the suspension flow properties. Secondly, the charged particles dispersed throughout the gas may induce a build-up of charge on parts of the conveying equipment with the subsequent risk of explosion. Investigations into the industrial hazards have been carried out by Cooper¹¹⁴ and Rose¹¹⁵, whilst Henry¹¹⁶ suggests means for overcoming the difficulties.

The present series of investigations was undertaken to obtain reliable and sufficient experimental data, which would facilitate discrimination between some of the large number of variables in order to establish which exert the major influences. It was considered desirable to relate, wherever possible, the work to industrial applications of pneumatic transportation.

1.3 Outline of the Main Contents of the Thesis

In Chapter 2, the motion of the solid phase is discussed with reference to the literature available, and some mention is made of the problems of agglomeration and electrostatic charge effects. The basic flow theory is developed which leads to an approach to the problem using dimensional analysis.

In Chapter 3, the design and construction of the basic experimental facility is described. The method of plant operation is outlined with suggestions for improving the equipment.

In Chapter 4, a detailed account is given of the experimental measurements of the overall flow parameters, together with an evaluation of the routine powder property determinations.

In Chapter 5, the first full experimental investigation is reported. This concerns the pressure drop for different sized alumina particles flowing vertically upwards through perspex ducts of one, two and three inches diameter.

In Chapter 6, the motion of solids entering a horizontal duct, preceded by a 90 degree bend, is examined. Recommendations are made for the location of static pressure tappings in this region of deviating flow.

In Chapter 7, a brief explanation of the suspension flow behaviour for six bends of different dimensions is presented. The amount of data acquired is so extensive that only a limited treatment has been dealt with in this thesis. It is proposed to scrutinize these results at a later date and submit them for publication.

In Chapter 8, the erosion of 90 degree bends by pneumatically-conveyed alumina particles is examined

quantitatively. The mechanism of erosion is discussed and the data analysis expresses bend wear as a function of superficial air velocity and solids-to-air mixture ratio. The results are related to industrial applications.

In Chapter 9, general conclusions from the experiments are stated.

Appendix 1 includes all the computer programs used to evaluate the basic data. Appendix 2 contains a paper on screw feeding equipment, whilst Appendix 4 illustrates the author's industrial interest by presenting a short investigation into the handling characteristics of china clay.

1.4 Research Policy

The work reported in this thesis is intended to be the start of a systematic series of investigations into many aspects of pneumatic conveying. The versatility of the apparatus has been demonstrated by the diversity of the experiments reported in this thesis. Further benefit has been derived from this flexibility in that the equipment has recently been adapted for a full-scale investigation into the heat transfer characteristics of flowing gas-solid suspensions.

Work scheduled for the immediate future, and to be performed by the author in collaboration with colleagues and research students, include the application of laser techniques for the measurement of particle velocity, the use of a pressure transfer vessel to examine the transition from dilute to dense-phase conveying, the performance of an air-slide, some aspects of electrostatic charging and further work on bend erosion. Negotiations with several firms are in an advanced state for the use of their large scale plant on which to carry out tests and to assess the practical relevance of the laboratory

investigations.

1.5 Publication Policy

Part of this study is now published in the following references which are bound in as part of this thesis.

1. "Comparison of Friction Factors in Pneumatically-Conveyed Suspensions using Different-Sized Particles in Pipes of Varying Size", Pneumotransport 1, B.H.R.A. Conference, Cambridge, (September 1971).
2. "Performance of a Calibrated Screw-feeder", I. Mech. E. Conference on Bunker Extraction Gear, (October 1971).

The author delivered both of these papers at the respective conferences.

A substantial part of Chapter 8 has been accepted for publication in Summer 1972, by the Journal of Powder Technology, the title being "The Erosion of Bends by Pneumatically-Conveyed Suspensions of Abrasive Particles".

It is proposed to prepare papers for publication on some of the material presented in this thesis, the most interesting work should evolve from a more comprehensive analysis of the investigations reported in Chapter 7 on the pressure drop around bends.

CHAPTER 2

FLOW THEORY

2.1 Introduction

The study of two phase gas-solid flows is exceptionally involved and the following complex phenomena demand consideration:-

- (i) The flow is turbulent and as the motion of the fluid for such flows cannot be satisfactorily described, it is unpromising to theorise on the motion of individual particles. Exact particle trajectories can be determined for laminar flow but this is an unusual practical situation.
- (ii) In the case of a fine particle suspension the smallest particles generally have a greater influence on the flow than the larger ones compared on a weight-to-weight basis. It is possible that during solids circulation the particle size distribution will alter, either through attrition or the finest particles becoming agglomerated. Consequently, a continuous understanding of the size distribution of particles in the flow would be advantageous. The particle Reynolds' number, $\frac{(\bar{u}_f - \bar{u}_p)\rho_f d_p}{\mu}$, will also alter; for large values of this parameter the validity of Stokes' law is questionable.
- (iii) Particles in close proximity create further difficulties in that the forces between them cannot be adequately described with a rigorous analysis.

2.2 Motion of the Solid Phase

The general frictional behaviour of suspensions often depends largely upon particle size, although this is only one of several relevant factors. In many earlier studies (see sections 5.2, 6.2 and 7.2) the particles were relatively coarse compared with the particles used in the present work. Systems in which the particles are fine exhibit completely different flow behaviour from systems in which the particles are coarse. The phenomena of agglomeration and electrostatic charging are likely to have entirely different effects upon these two rather broad categories of flow behaviour in pneumatic conveyors.

2.2.1 Coarse Particle Suspensions

Conveyed material which is of a granular nature will tend to move along a pipe in a series of relatively smooth trajectories, suffering a number of oblique impacts with the pipe wall in the process⁴⁸⁻⁵³. In this case the turbulent motion of the fluid has negligible effect on the trajectories, and at moderate loadings (i.e. $W_p/W_f < 12$ or so) it is normally observed for constant flow conditions that:-

$$\frac{\lambda_s}{\lambda_0} \equiv \frac{\Delta P_T}{\Delta P_0} = 1 + \alpha \cdot \frac{W_p}{W_f} \quad (1)$$

where α is a constant which depends upon the velocity of flow, pipe size, particle size, etc., but is independent of W_p/W_f . Successful predictions of α in terms of the Froude number, \bar{u}_f^2/gD , have been achieved^{21,48,49}.

For these low solids loadings it is reasonable to assume that the particles do not interfere with the large scale turbulence structure of the conveying gas, simply

because they are too widely spaced to resist the motion of the surrounding eddy. Inevitably a considerable number of smaller eddies may be created (due to vortex formation behind the particularly large particles) by the relatively local slip velocity ($\bar{u}_f - \bar{u}_p$). These small eddies are superimposed on the larger eddies which are characteristic of normal single phase flow turbulence. Nevertheless the larger eddies will travel in much the same way as in the absence of particles. The larger eddies in mid-stream determine the level of the wall-shear stress, and so it may be assumed that ΔP_0 is the same both when particles are present and also when they are absent.

These relatively large particles will, however, induce a further loss of pressure which may be interpreted in terms of wall impacts and the consequent loss of momentum. Alternatively these extra pressure losses may be evaluated from the slip velocity and the particle drag coefficient.

It is concluded therefore that the turbulence suppression mechanism takes place in coarse particle suspensions, but is not in evidence at moderate solids loadings simply because the particles are too widely dispersed to restrain the motion of the eddy.

2.2.2 Fine Particle Suspensions

When conveyed pneumatically fine particles behave differently compared with much coarser material, since they will tend to follow the random motion of the fluid eddy more closely, rather than restrain its motion. A characteristic property which these suspensions exhibit is a non-linear relationship between λ_s/λ_0 and W_p/W_f , this is particularly

in evidence at low solids loadings and may even cause a minimum of λ_s/λ_0 to be observed (see section 5.2, equation (5)) and references 1, 54 and 55. Thus, because of their closer spacing, fine particles may interfere much more with the gas turbulence mechanism generation⁵⁶ than is possible with coarser particles at the same solids loading. In this case it may be incorrect to assume that the frictional losses due to the conveying gas cause a pressure drop ΔP_0 when solids are present in the flow.

2.2.3 Agglomeration

Fluid flow properties depend upon the size spectrum of the particles and so agglomerate formation in turbulent flow is an important consideration. The effective particle size spectrum in the flow is influenced by particle and floc (i.e. an agglomerate of particles) collisions and the disruption of the flocs, the latter being dependent upon the internal binding effect of cohesive forces and the shear forces of the turbulent motion.

Boothroyd³⁰ has pointed out that agglomeration of particles depends upon the degree to which they differ in size and that it is also a function of position in the pipe. One expects large eddies on the duct centre-line and hence considerable agglomeration of very fine cohesive particles, whereas at the wall of the pipe, where there exists a state of highly energetic turbulence, considerable deagglomeration. This turbulence is still not sufficient to remove the build-up of particles at the wall, this being effected by interparticulate collisions⁵⁷. Basic particle size has an effect on the agglomeration tendency and it would appear that only the larger agglomerates have

an effect on the diffusion properties⁵⁸. Other important factors are electrostatic effects⁵⁹ and interparticle collisions⁶⁰.

A sound knowledge of the state of agglomeration of the flow would be of great value, especially in optical techniques where agglomerative tendencies render suspect the values of the dispersed density obtained³⁰. The industrial practice of pneumatically conveying a solid phase composed of fine particles having entirely different chemical and physical properties, presents an area of study in which a rigorous fundamental solution holds little promise.

2.2.4 Electrostatic Charging

The degree to which a flowing gas-solid suspension becomes electrostatically charged warrants investigation because the quantity of charge is likely to influence all aspects of the flow. The reliability of data from experiments on pneumatic conveyance was first seriously questioned, from an electrostatic viewpoint, following research into the nature of electrostatic charging by Richardson and McLeman⁶¹, who noted high increases of pressure drop during the course of their experiments, which they attributed to electrostatics. It seems likely that electrostatic charging must have been prominent in previous studies, although rarely has it been mentioned.

Soo^{62,63} has contributed considerably to this field, particularly by drawing analogies with similar problems in other better established fields of study. In a detailed article Montgomery⁶⁴ has included a complete survey of the more important points in static electrification. Various

methods of charge transfer are discussed and the importance of surface states in contact electrification is stressed. Many references^{64,65} mention that higher velocities at the moment of contact produce greater electrification but no explanation of this phenomenon is given.

The influence of charge effects in the present work has only been observed qualitatively.

2.3 Basic Flow Description

The difficulties in attaining even an approximate understanding of the fundamental behaviour of two phase gas-solid flows are overwhelming since the flow is turbulent. The structure of turbulence, even in single phase pipe flow of a Newtonian fluid is barely understood⁶⁶. Bakhmeteff⁶⁷ is typical of the many references which present the main features of turbulent gas flows in a pipe. It is generally assumed for flow through pipes that there is axial symmetry and that the flow is invariant with time. In order to give a more complete picture it is necessary to introduce the Reynolds' stresses derived from the non-linear terms of the Navier-Stokes equations. A non-dimensional equation can be developed which defines the pressure drop^{68,69,70,71} along the pipe in terms of the Reynolds' normal stress. Further analysis of the equation establishes the fact that the pressure gradient is linear, and Nikuradze's experimental work is quoted⁷¹ to substantiate this theory. Thus, there is a significant departure from two phase gas-solid flow experience in which the linear pressure gradient does not hold, particularly for very small particles.

It is not proposed in the present study to become involved with the mathematical complexities associated with

single phase and two phase flow turbulence. Thus the reader is referred to Pai⁶⁸ for a very clear mathematical presentation of the Reynolds' equations of motion for the turbulent flow of an incompressible fluid through a circular pipe. Moving on to suspension flow Baw and Peskin⁷² have produced a mathematical analysis of gas-solid flow at low solids concentration, continuing the work of Pai.

In two phase gas-solid flow it is concluded that even if the detailed motion of the carrier fluid were understood, calculation of the solids turbulence from the fluid motion would still be prohibitively involved.

2.4 Dimensional Analysis

It has been indicated that any purely theoretical approach to the understanding of momentum transfer in two phase pipe flow must be particularly unpromising. The work of Duckworth and Rose^{34,35} is typical of many attempts to obtain a simple theoretical analysis by applying the principle of momentum to an elemental volume of the suspension. Despite many simplifying assumptions such analyses are limited and an approach based upon dimensional analysis holds out most chance of success.

Although a large number of variables are involved in the problem of gas-solid suspension flow, it is quite likely that in many cases only a limited number of these parameters influence the system significantly. Thus different flow regimes are appropriate to particular situations and so partial modelling may be pertinent.

Boothroyd¹ deduced by a physical argument that the friction factor, λ_g , for suspension flow is related to that found without solids, λ_0 , by the functional equation:-

$$\frac{\lambda_s}{\lambda_0} = \phi \left[R_e; \frac{W_p}{W_f}; \frac{\rho_f D^2}{\rho_p d_p^2} \right] \quad (2)$$

On the basis that it is the most reliable way to derive a realistic dimensional relationship for a system, Boothroyd³⁰ used the basic differential equations describing the behaviour of the suspension to substantiate equation (2). This conclusion was then extended in reference 30, where a distinction was drawn between flow phenomena near the wall and in the more central parts of the duct. It was recommended for data correlation purposes, that for flow near the wall, $\rho_f D^2 / \rho_p d_p^2$ be replaced by $\rho_f D^2 / \rho_p d_p^2 R_e^2$ and for core flow by $\rho_f D^2 / \rho_p d_p^2 R_e$. Boothroyd³⁰ concludes that for fine particles, frictional momentum transfer in a pipe may be described by:-

$$\frac{\lambda_s}{\lambda_0} = \phi \left[R_e; \frac{W_p}{W_f}; \frac{\rho_f D^2}{\rho_p d_p^2 R_e} \right] \quad (3)$$

neglecting any electrostatic charge transfer effects.

Whereas for coarse particles:-

$$\frac{\lambda_s}{\lambda_0} = \phi \left[R_e; \frac{W_p}{W_f}; \frac{\rho_p}{\rho_f}; \frac{d_p}{D} \right] \quad (4)$$

A more orthodox approach using dimensional analysis has been adopted by many workers, perhaps the most thorough being the studies of Duckworth and Rose^{34,35}. Their work relates to the regime in which the particles have ceased to accelerate and have attained a constant velocity condition. Duckworth and Rose analyse successively the controlling variables in a flowing gas-solid system, namely, suspension friction factor, pressure drop due to acceleration of the solids, velocity of the solids, acceleration length and

minimum transport velocity. Their correlations apply in particular to coarse particle flow and so equation (4) may be used to compare the relationships of Boothroyd and Duckworth. The expressions of Duckworth and Rose for fluid friction factor, λ_0 , and the solid particles friction factor, λ_p , are given in the form:-

$$\lambda_0 = \phi_1 \left[R_e; \frac{k}{D} \right] \quad (5)$$

where k is the pipe roughness, and

$$\lambda_p = \phi_2 \left[R_e; F_R; \frac{W_p}{W_f}; \frac{\rho_p}{\rho_f}; \frac{d_p}{D}; \frac{k}{D}; \epsilon; Z; \beta; \theta \right] \quad (6)$$

where ϵ is the coefficient of restitution of the particles;

Z is the particle shape factor;

β defines the particle size distribution; and

θ is the angle of inclination of the pipe.

Boothroyd's basic assumptions were that the flow occurred in smooth pipes of fixed orientation. Thus, for a solid phase consisting of perfectly elastic and spherical particles of uniform size, equations (5) and (6) reduce to:-

$$\lambda_0 = \phi_1 [R_e] \quad (7)$$

and
$$\lambda_p = \phi_2 \left[R_e; F_R; \frac{W_p}{W_f}; \frac{\rho_p}{\rho_f}; \frac{d_p}{D} \right] \quad (8)$$

Thus, defining the suspension friction factor, λ_s , by:-

$$\lambda_s = \lambda_0 + \lambda_p$$

it can be seen that:-

$$\frac{\lambda_s}{\lambda_0} = \phi \left[R_e; F_r; \frac{W_p}{W_f}; \frac{\rho_p}{\rho_f}; \frac{dp}{D} \right] \quad (9)$$

Comparing equation (4) and (9) it is quite evident that the only variation is the omission of the Froude number parameter from Boothroyd's relationship. Barth^{9,20} and Hitchcock and Jones²¹ both acknowledge that Froude number is more significant than Reynolds' number when correlating the gas-solid flow of coarse particles (see section 5.2). In a more recent article Duckworth et al⁵ have applied their analysis to the transport of closely sized particles in the range 40 microns to 3000 microns. They report that the functional relationship for the solids friction factor is markedly affected by the dp/D ratio.

CHAPTER 3

EQUIPMENT DESIGN

3.1 Introduction

It is evident from the discussion in Chapter 2 that only limited progress can be achieved by an entirely theoretical approach to two phase gas-solid flow through pipes. The more acceptable theories merely postulate that certain phenomena may occur in suspension flows, rather than produce reliable design relationships. Thus priority should be given to an empirical approach requiring the acquisition of experimental data. As a consequence of this, it was realised that a more sophisticated pneumatic conveying system than is normally required for most industrial operations was necessary.

In the initial planning of the research programme it was decided that the experimental investigations should be concerned with many different aspects of suspension flow, such as pressure drop, velocity profiles, turbulent dispersion, electrostatic charging and at a later date heat transfer. It was also evident that the system orientation should not impose physical restrictions on the scope of the investigation. Thus a rig should be constructed to facilitate studies into the effect of the above parameters on flow through vertical and horizontal ducts, and around bends of varying geometries. Following an extensive literature survey (see section 5.2 in particular) it was apparent that little information was available for the pneumatic transport of "real" powder in the particle size range well below 100 microns diameter. There is a definite trend in many industrial processes towards the use of finer particles,

which often have many advantages in material processing. An increased surface area for chemical reactions is an obvious example of interest. Consequently it was decided to circulate different batches of alumina particles of mean diameter in the fine particle size range. It was realised that the flow circuit ducting could be satisfactorily cleaned by purging with high velocity air, however, the duct extraction system, hoppers, etc., should be sufficiently accessible to enable them to be completely cleaned between different batches of powder.

Permutation of the different aspects of suspension flow with the various system orientations and a variety of particle sizes amounts to a considerable quantity of work. However, being relatively undaunted it was decided to design a rig which would be both sufficiently flexible and versatile to allow simple adaptation to accommodate all these studies.

The present study has been quantitatively concerned with pressure drop measurements for a range of powders flowing through vertical and horizontal ducts and various bends. The turbulent dispersion aspect has only been assessed qualitatively; tracer gas techniques have not been used. The rig has recently been adapted for a detailed investigation into the heat transfer characteristics of a flowing gas-solid suspension, but this work is not part of the present study. Suggestions for further work of immediate interest are given in sections 5.7, 6.7, 7.7 and 8.6.

3.2 Flow System Specification

The basic requirements of a flow loop for a positive pressure pneumatic conveying system is shown below:-

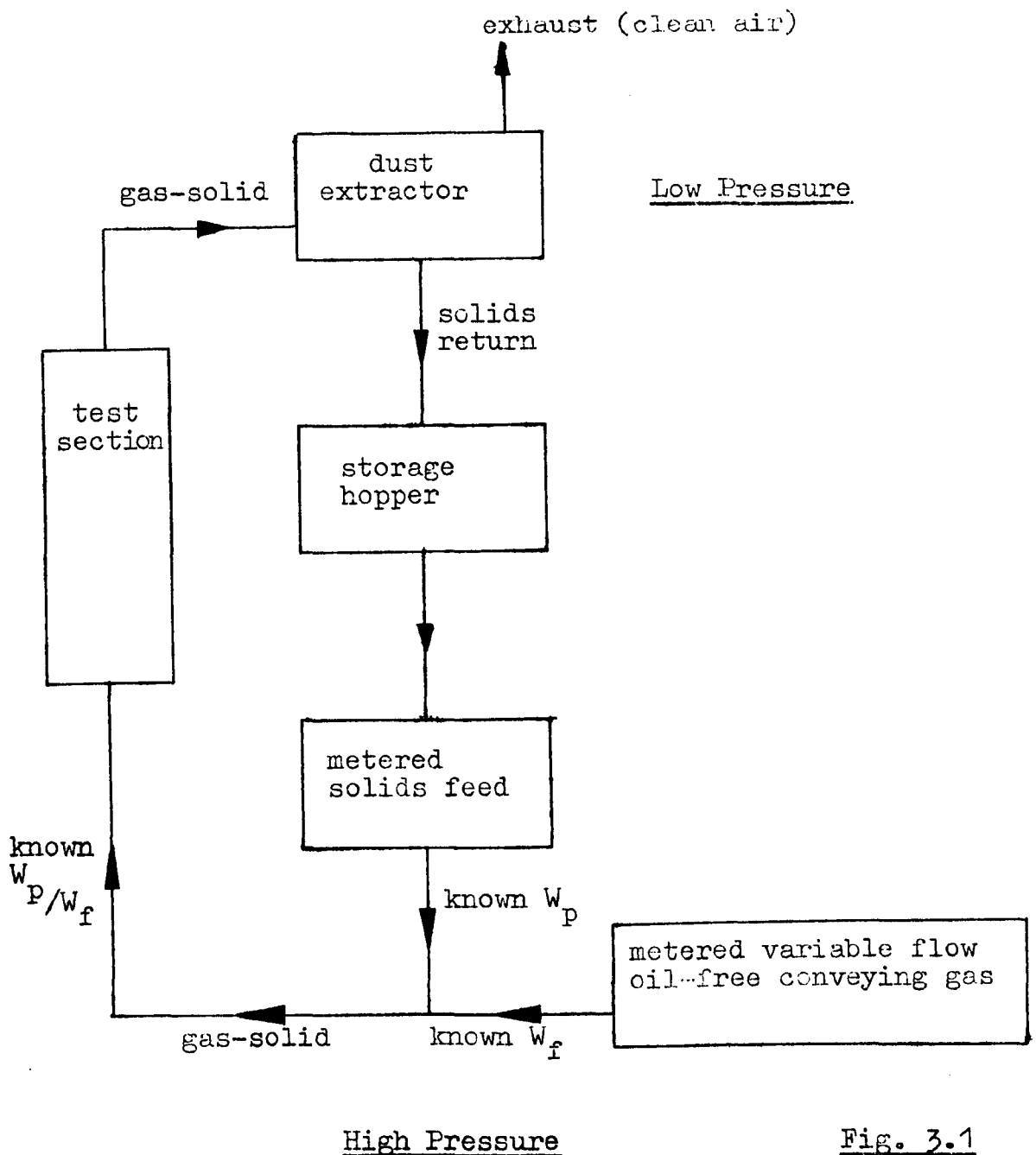


Fig. 3.1

The doubtful reliability and accuracy of the limited number of instruments available for measuring flowing aerosols indicated that, for precise metering of the two phases, it was necessary that each phase was separate during the flow measurements. The solids were metered with a calibrated screw-feeder having interchangeable screw-flights (see appendix A.2) and the air by an orifice-plate. It was essential that the air flow remained uncontaminated otherwise the cohesive properties of the solids may be affected, and so

an oil-free compressor was obligatory.

The acquisition of reliable data necessitates lengthy experiments and so the solids must be recirculated on account of cost and also that their properties remain constant, for example, the moisture content of circulated powder and new powder could be significantly different. Thus the system had to permit continuous circulation of the solids with minimum deterioration of the particulate matter. This was provided by a pair of cyclones at the low pressure end of the flow loop feeding back into the screw-feeder at the high pressure end via a pressure-lock arrangement of hoppers.

The whole system was designed to create steady flow conditions, pressure fluctuations being kept to a minimum, within the limits set by the compressor (see section 3.3.1). To enable visual observation of the flow to be undertaken large sections of the flow loop were made from perspex.

Detailed attention to the layout of controls, location of instrumentation and test-section made it possible for one person to operate the plant, take readings and observe the flow behaviour during the course of a test run.

3.3 Outline Description of Equipment

The apparatus is shown in plates 1 and 2, whilst the main features of the plant are shown in Figs. 3.2 and 3.3. The use of the figures in conjunction with the plates allows the location and size of individual components to be estimated. These illustrations share the same key notation in the description of this section. Plates 3 and 4 show much of the remainder of the equipment which is either obscured in the other two plates or was modified at a later date. It

is felt that these illustrations are sufficiently well-explained by their titles. For easier reading, a simplified description of the apparatus, together with a line diagram, Fig. 1., is given in section 5.8. The plant comprises basically three circuits: air alone, the solids feed, and the two phase fluid section.

3.3.1 Compressor

It has been mentioned that the air supply must be oil-free and without pressure pulsations at both the inlet and the outlet. For the positive low-pressure system required the air must be delivered at about 200 ft³/min f.a.d., and at a gauge pressure of at least 8 to 10 lbf/in². There are a large number of oil-free machines available but the requirement of minimum pressure pulsations narrows the field considerably to two possible types of compressor:-

(i) A rotary positive displacement sliding vane compressor;

and (ii) A Lysholm compressor.

The Lysholm has a high lobe-rotor speed which is ideal for attenuating the pulsations to a very low level, and it can easily be uprated if required by modifying the belts and pulleys. Unfortunately it is approximately double the cost of a sliding-vane machine of similar rating. Messrs. Alldays and Onions make an eccentric-rotor sliding vane machine having a capacity of 200 ft³/min free air delivery at 10 lbf/in² gauge. Oil-free conditions are obtained by having the non-lubricated blower fitted with four graphite impregnated blades. Alldays recommend that the blades should be inspected every three months for wear, and so contamination of the circuit was an initial concern. The

end plate of the blower was removed several times during the few months of commissioning the rig and minimal wear was observed. In fact, during three years of relatively heavy duty the blades have only been renewed on one occasion, and this was during a periodic planned maintenance inspection. The blower was not equipped with water-cooling and after discussions with the manufacturers it was decided that the maximum duration of continuous operation of the compressor should be two hours. Experience revealed, however, that operation for two hours was only satisfactory for normal duty; defined as conveying solids through the two inch and three inch diameter pipes. For high solids flow rate through the one inch diameter pipe over-heating of the compressor was soon evident and test-runs were restricted to a maximum of one hour.

3.3.2 Air Flow Distribution

Most of the circuitry for air alone is in three inch nominal bore mild steel gas pipe, with bends and other pipe fittings of similar material. The whole of this circuit is only a short distance from the concrete floor of the laboratory, thus enabling it to be securely positioned with the aid of standard pipe supports screwed into the concrete. Like the rest of the rig, all parts of this circuit were pressurised and leaks were then eliminated by the soap-bubble procedure. The use of flexible conduits throughout any part of the circuit was avoided (see section 3.3.3).

Air is drawn into the compressor (B) through the inlet filter and silencer (A) via a safety valve of the dead-weight type (C). The three inch air-operated Saunders diaphragm valve (D) is used to regulate the air supply by

short-circuiting a known proportion of air back to the inlet (A). The air flows from the compressor along a straight length of pipe to an orifice plate (E), through a three inch manually-operated Saunders valve (F) to a reducing section (G) and finally mixes with the solid phase in the fluidising unit at (H). The lengths of pipes either side of the orifice plate, the orifice plate itself, and the reducer (G), were all designed in accordance with B.S.1042. The valve (F) is only used for testing the proper functioning of the relief valve (C) and for pressurising the air flow circuit to facilitate testing for leaks.

A one inch diameter air bleed-off line leads to three one inch air-operated Saunders diaphragm valves (K), which are used for venting or pressurising the system of hoppers.

3.3.3 Gas-Solid Flow Circuit

The rest of the flow loop consists of two inch diameter mild steel ducting (L) connecting the fluidising unit to the vertical perspex test sections (M) of three, two and one inch diameter and the mild steel return ducting (N) leading to the air filtering plant.

The initial experiments were concerned with vertical flow only and so the return ducting (N) was of no particular interest. To adapt the rig in order that the pressure drop around bends having different geometries, and along the horizontal immediately following these bends, may be investigated, it was only necessary to modify the flow loop at (N). At the conclusion of the bend pressure drop tests, a perspex bend of identical dimensions to one of the steel bends was installed at (N), so that suspension flow around the bend could be visually observed.

The selection of the compressor was largely based upon the essential consideration of pulsation-free flow, however, the use of unsuitable ducting in the suspension flow loop is another possible source of pressure pulsations. If the velocity is too low, saltation may occur in the horizontal pipes at (L) and (N), resulting in pressure surges due to particle deposition and intermittent re-conveying of partial slugs of material. This problem was resolved by continuous visual observation of the flowing suspension in (M), thus avoiding the difficulty encountered when opaque ducting only is used. The part of the flow loop (L) was necessarily mild steel because of the erosive nature of the alumina particles, and the circuit configuration was required so as to allow for the maximum length of vertical test section. It is also recommended that the use of flexible ducting should be avoided in the flow loop on account of vibration being induced by the flowing suspension on the ducting, and the resulting motion of the ducting causing possible minor pressure pulsations or even disrupting the nature of the flow.

Apart from any resultant pressure pulsations rendering the measurements of ΔP_m difficult due to fluctuating manometer levels, it was also experienced that the achievement of steady suspension flow was essential if manometer tappings were not to become prematurely blocked. There is also a possibly valid criticism that pulsations may exert a direct influence on the nature of the flow in the test section.

Some initial concern was that unsteady suspension flow may be induced by the geometry of the fluidising unit (H). Consequently a number of hard wood inserts were constructed

to reduce the internal dimensions of the mixing unit and increase the flow velocities there. The reasoning for this procedure was that any possible hold-up of solids in the unit would be reduced, thus lessening the time required for the re-establishment of steady flow conditions after the speed of the screw-feeder has been adjusted. The transparent walls of the mixing unit and the transparent vertical test section enable the performance of the mixing unit to be observed. It would appear that the initial design of the mixing unit and the inadvertent selection of two inch diameter conduit of unusual configuration at outlet from the mixing unit were completely fortuitous, since the presence of any of the inserts usually worsened the flow situation.

3.3.4 Solids Circulation

The main solids storage hopper (R) discharges the solids via a double-sleeve pinch valve into the pressure hopper (S), which supplies the solids supply bunker (T) via a second pinch valve. The bunker (T) is situated directly above the variable speed screw-feeder (U), which discharges solids into the fluidising unit where it interacts with the metered air from the air supply circuit. The screw-feeder is of conventional design apart from having the facility of interchangeable screw-flights, thus providing for accurate injection of powder over a wide range of mass flow (see section 4.5). The screw-feeder bearing and drive-shaft seals are discussed in appendix A.3. Further details of the design and performance of the screw-feeder are given in appendix A.2.

The hoppers (R) and (S) were constructed in mild steel with conical discharge outlets having a wall angle of 70

degrees to the horizontal. These hoppers were designed in accordance with Jenike's theories in order to ensure free flow of the alumina particles. Using the simple laws of thermodynamics it was calculated that the time required to pressurise hopper (S) by the bleed-air from (J) was of the order of six seconds.

The two pinch valves for controlling the flow of solids between the hoppers were remotely operated from the central control point. These valves were manufactured by Mucon Ltd., and are ideally suited for handling abrasive materials. The double-sleeve type was selected because of their ability to withstand a pressure differential of up to 10 lbf/in² gauge.

The structural support and access facilities for the hoppers, dust extraction plant, suspension flow loop and other ancillary equipment was provided for by Dexion Speedlock beams and open steel plank walkway, and proved satisfactory for the present study.

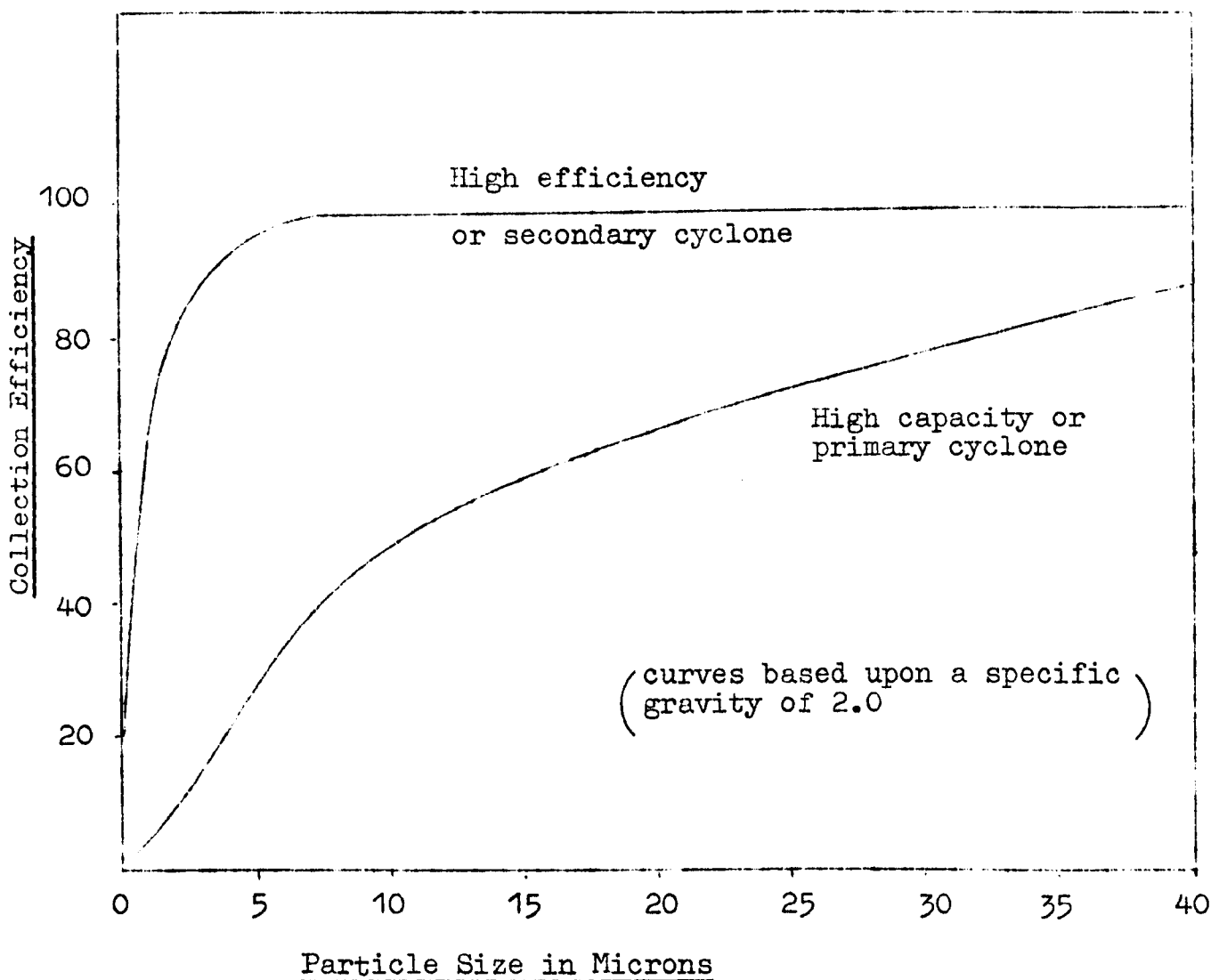
3.3.5 Air Filtration Plant

A previous study²⁹ had indicated that the use of a conventional bag filter, either within the main hopper or mounted on top of it, possibly suffers from three sources:-

- (i) When cleaning the filter bags the dislodged filter cake falls in bulk and could induce pressure pulsations.
- (ii) If the bag filter is cleaned by reverse air jets, typically at 100 lbf/in² gauge, then pressure pulsations in the circuit may result with consequent disturbance of test readings.

(iii) The reliability of filter bags is suspect for relatively high solids loading ratios ($W_p/W_f > 6$).

It was decided that a two-stage cyclone unit with an external bag filter would filter an air volume of 200 ft³/min containing up to 70 lb/min of alumina dust of particle size between 10 and 70 microns.



Cyclone Performance Curves

Fig. 3.4

The above performance curves were provided by the cyclone manufacturers Airfilco Ltd., who gave assurances that even with the alumina powder having a specific gravity of 3.94 the following collection efficiencies and pressure drops would be obtained:-

(i) Six inch diameter primary cyclone:-

55 to 60% for 15 micron particles,
 80% for 40 micron particles,
 90% for 70 micron particles,
 3 inches water gauge pressure drop.

(ii) Ten inch diameter secondary cyclone:-

99% for 15 micron particles,
 99.8% for 40 micron particles,
 100% for 70 micron particles,
 5 inches water gauge pressure drop.

The maximum solids flow rate of approximately 60 lb/min produces the following table:-

Powder mesh	Mean particle diameter microns	Cyclone Efficiency		Solids loading lb/min	Powder still in air, lb	
		Primary(P)	Secondary(Q)		after P	after Q
500	15	60	99	60	24	0.24
320	40	80	99.8	60	12	0.024
240	70	90	100	60	6	nil

Thus a thirty minute test run at 60 lb/min of 500 mesh powder results in 7.2 lb being collected in the bag filter (X), whilst with 320 mesh powder less than 1 lb arrives at the bag filter. The bag filter unit consists of four cotton bags

six inches diameter by six feet long providing an air/cloth ratio of 5 to 1. The bags are suspended vertically and the dusty air enters the hopper beneath the bags before passing upwards through the filter bags and defusing through the material to atmosphere. It was only necessary to clean the bags by mechanical shaking at the end of a test run. The powder removed from this hopper contained a high proportion of fines and so was periodically discarded.

The cyclone arrangement was satisfactory in that the filtration was relatively pulsation-free, due to the scroll-type inlet introducing the gas-solid flow into the body of the cyclone with minimum disturbance. The disadvantages of the cyclones appear to be:-

- (i) Loss of fines from the bulk of the powder.
- (ii) Possible attrition of the particular matter.
- (iii) Doubtful collection efficiency for very small particles.
- (iv) Erosion of the primary cyclone at inlet by the abrasive particles, in fact, this cyclone had to be reinforced with 0.5 inch mild steel plate.

3.4 Method of Plant Operation

The main features of plant control are as follows:-

- (i) Control of air flow;
 - (a) Adjust the four Enots pressure reducing valves, which supply air from the laboratory's hydro.. vane compressor to the Saunder's flow control valve (D) and the three one inch Saunder's valves (K), so that the valve (D) is fully open and the valves (K) completely closed.

- (b) Switch on the sliding vane compressor, which starts effectively in a "no-load" condition.
- (c) Gradually close valve (D) until the required air mass flow through the loop is indicated on the orifice-plate manometer.
- (d) Allow air only to flow through the plant for about 20 minutes, that the plant has settled down is determined from the air temperature at (E).

The valve at (F) remains open throughout.

(ii) Solids supply to screw-feeder;

- (a) With a charge of about 300 lb of powder in the main hopper (R) and both pinch valves closed, vent hopper (S) to atmosphere by regulating the appropriate Enots valve.
- (b) Open the top pinch valve and allow the powder to discharge into the hopper (S).
- (c) Close the top pinch valve and pressurise the hopper (S) using bleed-air from the sliding-vane compressor via the appropriate Enots valve.
- (d) Open the bottom pinch valve to discharge the powder into the solids supply bunker (T).

This valve is left open throughout a test run and the pressure between (T) and the fluidising unit (H) kept balanced.

This entire powder transfer sequence is performed from the central control point and requires approximately one minute.

(iii) Control of solids flow;

- (a) Switch on the screw-feeder motor, (appendix A.2).
- (b) Adjust the speed of rotation of the previously calibrated screw-flight with the hand-wheel on the Kopp variable speed system.
- (c) Re-adjust the air flow setting to allow for the additional energy required in transporting the solids. The particular Enots valve for regulating (D) needed careful attention to avoid any variation in the air flow rate.

(iv) Filtration and cleaning;

- (a) The cyclones automatically re-circulated a very high percentage of the powder back to the main hopper (R).
- (b) At the conclusion of each test run clean the filter bags by agitating them by operating the mechanical cleaning mechanism.

3.5 Problems Associated with Plant Operation

The highly abrasive alumina powder caused wear of the part of the screw-flight within the mixing unit, the inlet to the primary cyclone, the one inch to two inch diffuser at exit from the mixing unit, and erosion of all bends, to varying degrees, was observed (see Chapter 8). The wear was particularly excessive on the bends incorporated into the two inch diameter mild steel ducting preceding the vertical perspex test section. Some of these nine inch radius bends were "holed" after only four hours of circulation of the solids. Consequently, these bends were fitted with 0.5 inch thick mild steel backing plates.

Slight leakage of powder eventually occurred at the seal of the screw-feeder drive-shaft. This involved stripping down the seal assembly and replacing 'O' rings and felt washers. On one occasion the wear on the drive-shaft was sufficient to warrant replacement with a new primary shaft manufactured in harder steel.

In the early stages of operation of the plant, 'choking' of the test section occurred several times, but experience in recognising the warning symptoms of the nearness of choking completely eliminated this inconvenient and somewhat embarrassing problem.

At low air flow rates and high solid flow rates severe fluctuation of the manometer levels precluded the acquisition of reliable quantitative measurements.

3.6 Suggestions for Improvement to the Equipment

- (i) The limited rating of the compressor tended to be frustrating and a Lysholm compressor would be preferable.
- (ii) Air flow control with the three inch Saunder's diaphragm valve was not satisfactory, since continual attention to the Enots regulating valve was required to ensure constant air flow rate for a particular solids flow rate. Variation of the solids flow rate by adjusting the Kopp variator setting altered the circuit resistance and the air flow rate changed despite the Enots valve remaining constant. As a consequence of this, a particular test run consisting of a fixed Enots setting for a full range (usually fourteen) of solids flow rates, produced individual results at

different air flow velocities and hence different Reynolds' and Froude number values. The graphical plotting of results presented in this way is difficult, tiresome and should be avoided.

It is recommended that the air flow control be effected by a differential control valve which is regulated by the pressure difference across an orifice plate installed in the air flow loop. Thus any variation in the circuit resistance is reflected in a change in the orifice plate pressure drop which automatically adjusts the differential control valve to the original pre-set value. So the flow behaviour over a wide range of solids loadings can be obtained at any desired value of Reynolds' number or Froude number.

- (iii) The temperature rise of the system prevented test runs in excess of two hours from being carried out. It is recommended that a heat exchanger is incorporated into the air flow circuit at outlet from the compressor.
- (iv) Due to the erosion of the primary cyclone, possible attrition of the particles by the cyclone arrangement, and the doubtful collection efficiency for solids below about 30 microns diameter leading to a loss of fines, it is thought that a bag filter of the type manufactured by Dust Control Equipment Ltd., may be advantageous.

Note: Very recent adaptation of the rig for investigating the heat transfer characteristics of flowing suspensions has included recommendations (ii), (iii) and (iv).

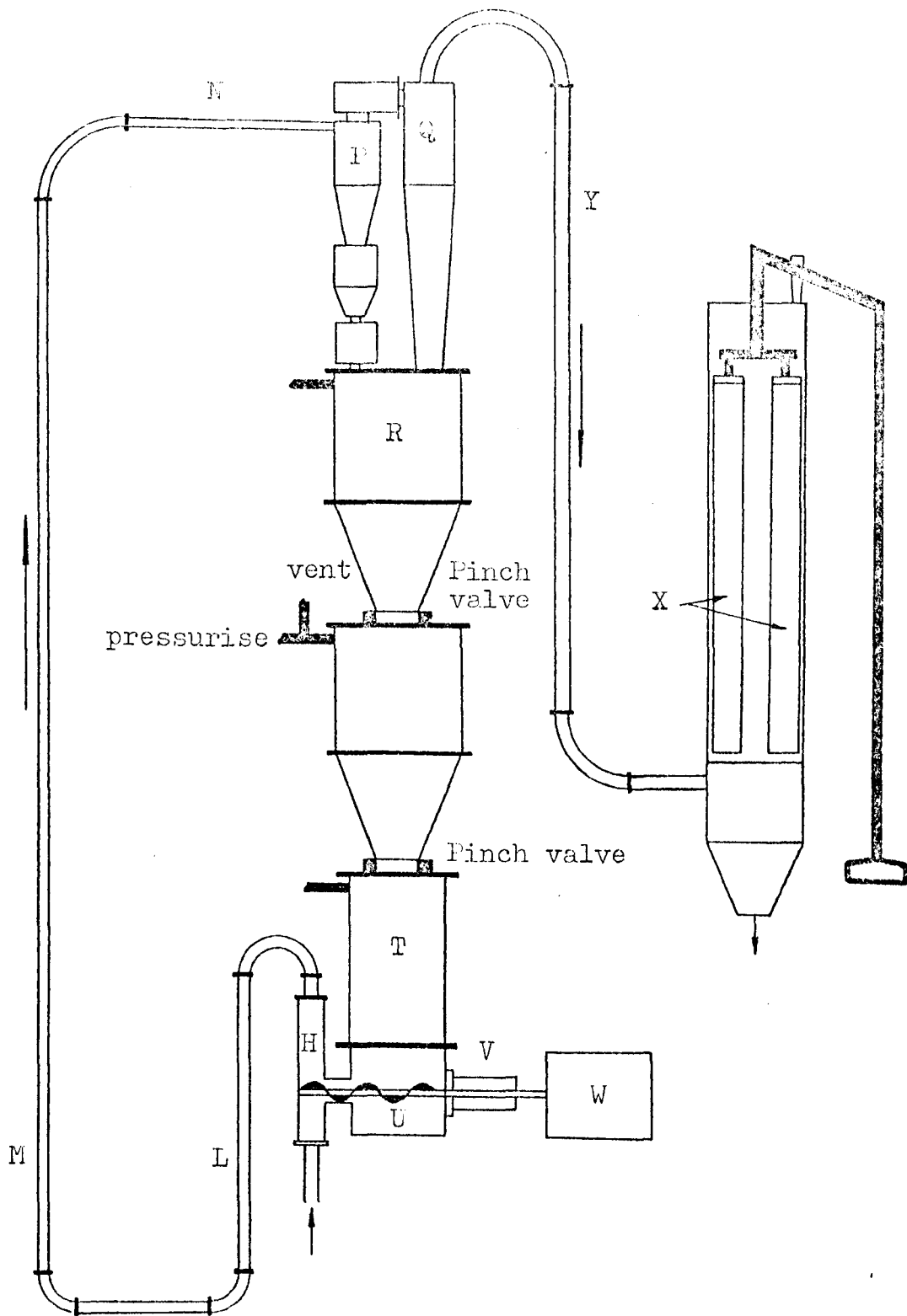


Fig. 3.2 Plant Layout (elevation)

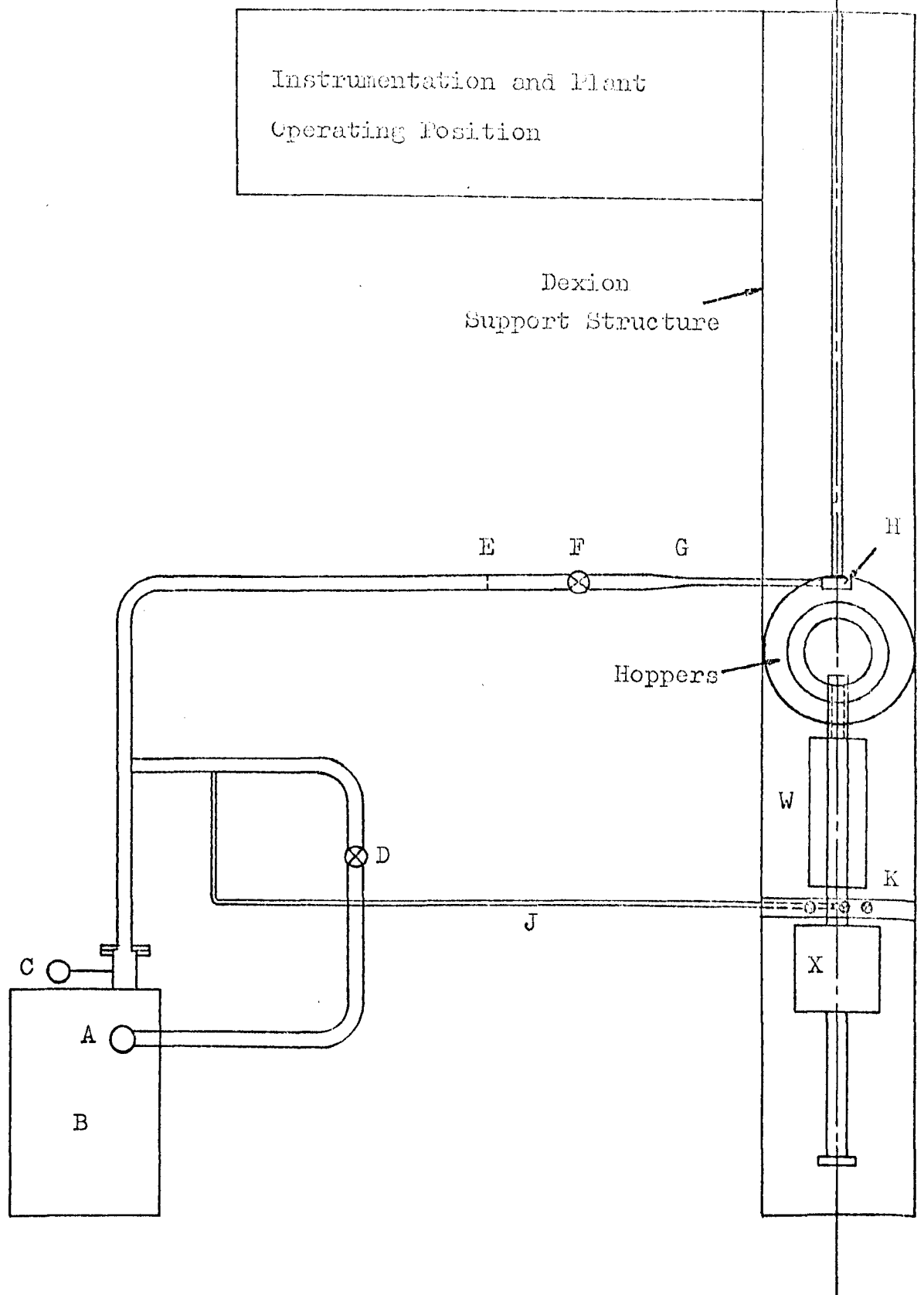
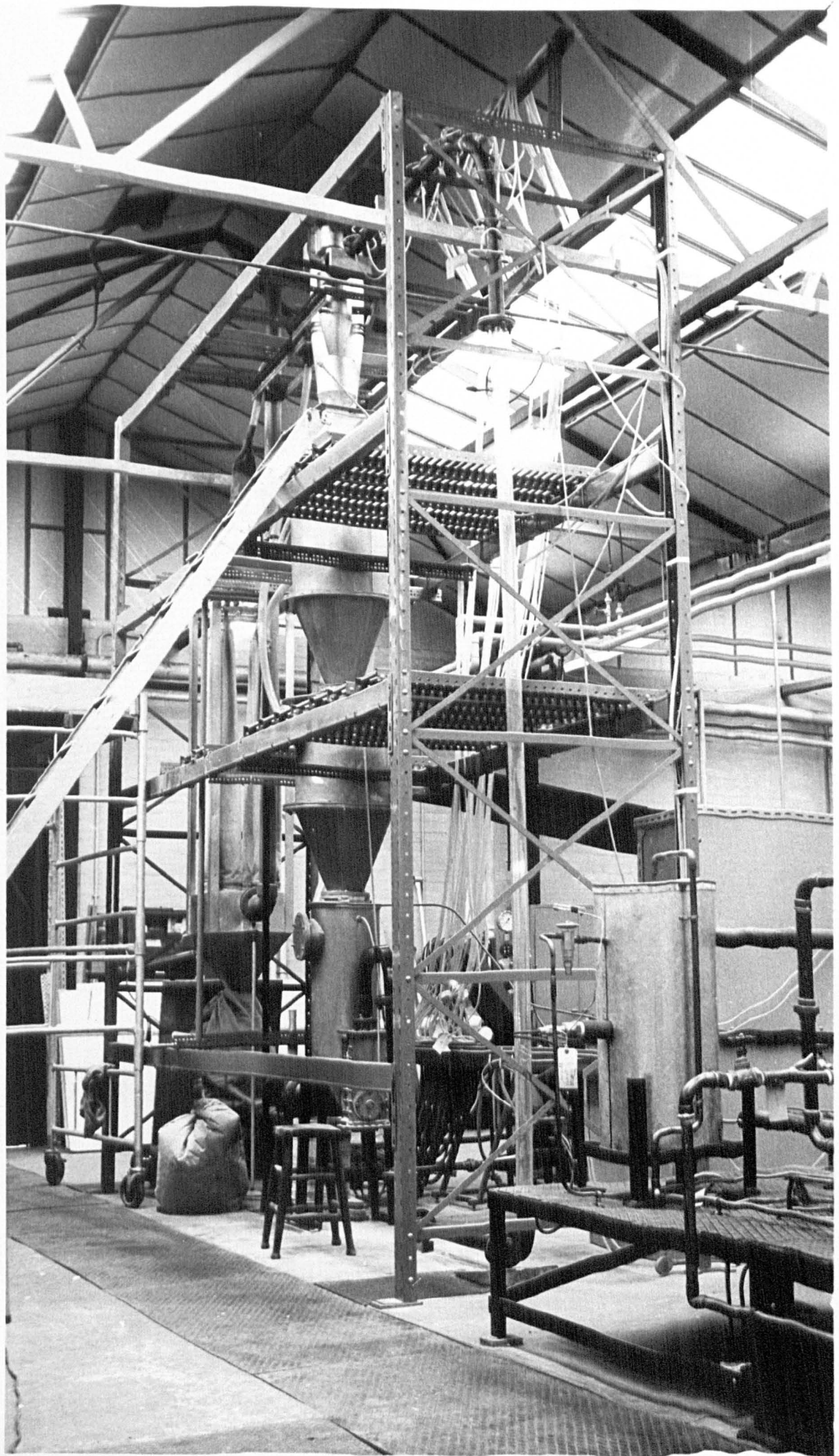


Fig. 3.3 Plant Layout (plan view)

N
P
R
S
X Y
J T
H M
L

Plate I : Gas-Solids Flow Rig.



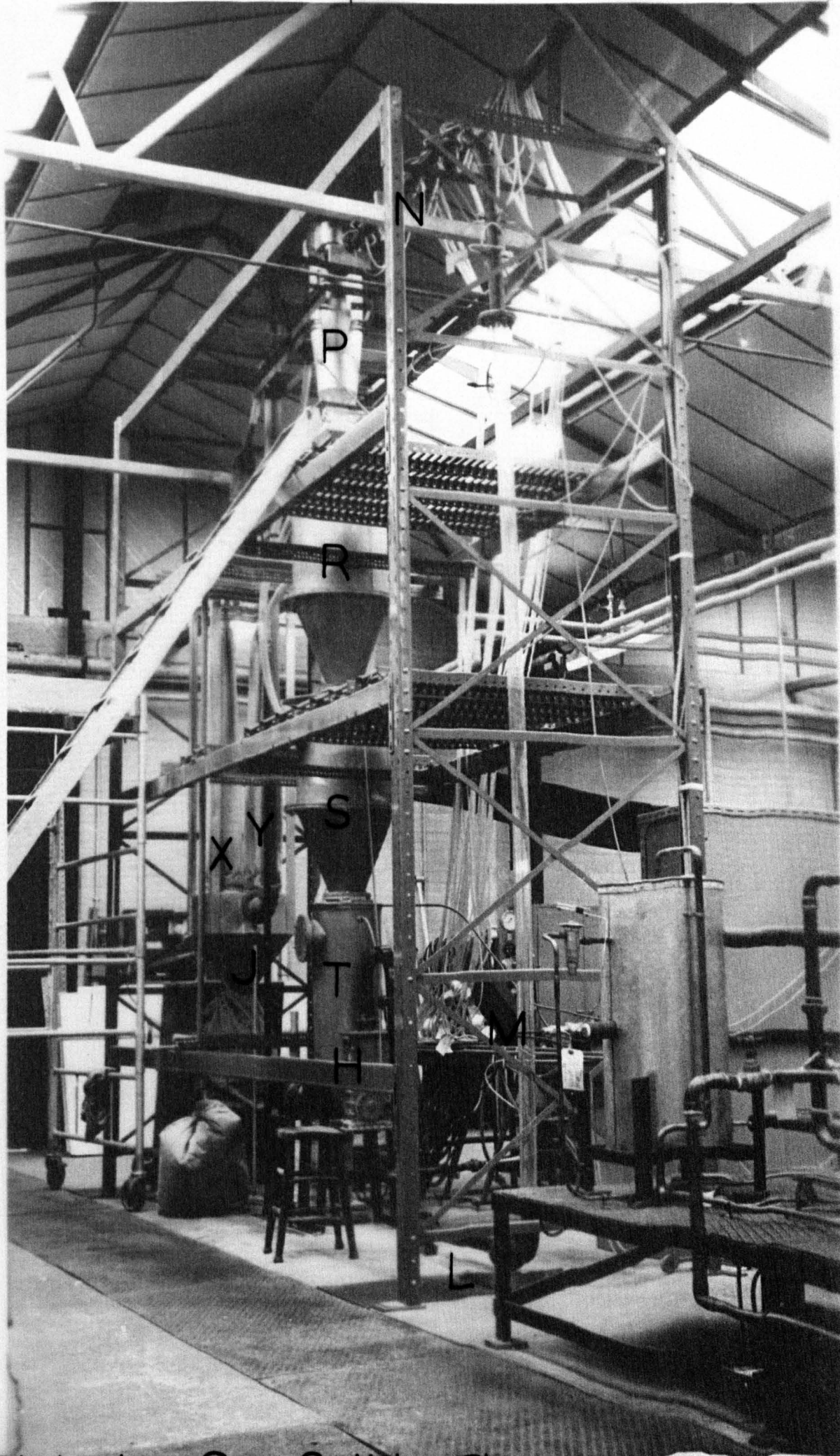


Plate I: Gas-Solids Flow Rig.

Q

R

S

M

T



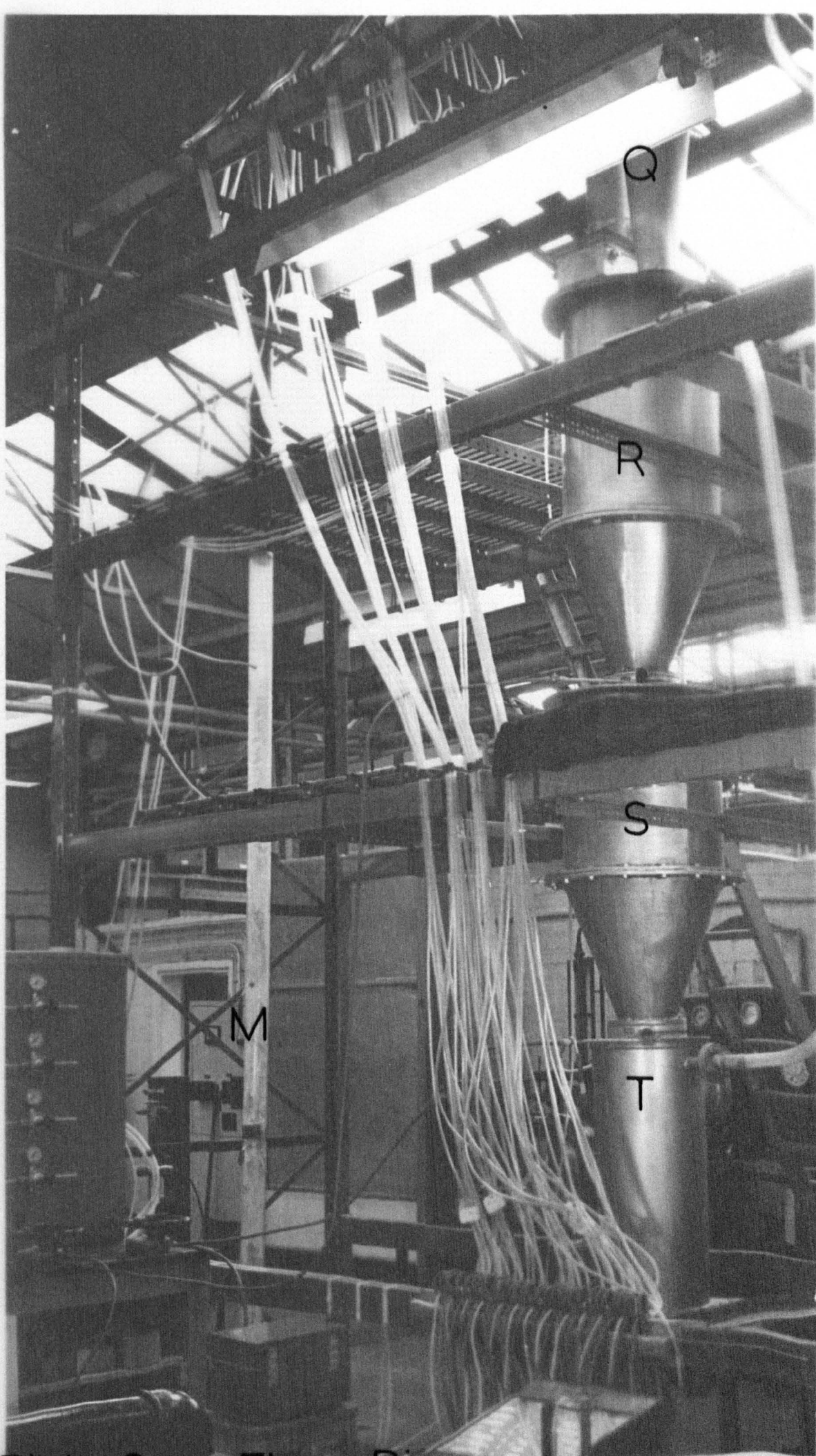


Plate 2 : Flow Rig.

N

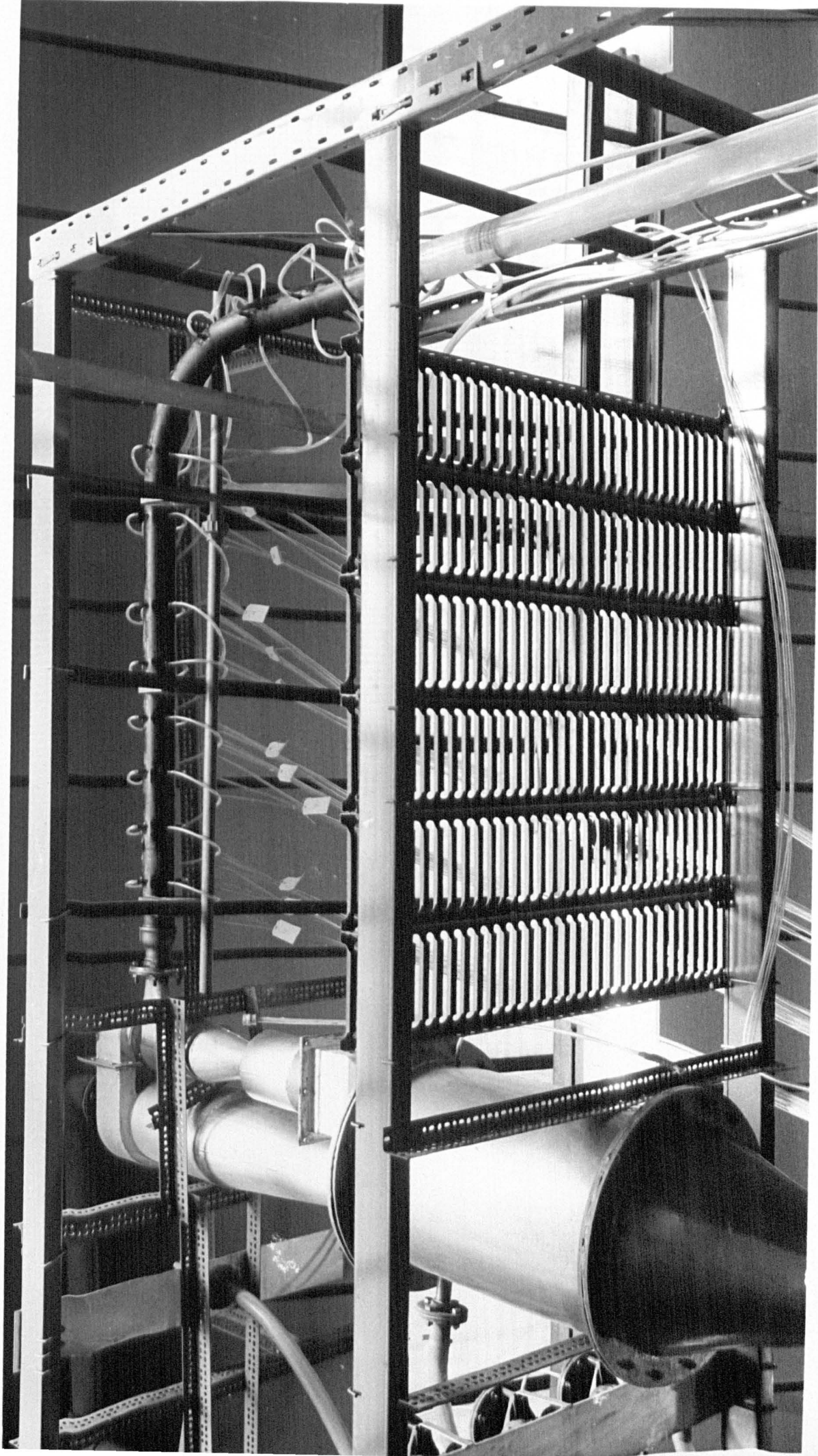
P

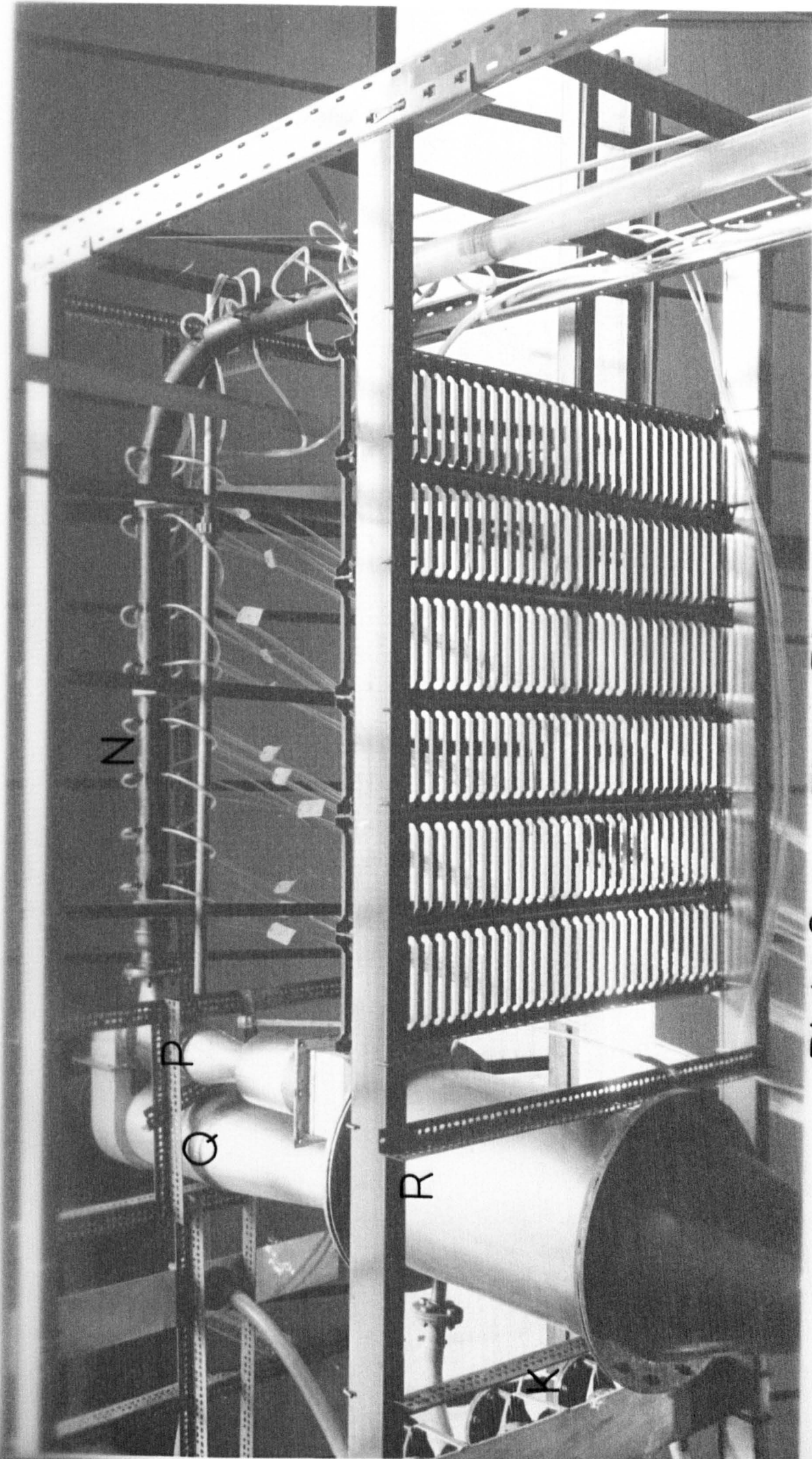
Q

R

K

Plate 3 : Flow Rig.





N

Q

R

R

X

Plate 3 : Flow Rig.

A

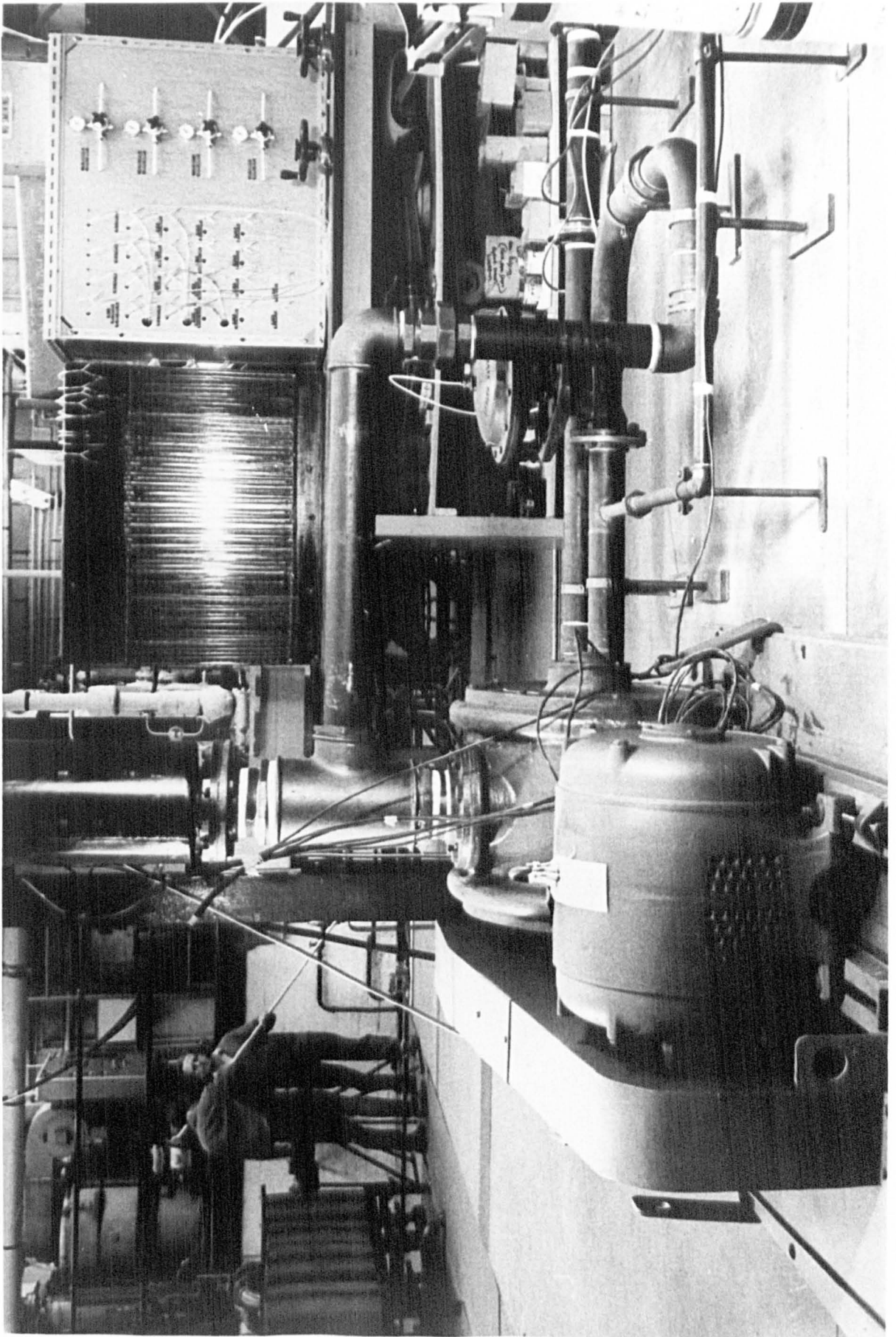
B

D

E

J

Plate 4: Air Supply.



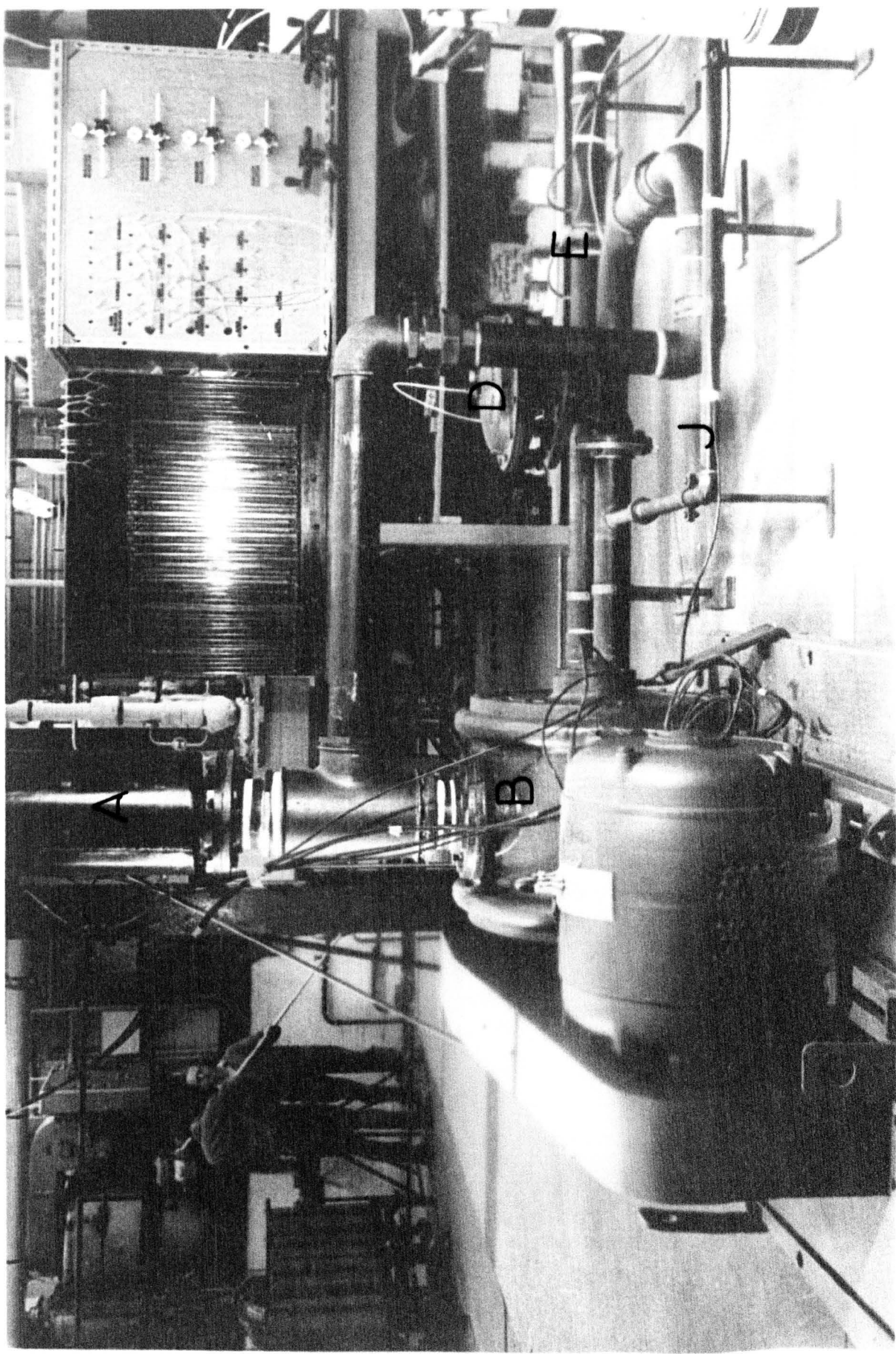


Plate 4 : Air Supply.

CHAPTER 4

EXPERIMENTAL MEASUREMENTS

4.1 Introduction

An investigation into gas-solid suspension flow may require measurement techniques for the determination of pressure drop, mass flow rate of the solids phase, density of the dispersed solids, particle temperature, velocity of the particles at a particular spatial point, electrostatic charge, particle size spectrum and the agglomerative state of the particulate matter. These are additional to the relatively easy determinations of the usual variables for single phase flow. Some general comments on the many problems which may arise in measuring the various parameters which describe a particular gas-solid flow situation are:-

- (i) Measurements in a flowing suspension generally depend upon some measurable physical effect which derives entirely from one of the phases and not from the other. Unfortunately traditional single phase flow measuring instruments are strongly sensitive to the presence of the solids and so the influences of either phase is difficult to interpret.
- (ii) The suspension is a hostile medium to any instrument placed in the flow due to both abrasion and dust deposition. The abrasive effects lead to the degradation of optical surfaces used in some instruments, apart from the necessity that such equipment must be robust enough to withstand the impact and frictional forces from the solid flow. Dust deposition may alter the surface properties

of electrostatic instrumentation, reduce insulation levels and render the traversing systems of detector probes liable to seizure.

- (iii) The taking of point measurements with a probe may be questionable on account of flow disruption by the probe. However, minimal flow interference necessitates the use of miniaturised instruments, but on account of (ii) these must also be durable.
- (iv) In a fairly dense fine particle suspension problems are likely to arise due to particle agglomeration, and also the application of optical equipment requires a high light flux level to penetrate such a suspension.

Two review articles by Boothroyd and Goldberg^{73,74} provide a clear assessment of both the industrial and research requirements and achievements in the measurements of flowing gas-solid suspensions. The papers contain a considerable bibliography relating to this subject and a detailed account of isokinetic sampling techniques is presented. Isokinetic sampling requires a bent sampling tube (typically 0.25 inches diameter) placed in the flow and a sample is aspirated at a known velocity, usually based upon a knowledge of the carrier gas velocity profile. The mass, m , of the dust sample is measured and further analysis provides information as to particle size distribution, shape, dryness, and electrostatic charge, q . Thus, the average charge per particle, q/m , can be derived, assuming all the particles receive charge of the same sign. It does appear, however, that the reliability of these probes is questionable, for example, the turbulence in pipes of normal industrial size is such that it is not

feasible to sample isokinetically at all times.

A recent extensive programme of work into instrumentation for measurements in relatively dense flowing suspensions of fine particles has been carried out by Arundel⁷⁵. This research reports on measurements of the particle dispersed density, particle velocity, charge to mass ratio in the flow and humidity effects. The investigation is typical of many researches which illustrate the difficult obstacles that have to be overcome in devising adequate instrumentation for investigating the behaviour of a flowing gas-solid suspension.

It has been mentioned previously that the objective of the present study is to obtain quantitative information on the pneumatic conveying of particulate matter, which would hopefully contribute to the industrial design of such plant. Thus it was essential that the study did not deviate to either a purely theoretical approach or become totally re-directed to developing instrumentation. Examination of the minimum number of variables needed to carry out the study showed that a knowledge of the following parameters would be indispensable:-

- (i) Density of the carrier fluid, ρ_f , in the test-section. This requires a knowledge of the absolute pressure in the test-section and the temperature of the fluid (see section 4.2).
- (ii) Dynamic viscosity of the carrier fluid, μ , in the test-section. This calls for temperature measurement and use of the appropriate property tables (see section 4.2).

- (iii) Mean air flow velocity, \bar{u}_f , and mass flow rate of the carrier fluid, W_f , (see section 4.3).
- (iv) Pressure differentials of the fluid phase only, ΔP_0 , and of the flowing suspension, ΔP_m , (see section 4.4).
- (v) Geometry of all test-sections and spatial position of static pressure tapings (see section 4.4).
- (vi) Mass flow rate of the solid particles, W_p . The difficulty in measuring accurately the mass flow rate of the solids phase in a two phase flow was resolved by monitoring the solids flow rate prior to it becoming diffused with the carrier gas (see section 4.5).
- (vii) Powder property determinations. The physical character of the conveyed material is a significant criterion in any transportation system, but becomes of paramount importance when the particles are re-circulated (see section 4.6).

An understanding of these overall total flow properties in a duct facilitates the derivation of the principle dimensionless groups (section 2.4) which enable correlations to be established for the prediction of system design data.

4.2 Temperature Measurement of the Gaseous Phase

4.2.1 Introduction

A direct measurement of the temperature of the gaseous phase alone within a flowing gas-solid suspension is difficult to accomplish. Even the temperature determination of the two phase flow itself is fraught with many problems. A thermocouple inserted in the flow is likely to record an

exceptionally high temperature owing to the particles losing their kinetic energy to produce heat by direct impact. If the thermocouple was shielded then the impacting solids may have a tendency to deposit on the surface and resist it from being cooled by the surrounding flow. Peskin and Brillier⁷⁶ used a 'bucket probe' to measure the temperature of solids. Their technique was to arrange for the probe to periodically collect a sample of solids and record the temperature before heat losses occur.

A thermocouple shielded from impingement of the particles by an aerofoil shape and so arranged that the carrier fluid only flows to the instrument was described by Dean⁷⁷. The basic requirement of the instrument is that the solid phase contributes nothing to the measurement. However, even though the design of the shield will minimise the heat generated through degradation of the kinetic energy of the particles, this relatively small amount of heat may be substantially increased by slight mis-alignment of the shield.

On account of the above difficulties in the temperature measurement of the carrier fluid, the knowledge of which was to be used in evaluating variables of second order importance, namely fluid density and viscosity, a simple indirect technique was employed.

4.2.2 Experimental Arrangement and Procedure

A copper-constantan thermocouple was placed in the air flow loop just upstream from the orifice plate, care being taken to ensure that the thermocouple head was centrally situated in the duct. A second thermocouple was located centrally in the airstream and equidistant from the first and last static pressure tappings of the test section, measured

longitudinally. The two thermocouples were connected to a potentiometer situated at the control point.

The compressor was switched on and the air flow control valve adjusted to allow the maximum quantity of air to flow through the test section. The two thermocouple milli-volt values and the ambient temperature were recorded from the potentiometer at appropriate time intervals (see tables 4.1 and 4.2).

Graphs of milli-volt versus time were drawn which illustrated that a steady state had been achieved (see Figs. 4.1, 4.3 and appendix A.5., Figs. A.5.1., A.5.2., A.5.3.). The correlations between the milli-volt readings in the test section and at the orifice plate were drawn (see Figs. 4.2, 4.4 and appendix A.5., Figs. A.5.4. to A.5.7.), and calibration equations deduced in the following manner:-

- (i) From Fig. 4.2, representing the three inch diameter bend having a radius of curvature of 18 inches, the following information can be obtained;

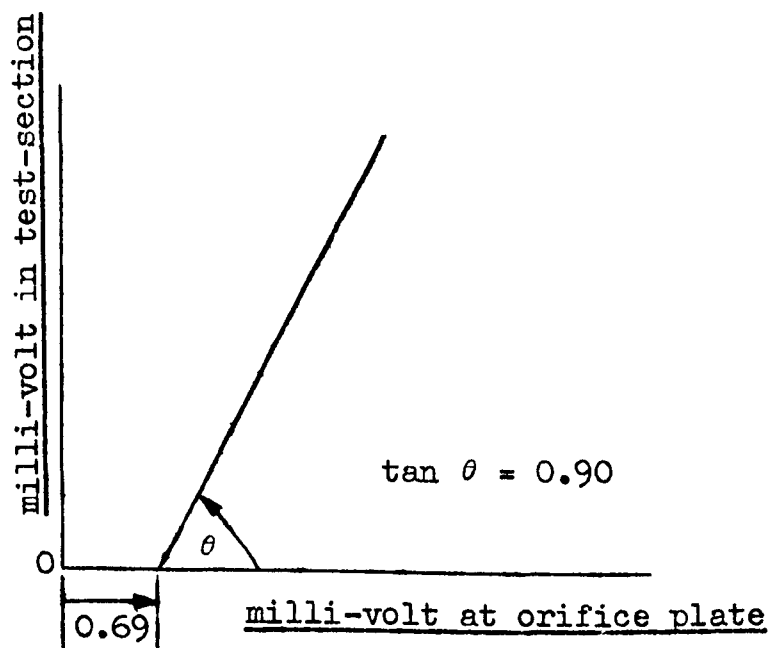
Table 4.1

Temperature Calibration for Three inch Bend having a
Radius of Curvature of 18 inches

Time (minutes)	Thermocouple Readings		Ambient temperature (°C)
	at orifice-plate (mV)	in test section (mV)	
2	1.03	0.28	21.0
4	1.20	0.41	21.0
6	1.33	0.53	21.1
8	1.44	0.64	21.2
10	1.52	0.73	21.3
12	1.62	0.81	21.4
14	1.68	0.89	21.5
16	1.76	0.96	21.6
18	1.82	1.02	21.7
20	1.88	1.08	21.8
24	1.99	1.18	21.9
28	2.08	1.27	21.9
32	2.16	1.36	21.9
36	2.23	1.42	22.0
40	2.30	1.48	22.0
50	2.44	1.59	22.3
60	2.54	1.69	22.6
80	2.66	1.80	23.0
100	2.76	1.86	23.3
120	2.82	1.91	23.6
150	2.85	1.93	23.9

Temperature Calibration for One inch Bend having a
Radius of Curvature of 10 inches

Time (minutes)	Thermocouple Readings		Ambient temperature (°C)
	at orifice-plate (mV)	in test section (mV)	
2	1.11	0.10	17.0
4	1.37	0.33	17.1
6	1.55	0.48	17.2
8	1.74	0.59	17.3
10	1.86	0.71	17.5
12	2.01	0.80	17.6
14	2.15	0.90	17.8
16	2.23	0.99	17.9
18	2.36	1.07	18.0
20	2.45	1.16	18.1
24	2.63	1.29	18.2
28	2.78	1.42	18.4
32	2.94	1.53	18.7
36	3.07	1.64	18.9
40	3.20	1.73	19.0
50	3.45	1.92	19.6
64	3.70	2.11	20.0



$$\text{So, } (mV)_{\text{test-section}} = \left\{ (mV)_{\text{orifice-plate}} - 0.69 \right\} 0.90 \quad (1)$$

The correlation curve for air temperature expressed in milli-volts (mV) and degrees Kelvin ($^{\circ}\text{K}$) (Fig. 4.5) gives:-

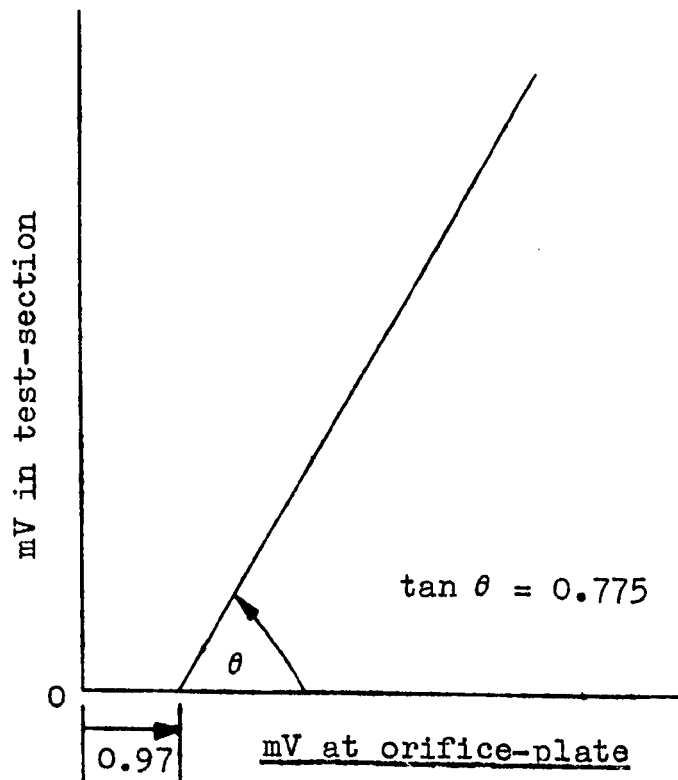
$$\text{Air temperature in } ^{\circ}\text{K} = 273.9 + 24.2(mV) \quad (2)$$

Equations (1) and (2) give the test section air temperature relative to ambient conditions, so designating the mean ambient temperature in $^{\circ}\text{C}$ by t_a , the final equation is obtained:-

Test section carrier fluid temperature in $^{\circ}\text{K}$,

$$T_f = \left[273.9 + 24.2 \left\{ (mV)_{\text{orifice-plate}} - 0.69 \right\} 0.90 + t_a \right] \quad (3)$$

(ii) A repeat example for comparative purposes, using Fig. 4.4, one inch diameter bend and 10 inches radius of curvature, is as follows:-



$$\text{So, } (mV)_{\text{test-section}} = \left\{ (mV)_{\text{orifice-plate}} - 0.97 \right\} 0.775 \quad (4)$$

From equations (2) and (4) and taking t_a into account:-

$$T_f(^{\circ}K) = \left[273.9 + 24.2 \left\{ (mV)_{\text{orifice-plate}} - 0.97 \right\} 0.775 + t_a \right] \quad (5)$$

Numerical example:

Substituting $(mV)_{\text{orifice-plate}} = 2.0$ and $t_a = 20^{\circ}C$ into equations (3) and (5), the test section air temperatures obtained are:-

$$T_f = 322.4^{\circ}K \dots\dots\dots \text{from (3),}$$

$$T_f = 313.2^{\circ}K \dots\dots\dots \text{from (5).}$$

Thus a percentage variation of less than 3% in evaluating T_f from two equations relevant to completely different physical situations. The above procedure was repeated on nine occasions (see appendix A.5), that is, for the three vertical pipes and then for the six bends.

The test section thermocouple was removed and solids allowed to flow through the suspension flow loop. The millivolt reading at the orifice-plate was recorded for every individual flow condition and the equivalent temperature of the gaseous phase of the flowing suspension deduced from the appropriate calibration equation. Highly accurate determination of T_f was not expected, although the value of T_f must be of the correct order of magnitude. To confirm that the approach was adequate, well-lagged thermometers were placed at different positions along the outside wall of the test section, and the temperatures recorded for a high proportion of the vertical pipe tests. Knowing the thickness of the

perspex wall of the duct and its thermal conductivity, a simplified heat transfer calculation justified the above indirect approach.

4.2.3 Density of the Gaseous Phase

In the evaluation of the fluid density, ρ_f , the absolute pressure in the test section, P_A , (see section 4.3) was also required. Thus, from the Equation of State:-

$$\rho_f = \frac{P_A}{R T_f}, \quad (6)$$

where R is the gas constant.

Since T_f and P_A were known for every single flow situation, a reasonably accurate knowledge of ρ_f could be calculated. During the first 90 test runs on the vertical pipes, taken over a period of four months, ρ_f varied from 0.073 lb/ft³ to 0.060 lb/ft³, that is, a variation of 18%.

4.2.4 Viscosity of the Gaseous Phase

The dynamic viscosity, μ , of the gaseous phase was deduced from T_f and the viscosity versus temperature correlation curve (Fig. 4.6). From Fig. 4.6, obtained from standard tables of physical properties, the following relationship can be obtained:-

$$\mu = [7.46 + 0.018(T_f - 300) \times 10^{-4}] \text{lb/ft min} \quad (7)$$

The variation in μ for the vertical pipe tests was from 0.00089 lb/ft min to 0.00076 lb/ft min, that is, a variation greater than 14%.

It must be remembered that these seemingly wide deviations cover a large number of tests concerned with ducts having diameters of one, two and three inches.

4.3 Measurement of the Superficial Velocity of the Gaseous Phase

4.3.1 Introduction

Although the orifice-plate situated in the air flow loop was made according to B.S. 1042 (see Fig. 4.7), the screw threads on the three inch nominal bore steel tubing, necessary for accommodating the two screwed flanges clamping the orifice-plate in position, made the accurate and secure location of the static pressure tapings difficult (see Fig. 4.7). As a result, the pressure tapings were conveniently positioned either side of the orifice-plate, which then required calibrating. It could be suggested that the interference of the screw threads was a minor detail, however, it was also felt that calibrating the orifice plate by a pitot-traverse in the test section was sound practice.

4.3.2 Orifice-Plate Calibration Procedure

A stainless steel pitot tube, with an outside diameter of 0.06 inches, was positioned in the three inch diameter vertical test section approximately forty diameters above the start of the straight vertical duct. The total head tube was mounted on a traversing system which enabled the tube to traverse the air stream in increments of 0.1 inches. At every station the pressure differential between the total head tube and a wall static pressure tapping in line with the pitot tube head was measured with an inclined manometer. Simultaneously, the pressure differential across the orifice-plate, absolute pressure in the test section and temperature of the flowing air were recorded (see Table 4.3).

4.3.3 Analysis and Results of Pitot-tube Traverse

The error in assuming that the air flow is incompressible

Table 4.3

Pitot-tube Traverse in Vertical Three inch diameter DuctTest No. 512

Traverse distance (in)	Pressure Differential (cm)		Test section absolute pressure cm water	Air temperature at orifice plate (mV)	Room temperature (°C)
	Pitot tube	Orifice Plate			
0	15.00	20.1	47.1	2.44	18.8
0.1	16.10	20.1	47.1	2.44	18.8
0.2	16.85	20.1	47.1	2.44	18.8
0.3	17.60	20.1	47.2	2.44	18.8
0.4	18.25	20.1	47.2	2.45	18.8
0.5	18.85	20.1	47.2	2.45	18.8
0.6	19.30	20.1	47.3	2.45	18.8
0.7	19.65	20.1	47.3	2.45	18.8
0.8	20.15	20.1	47.3	2.45	18.9
0.9	20.45	20.1	47.3	2.45	18.9
1.0	20.75	20.1	47.4	2.46	18.9
1.1	21.05	20.1	47.4	2.46	18.9
1.2	21.05	20.1	47.5	2.46	18.9
1.3	21.35	20.1	47.5	2.46	18.9
1.4	21.35	20.1	47.6	2.46	18.9
1.5	21.30	20.1	47.6	2.46	18.9
1.6	21.30	20.1	47.6	2.46	19.0
1.7	21.15	20.1	47.6	2.46	19.0
1.8	21.00	20.1	47.6	2.46	19.0
1.9	20.70	20.1	47.6	2.46	19.0
2.0	20.40	20.1	47.6	2.47	19.0
2.1	20.10	20.1	47.6	2.47	19.0
2.2	19.75	20.1	47.4	2.47	19.0
2.3	19.30	20.1	47.4	2.47	19.0
2.4	18.70	20.1	47.4	2.47	19.0
2.5	18.30	20.1	47.4	2.47	19.0
2.6	17.55	20.1	47.4	2.48	19.0
2.7	16.55	20.1	47.4	2.48	19.0
2.8	15.60	20.1	47.4	2.48	19.0
2.9	14.95	20.1	47.4	2.48	19.0

at Mach number values of less than 0.2 is below 1%. Since a Mach number, M , of 0.2 is equivalent to over 200 ft/s, then the incompressibility assumption is quite valid for the two inch and three inch diameter pipes, and also for part of the one inch tests. The maximum air flow velocity in the one inch duct during the present study was equivalent to a Mach number below 0.4. Using the well-known form of Euler's equation when applied to a pitot-tube placed in a subsonic gas stream:-

$$\frac{P_s - P}{\frac{1}{2}\rho_f u_f^2} = \left[1 + \frac{M^2}{4} + \frac{(2 - \gamma)}{24} M^4 + \dots \right] \quad (8)$$

where P_s is the stagnation pressure of the gas stream,

P is the static pressure of the gas stream,

γ is the ratio of the specific heats.

For a completely incompressible fluid the right-hand side of equation (8) reduces to unity. When $M = 0.2$, the term in square brackets is approximately 1.01 and when $M = 0.4$ it becomes 1.04. It was decided that these errors of 1% and 4% were acceptable and so the following relationship was assumed for all flow conditions:-

$$(P_s - P) = \frac{1}{2}\rho_f u_f^2 \quad (9)$$

where $(P_s - P)$ is the pressure differential recorded by the pitot-tube manometer for a particular fluid of density ρ_f travelling with a velocity u_f . The velocity u_f is the value at a particular distance from the longitudinal centre-line of the duct, that is, at a radius r , and is represented by $(u_f)_r$.

A graph of the fluid velocity versus the duct radius (or traverse distance), for one particular mean flow rate, is shown in Fig. 4.8. This graph was compared with the accepted work of Nikuradse⁷⁸ who produced velocity distribution curves

for smooth pipes at Reynolds' number values of 2.3×10^4 and 1.1×10^5 . The diagram in Fig. 4.8 is a mean of the two Nikuradse curves, and so is appropriately in the same Reynolds' number range as the present study. The principle deviation of the experimental curve from Nikuradse's curve was near the pipe-wall surfaces.

Fig. 4.9 shows a graph of $(u_f)_r \cdot r$ versus r for the two traverses, wall to pipe centre and pipe-centre to opposite wall. The area under the curve is related to the volumetric fluid flow rate, V_f , by the expression:-

$$\dot{V}_f = 2\pi \int_0^{D/2} (u_f)_r \cdot r \, dr \quad (10)$$

The curves in Fig. 4.9 give \dot{V}_f values of $2.59 \text{ ft}^3/\text{s}$ and $2.78 \text{ ft}^3/\text{s}$, and so the mean $\dot{V}_f = 2.69 \text{ ft}^3/\text{s}$, from which the mean air velocity, $\bar{u}_f = 54.8 \text{ ft/s}$, this velocity corresponds to a particular pressure drop across the orifice-plate. The variation in the \dot{V}_f values is partially due to end errors on account of the thickness of the pitot tube, and partially due to inaccurate location of the pipe centre-line.

The first series of pitot-tube traverses (tests 501 to 509) covered a range of nine values of air flow rate. The data was evaluated using a computer program (see appendix A.1.1), the area under the $(U_f)_r \cdot r$ versus r curves being determined by the trapezoidal rule. A typical print-out (test 504) of the results is illustrated in Table 4.4.

In view of the illustrations shown in Figs. 4.8 and 4.9 it was decided to repeat the pitot-tube tests and a new pitot-tube was constructed. This second series of tests (tests 510 to 518) were also carried out in the vertical three inch diameter duct. A results print-out (test 512) is

Table 4.4

Pitot-tube Traverse Results

DATE	71070
TEST NO	504
PIPE DIA	3 INCHES
ATMOS PRES	29.37IN HG
ROOM TEMP	15.4DEG C
ENOTS	7.80
AV DENSITY	.0697LB/CU FT
VISCOSITY	.000787
REYNOLDS NO	67694
ORIFICE PD	3.87IN. WATER
AV VELOCITY	50.9FT/S
VEL A	53.7FT/S
VEL B	48.2FT/S
MASS FLOW	0.175LB/S
MF A	0.183LB/S
MF B	0.166LB/S

RAD	VEL	VEL*RAD	TEMP	ROE
1.5	47.5	71.24	325.8	0.0695
1.4	49.1	68.79	325.6	0.0695
1.3	51.6	67.07	325.6	0.0695
1.2	53.1	63.72	325.4	0.0696
1.1	54.4	59.87	325.1	0.0696
1.0	55.5	55.49	325.1	0.0696
0.9	56.4	50.74	324.9	0.0697
0.8	57.1	45.69	324.6	0.0697
0.7	57.7	40.41	324.4	0.0698
0.6	58.3	35.00	324.1	0.0698
0.5	58.8	29.40	323.9	0.0699
0.4	59.4	23.76	323.7	0.0699
0.3	59.6	17.88	323.4	0.0700
0.2	60.0	11.99	323.2	0.0700
0.1	60.1	6.01	322.9	0.0701
0.0	59.7	0.00	322.7	0.0701
-0.1	59.5	-5.95	322.5	0.0702
-0.2	59.3	-11.85	322.2	0.0702
-0.3	58.4	-17.51	322.0	0.0703
-0.4	58.0	-23.20	321.7	0.0704
-0.5	56.8	-28.41	321.2	0.0705
-0.6	55.8	-33.47	321.0	0.0705
-0.7	54.9	-38.40	320.8	0.0706
-0.8	52.8	-42.27	320.5	0.0706
-0.9	52.1	-46.92	320.3	0.0707
-1.0	49.5	-49.46	320.3	0.0707
-1.1	46.9	-51.61	320.0	0.0707
-1.2	45.0	-54.04	319.8	0.0708
-1.3	41.2	-53.58	319.6	0.0708
-1.4	39.2	-54.95	319.3	0.0709
-1.5	47.5	-71.24	319.3	0.0709

Table 4.5

Pitot-tube Traverse Results

DATE 161070
 TEST NO 512
 PIPE DIA 3 INCHES
 ATMOS PRES 30.32IN HG
 ROOM TEMP 18.9DEG C
 ENOTS 8.20
 AV DENSITY .0683LB/CU FT
 VISCOSITY .000816
 REYNOLDS NO 63775
 ORIFICE PD 3.87IN. WATER
 AV VELOCITY 50.8FT/S
 VEL A 51.7FT/S
 VEL B 49.8FT/S
 MASS FLOW 0.171LB/S
 MF A 0.174LB/S
 MF B 0.167LB/S

RAD	VEL	VEL* RAD	TEMP	ROE
1.5	42.1	63.12	338.5	0.0689
1.4	45.8	64.06	338.5	0.0689
1.3	48.1	62.54	338.5	0.0689
1.2	50.3	60.41	338.5	0.0689
1.1	52.2	57.44	338.8	0.0688
1.0	53.9	53.88	338.8	0.0688
0.9	55.1	49.59	338.8	0.0688
0.8	56.0	44.82	338.8	0.0688
0.7	57.3	40.12	338.8	0.0688
0.6	58.1	34.85	338.8	0.0688
0.5	58.9	29.43	339.0	0.0688
0.4	59.6	23.84	339.0	0.0688
0.3	59.6	17.88	339.0	0.0688
0.2	60.3	12.07	339.0	0.0688
0.1	60.3	6.03	339.0	0.0688
0.0	60.2	0.00	339.0	0.0688
-0.1	60.2	-6.02	339.0	0.0688
-0.2	59.8	-11.97	339.0	0.0688
-0.3	59.5	-17.84	339.0	0.0688
-0.4	58.7	-23.49	339.0	0.0688
-0.5	58.0	-29.00	339.3	0.0687
-0.6	57.2	-34.34	339.3	0.0687
-0.7	56.3	-39.43	339.3	0.0687
-0.8	55.1	-44.11	339.3	0.0687
-0.9	53.5	-48.16	339.3	0.0687
-1.0	52.4	-52.40	339.3	0.0687
-1.1	50.3	-55.29	339.5	0.0687
-1.2	47.2	-56.70	339.5	0.0687
-1.3	44.2	-57.44	339.5	0.0687
-1.4	42.0	-58.75	339.5	0.0687
-1.5	42.1	-63.12	339.5	0.0687

shown in Table 4.5 and comparison of the average velocity corresponding to the orifice-plate pressure drop for tests 504 and 512 is quite convincing. The equivalent \bar{u}_f , W_f and orifice-plate pressure differentials were extrapolated from these latter tests and incorporated in a pre-data tape to the computer program (see appendix A.1.3).

At the end of the gas-solid flow experiments the three inch pipe was replaced by a two inch diameter vertical pipe and a third series (tests 520 to 528) of pitot-tube transverses were carried out. The results from these tests confirmed that applying the Continuity Equation to the three inch, two inch, and one inch pipes, and using the \bar{u}_f correlation from the second series of traverses, gave satisfactory accuracy for the determination of the mean superficial air velocity.

4.3.4 Alternative Method of Ascertaining the Superficial Air Velocity

Since \bar{u}_f and W_f are of primary importance, appearing in most dimensionless groups, it was decided to attempt to confirm the conclusions of section 4.3.3. The technique was to use the pressure drop along the duct in a relationship derived by relating the familiar Fanning equation for the turbulent flow of a single phase fluid to Blasius's smooth pipe law:-

$$\text{From Fanning; } \Delta P_o = \frac{4L \rho_f \bar{u}_f^2}{2D} \cdot \lambda_o \quad (11)$$

$$\text{that is, } \frac{\Delta P_o}{\rho_f g} \cdot \frac{gD}{2L\bar{u}_f^2} = \lambda_o$$

$$\text{or } h_o \cdot \frac{gD}{2L\bar{u}_f^2} = \lambda_o \quad (12)$$

where h_o is the pressure head loss due to fluid friction.

From Blasius; $\lambda_0 = \frac{0.079}{R_e^{0.25}}$ for $R_e < 10^5$ (13)

where $R_e = \frac{\rho_f \bar{u}_f D}{\mu}$

Equating (12) and (13):-

$$\bar{u}_f = \left(\frac{g}{2 \times 0.079} \right)^{4/7} \cdot \left(\frac{h_0}{L} \right)^{4/7} D^{5/7} \cdot \left(\frac{\rho_f}{\mu} \right)^{1/7} \quad (14)$$

To convert h_0 from units of fluid flowing to units of water, h_0 in (14) must be multiplied by ρ_f/ρ_w , where ρ_w is the density of water. Thus, if H_0 represents the pressure drop along the pipe in units of water, then equation (14) becomes:-

$$\bar{u}_f = \left(\frac{g}{2 \times 0.079} \right)^{4/7} \cdot \left(\frac{H_0}{L} \right)^{4/7} \cdot \frac{\rho_w^{4/7}}{\rho_f^{4/7}} \cdot \frac{D^{5/7}}{\mu^{1/7}} \quad (15)$$

Substituting the relevant conversion factors to obtain units appropriate to the present study:-

$$\bar{u}_f = \frac{9.552 D^{5/7} H_0^{4/7}}{L^{4/7} \mu^{1/7} \rho_f^{3/7}} \quad (16)$$

where \bar{u}_f is in ft/s;

D is measured in inches;

μ in lb/ft min;

ρ_f in lb/ft³;

L in ft; and

H_0 in cm of water.

Equation (16) was written into the computer program (see appendix A.1.2), and comparison between the approaches indicated by sections 4.3.3 and 4.3.4 is as follows:-

Test No. 63 (one inch diameter duct)

Pitot-tube/ orifice-plate velocity, ft/s	480.2	473.8	450.7	394.6	357.9	309.3	245.3	152.8
\bar{u}_f from equation(16) ft/s	493.1	482.9	460.9	398.1	355.0	297.1	236.1	135.5
Percentage difference	2.7	1.9	2.3	0.9	0.8	3.9	3.0	11.3

The close comparison is well within the experimental accuracy of determining H_o . It is only when H_o has become relatively small does the deviation in \bar{u}_f become unreasonable.

Test No. 1 (two inch diameter duct)

Pitot-tube/ orifice-plate velocity, ft/s	136.4	133.8	125.9	116.9	103.9	88.1	76.0	51.3
\bar{u}_f from equation (16) ft/s	139.6	137.1	128.7	120.1	105.0	83.9	66.1	45.1
Percentage difference	2.3	2.5	2.2	2.7	1.1	4.8	13.0	12.1

This confirms that the pitot-tube analysis for the determination of \bar{u}_f , represented on the pre-data sheet (appendix A.1.3), produces an adequate correlation between the pressure drop across the orifice-plate and the superficial air velocity in the test section.

Fig. 4.10 shows the difference between the air mass flowrate, W_f , calculated from the pressure drop results of

tests 1 and 63, in relation to the orifice-plate differential pressure. The small variation is possibly due to constant values for ρ_f and μ being assumed for the W_f values from 1 and 63.

4.4 Pressure Drop Measurements

4.4.1 Introduction

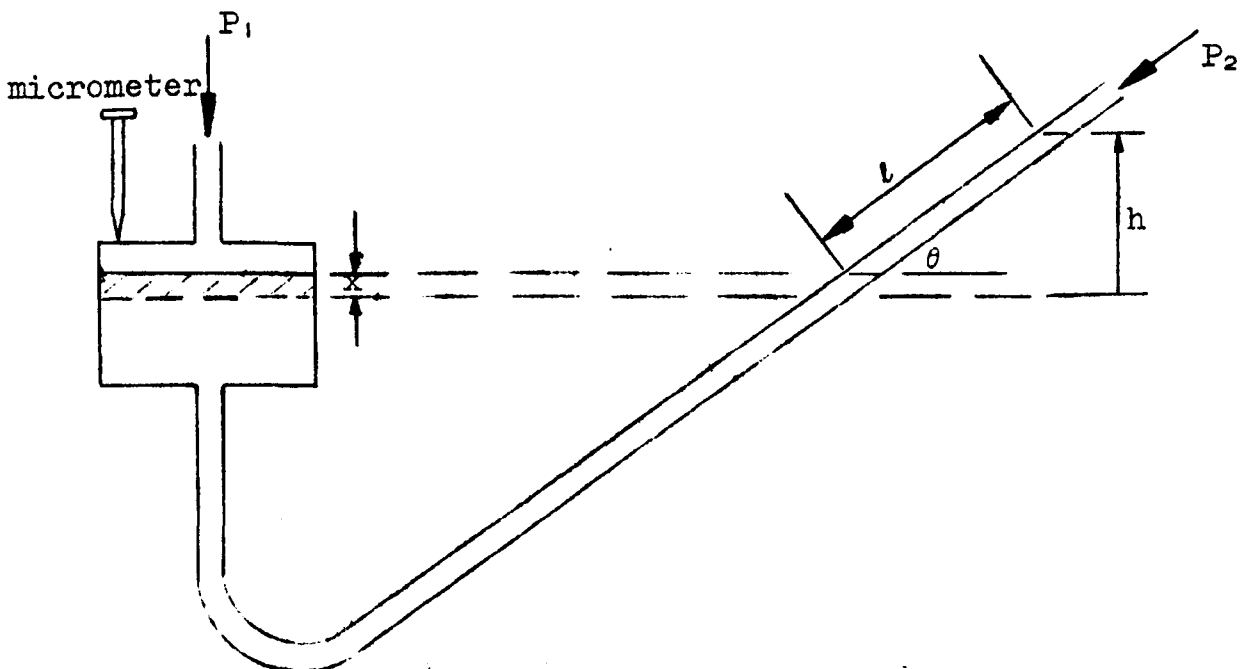
A fortyeight point pressure-scanning valve with a built-in transducer and amplifier arrangement was available for the present investigation. The transducer was of adequate sensitivity and its scanning speed very acceptable, however, some concern was expressed about the possible ingress of the abrasive alumina particles along the manometer lines and so causing damage to the delicate transducer diaphragm. This type of occurrence was likely to happen during a limiting flow condition when slugging and even "choking" was imminent. Two further disadvantages of the electronic scanning valve are that a point reading would be recorded for a fluctuating pressure and secondly there would be no indication that a particular pressure tapping was blocked with powder. As a result two different types of differential manometer were used, each being appropriate to a particular series of experiments (see sections 4.4.2 and 4.4.3).

4.4.2 Pressure Measurements in a Vertical Duct

The first full-scale part of the present study was concerned with the pressure drop, for a range of gas-solids loadings, of a suspension flowing upwards through a vertical duct. The pressure drop was measured along a length of 4 ft of pipe for the one inch and two inch diameter pipes, and 2 ft for the three inch pipe, the particles having travelled along a straight vertical section of uniform bore

pipe for at least 8 ft before the first static pressure tapping. A tendency for the flowing suspension to "swirl" for some flow conditions was observed visually in the three inch pipe and the flow was only considered acceptably homogeneous after a minimum distance of 10 ft along the vertical duct.

The pressure tappings in the vertical tube and across the orifice plate were connected to sensitive inclined manometers filled with fluid of specific gravity 0.810 and having relatively large reservoirs accurately adjusted by micrometers. It was necessary to apply a correction to the manometer reading in order to allow for the difference in surface levels between the liquid in the reservoir and in the inclined tube:-



Cross-sectional area of manometer tube = 'a' and of the circular reservoir = A. Due to the pressure differential ($P_1 - P_2$) a volume of fluid flows from the reservoir into the manometer with the result that the equilibrium surface level of the reservoir falls a distance x, where $x = \ell a/A$. Thus the vertical manometer reading, h, is given by the equation:-

$$h = \ell \sin \theta + x$$

$$\text{or } h = \ell \{ \sin \theta + a/A \}, \quad (17)$$

where $a/A = 0.01563$.

Since ℓ is measured in cm then h has units of cm of manometric fluid, and converting, h, to cm of water equation (17) becomes:-

$$h = \ell \{ \sin \theta + 0.01563 \} \times 0.810 \quad (18)$$

for an inclination of 20° , $\sin \theta = 0.3420$, and

$$h = 0.2897\ell \quad (19)$$

The value of θ varied from 10° to 50° for the pressure drop tests with the two inch and three inch diameter ducts. Due to the considerable errors possible at low values of θ for a marginally incorrect slope, the micrometer was used to determine the precise inclination of the manometer tube.

The magnitude of the pressure differential across the 2 ft length of three inch diameter tube varied from 0.03 to 1.16 cm H_2O , and across the 4 ft length of two inch diameter tube from 0.6 to 8.7 cm H_2O . The pressure differential across the 4 ft of one inch diameter tube varied from 8.4 to 88.3 cm H_2O and so the inclined manometer was replaced by a conventional vertical U-tube manometer.

4.4.2.1 Experimental Procedure

The experimental routine was briefly as follows.

The plant was allowed to settle down by passing air only through the test section for about 20 minutes, and then the Enots regulating valve, controlling the air flow control valve, was adjusted to a particular value. The screw-feeder was then started and a series of pressure drop readings were taken for various values of solids flow rate, the Enots valve being maintained constant throughout. Only about 30 seconds are required after altering the screw-feeder for the re-establishment of steady flow conditions. The continuous nature of data acquisition allowed speedy completion of a test run. For each Enots setting, measurements were taken as follows:-

- (i) Test section pressure drop.
- (ii) Test section absolute pressure.
- (iii) Orifice-plate pressure drop.
- (iv) Screw-feeder size and Kopp variator setting.
- (v) Air temperature at the orifice-plate.

The following subsidiary data were also taken:-

- (a) Absolute pressure at the orifice-plate.
- (b) The ambient temperature and pressure.
- (c) Humidity measurements were taken as a precaution in case any spurious data were found later on analysing the results. As the equipment was in frequent use during the experimental programme, the moisture content of the particulate matter and hence its agglomerative properties may be expected to depend only on the carrier fluid.

- (d) Note of the particular batch of powder being conveyed was made and a sample of the powder taken at routine intervals during a programme of work.
- (e) Overall running time of the compressor. This was very necessary to avoid possible malfunction due to overheating and to carry out the planned maintenance scheme efficiently.

4.4.2.2 Blocked Manometer Tappings

The problem of solid particles flowing into the manometer lines and tending to block them has been mentioned in a previous investigation⁴. In this study⁴, the difficulty was resolved by continuously purging the lines with air via water in a transparent vessel. Prior to taking the manometer reading, the purging flow was cut off, this being indicated by the cessation of bubbling. In the present work, however, the manometer lines are rather long, and considerable time would be necessary after stopping the purge gas to enable the manometer levels to become steady and indicate the correct reading.

It was found to be satisfactory in this study to make no special provision for preventing the blocking of the lines; it sufficed merely to blow out any deposited solids at 30 minute, 1 hour or 2 hourly intervals. This was easily done because of the free-flowing properties of the solids. Close to the limiting condition of choking the manometer lines tended to block after only a few minutes of use. However, prior to choking the dense phase flowing suspension caused the manometer levels to fluctuate and cessation of the fluctuations was often an indication that the line was blocked. Thus the blocking of lines was aggravated by any

form of unsteady flow, rather than a gradual build-up of solids. It is true that there was some evidence of slow blocking but this rarely affected a manometer reading.

4.4.3 Bend, Vertical and Horizontal Pipe Circuit Pressure Measurement

The second part of the present study was originally intended to be concerned with the pressure drop characteristics due to a gas-solid suspension flowing around several bends of different geometry. It was ultimately decided to extend the proposed investigation to include the vertical duct preceding the bend and a horizontal pipe immediately following the bend.

The range of bends and duct diameters were as follows:-

- (i) 3 inches diameter, 30 inches radius of curvature, that is, $\lambda = 20$;
- (ii) 2 inches diameter, 20 inches radius of curvature, that is, $\lambda = 20$;
- (iii) 1 inch diameter, 10 inches radius of curvature, that is, $\lambda = 20$;
- (iv) 3 inches diameter, 18 inches radius of curvature, that is, $\lambda = 12$;
- (v) 2 inches diameter, 12 inches radius of curvature, that is, $\lambda = 12$;
- (vi) 3 inches diameter, 20 inches radius of curvature, that is, $\lambda = 13.3$;

where λ is the ratio of the radius of curvature of the bend to the radius of the pipe.

The location and number of static pressure tappings, around the bends in particular, demanded careful consideration and it was decided to have four tappings at each cross-section for the bend, the horizontal section and the reference point,

R, (see Fig. 4.11 and appendix A.5., Figs. A.5.8 to A.5.12). The tappings were arranged at 22.5 degree intervals around the bends and approximately six inches apart along the horizontal pipe. The configuration of each set of four tappings is shown in Fig. 4.11, together with the arrangement used for static pressure measurement with a pipe-wall fitting. The centre tappings, denoted by 'a' in Fig. 4.11, were inter-connected and so there were three manometer lines coming from each station. It can be seen from Fig. 4.11 that there were five stations around each bend and six along the horizontal section, thus providing thirtythree manometer lines. Three single pressure tappings were positioned along the vertical pipe and the total thirtysix manometer lines lead to a multi-tube manometer. The reference point, R, was inter-connected at R and the single manometer line from here connected to the reservoir of the manometer. Thus all pressure drops were measured relative to R and it was particularly vital that this line was frequently checked for leaks and deposition of solids.

4.4.3.1 Experimental Procedure

The experimental routine was similar to that outlined in section 4.4.2.1. The principal differences being that there were many more pressure readings to record and a considerable number of manometer lines to be cleaned after each test run. Apart from the physical difficulty of reading thirtysix closely-spaced manometer levels, which may be fluctuating slightly, it was felt that the flow conditions may vary between estimating the first and last manometer reading. To overcome this problem a 35 mm camera was mounted on a tripod and positioned one metre from the sloping multi-tube

manometer. Successful negatives were only produced after many attempts to eliminate the reflections, in the glass front of the manometer, from fluorescent lights and laboratory skylights, by sufficient and carefully placed black-out screening which allowed enough light to expose the film. The film itself needed to have a high contrast and the exposure times were appropriately varied to suit the laboratory lighting conditions. The technique was finally mastered and the thirtysix manometer readings were recorded by the camera in less than one second. The film was developed in the laboratory immediately following a test run in case of a mishap requiring a repeat of the test, this fortunately only occurred once in over one hundred and fifty tests. Though this procedure was admirable for the speedy completion of experiments, the reading of the projected negative was unbelievably laborious and over ninety thousand readings were recorded in this manner. Many of the negatives were so good that the bottom of the meniscus could be clearly seen (see Plate 6), however, photographing a fluctuating level inevitably produced a blurred result but the mean value was relatively easy to assess.

The manometric fluid in the multi-tube manometer had a specific gravity of 1.00, and an inclination of 18 degrees to the horizontal was used for all the three inch bend tests, whilst 45 degrees was used for the two inch bends. The one inch bend presented an immediate problem since the pressures were outside the manometer range, however, mercury was used as the manometric fluid and with a slope of 19 degrees it was equivalent to having a vertical manometer with fluid of specific gravity 4.4.

The flexible manometer tubing needed to be heated in very hot water before being fitted onto the 1.25 inches long pipe-wall tubes. This was very effective in avoiding leaks but it was out of the question to remove them whilst cleaning out deposited solids after a test run. Consequently a novel and simple purging system was devised (see Plate 5). On completion of a test the manometer was clamped, and using a manifold system, all the manometer lines were purged clean with nitrogen at 2000 lbf/in². This purging procedure was carried out in less than thirty seconds and could be performed whilst the rig was still operating.

A typical set of the measurements taken for one test is shown in Fig. 4.12, and the similarity with the measurements described in section 4.4.2.1 is evident.

4.4.4 Pressure Drop due to Air Only Flowing, ΔP_0

It was realised that the contribution of the fluid phase to the total pressure drop associated with a gas-solid flow is likely to be affected by the presence of the solids. As a result, the data processing for this investigation has defined the specific pressure ratio as $\Delta P_T / \Delta P_0$, where $\Delta P_T = \Delta P_m$ in an experimental study. The determination of ΔP_0 is as follows:-

From the Equation of Continuity and equation (11):-

$$\Delta P_0 = \frac{2L}{D\rho_f} \cdot \lambda_0 \cdot \rho_f^2 \bar{u}_f^2 = \frac{2L}{D\rho_f} \cdot \left(\frac{W_f}{A}\right)^2 \cdot \lambda_0 \quad (20)$$

Assuming the perspex tube to be smooth and using Nikuradse's relationship between friction factor and Reynolds' number, that is:-

$$\lambda_0 = \left\{ 0.0008 + \frac{0.055}{R_e^{0.237}} \right\} \quad (21)$$

an expression for ΔP_0 can be derived:-

$$\Delta P_0 = \frac{3.404 W_f^2 L}{\rho_f D^5} \cdot \left\{ 0.0008 + \frac{0.055}{R_e^{0.237}} \right\} \quad (22)$$

where ΔP_0 is given in cm H₂O;

L in ft;

D in inches;

ρ_f in lb/ft³; and

W_f in lb/min.

The calculated ΔP_0 values are compared with the experimental quantities obtained when air only was flowing through the vertical one inch and two inch diameter ducts. The curves (see Figs. 4.13 and 4.14) justify the inclusion of equation (22) into the computer program (see appendix A.1.2).

4.5 Measurement of Solids Mass Flow Rate

4.5.1 Introduction

There are many commercially obtainable devices⁷⁹ which can be used for discharging solids into an airstream. These include various types of rotary valve, gravity feed devices, screw-feeders, fluidised beds and hybrid combinations of these. The present requirement for a steady, adjustable and accurately calibrated delivery rate of an abrasive powder that may be slightly cohesive severely restricts the choice. The abrasion factor rules out rotary valves, the cohesive property eliminates a gravity feed device as used by Farbar⁷, whilst the more positive delivery characteristics of the screw-feeder are ideally suited to the present application. As shown in appendix A.2., Fig. 1,

the feeder delivers the solids uniformly into a mixing unit where it becomes intimately mixed with a previously metered air-stream.

4.5.2 Screw-feeder Arrangement and Calibration Procedure

It was important that the screw-feeder should be capable of discharging the solids over a large range of delivery rates without sacrificing accuracy. As a result, the screw-feeder, which was rotated by a Kopp variator having an infinitely variable speed range from 0 to 180 rev/min, was designed to accommodate several interchangeable sizes of screw-flight. Three flights were manufactured, classified simply as small, medium and large, but the small flight was not used due to the medium flight being able to deliver the solids at 2 to 3 lb/min for a shaft speed of 30 rev/min. The small flight will be useful for tests performed at extremely dilute conditions, say $W_p/W_f < 0.4$. The difference between the medium and large flights is evident from Table 4.6:-

Table 4.6 Screw-flight Geometry

Screw Classification	Shaft diameter (in)	Flight thickness (in)	Overall length (in)	Flight diameter (in)	Mean pitch diameter (in)	Number of flights
Medium	0.625	0.125	16.1	1.69	1.31	9½
Large	0.625	0.125	16.1	2.50	1.81	6½

The calibration procedure was as follows:-

- (i) With the particular screw-flight in position, fill the solids supply bunker with the appropriate powder through the access hole in the side of the

bunker; the bunker will hold about 300 lb of alumina.

- (ii) Remove the base of the mixing unit and place an empty container of known weight beneath the unit.
- (iii) Switch on the Kopp variator, carefully adjust the speed of rotation and collect the solids in the container over a selected period of time. Repeat for a full range of Kopp speeds.

Typical calibration curves are shown in Figs. 4.15 to 4.22, and Table 4.7 is a representative set of data.

The relationship between the Kopp handwheel setting and the output shaft speed was established by two different methods:-

- (a) Using a tachometer having a full-scale range of 0 to 200 rev/min.
- (b) The input speed of the variator was constant at 1460 rev/min. With the rear cowl of the variator removed the number of turns of the fan for one turn of the output shaft was recorded. Thus, the input speed divided by number of turns of fan is equivalent to the output shaft speed.

The calibration accuracy is evident by reference to Table 4.8 and the calibration curve shown in Fig. 4.23.

Table 4.7

Medium Screwfeeder Calibration after Test 6

Powder mesh: 240

5th May 1970

Remarks	Kopp Variator Setting	Shaft Speed rev/min	Weight of powder, lb	Time min.	$\frac{W}{P}$ lb/min
static powder height 15 in above hopper base at start and about 9.5 in above at end of the calibrations except for Kopp settings 60 and 70. static powder height at end of calibration 7" above hopper base 1" above hopper base at end of calibration	0	30.0	23.5-9.1=14.4	5	2.88
	10	41.5	28.7-9.1=19.6	5	3.92
	20	52.5	34.3-9.1=25.2	5	5.04
	30	63.5	39.0-9.1=29.9	5	5.98
	40	74.5	45.4-9.1=36.3	5	7.26
	50	86.0	43.0-9.1=33.9	4	8.48
	60	98.0	37.9-9.1=28.8	3	9.60
	70	110.0	41.9-9.1=32.8	3	10.93
	80	123.0	45.8-9.1=36.7	3	12.23
	90	136.0	49.4-9.1=40.3	3	13.43
	100	150.5	53.5-9.1=44.5	3	14.83
	110	166.0	57.6-9.1=48.5	3	16.17
120	182.5	61.5-9.1=52.4	3	17.47	

9.1lb = weight of empty container.

Table 4.8

Kopp Variator Calibration

Kopp hand-wheel setting	Number of turns of fan for one turn of output shaft	Output shaft speed for constant input speed of 1460 rev/min	
		calculated	from tachometer
0	48.3	30.2	30.0
10	35.0	41.7	41.5
20	27.7	52.7	52.5
30	23.0	63.5	63.5
40	19.8	73.7	74.5
50	17.0	85.9	86.0
60	14.9	98.0	98.0
70	13.2	110.6	110.0
80	11.9	122.7	123.0
90	10.7	136.4	136.0
100	9.7	150.5	150.5
110	8.8	165.9	166.0
120	8.0	182.5	182.5

4.5.3 Discussion and Results

The calibration procedure explained in section 4.5.2 was performed with zero pressure differential between the solids discharge and the top of the powder in the solids supply bunker. To avoid invalidating the screw-feeder calibrations it was necessary to balance the pressure between the mixing unit and the top of the powder in the bunker. This was effected by connecting a length of manometer tube between the unit and the centre hopper, the bottom Mucon valve remaining open throughout a test run.

The phenomenon of "rat-holing" is one of the hazards

often encountered in the use of a calibrated screw-feeder. In the present study there was no evidence of rat-holing due to the solids being relatively free-flowing and a fairly high level of solids being maintained in the supply bunker to the screw-feeder, this latter precaution was particularly important to avoid starvation of the feeder.

Calibration of the screw-feeder was found to be independent of the height of the powder bed in the supply bunker, this characteristic has been reported previously by Richards⁸⁰, unless the screw-feeder was severely starved of solids.

The problem of sealing the screw-feeder drive shaft, which is rotating in a bed of abrasive powder and across which a pressure differential exists, is discussed in appendix A.3.2.

Fig. 4.15 shows that the medium screw calibration for the 240 mesh powder only increased by approximately 5% from test 1 to test 230, which represents a period of over one year during which time the rig was used extensively. The two curves illustrated, effectively portray the boundaries which enclose the results of several other calibrations. Thus the error in the solids flow rate for all test runs is estimated to be not greater than 1%. The 320 mesh calibrations shown in Fig. 4.16 are very similar, whereas the 500 mesh results in Fig. 4.17 indicate a large variation of 15% between tests 17 and 88. The deviation for the 500 mesh powder was on account of the test 17 calibration being performed with new powder, and the graph justifies the procedure used in this study of circulating new powder around the rig several times before carrying out calibrations

or pressure drop tests.

Fig. 4.18 shows the large effect of particle size upon the screw-feeder performance, and Figs. 4.19 to 4.22 illustrate that the characteristics of the large screw-flight are almost identical to the medium screw. It is interesting to note that the solids delivered increases with time, possibly indicating that a loss of fines out of the original batch of powder has effectively increased the screw-feeder efficiency. On the other hand it partially conflicts with the concept that attrition of the particles is a consequence of circulation and of passing through the screw-feeder.

At the conclusion of the vertical pipe tests, that is, after about four months of continuous use, the section of the screw-feeder drive shaft which was central in the mixing chamber had eroded from 0.625 inches to 0.25 inches diameter.

4.6 Powder Property Determinations

4.6.1 Introduction

The "white bauxilite abrasive" or white fused alumina used in this investigation is manufactured by the Universal Grinding Wheel Company. The sub-sieve sizes (240 to 1200 mesh) are made under laboratory controlled conditions to give powders of the closest possible range of particle sizes. The mesh sizes selected from the above range were 240, 320 and 500 mesh, which have respectively, mean particle diameters of 53, 30 and 14 microns. A chemical analysis shows the powder to contain more than 99% Al_2O_3 , whilst a physical analysis gives a specific gravity of 3.94 and a hardness factor (Knoop, K100) of 2,100.

4.6.2 Routine Analysis of Powder Samples

The particle size analyses and various other powder

property evaluations were carried out by the School of Pharmacy, Liverpool Polytechnic. Table 4.9 presents a brief summary of this work, except for the particle size analyses which are mentioned in section 5.8, Figs. 2a and 2b.

Table 4.9 Bulk Density and Angle of Repose Measurements

Powder Classification	Maximum bulk density (g/cm ³)	Poured Angle of Repose (degrees)
240 mesh; after test 79	2.33	30
240 mesh; after test 128	2.44	35
320 mesh; original powder	2.06	39
320 mesh; after test 46	2.10	35
320 mesh; after test 71	2.22	35
500 mesh; original powder	1.85	49
500 mesh; after test 41	1.95	40
500 mesh; after test 110	1.96	40

Powder properties are also discussed in section 8.4.5 of this study and reference should be made to Table 8.2 for further details about the 240 mesh powder, and to Figs. 8.8 to 8.11 which clearly illustrate the change in particle shape and size distribution due to re-circulation.

Examination of the particle size spectra illustrated in Figs. 4.24 to 4.26 shows that re-circulation of the relatively large particles (240 mesh) results in a higher percentage number of fines through attrition of the particles. Converting the ordinates of these Figs. from percentage number frequency to percentage weight masks this observation simply

because the very fine particles weigh so little. Conversely, Fig. 4.26 shows that re-circulation of the 500 mesh powder reduces the percentage number of very fine particles, this is explained by the limitation of the cyclone separators. Despite these anomalies, it is quite remarkable that the mean particle size of the three powders, as determined from the percentage weight versus particle size curves, changed so marginally throughout the investigation.

The repeatability of the screw-feeder calibrations is also confirmation that the nature of the powders did not change so drastically as to render the pressure drop experiments of doubtful value.

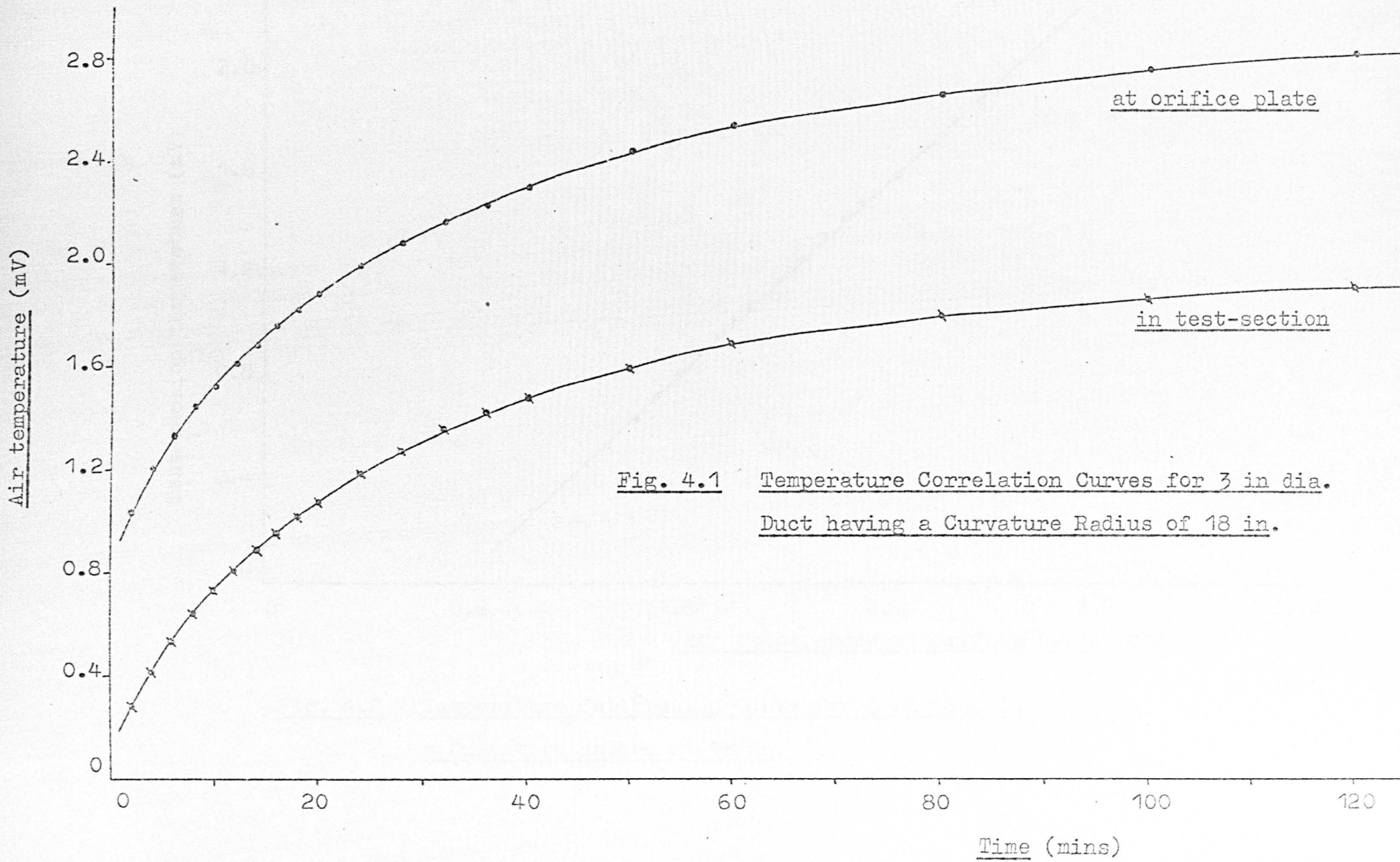


Fig. 4.1 Temperature Correlation Curves for 3 in dia.
Duct having a Curvature Radius of 18 in.

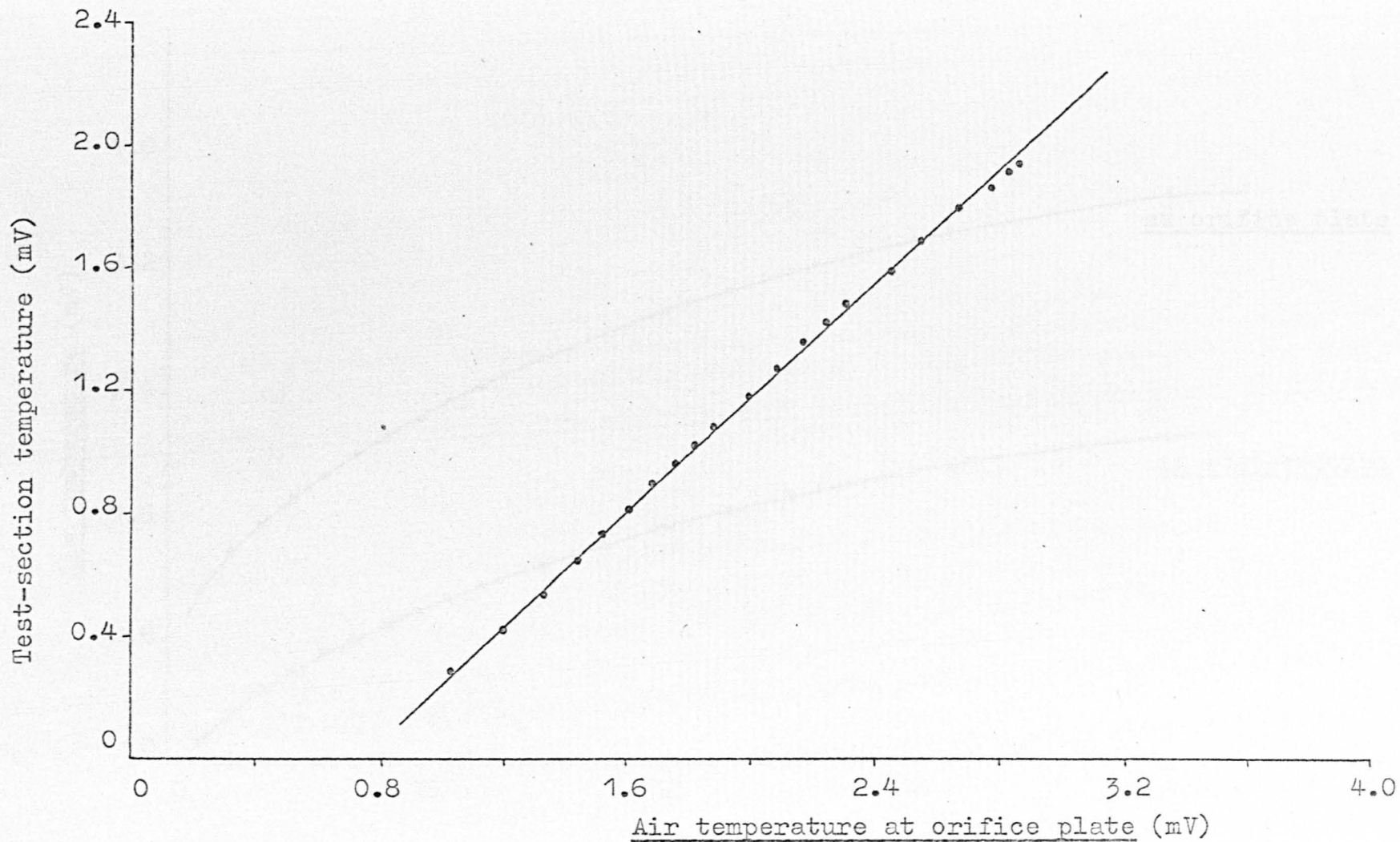


Fig. 4.2 Temperature Calibration Curve for 3 in dia. Duct having
a Curvature Radius of 18 in.

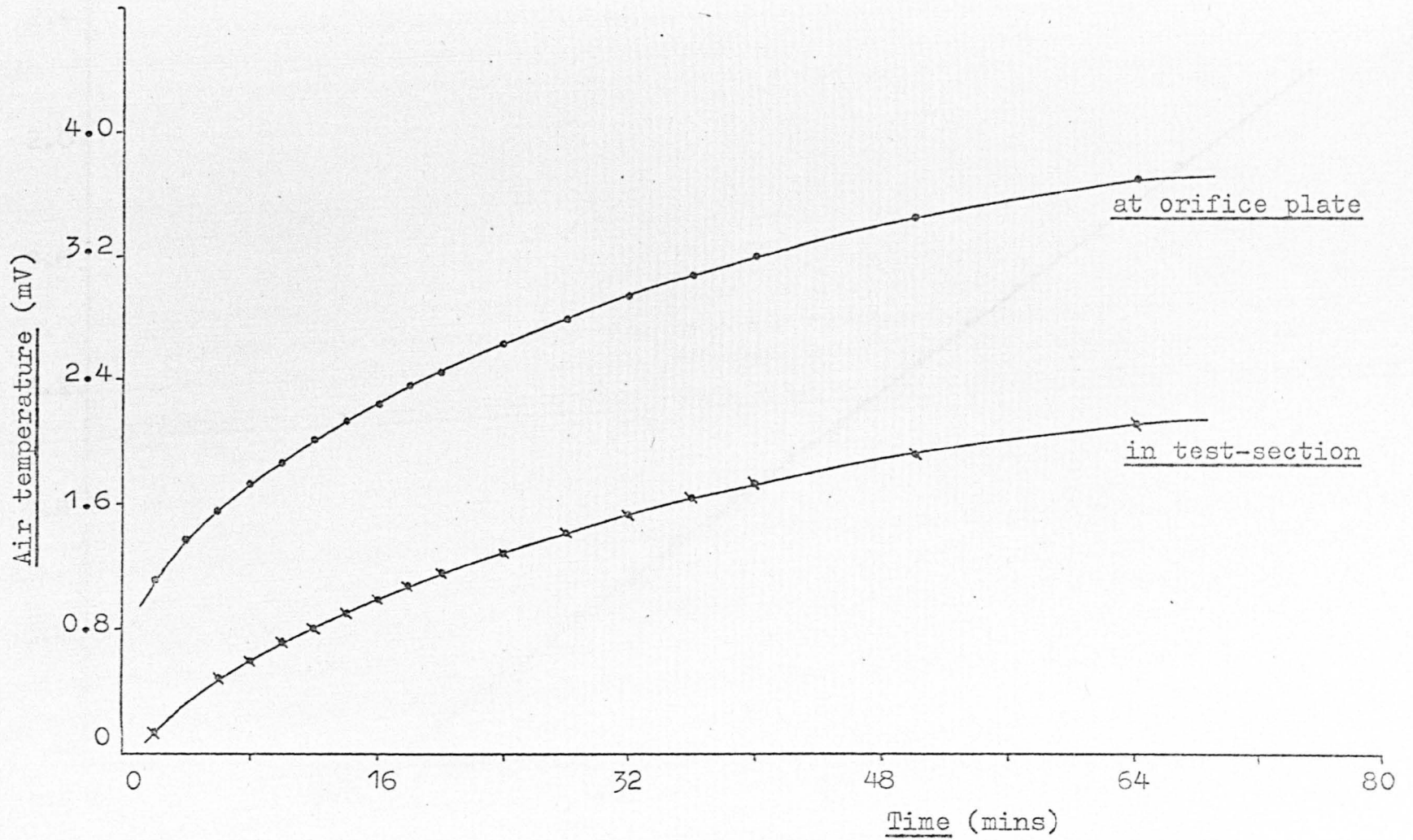


Fig. 4.3 Temperature Correlation Curves for 1 in dia. Duct having a Curvature Radius of 10 in.

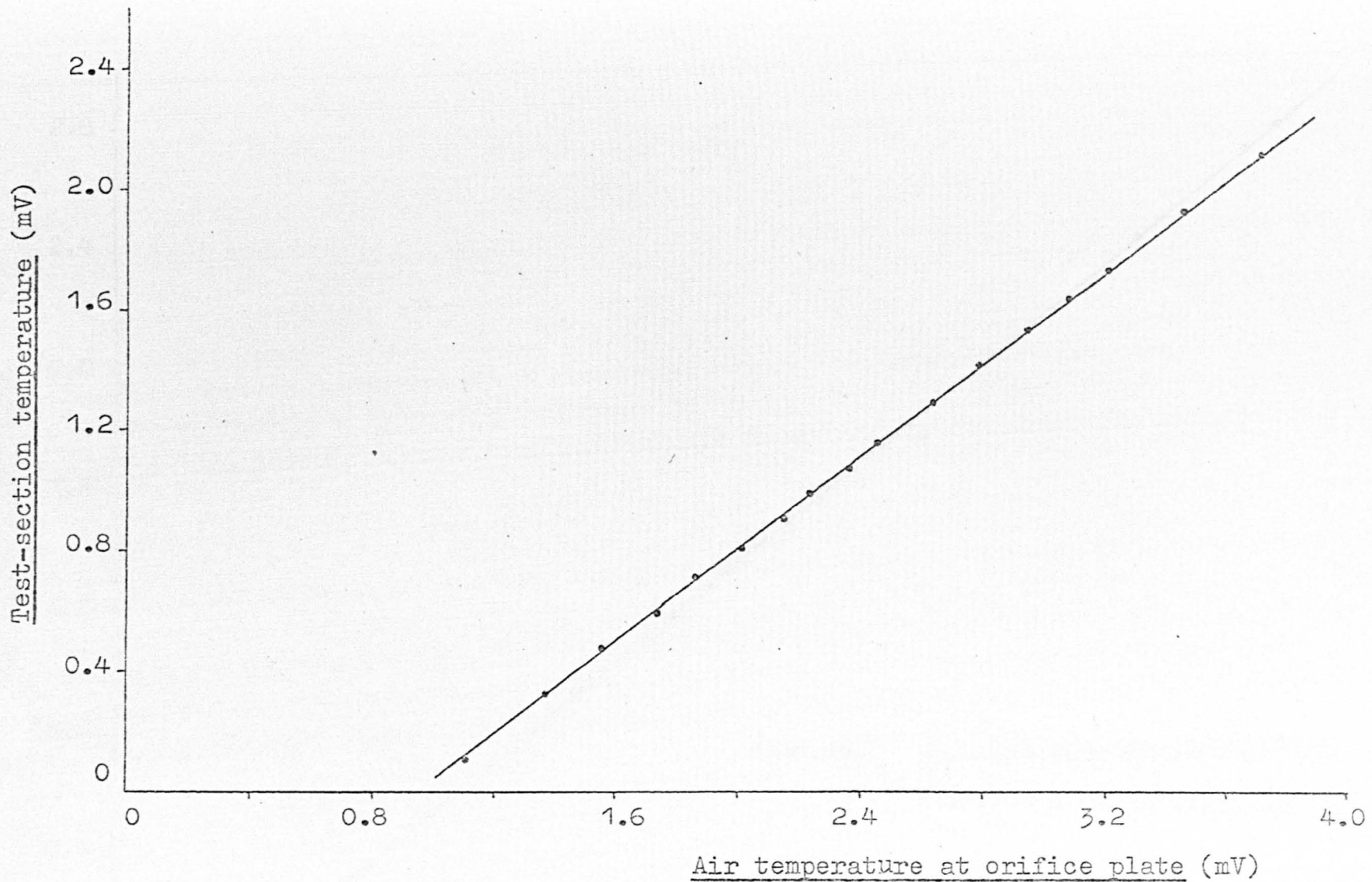


Fig. 4.4 Temperature Calibration Curve for 1 in dia. Duct having
a Curvature radius of 10 in.

- 08 -

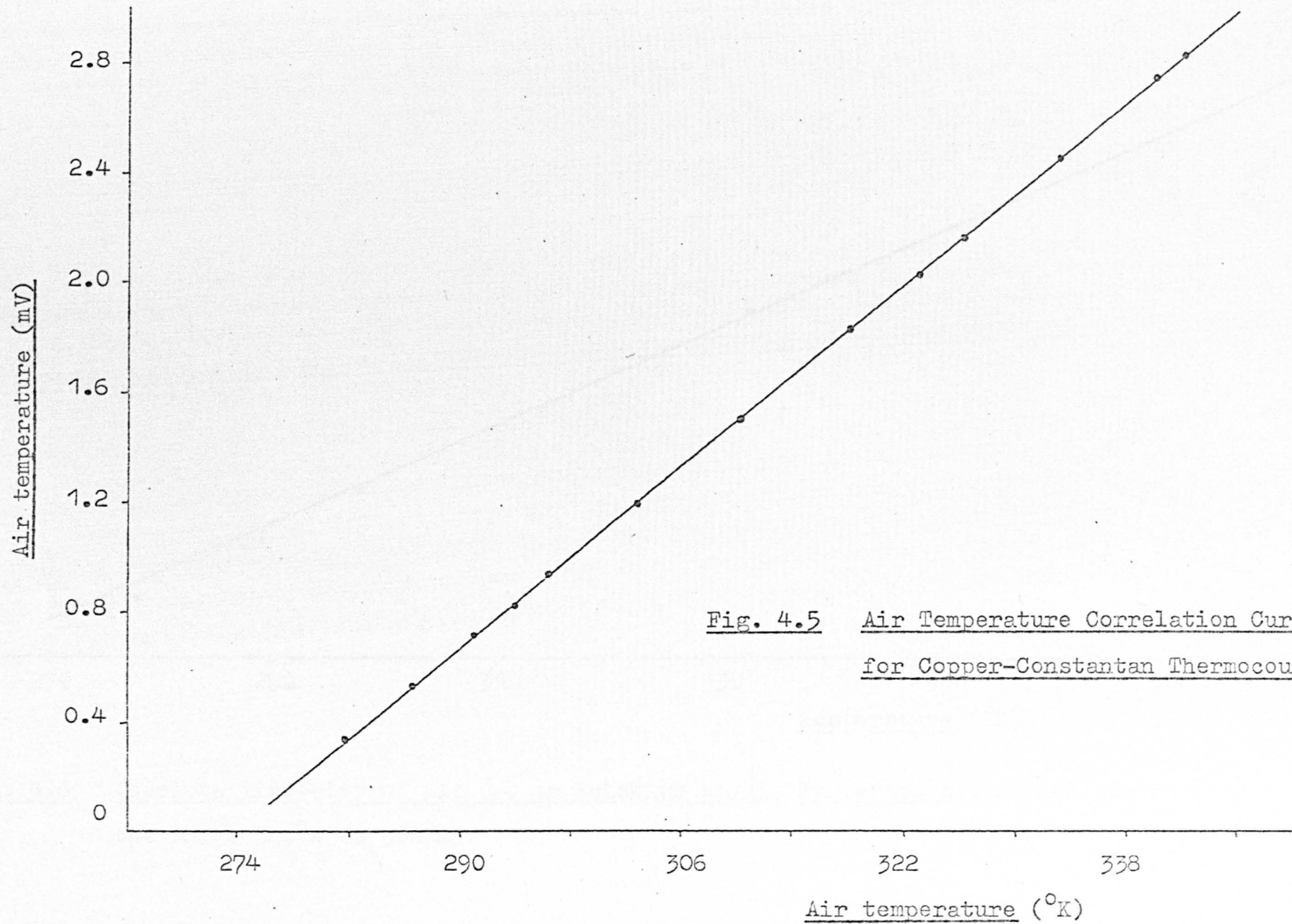


Fig. 4.5 Air Temperature Correlation Curve
for Copper-Constantan Thermocouple

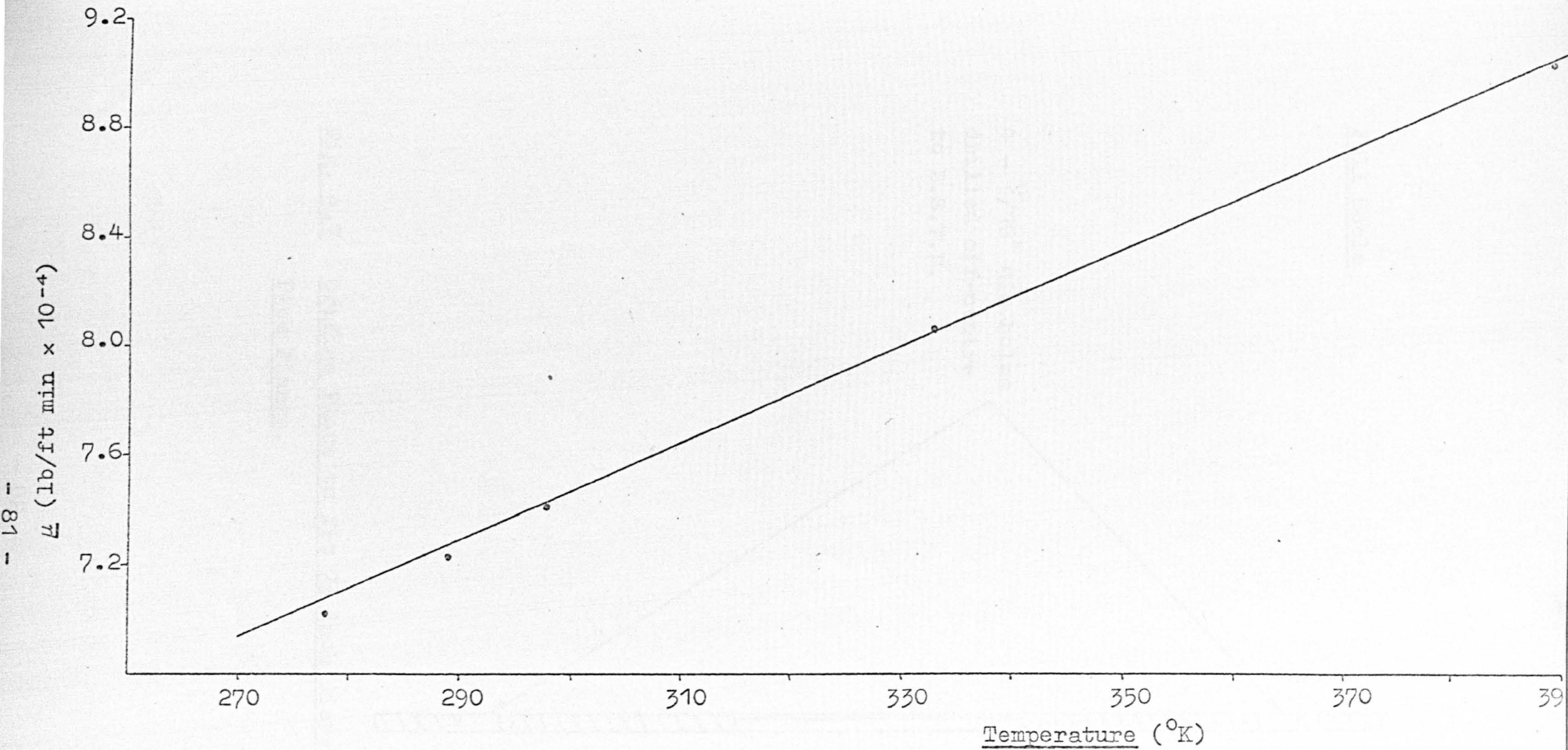


Fig. 4.6 Absolute Viscosity of Air (μ) in Relation to Air Temperature (assumed linear in the range 310°K to 360°K).

Full Scale

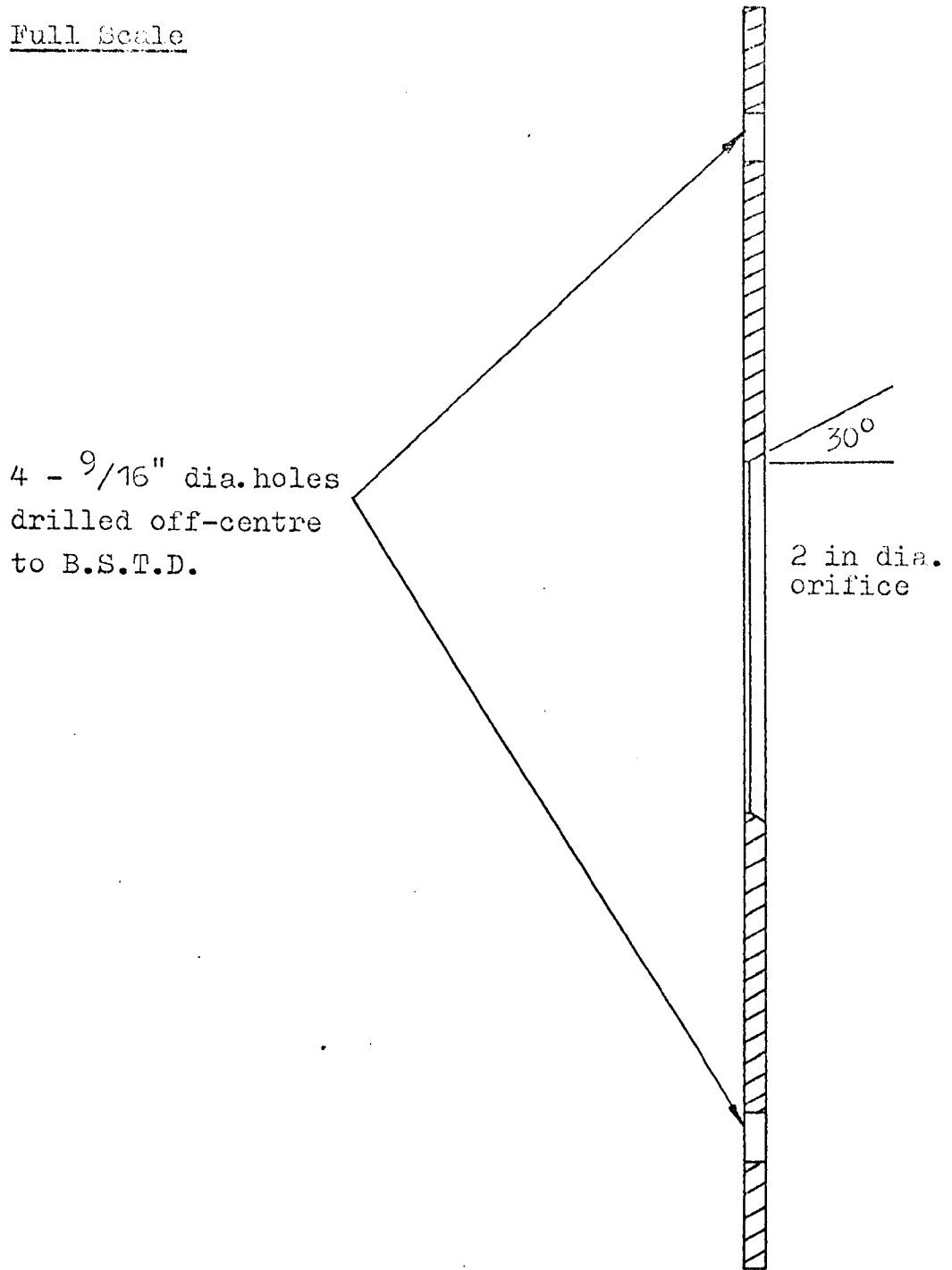


Fig. 4.7 Orifice Plate to fit 7 1/4 inch diameter Pipe Flange.

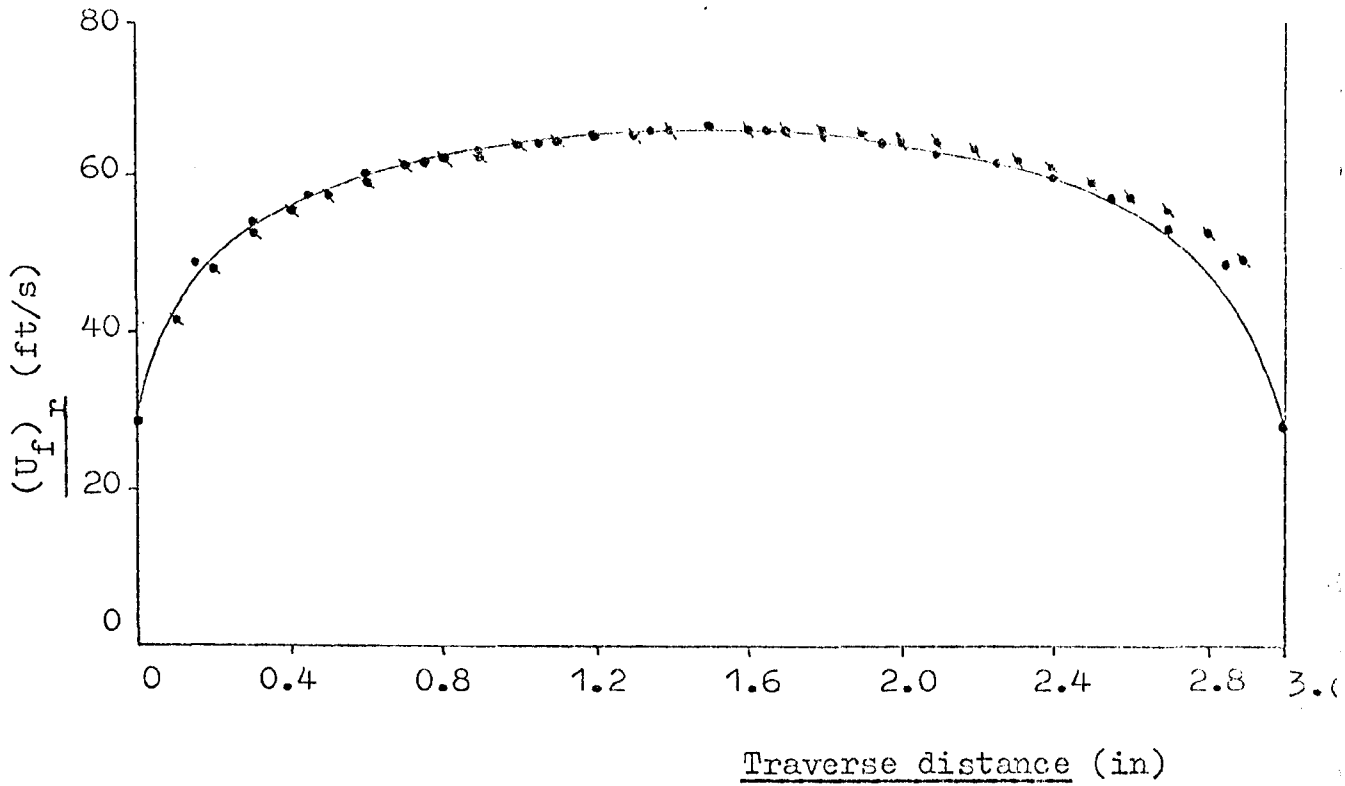


Fig. 4.8 Pitot-tube Traverse Relating Air Velocity in a 3 inch diameter Vertical Duct to Distance from Duct Wall measured along the Duct diameter.

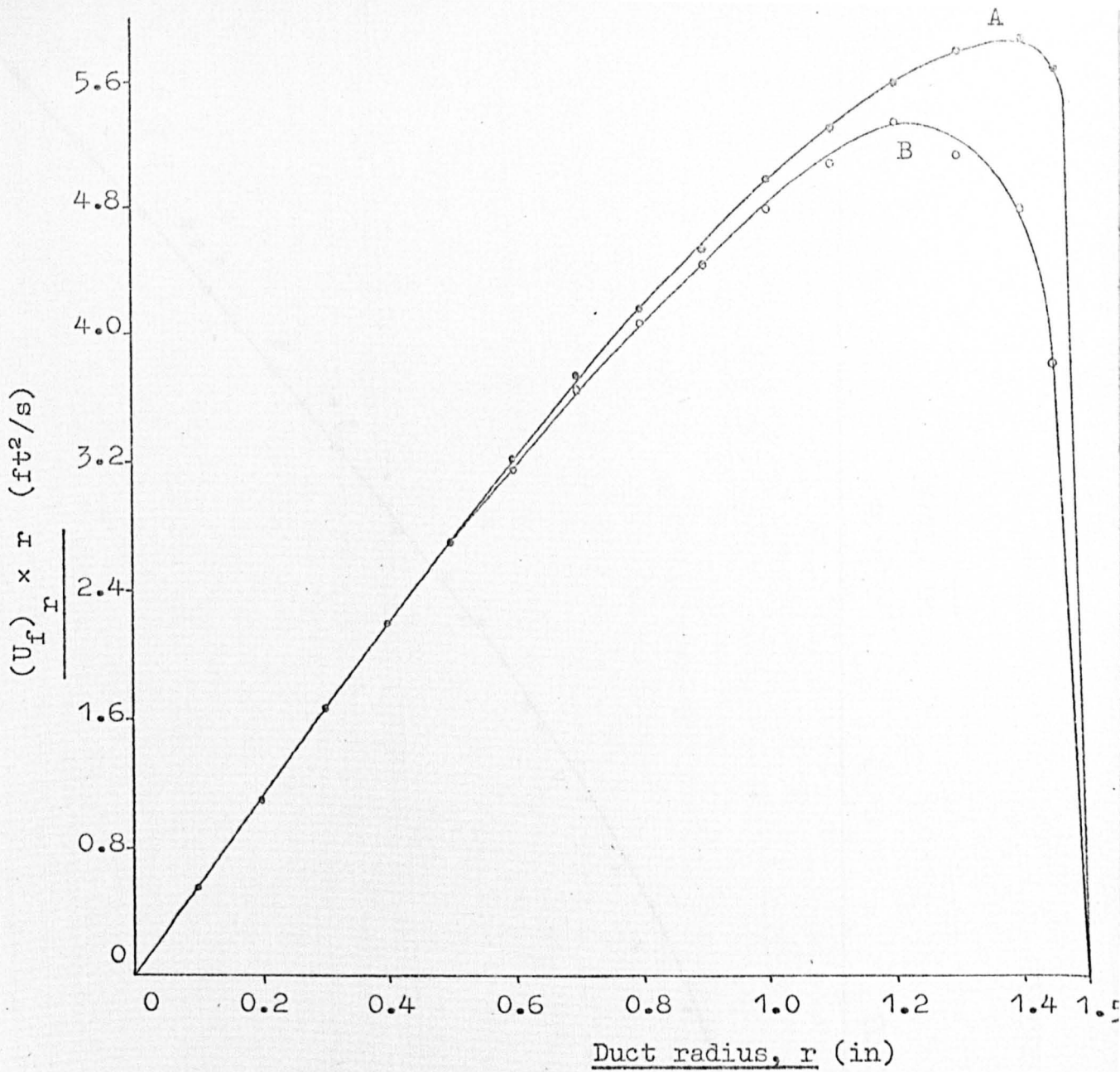


Fig. 4.9 Graphical Analysis of Pitot-tube Traverse in 3 inch diameter Duct.

From curve A : $\dot{V}_f = 2.59 \text{ ft}^3/\text{s}$

From curve B : $\dot{V}_f = 2.78 \text{ ft}^3/\text{s}$

Mean $\dot{V}_f = 2.69 \text{ ft}^3/\text{s}$, which is equivalent to
 $\bar{u}_f = 54.8 \text{ ft/s}$.

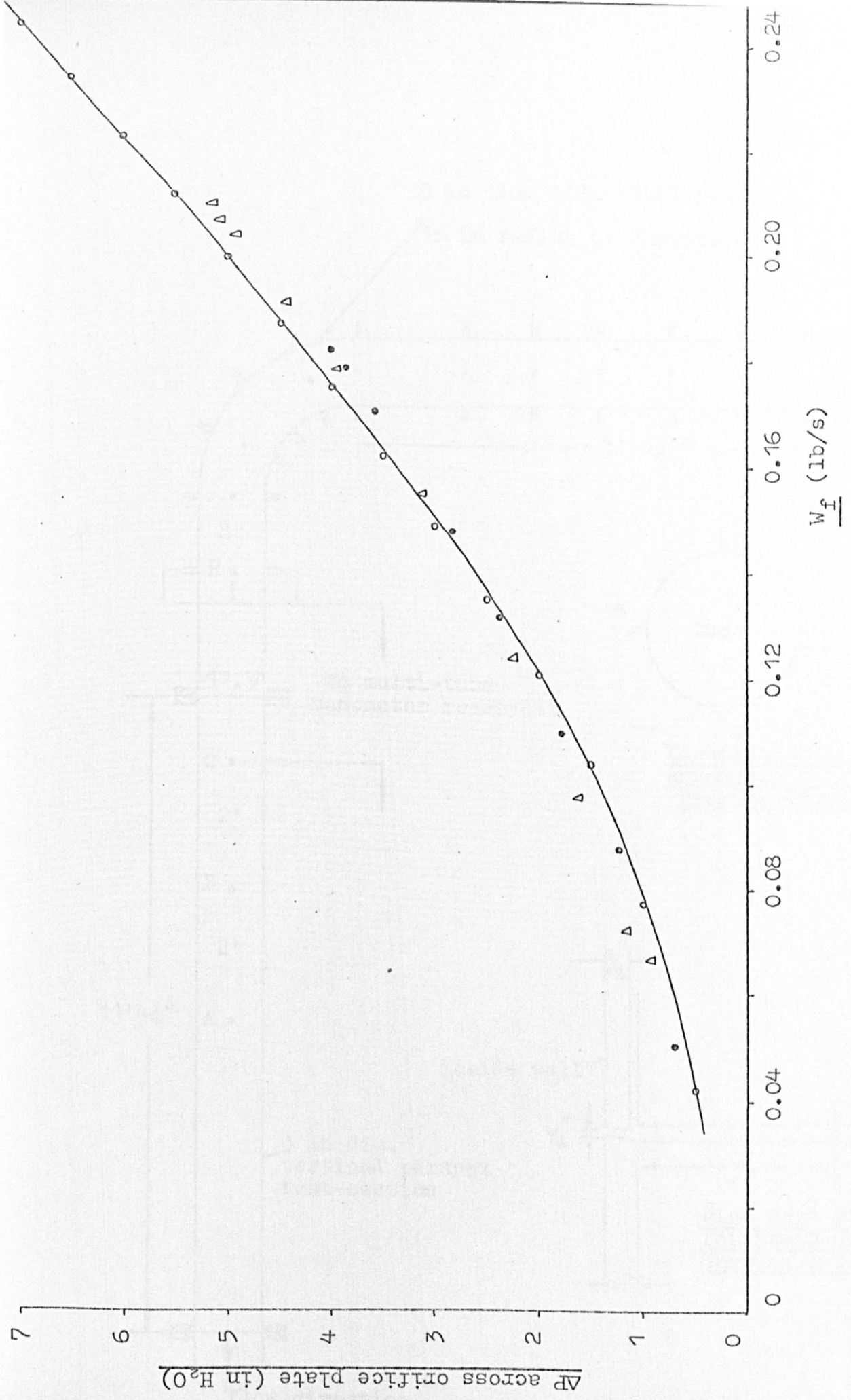


Fig. 4.10 Orifice Plate Calibration

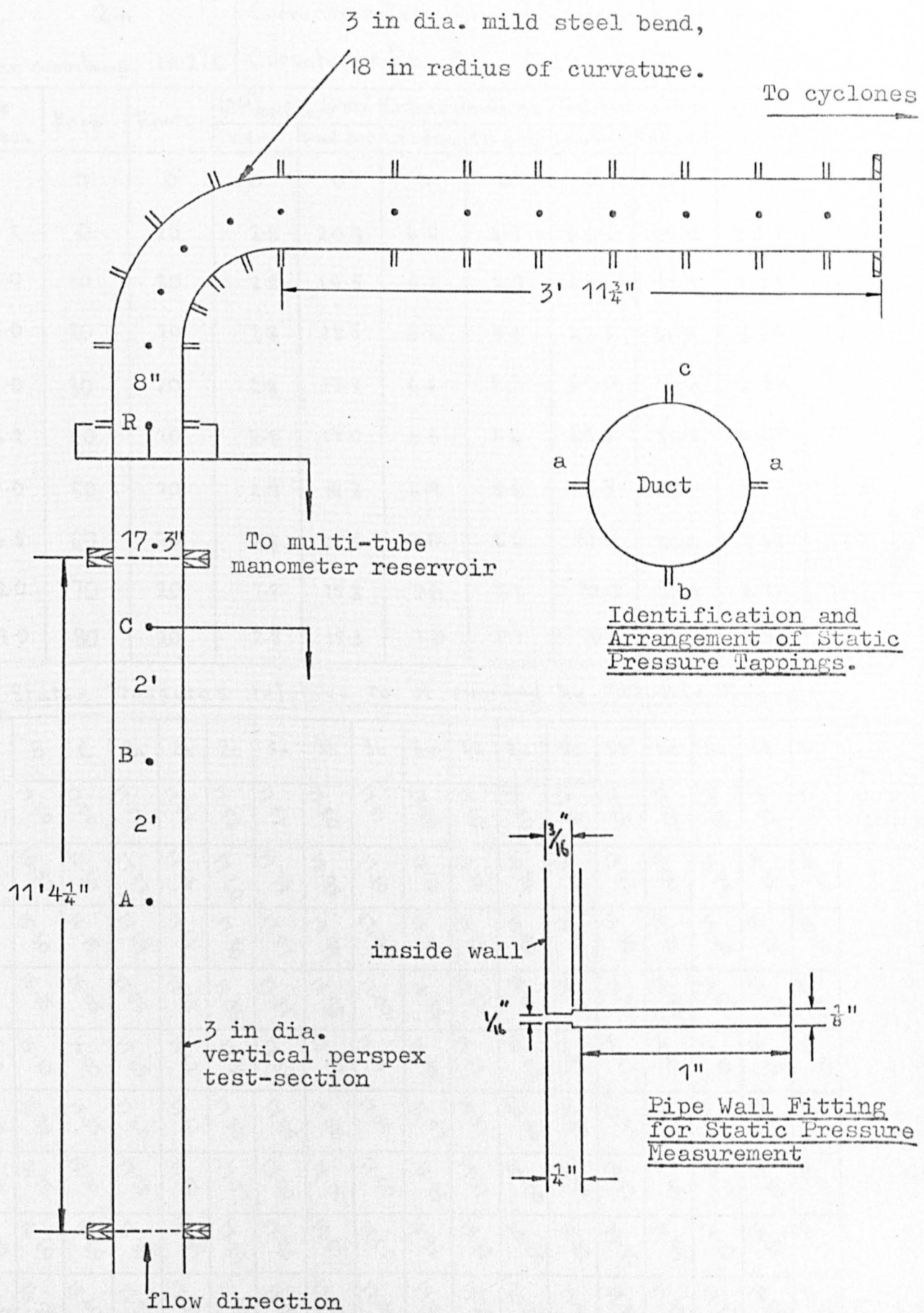


Fig. 4.11 Test Section Geometry.

Typical Observations for Bend Tests.

Test No. 245	Bar. pressure. 29.81 inHg	Compressor start: 1740
Date. 100671	Powder mesh. 500/7	Tests start: 1805
Dia. 2in	Curvature radius. 12 in.	Compressor shut down: 1940
Mean roomtemp. 18.2°C	Curvature ratio. 12	W.B. 56°F ; DB. 65°F.

Wp lb/min.	Kopp	Enots	(ΔP) orifice @ 50°		Orifice plate abs. press.		Test-section abs. press.		mV at orifice plate	ambient temp. °C
			zero	final (cm)	L.H. column	R.H. (inHg)	L.H. column	R.H. (cm H ₂ O)		
0	0	0	0	0	0	0	0	0	0	0
10.1	0	20	2.8	20.3	6.0	4.8	68.0	32.0	2.08	18.0
14.0	10	20	2.8	19.5	6.2	4.9	68.5	31.5	2.19	18.0
18.0	20	20	2.8	18.5	6.4	5.1	68.5	31.5	2.29	18.0
22.0	30	20	2.8	17.7	6.6	5.3	69.0	31.0	2.38	18.0
26.2	40	20	2.8	17.0	6.6	5.4	69.5	30.5	2.47	18.1
31.0	50	20	2.8	16.2	6.9	5.6	69.5	30.0	2.57	18.2
36.5	60	20	2.8	15.6	7.0	5.6	70.0	30.0	2.68	18.3
42.0	70	20	2.8	15.3	7.0	5.7	70.0	30.0	2.77	18.3
48.0	80	20	2.8	15.3	7.0	5.7	70.0	30.0	2.83	18.6

Static Pressures relative to 'R' recorded by Multi-tube Manometer

A	B	C	2a	2b	2c	3a	3b	3c	4a	4b	4c	5a	5b	5c	6a	6b	6c	Tapping identification
17.50	17.50	17.50	17.51	17.51	17.52	17.51	17.50	17.51	17.50	17.50	17.50	17.49	17.49	17.50	17.50	17.51	17.51	zero readings
14.80	15.50	16.30	17.58	17.68	17.40	17.79	18.98	17.10	18.78	19.18	19.70	19.68	19.82	19.50	19.58	19.33	20.00	
14.50	15.30	16.15	17.49	17.61	17.30	17.87	18.99	17.00	18.80	19.22	19.90	19.75	19.90	19.70	19.60	19.38	20.10	
14.30	15.15	16.05	17.55	17.68	17.35	17.88	18.98	17.00	18.88	19.24	19.90	19.75	19.90	19.85	19.65	19.40	20.20	
14.10	15.10	16.00	17.45	17.62	17.35	17.89	18.99	17.05	18.94	19.28	20.02	19.85	19.97	19.98	19.70	19.48	20.20	
13.90	14.90	15.85	17.40	17.61	17.30	17.95	19.00	17.00	18.97	19.31	20.00	19.85	19.98	20.00	19.73	19.50	20.20	
13.60	14.75	15.70	17.38	17.58	17.27	17.90	19.00	17.00	18.98	19.37	20.00	19.79	19.87	19.99	19.71	19.50	20.17	
13.50	14.60	15.60	17.39	17.59	17.29	17.95	19.05	17.00	18.98	19.39	20.00	19.82	19.90	19.99	19.72	19.51	20.17	
13.40	14.50	15.60	17.39	17.61	17.30	18.21	19.10	17.16	19.00	19.45	20.00	19.80	19.89	19.98	19.73	19.60	20.15	
13.30	14.45	15.55	17.30	17.50	17.20	18.20	19.10	17.05	18.98	19.44	20.00	19.80	19.89	19.99	19.75	19.58	20.11	

Fig. 4.12

Test 245 (continued)

Static Pressures along Horizontal Duct

Kopp	7a	7b	7c	8a	8b	8c	9a	9b	9c	10a	10b	10c	11a	11b	11c	12a	12b	12c
0	17.50	17.50	17.50	17.50	17.49	17.49	17.49	17.49	17.50	17.50	17.50	17.49	17.49	17.50	17.50	17.51	17.50	17.50
0	19.99	19.70	19.76	20.60	20.75	20.40	20.86	21.60	21.48	22.70	22.60	22.30	23.70	23.80	22.90	23.40	23.90	23.50
10	20.00	19.72	19.79	20.65	20.86	20.48	21.08	21.82	21.78	23.20	23.17	22.68	24.40	24.35	23.40	24.50	24.60	24.40
20	20.00	19.70	19.84	20.64	20.74	20.50	21.20	21.90	21.89	23.60	23.45	23.05	24.80	24.80	23.90	24.90	25.50	25.20
30	20.00	19.76	19.89	20.65	20.80	20.55	21.20	21.93	21.93	23.80	23.50	23.15	25.10	25.15	24.20	25.20	25.85	25.60
40	20.03	19.79	19.90	20.65	20.80	20.50	21.20	21.93	21.93	23.80	23.10	23.10	25.00	25.30	24.30	25.30	26.20	25.90
50	19.98	19.71	19.81	20.49	20.50	20.35	20.90	21.70	21.65	23.50	23.00	23.00	25.10	25.40	24.30	25.40	26.50	26.20
60	19.98	19.72	19.88	20.50	20.58	20.39	20.99	21.71	21.68	23.50	23.30	23.00	25.20	25.40	24.40	25.70	26.65	26.20
70	19.95	19.72	19.90	20.41	20.46	20.30	20.85	21.70	21.50	23.40	23.00	22.87	25.10	25.30	24.30	25.50	26.65	26.20
80	19.95	19.72	19.89	20.39	20.40	20.28	20.75	21.45	21.30	23.10	22.80	22.80	25.20	25.20	24.00	25.60	26.80	26.40

Fig. 4.12

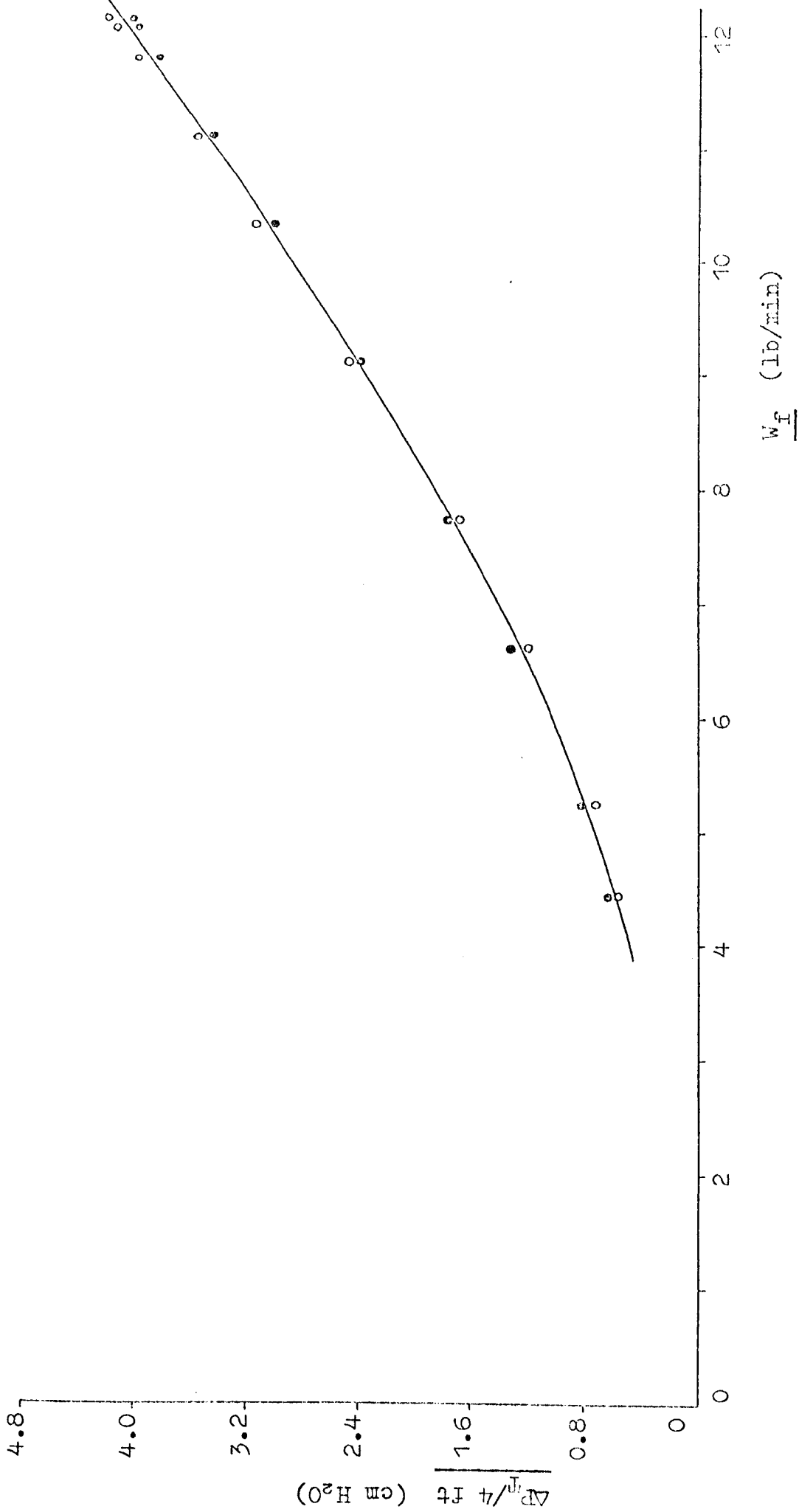


Fig. 4.13 Relationship between Pressure Gradient and Air Mass Flowrate for Air Flowing Alone up a Two inch diameter Vertical Duct.

- 06 -

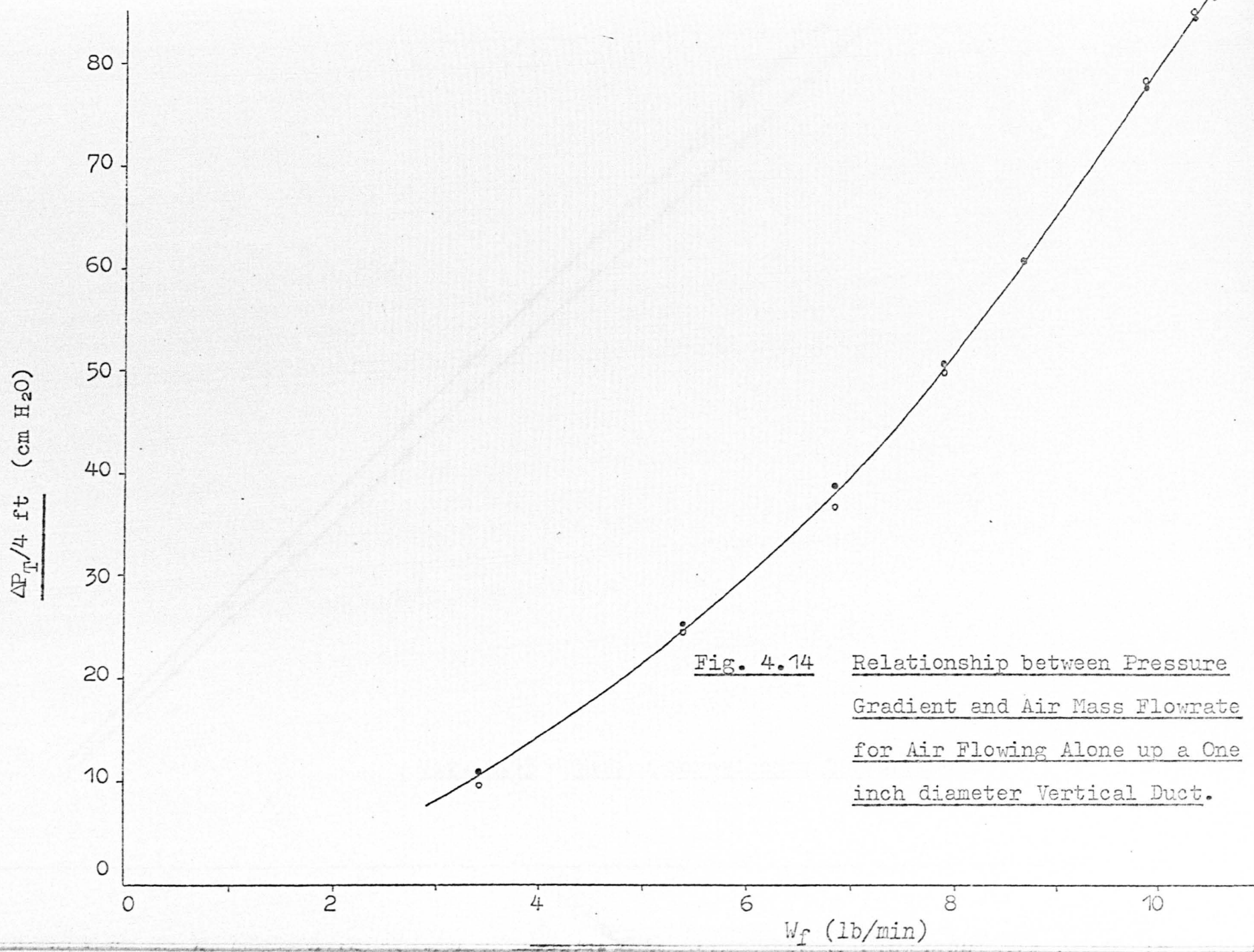


Fig. 4.14 Relationship between Pressure Gradient and Air Mass Flowrate for Air Flowing Alone up a One inch diameter Vertical Duct.

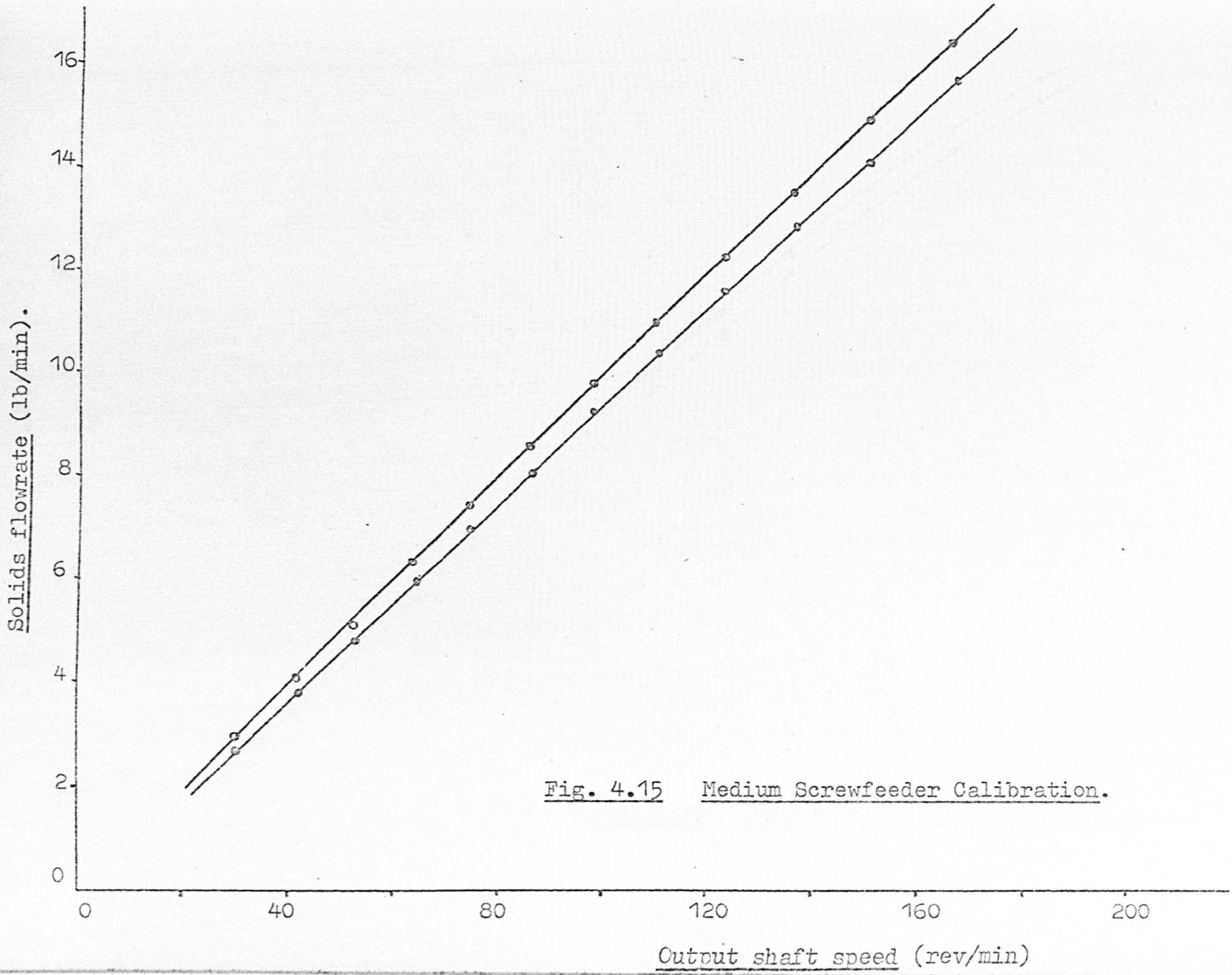


Fig. 4.15 Medium Screwfeeder Calibration.

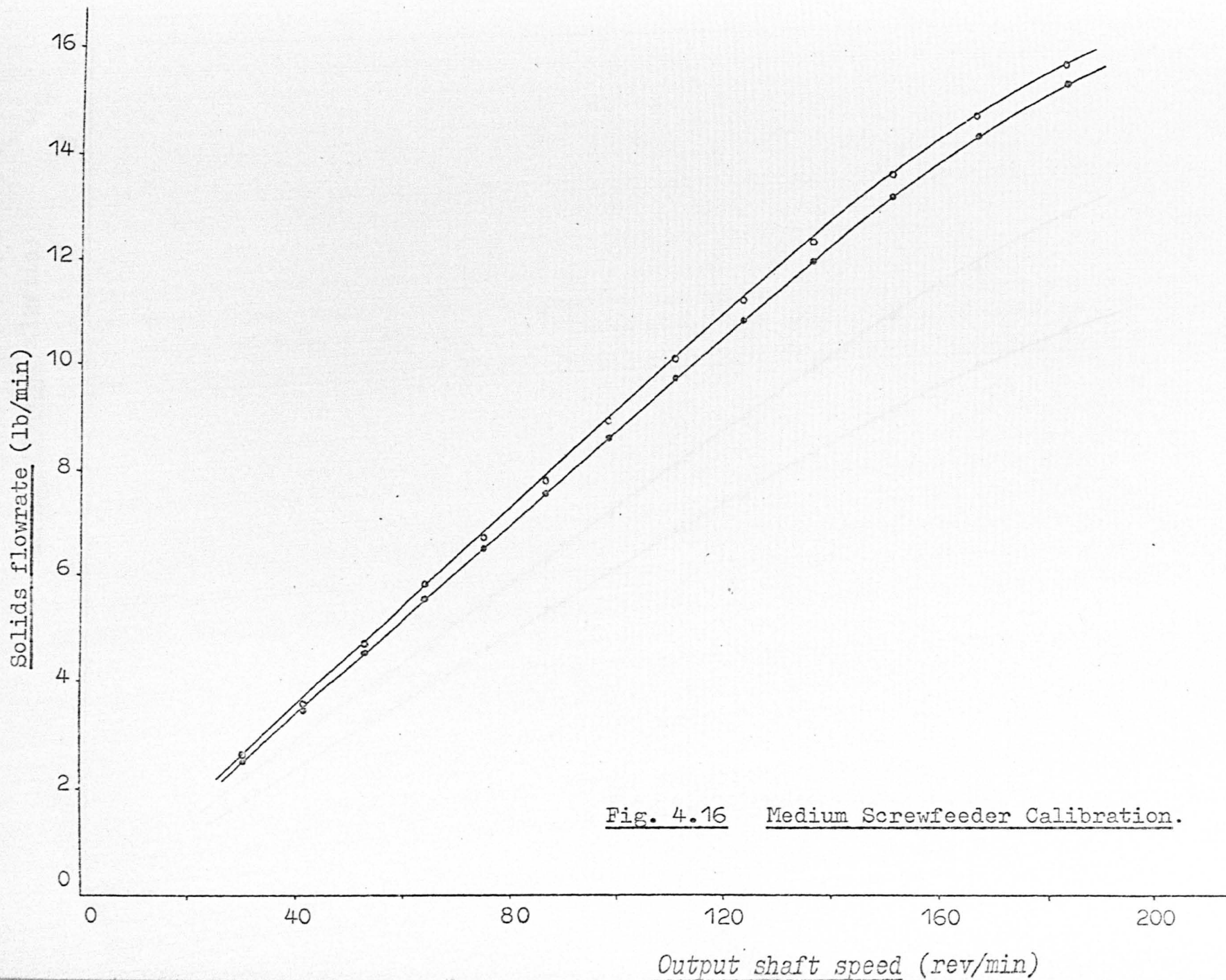


Fig. 4.16 Medium Screwfeeder Calibration.

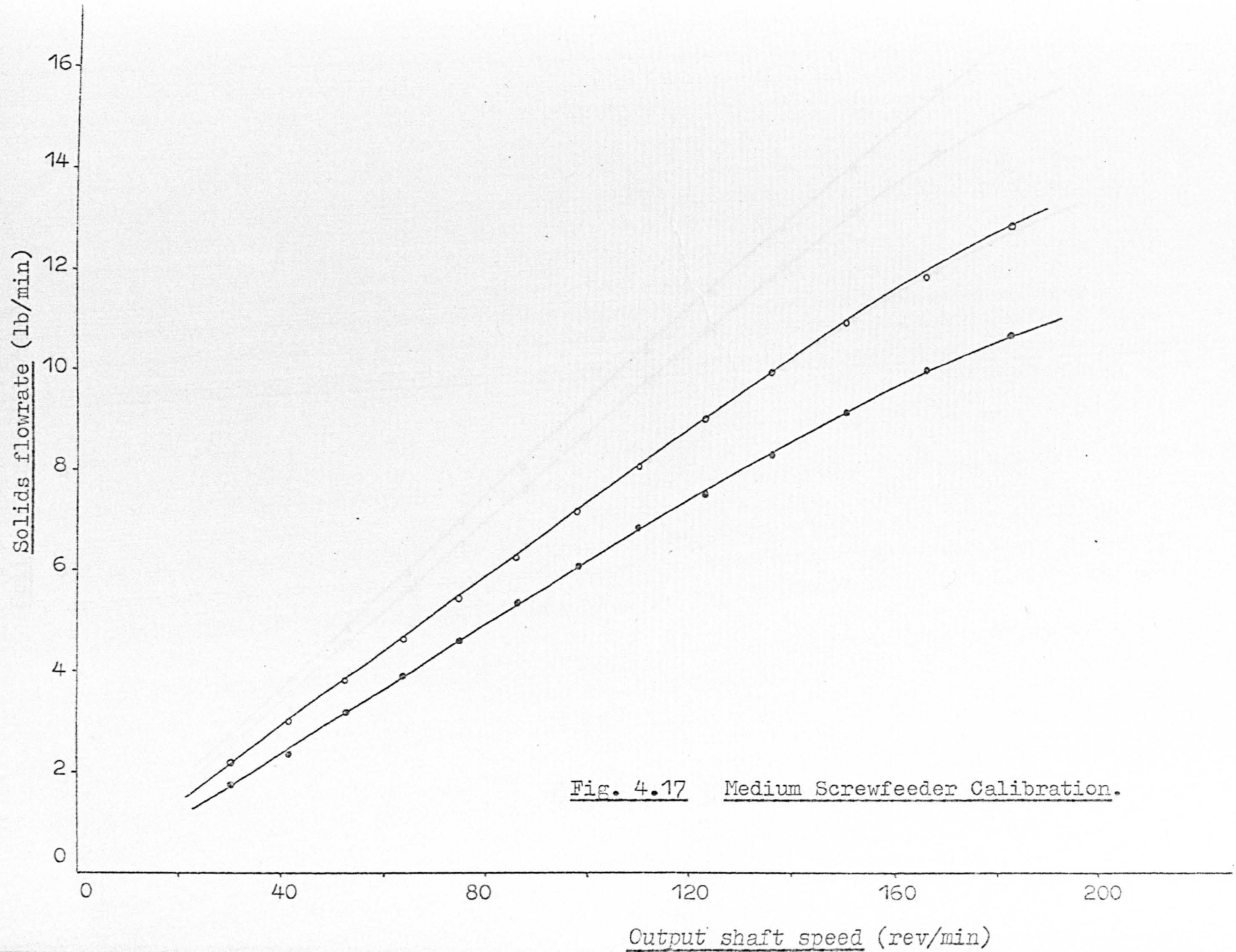


Fig. 4.17 Medium Screwfeeder Calibration.

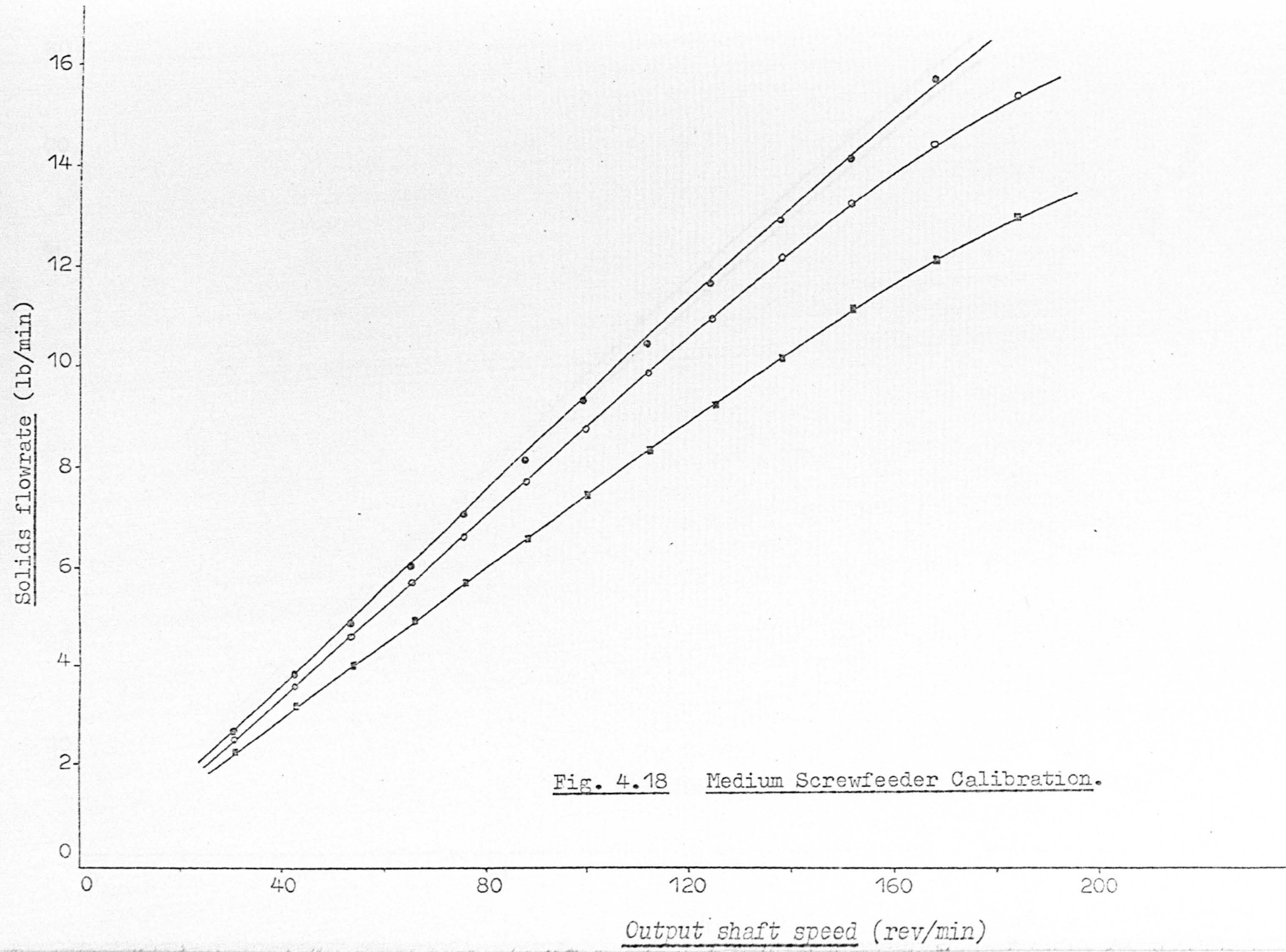


Fig. 4.18 Medium Screwfeeder Calibration.

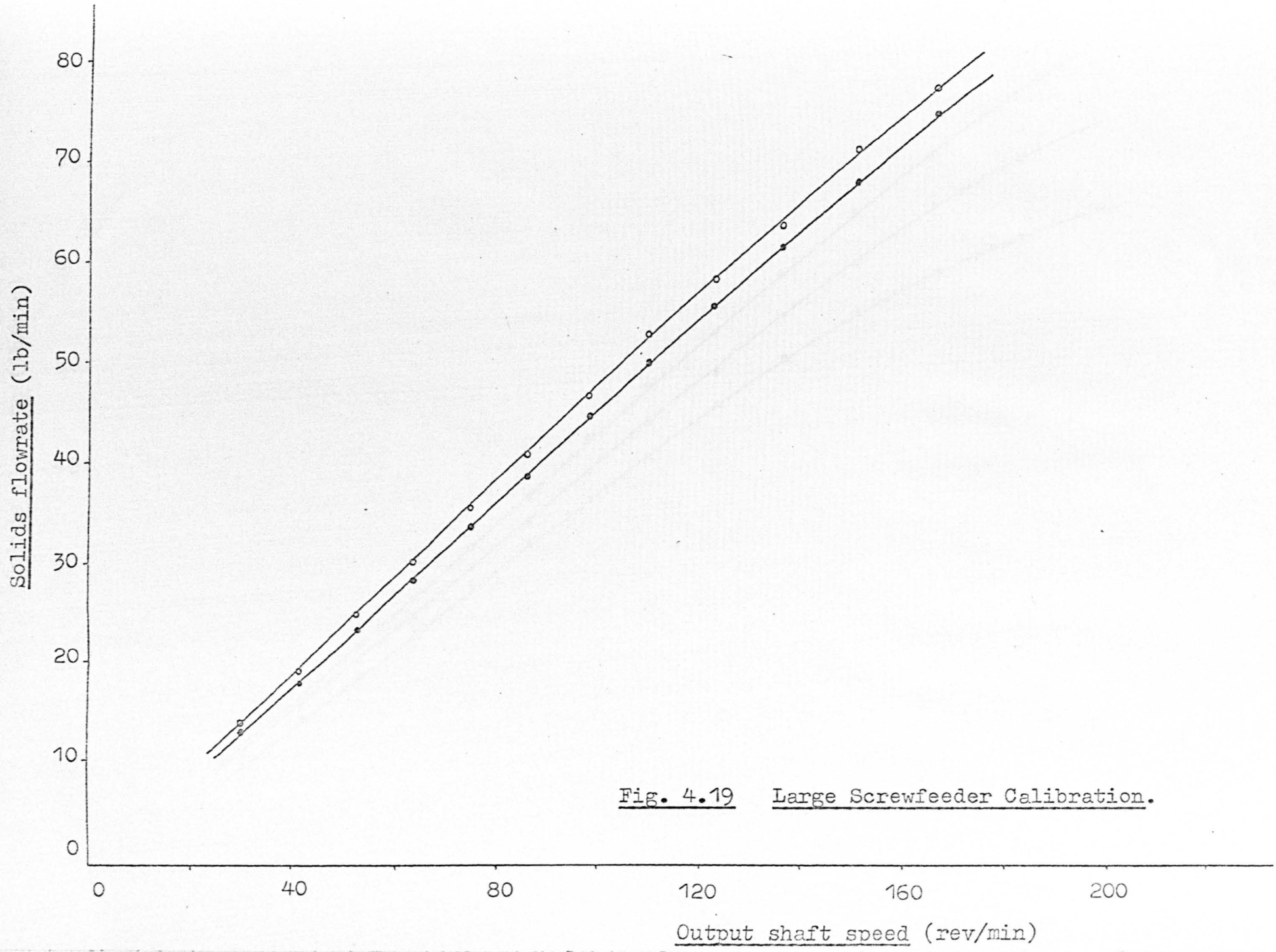


Fig. 4.19 Large Screwfeeder Calibration.

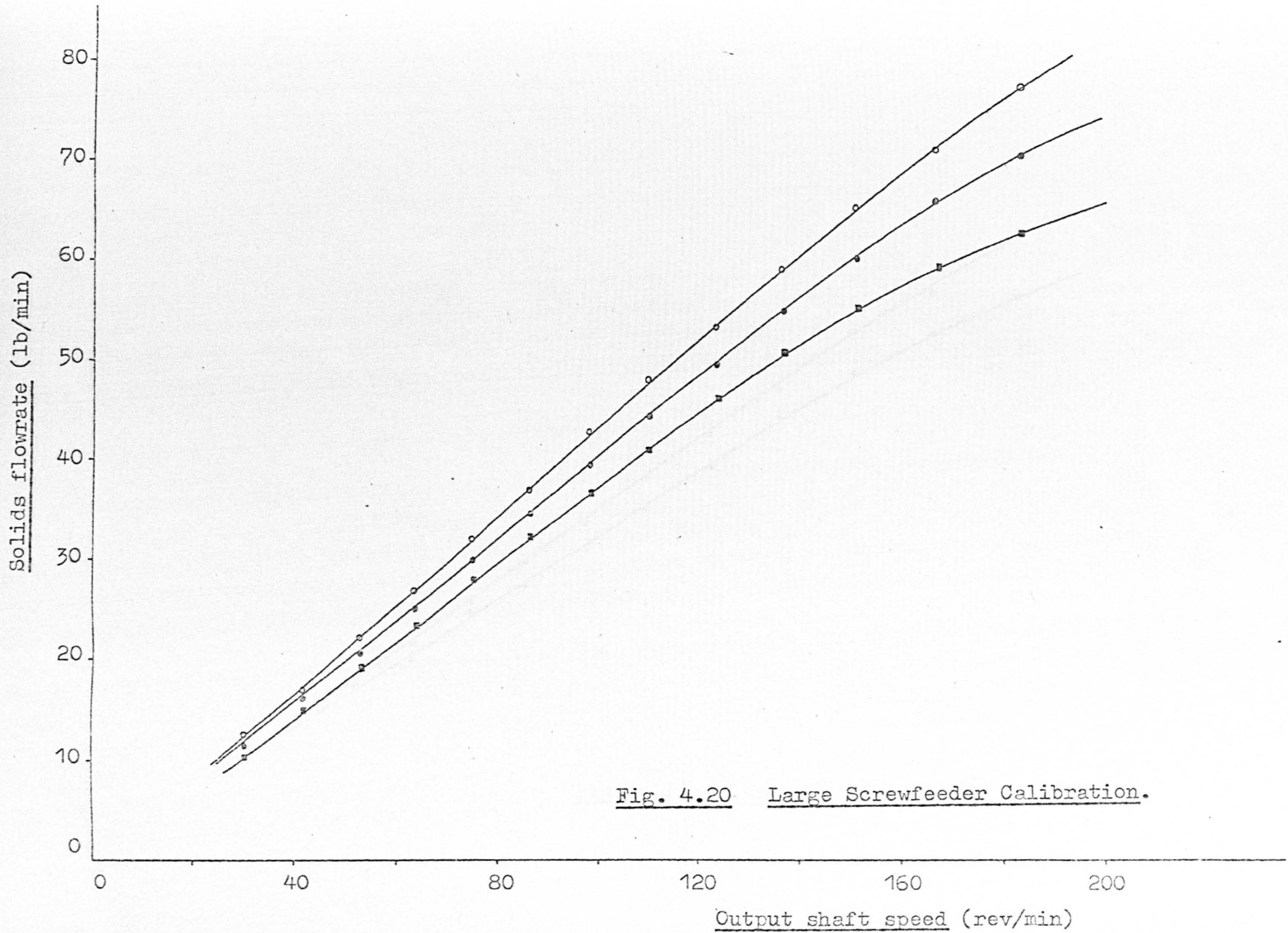


Fig. 4.20 Large Screwfeeder Calibration.

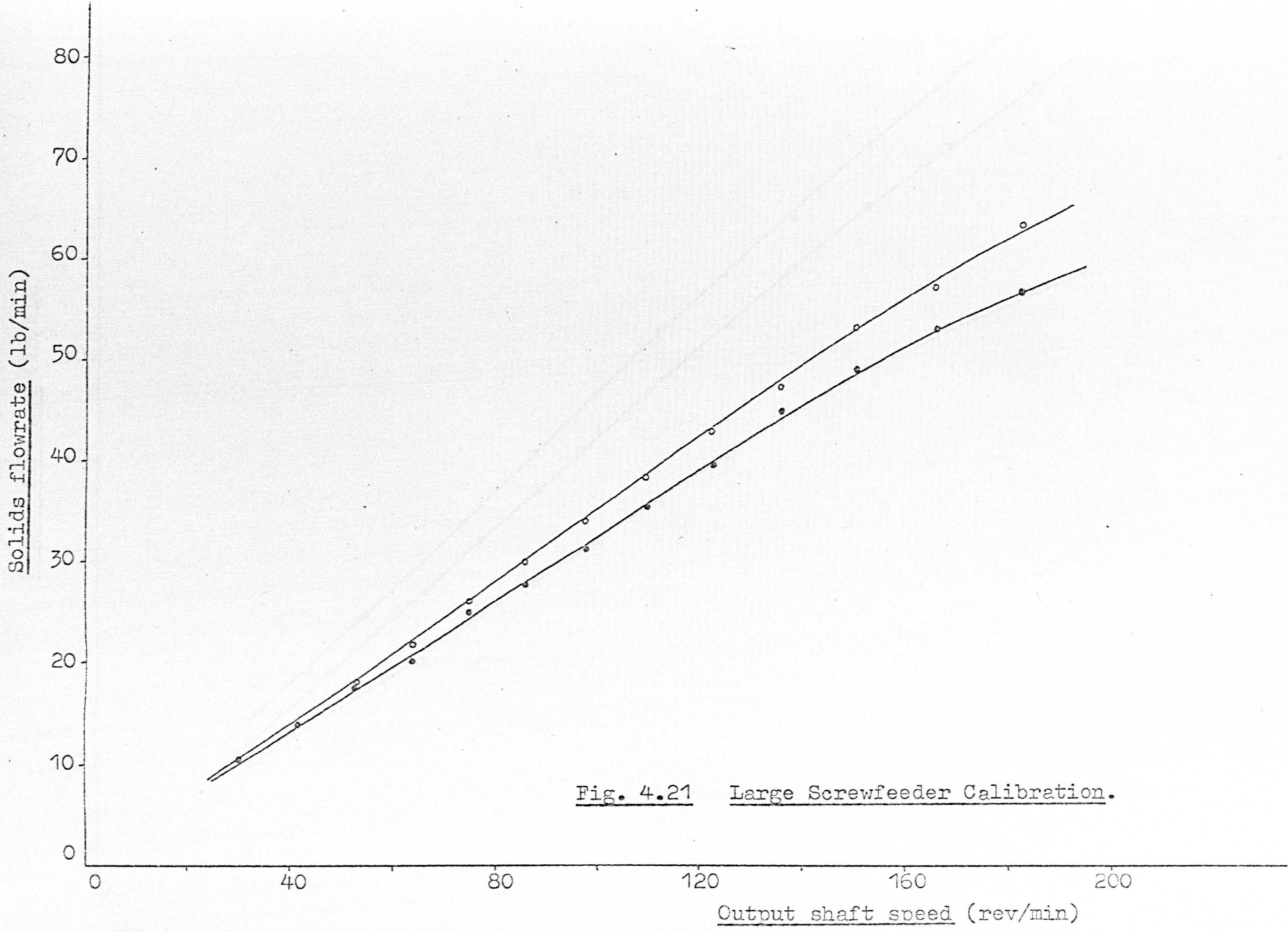


Fig. 4.21 Large Screwfeeder Calibration.

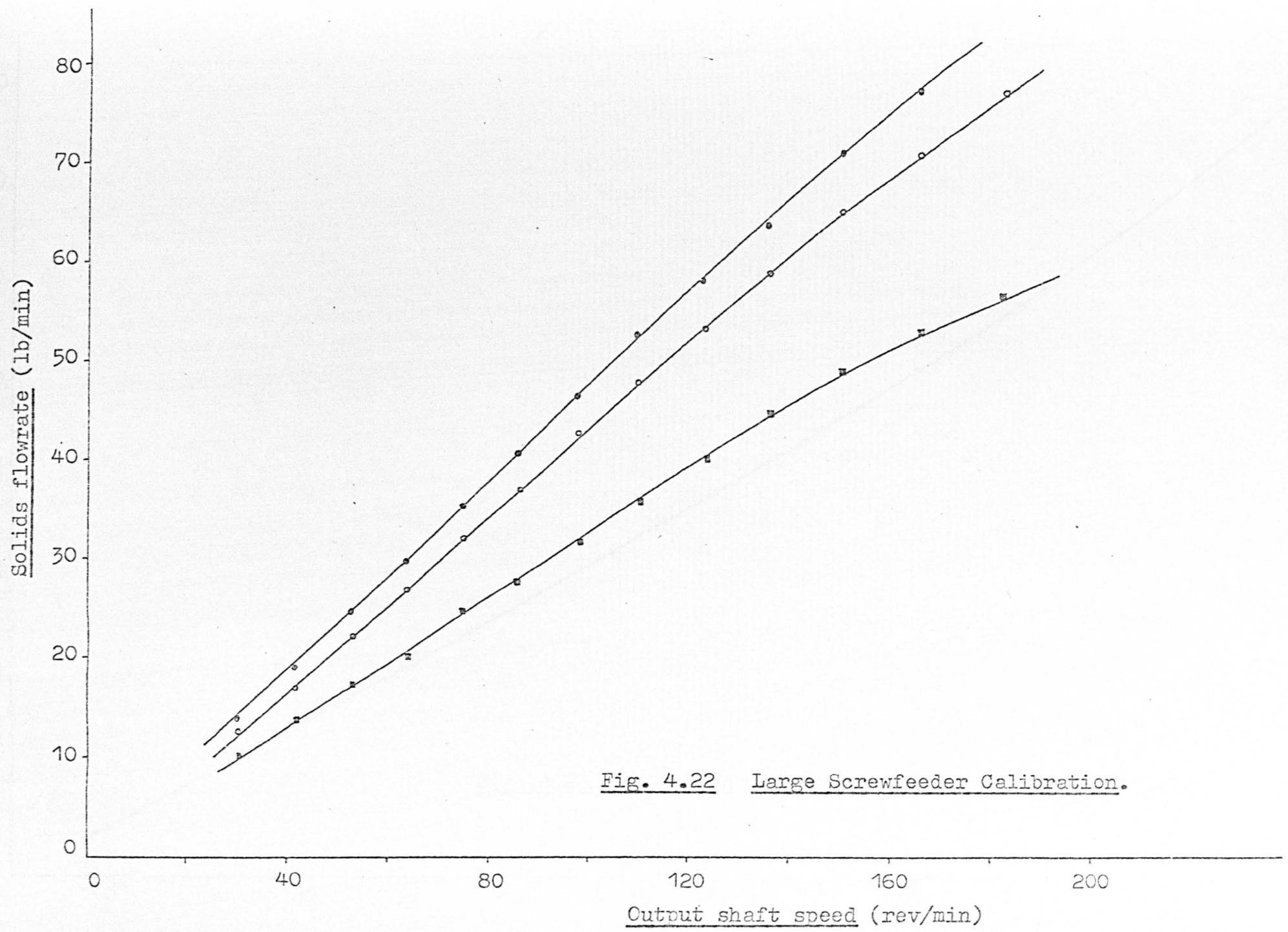


Fig. 4.22 Large Screwfeeder Calibration.

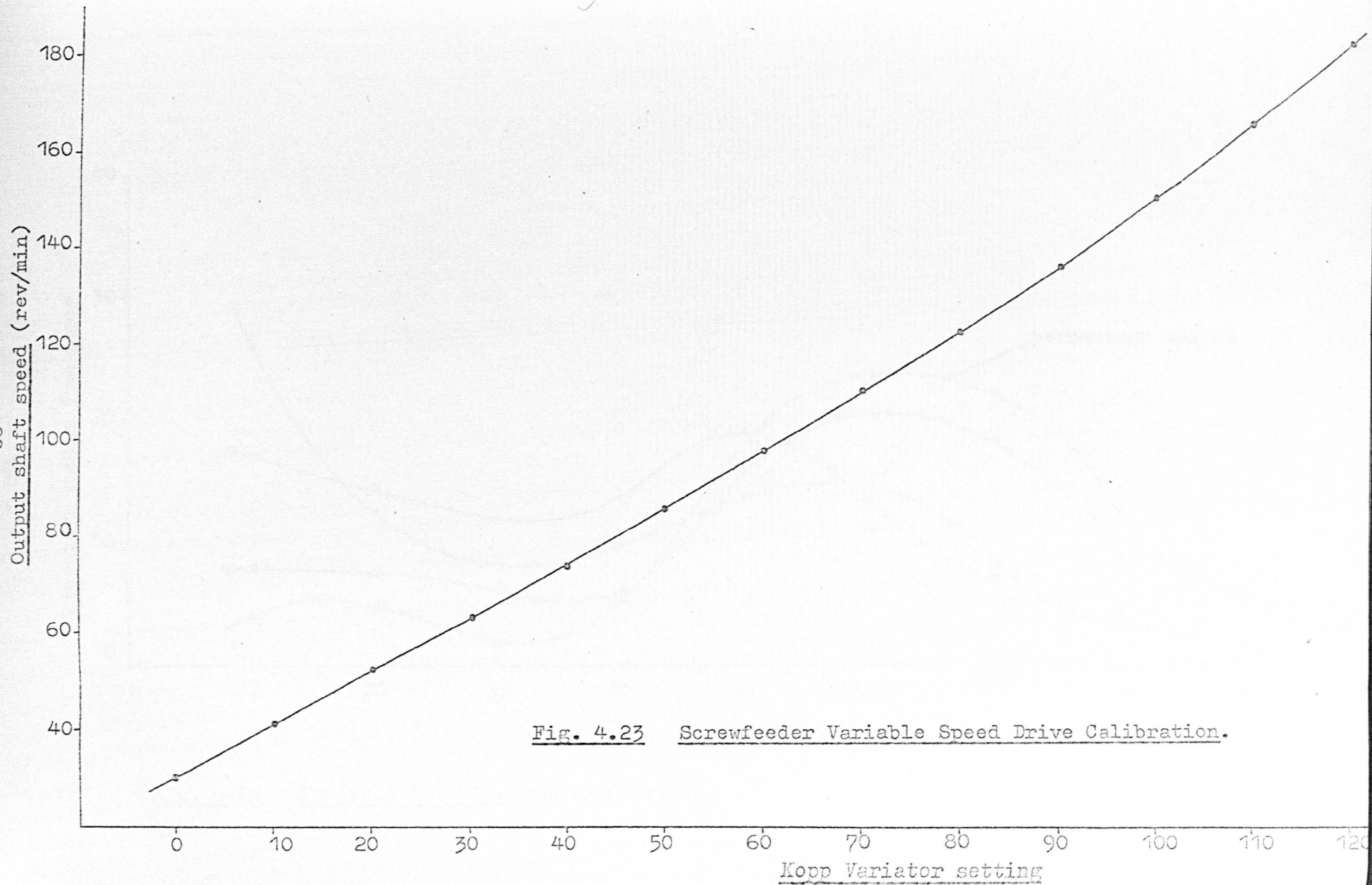


Fig. 4.23 Screwfeeder Variable Speed Drive Calibration.

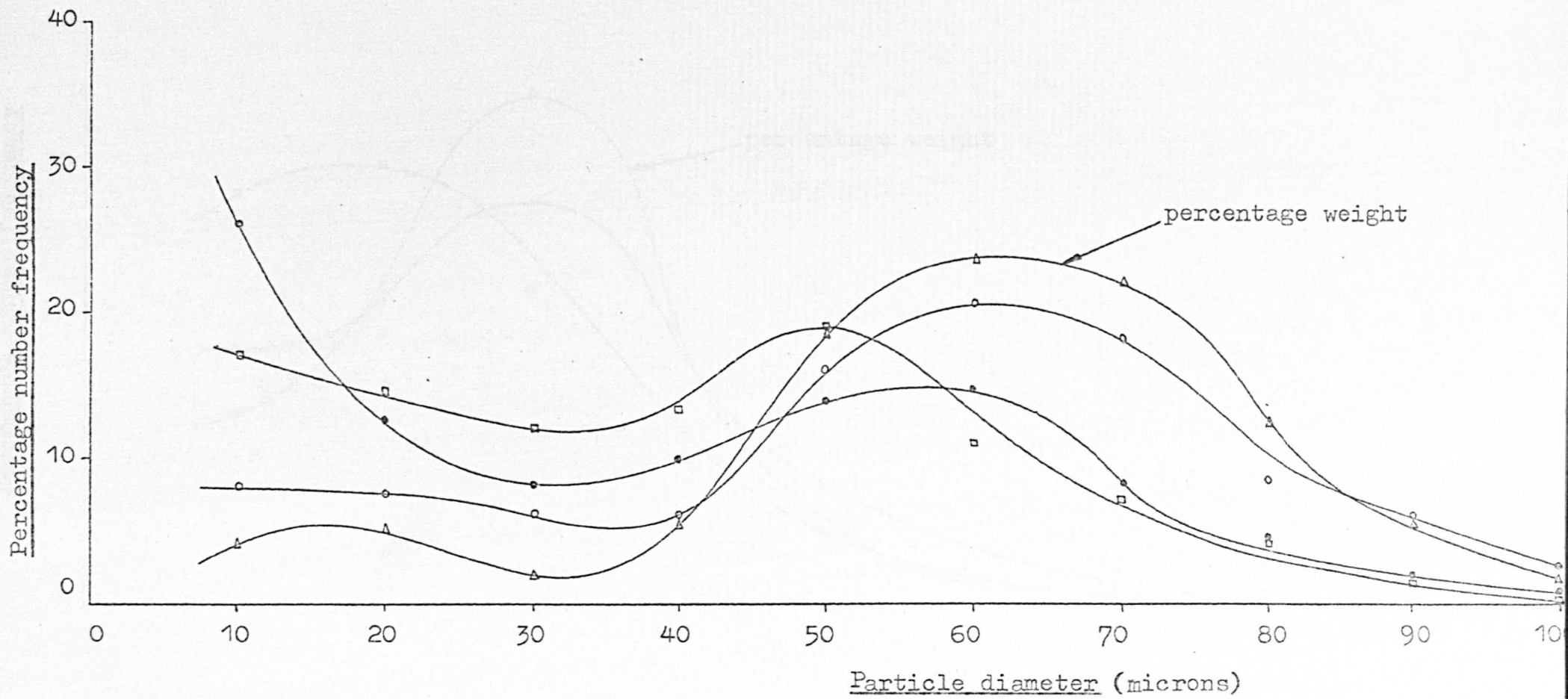


Fig. 4.24 Particle Size Spectra (240 mesh)

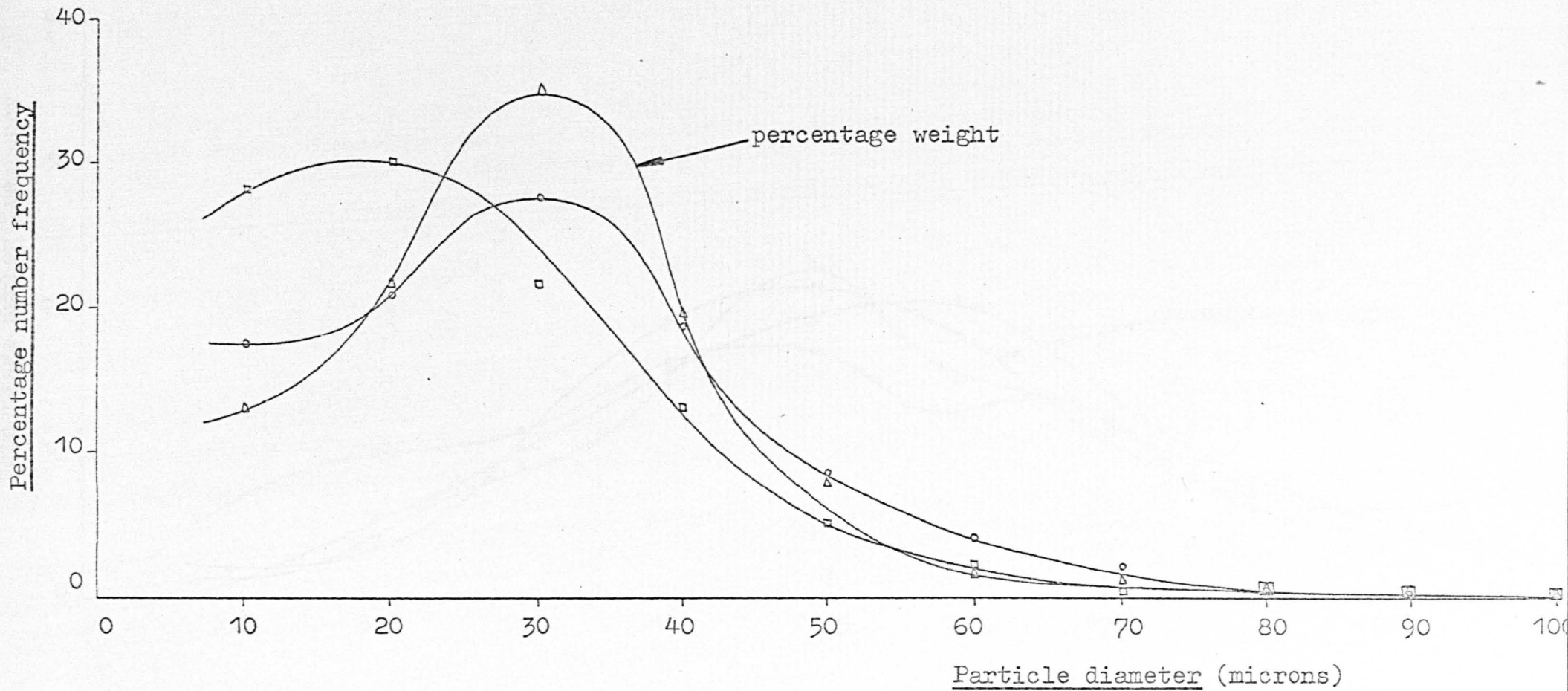


Fig. 4.25 Particle Size Spectra (320 mesh)

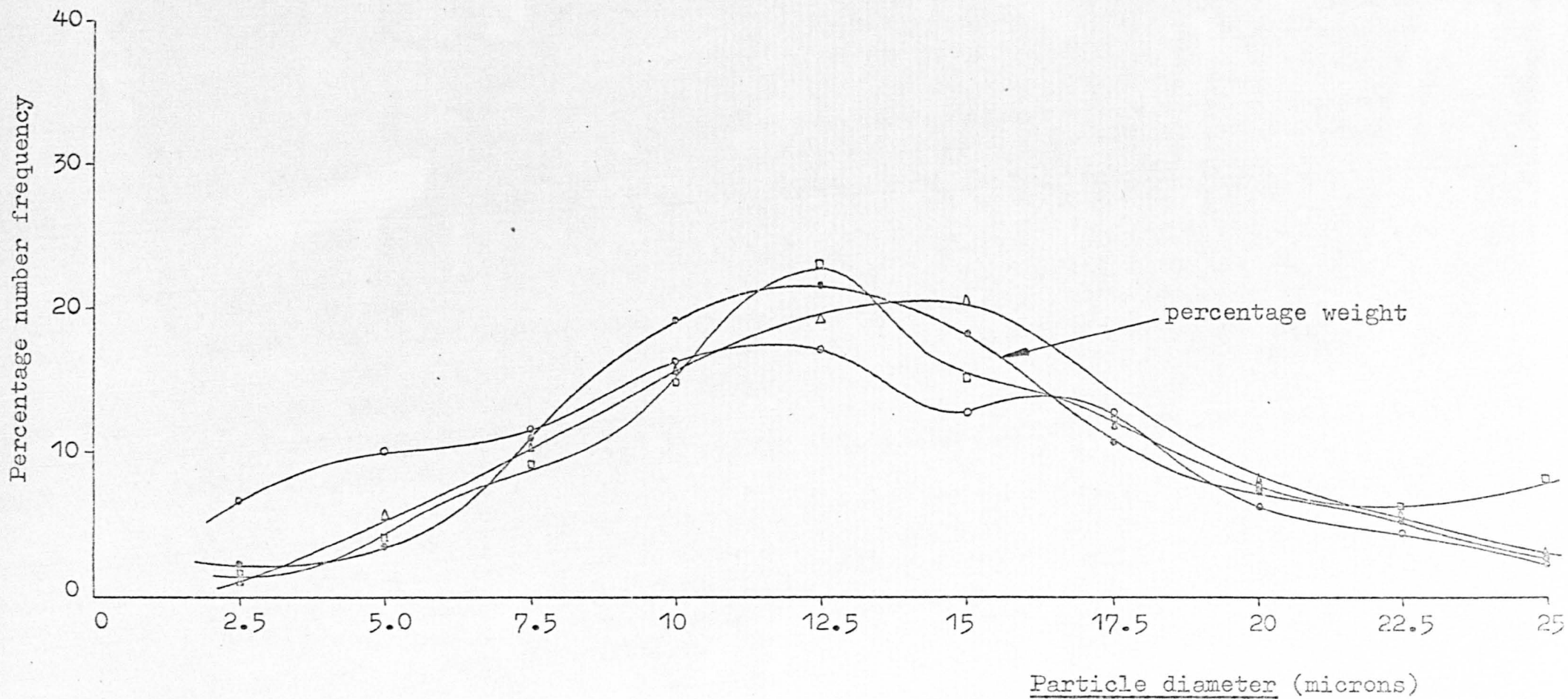
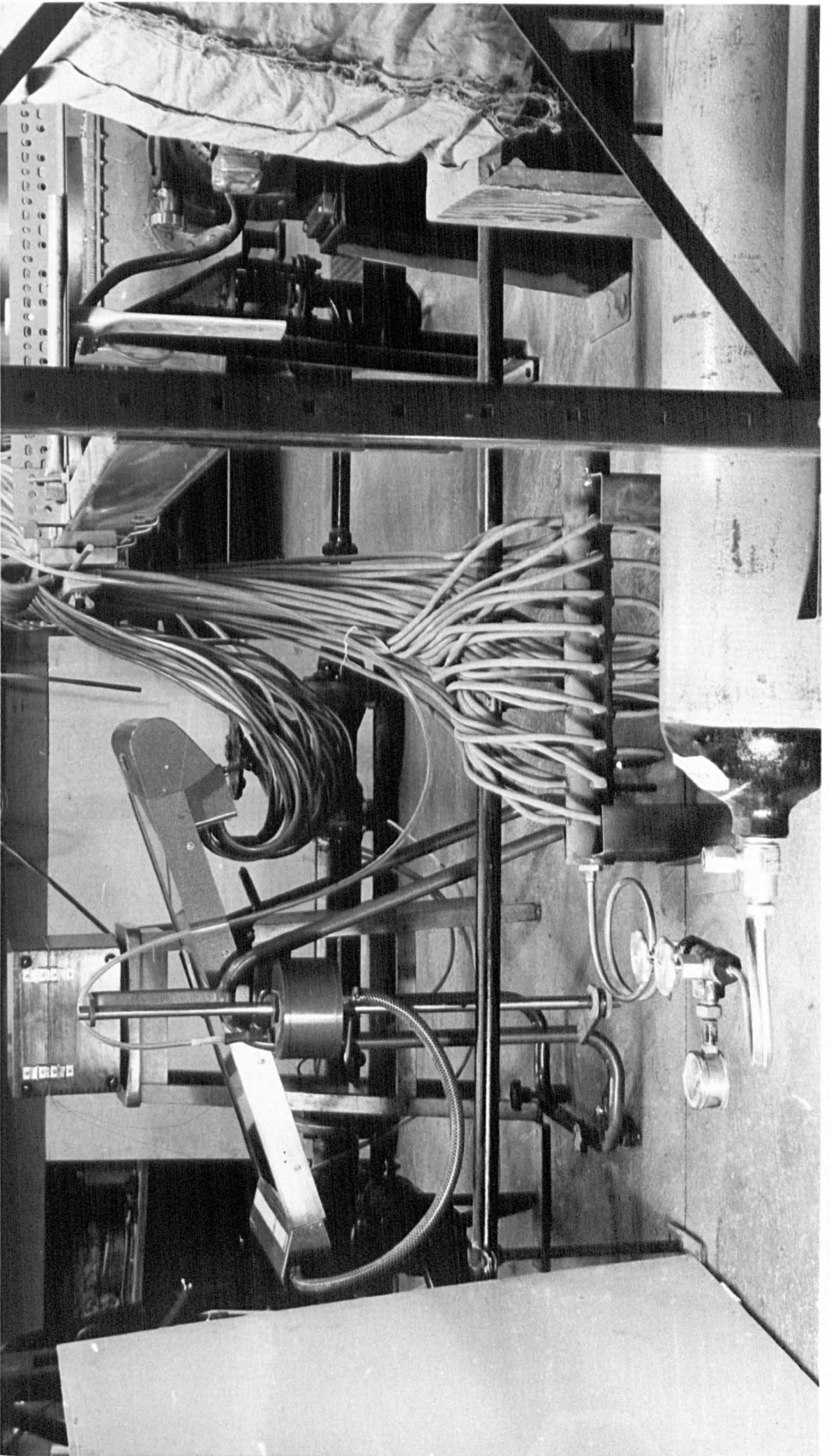


Fig. 4.26 Particle Size Spectra (500 mesh)

Plate 5: Purging System.



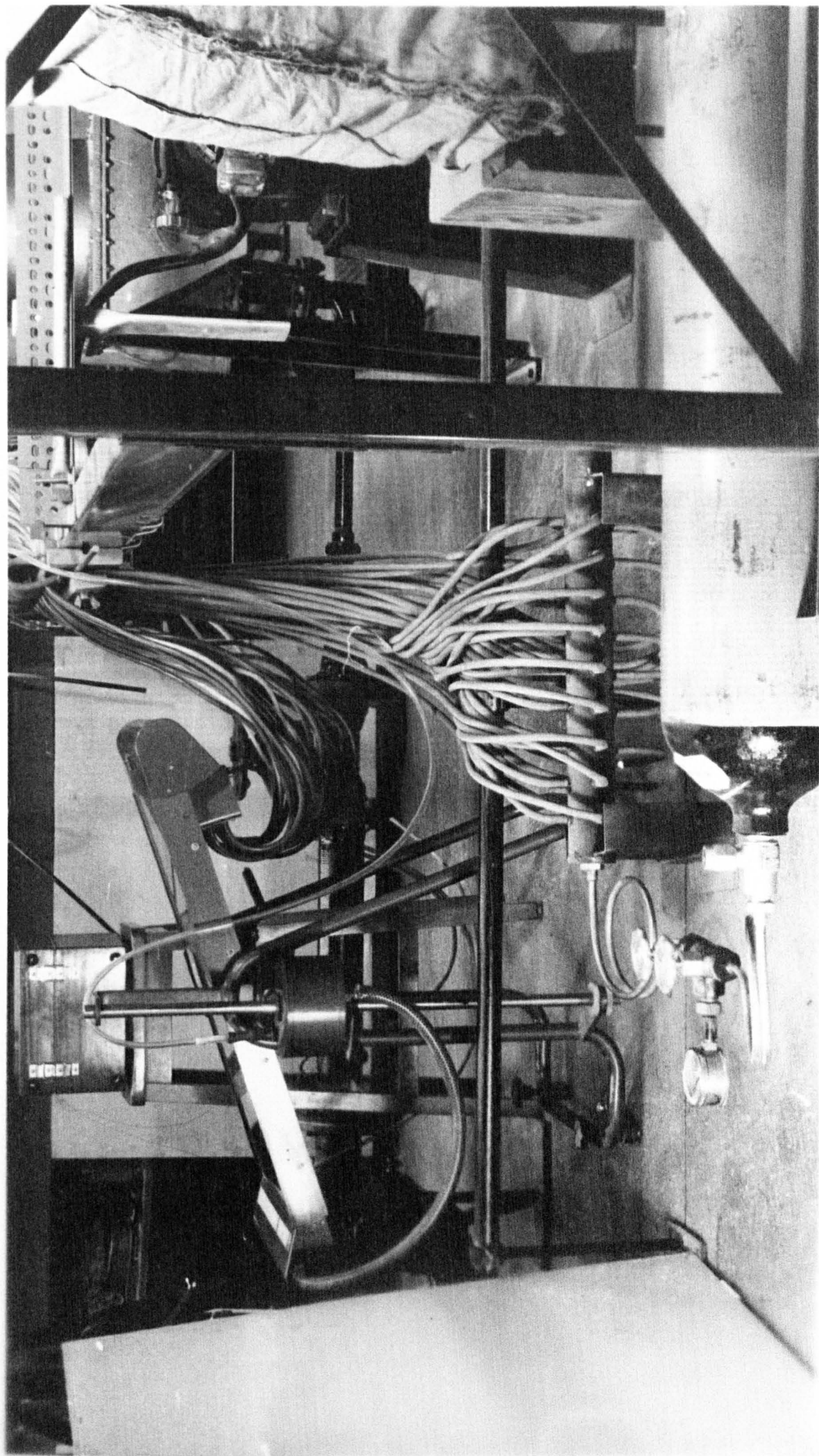
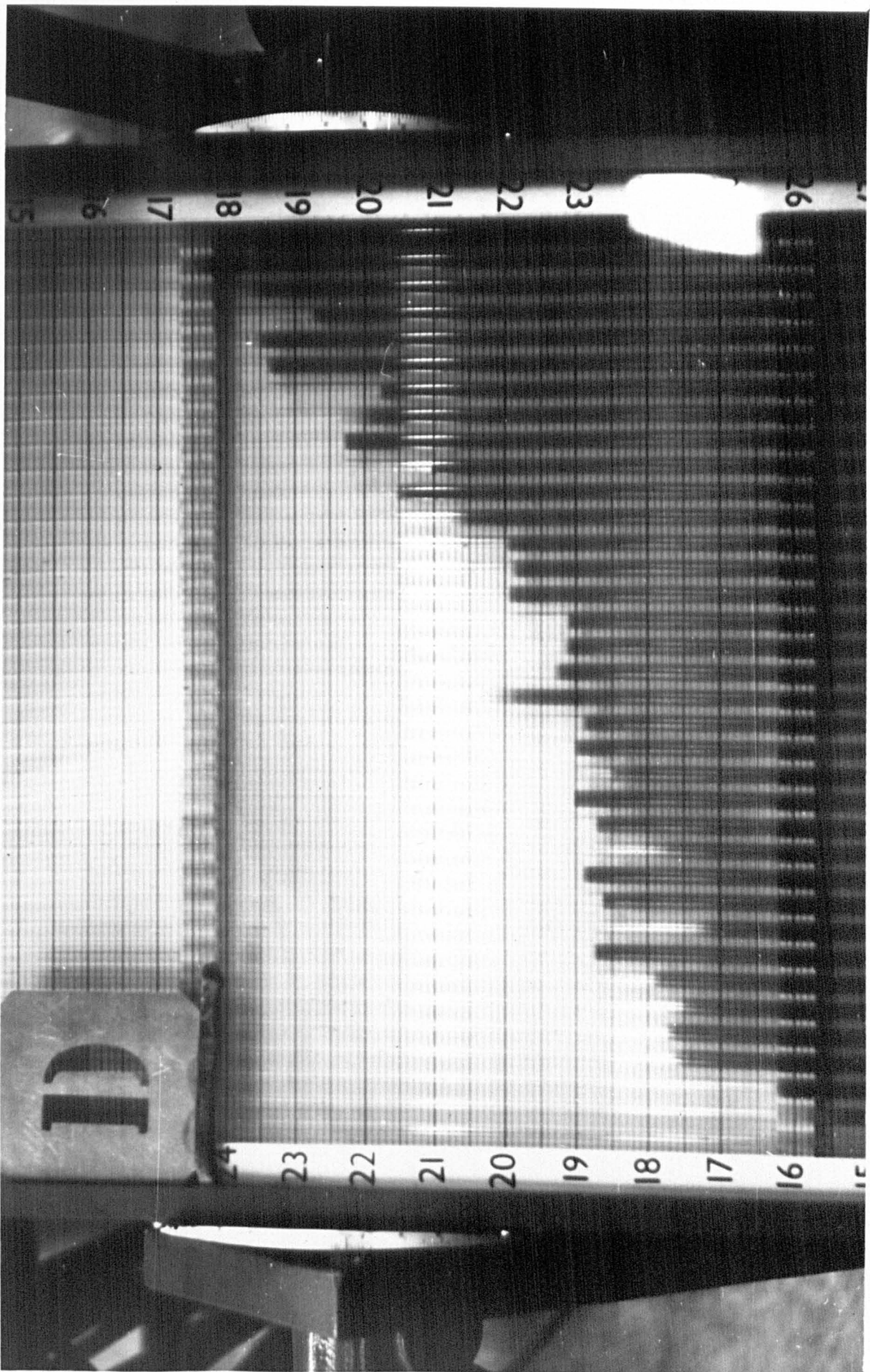


Plate 5: Purging System.

Plate 6: Manometer Readings.



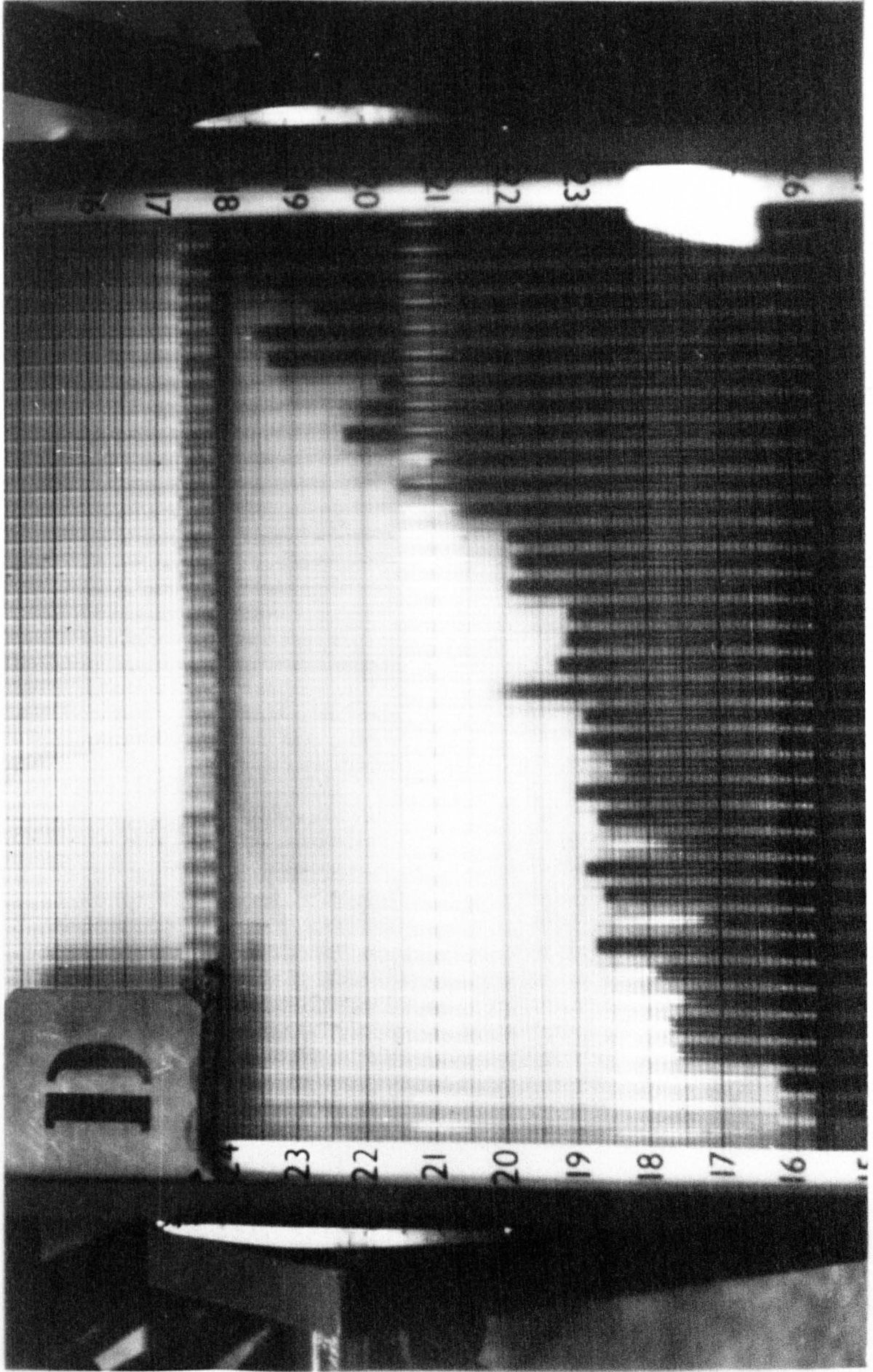


Plate 6: Manometer Readings.

CHAPTER 5

GAS-SOLID FLOW THROUGH VERTICAL DUCTS

5.1 Introduction

The pneumatic transport of granular materials had been exploited commercially for many years before the advent of fluid catalyst processes, which focussed attention on the acute shortage of reliable and quantitative information on the pressure differentials needed to produce the flow of suspensions of solids in gases through pipelines. The resulting studies generally attempted to develop correlations for predicting the effects of variations in solids flow rate, velocity, particle characteristics, duct diameter and numerous dimensionless relationships, on flow behaviour or power requirements.

Examination of the vast literature covering gas-solid two phase flow emphasises that the science remains inadequate. The mere presence of particles in a gas yields a large number of parameters which renders the problem too complex for complete solution, and the technological difficulties of circulating solids makes the study unattractive. The parallel case of circulating solids in liquids is relatively easy, since the smaller difference in density between the phases allows the suspension to be more stable at low velocities.

The fundamental aspects of gas-solid flow were reviewed by Torobin and Gauvin¹⁴ in a detailed survey which confirms that the field of gas-conveyed solids is a most unsatisfactorily studied aspect of gas-solid two phase flow. However, the mechanics of the turbulent flow of single phase fluids are so complex that empirical methods have been more effective in correlating the relations involved. When solids

are present within a fluid phase flowing turbulently, it becomes necessary to describe the solid phase by variables such as the mean particle diameter, particle density, particle shape, the ratio of solids to fluid in the flowing suspension, and so on.

In the literature survey which follows, fundamental approaches to gas-solid flows have generally been omitted and the possibly more rewarding area of empirical analysis examined in some detail. The literature survey is followed by a brief reference to the experimental work (section 5.3), whilst the simple theoretical approach used in the present study is considered in section 5.4.

5.2 Literature Survey

Although it is not completely exhaustive, this review is intended to be discriminative and cover all important previous contributions in this field of dilute phase, gas-solid flow through vertical ducts.

Most investigators of pneumatic transport have focussed attention on the region in which the particles travel as a well-dispersed phase, the controlled flow conditions remaining stable for a range of solids and air flow rates.

Probably the earliest work of significance is that of Cramp^{15,16} who investigated the vertical conveying of cereal seeds. Cramp considered that the force on a particle was proportional to $(U_f - U_p)^2$, and the difference between this force and the weight of the conveyed solids provided the force to accelerate the particles up the duct. By assuming the particle to be continuously accelerating, he obtained a relationship between U_f and U_p for a given distance of

particle travel. Cramp and Priestly¹⁷ continued experimental work on the vertical conveying of grain, and they developed an expression describing the frictional resistance of the grains.

Vogt and White⁸ investigated the dilute phase conveying of sand, steel shot, clover seed and wheat through both horizontal and vertical 0.5 inch nominal bore steel pipes. They derived a correlation in terms of the ratio of pressure drop with the suspension flowing to that obtained with the carrier gas alone, the mass ratio of solids flow to gas flow, and properties of the solid and gas. The interpretation of their work for vertical pipes presents some difficulty in that an allowance for static head is not evident.

Hariu and Molstad¹¹ measured the pressure drop in the transport of sands and silica-alumina cracking catalyst through vertical glass tubes of 0.267 and 0.532 inches diameter. Unfortunately, their results are obscured by the initial disregard of pressure drop due to acceleration, and they acknowledge that later measurements showed that the major portion of the apparent friction was due to particle acceleration in the test section.

The vertical transport of spherical catalyst through steel pipes of 0.473 and 1.023 inches diameter has also been investigated by Belden and Kassel¹⁸. From dimensional analysis they considered the longitudinal pressure gradient to be a function of Re , F_r , ρ_p/ρ_f , d_p/D , and the ratio of particle mass velocity to gas mass velocity. Their final correlation for the frictional pressure drop is independent of the particle diameter and density, also confirmed by Korn¹⁹, and they question Vogt and White's dependence of the

pressure drop upon $\left(\frac{D}{d_p}\right)^2$.

The work of Farbar⁷ is of particular interest since he conveyed mixed sized particles of a silica-alumina catalyst through a vertical glass tube of 17 mm diameter. His results, which are presented in the form of specific pressure drop $\left(\frac{\Delta P^m}{\Delta P_0}\right)$ plotted against the ratio of mass of solids to mass of gas, show a departure from the linear relationship between these variables reported by Gasterstädt⁶ and Vogt and White⁸.

More progress towards understanding the dynamics of the transport of solid particles by gases resulted from the work of Mehta et al⁴. They correlated the pressure drop data by adding the contributions associated with wall friction, particle friction, particle and air acceleration, and support of the particles. Mehta observed completely different flow behaviour of the solid particles for the two sizes of glass beads tested. The pressure drop correlation is expressed as a modified Fanning equation which includes particle velocity. Although they emphasise the importance of particle velocity, their indirect method of its determination is somewhat crude.

Bannister²⁴ reviewed the literature on pneumatic systems in 1959, and he concluded that the correlation of variables based upon empirical relationships provides the only means available for design. He states that the best approaches to pneumatic conveying are those of Clark et al²⁵ and Coulson and Richardson²⁶. The latter developed the following equation for vertical pipe flow from mathematical considerations:-

$$\Delta P_p \cdot A = \frac{W_p \cdot L}{\bar{u}_p} \cdot g \left\{ \left(1 - \frac{\rho_f}{\rho_p} \right) \left(\frac{\rho'}{\rho_f} \right) \left(\frac{\bar{u}_f - \bar{u}_p}{u_0} \right) - \left(1 - \frac{\rho'}{\rho_p} \right) \right\}, \quad (1)$$

where ρ' appears to be the average density of the suspension and u_0 is the terminal velocity of the particles. The proportion of the total pressure loss caused by the presence of the solid particles, ΔP_p , can, however, only be evaluated from equation (1) if the particle velocity and density of the dispersed solids are known, the other variables in equation (1) being relatively easy to determine. Clark et al used this equation and obtained a general correlation between friction factor and a modified R_e .

The extensive researches of German workers up to 1960 are summarised by Barth^{9,20}. Barth initially proposed that gas-solid transport systems be compared on a basis of similar Reynolds' and Froude numbers, and similar ratios of geometric sizes, densities and viscosities. Barth latter reported that that gas-solid flow phenomena in the vertical plane are more dependent upon Froude number than upon Reynolds' number, this was independently supported by Hitchcock and Jones²¹. Consequently, the results of several German investigators are presented as resistance coefficients versus Froude number for different solids-to-air loading ratios. Their general approach to evaluating the pressure drop data is to sum the different contributions in a manner similar to Mehta et al⁴. However, the portion of the total pressure difference caused by the presence of the solid particles is presented in a slightly modified form. They include terms to represent the pressure loss due to the particles striking the pipe walls and that due to interparticulate collisions, whilst Mehta et al simply refer to particle-particle friction loss. Since the remaining pressure loss contributions of the Germans and Mehta are the same, it becomes difficult to reconcile the

differences. It is possible that for a steady flowing suspension of solid particles the wall impact losses are minimal. Also, the loss due to interparticulate collisions may be considered negligible, since the total energy of the travelling particles will remain essentially constant, the only losses incurred being those due to attrition, non-elastic collisions, and the generation of alternative forms of energy. Similarly, the particle-particle friction term of Mehta is of doubtful overall importance, particularly for very fine particles. Thus the magnitudes of these specific contributions are probably so small compared with the total pressure loss, that any fundamental differences between both approaches are not highlighted in experimental programmes.

Previous research work had generally been confined to small bore pipes, although the validity of some of the equations developed has been tested by using data from industry⁹. Stemerding²² conveyed a fine cracking catalyst through two inch diameter vertical ducts, and obtained an empirical relationship between total pressure drop and several characteristic variables. He justifies his investigation on the grounds that earlier work had been confined to the transport of granular solids or very coarse materials flowing through horizontal pipes.

Experiments on the transportation of maize, wheat and granulated cork through two, three and four inch diameter steel pipes were reported by van der Lingen and Koppe²⁷. Their results are presented as specific pressure ratio, $\Delta P_m / \Delta P_o$, versus mass of solids to mass of air for a range of constant air velocities, and a relative resistance number against material Froude number. The scatter of points in

their graphs reflects their comment that the limited number of conclusions are rather tentative.

Uematsu et al²⁸ transported millet seed through 2.88 cm diameter steel tubing, and from the data they derived an empirical expression for the pressure gradient in a vertical duct. Their expression relates to the region where the particles have been accelerated to a steady velocity, and requires only a knowledge of R_e , D , L , ρ_f , \bar{u}_f and W_p/W_f .

Jones et al² stated that their objective was to develop expressions for the prediction of pressure drop in vertical tubes using only easily determined physical properties of the solid particles. Their approach consisted of separating the pressure drop into individual components and applying the following relationship:-

$$\frac{\Delta p_f^*}{h} - \lambda_f = \lambda_p = 1.89 \times 10^{-6} \frac{A_o}{x^{1/2}} \cdot \theta^x \quad (2)$$

where ΔP_f^* = total pressure drop due to friction only per one diameter of pipe length;

h = velocity head of the carrier fluid;

λ_f = friction factor for air;

λ_p = friction factor for solids;

A_o = surface area of solid particles per unit volume;

θ = specific loading, lb of solid/lb of air;

x = dimensionless surface shape factor of the solid particles.

The expression $\frac{\Delta P_f^*}{h} = \frac{\Delta P_{FS} \cdot D/L}{\frac{1}{2} \rho_f \bar{u}_f^2}$, which is the well known form of the friction factor of the suspension, λ_s , and so, like many other workers⁵, they have assumed that the friction factor for the solids may be defined by the equation:-

$$\lambda_p = \lambda_s - \lambda_f.$$

The purpose of equation (2) was to determine the value of λ_p , which could then be used in the following total pressure drop equation, which includes acceleration effects:-

$$\Delta P_T = \frac{\rho_{ds} \bar{u}_p^2}{2g} + \frac{\rho_f \bar{u}_f^2}{2g} + \rho_{ds} \cdot L + (\lambda_f + \lambda_p) h \cdot \frac{L}{D}. \quad (3)$$

Unfortunately the precise definition of the surface shape factor is not explained, it is probable that $\chi = \frac{\pi d_p^2}{4} / A_p$, which reduces to unity for spherical particles. They recommend use of equation (1) for the range of A_o from 6,300 to 20,000 ft²/ft³, compared with the present study in which $A_o \approx 15,000$ ft²/ft³ for the 240 mesh alumina powder and $A_o \approx 60,000$ ft²/ft³ for the 500 mesh powder. However, deviation of their experimental and calculated values was in the majority of cases less than 5%, and their experimental data correlated satisfactorily using Hinkle's²³ relationship.

Jones et al state that fluid rate and density, duct diameter, solids rate, density, surface area and surface shape factor are the only quantities which need to be known for the prediction of the total pressure drop. They make no reference to the determination of particle velocity, \bar{u}_p , which is an essential parameter in equation (3), and their determination of the dispersed density of the solids, ρ_{ds} , is questionable. Despite these and certain other deficiencies the concept is quite original and the wide range of solid particles of diameters varying from 200 to 765 microns used in the investigation deserves recommendation.

An impressive contribution towards understanding the turbulent flow properties of gaseous suspensions of fine

particles flowing vertically upwards through ducts has been made by Boothroyd^{1,29,30,31,32}. Boothroyd's work is generally concerned with the effect on fluid turbulence by the presence of the solids. He shows that the frictional pressure drop for gas-solid flow through a one inch diameter pipe is less than that for air alone, whereas the pressure drop in larger diameter pipes was usually higher than that for air alone. This is supported by the present study³ for the flow of alumina particles of similar size distribution as Boothroyd's zinc dust. Boothroyd¹ deals with the problem of correlating pressure drop data for design purposes by a theoretical approach based upon dimensional analysis and supported by experimental data.

A most interesting investigation of gas-solids flow at high Reynolds' number (10^5 to 10^6) and low solids loading ($\frac{W_p}{W_f} < 0.6$) through a one inch diameter tube, in which acceleration effects were small, has been carried out by McCarthy and Olson³³. They report that the two phase friction factor decreased with increased solids loading, as seen clearly in my reference (3). The friction factor correlation proposed by McCarthy and Olson is:-

$$\frac{\lambda_s}{\lambda_f} = 1.0 - 0.8 \frac{W_p}{W_f} + 0.5 \left(\frac{W_p}{W_f} \right)^2 \quad (4)$$

and since
$$\frac{d(\lambda_s/\lambda_f)}{d(W_p/W_f)} = -0.8 + \frac{W_p}{W_f} \quad (5)$$

then the rate of decrease in the friction factor decreases with increasing solids loading, which is consistent with the fact that zero friction loss is not possible. Since the second derivative of equation (5) is positive, then equating

$\frac{d(\lambda_s/\lambda_f)}{d(W_p/W_f)}$ to zero produces a minimum of λ_s/λ_f at $W_p/W_f = 0.8$. They quote a standard deviation of ± 0.4 for W_p/W_f , and so the minimum value of λ_s/λ_f occurring at $W_p/W_f = 0.8$ should be used with caution. The results from the present study, as reported in reference (3), gave minimum values of λ_s/λ_f at W_p/W_f in the range 0.3 to 0.7 for the flow of alumina particles, having a mean diameter of 15 microns, through a two inch diameter duct. Similar results were obtained for flow through a three inch diameter duct, but these minima are very dependent upon particle size and probably do not exist for particles above 100 microns. The increase in friction factor at higher solids loading shown in reference (3), are possibly due to particle-particle and particle-wall impacts becoming important.

Boyce and Blick³⁶ state that one of the most important characteristics of gas-solid flow is its frictional energy dissipation ability. They were quite satisfied that this characteristic had been extensively investigated for liquid-solid flows but concluded, after an extensive literature search, that work in the gas-solid flow region had been rather limited in the number and range of parameters investigated. Their work involved measuring pressure gradients for the gas-solid flow through a 2.75 inch diameter tube of plexiglas, for a range of solids-to-gas mass flow ratio, W_p/W_f , from 0 to 3, and a Reynolds' number range from 0.9×10^4 to 6.3×10^4 . The scope of their work appears to be more restricted than many earlier workers, and their claim that this extensive variation of the important parameters has given a fuller understanding of the fluid flow phenomena in dusty air is difficult to appreciate. They did, however,

circulate five different particle sizes, which varied from silica dust having a size distribution from 2 to 60 microns to glass beads of 100, 200, 840 and 1680 microns mean diameter. Their results are represented as percentage reduction of skin friction drag versus weight flow of particles for different ranges of Reynolds' number. They concluded that the maximum reduction of the skin friction coefficient occurred in the low end of the fully developed turbulent flow region.

A recent paper by Chandok and Pei³⁷, who transported spherical glass beads, 150 to 500 microns, through a 10 cm diameter vertical pipe, stated that the air velocity profile and the pressure drop due to air alone are unaffected by the presence of solids up to a solids loading ratio of 3 - the limit of their experimental programme. Their results indicate that total pressure drop is independent of particle diameter, and the slope of the pressure drop lines at different pipe Reynolds' number is constant, with the intercepts on the $W_p = 0$ line corresponding to the pressure drop due to air alone. Unfortunately the pressure drop relationships are not shown in their paper, however, they give the very simple relationship:-

$$\Delta P_{p/L} = 0.0424W_p \quad (6)$$

where the pressure drop due to the presence of the solids, ΔP_p , is measured in cm H₂O, the pipe length, L, in metres, and the solids flow rate in kg/min. They quote a standard deviation of ± 0.0425 cm H₂O/m, which is equivalent to ± 0.0130 cm H₂O/ft, whilst equation (6) can be written as:-

$$\Delta P_{p/L} = 0.3064W_p \quad (7)$$

where ΔP_p is in cm H₂O, L in ft and W_p in lb/min, which are the units employed in the present study. The relevance of equation (7) to the present work is discussed in section 5.6.

Some recent work by Leung et al⁴⁷ develops a design procedure for calculating pipe size, air flow rate and pressure drop in steady state vertical pneumatic conveying. Their pressure drop correlation is based upon the work of Hinze⁴⁶ and Jones et al², and is applicable to dilute phase flow:-

$$\Delta P_T = \left[\frac{\rho_f \epsilon U_{af}^2}{g} + \frac{\rho_p (1 - \epsilon) U_{ap}^2}{g} \right]_0^L + \int_0^L \rho_f \epsilon dz + \rho_p \int_0^L (1 - \epsilon) dz + (\lambda_f + \lambda_p) \frac{\rho_f U_{af}^2}{2g} \cdot \frac{L}{D} \quad (8)$$

where ϵ = voidage,

z = vertical pipe axial coordinate,

U_{af} = actual average gas velocity = $\bar{u}_f / (1 - \epsilon)$,

U_{ap} = actual average solids velocity = $\bar{u}_p / (1 - \epsilon)$.

The two terms in the square brackets represent the acceleration losses of the flowing suspension, the next two quantities are concerned with supporting the gas and solid in the test-section, whilst the final term describes the total frictional losses. It is reasonable to assume for uniform suspension flow of very fine particles that:-

- (i) ρ_f is sensibly constant throughout the test-section;
- (ii) $U_{af} = U_{ap}$, that is, $\bar{u}_f = \bar{u}_p$; and
- (iii) the voidage, ϵ , is invariant.

Thus, equation (8) reduces to:-

$$\Delta P_T = \left[\frac{\rho_f \epsilon}{g} \cdot \frac{\bar{u}_f^2}{(1 - \epsilon)^2} + \frac{\rho_p (1 - \epsilon) \bar{u}_p^2}{g(1 - \epsilon)^2} \right]_0^L$$

$$+ \rho_f \epsilon L + \rho_p (1 - \epsilon) L + (\lambda_f + \lambda_p) \cdot \frac{\rho_f \bar{u}_f^2}{2g(1 - \epsilon)^2}$$

$$\text{i.e. } \Delta P_T = \frac{\bar{u}_f^2}{g(1 - \epsilon)^2} \left[\rho_f \epsilon + \rho_p (1 - \epsilon) \right]_0^L + L \left\{ \rho_f \epsilon + \rho_p (1 - \epsilon) \right\} \\ + (\lambda_f + \lambda_p) \frac{\rho_f \bar{u}_f^2}{2g(1 - \epsilon)^2}$$

but, the density of the dispersed solids, $\rho_{ds} = \rho_f \epsilon + \rho_p (1 - \epsilon)$,

$$\text{so, } \Delta P_T = \frac{\rho_{ds} \bar{u}_f^2}{g(1 - \epsilon)^2} + \rho_{ds} L + (\lambda_f + \lambda_p) \frac{\rho_f \bar{u}_f^2}{2g(1 - \epsilon)^2} \quad (9)$$

Comparing equations (3) and (9), it can be seen that the difference between the correlations of Jones et al² and Leung et al⁴⁷ is the factor $(1 - \epsilon)^2$ in the denominators of the acceleration and frictional terms of equation (9). Since $(1 - \epsilon)^2$ reduces to unity for dilute phase flow having a low solid concentration, it is apparent that comparison of equations (3) and (8) would result in only minor differences in the predicted total pressure drop for dilute phase flow of fine particles.

A selection of the more theoretical, as distinct from fundamental or empirical, approaches to the analysis of gas-solids flows are those of Stannard⁴³, Kovacs⁴⁴ and Chand⁴⁵.

This survey has attempted to be in chronological order and yet the extensive researches of Zenz^{38,39,40,41} have not been reported. The justification is that Zenz was more concerned with the limiting conditions of "choking" for vertical pipes and "saltation" for horizontal flow. He states that the

region of greatest interest to the designer is that at gas velocities just above choking and saltation, a review of the literature relevant to this region has been carried out by Doig and Roper⁴².

5.3 Experimental Procedure

The method of plant operation is described in section 3.4, the arrangements for pressure drop measurements in a vertical duct explained in section 4.4.2 and the experimental procedure detailed in section 4.4.2.1. A simplified account of the experimental work is outlined in the paper in section 5.8 at the end of this chapter.

5.4 Data Analysis

The pressure drop in the vertical transportation of solid particles may be attributed to six factors:-

- (i) The pressure drop due to acceleration of the solid particles, ΔP_{ap} , which may be determined by application of the momentum principle to gas-solid flow through an annulus of width dr at a radius r , in which the particles have a velocity u_p :-

$$\Delta P_{ap} = 2\pi \left\{ \left[\int_0^{D/2} r \rho_{ds} U_p^2 dr \right]_2 - \left[\int_0^{D/2} r \rho_{ds} U_p^2 dr \right]_1 \right\} \quad (10)$$

This cannot be evaluated without details of the solids velocity and density of the solid phase dispersion in the carrier fluid. Earlier evidence¹ indicates that for the flow conditions under investigation, equation (10) can be replaced, with significant loss of accuracy, by:-

$$\Delta P_{an} = \Delta P_{af} \cdot \frac{W_p}{W_f} \quad (11)$$

since for these very fine particles $\frac{\partial \bar{u}_f}{\partial x} \approx \frac{\partial \bar{u}_p}{\partial x}$ along the upper part of the test section.

(ii) Similarly, the pressure drop due to fluid acceleration, ΔP_{af} , may be expressed in the form:-

$$\Delta P_{af} = 2\pi \left\{ \left[\int_0^{D/2} r \rho_f U_f^2 dr \right]_2 - \left[\int_0^{D/2} r \rho_f U_f^2 dr \right]_1 \right\} \quad (12)$$

For calculation purposes, equation (12) can be approximated by considering the change of momentum between two sections distance L apart:-

$$\Delta P_{af} \cdot A = (W_f)_2 (U_f)_2 - (W_f)_1 (U_f)_1.$$

Applying the Continuity Equation:-

$$\Delta P_{af} \cdot A = (\rho_f A U_f^2)_2 - (\rho_f A U_f^2)_1,$$

$$\Delta P_{af} = (\rho_f U_f^2)_2 - (\rho_f U_f^2)_1. \quad (13)$$

From the Equation of State:-

$$\frac{P_1}{(\rho_f)_1} = RT_1 \quad \text{and} \quad \frac{P_2}{(\rho_f)_2} = RT_2$$

$$\frac{1}{(\rho_f)_2} - \frac{1}{(\rho_f)_1} = R \left[\frac{T_2}{P_2} - \frac{T_1}{P_1} \right] \quad (14)$$

$$\text{now } \Delta P_{af} = \frac{(\rho_f U_f)_2^2}{(\rho_f)_2} - \frac{(\rho_f U_f)_1^2}{(\rho_f)_1}$$

$$\text{but } \frac{W_f}{A} = (\rho_f U_f)_1 = (\rho_f U_f)_2$$

$$\text{so } \Delta P_{af} = \left(\frac{W_f}{A} \right)^2 \left[\frac{1}{(\rho_f)_2} - \frac{1}{(\rho_f)_1} \right] \quad (15)$$

substitute (14) into (15):-

$$\Delta P_{af} = R \left(\frac{W_f}{A} \right)^2 \left[\frac{T_2}{P_2} - \frac{T_1}{P_1} \right] \quad (16)$$

- (iii) The pressure loss due to supporting a column of air, $\Delta P_{\rho f}$, which may be evaluated from direct measurements of temperature and pressure in the test section using

$$\Delta P_{\rho f} = R \int_0^L \frac{P}{T} \cdot dx \quad (17)$$

- (iv) The pressure loss due to the static head of the solid particles $\Delta P_{\rho p}$, which may be estimated from:-

$$\Delta P_{\rho p} = \frac{W_p}{W_f} \cdot \Delta P_{\rho f} \quad (18)$$

on the basis that the mean velocity ratio of the gas and solids, $\frac{\bar{u}_f}{\bar{u}_p} \rightarrow 1$, for all but the very lowest values of Reynolds' number. This assumption was used in all the routine computer calculations for the present study. The difference in axial velocity between the two phases results in equation (18) generally underestimating the value of $\Delta P_{\rho p}$. However, the fine particles were observed to be in a highly fluidised state and so the slip ratio would not affect the value of $\Delta P_{\rho p}$ by more than one or two percent.

- (v) The frictional losses due to the carrier fluid flowing through the pipe is frequently determined from standard Fanning friction factor equations⁽²⁾. This presupposes that the air friction factor is the same for air alone flowing through the pipe, as it is when the air is conveying solid particles. The actual air friction factor is dependent upon the turbulence level in the

flowing gas-solid suspension. This is influenced by Reynolds' number, pipe roughness and the nature of the transported particles, which may even suppress the level of turbulence³.

- (vi) The pressure drop due to additional frictional losses caused by the presence of the solids. This contribution to the overall pressure drop may be due to collisions between particles and between particles and the pipe wall. This phenomenon has been analysed using a drag coefficient approach⁴, and also using the concept of a solids friction factor^{3,5}. It is often assumed that the pressure drop due to solids friction, ΔP_{Fp} , can be represented by a Fanning-type expression:-

$$\Delta P_{Fp} = \frac{2\lambda_p \rho_{ds} \bar{u}_p^2 L}{D} \quad (19)$$

where λ_p is a solids friction factor. The evaluation of ΔP_{Fp} from equation (19) requires a knowledge of λ_p , ρ_{ds} and \bar{u}_p , all of which present some difficulty.

Several attempts to simplify the evaluation of (19) have used the relationship:-

$$\text{Specific pressure ratio, } \frac{\Delta P_T}{\Delta P_0} = 1 + \frac{\lambda_p u_p}{\lambda_f u_f} \cdot \frac{W_p}{W_f} \quad (20)$$

This equation is applicable to a system in which the acceleration is zero, the manometer lead lines contain the same fluid as that in the test section (thus, $\Delta P_{\rho f} = 0$), and the duct is horizontal (thus, $\Delta P_{\rho p} = 0$). So, the slope of a curve of $\frac{\Delta P_T}{\Delta P_0}$ against $\frac{W_p}{W_f}$ is equal to $\frac{\lambda_p u_p}{\lambda_f u_f}$. Gasterstadt⁶ determined the slope to be constant for a given air velocity, but other studies^{7,8} have shown this not to be generally true.

In an attempt to avoid the anomalies inherent in evaluating the frictional pressure drop due to air in a flowing gas-solid suspension, and that caused by the solids themselves, the following procedure was adopted:-

$$\Delta P_T = \Delta P_m = \Delta P_{af} + \Delta P_{ap} + \Delta P_{\rho p} + \Delta P_{\rho f} + \Delta P_{Fp} + \Delta P_{Ff}$$

where the pressure drop due to the composite fluid friction, ΔP_{Fs} , = $\Delta P_{Fp} + \Delta P_{Ff}$

$$\text{so, } \Delta P_{Fs} = \Delta P_m - \Delta P_{af} - \Delta P_{ap} - \Delta P_{\rho p} - \Delta P_{\rho f} \quad (21)$$

In the present investigation, the fluid in the manometer lines and the test section was air at similar conditions of pressure and temperature, and so equation (21) can be written:-

$$\Delta P_{Fs} = \Delta P_m - (\Delta P_{af} + \Delta P_{ap}) - \Delta P_{\rho p} \quad (22)$$

where $(\Delta P_{af} + \Delta P_{ap})$ is determined from equations (11) and (16), whilst $\Delta P_{\rho p}$ is estimated from (17) and (18).

The friction factor of the suspension, λ_s , is defined as:-

$$\lambda_s = \frac{\tau_s}{\frac{1}{2}\rho_f \bar{u}_f^2} = \frac{\Delta P_{Fs} \cdot D}{2\rho_f \bar{u}_f^2 \cdot L} \quad (23)$$

whilst the friction factor, λ_o , for the flow of gas alone in smooth pipes, is defined as:-

$$\lambda_o = \frac{\tau_o}{\frac{1}{2}\rho_f \bar{u}_f^2} = \frac{\Delta P_o \cdot D}{2\rho_f \bar{u}_f^2 \cdot L} \quad (24)$$

It is pointed out that the combined solid-fluid friction factor has been based upon the velocity and density of the fluid phase alone, in agreement with other researchers⁹.

Thus,

$$\frac{\lambda_s}{\lambda_o} = \frac{\Delta P_{Fs}}{\Delta P_o} \quad (25)$$

$$\text{and } \frac{\lambda_s}{\lambda_0} - 1 = \frac{\text{friction factor due to solids phase only}}{\text{friction factor for air only flowing}} \quad (26)$$

The friction coefficient is quite frequently defined as⁵:-

$$\lambda = \frac{\tau}{\frac{1}{8}\rho_f \bar{u}_f^2} = \frac{\Delta P}{\frac{1}{2}\rho_f \bar{u}_f^2} \cdot \frac{D}{L} \quad (27)$$

which has the advantage of expressing the friction coefficient more clearly in terms of the dynamic pressure, $\frac{1}{2}\rho_f \bar{u}_f^2$, of the conveying air. Thus, equations (23) and (24) may be written as:-

$$\lambda_s = \frac{\Delta P_{Fs}}{\frac{1}{2}\rho_f \bar{u}_f^2} \cdot \frac{D}{L} \quad (28)$$

$$\text{and } \lambda_0 = \frac{\Delta P_0}{\frac{1}{2}\rho_f \bar{u}_f^2} \cdot \frac{D}{L} \quad (29)$$

The definition of friction coefficient producing equations (28) and (29) will be used in this study. It is quite evident that equation (25) is independent of the particular definition adopted, and so the graphs shown in section 5.8 are unaffected. An additional non-dimensional coefficient which has been used by many German investigators is simply called a resistance number, ψ , and it is defined as:-

$$\psi = \frac{\Delta P_m}{\frac{1}{2}\rho_f \bar{u}_f^2} \cdot \frac{D}{L} \quad (30)$$

It is clear from equations (28) and (30) that the suspension friction coefficient and the resistance number are equal for non-accelerating flow, that is, when $\Delta P_m (= \Delta P_T)$ becomes equal to ΔP_{Fs} .

5.5 Results and Discussions

The pressure drop data for the vertical test sections have been illustrated in different ways in an attempt to

produce some useful correlations and a better understanding of the flow behaviour. Figs. 5.1 to 5.3 show the pressure drop per unit length of pipe expressed as a function of the superficial air velocity for several solids-to-air flow ratios. The slope of the curves indicate the influence of fluid friction in a mixed phase system. The almost linear relationship between pressure drop and velocity of the carrier fluid at higher solids loading, particularly for the one and two inch diameter pipes, indicates the constancy of solids frictional effects and the linear correlation between pressure drop and an increasing superficial velocity. The distribution of solids in the flowing suspension appeared to be most uniform for the two smaller pipes, whilst the flow in the three inch pipe was characterised by a swirling stream of dense phase flow induced by the 90 degree bend at the bottom of the vertical pipe.

The $\Delta P_m/L$ versus \bar{u}_f curves for constant W_p/W_f shown in Fig. 5.1 illustrate clearly a particle size effect, but no significant influence of W_p/W_f in the one inch pipe. The 240 mesh powder shows an almost identical characteristic curve as that for air only at the higher values of \bar{u}_f , which infers that even with relatively large particles suppression of turbulence occurs, this confirms the conclusions from the λ_s/λ_0 versus W_p/W_f curves illustrated in Fig. 7 of the paper in section 5.8. Turbulence suppression is distinctly more evident with the 500 mesh powder, the curve being well below the results for air only. These curves are very similar to those shown in Fig. 6 of reference (4), which are for 36 micron particles flowing through a 0.5 inch diameter pipe, but at much lower air velocities than those of the present

study.

Fig. 5.2 illustrates that particle size affects the flow throughout the entire range of \bar{u}_f , except for the very dilute phase situation when $\bar{u}_f > 110$ ft/s. It is possible that the presence of relatively few solid particles has little influence on the flow at high velocities and so there is no significant difference between the effect of the 240 and 500 mesh powders. For lower velocities the finer particles suppress the turbulence level quite markedly, the curve following closely to the "air only" curve, whereas the curve for the larger particles begins to diverge upwards, away from the "air only" curve, and indicates that the condition of "choking" will be reached sooner with the 240 mesh powder. It was visually observed throughout all the pressure drop tests, that the ability of the air to convey the finer particles was greater than that to transport larger particles. The superficial air velocity was reduced until the particles were observed falling back down the duct distances of up to four feet before being arrested and re-conveyed. For this flow situation of "near-choking" the manometer levels fluctuated violently and it was not possible to record reliable pressure drop measurements. However, the visual observations can be related qualitatively to Figs. 5.2 and 5.3, in that if the curves were extrapolated for decreasing \bar{u}_f it would be expected that the pressure drop would increase suddenly and the curves would exhibit the characteristic "hook" or "cup" shape reported by Zenz³⁸.

The three inch pipe results in Fig. 5.3 illustrate a distinct particle size effect upon the flow for W_p/W_f in the range 4.0 to 5.0, however, particle size has little

influence for $W_p/W_f < 3.0$. This substantiates the swirling motion mentioned earlier, in that this phenomenon has more consequence on the flow behaviour than the ability of the particles to suppress turbulence. As W_p/W_f increases, the phase density is such that the solids burden effectively dampens down the longitudinal eddying or swirling motion, the flow becomes more uniform and turbulence suppression by the 500 mesh particles is evident in reducing the overall pressure drop for the same values of air velocity and solids loading. Another possible explanation is that in the three inch pipe the time-scales of eddies near the wall are quite large, thus enabling fine particles to follow the fluid motion more easily and suppress the turbulence much less. It is interesting to note that for very dilute phase flow in the three inch pipe, that is $W_p/W_f < 0.5$, the pressure drop is less with solids present than for air only, this tends to support the minimum λ_g/λ_o concept which is shown in section 5.8, Fig. 9, and is also referred to by McCarthy and Olson³³ (see section 5.2). The curves in Fig. 5.3 for higher W_p/W_f values exhibit remarkable tendencies for air velocities in the range 40 to 50 ft/s. For a marginal increase in the velocity of the conveying air the pressure drop increases rapidly, resulting in a highly inefficient transport system.

The relationships shown in Figs. 5.1 to 5.3 indicate how the pressure drop varies when the system parameters are changed and it is clearly erroneous to suggest that particle size, duct diameter or solids loading generally has a particular effect or otherwise upon the pressure drop.

The system parameters of Chandok and Pei³⁷ give a maximum value for dp/D of 0.005 and so, according to Duckworth⁵, their flow conditions throughout were likely to be in the form of a homogeneous suspension. The relationship produced by Chandok (see section 5.2, equation (7)), $\Delta P_p/L = 0.3064W_p$, suggests that the contribution of the solid particles to the overall pressure drop varies linearly with the solids flow rate. It is difficult to believe that the correlation is so elementary, since reference to Figs. 5.4 to 5.9 shows clearly that not only is there a duct size effect, but that different particle sizes inhibit the two phase flow in a variety of ways. In fact, the response of the solid particles to the turbulent movement of the fluid is probably of prime importance.

Fig 5.4 to 5.9 illustrate the variation in pressure drop per unit length as a function of solids flow rate for a range of mixture densities. The one inch pipe results (Figs. 5.4 and 5.5) indicate a linear increase in pressure drop for increasing solids flow rate, with a very large air flow rate effect. It is quite noticeable that transporting the finer powder produces less pressure drop, which may possibly be attributed to turbulence suppression. The two inch pipe tests with the 240 and 320 mesh particles only exhibit the above linearity for higher values of solids flow rate, in fact, an actual minimum pressure drop is observed for particular flow conditions, this minimum increasing with increasing solids and air flow rates. These correlations are quite similar to those obtained by Farbar⁷, whilst a linear relationship was obtained by Hariu¹¹. Fig. 5.8 shows the pressure drop characteristic for the 500 mesh

powder flowing through the two inch pipe, the minimum pressure drop phenomenon is clearly evident and there appears to be a definite tendency towards the independence of pressure drop with respect to solids loading for the higher solids flow rates. This trend indicates the prominent part played by very fine particles in suppressing turbulence and increasing their conveyability. The three inch pipe results shown in Fig. 5.9 do not indicate the same dependence of pressure drop upon air flow rate, in fact, the single curves are drawn for air flow rates varying from 7.0 to 9.5 lb/min, that is, almost 40% variation. The 240 and 320 mesh curves in Fig. 5.9 are very similar to those of Farbar⁷ with $\partial P/\partial W_p$ increasing as W_p increases. As the solids flow rate of the 500 mesh powder increases, the numbers of very fine particles in the two phase flow markedly affect the turbulence level and $\partial P/\partial W_p$ starts to decrease in a similar way to that shown in Fig. 5.8 for the two inch pipe, but not as dramatic.

The curves illustrated in Figs. 5.10 to 5.12 relate the resistance number or total friction coefficient, ψ_v , to Reynolds' number for various solids-to-air flow ratios. All the results indicate that the friction coefficient of a flowing gas-solid suspension becomes independent of Reynolds' number at high values of Reynolds' number, but is very definitely dependent upon Reynolds' number at low values. These curves are in the dp/D range where $0.0027 > dp/D > 0.0002$, which according to Duckworth⁵ clearly classifies the flow as being in the form of a homogeneous suspension. Thus the frictional resistance will arise primarily from the exchange of momentum between the particles and the carrier air, rather than from particles impinging

on the pipe walls. Although it is not clear in reference (5) whether Figs. 4 to 7 refer to suspension flow through horizontal or vertical pipes, they nevertheless show similar trends to the present investigation despite substantial differences in system parameters.

Mehta⁴ shows in Fig. 11 the suspension friction factor as a function of Reynolds' number for two particles sizes, 97 and 36 microns, flowing through a 0.5 inch diameter pipe. He classifies the flow behaviour of the larger particles as "bouncing flow" and that of the smaller particles as "suspension flow", the dp/D in the latter case being 0.0028, which is almost identical to the dp/D ratio for the 240 mesh curve shown in Fig. 5.10 of the present investigation. Unfortunately Mehta's results are so scattered that he could only suggest that the friction factor becomes constant at high Reynolds' number. He also postulated that the suspension friction coefficient is essentially the same for both vertical and horizontal flow and independent of solids flow rate, this latter conclusion is refuted by the present study.

It is evident from Figs. 5.10 to 5.12 that particle size has little influence on the resistance coefficient in the three inch pipe and a significant effect in the one inch pipe, this confirms the conclusions derived from the $\Delta P_m/L$ versus \bar{u}_f curves shown in Figs. 5.1 to 5.3.

The relation between the resistance coefficient for a upward flowing suspension and the Froude number is illustrated in Figs. 5.13 to 5.15. The results for both the one inch and two inch pipes show that this coefficient rises rapidly as the Froude number decreases, the rate of increase being more emphatic for higher values of solids-to-air ratios.

The relationship is reversed at high Froude number, for which the resistance coefficient assumes a constant value for a particular flow situation. Although Barth's⁹ results are for coarse particles his correlations between friction coefficient and Froude number were not dissimilar to those portrayed in Figs. 5.13 to 5.15.

It is not clear from Figs. 5.13 to 5.15 whether or not a Reynolds' number effect is inherent in the trends illustrated, which are so similar to those shown in Figs. 5.10 to 5.12. In an attempt to obtain a better correlation a relative resistance coefficient, $\psi_v \frac{W_p}{W_f}$, is expressed as a function of Froude number, for different ranges of Reynolds' number, in Figs. 5.16 to 5.17. It is apparent from Fig. 5.16 that there is a prominent Reynolds' number effect, which can be seen more clearly by reference to Fig. 5.18. An apparent minimum value of $\psi_v \frac{W_p}{W_f}$ is obtained, for flow through the two inch pipe, which is possibly independent of particle size (compare Figs. 5.17 and 5.18). It is suggested that as Froude number decreases the curves would pass through the minimum value of $\psi_v \frac{W_p}{W_f}$ and then begin to increase rapidly, since the resistance coefficient would increase more rapidly than W_p/W_f as the condition of "choking" is approached.

Boothroyd³⁰ suggested that the ratio of the time scale of eddies near the pipe wall and the particle response time may influence an upward flowing suspension of fine particles. Continued analysis lead to the conclusion that the flow behaviour depended upon both the ratios, $\rho_f D^2 / \rho_p d_p^2 R_e$ and $\rho_f D^2 / \rho_p d_p^2 R_e^2$, the latter ratio being more appropriate for correlating flow near the wall. A brief attempt is made in Figs. 5.19 and 5.20 to assess the above correlation procedure

and in both instances straight line relationships were obtained for a wide range of solids-to-air flow ratios, for the 320 mesh and 500 mesh particles flowing through the one inch pipe. The results are insufficient to establish any recommended functional relationship between these variables. The two inch pipe tests produced a considerable scatter of points for the same axes as Figs. 5.19 and 5.20, which indicated that no simple relationship exists. It is proposed to pay some detailed attention to this suggested correlation procedure in the near future.

5.6 Conclusions

It is apparent from the results that there is no justification for assuming that the flow properties of a suspension of fine solid particles in gas will resemble those exhibited by the flow of gas alone. The very fine particles appear to stabilise eddy formation and so suppress the level of turbulence rather than generate turbulence.

In the application of dimensionless scaling ratios it is generally accepted that similar particulate material must be used in the systems being compared. The present investigation indicates that it is not adequate to account for particle size by incorporating the mean particle diameter into one or several dimensionless groups. It is considered that the use of scaling ratios be restricted to material of the same nature and similar particle size distribution.

Description of a gas-solid flow by a correlation curve of resistance coefficient and Froude number, for known solids-to-air flow ratios, is of limited value owing to this correlation varying with Reynolds' number. It is proposed that a more useful correlation is that of a relative

resistance coefficient, $\psi_v \frac{W_p}{W_f}$, with Froude number for a particular value of Reynolds' number.

5.7 Suggestions for Further Work

It is proposed to scrutinize the data obtained from this investigation, and not presented here, in an attempt to derive an expression for predicting the total pressure drop due to a gas-solid suspension flowing vertically upwards. The author intends to arrange with industry for the personal acquisition of data from large scale plant and thereby verifying or otherwise the validity of the pressure drop equation.

It is believed that further progress in the study of solid transport behaviour depends upon a deeper understanding of the following factors:-

- (i) Particle velocity; it is proposed to use a laser-doppler arrangement to measure the particle velocity profile in a dilute-phase suspension flowing up a vertical pipe.
- (ii) Density of a dispersed gas-solid suspension; for dilute-phase suspensions it should be possible to obtain a correlation between the dispersed phase density and the attenuation of a laser beam.
- (iii) Particle size distribution in a flowing suspension; it has often been suggested that the larger particles in a mixed-size two phase flow travel along the central core of a vertical pipe, whilst the finer particles occupy the region of high shear stress near the pipe wall. This feature, together with the industrial problem of particle segregation and the effect of particle agglomeration may possibly be examined using holographic techniques.

(iv) Electrostatic charging; this has recently become the subject of serious consideration, but the contribution of electrostatics to the total pressure drop and to other flow phenomena remains somewhat of a mystery. The explosion hazard alone should be sufficient incentive to warrant an extensive examination of this phenomenon.

It is generally concluded that this subject should be examined by a programme of careful experimental studies which should be extended to tests on full scale plant.

5.8 Comparison of Friction Factors

In section 5.5 and in Figs. 5.1 to 5.20 there has been no mention of the relationship between λ_s/λ_o and the solids loading ratio. This part of the present work was reported in a paper given at the British Hydromechanics Research Association's conference, "Pneumotransport 1", held at Churchill College, Cambridge, 5th to 8th September 1971. The presentation here is in preprint form. The nomenclature for the paper is marginally different from that used in the remainder of this thesis and so attention is drawn to the nomenclature given on page C1-2 of the paper.

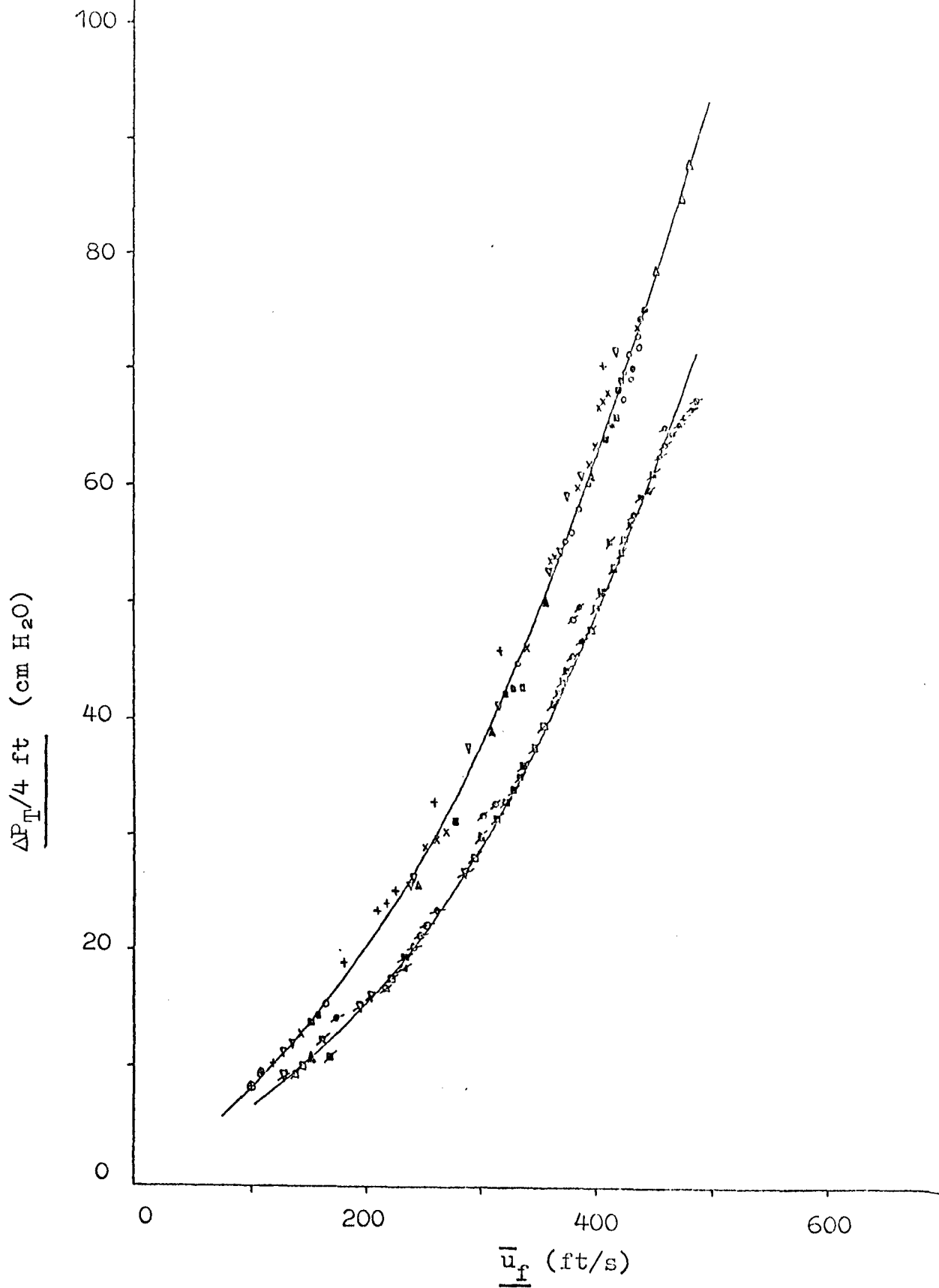


Fig. 5.1 Variation of Axial Pressure Gradient along
One inch Vertical Duct with Mean Air
Velocity, \bar{u}_f .

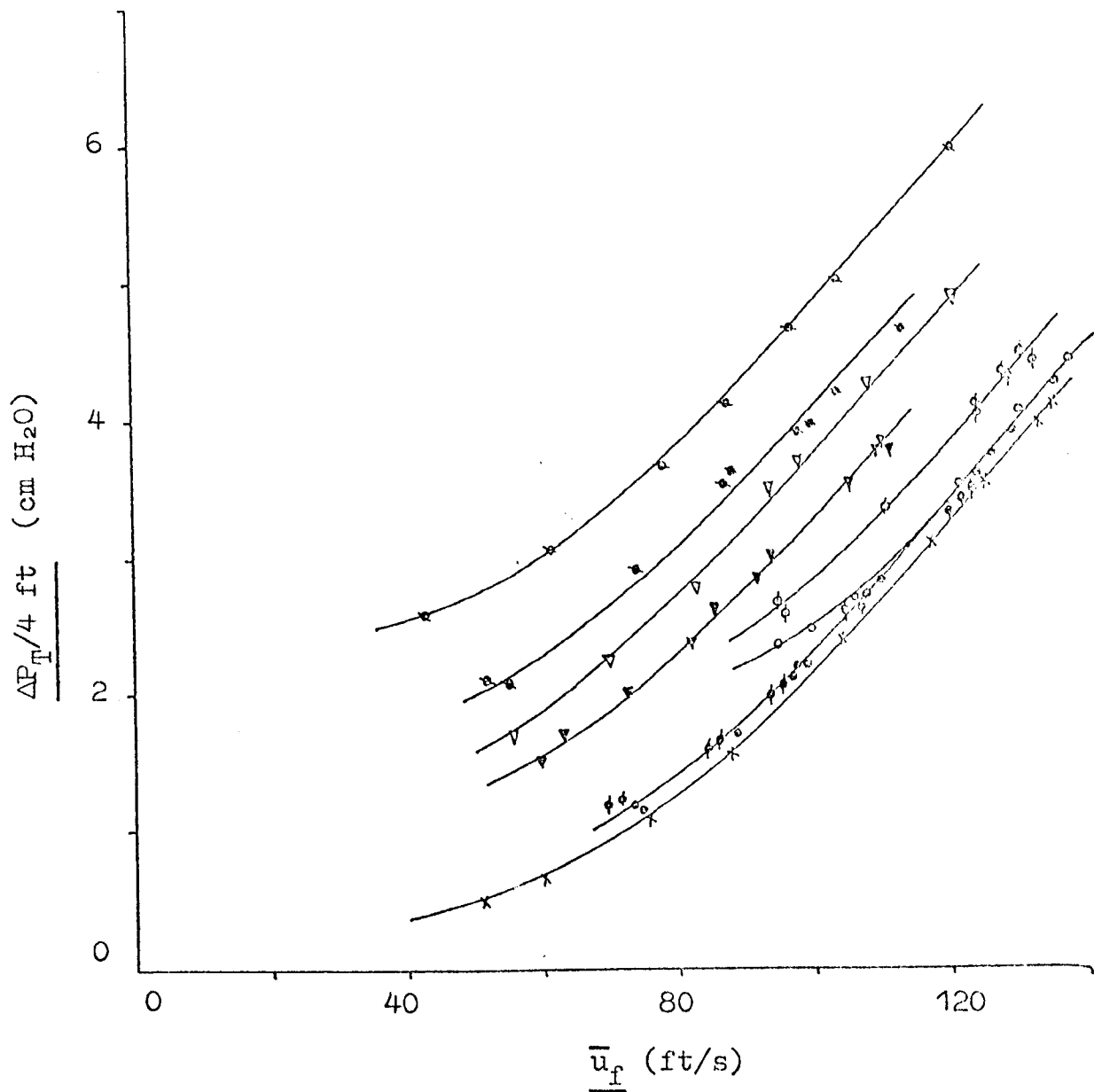


Fig. 5.2 Variation of Axial Pressure Gradient along
2 inch Vertical Duct with Mean Air
Velocity, \bar{u}_f .

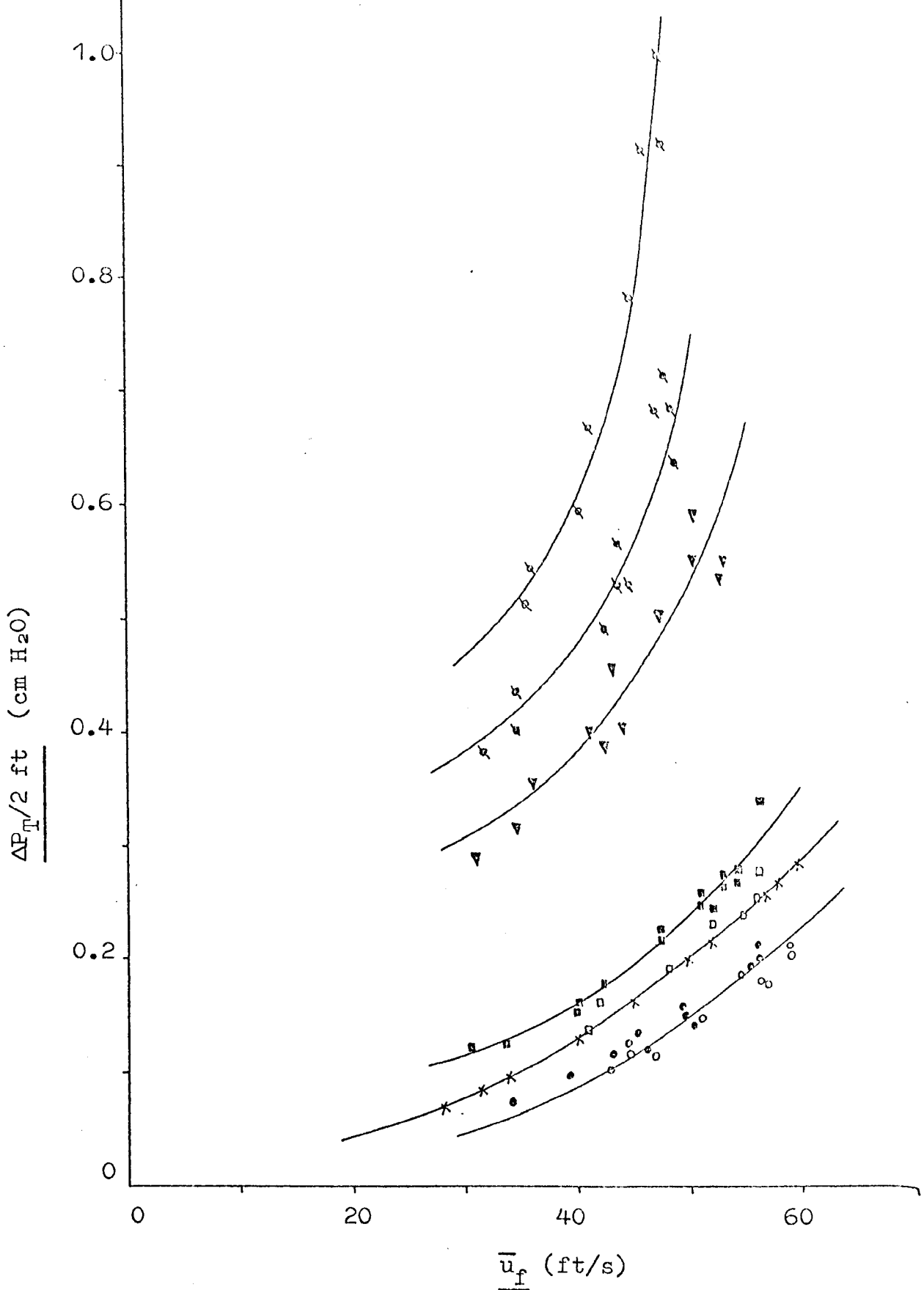


Fig. 5.3 Variation of Axial Pressure Gradient along
3 inch Vertical Duct with Mean Air
Velocity, \bar{u}_f .

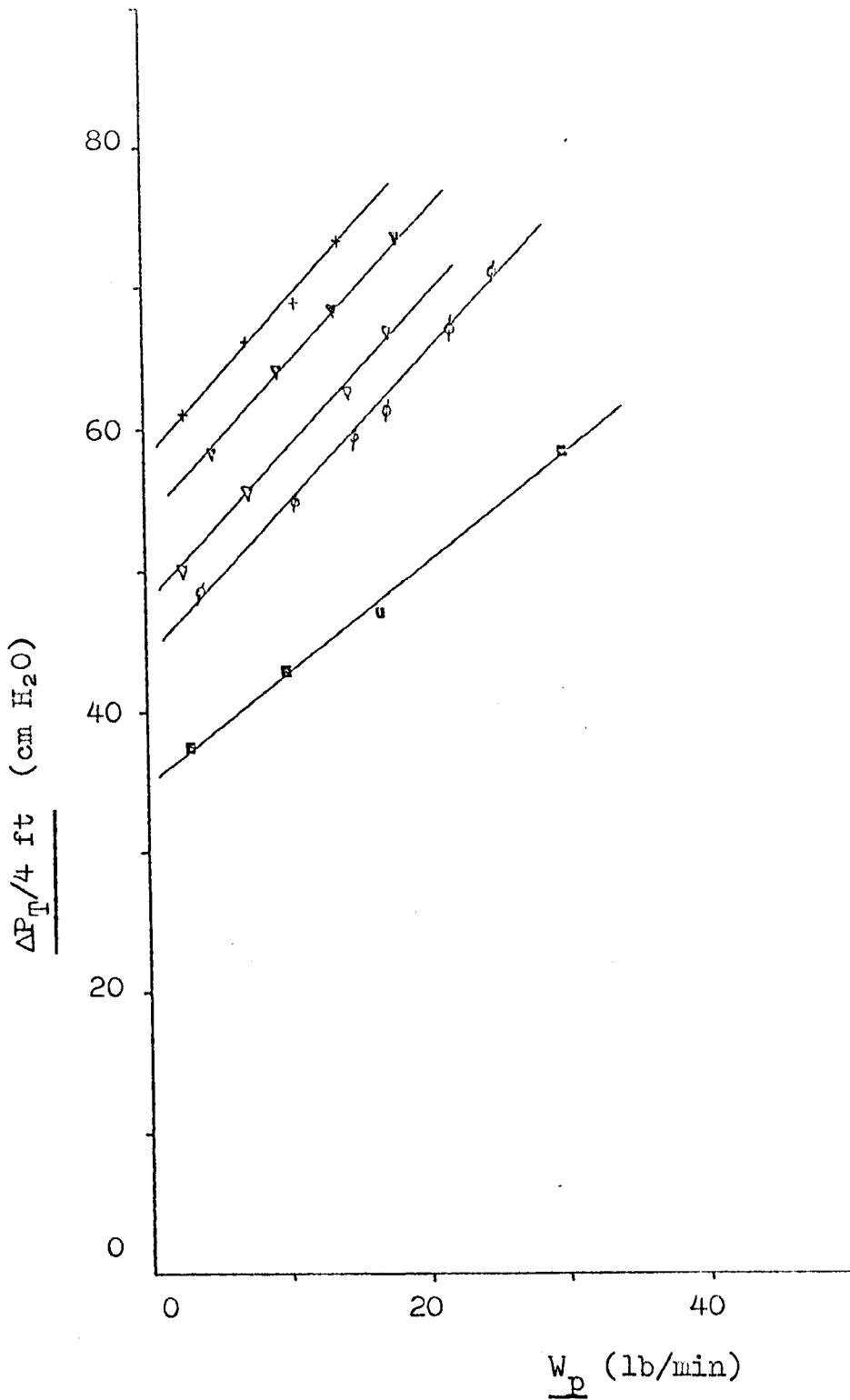


Fig. 5.4 Variation of Axial Pressure Gradient along
One inch Vertical Duct with Solids flowrate, W_p .

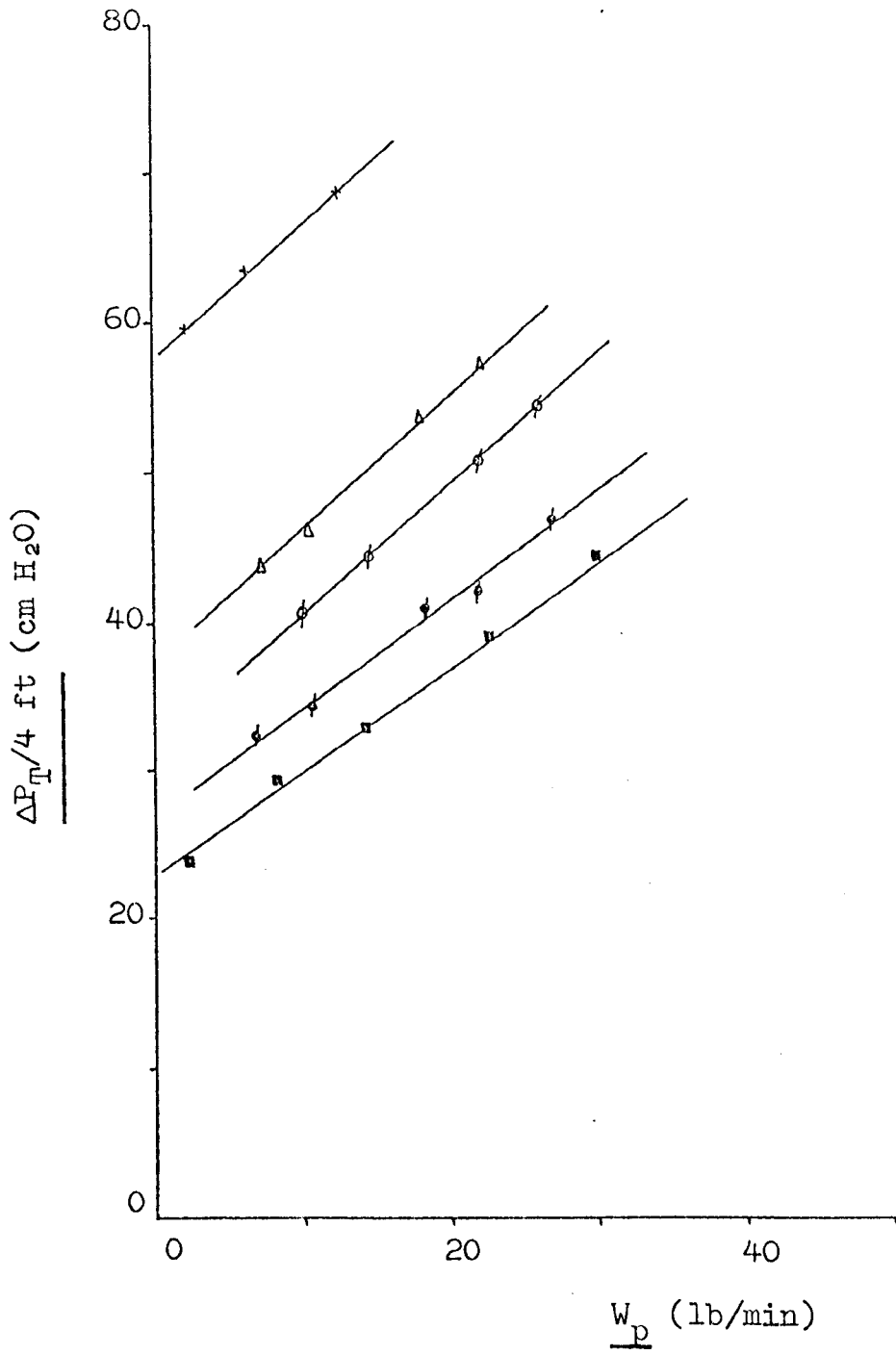


Fig. 5.5 Variation of Axial Pressure Gradient along One inch Vertical Duct with Solids flowrate, W_p .

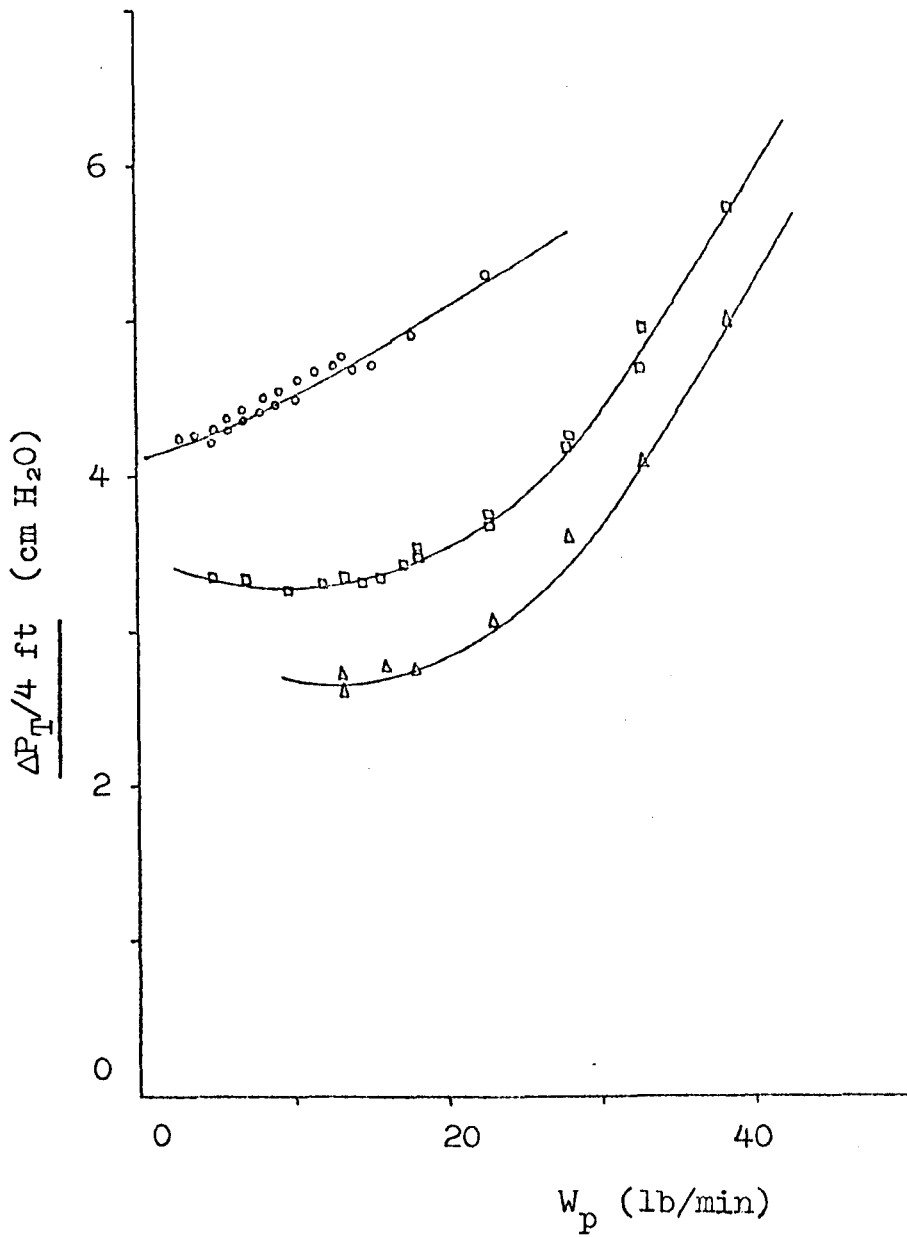


Fig. 5.6 Variation of Axial Pressure Gradient along a 2 inch
Vertical Duct with Solids flowrate, W_p .

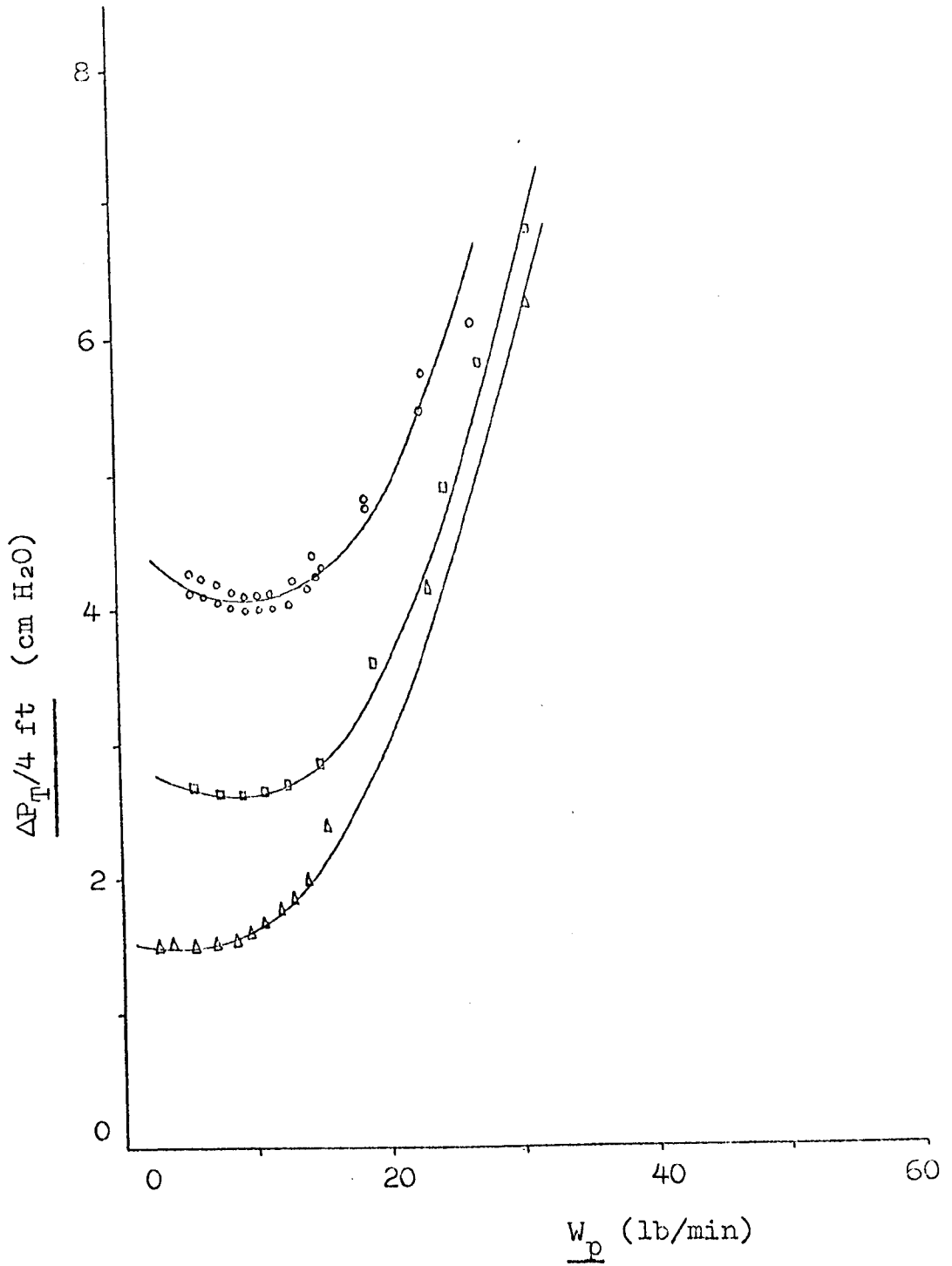


Fig. 5.7 Variation of Axial Pressure Gradient along a 2
inch Vertical Duct with Solids flowrate, W_p .

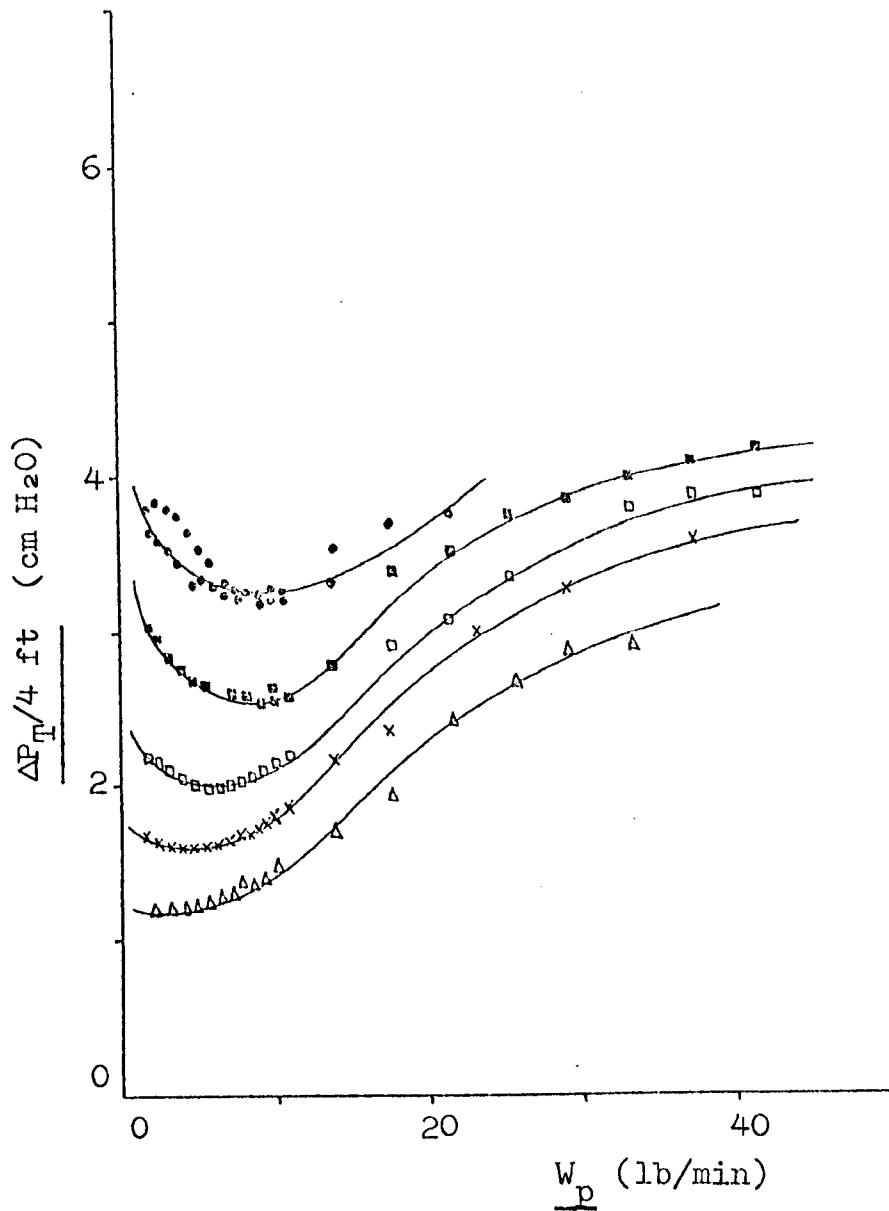


Fig. 5.8 Relationship between the Pressure Gradient for a Gas-Solid Suspension flowing through a 2 inch Vertical Duct and the Solids flowrate, W_p .

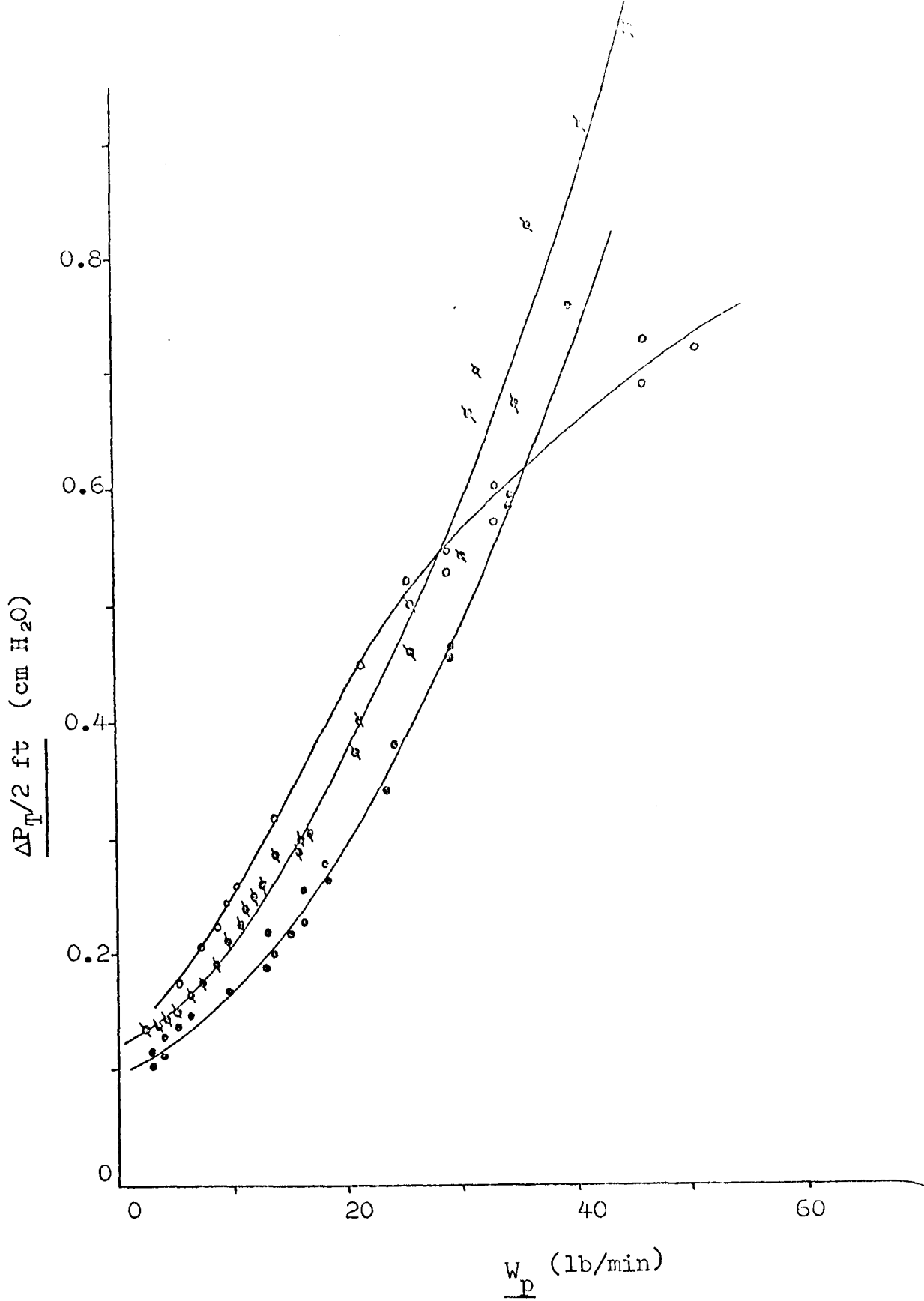


Fig. 5.9 Relationship between the Pressure Gradient for a Gas-Solid Suspension flowing through a 3 inch Vertical Duct and the Solids flowrate, W_p .

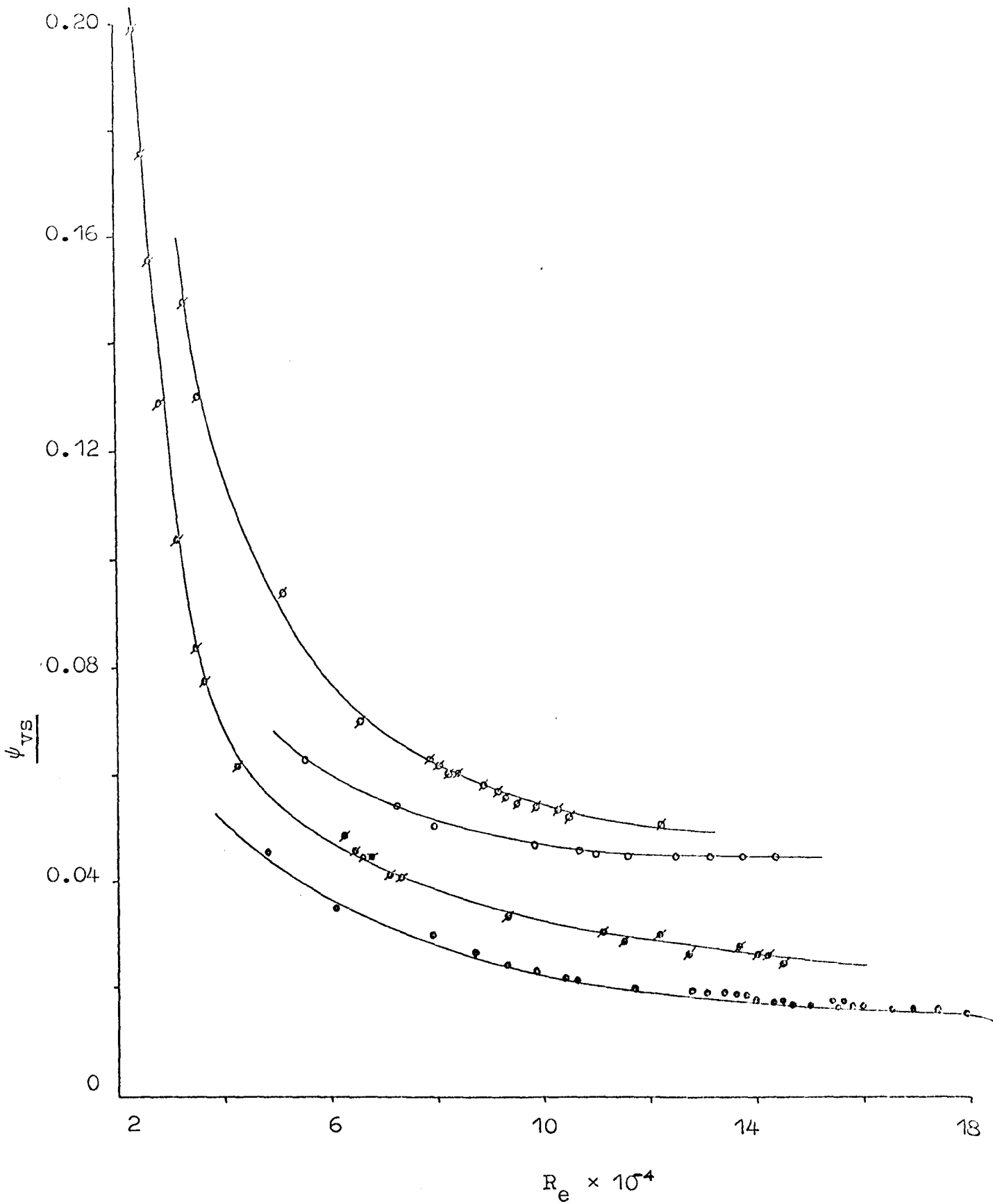


Fig. 5.10 Coefficient of Resistance for a Suspension flowing
vertically upwards, ψ_{VS} , through a One inch Duct,
Related to the Reynolds' number, R_e .

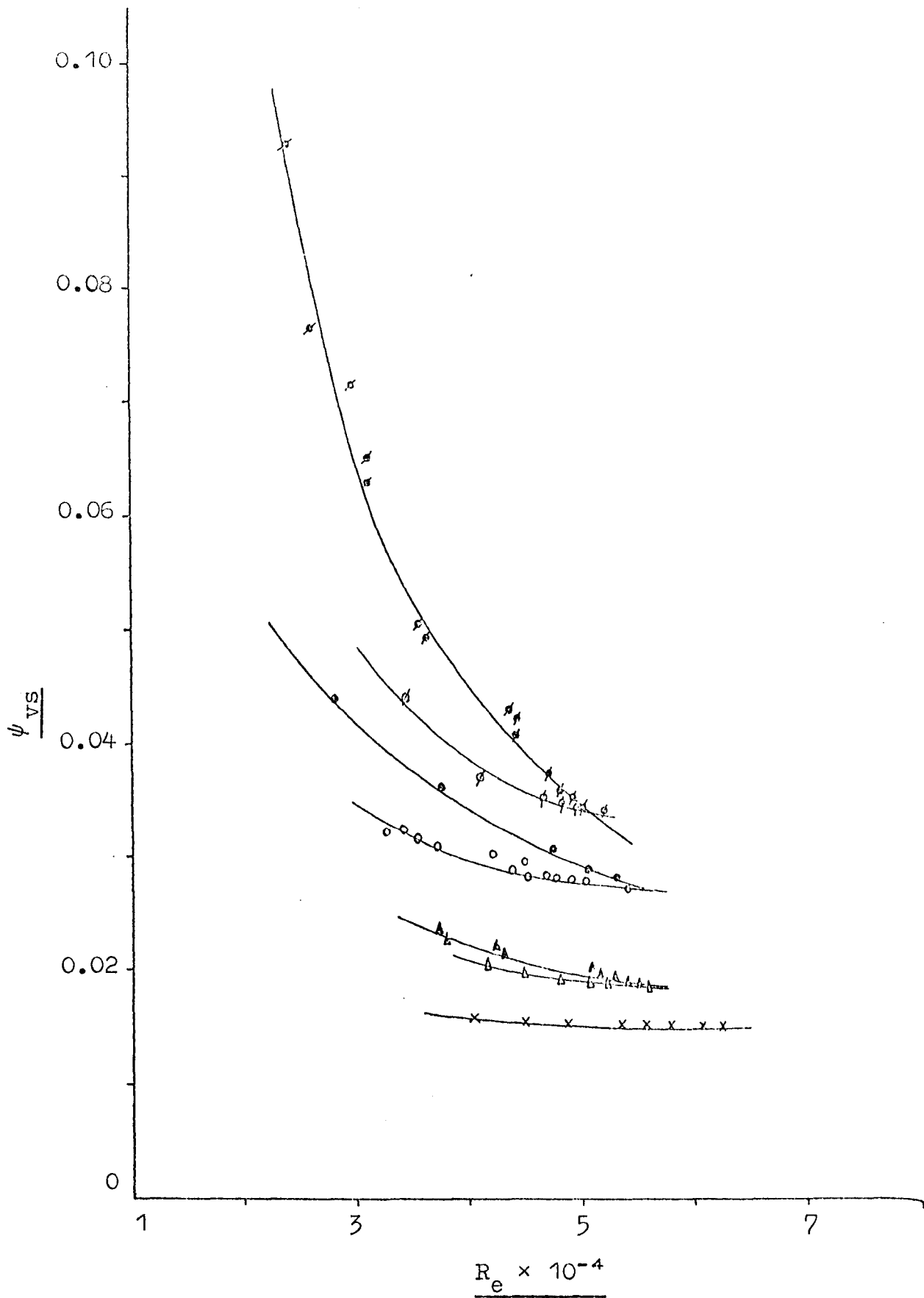


Fig. 5.11 Coefficient of Resistance for a Suspension flowing
vertically upwards, ψ_{vs} , through a 2 inch Duct,
Related to Reynolds' number, R_e .

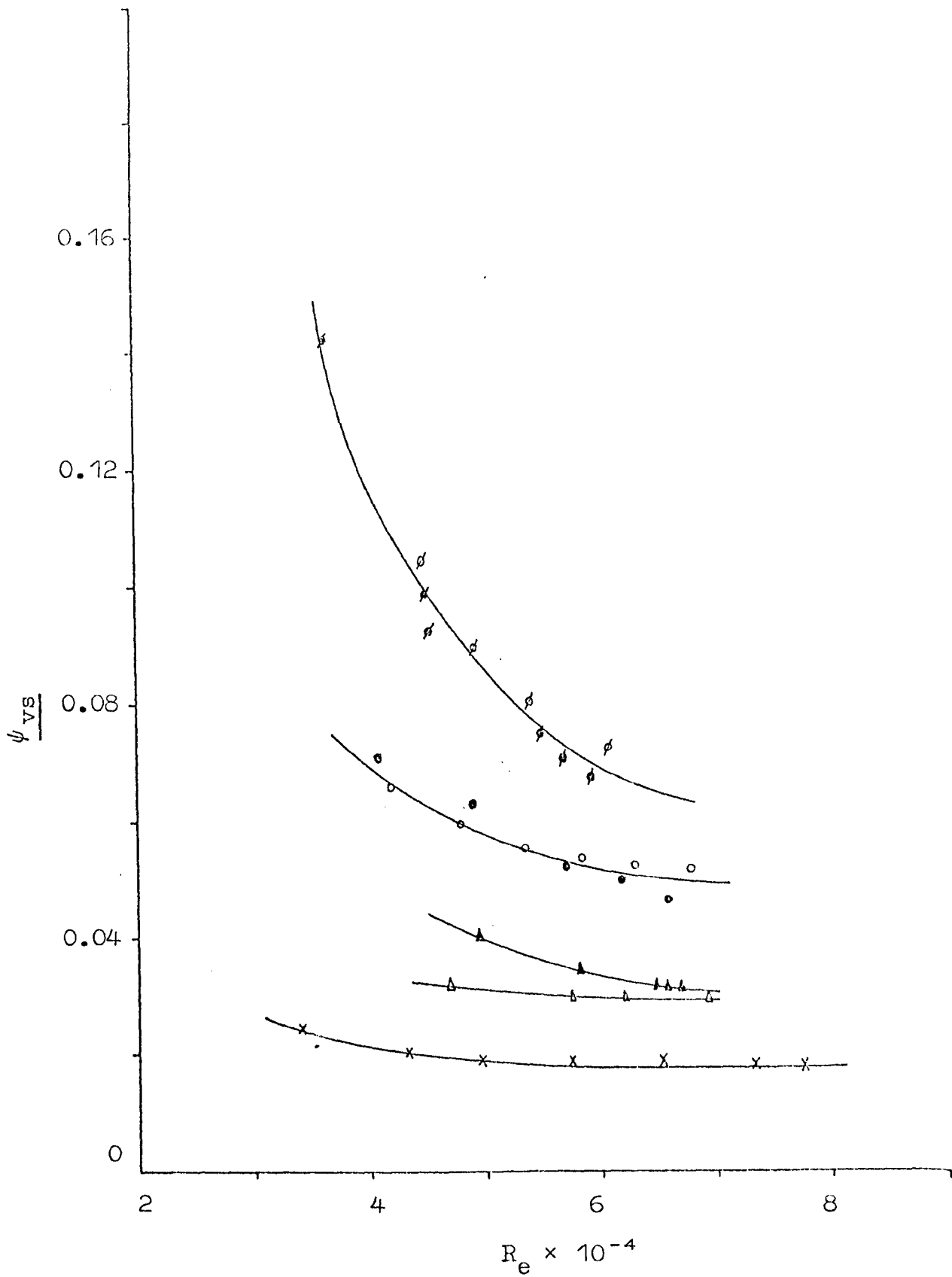
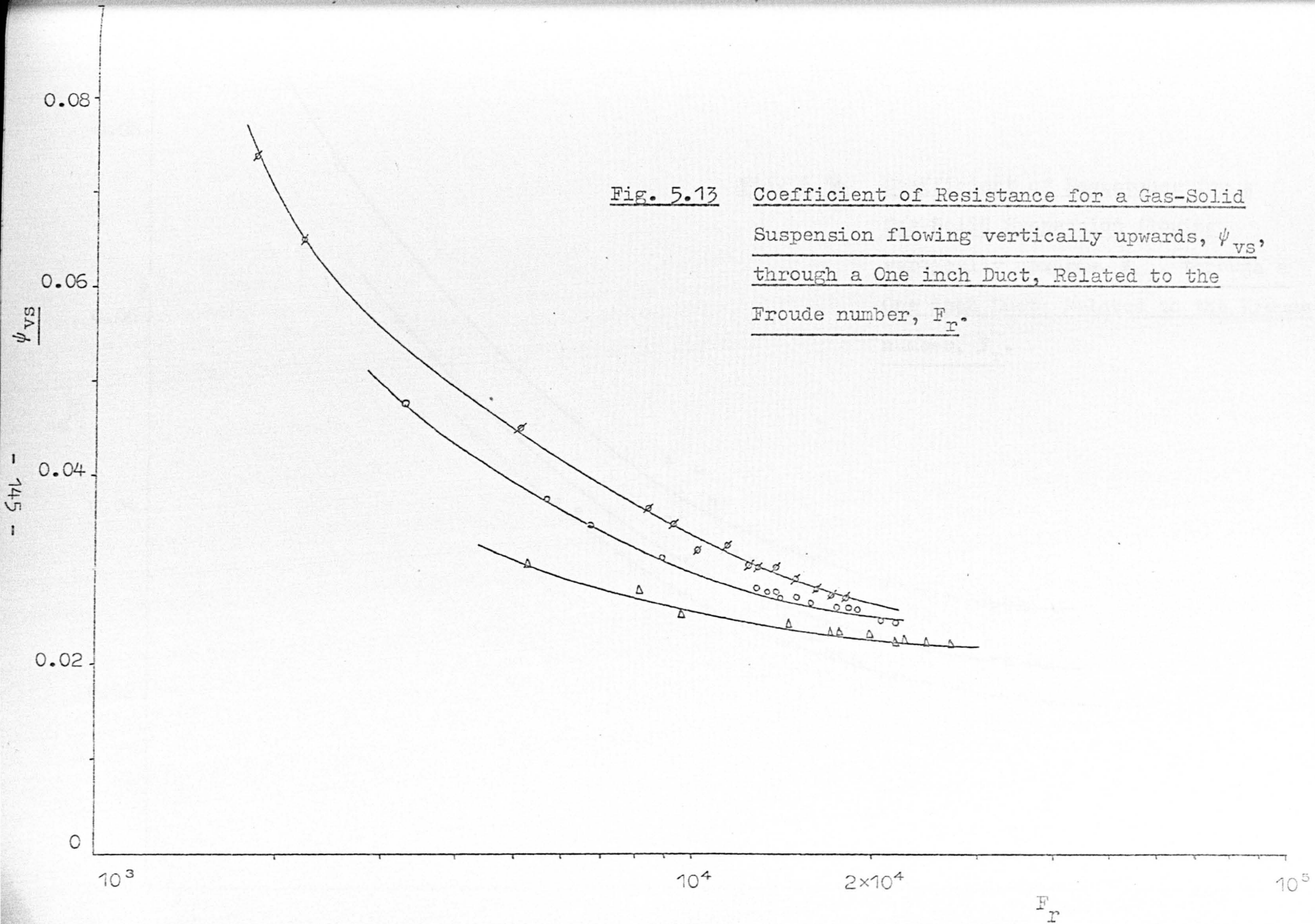


Fig. 5.12 Coefficient of Resistance for a Suspension
flowing vertically upwards, ψ_{vs} , through a
3 inch Duct, Related to Reynolds' number, R_e .

Fig. 5.13

Coefficient of Resistance for a Gas-Solid
Suspension flowing vertically upwards, ψ_{VS} ,
through a One inch Duct, Related to the
Froude number, F_r .



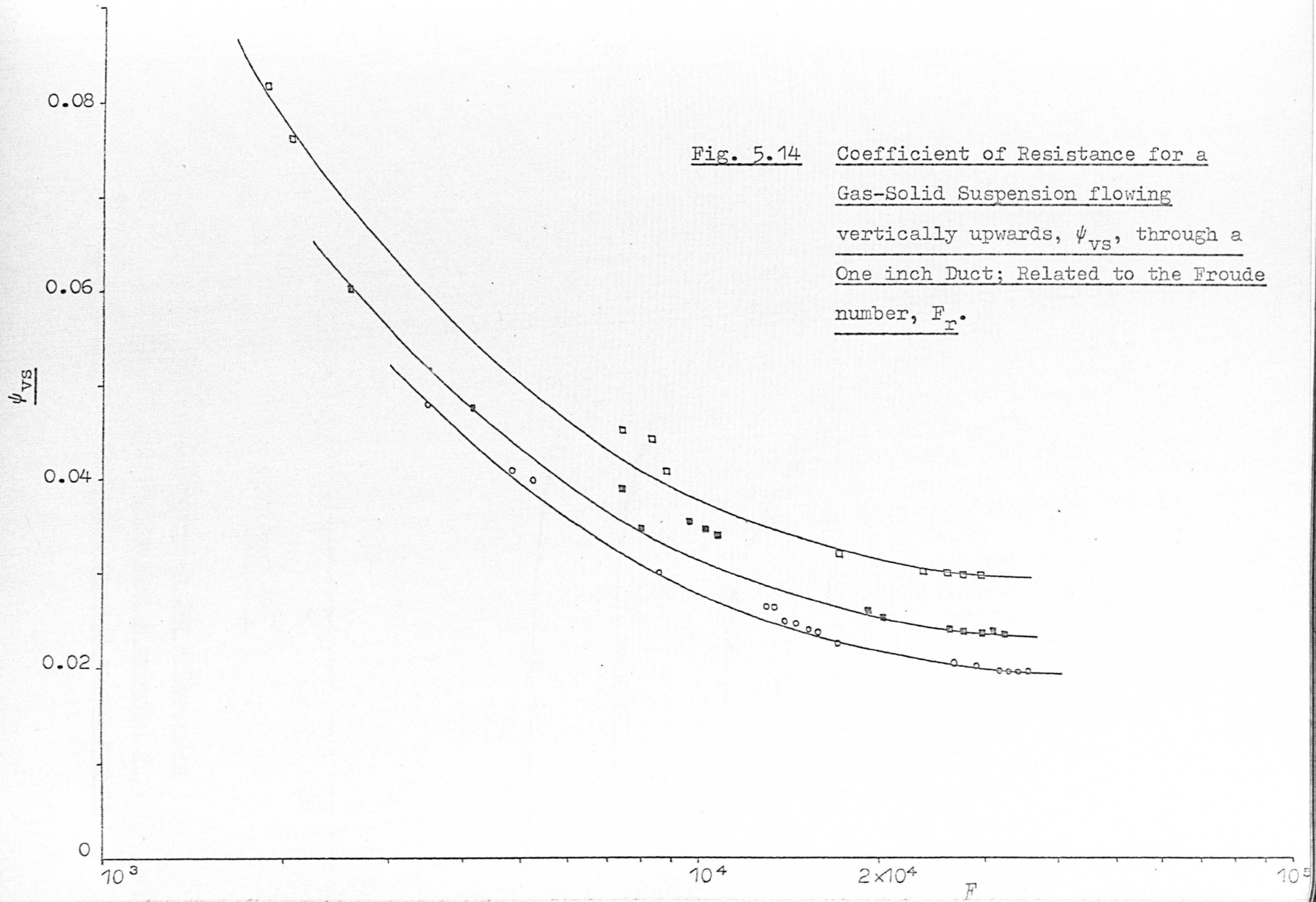


Fig. 5.14 Coefficient of Resistance for a
Gas-Solid Suspension flowing
vertically upwards, ψ_{VS} , through a
One inch Duct; Related to the Froude
number, F_r .

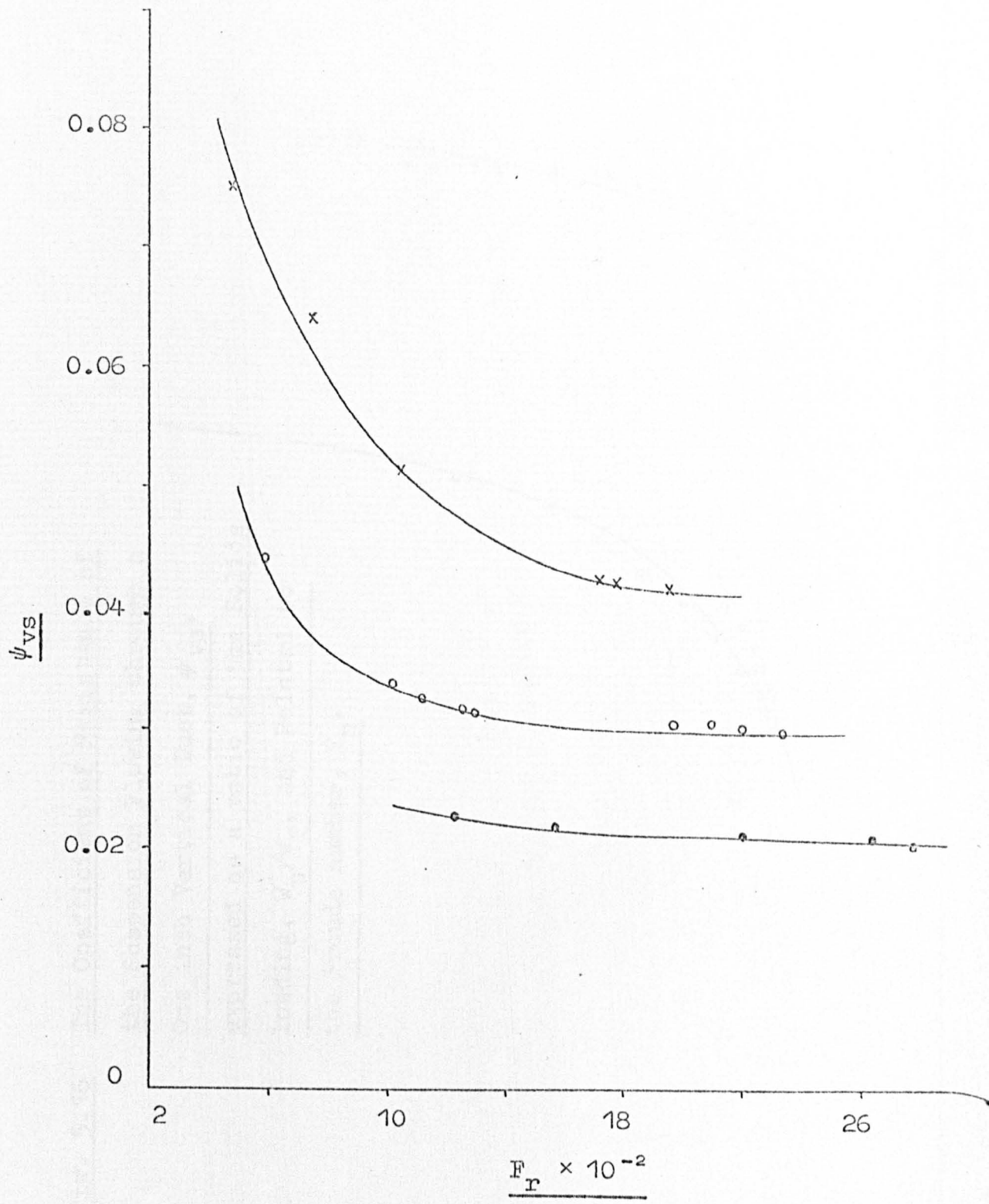
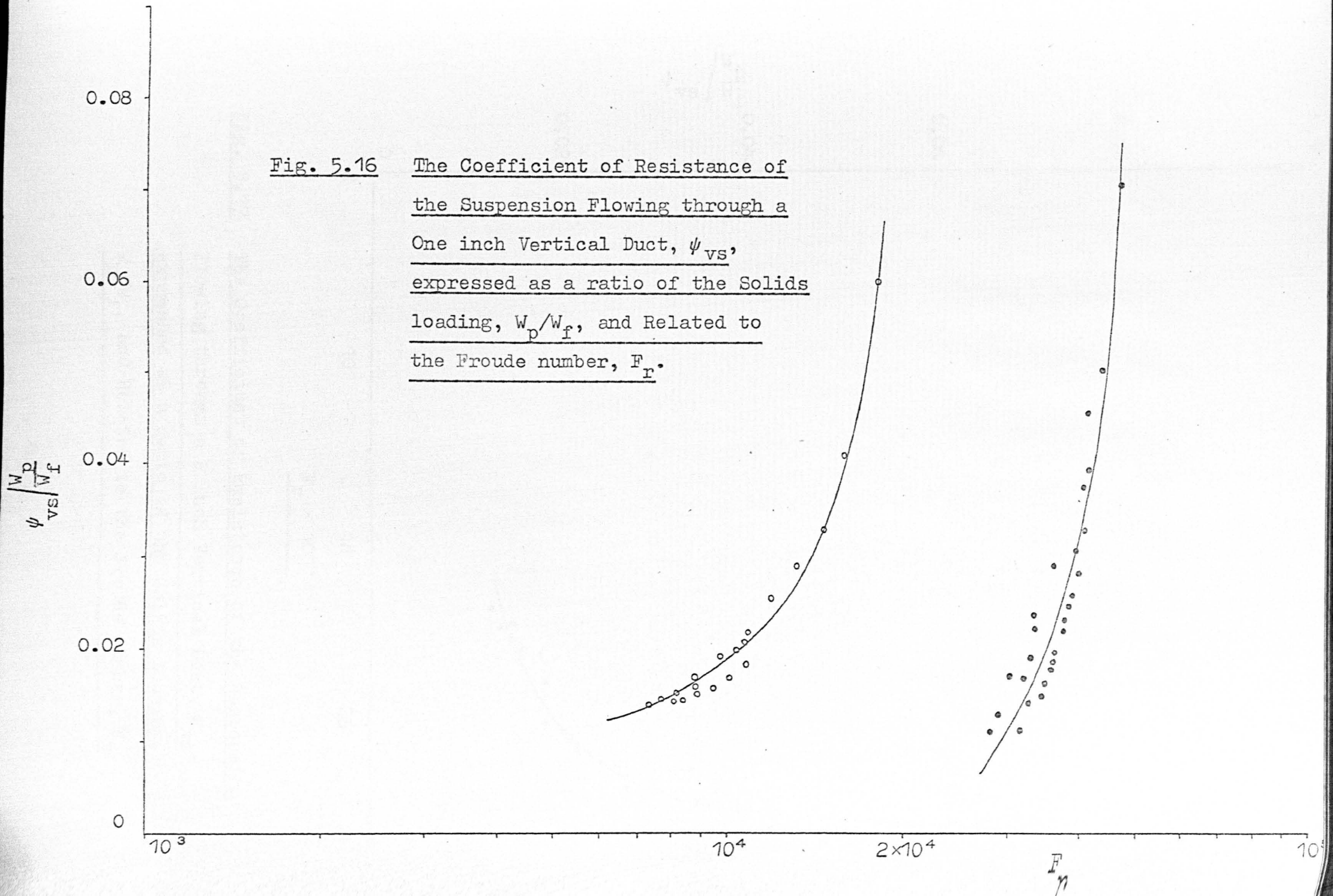


Fig. 5.15 Coefficient of Resistance for a Gas-Solid Suspension flowing vertically upwards, ψ_{vs} , through a 2 inch Duct, Related to the Froude number, F_r .

Fig. 5.16 The Coefficient of Resistance of
the Suspension Flowing through a
One inch Vertical Duct, ψ_{VS} ,
expressed as a ratio of the Solids
loading, W_p/W_f , and Related to
the Froude number, F_r .



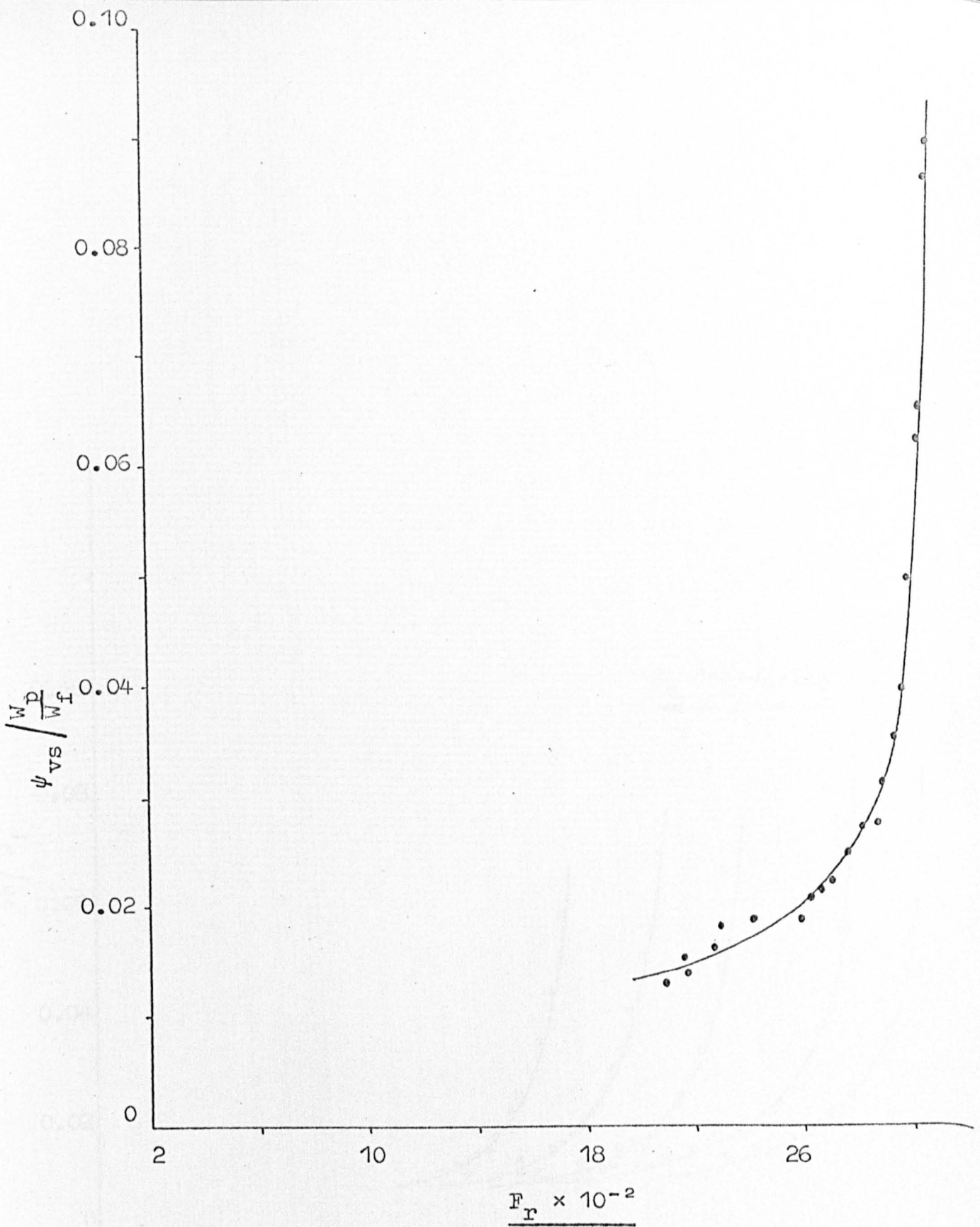


Fig. 5.17 The Coefficient of Resistance of the Suspension
Flowing through a 2 inch Vertical Duct, ψ_{VS} ,
expressed as a ratio of the Solids loading,
 W_p/W_f , and Related to the Froude number, F_r .

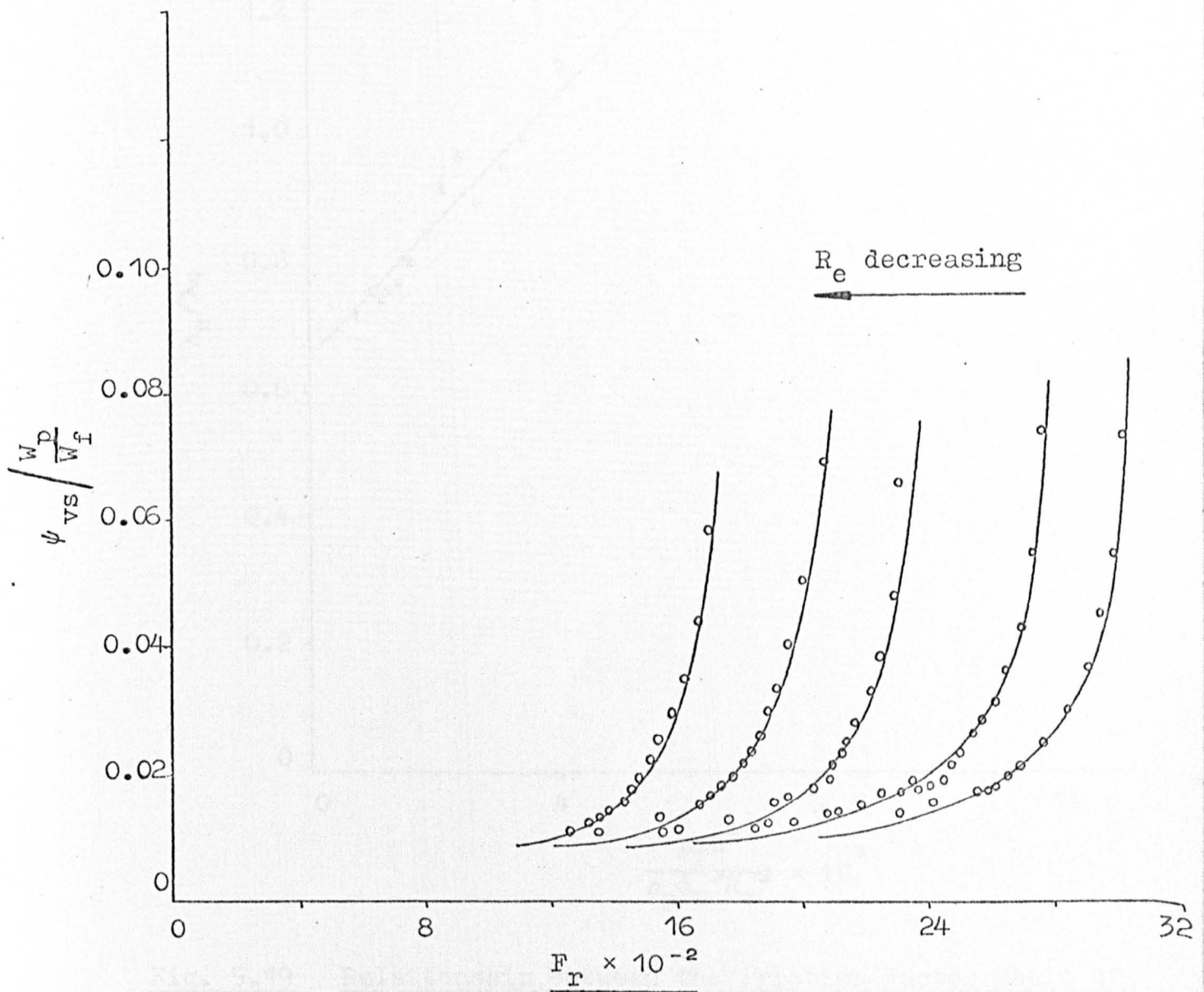


Fig. 5.18 The Coefficient of Resistance of the Suspension
Flowing through a 2 inch Vertical Duct, ψ_{vs} ,
expressed as a ratio of the Solids loading,
 W_p/W_f , and Related to the Froude number, F_r .

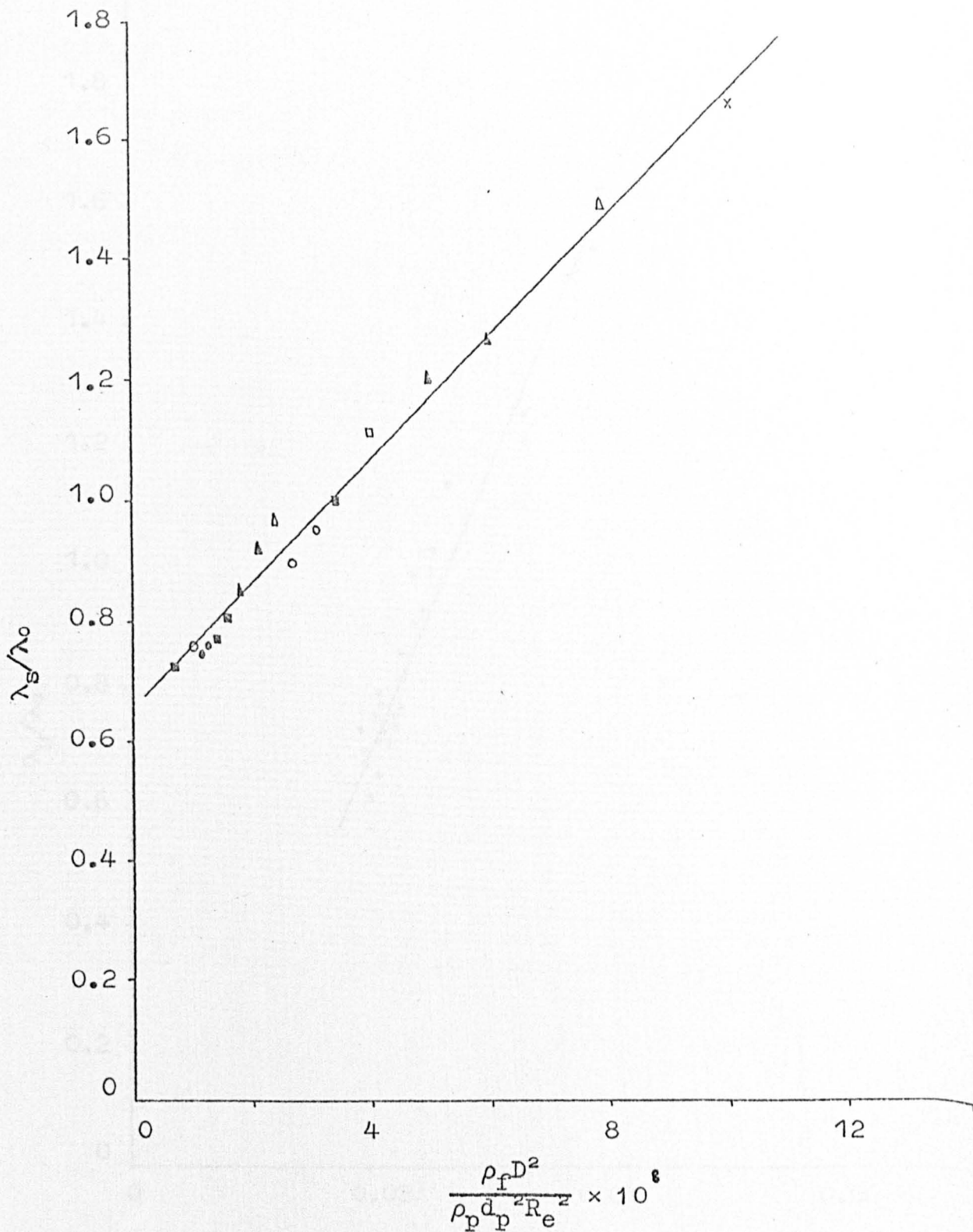


Fig. 5.19 Relationship between the Friction Factor Ratio of the Flowing Suspension, λ_s , and Air Alone, λ_o , with the Non-dimensional Group $\rho_f D^2 / \rho_p d_p^2 Re^2$ for a One inch Vertical Duct.

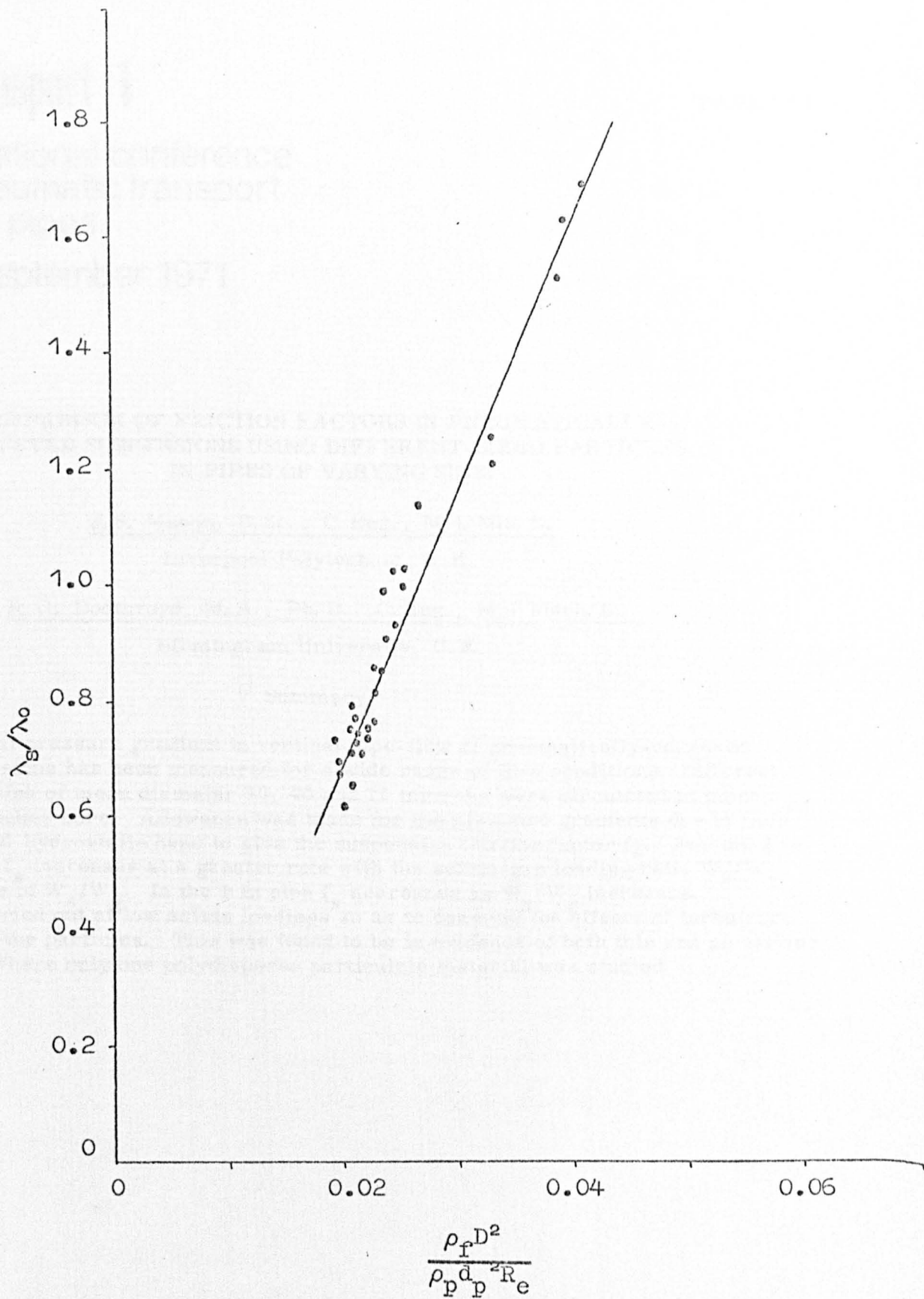


Fig. 5.20 Relationship between the Friction Factor Ratio of the Flowing Suspension, λ_s , and Air Alone, λ_o , with the Non-dimensional Group $\rho_f D^2 / \rho_p d_p^2 Re$ for a 2 inch Vertical Duct.

CHAPTER 6

GAS-SOLID FLOW THROUGH HORIZONTAL DUCTS

6.1 Introduction

It has frequently been stated that there are two principal categories of solids flow encountered in pneumatic transport through horizontal ducts:-

- (i) When the solid particles are conveyed in a uniformly dispersed phase; and
- (ii) when the transported material mainly occupies the lower part of the conveying line and assumes the form of a moving layer, or moving "dunes" or "balls" of solid particles^{9,25,38,41,61}.

The transition from (i) to (ii) occurs when the air velocity is decreased or the solids flow rate increased, due to the continual deposition of solids from the two-phase flow.

The above classification has been named "dilute-phase" for transport in the dispersed phase, and "dense-phase" when the conveying air velocity is below that at which "saltation" (analogous to the "choking" phenomenon in vertical transport lines) occurs.

Examination of the literature reveals that considerable work has been carried out to establish correlations for frictional pressure differentials, and some recent work^{34,35} has developed a technique for calculating the length of circular pipe required to ensure that the solid particles in a flowing suspension have been accelerated to a steady velocity. Since the total pressure differential is the addition of the pressure drop contributions in the acceleration zone and in the region where the flow conditions are established, it appears relatively straightforward to be able

to predict the overall pressure drop using the procedure outlined by Duckworth and Rose^{34,35}. However, Duckworth's work was concerned with granular materials flowing through a 1.26 inch diameter pipe, and an appropriate extension of this investigation would be to acquire transport data for the suspensions of fine particles flowing through different diameter pipes.

The limitations of the apparatus used in the present study prevented long horizontal runs of ducting from easily being incorporated into the design. As a result, the emphasis of this part of the work is concerned with the flow behaviour and pressure drop along a horizontal duct immediately following a 90 degree bend.

The introductory remarks made in section 5.1 apply equally to this section and the literature survey which follows attempts to avoid any duplication of the survey reported in section 5.2.

6.2 Literature Survey

This survey is a brief summary of the more important contributions to the field of gas-solid flow through horizontal ducts. Particular attention has been given to studies which have been largely concerned with flow behaviour in the acceleration zone.

Gasterstadt's⁶ investigation into the horizontal transportation of wheat appears to be the first detailed study indicating the possibility that a relationship may exist between the pressure drop of a single gaseous phase flowing through a duct, with that encountered for a multi-phase system. Unfortunately, Gasterstadt assumed the acceleration pressure drop to be independent of solids loading.

Farbar⁷ observed for horizontal transport that at low solids concentration the solid particles appeared to travel in a sinuous path, that is, clusters of particles or dense masses strike the bottom wall of the duct and then deflect back into the main stream. The wave length of this motion increasing with increasing air flow, but decreasing with increasing solids flow rate until two distinct flow categories become apparent; a dense phase moving in the lower half of the duct and a dilute phase in the upper part of the duct. Farbar used material having a size distribution of 10 to 220 microns and he noted that the larger particles were prevalent in the dense phase. It was visually observed in the present study that, for 15 micron alumina particles flowing around a 30 inch radius bend into a three inch diameter horizontal duct, the suspension rapidly became uniformly distributed throughout the duct at an air velocity of 50 ft/s and a solids flow rate of 18 lb/min, giving a W_p/W_f value of 1.8. Increasing the solids flow rate to 34 lb/min caused a reduction in the air velocity to 45.6 ft/s with W_p/W_f becoming 3.6, and this flow was characterised by a high concentration of solids in the lower part of the duct with the dilute phase above the dense layer moving at a far greater velocity. The top layer of the moving bed of dense particles was continually disturbed by the turbulently moving particles above. The solids flow rate was increased to 63 lb/min, the air velocity becoming 42 ft/s whilst W_p/W_f increased to 7.5. The very dense lower layer was transported by a continual "turning-over" or scouring action by the fast moving dilute suspension in the upper part of the duct. Even at this high solids concentration none of the powder remained entirely static, although slight reduction in

the air velocity would undoubtedly have caused the tube to become blocked. The bend preceding the horizontal duct did induce the suspension to be deflected, but this "bouncing flow" was soon "damped-out" by the inertia of the suspension as it passed through the horizontal duct. There was no evidence of dense masses of particles being deflected from the bottom wall of the duct and back into the main stream as reported by Farbar. The author feels that it is unlikely that such deflected particles would have sufficient energy to penetrate through the thick lower bed of powder, although the previously mentioned scouring of the top surface may be mis-interpreted to be deflecting flow. However, Farbar's test section was only 0.67 inches diameter, compared with three inches used in this investigation, and he must have experienced considerable difficulties in making visual observations in such a small duct.

Clark et al²⁵ investigated the dilute phase conveyance of a number of different seeds, including cress, rye, rape, turnip and radish, through a one inch diameter horizontal pipe. They contend that the additional pressure drop due to the presence of the solids arises because energy is continuously transferred from the air to the particles, in order to overcome inertia and to accelerate the particles, and to compensate for energy losses occurring when particles collide with the wall or with each other. The rate of transfer of energy is greatest when the particles are being accelerated from rest, and decreases as the velocity of the particles increases. Clark et al derive an equation to calculate the pressure drop due to the solids in a region where the particles are fully accelerated, their expression reduces to zero if

there is no slip between the particles and the conveying air, and it is not valid when the particles are in contact with the pipe wall for a finite conveying distance. They observed that the particles were evenly dispersed at high rates of flow, and as the air velocity is reduced the particles travel preferentially in the lower half of the tube where they segregate into regions of alternately high and low solid concentration. As the air velocity diminishes further deposition of the particles results in the formation of small dunes, and transport is effected by the movement of particles from one dune to the next and by occasional sliding of the dunes along the bottom of the tube. The relationship between flow behaviour and pressure drop enabled the flow conditions for the onset of "slugging" to be evaluated.

Pinkus⁵³ studied the pneumatic transport of two sizes of sand in a one inch diameter horizontal steel pipe. He emphasises the care taken in avoiding the inclusion of the acceleration pressure losses in the data for frictional losses, and his experimental results indicate that acceleration effects ceased within a distance of eight inches from the solids feed point. Pinkus's particles were relatively large compared with the present study and so it can be expected that, according to Pinkus, the pressure loss due to acceleration of the particles will be contained in the overall pressure drop for the bend and a minimal contribution in the pressure drop along the horizontal. However, for some flow conditions the deposition of solids reduces the cross-sectional area available for flow and causes the airstream to accelerate continuously.

A theoretical examination of the starting section in

pneumatic grain conveying has been carried out by Papai¹⁰, who derives an equation for the evaluation of the pipe length required for grains to acquire the speed of uniform rate of delivery. He concludes that the equivalent pipe lengths for horizontal and vertical starting sections, under equal working conditions, are substantially different, with the smaller length being that for horizontal delivery. This contradicts the work of Pinkus and many other investigators, however, Papai did assume completely uniform flow situations for both horizontal and vertical transportation.

Some interesting correlations between several dimensionless groups encountered in pneumatic transport have been obtained by Hitchcock and Jones²¹. They conveyed large uniform particles through horizontal steel pipes two and three inches diameter and 100 ft long. The investigation was confined to that part of the pipeline in which the particles travelled with constant velocity.

The flow characteristics of dense solid-gas mixtures ($80 < W_p/W_f < 750$) flowing through $\frac{1}{4}$, $\frac{1}{2}$, $\frac{3}{4}$ and 1 inch diameter horizontal pipes have been examined by Wen and Simons⁸⁹. They observed that such flows are characterised by a large amount of slip between the gas and solids, typically 50%. It is particularly interesting to note that the primary factors influencing the total pressure drop were acknowledged to be the solids loading and the particle velocity, whilst particle shapes and sizes were of insignificant effect. Their justification for the latter statement is based upon the visual observation that the particles travel predominantly along the lower part of the pipe as agglomerated masses rather than as individually suspended particles. It is well known

that particle size has a direct influence upon the agglomerative properties of particulate matter, and it is likely that particle shape affects the tendency of the particles to rotate about their own axes and so producing a lift component. It is the author's view that insufficient data and a limited variation in the system parameters resulted in some rather dubious conclusions, although it is agreed that particle size and shape may well be of secondary importance in many instances. Zenz⁹⁴ maintains that lower air velocities are required to transport angular particles compared with spherical particles. He attributes this to the greater rebound of the angular particle when it grazes the bottom of the pipe, whilst the spherical particle tends to roll and any deflection is merely a function of its angle of incidence. Zenz compared other accepted studies^{95,96,97} from which it was concluded that the smallest particles may be the most difficult to convey. Although this latter observation is refuted by the present study, there seems little doubt that Wen's⁸⁹ disregard of particle size and shape is questionable. Trezek and France⁹⁸ reported a marked dependence of the gas-solid dynamic parameters upon a variation in particle size (110 to 390 microns); a viewpoint generally supported by the present study.

Patterson⁹² conveyed pulverized coal, having a particle size spectrum which allowed 99% to pass through 200 mesh and 90% through 325 mesh, along eight and twelve inch diameter pipes. He observes that friction factors for flowing gas-solid suspensions are difficult to determine because of the complications of drifting in horizontal pipes, and acceleration and retardation effects of particles travelling between dunes of material. The investigation was carried out at low values

of solids-to-air ratios, generally below unity, but such solids concentrations are typical in the transport between pulverizers and burner nozzles. In the operating range of Patterson's experiments, friction factors of 0.024 to 0.026 for the 12 inch pipe and 0.017 to 0.018 for the 8 inch pipe were obtained. An interesting examination of the drifting patterns following bends in various orientations, lead to the dubious conclusion that for upward flow 90 degree bends there was no tendency towards drifting regardless of the length of horizontal pipe following the bend.

Richardson and McLeman⁶¹ investigated the flow of a wide range of materials through a one inch diameter horizontal pipe having a length of 114 ft. The mean particle diameter of the materials varied from 230 to 3,800 microns and their work was confined to the non-accelerating flow region. The study is of particular interest since it attributes exceedingly high increases of pressure drop during the course of the experiments to the effects of charge transfer between the particles and the pipe wall. Although some electrostatic charging was evident in the present investigation, it was only after the installation of new ducting and the introduction of new powder did the fall in test-section pressure increase with time.

An experimental investigation of particle movement and velocity distribution in a pneumatic transport line by Uemata and Morikawa⁹³ revealed that the distribution of particles in a horizontal line is related to the turbulence of the conveying air. Their results indicate that the speed of fall of the particles is less than the fluctuations in velocity of the air flow.

A review of the considerable researches of such German workers as Weidner, Jung, Guenther, Hesse and Muschelknautz has been reviewed by Doig and Roper⁹⁹, whilst Barth's work is referred to in Chapter 5, section 5.2.

Recent papers by Jotaki et al¹⁰⁰ and Ikemori et al¹⁰¹ investigate the velocities of a variety of granules and the consequent pressure drop for flow through a horizontal conveying system. They relate the solids friction factor to the Froude number and Ikemori observes that the relationship is independent of solids-to-air mixture ratio providing that the latter is greater than unity.

This reasonably comprehensive survey discloses the fact that very little work has been carried out with non-spherical particles below 100 microns diameter, being transported through ducts of moderate diameter, say two and three inches. Patterson⁹² and Farbar⁷ both used relatively fine particles, but Patterson used very large conveying lines, whilst Farbar employed a duct well below one inch diameter. Since the present study illustrates that particle size and shape, and duct diameter, affects the behaviour of a flowing gas-solid suspension, then comparison of this work with that of other investigators can only be made somewhat tentatively.

6.3 Experimental Procedure

The method of plant operation is described in section 3.4, the arrangements for pressure drop measurements in a horizontal duct outlined in section 4.4.3 and the experimental procedure explained in section 4.4.3.1. The part of the suspension flow loop indicated by (N) in Fig. 3.2, was mild steel ducting for the entire series of pressure drop tests. This steel ducting was then replaced by perspex tubing to

enable a visual appreciation of the flow behaviour at various solids loadings and superficial air velocities to be executed.

6.4 Data Analysis

The pressure loss analysis for vertical transportation of solid particles was outlined in section 5.4. The procedure for horizontal transportation differs only in that the pressure drop contributions required for the support of a column of the suspension, represented by equations (8) and (9) in section 5.4, reduce to zero. Thus, the pressure drop due to the composite fluid friction (compare equation (12) in section 5.4), ΔP_{Fs} , may be evaluated from:-

$$\Delta P_{Fs} = \Delta P_m - (\Delta P_{af} + \Delta P_{ap}) \quad (1)$$

where ΔP_m is the total measured pressure differential, and $(\Delta P_{af} + \Delta P_{ap})$ is the pressure drop attributed to acceleration of the conveying air and the solid particles.

The resistance number defined by equation (20) in section 5.4 applies equally well to flow through horizontal conduits, provided that ΔP_m is the total pressure drop along a horizontal pipe of length, L, and diameter, D.

6.5 Results and Discussions

The direct experimental results, a plot of the total modified pressure drop, $\Delta P_m/L$, of a horizontal straight pipe, as a function of the mean gas velocity, \bar{u}_f , for different solids-to-air flow ratios, are shown in Figs. 6.1 to 6.6. According to these plots the relationship between $\Delta P_m/L$ and \bar{u}_f is always dependent upon W_p/W_f , the extent being dependent upon the duct diameter and particle size. Fig. 6.1 is of particular interest in that a distinct minimum of $\Delta P_m/L$ is obtained for the 500 mesh alumina powder flowing through a one

inch diameter pipe. At conveying velocities below that for this minimum, the solid particles will deposit on the bottom of the pipe with a consequent rise in $\Delta P_m/L$, as indicated in Fig. 6.1, and eventually the conveying line could become blocked. Since the air velocity must be greater than that at which saltation occurs, it is suggested that the optimum conveying velocity is that which corresponds to the minimum $\Delta P_m/L$ value, this is in agreement with Schuchart¹⁰³. The results depicted in Fig. 6.2 show no such minimum and yet they represent similar flow conditions to those just discussed and apply to the same one inch duct. The only system parameter which has been varied is the particle size, now being 320 mesh powder, that is, a mean particle diameter increase from 15 to 40 microns. The particle size effect is very apparent even for velocities greater than that at which the minimum $\Delta P_m/L$ occurs, for example, comparison of Figs. 6.1 and 6.2 illustrates that above 220 ft/s the 320 mesh curve for a W_p/W_f value of 0.65 is almost identical to the 500 mesh curve for W_p/W_f in the range 2.0 \rightarrow 4.0. The ability of the finer particles to suppress turbulence levels and consequently reduce the total pressure drop is once again demonstrated.

The $\Delta P_m/L$ versus \bar{u}_f curves for the 500 mesh powder flowing through a two inch diameter duct are shown in Fig. 6.3, this family of curves, which are similar to those of Mehta et al⁴ and Duckworth and Rose³⁴, exhibit a large W_p/W_f effect, particularly at low values of W_p/W_f . The interesting feature of Fig. 6.4 is that the 320 mesh alumina exhibits almost identical characteristics to those of the 500 mesh alumina, thus producing a minimal particle size effect for flow through two inch horizontal ducts.

Similar families of curves for flow through a three inch diameter pipe are shown in Figs. 6.5 and 6.6, the W_p/W_f effect for the 500 mesh particles diminishes as \bar{u}_f decreases. A particle size effect is possibly more evident than in the case of two inch duct flow, but again it is not as strikingly apparent as that for gas-solid flow through a one inch pipe.

The pressure drop data for the horizontal test sections are also shown in Figs. 6.7 to 6.11, as a function of the solids rate of flow for several different air flow rates. The spread in some of the points is due in part to each curve representing a range of air flow rate, W_f , and also to occasional erratic manometer readings for the higher solids flow rates, W_p . The curves for the one inch pipe, shown in Fig. 6.7, indicate a general trend of initial linearity with a decreasing slope for the upper values of W_p , this distribution of points was repeated for the 500 mesh powder and so the graph is not presented. Figs. 6.8 and 6.9 show very little particle size effect, as noted previously for flow through the two inch duct, and a fair linear relationship for $W_f > 8.0$ lb/min. The results differ considerably for $W_f < 8.0$ lb/min at relatively high solids flow rates, in that there is a definite tendency towards the independence of pressure drop with respect to solids loading. This phenomenon is repeated in Figs. 6.10 and 6.11 which represent the three inch test section results for the 500 and 320 mesh powders respectively; similar results were obtained by Farbar⁷, although the limitations of his equipment prevented him from establishing this "levelling-off" feature for more than one air flow rate. The latter two curves show a distinct particle

size effect, particularly for high values of W_p where the pressure differential for the finer particles is much lower than for the large particles.

It is generally beneficial to define the factors influencing gas-solid flows by appropriate non-dimensional characteristic data. In order to reduce the number of parameters to be examined it was thought advantageous to express resistance numbers, ψ , (defined in section 5.4) in terms of the concentration of the transported material, W_p/W_f . As a result, Figs. 6.12 to 6.14 are plots of $\psi/W_f^{0.5}$ versus Froude number for different ranges of Reynolds' number. The results for the two and three inch pipes show the virtual independence of $\psi/W_f^{0.5}$ upon Froude number at low values of Froude number. A family of curves is obtained in every case because of the large Reynolds' number effect, despite this the curves for a particular duct diameter all tend to a single minimum value of $\psi/W_f^{0.5}$. Figs. 6.14 and 6.15 indicate a minimum value of about 0.018 for $\psi/W_f^{0.5}$ occurring at a Froude number of 80. This value of Froude number corresponds to an air velocity of 25 ft/s through the three inch pipe, which is "equivalent" to 225 ft/s through a one inch pipe, whilst the optimum velocity indicated by Fig. 6.1 is approximately 200 ft/s, which shows such surprising similarity that it is possibly worthy of further investigation. These curves showed no particle size effect for both the two and three inch ducts.

The variation of resistance number with Froude number for different values of solids-to-air ratios is shown in Figs. 6.16 to 6.19. These curves are similar to the friction factor versus Froude number relationships of Ikemori et al¹⁰¹

and Duckworth et al⁵. Ikemori states that the relationship is independent of the solid-to-air ratio, for $W_p/W_f < 1.0$, whilst Duckworth shows a distinct dependence upon W_p/W_f for W_p/W_f between 1.0 and 5.0. The present work, which is concerned with far smaller particles than Duckworth and Ikemori, indicates that even values of W_p/W_f as low as 0.2 have a significant effect upon the relationship between ψ and F_R . Figs. 16 to 19 show that the Froude number, when low, has a considerable effect on the resistance number, this effect decreases as Froude number increases until the resistance number approximates to a constant value.

The correlation between resistance number and Reynolds' number, for 15 micron particles flowing through two and three inch horizontal ducts, is shown in Figs. 6.19 and 6.20. The data on these graphs are rather insufficient to make firm postulations, however, the trend indicated is that there is little dependence of resistance number upon Reynolds' number, except for relatively high solids-to-air ratios ($W_p/W_f > 3.0$); a conclusion reached previously by several investigators^{4,21,34}.

The location of static pressure tapplings at a particular cross-section of the test section has rarely been mentioned by previous workers, with the exception of Schuchart⁴⁹ who provided at certain intervals along the duct three pressure bores of one mm diameter. He interconnected the three tapplings for the purpose of determining the static pressure. The three tapplings were positioned such that two of them were centrally situated (similar to the "a" tapplings of the present work indicated in Fig. 4.11), but it is not clear whether the third pressure bore is along the bottom of the duct ("b" in Fig. 4.11) or along the upper surface of the test-section ("c" in Fig. 4.11).

The author assumes that Schuchart adopted this arrangement for pressure determination in the case of horizontal pipes as well as bends, although this is not clearly explained. In the present study it was considered reasonable practice to interconnect the two centre tapplings, although the presence of swirling or sinuous suspension flow would render these readings somewhat suspect, whilst the upper and lower static pressure values were recorded independently. The 90 degree bend preceding the horizontal test section causes the gas-solid flow to deflect as it enters the horizontal duct, the extent depending upon the bend geometry and the particular flow conditions. The curves in Figs. 6.21 to 6.27 fully justify the procedure of pressure determination adopted in this study, and cast doubt upon the reliability of Schuchart's data. These curves include the results for only ten flow situations out of the 2,000 performed, and since their selection was completely random, only tentative conclusions can be made at the present time.

The total pressure drop is plotted against the distance from the horizontal pipe entrance for fixed values of solids flow rate, W_p , and solids-to-gas mixture ratios, W_p/W_f , in Figs. 6.21 to 6.27. The flow of the 500 mesh powder through the one inch pipe, having a 10 inch radius bend preceding it, is illustrated in Fig. 6.21. The flow conditions of $W_p = 10.2$ lb/min and $W_p/W_f = 1.32$, show that the relationship between ΔP_m and L rapidly become linear. The very low pressure drop indicated by the upper tapping, after travelling only 8 inches from the pipe entrance, infers that the upward flowing suspension from the bend impacts upon the upper horizontal surface in the region of this tapping with the

result that a dynamic pressure contribution is incorporated in the "static" pressure reading. The expected longitudinal pressure distribution would be a continuous decrease in the pressure gradient from a maximum value at entrance to a constant value some distance downstream. The large pressure differentials in the upstream sections of the horizontal pipe being necessary to overcome the inertia forces of the particles associated with acceleration of the solid particles and the frictional and other forces present in these flows. A constant pressure gradient is only achieved after the particles have been accelerated to a steady velocity and the flow is uniformly dispersed so that the pressure gradient can be solely related to frictional effects. This rather simplified explanation of gas-solid flow behaviour does not take into account the effects of particle size and possible turbulent suppression, the effects of particle shape and the abrupt deviations of angular particles compared with the "rolling" motion of spherical particles, the direction of the two phase flow induced by the bend curvature at entrance to the test section, particle deposition as the solids flow rate increases with respect to the conveying air velocity, and so on. Fig. 6.22 differs from Fig. 6.21 in that the solids flow rate has been increased from 10.2 to 36.5 lb/min, resulting in W_p/W_f increasing from 1.32 to 5.00. Examination of the curves in Fig. 6.22 again reveals the dynamic pressure contribution reflected in the pressure reading of the first upper surface tapping. The linear relationship between ΔP_m and L only becomes established towards the end of the test section, this being related to the high solids loading. The flow did not deflect from the upper surface with a downward component

of sufficient magnitude to cause impingement of the flow on the lower surface, since this would have been indicated by a sudden fall in the pressure differential. It seems reasonable to assume that for a wide range of solids loadings, gas-solid flow through one inch horizontal pipes very quickly achieves a uniformly dispersed state.

The curves in Figs. 6.23 and 6.24 illustrate the ΔP_m versus L relationships for several solids loadings of 500 mesh powder flowing through a two inch diameter horizontal duct preceded by a bend having a radius of curvature of 20 inches. The initial pressure gradient for the more dense flows, Fig. 6.24, appears to be zero, along the upper surface of the duct, over the first 16 inches of test section, this is attributed to the previously mentioned dynamic pressure component. The results for the centre and bottom tappings are very similar along the entire length of pipe, although the initial pressure gradients are much less than anticipated. This may be explained by the fact that there was a downward flowing two phase portion of the flow and possibly some swirling motion induced by secondary flow phenomena associated with bends. The curves eventually exhibited a certain linearity. The total pressure drops, as recorded by the centre tappings, for the entire length of the horizontal test section were used for the results shown in Figs. 6.1 to 6.11, and for the determination of the resistance numbers used in Figs. 6.12 to 6.20. The overall pressure drop was 9.97, 9.93 and 9.55 cm H₂O for the centre, lower and upper tappings respectively, for the case shown in Fig. 6.24 when the solids flow rate was 30.0 lb/min, which represents a maximum variation of approximately 4%. This compares with 72.4, 68.4 and 68.5 cm H₂O

for the centre, lower and upper tappings of the one inch pipe shown in Fig. 6.21, which produces a deviation of 5%. The mean static pressure recorded by the two centre tappings was employed in the results illustrated in Figs. 6.1 to 6.20 on account of them being less affected by deflecting flow induced by the bend curvature, although it is accepted that they would still be susceptible to most forms of unsteady motion. Fig. 6.23 shows relationships for more dilute flows and these curves indicate that the gas-solid flow progresses along the horizontal duct in a series of gentle deviations.

The curves in Fig. 6.25 representing a very dilute gas-solid suspension of 500 mesh alumina particles in air, $W_p/W_f = 0.26$, flowing through a three inch duct preceded by an 18 inch radius bend, exhibit very similar characteristics to the larger 240 mesh particles shown on the same plot. The lower tapping shows distinct linearity over the greater portion of the test section, whilst the centre and upper pressure tappings indicate a series of small deflections as noted earlier. The overall pressure differentials for the centre, lower and upper tappings with the 500 mesh powder are 0.72, 0.58 and 0.78 inches H_2O respectively, which represents a large deviation of up to 25%. The curves for $W_p/W_f = 1.33$, with 240 mesh powder, shown in Fig. 6.26 illustrate similar trends to the above except for the final pressure differential along the upper surface, consultation of the data observation sheet revealed that the manometer line leading to this tapping had become blocked. Also shown in Fig. 6.26 are the curves for 500 mesh powder flowing at 34.5 lb/min with $W_p/W_f = 4.02$. The lower and centre tappings have produced very similar ΔP_m versus L curves, the early pressure differentials being low

due to the dynamic pressure influence followed by a linear relationship, except for the final tappings which were reported as blocked. Fig. 6.26 is of particular interest in that the upper tappings give a large negative pressure drop after entering 9 inches along the three inch duct. This is caused by the upward deflecting flow producing a large dynamic pressure effect along the upper path of the duct. The flow did not impact on the lower surface and it is noticeable that the three straight curves are parallel to each other.

Fig. 6.27 shows the characteristics obtained for 500 mesh powder flowing along a three inch horizontal duct which is preceded by a 90 degree bend of 30 inches radius of curvature. The solids flow rates are 1.8, 4.8 and 36.5 lb/min, corresponding to W_p/W_f values of 0.16, 0.44 and 3.97, and the percentage deviations in the total pressure drops are 27, 9 and 12. The significant difference between these curves and those shown in Figs. 6.25 and 6.26 is the form of the pressure-plot for the upper tappings. The more gradual curvature of this bend results in the solid particles occupying the outer region of the bend and sliding, rather than "bouncing", around it. The curvature induces a slight downward trend for the suspension flow as it enters the horizontal pipeline and a suction effect is experienced by the pressure tappings along the upper part of the horizontal duct. The flow finally becomes reasonably uniformly dispersed by the end of the horizontal section.

6.6 Conclusions

The distribution of 15 micron alumina particles when flowing through a three inch diameter horizontal duct has been visually observed for a range of flow conditions.

The conditions producing particle deposition along the lower part of the duct were characterised by a fast-moving dilute layer in the upper area of the test section, which continually disturbed the top surface of the moving bed of dense material.

The correlations between $\Delta P_m/L$ and \bar{u}_f are in agreement with other authors, although the relationship was always found to be dependent upon W_p/W_f . A definite particle size effect was evident for flow through the one inch duct, but this effect became minimal for the two and three inch test sections.

An independence of pressure drop upon solids loading was obtained from plots expressing the ΔP_m as a function of W_p for different air flow rates.

The curves defining the flow behaviour in terms of non-dimensional groups were generally of the expected form, except that the correlation between a modified resistance number and Froude number indicated a considerable Reynolds' number effect, which is in conflict with the observations of other investigators^{21,34,35}. It is the opinion of the author that, for very fine particles, dimensionless parameters should be correlated in terms of both Reynolds' number and Froude number.

It is recommended that examination of gas-solid flow downstream from a pipe transition, such as a bend, be effected by four static pressure tappings arranged at intervals along the test section and connected independently to a manometer. It has been shown that deflecting flow behaviour and possibly swirling flow can be interpreted from careful arrangement of pressure tappings. The danger in assuming that all manometer readings indicate the true static pressure of the flowing

suspension has been demonstrated, reference having been made to dynamic pressure contributions and suction effects generated by deflecting flows.

6.7 Suggestions for Further Work

A more detailed examination of the effect of bends, immediately upstream from a horizontal conduit, upon the flow behaviour in the horizontal section will eventually be obtained from the data already available in the present study. At the same time, the effect on the flow characteristics of varying the particle size spectrum will be scrutinized.

An interesting problem requiring extensive investigation is the flow of extremely dense phases of fluidised solids through horizontal conduits of several inches diameter. The author recommends the use of a pressure transfer vessel of capacity between 20 and 30 ft³, which would be capable of discharging over one ton of alumina powder in less than one minute. The author has recently acquired such a vessel and is currently designing a transport system which includes a 300 ft horizontal run. It is proposed to convey different materials at solids-to-air ratios varying from dilute to very dense phase.

There seems tremendous scope for research into the horizontal conveying of very fine particles over relatively long distances and through large diameter pipelines.

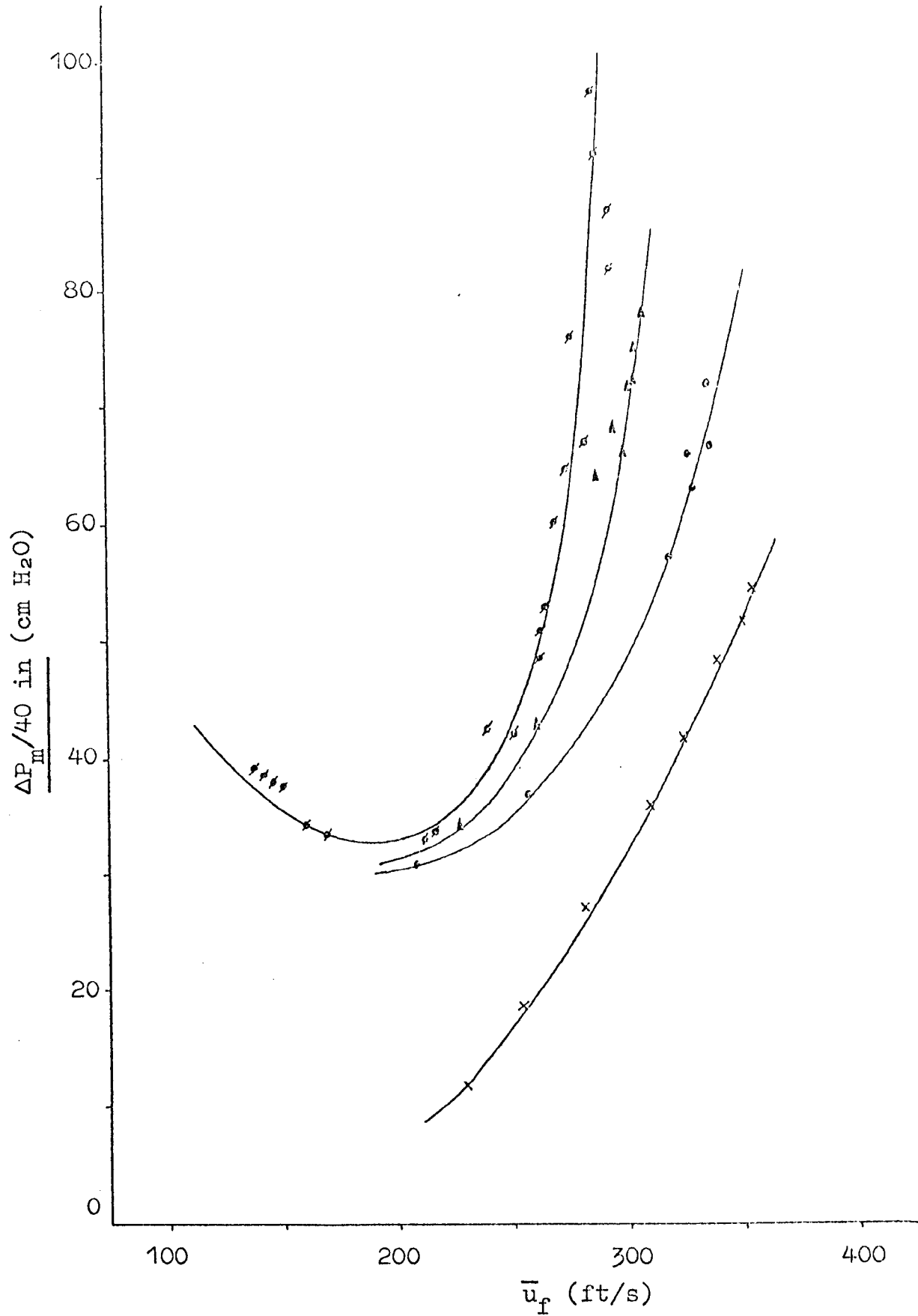


Fig. 6.1 Pressure Drop along a One inch diameter Horizontal Duct Related to the Mean Air Velocity, \bar{u}_f .

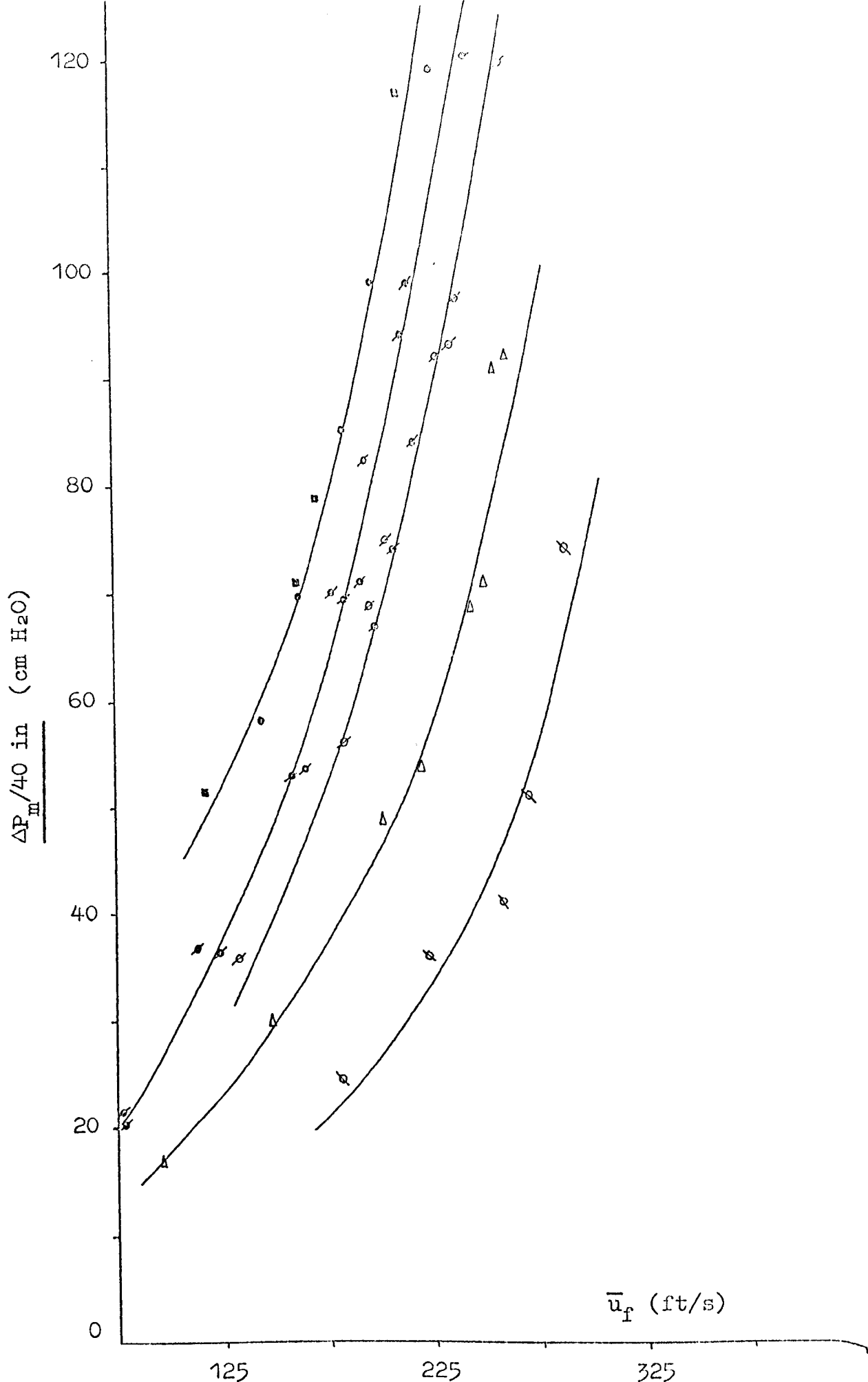


Fig. 6.2 Pressure Drop along a One inch diameter Horizontal Duct
Related to the Mean Air Velocity, \bar{u}_f .

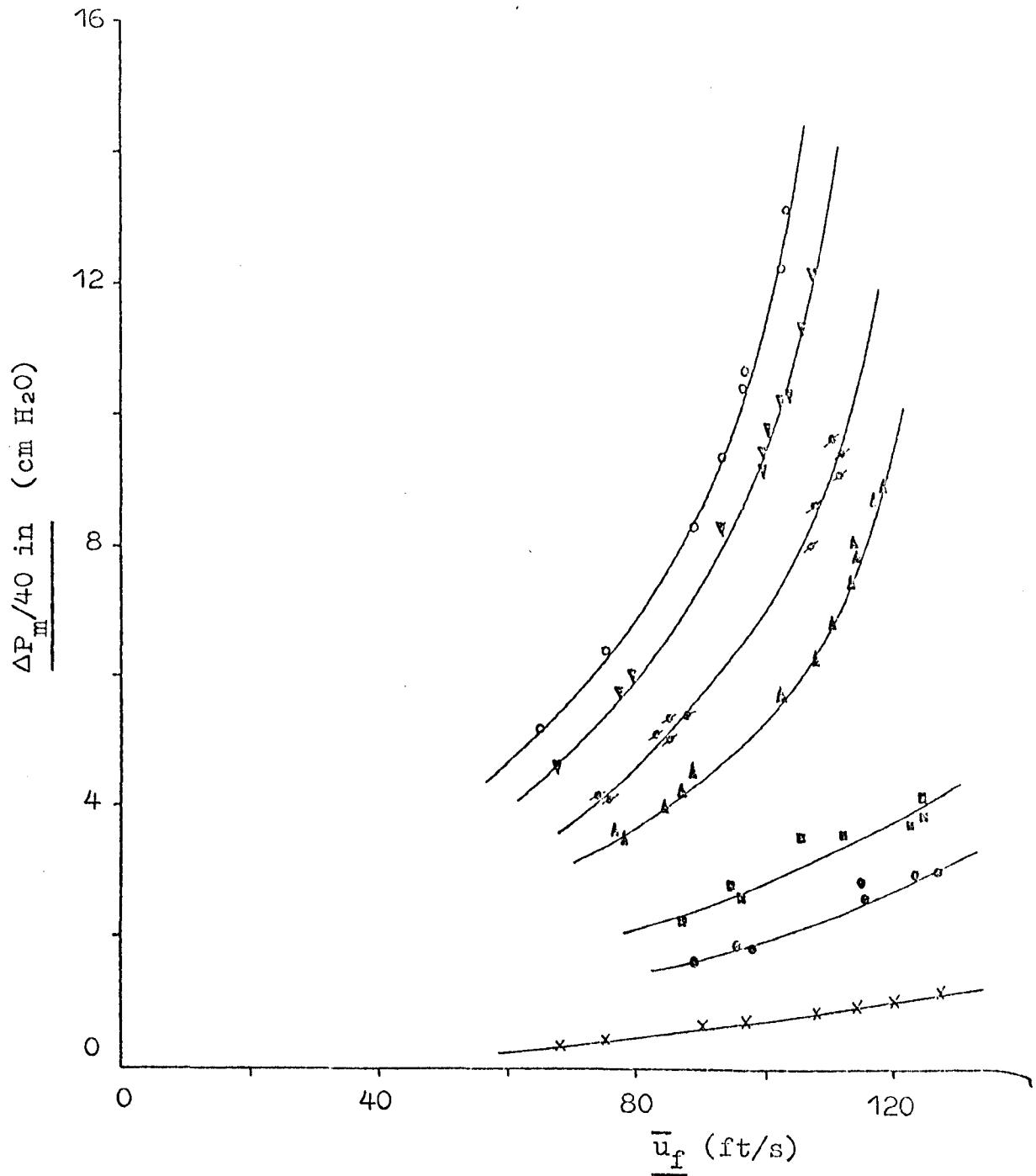


Fig. 6.3 Pressure Drop along a 2 inch diameter Horizontal Duct Related to the Mean Air Velocity, \bar{u}_f .

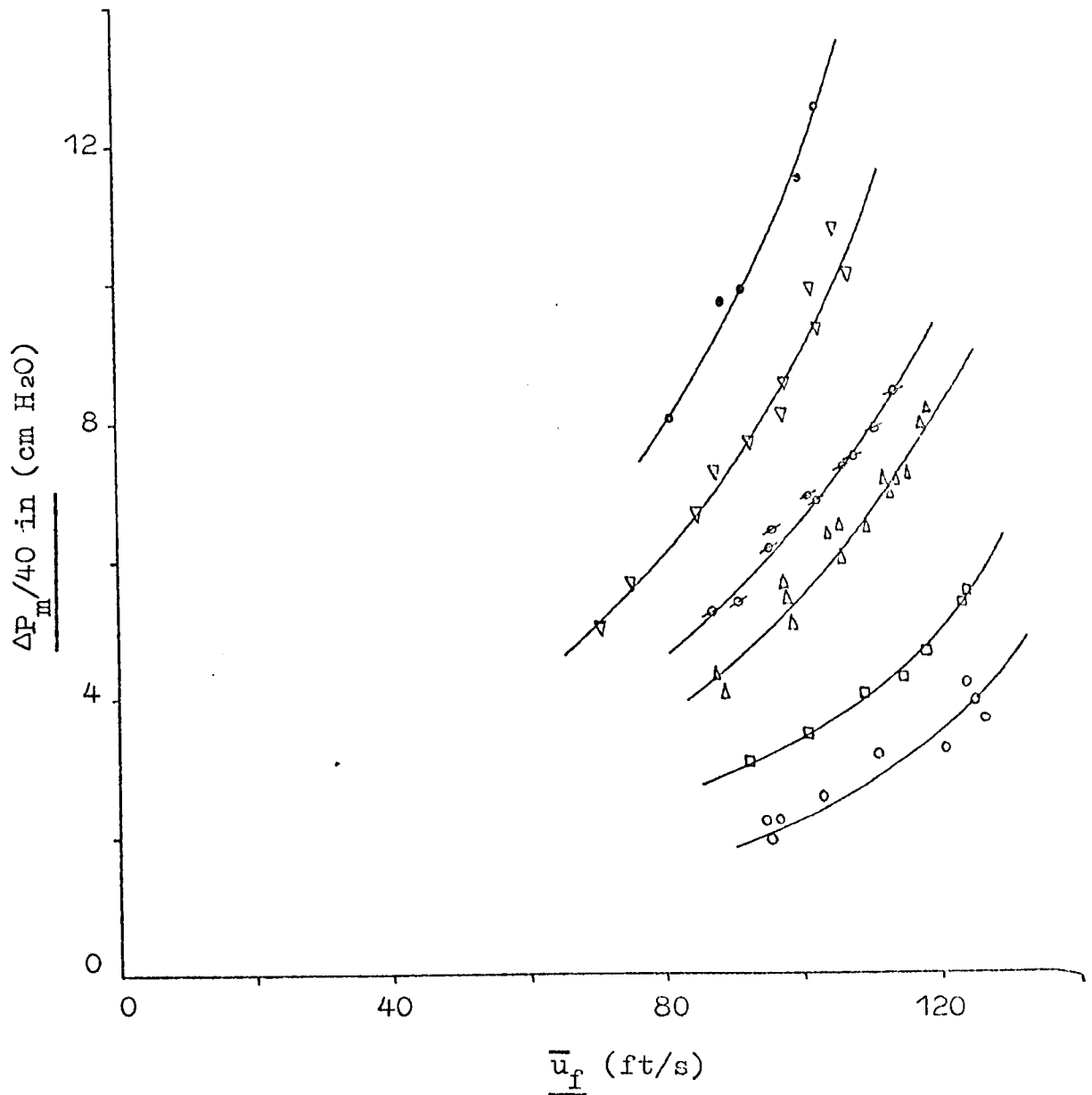


Fig. 6.4 Pressure Drop along a 2 inch diameter Horizontal
Duct Related to the Mean Air Velocity, \bar{u}_f .

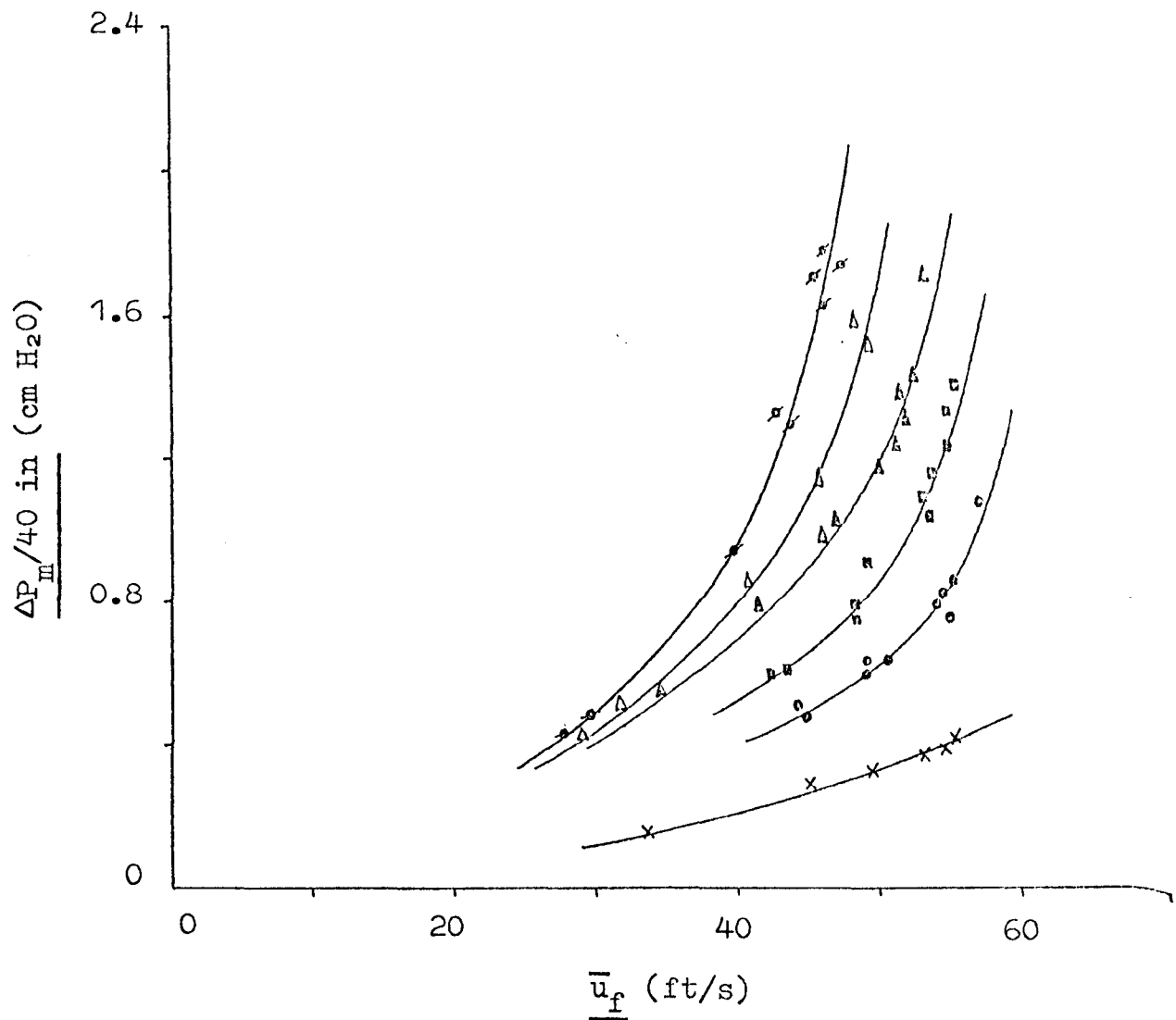


Fig. 6.5 Pressure Drop along a 3 inch diameter Horizontal
Duct Related to the Mean Air Velocity, \bar{u}_f .

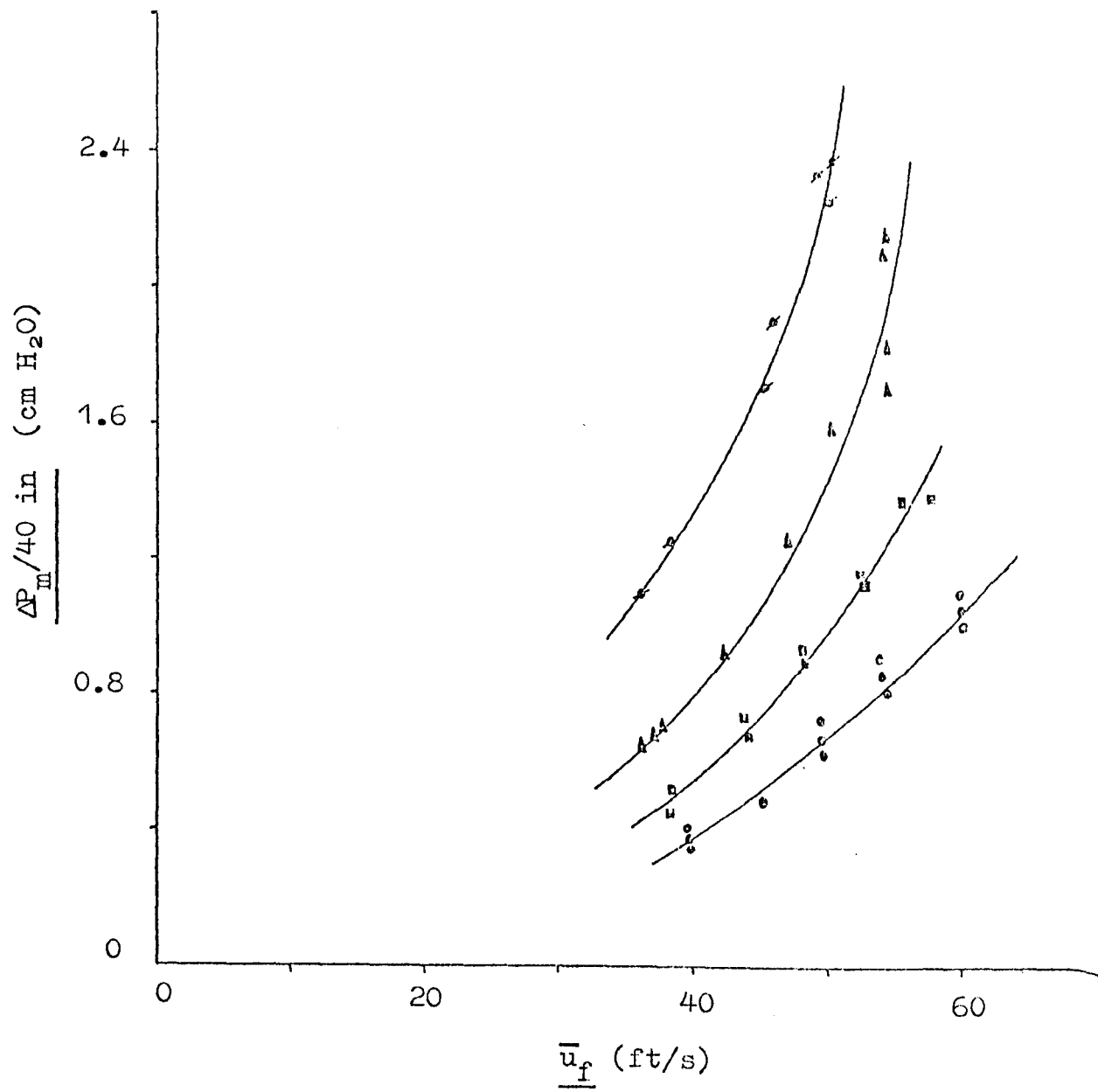


Fig. 6.6 Pressure Drop along a 3 inch diameter Horizontal Duct Related to the Mean Air Velocity, \bar{u}_f .

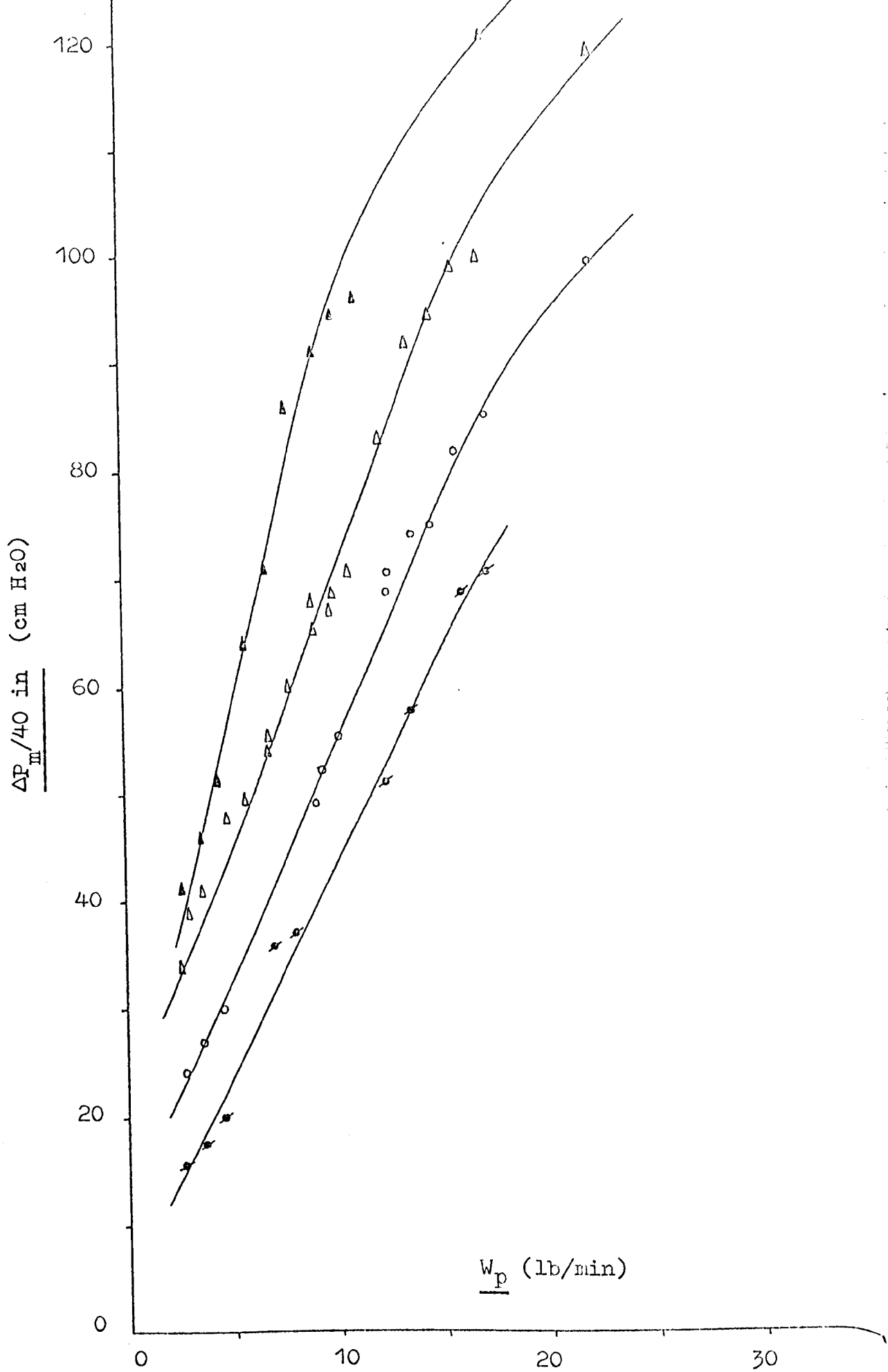


Fig. 6.7 Pressure Drop along a One inch diameter Horizontal Duct Related to the Solids Flowrate, W_p .

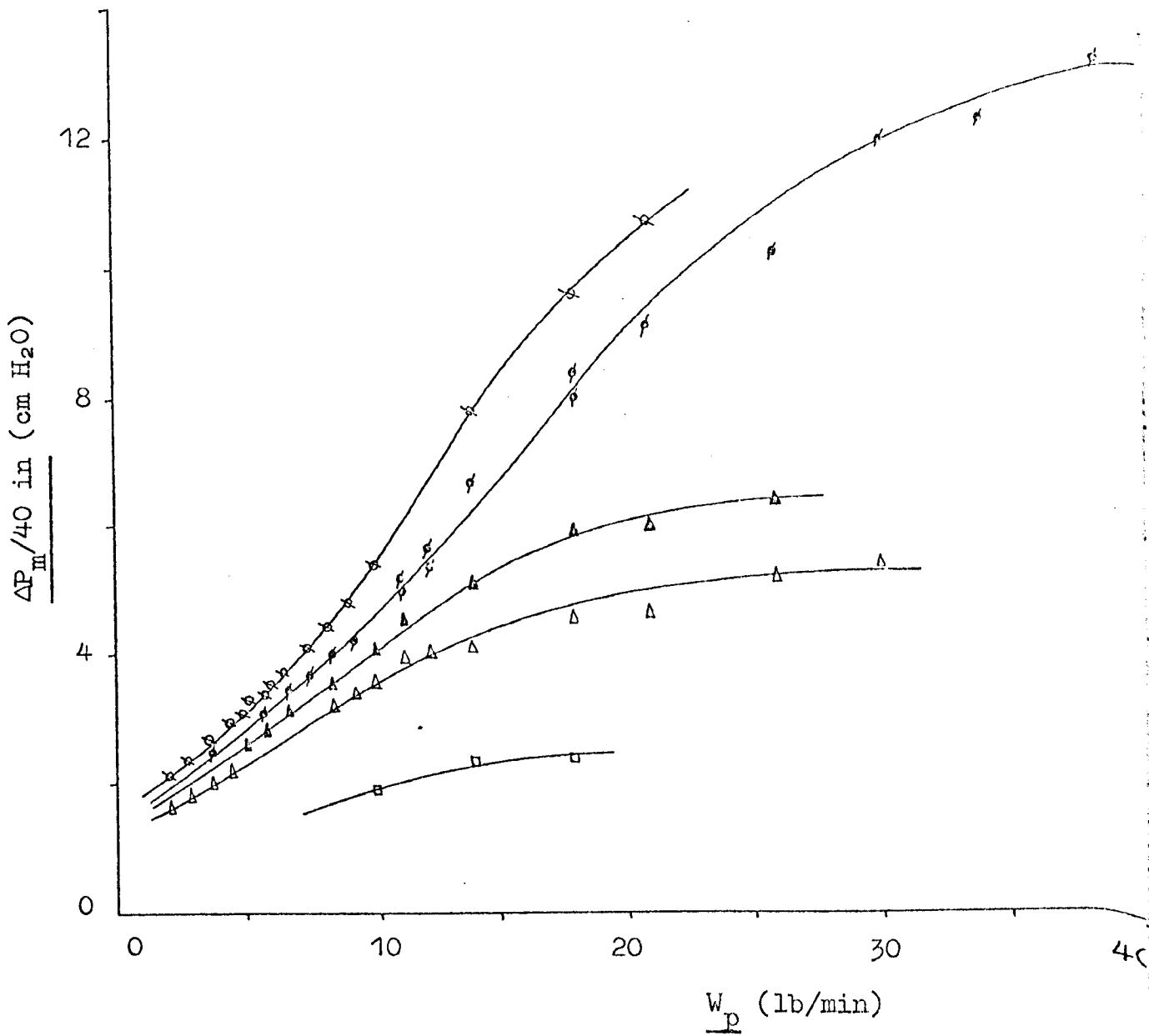


Fig. 6.8 Pressure Drop along a 2 inch diameter Horizontal
Duct Related to the Solids Flowrate, W_p .

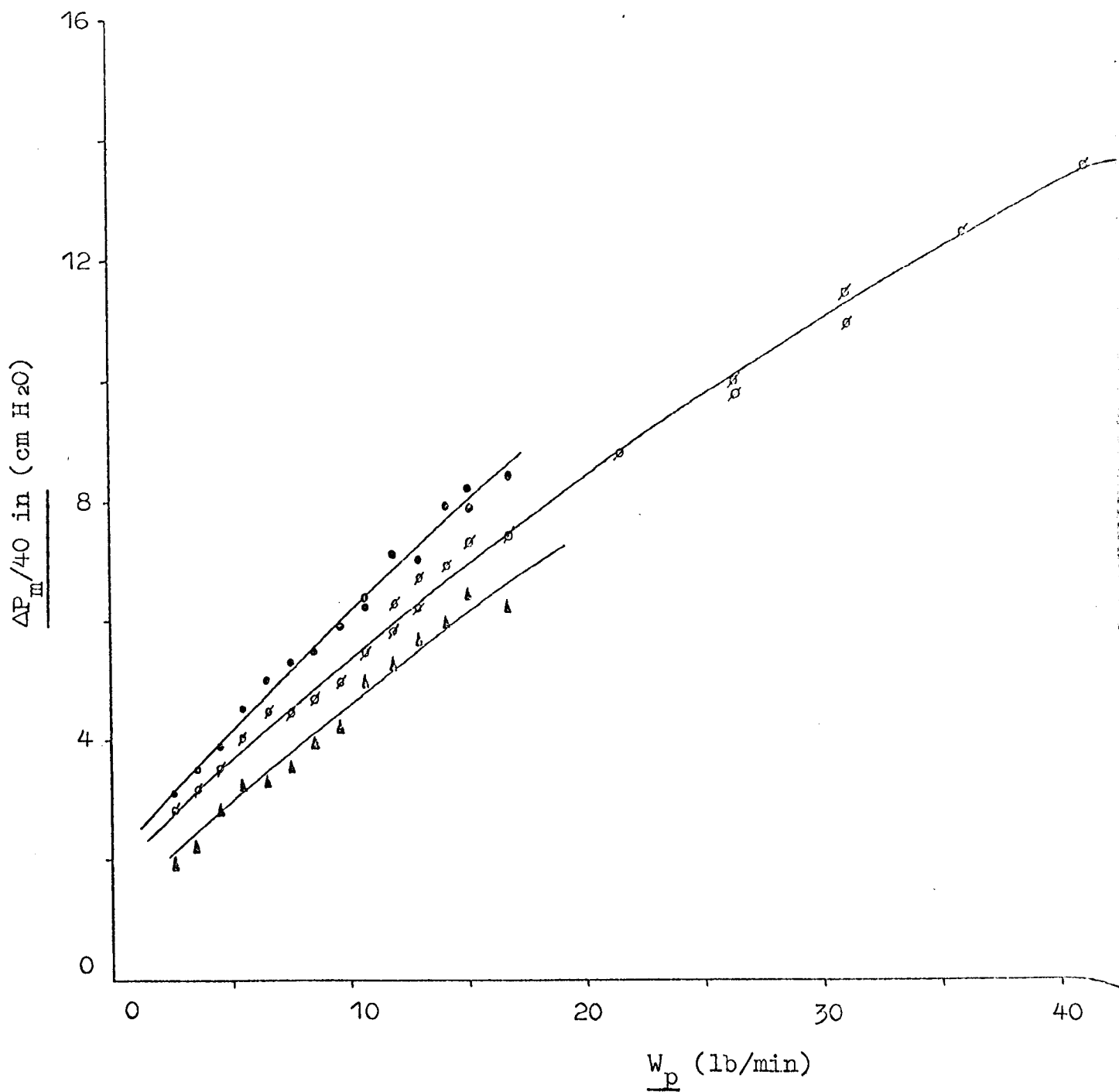


Fig. 6.9 Pressure Drop along a 2 inch diameter Horizontal
Duct Related to the Solids Flowrate, W_p .

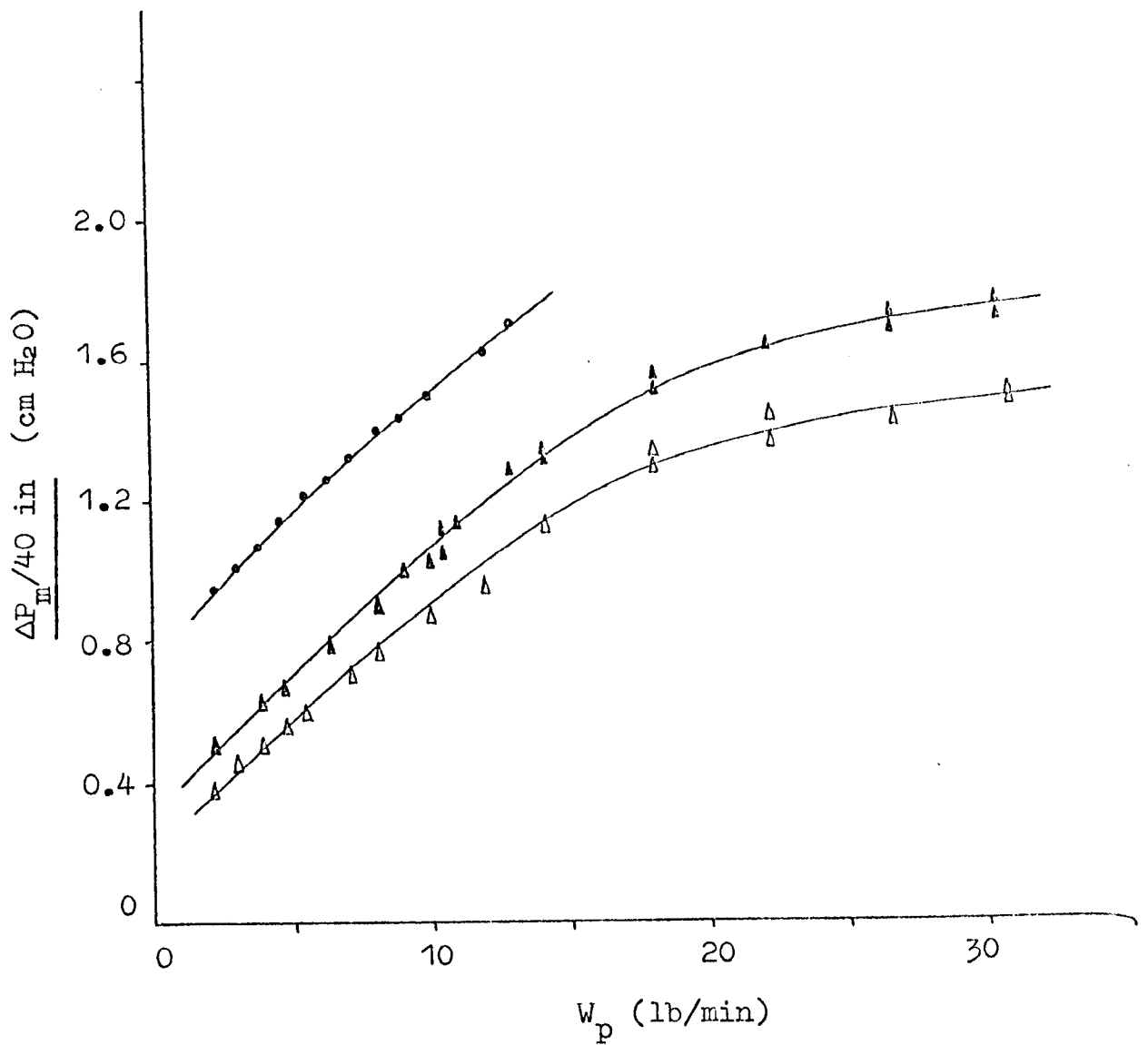


Fig. 6.10 Pressure Drop along a 3 inch diameter Horizontal Duct Related to the Solids Flowrate, W_p .

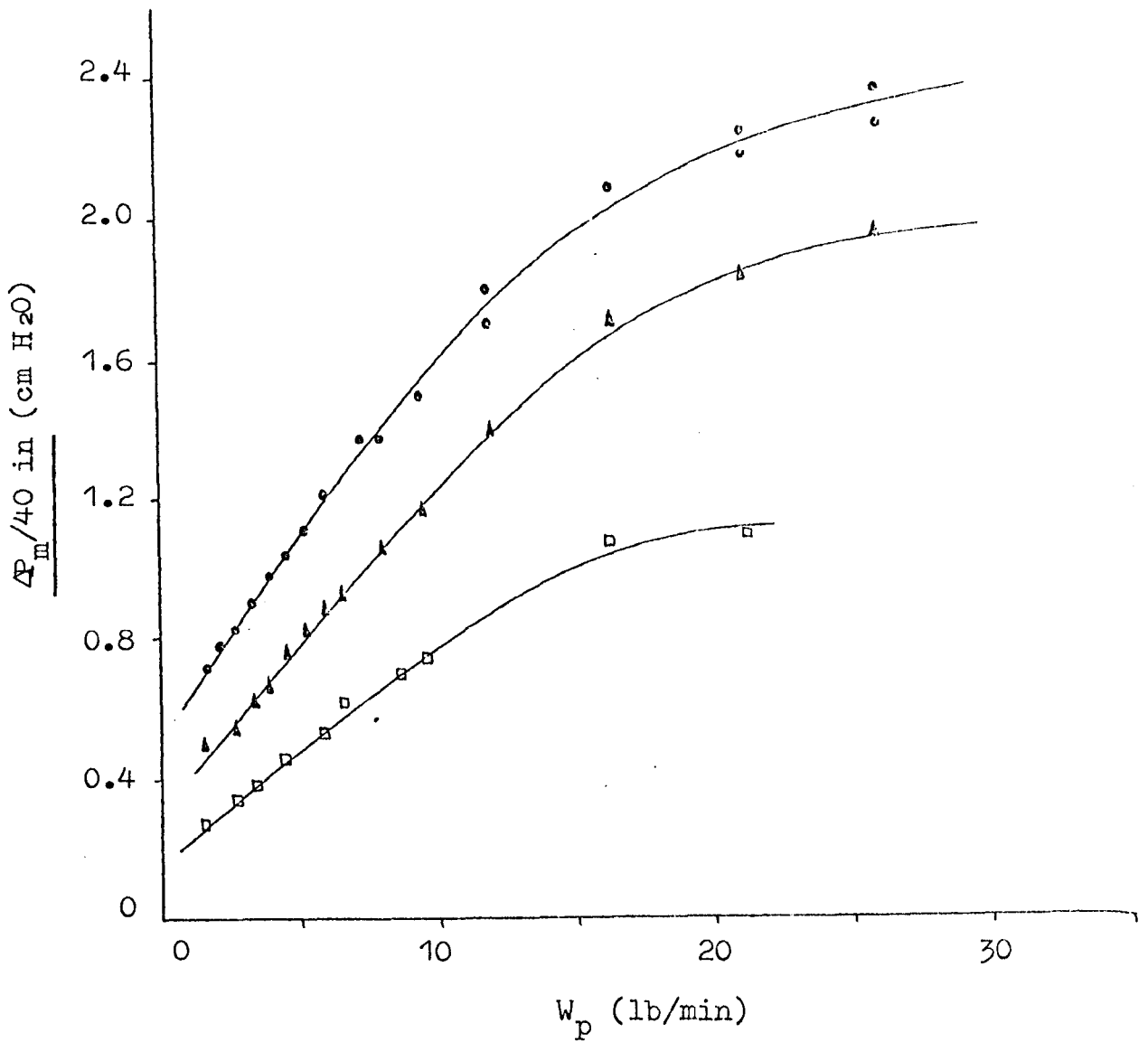


Fig. 6.11 Pressure Drop along a 3 inch diameter Horizontal Duct Related to the Solids Flowrate, W_p .

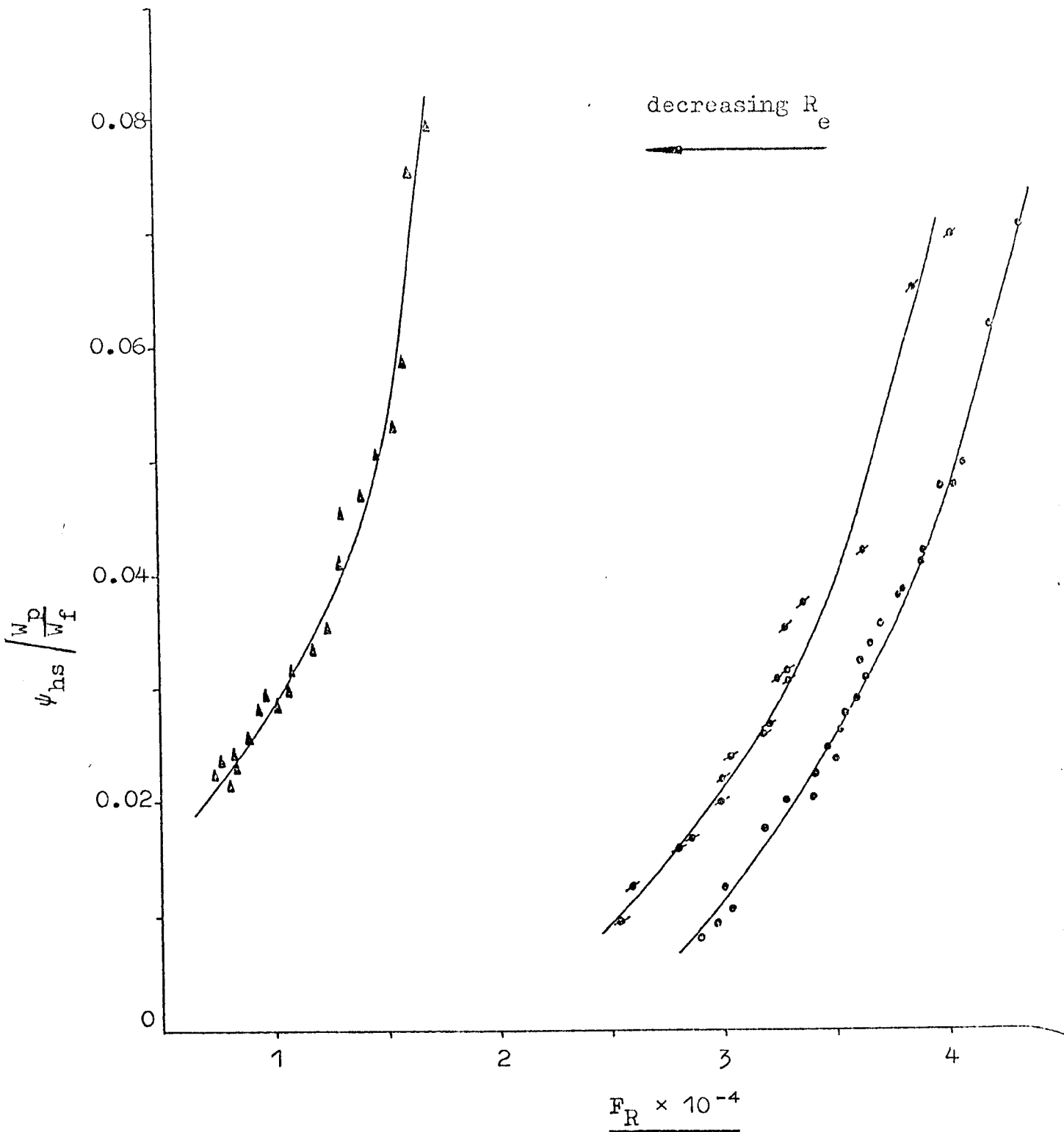


Fig. 6.12 Modified Resistance Number, $\psi_{hs} / \frac{W_p}{W_f}$, Related to Froude number, F_R , for Flow through a One inch diameter Horizontal Duct.

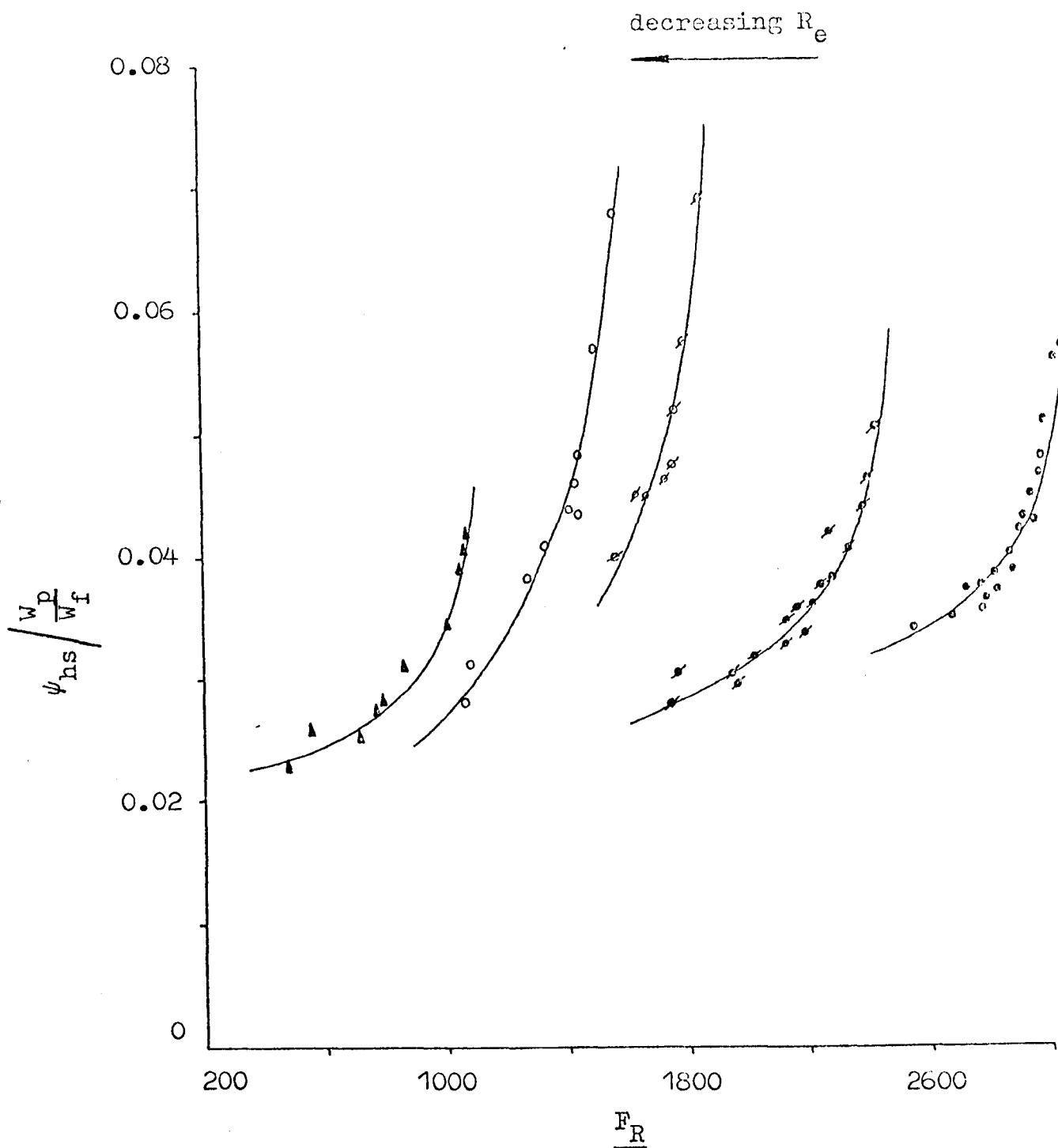


Fig. 6.13 Modified Resistance Number, $\psi_{hs} \frac{W_p}{W_f}$, Related to Froude number, F_R , for Flow through a 2 inch diameter Horizontal Duct.

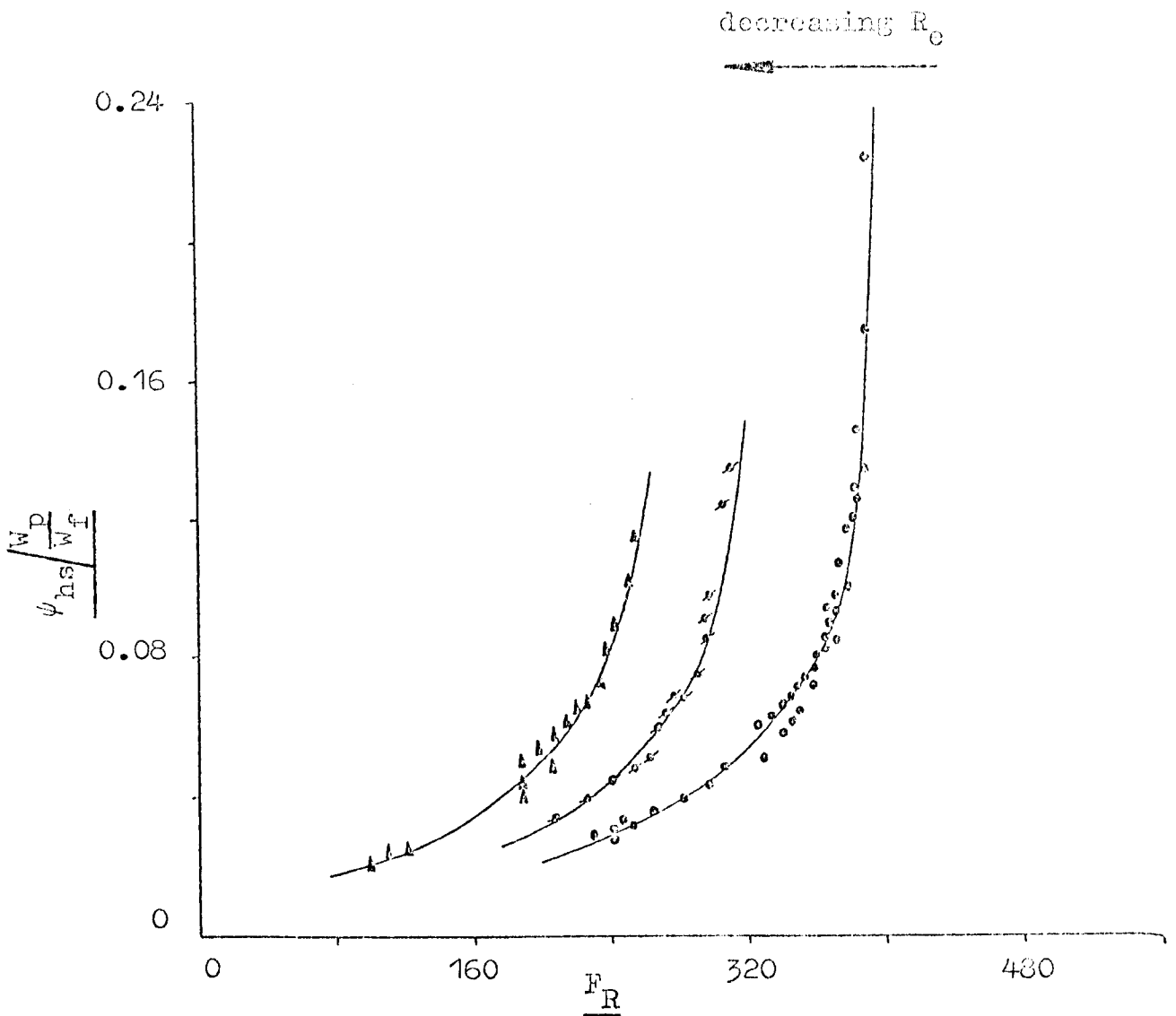


Fig. 6.14 Modified Resistance Number, $\psi_{hs} \frac{W_p}{W_f}$, Related to Froude number, F_R , for Flow through a 3 inch diameter Horizontal Duct.

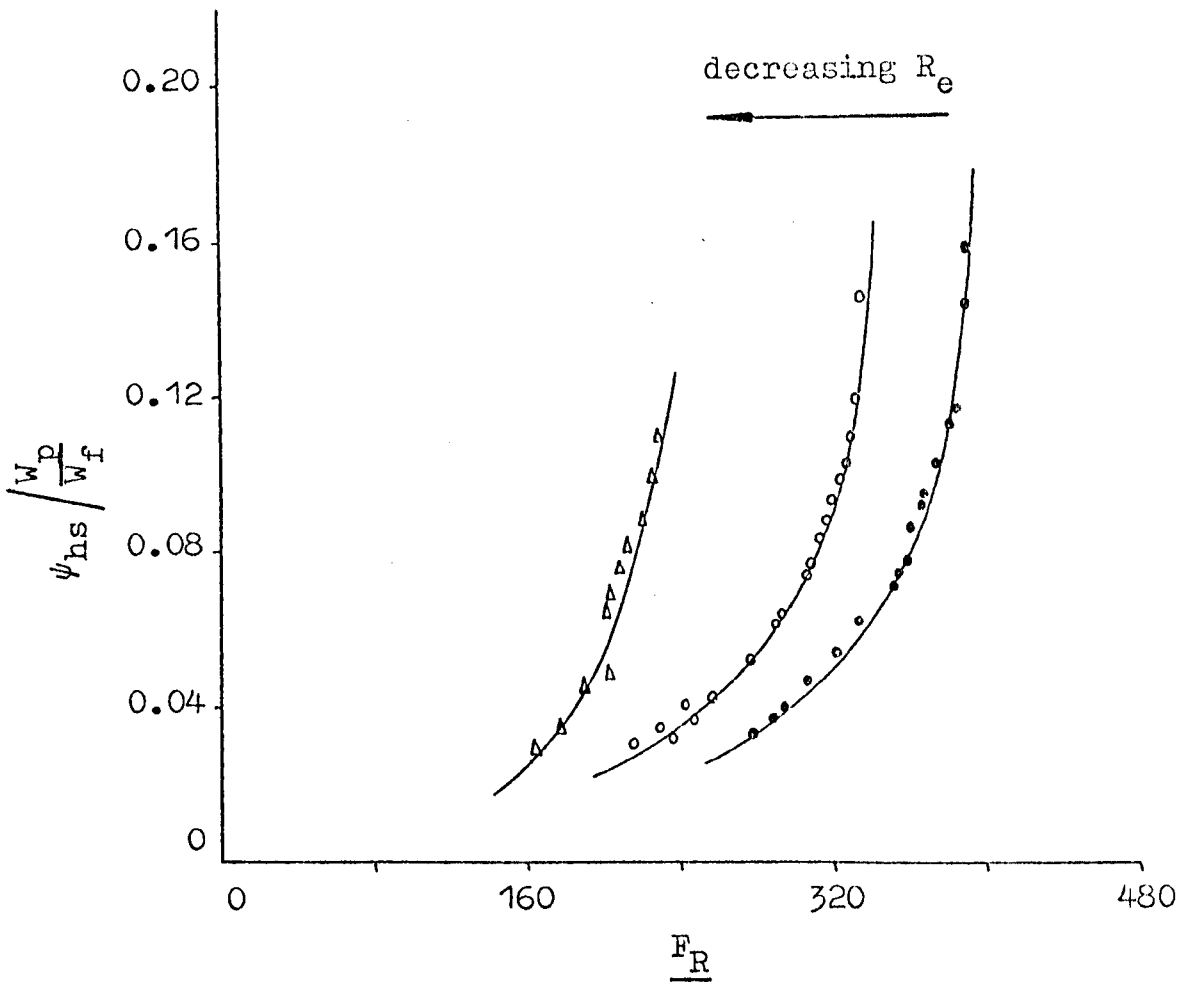


Fig. 6.15 Modified Resistance Number, $\psi_{hs} / \frac{W_p}{W_f}$, Related to Froude number, F_R , for Flow through a 3 inch diameter Horizontal Duct.

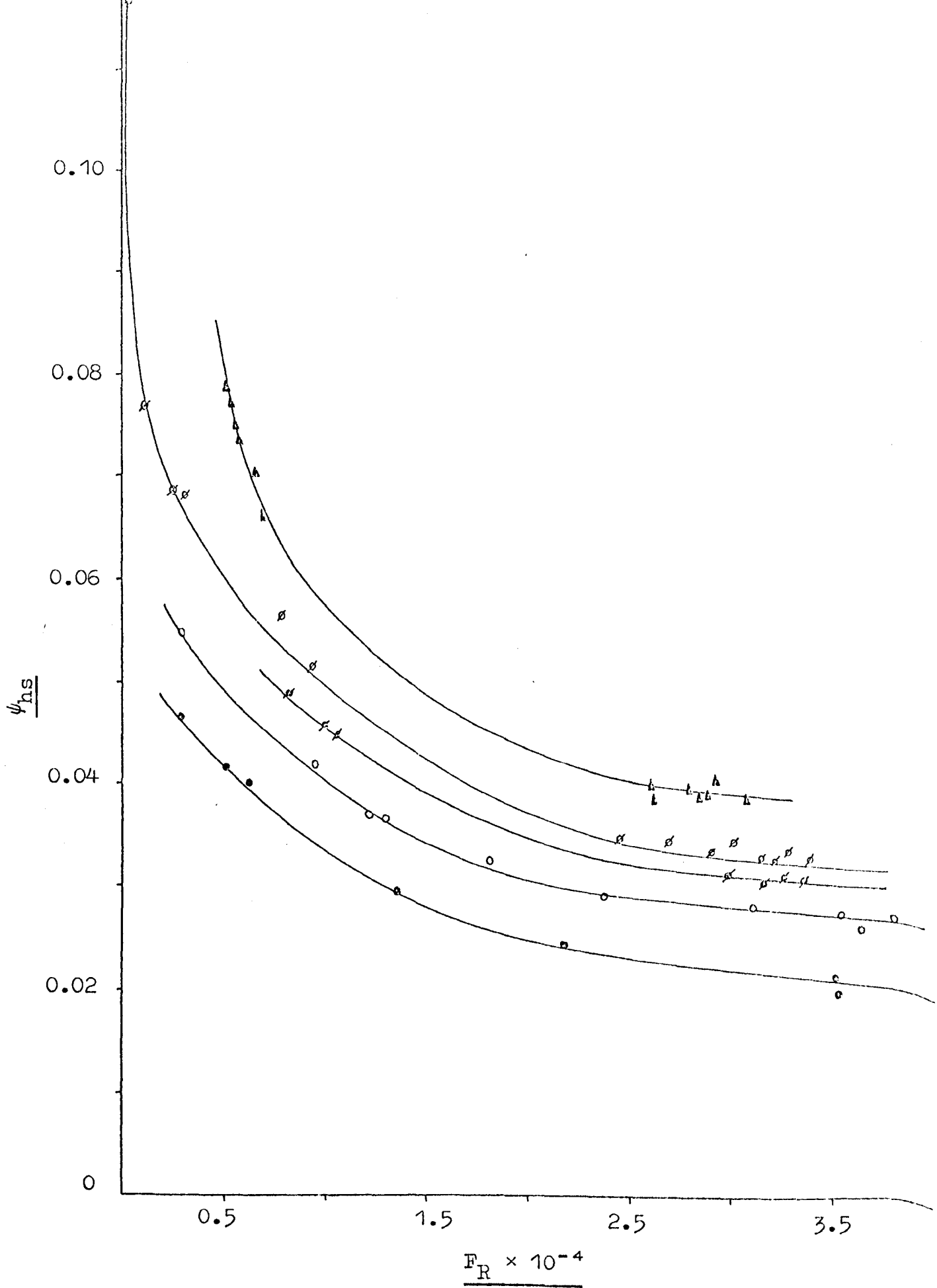


Fig. 6.16 Coefficient of Resistance for Flow through a One
inch diameter Horizontal Duct, ψ_{hs} , Related to
Froude number, F_R .

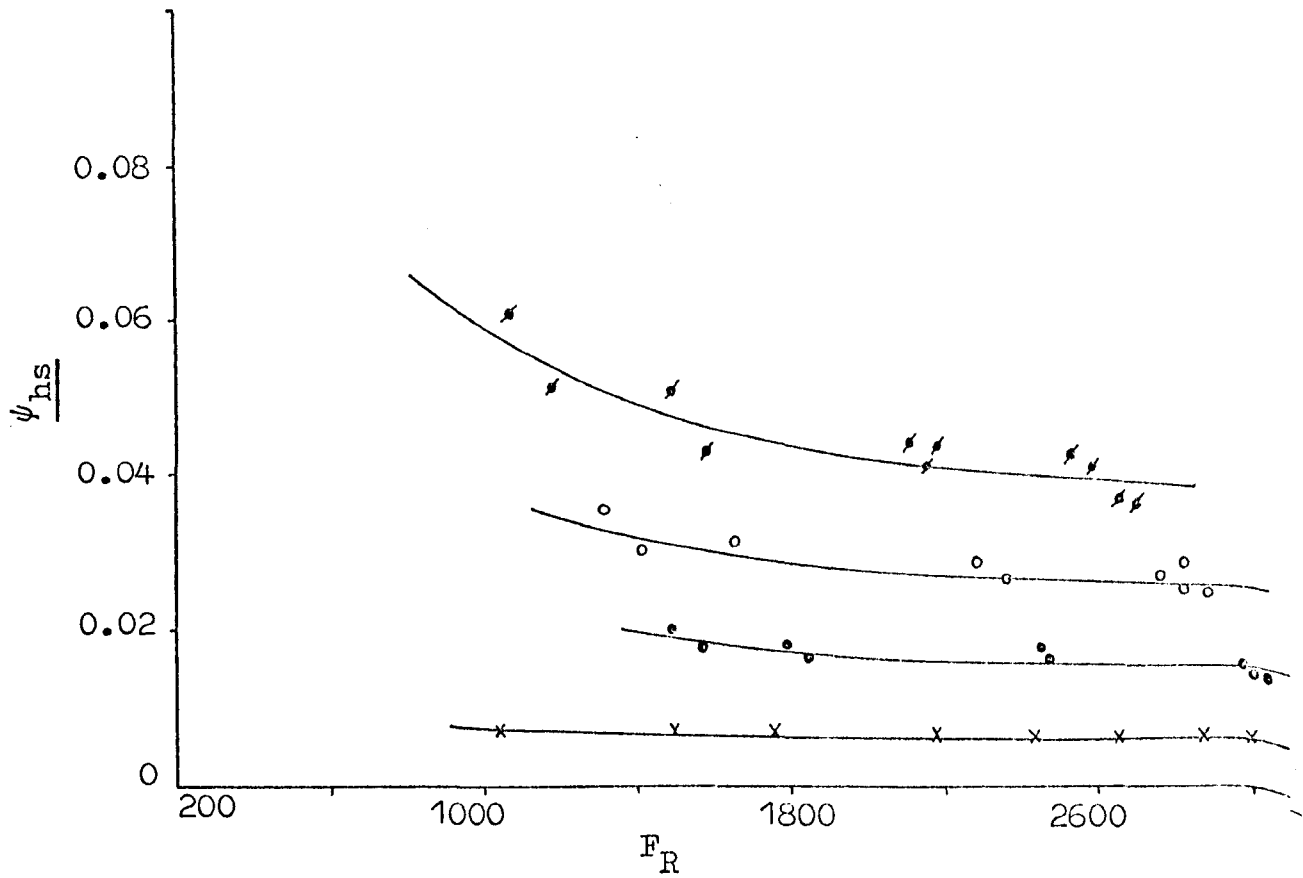


Fig. 6.17 Coefficient of Resistance for Flow through a 2 inch
diameter Horizontal Duct, ψ_{hs} , Related to Froude
number, F_R .

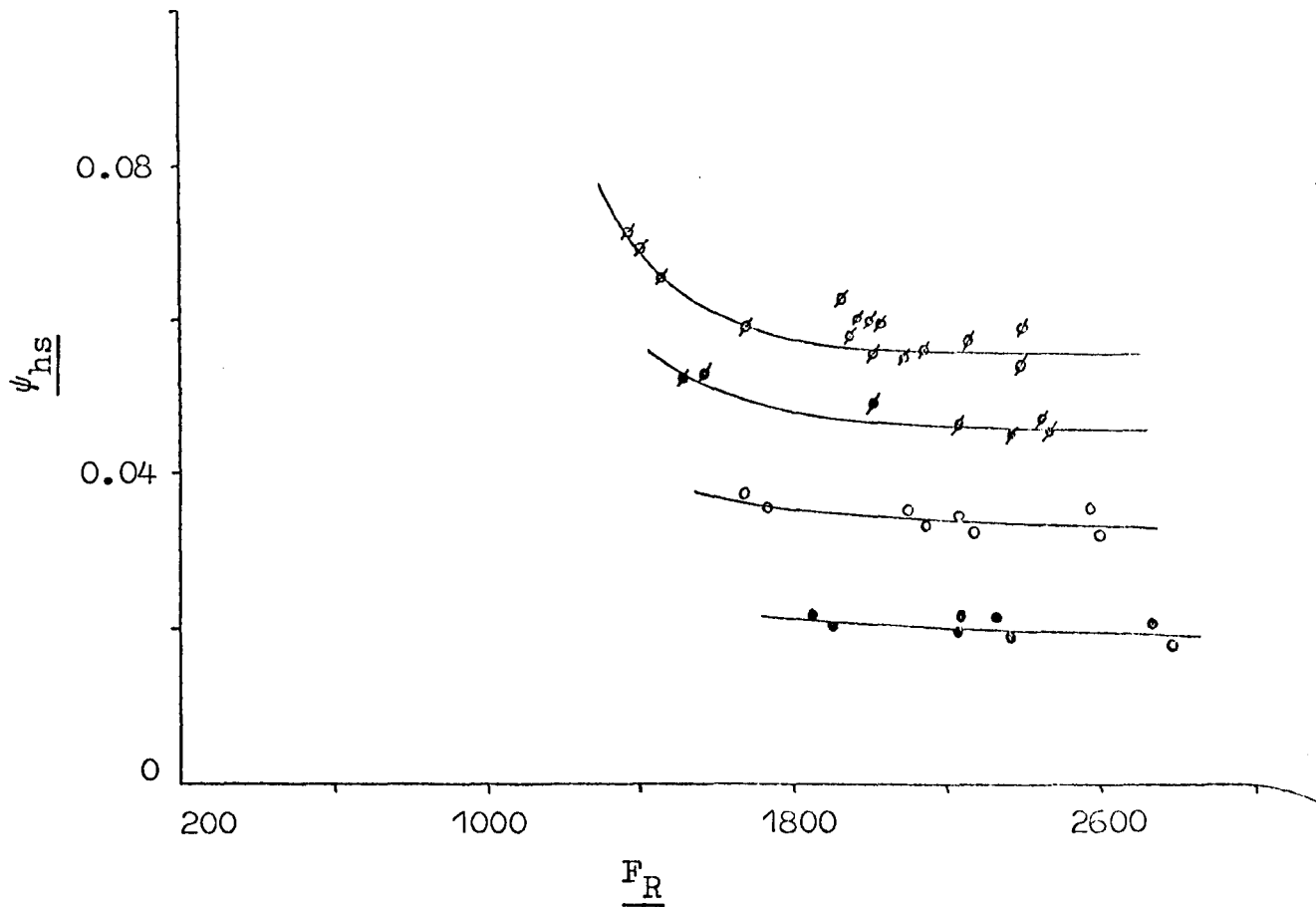


Fig. 6.18 Coefficient of Resistance for Flow through a 2 inch diameter Horizontal Duct, ψ_{hs} , Related to Froude number, F_R .

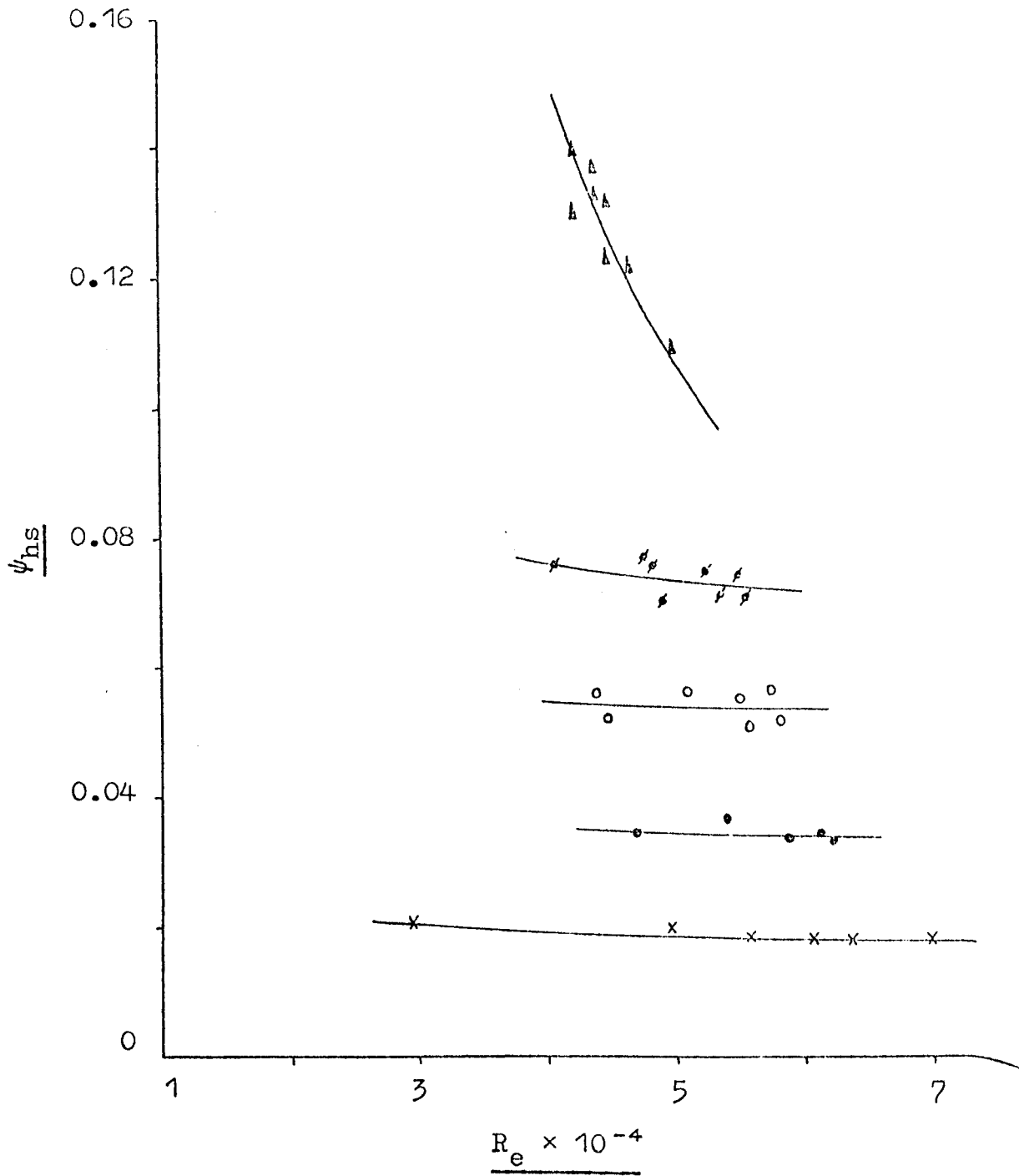


Fig. 6.19 Coefficient of Resistance for Flow through a 3
inch diameter Horizontal Duct, ψ_{hs} , Related to
Reynolds' number, R_e .

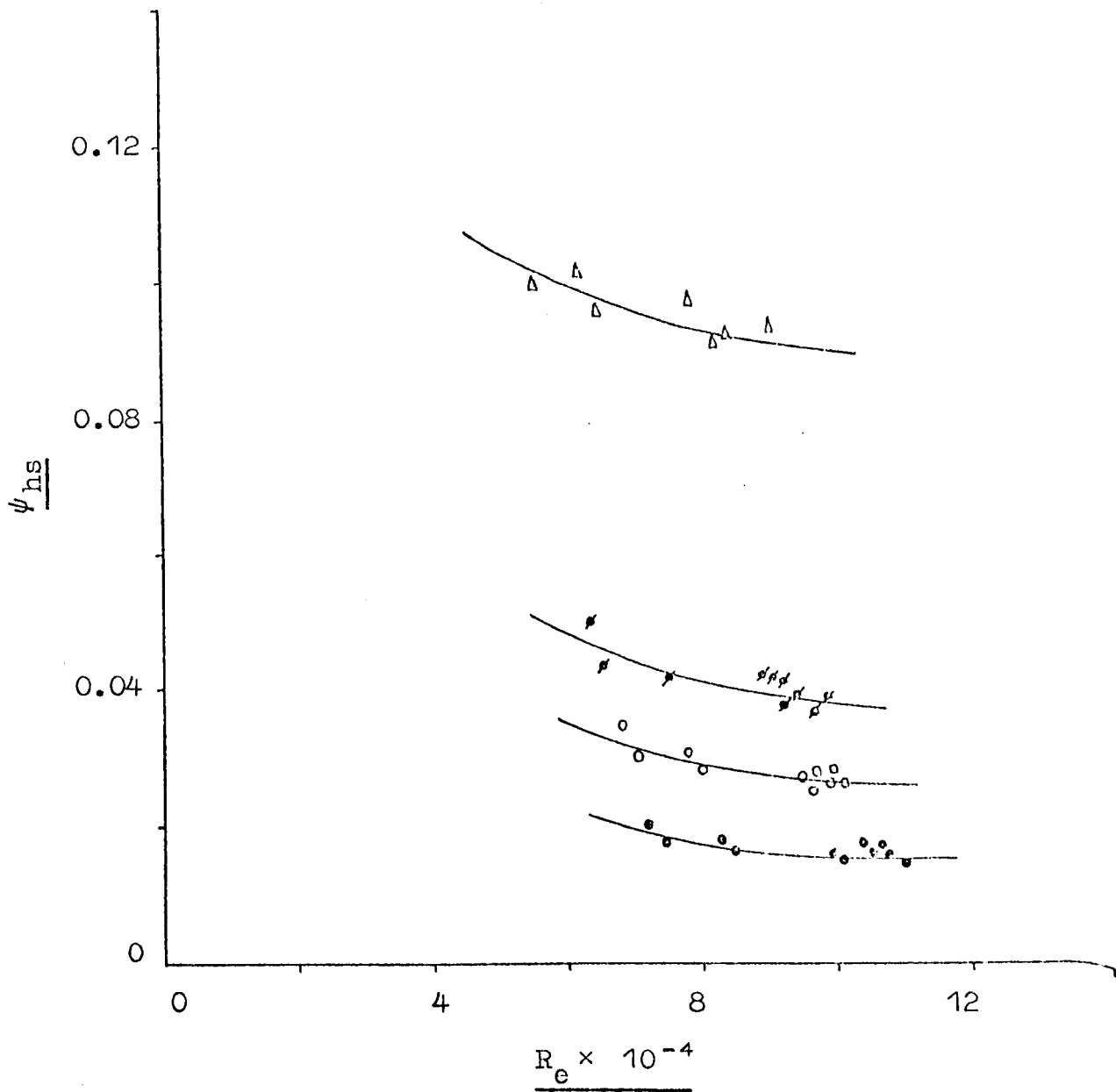


Fig. 6.20 Coefficient of Resistance for Flow through a 2
inch diameter Horizontal Duct, ψ_{hs} , Related to
Reynolds' number, R_e .

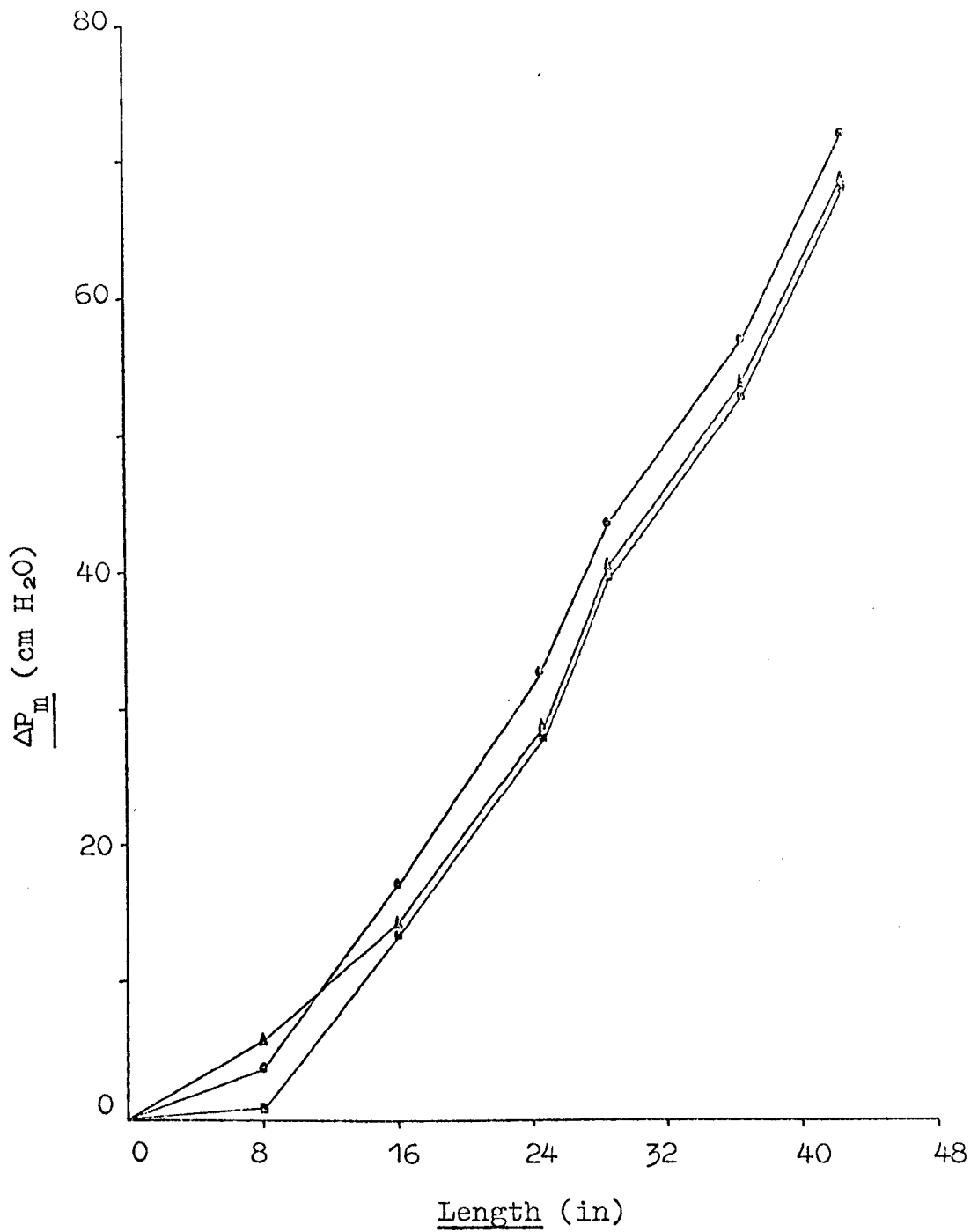


Fig. 6.21 Pressure Distribution along a One inch diameter
Horizontal Duct downstream from a Bend having a
Curvature Radius of 10 inches.

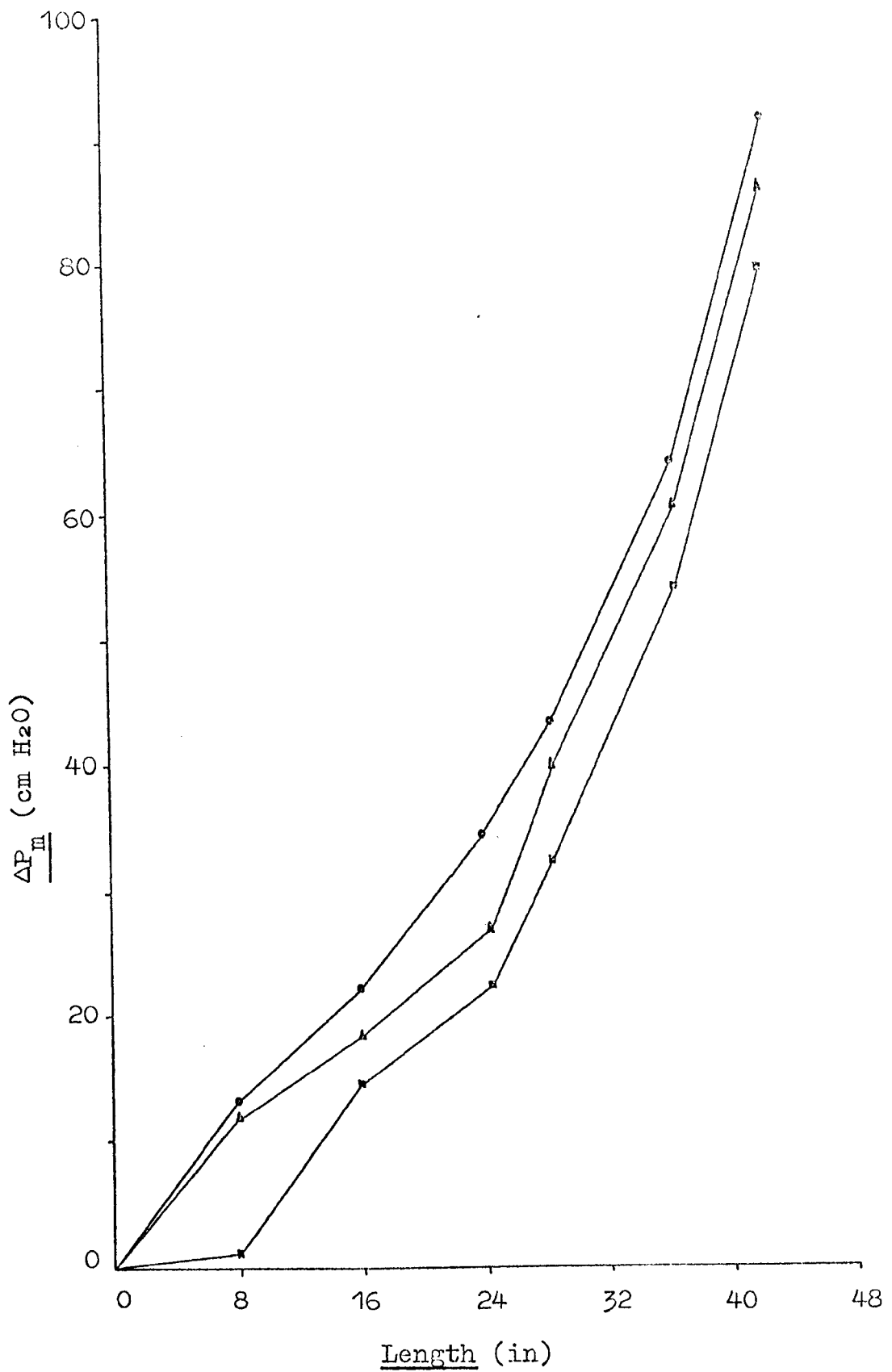


Fig. 6.22 Pressure Distribution along a One inch diameter
Horizontal Duct downstream from a Bend having a
Curvature Radius of 10 inches.

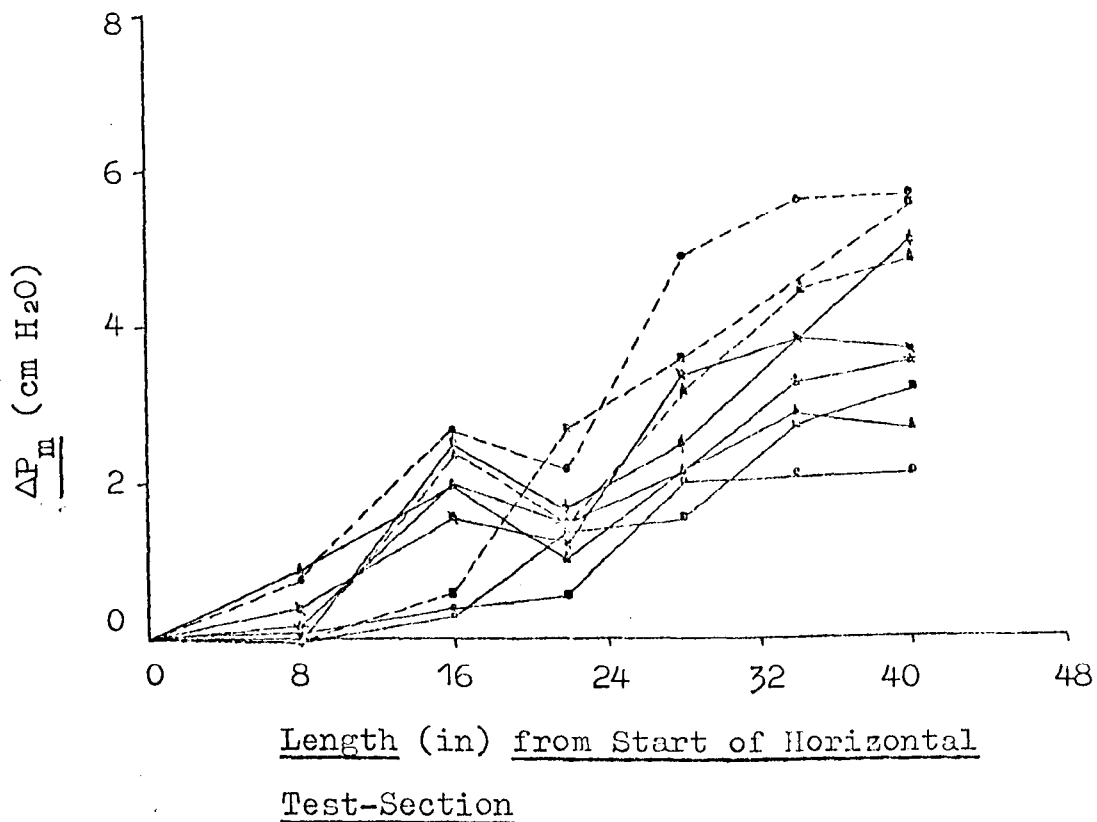


Fig. 6.23 Pressure Distribution along a 2 inch diameter
Horizontal Duct downstream from a Bend having a
Curvature Radius of 20 inches.

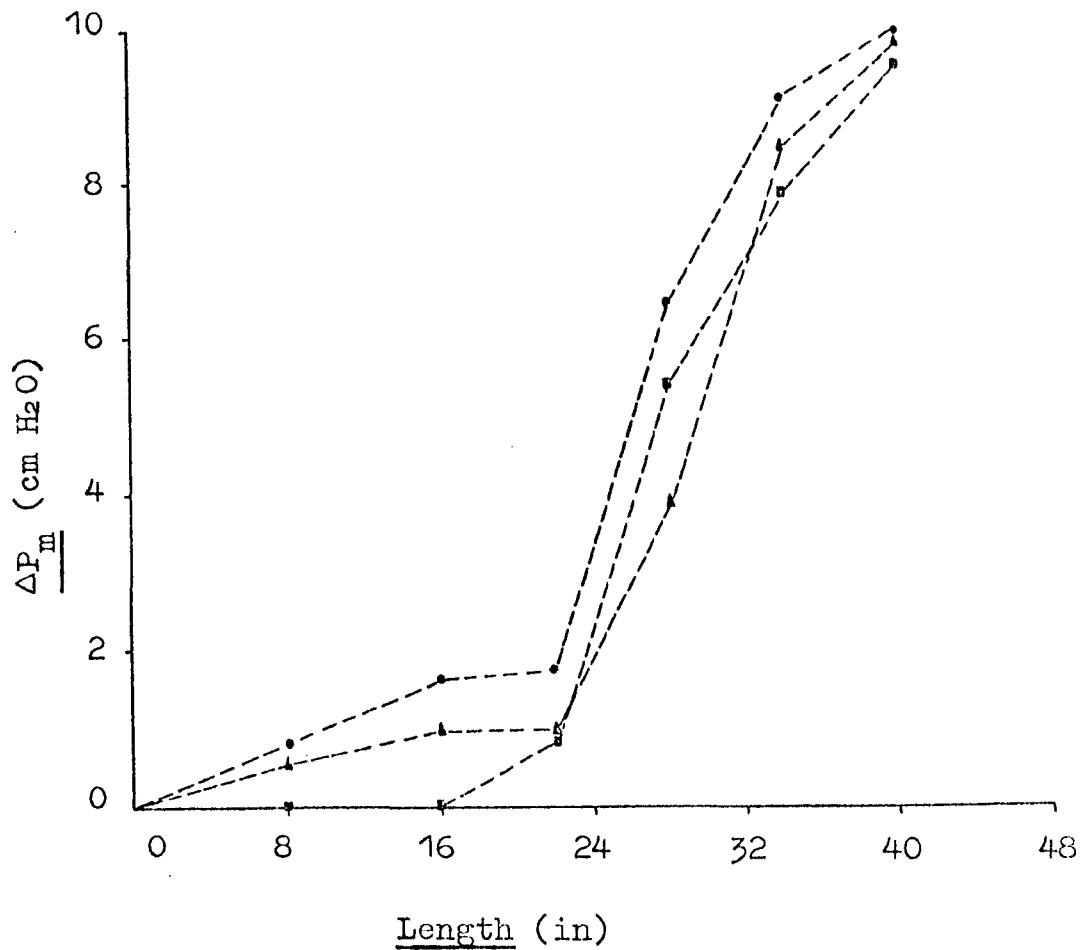
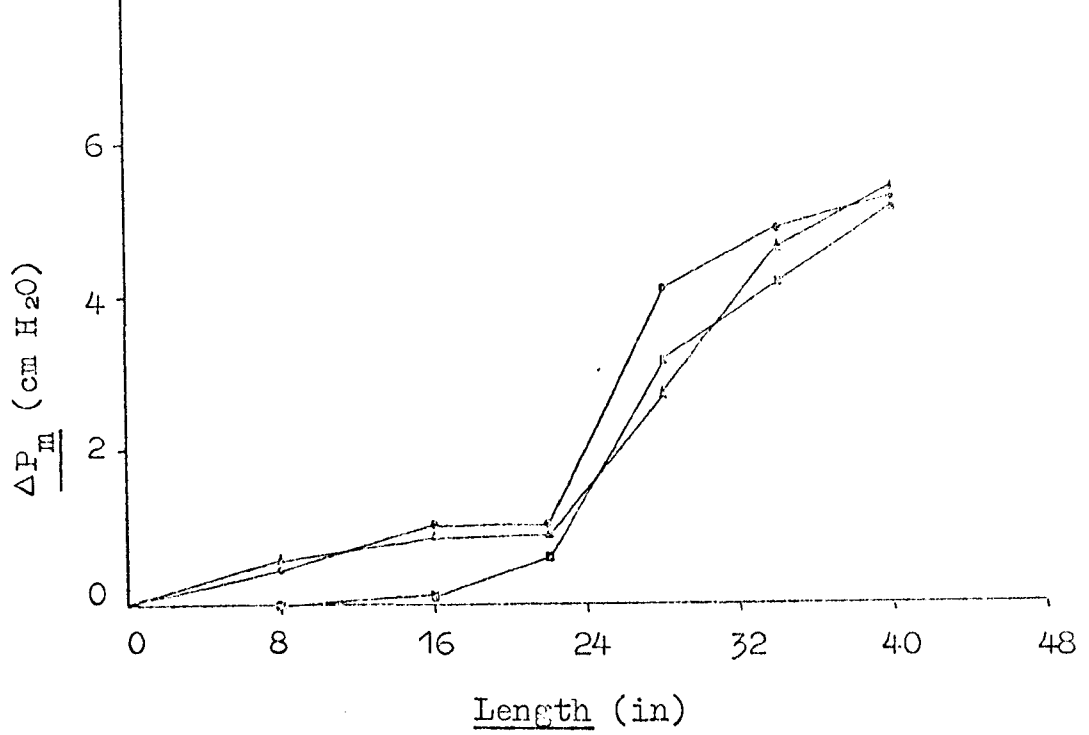


Fig. 6.24 Pressure Distribution along a 2 inch diameter
Horizontal Duct downstream from a Bend having a
Curvature Radius of 20 inches. - 213 -

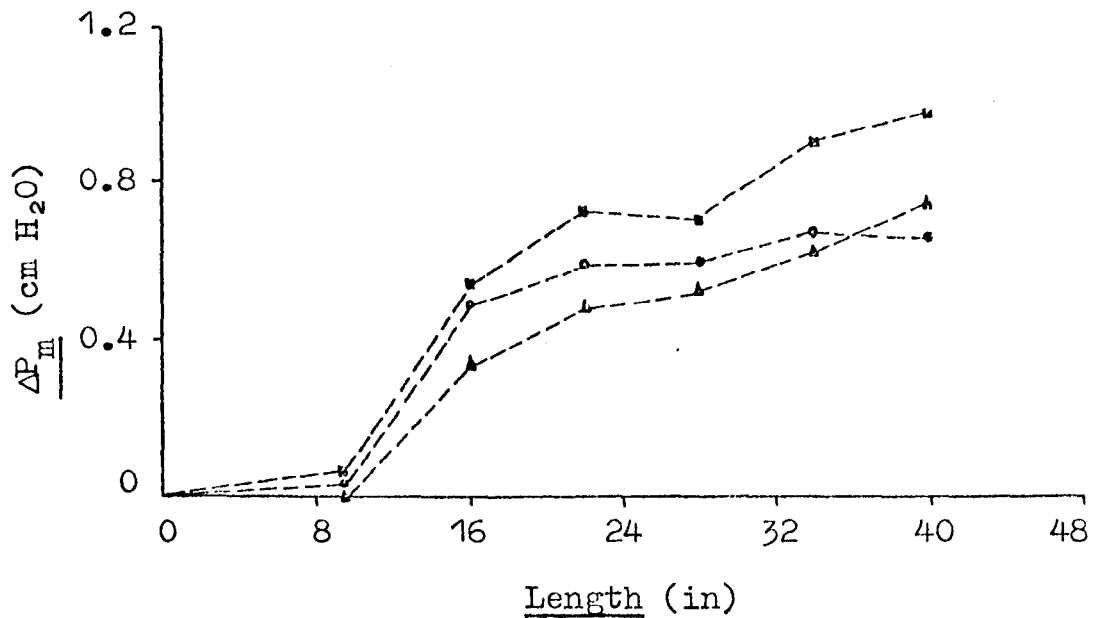
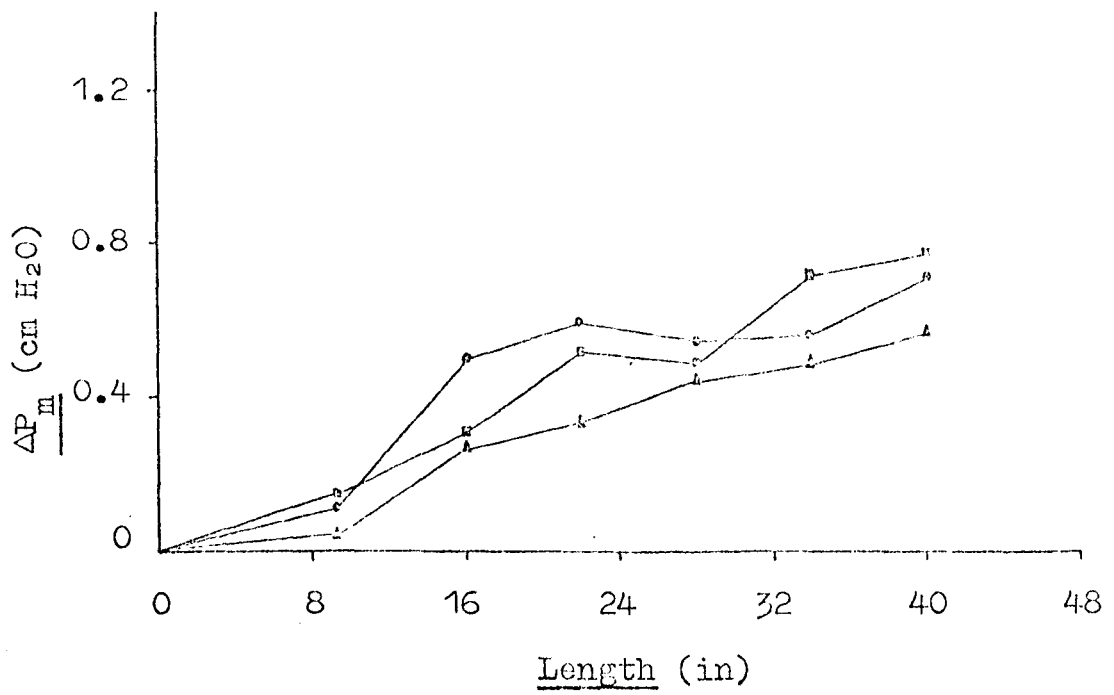


Fig. 6.25 Pressure Distribution along a 3 inch diameter
Horizontal Duct downstream from a Bend having
a Curvature Radius of 18 inches.

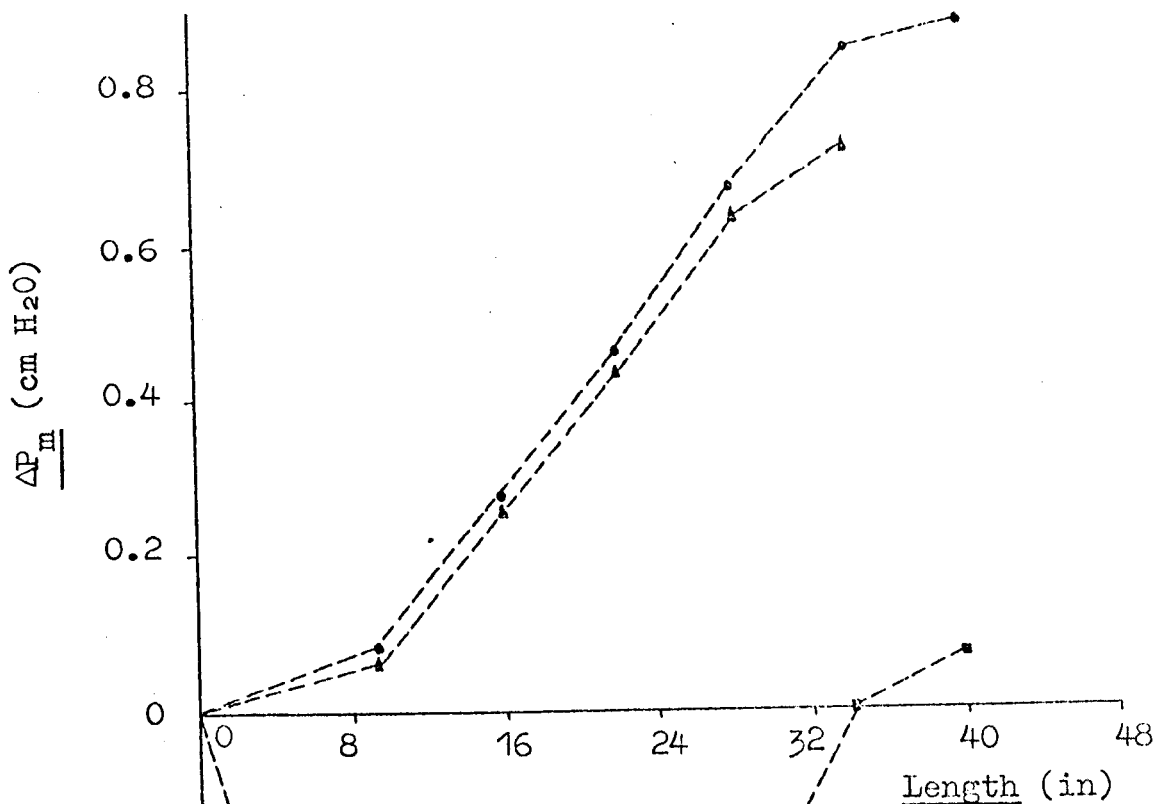
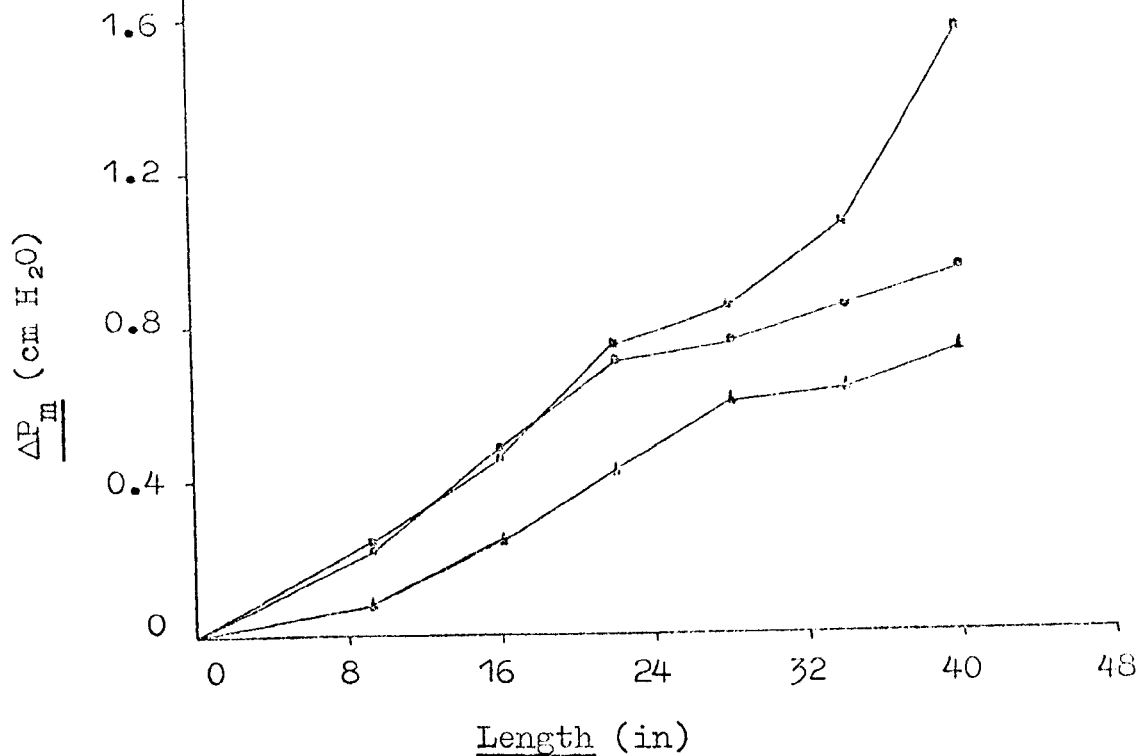


Fig. 6.26 Pressure Distribution along a 3 inch diameter Horizontal Duct downstream from a Bend having a Curvature Radius of 18 inches.

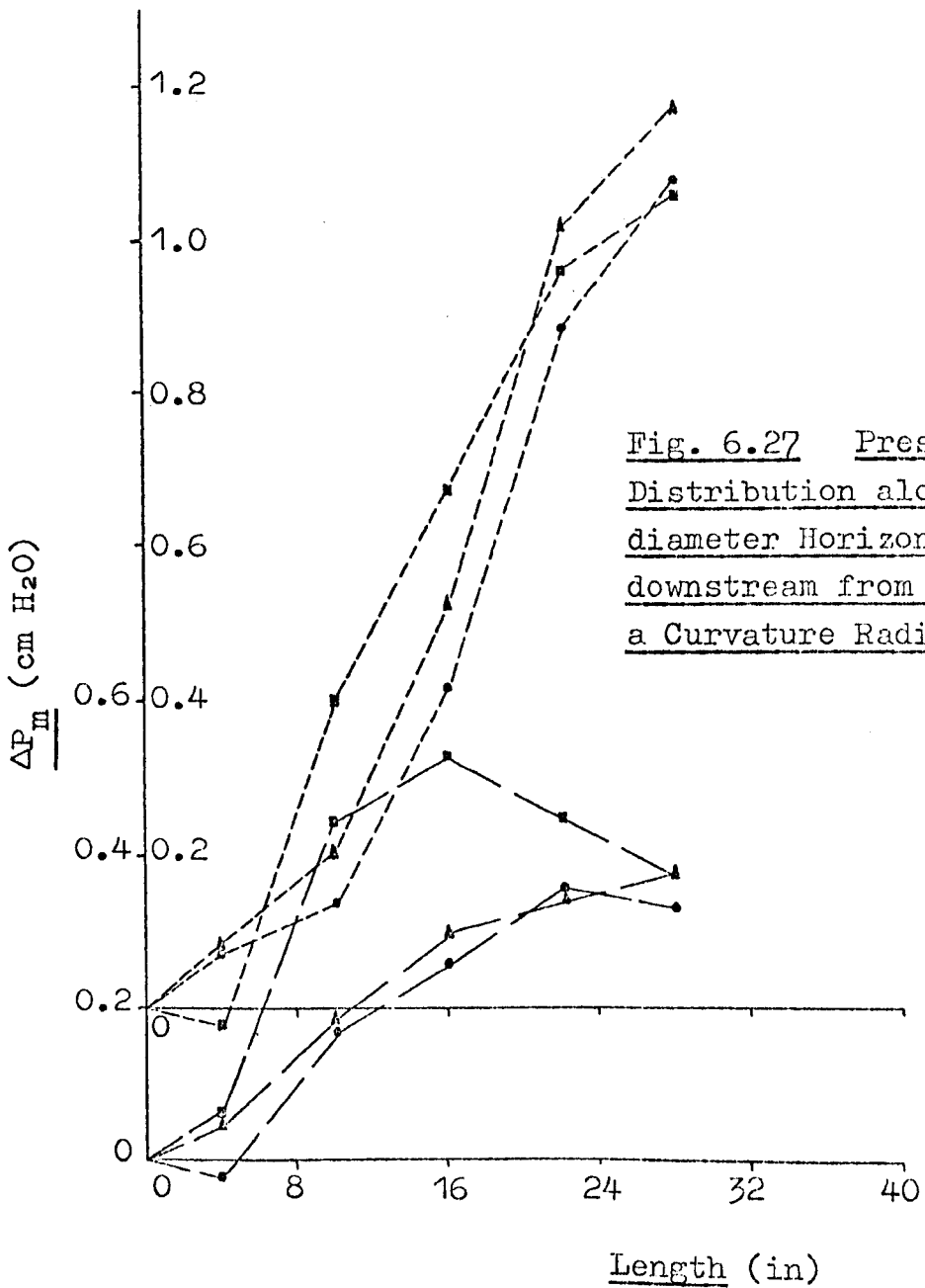
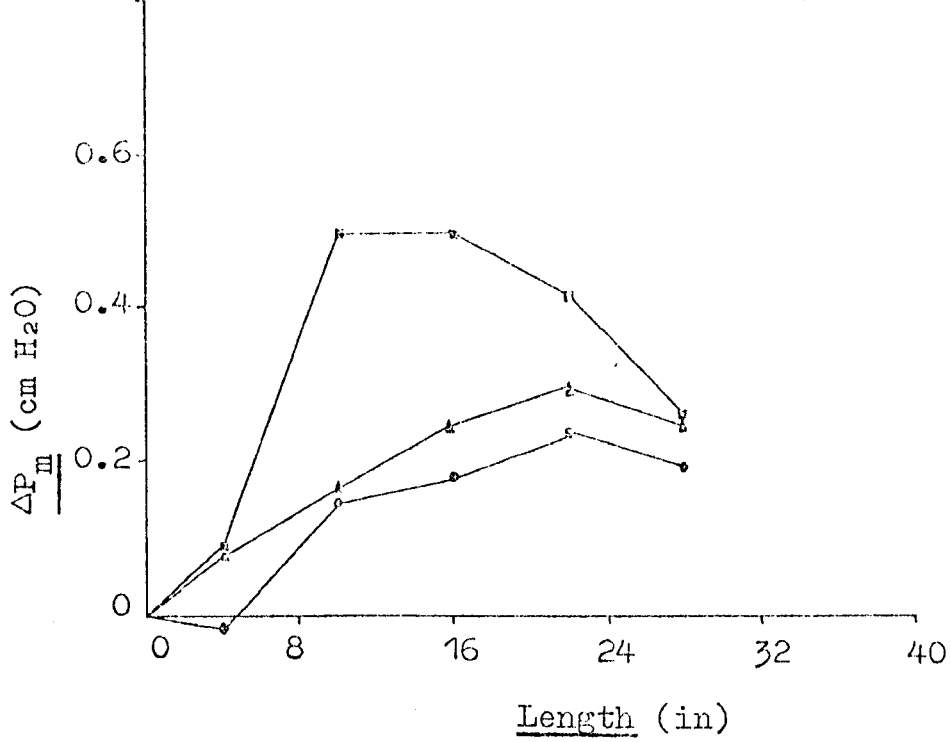


Fig. 6.27 Pressure Distribution along a 3 inch diameter Horizontal Duct downstream from a Bend having a Curvature Radius of 30 inches.

CHAPTER 7

GAS-SOLID FLOW THROUGH BENDS OF VARYING GEOMETRY

7.1 Introduction

The use of bends provides a pneumatic transport system with flexibility in layout but unfortunately introduces increased pressure losses, possible attrition of solid particles, and erosion of bends when the conveyed material is abrasive. The erosion aspects are discussed in Chapter 8, whilst this chapter examines the flow behaviour in bends of the solid particles and the resulting pressure drop.

Fundamental analysis of the problem is complicated by the secondary motion of the carrier fluid which is induced by centrifugal force effects. However, visual observations of the motion of particles has provided some understanding of the phenomena which occur in pipe bends. It has been reported³² that there are two basic categories of flow. Firstly the particles may slide around the outer radius of the bend as a relatively well-dispersed layer with the particles travelling much slower than the conveying air. The second category is usually restricted to large particles which suffer a number of collisions in traversing the bend, the particle trajectories between the particle-wall impacts sometimes being reported as straight lines³² and frequently as distinct curves⁴⁹. The actual motion of the solid phase undoubtedly depends upon particle velocity, phase density, bend geometry and orientation, and material properties, in addition to particle size.

Schuchart⁴⁹ summarises the work of Mühle¹¹⁷ who has studied extensively the paths followed by coarse particles when flowing around bends. Mühle states that particles

situated along the centre-line of the straight pipe preceding a bend, travel rectilinearly until they impinge upon the outer wall of the bend. The particles are then reflected at an angle which causes them to rebound from the outer wall of the bend several times. He states that the number of particle impacts is mainly dependent upon the curvature ratio (bend curvature diameter/duct diameter, β). The particles lose momentum on impact and are speeded-up after reflection by the flow medium. This sequence is repeated and, for a low initial velocity, the collisions may result in the particles eventually remaining in contact with the wall along which they slide at a decelerating rate.

Flow visualisation experiments performed during the present study with a vertical-to-horizontal 90 degree bend having a curvature ratio of 20, generally substantiates the observations of Mühle even though the present work used fine particles having a mean particle diameter of 15 microns. Deviating flow was not evident for a solids flow rate of 18 lb/min and a mean air flow velocity of 50 ft/s. This suspension appeared to be influenced by the bend curvature and a considerable proportion of the solids was well-distributed across the flow area, although there was a noticeable zone without moving particles along the inner bend surface. An interesting observation was the thin layer of static powder which had migrated to the inner wall and become deposited. The flow conditions were varied to 63 lb/min solids flow rate and 42 ft/s air velocity. The flowing suspension entering the bend progressed vertically upwards, the particles near to the outer wall became influenced by the bend and "cut-across" the main stream to impinge on the inner surface. The material

was then deflected towards the outer wall but had insufficient energy to penetrate the fast flowing main stream of particles. The deflections gradually became less severe but their influence was still apparent when the flow entered the horizontal pipe leading to the air filtering plant.

Relatively little information is available for the flow of single-phase Newtonian fluids in pipe bends, and it is a natural consequence that corresponding work for gas-solid suspension flows is particularly sparse. The following literature survey covers the majority of valuable contributions of which the author is aware.

7.2 Literature Survey

White's¹¹⁸ investigation into the flow of the Newtonian fluids, air, oil and water, through pipes having curvature ratios from 15 to 2050 at Reynolds' number values up to 4.1×10^4 , appears to be one of the first attempts to define the influence of curvature upon the resistance to flow. The experimental work was extensive and, despite the process of coiling the straight pipes causing some sections to become slightly oval, the overall accuracy of the results is impressive. White concludes his work with a simple empirical expression for the loss of head resulting from the flow of fluid in a coiled pipe.

The variation in the character of fluid flow due to secondary circulation has been examined mathematically for a perfect fluid in the absence of body forces by Hawthorne¹¹⁹. He noticed considerable deviations in the pressure loss coefficients for pipe bends obtained by different investigators and he attributed the discrepancies to differing velocity distributions at inlet to the bend. Further work concerning

the flow of single-phase fluids in bends and the associated secondary flow phenomenon is reported in references 120, 121 and 122.

Extensive measurements of the resistance numbers of pipe bends has been carried out by Ito^{102,123}, using water as the flow medium. Ito expresses concern over the conflicting correlations of many investigators and he suggests that a modified bend loss coefficient, $\Delta P_m / \frac{1}{2} \rho_f \bar{u}_f^2 \cdot \theta \cdot \beta^{\frac{1}{2}}$, expressed as a function of the non-dimensional number, R_e / β^2 , where β is the curvature ratio and θ the bend angle, provides a reliable correlation procedure and his experimental results seem to confirm this theory. Ito also draws attention to the fact that the influence of the bend produces substantial pressure losses in the downstream tangent.

The physical phenomena and the pressure drop which occurs when gaseous suspensions of solid particles are conveyed in bends have been studied by Segler¹², Weidner¹²⁴, Uematu and Morikawa¹²⁵, Haag¹²⁶, Uematu et al²⁸, Morikawa¹²⁷, Jung¹²⁸, Schuchart⁴⁹, Kriegel¹²⁹, and Kovacs¹³⁰.

Weidner developed equations for that portion of the total pressure drop for the bend, caused by the presence of the solid particles. He based his analysis on the assumptions that the material entering a bend is immediately thrown against the outer wall where it is decelerated by the frictional force between itself and the pipe wall; that the material receives no assistance from the gas stream as it travels around the bend, it relies solely upon its own kinetic energy; and that on leaving the bend it is re-accelerated to its original velocity by the conveying air. The final assumption is questionable since the material may continue to glide along

the wall of the ensuing straight section, losing momentum, before it becomes re-entrained by the gas stream. The first assumption is partly dependent upon the bend orientation and completely ignores the possibility of the particles re-bounding from the wall surface and become re-entrained by the gas stream whilst still in the bend. The last point also casts doubt upon the assumption that the particles rely entirely upon their own kinetic energy. The limited experimental confirmation of Weidner's pressure drop predictions and the dubious nature of his assumptions renders the work of uncertain value.

An experimental investigation into pressure drop relationships for granular materials flowing pneumatically around the bend of a horizontal conveyor has been performed by Uematu et al¹²⁵. The starting point of their data analysis is that the pressure drop due to fluid only flowing around a smooth bend, ΔP_{bf} , may be expressed as:-

$$\Delta P_{bf} = \psi_{bf} \cdot \frac{1}{2} \rho_f \bar{u}_f^2 \quad (1)$$

where $\psi_{bf} = \phi \{R_e, \theta, \beta\}$ (2)

ψ_{bf} is a coefficient of resistance for the bend, having an angle of deviation θ , through which a single phase fluid is flowing. Evidence is quoted that ψ_{bf} becomes a minimum for $4 < \beta < 6$, whereas the pressure loss rises hyperbolically for $\beta < 4$. Uematu was influenced by industrial practice and his 90 degree bends had β values of 12 and 20, which are precisely the same as used in the present study. The materials transported through the 2.74 cm diameter pipe network were millet seed and white sesame having mean particle diameter of 1630 microns. It is interesting to note that reference is

made to the difference in pressure levels at various points in the same cross-section of the bend, as determined from the four pressure tappings at each interval. The pressures were recorded independently, but according to Figs. 2 and 3 there appears to be almost insignificant variation in the values, which is somewhat confusing when one considers the quite definite observations by other investigators of "bouncing flow" with large particles. In fact, they recommend the use of only one pressure-recording point whether or not material is being transported, and in the remainder of their work they averaged the four pressures at each cross-section. These findings are completely at variance with the present study and although there is an enormous difference in the size of particles used in the two investigations, the author considers that the effects of flow deviation discussed in sections 6.5 and 7.5 would have been noticeable had Uematu used more than one series of tappings between $\theta = 0^\circ$ and $\theta = 90^\circ$. They conclude by observing that the effect of the bend on the upstream flow is insignificant, whilst part of the additional pressure loss induced by the bend occurs in the downstream straight section. The pressure loss attributed to the particles being transported is defined in the form of a resistance coefficient for the bend and particles, ψ_{bp} , being equal to $B \cdot W_p / W_f$, where B is a constant for a particular bend, for example, $B = 0.830$ when $\beta = 20$ and $B = 0.964$ when $\beta = 12$. This line of investigation was continued by Uematu et al²⁸ in a programme of work which again used millet seed and 2.88 cm bore tubing, but used six bends for the pressure loss tests having curvature ratios from 11.2 to 19.5. Their results showed that the pressure drop in a bend upwards from the

horizontal to the vertical is greater than in a bend from the vertical upwards to the horizontal. Morikawa¹²⁷ has simply reproduced the work contained in references 28 and 125.

Haag¹²⁶ produced an oversimplified analysis for pressure losses in bends, the work being based upon dubious assumptions leading to such questionable conclusions that short radius bends can produce less pressure drop than long radius bends.

An interesting series of extensive experimental tests with rather coarse particles (1490 → 2960 microns) flowing around bends of different curvature has been reported by Schuchart⁴⁹. He examined the resistance behaviour of the solids for horizontally situated 90° bends in an attempt to produce an appropriate resistance law. Analysis of the experimental data produced a simple empirical equation, applicable to the particular system parameters, in which only the curvature ratio is a variable:-

$$\psi_{bp}/\psi_{hp} = 210\beta^{-1.5} \quad (3)$$

ψ_{bp} is the resistance number of the bend for the solids phase only, and ψ_{hp} is the resistance number of the equivalent length of straight horizontal pipe for the solids phase. Apart from the elastic properties of the particulate matter and the material of the pipe wall, Schuchart considered that the pressure loss around a bend due to the flowing suspension is dependent upon R_e , F_R , W_p/W_f , ρ_p/ρ_f , d_p/D , and β . The total pressure loss, ΔP_m , being related to the resistance number, ψ , by the expression:-

$$\psi = \frac{\Delta P_m}{\frac{1}{2}\rho_f \cdot \bar{u}_f^2} \cdot \frac{D}{L} \quad (4)$$

The length, L , of a duct of diameter, D , becomes the arc length, $(\pi/4 \cdot \text{Curvature diameter})$, for a 90° bend. Schuchart noted that the solid particles accelerate well downstream from the bend and when evaluating the bend resistance number for the suspension flow, ψ_{bs} , he used the total pressure drop due to the change in flow direction in equation (4), refer to Fig. 3. This presupposes that the downstream straight duct is of sufficient length and that the upstream length is relatively unimportant.

Kriegel¹²⁹ related the results of his bend wear experiments to pressure loss calculations by assuming that the loss was directly proportional to the impulse of the boundary grains. These boundary grains are the solid particles at the extremities of the flowing solid phase, which Kriegel infers are solely responsible for the development of the wear trough. He ignores the mass of particles between these boundaries on account of them impinging upon grains already present at the bend wall. Kriegel's procedure for the bend pressure loss evaluation is independent of the orientation of the bend, disregards the solids intensity and distribution, and does not allow for particles being sufficiently deflected to become re-entrained by the conveying air. Kriegel deals at length with Ito's^{102,123} experiments and techniques of graphical interpretation, which influence his attempts to substantiate a theory derived entirely from the impulse loss concept of the impacting boundary grains. He does express concern that his equation for the bend coefficient of resistance of the solid phase does not include a description of the conveyed material characteristics, which are well known to be a decisive factor in the erosion process.

In a recent paper Kovacs¹³⁰ presents a mathematical approach for the calculation of pressure drop due to solids being conveyed around 90° bends having different orientations. His analysis assumes that the particles slide along the outer wall of the bend and become accelerated by the gas stream at exit from the bend. Consequently, the total pressure loss is a function of contributions from within the bend itself and in the downstream straight section. Kovacs concludes that the greatest pressure drop occurs with a vertical-to-horizontal bend, which completely contradicts Haag's¹²⁶ statement that a vertical bend with vertical approach is strongly recommended for pneumatic transportation, whilst horizontal bends should be avoided.

7.3 Experimental Procedure

The method of plant operation is described in section 3.4 and the technique of acquiring pressure measurements for the bend explained in section 4.4.3.1. Continual attention was paid to the manometer tubes connected to the outer wall pressure tappings, since these generally were the first tappings to become blocked. This undesirable feature was immediately evident in either total cessation of the normal small fluctuations of the manometric fluid or in a continually rising manometer reading. The technique explained in section 4.4.2.2 of purging the manometer lines with high pressure nitrogen was frequently carried out.

7.4 Data Analysis

The theoretical procedure outlined in Chapter 5, section 5.4 for gas-solid flow through vertical ducts applies also to this part of the study.

Additional parameters evaluated by the computer program

(see appendix A.1.2) included several dimensionless groups declared of some importance by other workers in this field. Ito^{102,103} used the following two groups for correlation purposes:-

(i) An "extended Reynolds' number"

$$= R_e / \beta^2, \text{ where } \beta \text{ is the curvature ratio.}$$

(ii) A "related resistance number"

$$= \frac{\Delta P_m}{\frac{1}{2} \rho_f \bar{u}_f^2 \cdot L/D \cdot \beta^2 \cdot \theta}$$

where θ is the bend angle and equal to $\pi/2$ for the 90° bends used in the present investigation.

The resistance number, as defined in section 5.4, was also evaluated for the bends, the pressure drop used being the difference in the static pressures recorded by the centre tappings at $\theta = 0^\circ$ and $\theta = 90^\circ$. Thus, the bend resistance numbers, ψ_b , referred to in this work do not include that part of the pressure loss induced by the bend which appears in the adjoining straight connecting pipes.

7.5 Results and Discussions

The results illustrated in Figs. 7.1 to 7.22 represent less than 10% of the data available from the experiments performed on six bends during the present investigation. It has been mentioned previously that it is proposed to analyse the remainder of these results at a later date and it is hoped that this initial report utilizes sufficient data to enable certain concepts to be formulated and to guide the more detailed analysis along the most fruitful directions.

The curves shown in Figs. 7.1 and 7.2, $\Delta P_m / \frac{1}{2} \rho_f \bar{u}_f^2$ versus L/D , reveal the transition between the state of the transported material ahead of and beyond the two inch diameter

bend having a curvature ratio of 20. The three curves shown in Fig. 7.1 represent flow conditions in which the phase density, defined by W_p/W_f , is increased from very dilute ($W_p/W_f = 0.24$) to relatively dense ($W_p/W_f = 3.28$), whilst the duct Reynolds' number is decreased from 10.98×10^4 to 6.20×10^4 . In all three instances the modified pressure gradient is linear for the suspension flowing vertically upwards from station A to station C. The gradient then increases from station C to station 2(a) due to the influence of the bend on the upstream pressure drop, the proportion, which increases with the solids-to-air ratio, is denoted by ΔP_{vb} in Fig. 7.1. The transported material retarded by the bend is then re-accelerated. The relatively linear pressure gradient between stations 6(a) and 12(a) for the downstream horizontal duct following the bend suggests that the particles are fully accelerated within the bend. As a result, part of the pressure drop due to the bend is not reflected in the ensuing downstream straight section which is contrary to the evaluation anticipated. Thus, the additional pressure loss brought about by the bend shows itself not only in the difference between the readings taken at the inlet and outlet of the bend, but also in the pressure distribution in the connected piping. The scatter of points in the bend section is explained during the discussion of Figs. 7.3 to 7.8. The gradient of the lines representing the overall pressure loss for the particular section is defined as the resistance number of the flowing suspension for that section.

The pressure distribution recorded by the centre, inside wall and outside wall static pressure tappings, denoted by 'a', 'b' and 'c' respectively, is shown in relation to the axial

distance around the bend in Figs. 7.3 to 7.8. Referring to Fig. 7.3 it can be interpreted for the very dilute suspension, that the gas-solid flow impinges on the outer wall surface at a bend angle of about 20° , resulting in a relatively high pressure being measured at station 3(c) due to a contribution to the normal static pressure from the dynamic pressure of the flowing suspension, causing an apparent gain in static pressure between stations 2(c) and 3(c) instead of the expected pressure loss. The flow deflects from the outer wall and station 4(c) experiences a suction effect which reflects in a large apparent pressure loss from 3(c) to 4(c), after which a linear pressure drop is obtained suggesting a well-dispersed flow from 4(c) to the bend exit at 6(c). Meanwhile, the centre tapplings indicate a large initial pressure drop from 2(a) to 3(a) and negligible pressure drop from 3(a) to 4(a), a similar distribution to that illustrated by the inside wall tapplings, due to the flow deflected from 3(c) impinging upon 4(b) and the static pressure loss from 3(b) to 4(b) being compensated by a dynamic pressure component. The flow deflects more gradually from 4(b) causing only a slight suction at 5(b) with the resulting excess pressure loss from 4(b) to 5(b). The centre tapplings, in like manner to the outer wall tapplings, record a relatively linear pressure distribution over the final section of the bend.

Increasing the solids flow rate from 2.8 to 11.2 lb/min for a slightly reduced air velocity results in only a slightly modified pressure distribution. The increased number of particles impinging in the region of 3(c) cause a measurable increase in the dynamic pressure contribution and substantial deflection of the flow is noticeable by the excessive pressure loss from 3(c) to 4(c) and the apparently zero pressure drop

from 3(a) to 4(a) and 3(b) to 4(b) for this dilute flow situation in which $W_p/W_f = 1.07$. The flow deviations become less severe with the solid phase fairly well-dispersed as it accelerates into the horizontal duct.

The third set of curves in Fig. 7.3 represent a fairly dense phase situation in which $W_p/W_f = 3.28$. The interesting feature is the linear pressure gradient shown by both the centre and inside wall tapplings. The outer wall tapplings conform to previous trends except for the final reading at 6(c), the data observation sheet noted that this tapping was becoming blocked and, in fact, the system was purged with high pressure nitrogen immediately following these recordings.

Comparing the three flow situations it is interesting to note that the pressure differential recorded by the static tapplings at inlet to and exit from the bend was similar for the very dilute and the relatively dense flows, the centre tapplings measuring 4.44 and 3.57 cm H₂O respectively. It appears that increasing the solids flow rate from 2.8 to 21.8 lb/min has a similar but reverse effect on the pressure loss to reducing the conveying air velocity from 128 to 76.3 ft/s. This observation illustrates the importance of operating a pneumatic transport system at the minimum safe conveying speed. The deflecting flow was evident for all the flow conditions, although there were indications that, with increased numbers of very fine particles moving relatively slowly, the deflecting flow subsequent to particle-wall impact and the secondary flow phenomenon induced by the centrifugal force was effectively suppressed and a linear pressure gradient, as reported for coarse particles, obtained.

Fig. 7.4 illustrates the effect of W_p/W_f and Reynolds'

number upon the pressure distribution obtained from the static pressure tappings situated around the bend. The expected large pressure differential towards the bend exit, due to the arrested particles becoming re-entrained by the conveying air and accelerated out of the bend, is obscured by the dominating influence of the deflecting flow characteristic of the suspension.

The pressure distributions for the three inch bend having a curvature ratio of 20, Fig. 7.5, and the one inch bend with a curvature ratio of 20, Figs. 7.6 to 7.8, can be analysed in a similar manner to the detailed case history just explained for the two inch diameter bend. The one inch bend pressure distributions are generally characterised by acceptably linear pressure gradients between stations 3 and 6. Fig. 7.8 clearly illustrates that the centre tappings at station 3 experience a pressure increase which substantiates that these "early" tappings do "benefit" from a dynamic pressure contribution.

The functional relationship between the bend resistance number, for either the flowing suspension or for the solid particles alone, and the solids-to-air mixture ratio has been reported as straight lines by Uematu et al^{125,28}, Morikawa¹²⁷ and Jung¹²⁸. It is not clear whether Jung's results are for suspension flow at a single value of Reynolds' number or not. He states that the only deviation from a linear relationship between the bend resistance number and the solids loading occurred for one bend only when $W_p/W_f > 0.6$. Jung's results covered the solids loading extent defined by $0.22 < W_p/W_f < 1.3$. Both Uematu and Morikawa plotted the bend resistance number for the solid particles only against solids loading for different values of the mean air flow velocity. Their results were

confined to the range $0.25 < W_p/W_f < 5.0$ for the two 90° bends having curvature ratios of 12 and 20. Although the points were well-spread there were sufficient of them to indicate general linear relationships having no dependence upon the air velocity, the gradients of these lines diminished as the curvature ratio increased and became very small for a curvature ratio of 20.

The resistance number for a gaseous suspension of fine alumina particles, ψ_{bs} , flowing around a bend, in relation to the solids loading, W_p/W_f , is shown in Figs. 7.9 to 7.13. These graphs represent the results for three bends, each having a curvature ratio of 20 and internal diameters of one, two and three inches. The two inch pipe tests, Figs. 7.9 and 7.10, show ψ_{bs} versus W_p/W_f to independent of Reynolds' number and becoming linear as W_p/W_f increases. The curves represented 240 and 500 mesh alumina particles and no evidence of a particle size effect is portrayed. The resistance number for air only was relatively constant at 0.027 throughout the entire range of solids loading, that is, $0.20 < W_p/W_f < 4.7$, thus enabling the resistance number for the particles only, ψ_{bp} , to be shown in relation to W_p/W_f . A definite particle size effect was evident for flow through the three inch bend with the very fine 500 mesh particles exhibiting a relationship between ψ_{bs} and W_p/W_f which is independent of Reynolds' number, Fig. 7.12. The curves for the larger particles, illustrated in Fig. 7.11, show a marked dependence upon Reynolds' number and do in fact display a good linear relationship between ψ_{bs} and W_p/W_f for higher values of Reynolds' number. The one inch bend results shown in Fig. 7.13 portray a similar pattern to Uematu and Morikawa, but it again becomes non-linear for low values of W_p/W_f .

The results obtained for the flow of pure air are shown in Fig. 7.16, in addition to some two-phase results, and are in complete agreement with Schuchart⁴⁹, however, these curves illustrate that the resistance number, ψ_{bs} , is independent of Reynolds' number over the particular range.

Ito^{102,123}, and later Kriegel¹²⁹, proposed a correlation procedure which relates the coefficient of resistance, ψ_{bs} , to the bend angle, θ , and the curvature ratio, β , and extends Reynolds' number by the curvature ratio. Thus the functional relationship between $\psi_{bs}/\theta \cdot \beta^{\frac{1}{2}}$ and R_e/β^2 is shown diagrammatically in Figs. 7.17 to 7.21. The linear relationship shown between these two parameters in Fig. 7.17 are the results for one particular test for a solids-to-air mixture ratio varying from 0.18 to 1.19. The results from other tests produced a family of straight lines more or less parallel to each other, a second such curve with W_p/W_f varying from 0.23 to 1.61, displaced because of a large Reynolds' number effect, is also shown in Fig. 7.17. These curves display similar trends to both Kriegel for gas-solid flow and Ito for single phase flow. Ito's curves, however, are effectively drawn for a constant value of W_p/W_f , that is, zero, and Fig. 7.18 illustrates the relationship between $\psi_{bs}/\theta \cdot \beta^{\frac{1}{2}}$ and R_e/β^2 for constant values of W_p/W_f . The flow of pure air produces results which show no dependence of $\psi_{bs}/\theta \cdot \beta^{\frac{1}{2}}$ upon R_e/β^2 , but the dependency increases with solids loading, as illustrated in Fig. 7.18. It is suggested that for a two inch bend having a curvature ratio of 20, the above procedure may provide an excellent correlation procedure for $W_p/W_f > 5$. This suggestion has been particularly qualified by specifying the bend geometry, since reference to Figs. 7.19 to 7.21 clearly illustrate that a general

correlation for all bends is most unlikely. However, the results displayed in Figs. 7.17 and 7.18 are sufficiently convincing to propose that further investigation along these lines is justified.

7.6 Conclusions

Measurements on bends have shown that an additional pressure loss is induced by a bend in the straight lengths of ducting upstream and downstream from the bend. The present study clearly showed an upstream pressure loss contribution but the expected downstream effect was either obscured by unreliable results due to a deviating flow or, less likely, that the solid particles became fully accelerated within the bend.

The four pressure tappings at intervals around the bend allowed the pattern of flow behaviour in several different situations to be ascertained. A clear picture was provided of the deflecting nature of the flow of fine particles, a theory previously attributed to relatively coarse particles only. The results of this investigation are at variance with the findings of Uematu and Morikawa, who reported negligible differences in the pressures recorded by an identical arrangement of pressure tappings to that used in the present work.

The linear relationship between the total resistance number for a suspension flowing around a bend and the solids-to-air mixture ratio, reported by other authors, is not generally confirmed. The relationship tends to become linear as W_p/W_f increases and there is a general independence of Reynolds' number, however, it is shown that the precise correlation depends very much on the system parameters.

The functional relationship between a related

coefficient of resistance, $\psi_{bs}/\theta \cdot \beta^1$, and an extended Reynolds' number, R_e/β^2 , holds some promise of providing a valuable correlation procedure for gas-solid flow in bends.

7.7 Suggestions for Further Work

The author of the present study was concerned at the complete disregard of other investigators in the variation of pressure distribution within the bend, and feels that further study with more bends and a wider variation of particle sizes is warranted. It is stressed that, where possible, transparent bends should be utilised and an attempt made to relate the visually observed flow behaviour of the particles to that predicted from the pressure distributions. This suggestion was followed to a very limited extent during this investigation.

A short-coming of the present equipment was the length of ducting downstream from the bend, and further experimental work should take this into account.

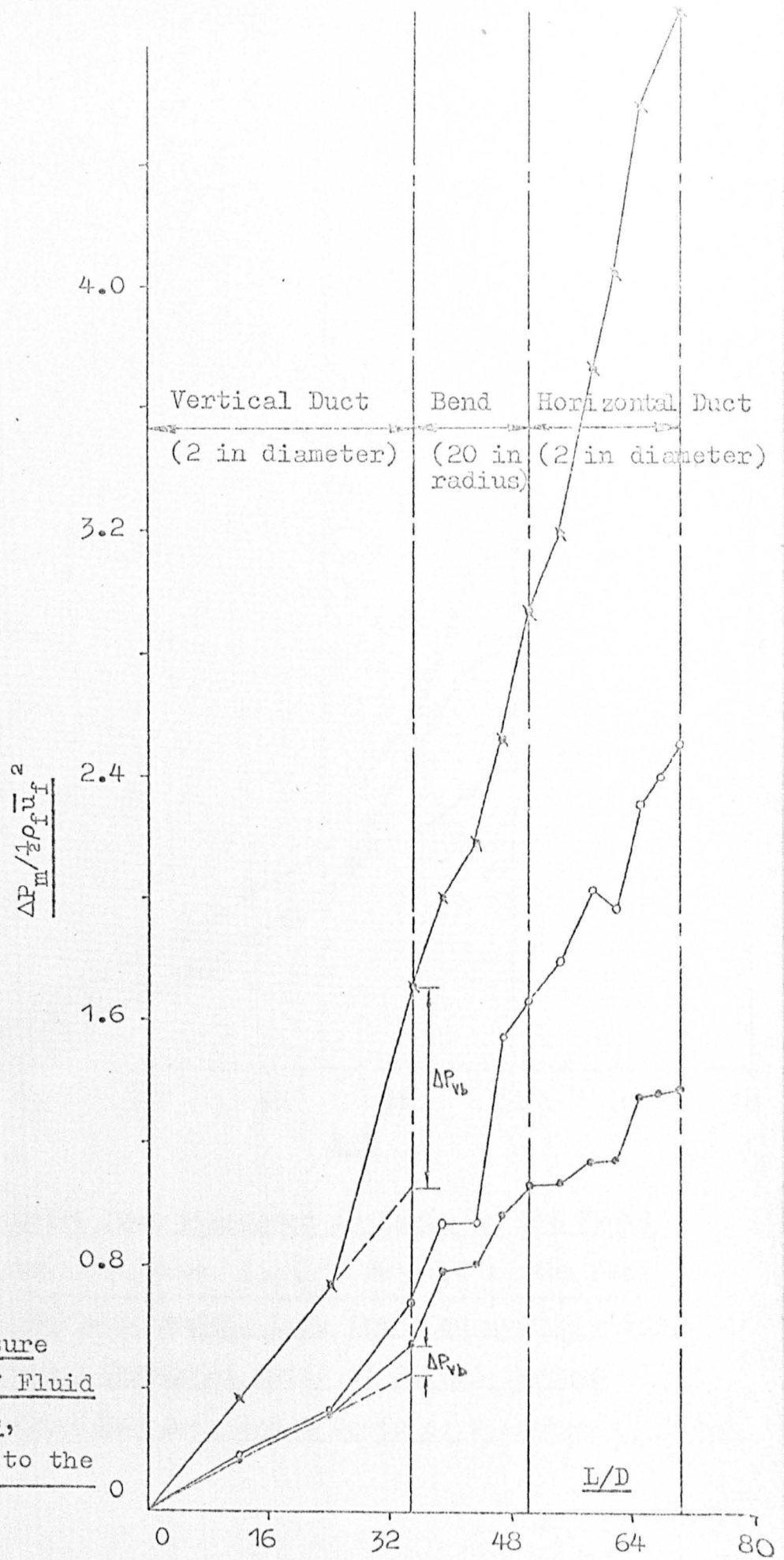


Fig. 7.1 Pressure Drop in terms of Fluid Dynamic Pressure, $\frac{1}{2}\rho_f \bar{u}_f^2$, related to the Non-Dimensional Length, L/D .

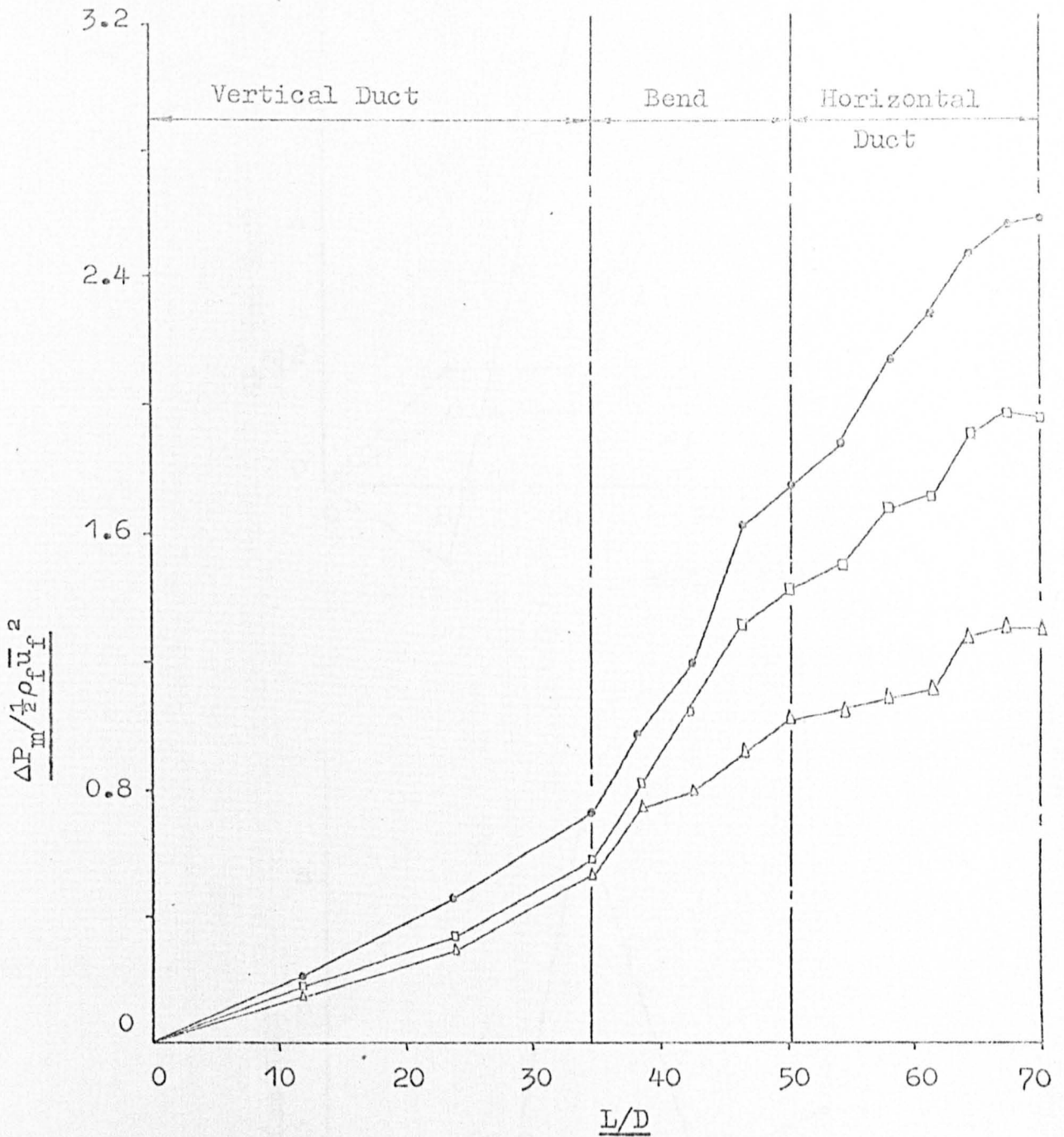


Fig. 7.2 Pressure Drop expressed in terms of the Fluid Dynamic Pressure, $\frac{1}{2} \rho_f \bar{u}_f^2$, related to the Non-Dimensional Length, L/D , for Flow around a Bend having a Curvature Ratio of 20 and through Vertical and Horizontal Ducts of 2 inches diameter.

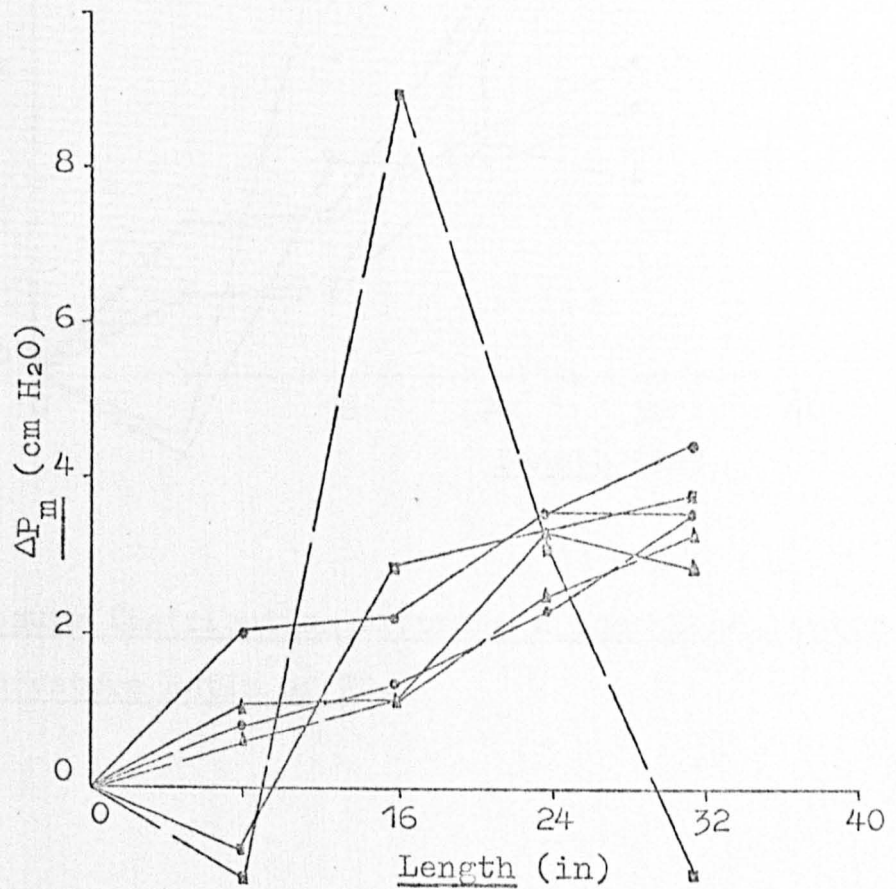
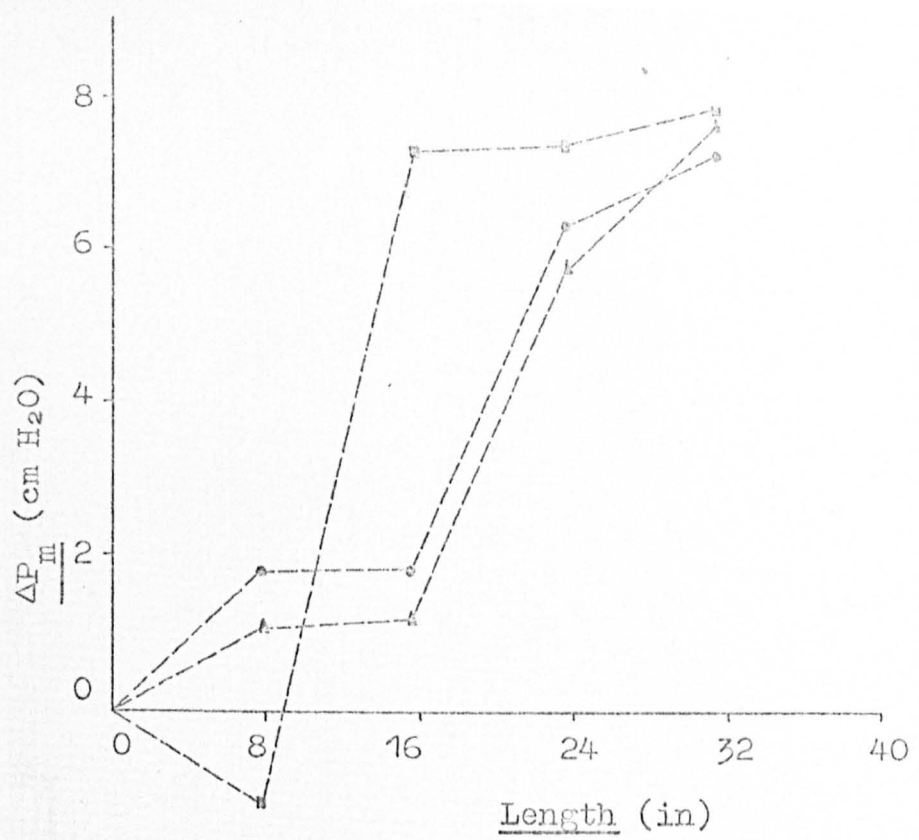


Fig. 7.3 Pressure Distribution around a 2 inch Bend having a Curvature Ratio of 20.

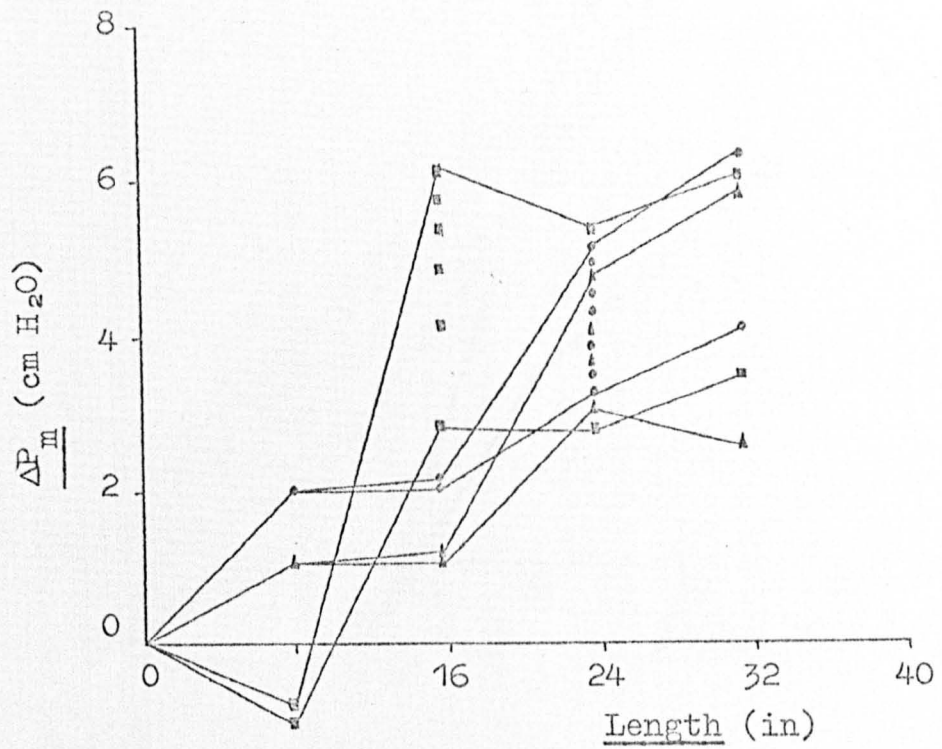


Fig. 7.4 Pressure Distribution around a 2 inch Bend having a Curvature Ratio of 20.

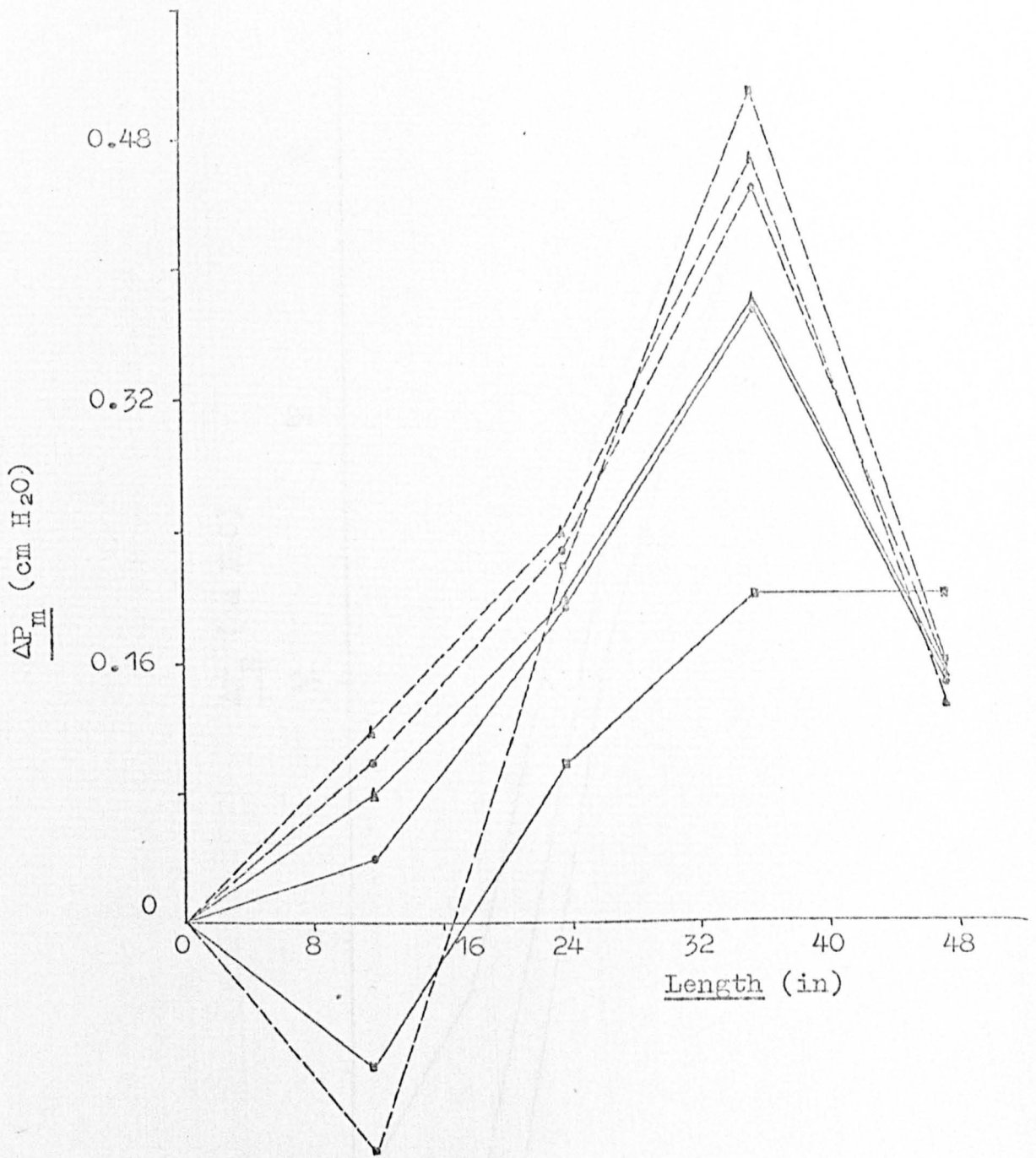


Fig. 7.5 Pressure Distribution around a 3 inch Bend having a Curvature Ratio of 20.



Fig. 7.6 Pressure Distribution around a One inch Bend having a Curvature Ratio of 20.

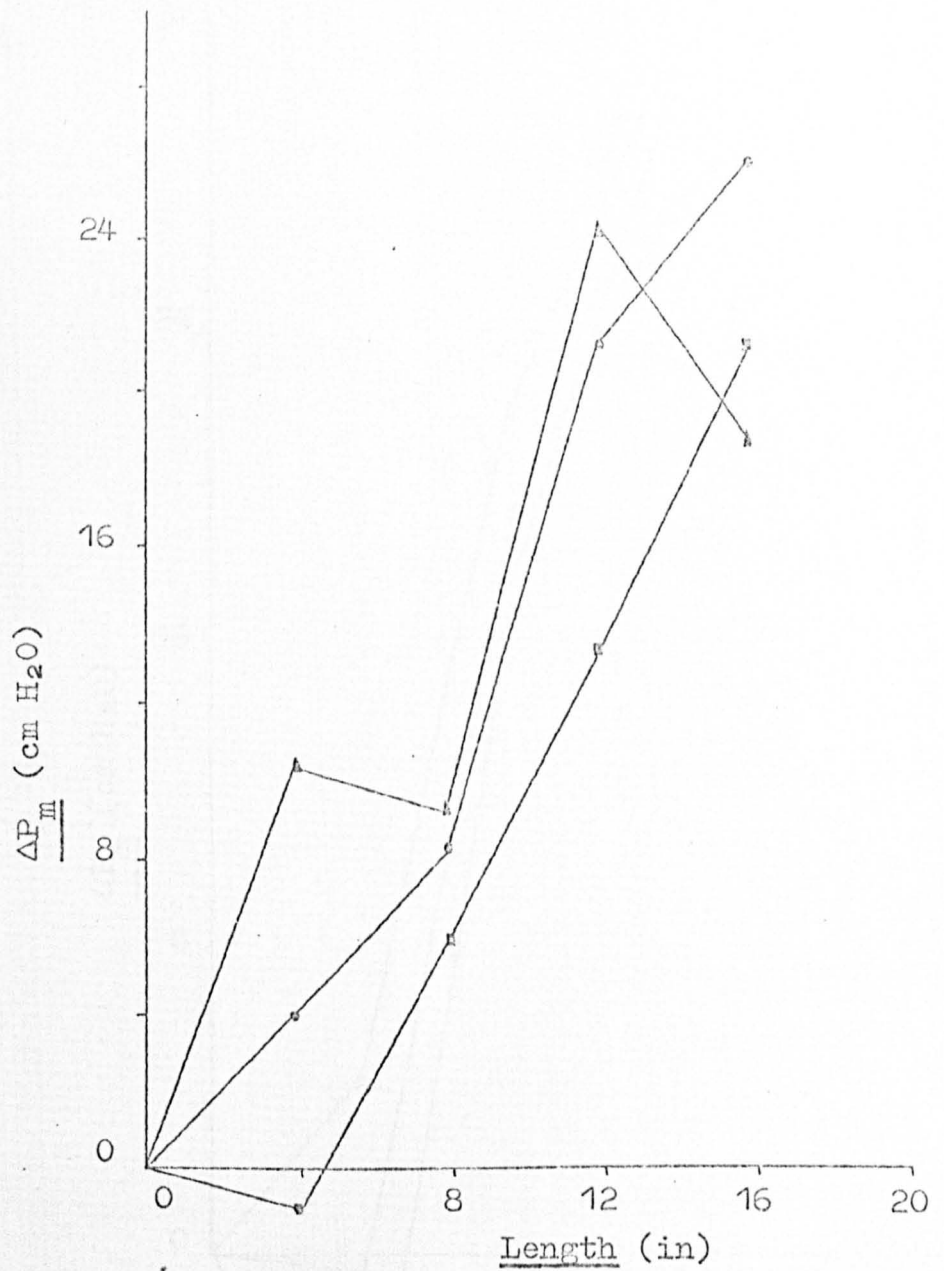


Fig. 7.7 Pressure Distribution around a One inch Bend having a Curvature Ratio of 20.

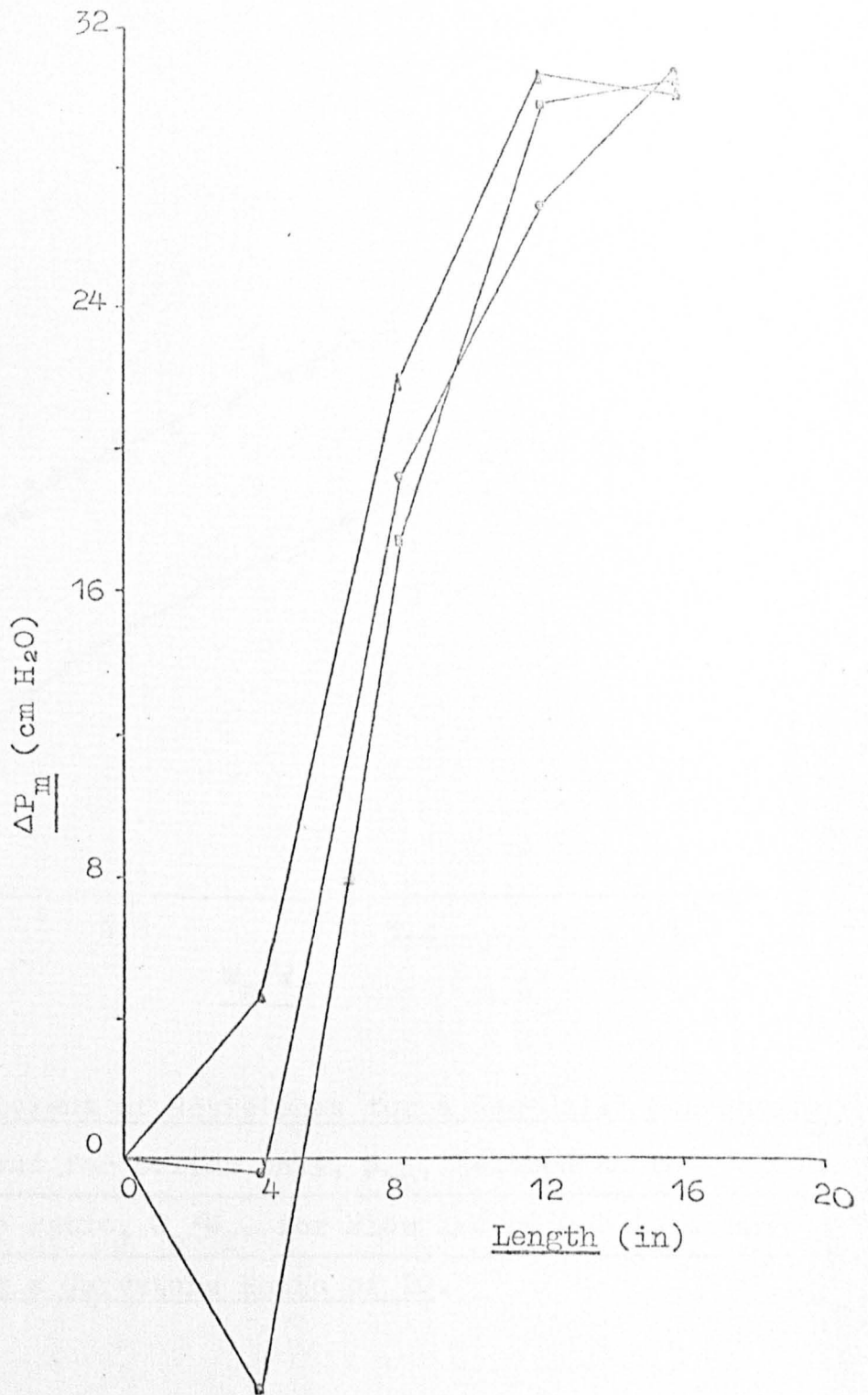


Fig. 7.8 Pressure Distribution around a One inch Bend having a Curvature Ratio of 20.

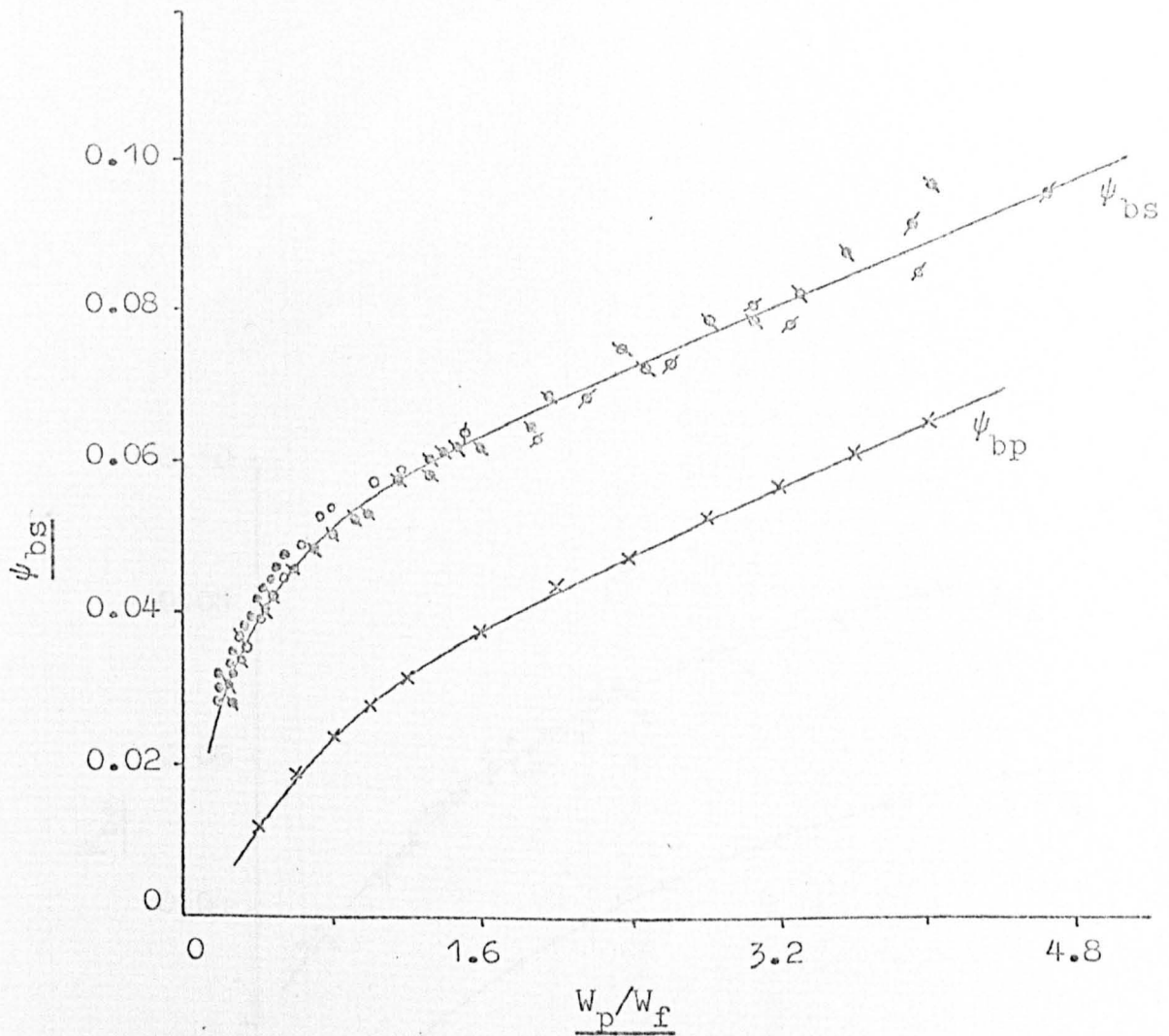


Fig. 7.9 Coefficient of Resistance for a Gas-Solid Suspension,
 ψ_{bs} , and for Solids only, ψ_{bp} , Related to the Solids-
to-Gas ratio, W_p/W_f , for Flow around a 2 inch Bend
having a Curvature Ratio of 20.

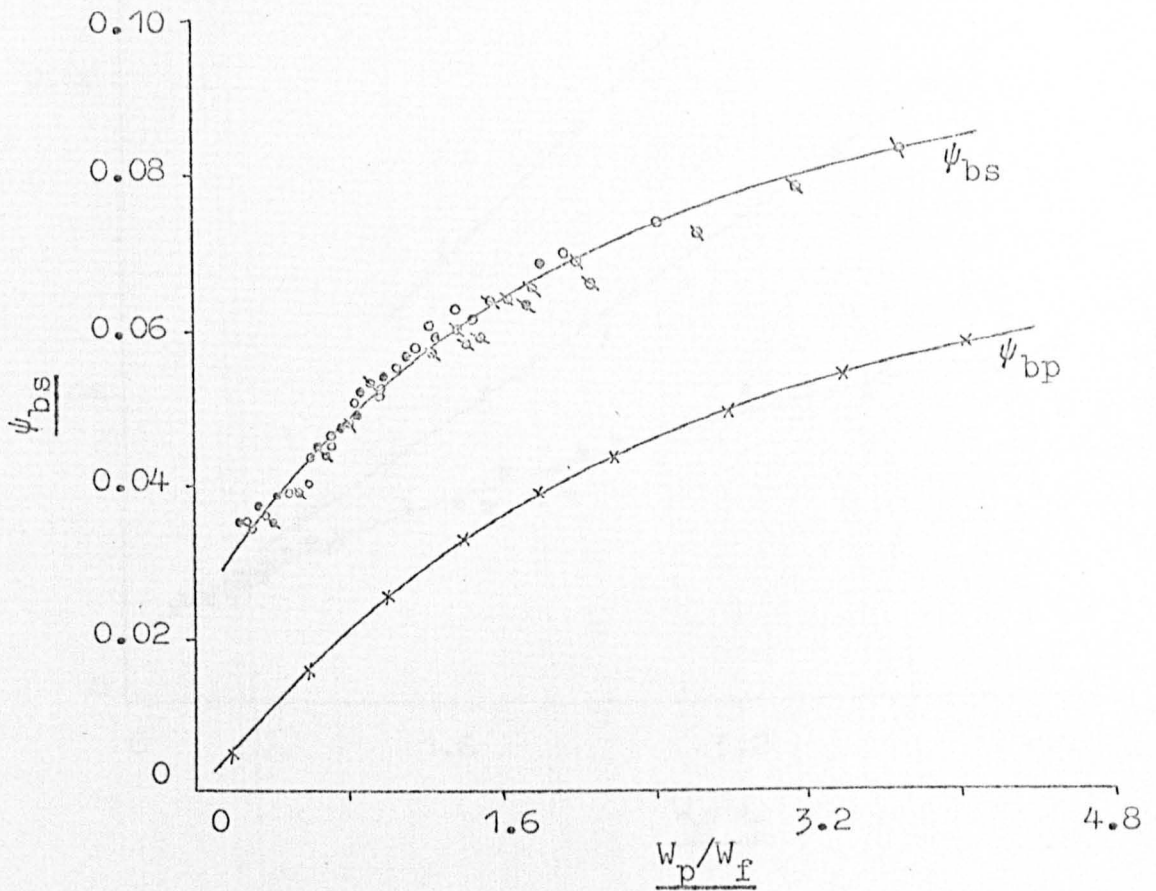


Fig. 7.10 Coefficient of Resistance for a Gas-Solid Suspension, ψ_{bs} , and for Solids only, ψ_{bp} , Related to the Solids-to-Gas ratio, W_p/W_f , for flow around a 2 inch Bend having a Curvature Ratio of 20.

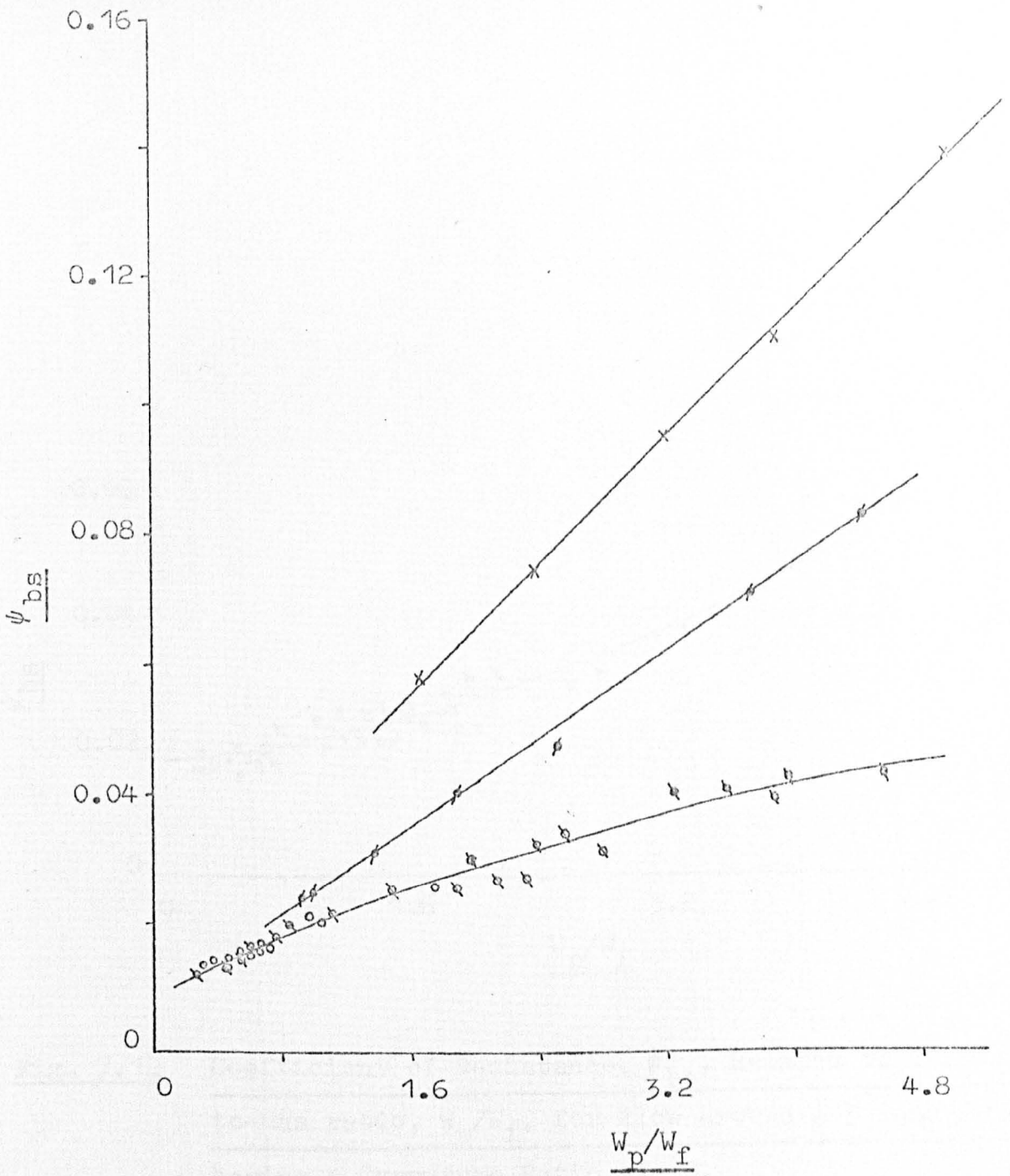


Fig. 7.11 Coefficient of Resistance, ψ_{bs} , Related to Solids-to-Gas ratio, W_p/W_f , for Flow around a 3 inch Bend having a Curvature Ratio of 20.

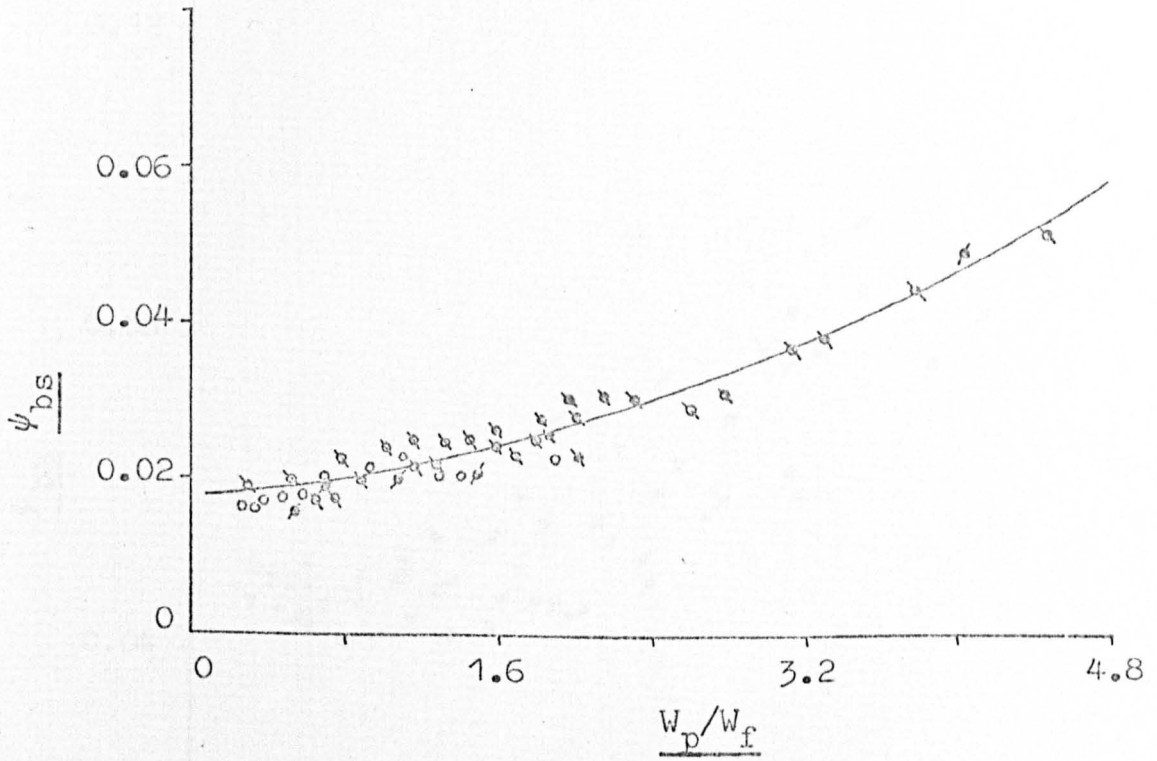


Fig. 7.12 Coefficient of Resistance, ψ_{bs} , Related to Solids-
to-Gas ratio, W_p/W_f , for Flow around a 3 inch Bend
having a Curvature Ratio of 20.

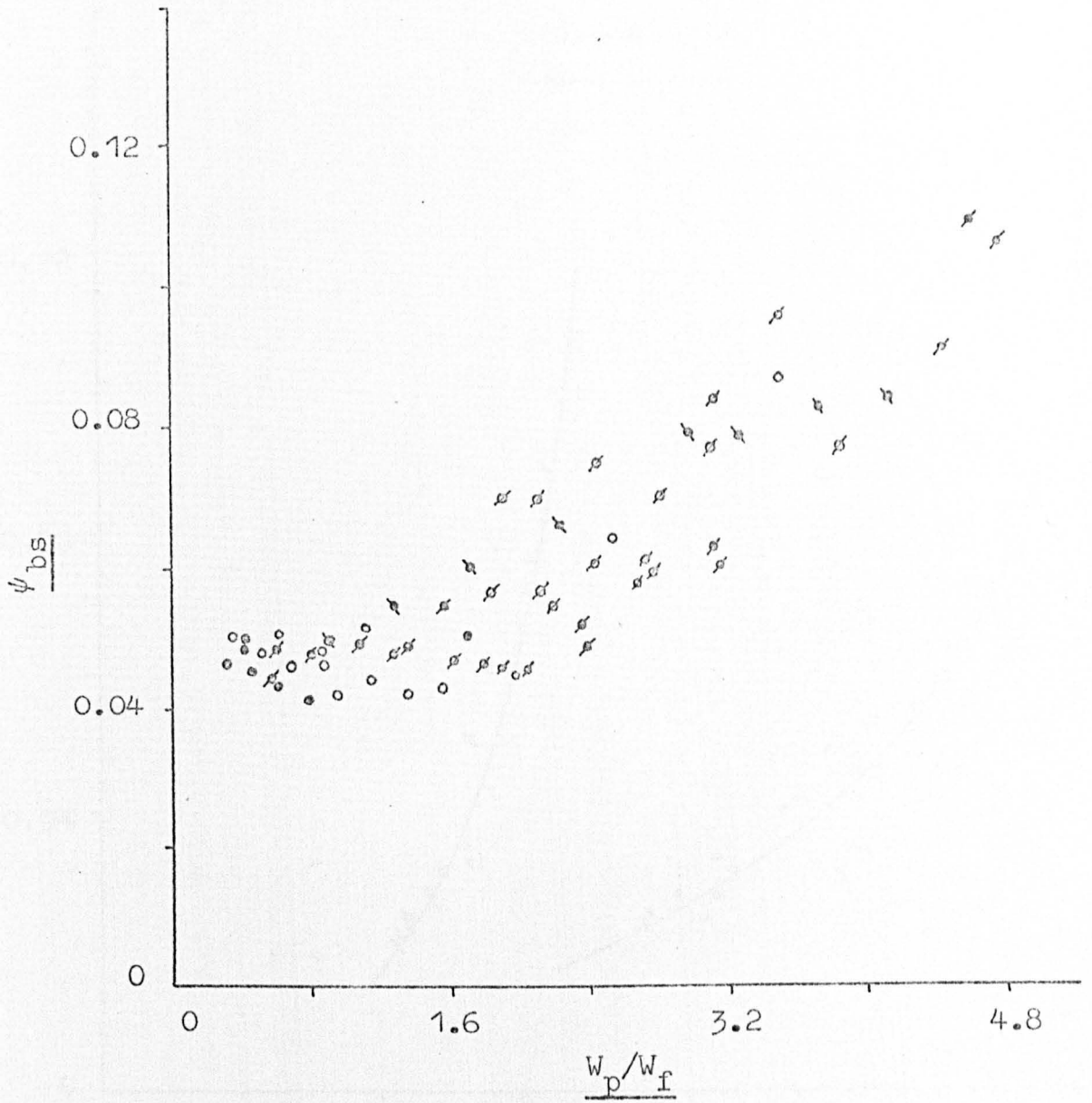


Fig. 7.13 Coefficient of Resistance, ψ_{bs} , Related to Solids-
to-Gas ratio, W_p/W_f , for Flow around a One inch
Bend having a Curvature Ratio of 20.

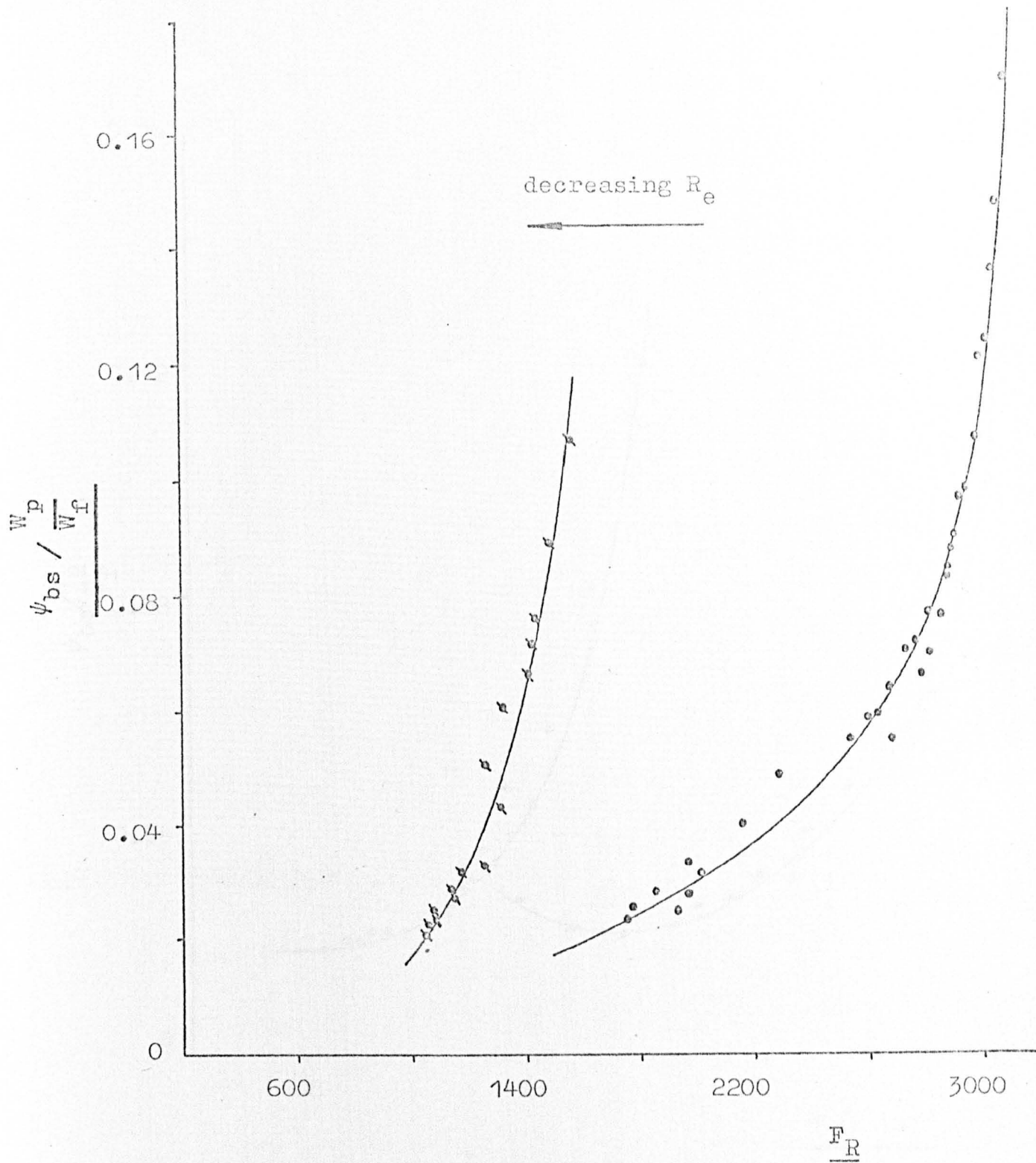


Fig. 7.14 Relationship between a Modified Resistance number, $\psi_{bs} / \frac{W_p}{W_f}$, and Froude number, F_R , for Flow around a 2 inch Bend having a Curvature Ratio of 20.

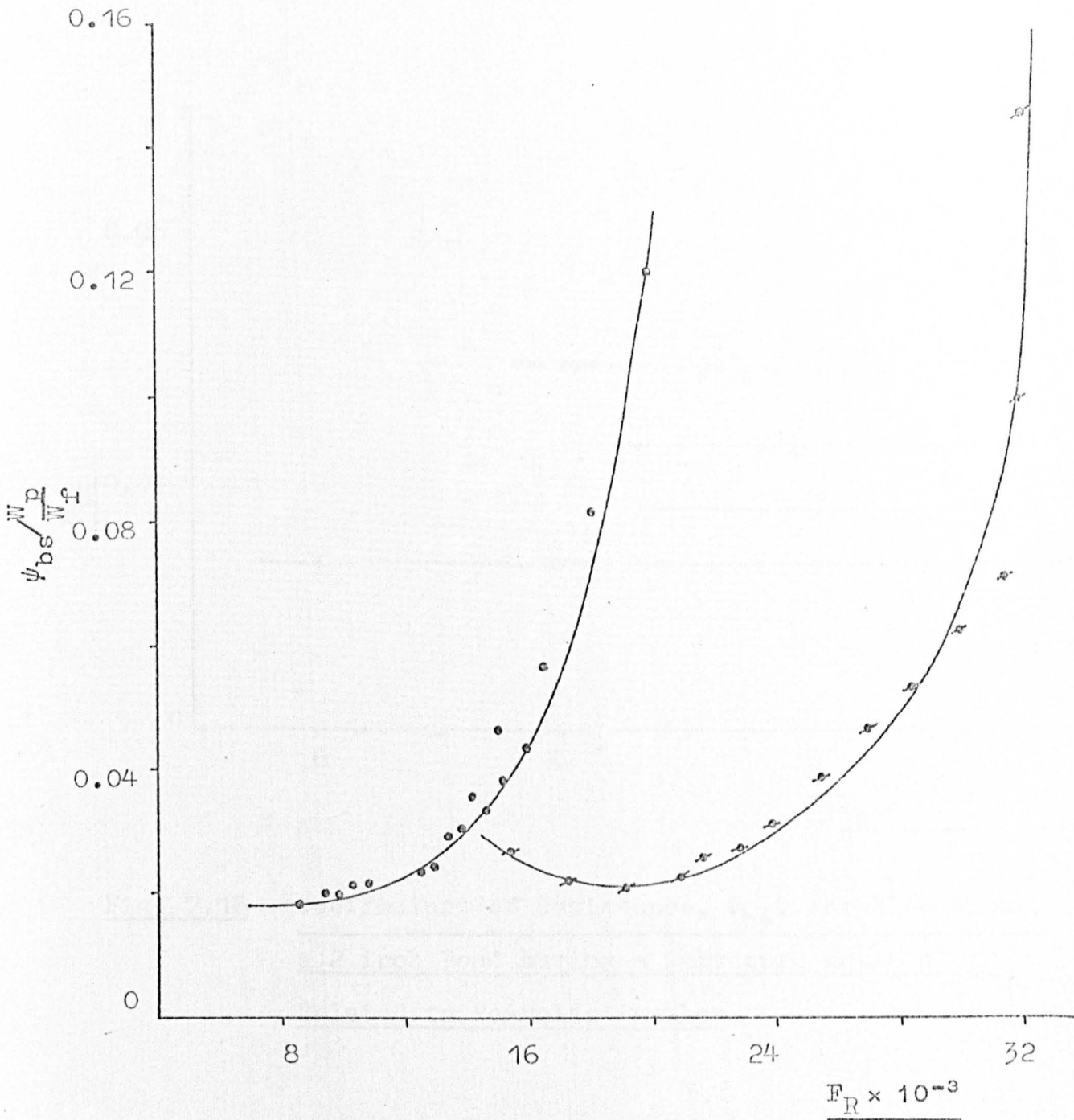


Fig. 7.15 Relationship between a Modified Resistance number, $\psi_{bs} \frac{W_p}{W_f}$, and Froude number, F_R , for Flow around a One inch Bend having a Curvature Ratio of 20.

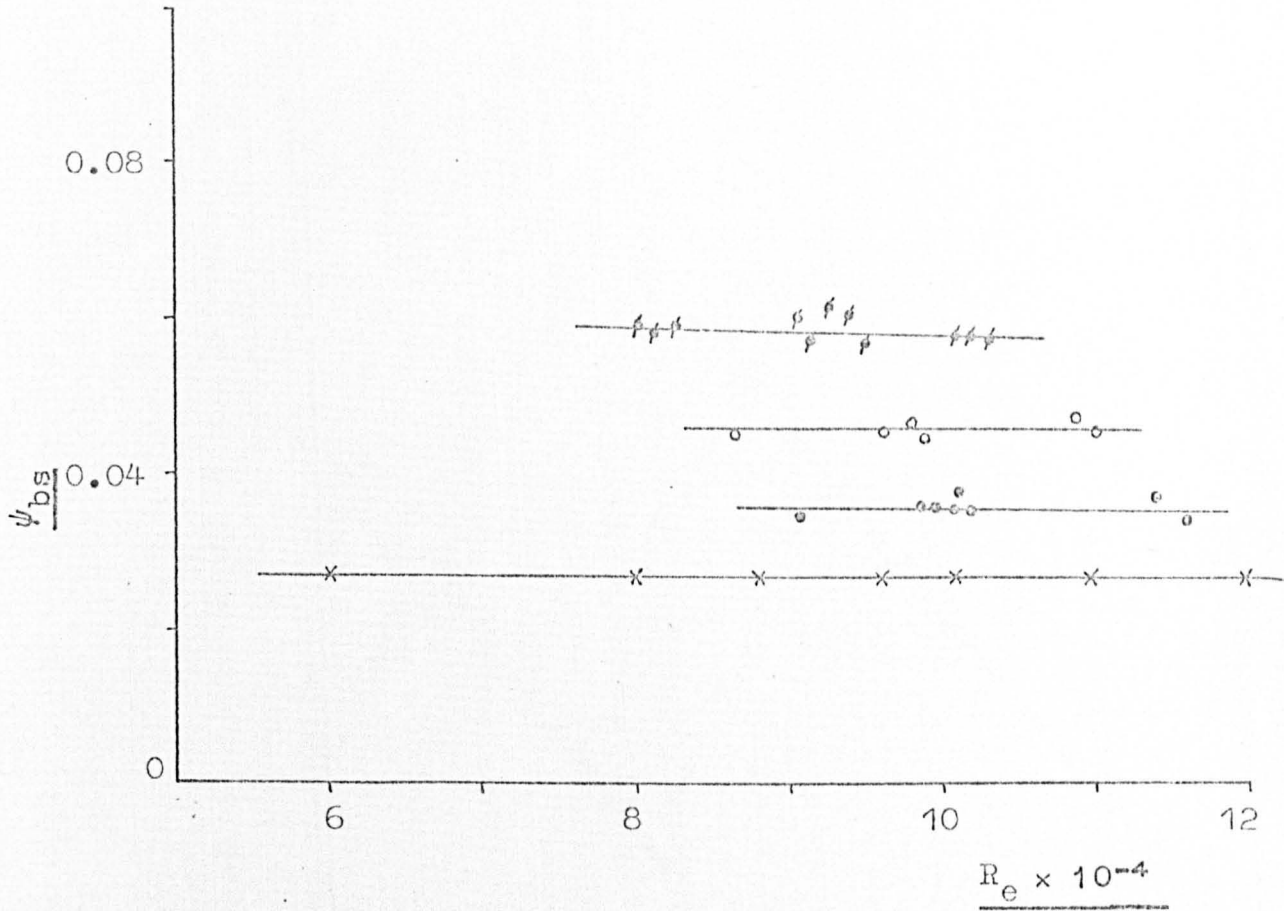


Fig. 7.16 Coefficient of Resistance, ψ_{bs} , for Flow around a 2 inch Bend having a Curvature Ratio of 20 Related to Reynolds' number.

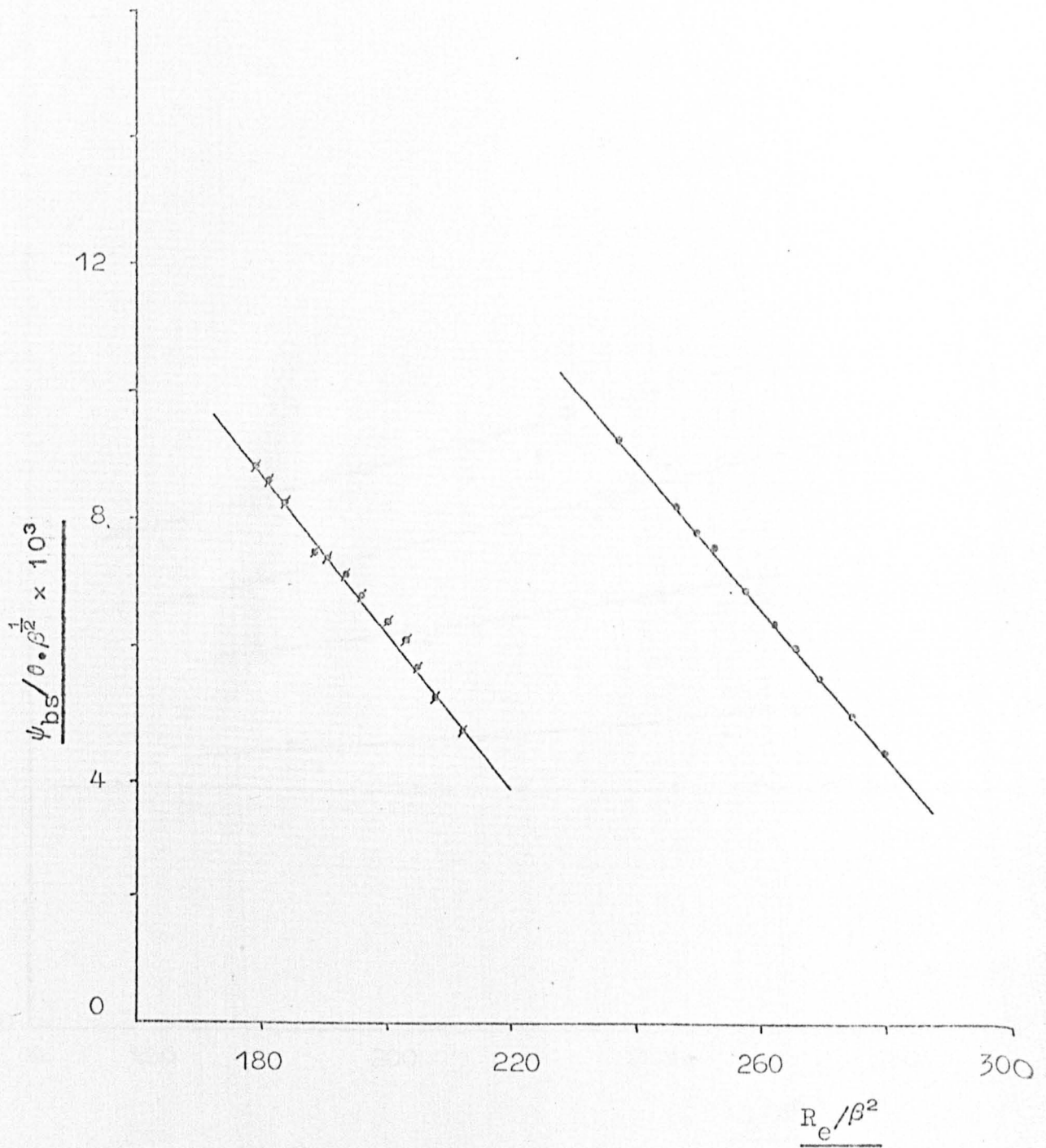


Fig. 7.17 Variation of a Related Resistance number,
 $\psi_{bs} / 0.0\beta^{1/2}$, with an Extended Reynolds' number index,
 R_e / β^2 , for Flow through a 2 inch Bend having a
Curvature Ratio, β of 20.

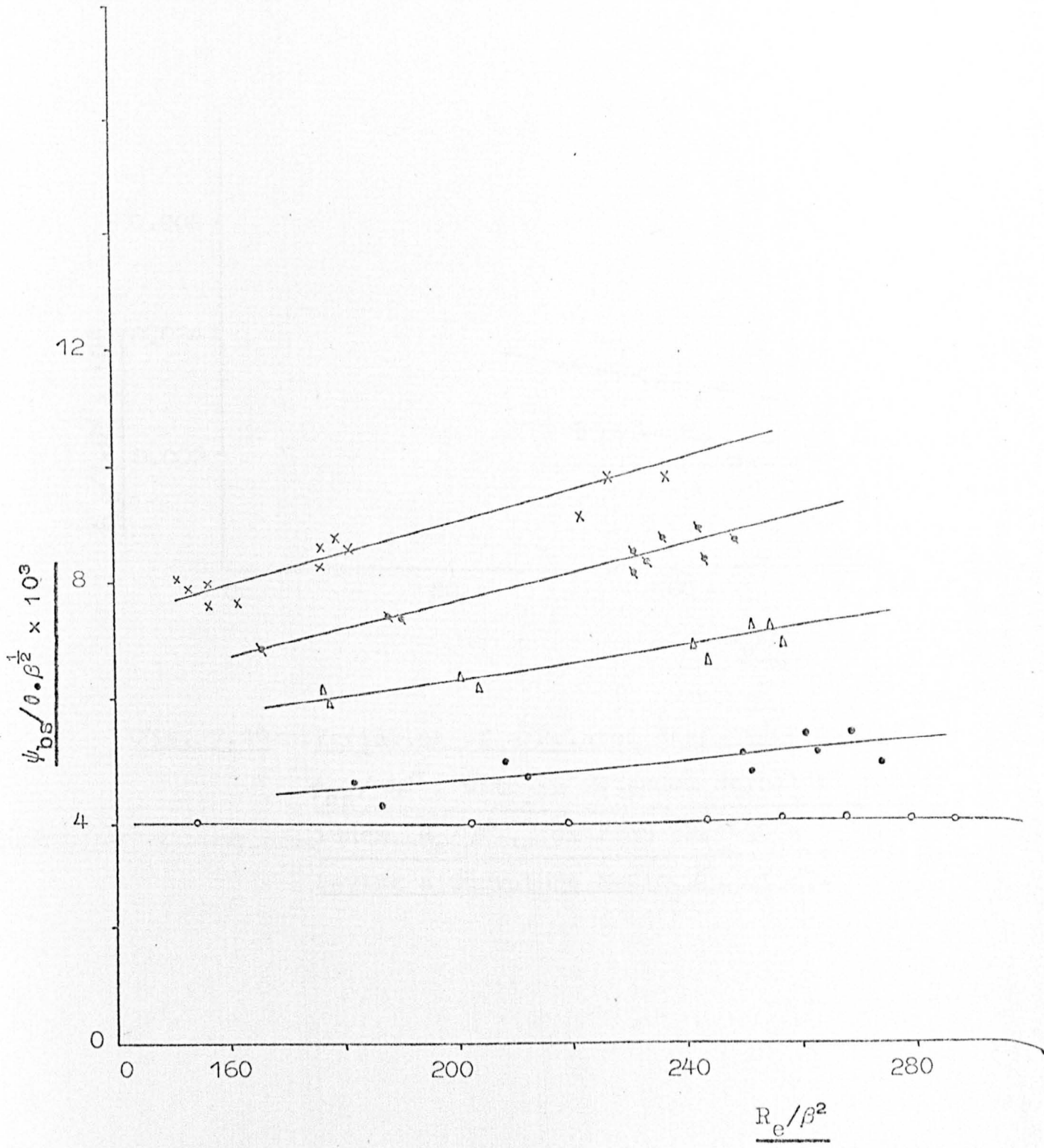


Fig. 7.18 Variation of a Related Resistance number, $\psi_{bs}/\theta \cdot \beta^{1/2}$, with an Extended Reynolds' number index, R_e/β^2 , for Flow through a 2 inch Bend having a Curvature Ratio, β , of 20.

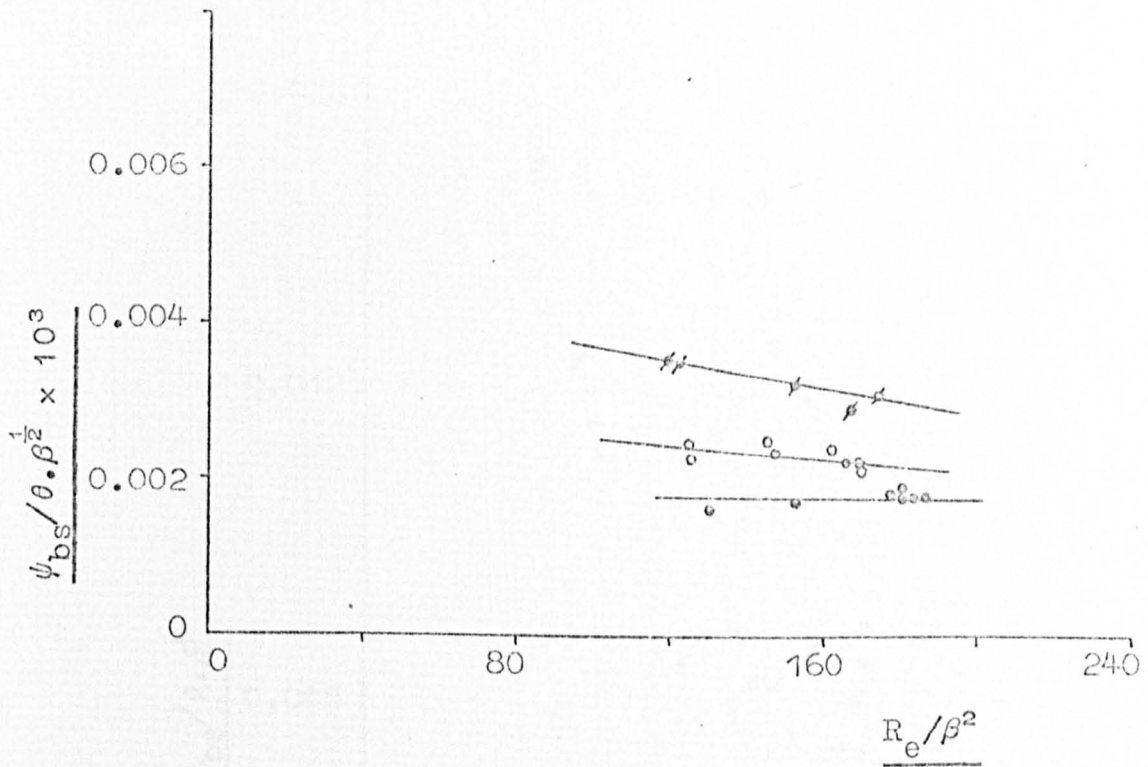


Fig. 7.19 Variation of a Related Resistance number,
 $\psi_{bs} / \theta \beta^{\frac{1}{2}}$, with an Extended Reynolds' number
index, R_e / β^2 , for Flow through a 3 inch Bend
having a Curvature Ratio, β , of 20.

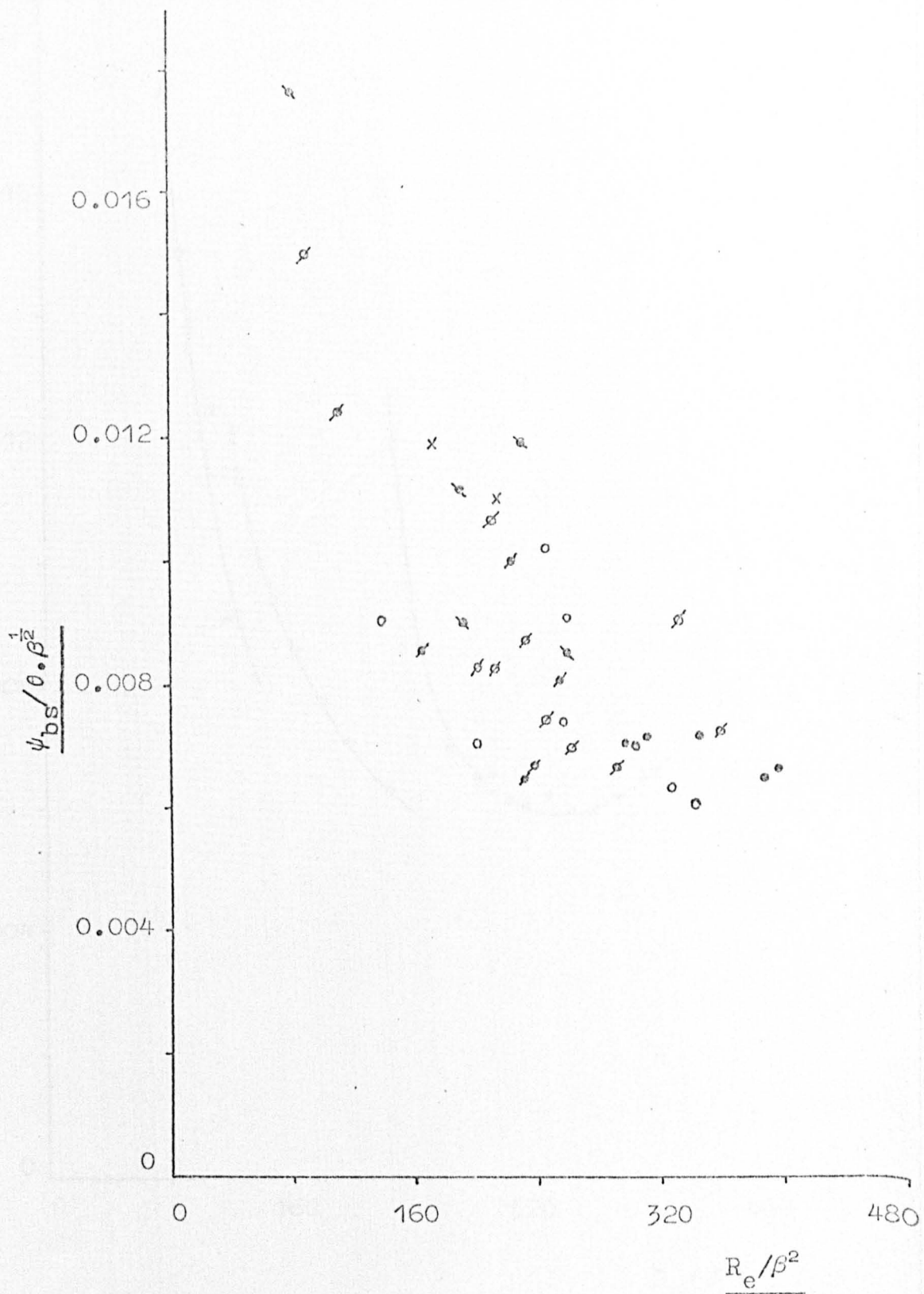


Fig. 7.20 Variation of a Related Resistance number, $\psi_{bs}/0.0\beta^{1/2}$, with an Extended Reynolds' number index, R_e/β^2 , for Flow through a One inch Bend having a Curvature Ratio, β , of 20.

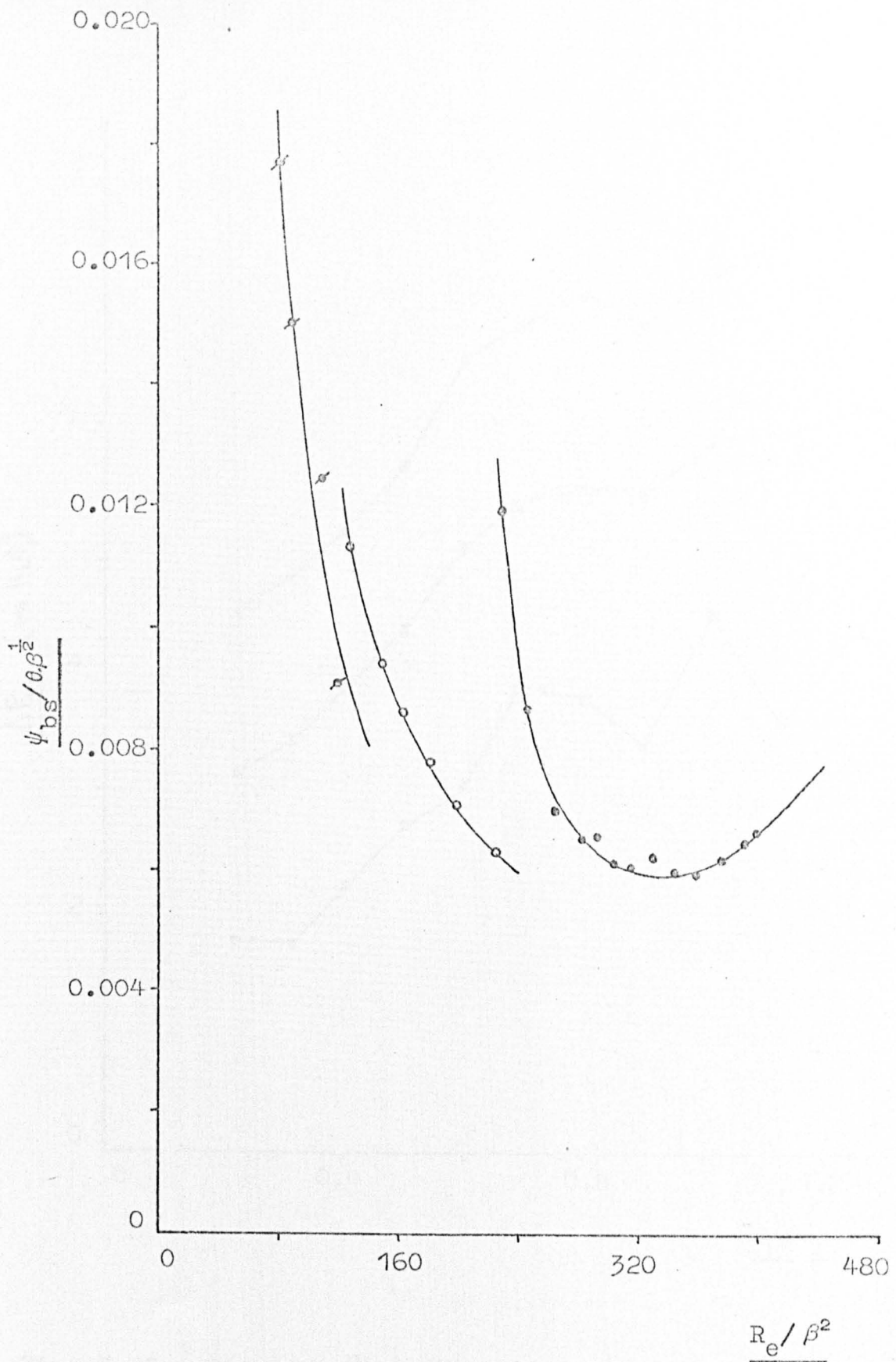


Fig. 7.21 Variation of a Related Resistance number,
 $\psi_{bs}/\alpha\beta^{1/2}$, with an Extended Reynolds' Number
index, R_e/β^2 , for Flow through a One inch
Bend having a Curvature Ratio, β , of 20.

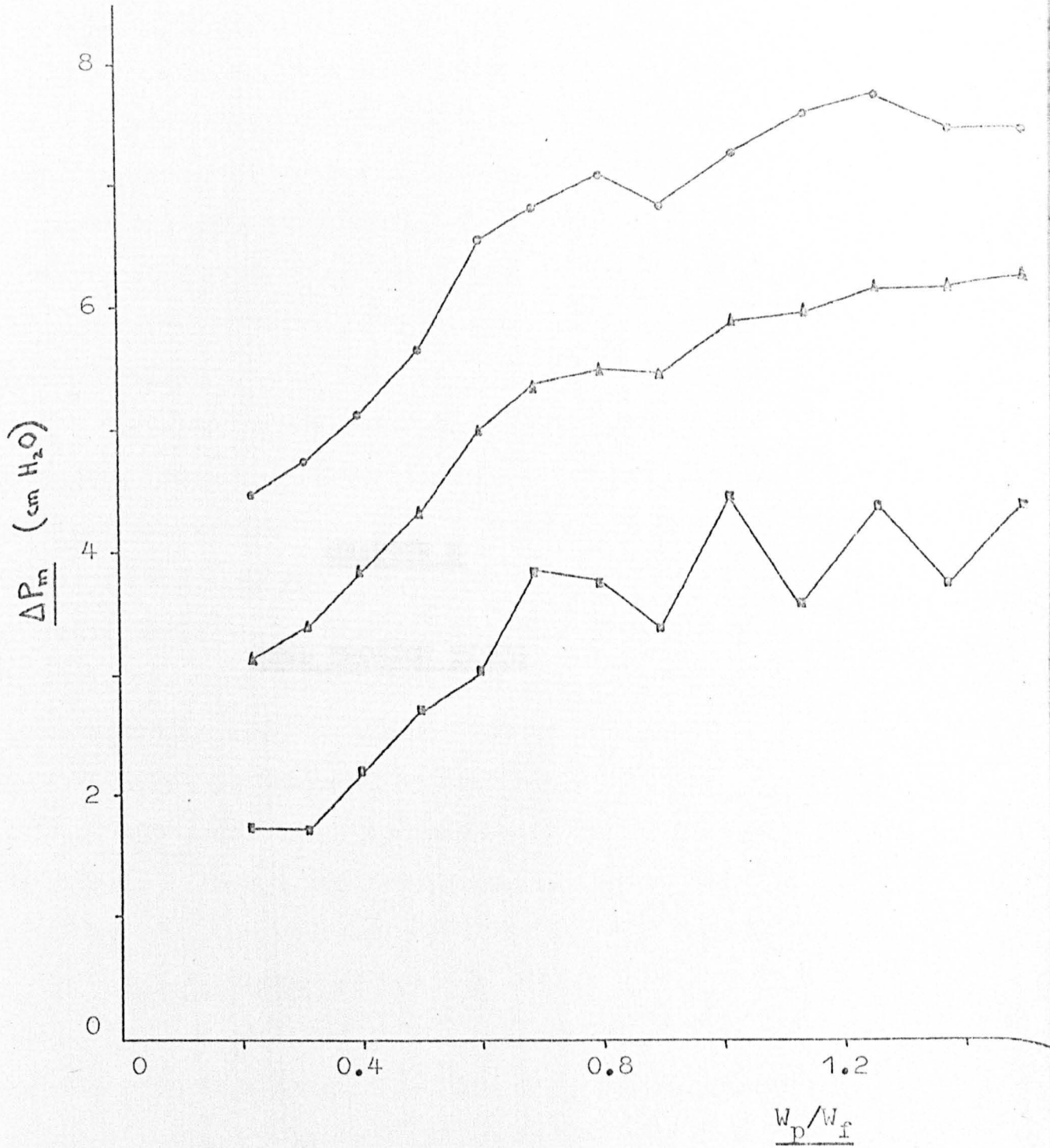


Fig. 7.22 Pressure Distribution around a 2 inch Bend
having a Curvature Ratio of 20 inches in
relation to the Solids-to-Gas ratio, W_p/W_f

CHAPTER 8

BEND EROSION TESTS

8.1 Introduction

The erosion of a surface by solid particles in a fluid stream is perhaps the dominant factor which makes industry reluctant to install pneumatic conveying systems for handling abrasive materials. However, the demands for environmental protection are likely to require that many more abrasive solids will ultimately be transported pneumatically.

The erosive action of particles depends upon their hardness, strength, particle shape and size, whilst the erosion of a surface by these particles depends upon the nature of the surface, the number of particles striking the surface, their velocity and their direction relative to impact. The flow conditions define the last three parameters, and erosion is more severe for sudden changes in flow direction, as encountered in pipe bends and valves. Erosion in straight runs of piping does occur but it is not normally as severe, although local turbulence, due to misaligned sections or roughened surfaces, may greatly increase erosion.

8.1.1 The Mechanism of Erosion

Earlier studies^{81,82,83} have shown that ductile and brittle materials exhibit distinctly different types of erosion behaviour. Tilly⁸⁴ illustrates in Fig. 8.1 the effect of impact angle on the erosion of different materials by sand particles sieved to 60-125 microns impinging at 340 ft/s. The glass (brittle) suffers little erosion at low impact angles and maximum erosion at an impact angle of 90°. The aluminium alloy (ductile) shows excellent resistance to

erosion at high impact angles, whilst the erosion is maximum at an angle of about 14° . The 11% chromium steel exhibits both types of erosion, maximum erosion occurring at about 20° with moderate erosion at 90° . This variation is because ductile materials suffer a volume loss by plastic deformation, the material being removed by the cutting action of the eroding particles; whilst the mechanism of brittle erosion is probably due to the Hertzian stresses generated by the impinging particles resulting in fracture and removal of material during subsequent impacts.

8.1.2 Physical Properties of the Abrasive

Finnie⁸¹ states that the influence of the eroding particle depends upon its shape, hardness and strength. However, the angle for maximum erosion is not particularly dependent upon shape, and if the particle is harder than the pipe surface then variation in abrasive hardness assumes little importance. The strength of the particle determines the extent to which they cut as a single entity or fracture internally while cutting and so influence the degree of erosion.

8.1.3 Results of Previous Researchers

The works documented in references 81 to 87 are concerned with the impact of different materials over a range of particle sizes and velocities impinging on flat surfaces at various angles.

Finnie⁸² states that erosion is proportional to $(\text{velocity})^2$ for ductile materials, whilst the exponent could be as high as 6 for brittle materials. Finnie et al⁸³ consider erosion as a machining process and assume that the only energy available is the translational kinetic energy

of the particles. They state that the energy required per unit volume removed by erosive cutting is approximately eight times that of conventional cutting tools. The discrepancy is accounted for by concluding that only about half of the eroding particles are effective in removing material, that about three-quarters of the initial translational kinetic energy is converted to rotational kinetic energy during impact, and only about one-quarter of the initial kinetic energy being available to produce plastic deformation in the surface. For several types of steel, and with particle velocities ranging from 250 to 450 ft/s, the exponent n (in the relationship, volume removed \propto velocity ^{n}) varied between 2.28 and 2.38 with silicon carbide particles of 60 mesh at an impact angle of 20°.

Bitter^{85,86} confirms that the severe erosion in transport lines for solids comprises two types of wear:-

- (i) that caused by repeated deformation during collisions; and
- (ii) that caused by the cutting action of the free-moving particles.

He observes that erosion is dependent upon whether the eroded surface is ductile or brittle, the latter being more resistant at low impact angles, whilst at high impact angles the more resilient material was less affected. Thus, the mechanical properties of the eroded material determines the type of erosion which prevails. Bitter states that no erosion of glass (brittle) due to repeated deformation can occur at impingement angles smaller than about 19°.

Tilly's⁸⁴ experiments were carried out with 60 to 125 micron sand particles at 340 ft/s. He noted that

temperature had little effect on erosion, which is in agreement with my observations, in fact, Tilly mentions that elevated temperatures can result in decreased erosion. This is contrary to the work referred to by Boothroyd⁸⁸, in which evidence was quoted of material removal being due to the micro-smearing effect of a molten surface. Tilly agreed that the degree of erosion is influenced by the pattern of airflow approaching the impact point and he states that particles less than 5 microns cause no significant erosion, while 5 to 20 micron particles cause substantially less damage than 60 to 125 microns being influenced by the deflecting forces of the airstream curvature to the extent that they may miss the surface altogether. This reasoning tends to conflict with Finnie⁸¹, who states that the result of particles fracturing into smaller particles on impact could be that, with their increased ratio of surface area to mass, an alteration in cutting conditions prevails which leads to an increase in volume removal by unit mass of abrasive.

The energy involved in damage due to ductile erosion results in temperature rises of about 190°C ⁸⁴. This explains the minimal effect on the extent of erosion of using heat treatment to give different hardnesses.

Neilson and Gilchrist⁸⁷ produced equations to predict surface erosion by impinging particles. Their experiments used aluminium oxide particles impinging upon different surfaces at velocities between 354 ft/s and 494 ft/s. Their results showed that cast iron has similar erosion characteristics as perspex, which is neither typically brittle nor typically ductile and so neither cutting wear nor

deformation wear predominated.

Thus, it is generally believed that increase in surface hardness increases wear resistance for low impact angles, since these glancing impacts involve lower stresses than normal impacts. Whereas, erosion at normal impacts increases with hardness, and since decreased hardness may be associated with increased ductility, these impact stresses are relieved by the plastic deformation in the region of impact.

8.2 Experimental

8.2.1 Apparatus

The experimental equipment shown in Fig. 8.2 has been described in detail in an earlier paper³, this can be briefly summarised as follows. Alumina particles were introduced into a metered airstream by a calibrated screw-feeder. The air-solid suspension was then passed vertically upwards through a 12 ft long perspex pipe of 1 in or 2 in internal diameter. The suspension then entered the 1 in or 2 in square-section 90° perspex bend, as shown in Plate 8. Three 1 in bends and one 2 in bend were used for these experiments. The suspension passed through the vertical-to-horizontal 90° test-bend into a horizontal pipe leading to an air filtering system consisting of two cyclones and a bag filter. The solids then passed from the cyclones into a combination of hoppers separated by pinch valves, before returning to the screwfeeder supply bunker.

The perspex bends were constructed with substantial backing-pieces in order that the change in flow pattern of the suspension, due to the deflection caused by the "rippled" surface of the eroded bends, could be visually observed.

In addition to the quantitative measurements recorded from the perspex bend tests, the 2 in diameter mild steel ducting preceding the vertical pipe, as shown in Fig. 8.2, contained 9 in radius bends, some being fitted with 0.5 in. thick mild steel backing plates. These bends were removed from the rig at appropriate intervals and the development of wear is shown in Plates 9 and 10. The "pocketing" effect of the mild steel shown in Plate 10 being similar to that at the primary wear point of the perspex test-bends.

8.2.2 Experimental Procedure

The air flowrate was adjusted to provide a velocity of 280 ft/s through the first 1 in test-bend, and for this mass flowrate of air the screwfeeder delivery was controlled to yield a mass of solids to mass of air ratio, W_p/W_f , equal to 3.3. These flow conditions were maintained throughout each test on this particular bend. At intervals during a test run of approximately 75 minutes, a sketch of the flow behaviour around the bend was recorded and various pressure measurements taken. At the end of each test, detail measurements of the erosion at many intervals around the bend were carried out.

Tests on the second 1 in bend were carried out at an increased velocity and at a very dilute phase, W_p/W_f being 0.5. The flow conditions were again modified for the third and final 1 in bend. However, with this bend the air velocity and phase density were varied at appropriate intervals, as is evident by reference to Fig. 8.5.

The 2 in bend was then tested and a total 100,000 lb alumina was circulated through the bend at a velocity of 96 ft/s and a W_p/W_f value of 3.3.

The material used throughout all the tests was highly abrasive alumina powder having a mean particle diameter between 50 and 60 microns. Samples of the charge of 300 lb of alumina were taken at routine intervals throughout the tests, the change in particle shape as the tests progressed is shown in Plates 11 and 12. In addition to particle shape and particle size distribution, the "poured" and "drained" angle of repose and the bulk density of each sample were determined.

8.3 Data Analysis

The factors which influence the erosion rate of a surface may be expressed as follows:-

Erosion = ϕ (mass of particles, velocity of impinging particles, impingement angle, mechanical and physical properties of the abrasive particles and eroded body, bend geometry, bend orientation) (1)

In order to establish a simple relationship which will define erosion, the above factors will be briefly examined.

8.3.1 Erosion

Previous researches have generally defined erosion as the volume of material removed or the weight loss per unit mass of eroding particles. It is the author's belief that industry, using pneumatic conveying to transport abrasive solids, is more concerned with the depth of wear in bends and pipe-lines, and the ability to be able to predict the location of the major wear points. Consequently, I have defined the mean wear rate w , as that quantity of powder which, when pneumatically conveyed around a 90° bend, results in unit depth of wear at the primary wear point.

8.3.2 Mass and Velocity of Impinging Particles

The mass of particles in the flowing suspension is important, due to the possible shielding action of particles which are in contact with the surface - this effect can best be defined by W_p/W_f .

The erosion of a surface is often stated as being proportional to the (particle velocity)ⁿ, the exponent n being in the range $2 < n < 2.5$ for ductile materials, whilst for brittle materials it can be much larger. The particle velocity is a parameter which industry particularly would experience much difficulty in measuring and so I will consider the velocity to be that of the superficial air. The particle velocity and air velocity for particles less than about 20 microns can reasonably be assumed equal and provided the particles are less than about 100 microns the error incurred from an industrial viewpoint should be acceptable. From the definition of mean wear rate, the bend erosion will be inversely proportional to v^n .

8.3.3 Angle of Particle Impingement, θ

As illustrated in Fig. 8.1, the angle of impingement of particles has an important effect on the erosion rate. Very brittle materials are highly resistant to oblique impact and suffer most at high angles of incidence of the particle stream. For ductile materials the maximum erosion occurs at a relatively low angle of incidence. The perspex bends behaved in a ductile manner and the above definition of mean wear rate includes the value of θ which produces maximum depth of wear.

8.3.4 Properties of the Particles and Eroded Surface

The particle size and shape remained reasonably

unaffected during the tests, as can be seen from Table 8.2. Also, the material of the four test bends was the same for all the tests. Thus, any formula which does not include these parameters can only be used when the particles are similar to those used in these tests and the surface material has similar ductile properties.

8.3.5 Bend Geometry and Orientation

The formula developed is applicable to bends in a vertical-to-horizontal orientation having a square-section and a D/d_p ratio of 20. Mehring⁹⁰ states that values of $D/d_p > 24$ are desirable when handling abrasives - the implications of this statement, though reasonably true, are discussed later on in this report.

8.3.6 Analysis of Experimental Results

Within the restrictions imposed by the experimental work, equation (1) becomes:-

$$\text{mean wear rate} = \phi (W_p/W_f, v, D/d_p)$$

$$\text{i.e. } w = \frac{ab (W_p/W_f)^m}{v^n} \quad (2)$$

where 'a' is a constant depending upon the materials of the surface and particles and 'b' is a constant which defines the bend geometry D/d_p . Thus comparing bends 1 and 2, equation (2) yields:-

$$\frac{w_1}{w_2} = \left[\frac{(W_p/W_f)_1}{(W_p/W_f)_2} \right]^m \times \left[\frac{v_2}{v_1} \right]^n \quad (3)$$

where suffix 1 refers to bend 1 and suffix 2 to bend 2;

$$\text{similarly } \frac{w_1}{w_3} = \left[\frac{(W_p/W_f)_1}{(W_p/W_f)_3} \right]^m \times \left[\frac{v_3}{v_1} \right]^n \quad (4)$$

The particular test conditions and the graphs illustrated in Figs. 8.3 to 8.6 produced the results shown in Table 8.1, and substituting these values into equations (3) and (4) and solving for m and n we obtain:-

$$m = 1.36 \text{ and } n = 2.25$$

$$\text{i.e. } w = ab \frac{(W_p/W_f)^{1.36}}{v^{2.25}} \quad (5)$$

The constants 'a' and 'b' cancelled out in equations (3) and (4) since these equations were concerned with three bends of identical geometry, similar material and were eroded by similar particles. It must be remembered that the exponents m and n are time-dependent factors, as determined by the definition of mean wear rate.

The product 'ab' can be evaluated by substituting the results of bend 1, bend 2 or bend 3 into equation (5) thus:-

$$'ab' = 7.13 \times 10^8 \text{ if } w \text{ is measured in lb/in, and } v \text{ in ft/s.}$$

So, equation (5) becomes:-

$$w = 7.13 \times 10^8 \times \frac{(W_p/W_f)^{1.36}}{v^{2.25}} \quad (6)$$

Consider now the 2 in square-section bend, that is, bend 4. This bend has a D/d_p value of 12, whilst equation (6) is based upon a D/d_p value of 20. However, Mehring⁹⁰ shows that the impact angle for bends with $D/d_p = 20$ and $D/d_p = 12$ are very similar and so the erosion at their primary wear points may be assumed similar. Thus, substituting the values from Table 8.1 for bend 4 into equation (6), the left-hand side yields:-

$$7.13 \times 10^8 \times \frac{(3.3)^{1.36}}{(96)^{2.25}} = 126,000 \text{ lb/in}$$

this is the predicted mean wear rate at the primary wear point for bend 4. However, the actual mean wear rate, as determined from the graph shown in Fig. 8.6 is 128,000 lb/in.

The close agreement justifies the author's belief that phase density, as defined by W_p/W_f , should be considered, as well as velocity, when considering bend erosion.

If W_p/W_f had been ignored and the relationship $w \propto 1/v^n$ assumed, the following results would have been obtained.

- (a) from $w_4/w_2 = (v_2/v_4)^n$; $n = 4.0$
- (b) from $w_4/w_3 = (v_3/v_4)^n$; $n = 2.1$
- (c) from $w_4/w_1 = (v_1/v_4)^n$; $n = 2.5$.

The wide variation in n can be explained by comparing the corresponding W_p/W_f values, which show that the largest discrepancy in n , from the usually accepted values for ductile materials of between 2.0 and 2.5, occurs when the difference in phase density is large. For example, for case (a) above, $(W_p/W_f)_4 = 3.3$ whilst $(W_p/W_f)_2 = 0.5$, thus confirming that w is dependent upon W_p/W_f as well as upon v .

8.3.7 Examination of the Mean Wear Rate Equation

$$\text{From equation (2) } w = ab \frac{(W_p/W_f)^m}{v^n}$$

where 'a' and 'b' are constants for particular surface materials, particles and bend geometry, thus:-

$$w \propto \frac{(W_p/W_f)^m}{v^n} \quad (7)$$

(a) Consider v constant and W_p/W_f variable:-

- (i) as $W_p/W_f \rightarrow \infty$, $w \rightarrow \infty$, that is, no wear occurs for the flow conditions of maximum theoretical dense phase;

(ii) as $W_p/W_f \rightarrow 0$, $w \rightarrow 0$, that is, maximum erosion occurs when air only is flowing. The anomaly which these latter boundary conditions suggest, infers a minimum value of w at a critical value of W_p/W_f , assuming a constant velocity condition; see Fig. 8.7.

(b) Consider W_p/W_f constant and v variable; see Fig. 8.8:-

as $v \rightarrow 0$, $w \rightarrow \infty$, that is, no wear; and

as $v \rightarrow \infty$, $w \rightarrow 0$, that is, infinite wear.

The observations represented in Figs. 8.7 and 8.8 may be integrated as follows:-

(i) For $W_p/W_f > (W_p/W_f)_{\text{critical}}$, equation (7) is in

the correct form, i.e. $w \propto \frac{(W_p/W_f)^m}{v^n}$

(ii) For $W_p/W_f < (W_p/W_f)_{\text{critical}}$, equation (7) becomes,

$w \propto \frac{1}{(W_p/W_f)^m \times v^n}$, thus

as $W_p/W_f \rightarrow 0$, then $w \rightarrow \infty$, that is, no wear for air only flowing.

The latter relationship for w also infers that if W_p/W_f is very small (that is, very dilute phase) then the erosion will be minimal, since w will be large.

8.4 Results and Discussions

8.4.1 Erosion History for Bend 1

8.4.1.1 Nature of the Flowing Suspension

The superficial air velocity in this one inch bend was 280 ft/s and the solids-to-air ratio was 3.3.

8.4.1.2 Wear Development

It can be seen by reference to Figs. 8.9 and 8.13 that

erosion first occurred at a bend angle of 21° , which very soon became the primary wear zone. The primary wear point did ultimately move to a bend angle of 22° . After a certain depth of wear pocket had been achieved, the air-solid flow became deflected sufficiently to promote wear on the inside of the bend - this is evident by comparing the results for tests 5 and 16 shown in Fig. 8.9. The suspension was then deflected back to the outside of the bend and a secondary wear point developed at a bend angle of 76° . A small tertiary wear point was subsequently created at an angle of 87° . The flow which deflected from these latter wear points would probably result in erosion of the horizontal pipe immediately down-stream from the bend. Fig. 8.3 illustrates that the depth of wear at the primary wear point increases rapidly until a particular depth of wear is achieved. This apparent limit to the depth of the wear pocket is possibly because the effective impingement angle of the particles had continually increased to over 80° . The perspex then behaved in a ductile manner so that the plastic deformation of the surface relieved any high stresses which could have induced surface fracture. In addition, the dynamic layer of powder moving slowly within the pocket protected the area from the direct impact of the solid particles.

Fig. 8.3 also illustrates clearly that the depth of the secondary wear point increases quite dramatically once the primary wear point has been established. This is definite confirmation of severe deflection of the suspension by the primary pocket being required before the flow can "re-bound" from the inner surface with sufficient momentum to promote the severe secondary wear condition.

8.4.1.3 Flow Pattern

The flow pattern during Test 1 is shown in Fig. 8.17 and immediately suggests the location of the initial wear zone and that no wear on the inside of the bend is likely. Fig. 8.18 shows the flow pattern, after the primary, secondary and tertiary wear pockets have become established, for the flow conditions which had been maintained throughout these tests. It is quite evident that wear will eventually result on the inside of the bend at an angle of 80° to 90° , and that wear on the bottom of the horizontal pipe is probable. Fig. 8.19 shows the effect of reducing the solids flowrate for the same superficial air velocity. The momentum of the "dusty air" flowing along the inside of the bend is now sufficient to deflect the suspension flowing from the primary wear pocket and so erosion of the inside of the bend would not occur for these flow conditions of 280 ft/s and solids-to-air ratio of 2.6.

Fig. 8.20 shows the flow pattern when the solids-to-air ratio is reduced still further to 1.8 for the same velocity. This very much more dilute phase confirms that no wear on the inside of the bend will occur for these flow conditions and bend geometry. However, the most remarkable feature is that it shows that erosion of the bottom surface of the horizontal pipe will occur much further downstream.

8.4.2 Erosion History for Bend 2

8.4.2.1 Nature of Flowing Suspension

For the second one inch bend the superficial air velocity was increased to 330 ft/s and the solids-to-air ratio reduced dramatically to 0.5.

8.4.2.2 Wear Development

The very dilute phase and high velocity flow conditions resulted in remarkably high initial erosion rates at the primary and secondary wear points, as shown in Fig. 8.4. The characteristic "levelling-off" at a certain depth of wear at the primary zone was again evident. The bend angles defining the primary and secondary wear points were approximately 28° and 80° respectively. The excessive depth of pocket at the primary point resulted in severe flow deflection which caused considerable wear of the inside bend and the corresponding deflection here resulted in the secondary wear point becoming almost "primary". The deflection from the secondary wear point induced considerable erosion along the bottom of the horizontal pipe, as shown in Fig. 8.14. The severity of bend erosion for these flow conditions is shown in Plate 13. The peak wear of the inside of the bend occurred at a bend angle of about 45° .

8.4.3 Erosion History for Bend 3

8.4.3.1 Nature of the Flowing Suspension and Wear Development

The initial flow conditions for the third and final one inch bend were 290 ft/s air velocity with a solids-to-air ratio of 3.8. After ten tests, represented on Fig. 8.5 by point A, the solids-to-air ratio was reduced to 0.5 whilst the air velocity was kept at 290 ft/s. The wear at the primary point, having previously approached its limiting value, began to increase again until it achieved its ultimate depth of wear for the particular flow conditions. The flow conditions were again modified after test 13, point B on Fig. 8.5, to an air velocity of 330 ft/s whilst the solids-to-air ratio remained at 0.5. A sudden increase in depth of

wear at the primary point again occurred, until finally the third "levelling-off" characteristic was achieved.

The secondary wear point showed little erosion until after the primary wear pocket had been established, this being in close agreement with bend 1. However, the secondary wear point increased very rapidly after the tenth test and was seemingly unaffected by the various modifications to the flow conditions. The dramatic wear here was such that it ultimately exceeded the primary wear depth, as illustrated in Figs. 8.5 and 8.11 and Plate 14.

The bend angles defining the primary and secondary wear points are approximately 26° and 76° respectively. The peak wear on the inside of the bend occurred at 41° , which is in fairly close agreement with bends 1 and 2.

Fig. 8.11 illustrates the secondary and tertiary wear points developed after test 13, as experienced with bend 1. However, for bend 3 the secondary and tertiary wear points became one complete wear zone following further excessive erosion.

8.4.4 Erosion History for Bend 4

8.4.4.1 Nature of the Flowing Suspension

This was the only 2 inch square-section bend which was tested, the flow conditions prevailing throughout being 96 ft/s air velocity with a solids-to-air ratio of 3.3.

8.4.4.2 Wear Development

Wear only became evident after several thousand lb of alumina had been conveyed around the bend. The first indication of wear occurred at a bend angle of 17° and this became the primary wear point for the whole series of tests. The initial wear pattern was characterised by several peaks

across the 2 inch wide section, extending in the direction of flow. These triangular wear peaks were more severe along a 1 inch wide central zone, although they ultimately became moderately uniform across the full 2 inch wide section. The conveying rate of the 240 mesh alumina was 30 lb/min and a total of 100,000 of powder was transported around the bend.

Fig. 8.6 shows an initial rapid erosion rate, followed by a limiting depth of wear at the primary wear point, thus confirming that "scale-up" does not destroy the information acquired from the one inch bend tests. Fig. 8.12 shows no definite secondary wear point, the erosion after the primary wear point being characterised by a regular series of small peaks, as confirmed by Fig. 8.16. It is probable that these peaks would eventually merge and a definite secondary wear point develop at a bend angle of approximately 70° to 75° .

8.4.4.3 Flow Pattern

The flow patterns were very similar to those for bend 1 as represented by Figs. 8.17 and 8.20. The essential difference, compared with Fig. 8.17, was that an even greater proportion of the solids was concentrated within a small area along the outside of the bend. After the peaks had developed around the outside of the bend, powder issued from these very small pockets as dense "jets" of deflected powder. The momentum of these jets was not sufficient to "penetrate" the dusty air flow occupying the inner area of the bend. These denser streams of powder were then re-directed to the outside of the bend which explains the "bouncing" flow that produced the series of wear points extending around the bend.

8.4.4.4 Pressure Loss

The pressure drop around the bend after test 7 was

6.5 in water, when the depth of wear at the primary point was 0.20 in. An increase in the depth of wear to 0.43 in, produced a pressure drop of 7.0 in water, which is an increase of almost 8% in the pressure drop.

8.4.5 Powder Property Determinations

Table 8.2 illustrates the properties of a few of the many samples of powder taken throughout the tests.

The design of the apparatus required the initial charge of 300 lb of alumina powder to be continuously re-circulated throughout the tests. In order to analyse the quantitative measurements with some confidence, it was essential to know the nature of the powder at all stages. Plates 11 and 12 show that the same "blocky" but sharp-edged particle shape is retained even after over 24,000 lb of powder had been conveyed around the three one-inch test bends. Degradation of the particles is evident and the increasing proportion of fines accounts for the powder becoming more cohesive. The final sample shown above has achieved its ultimate form, it has still retained its "blocky" shape but the corners have been "rounded-off". This situation only arose after a further 100,000 lb of powder had been circulated and the reduction in erosive potential of these particles was avoided in the data analysis.

8.4.6 Relevance to Industry

Wear rates for sand in an industrial plant for a 4 inch nominal bore, 90° mild steel bend of 4 ft 6 in radius, were 300 tons/in for a non-pocketed bend and 1700 tons/in for a pocketed bend⁹¹. Thus "pocketing" appears to increase the wear resistance of mild steel which confirms the observations of the present investigation. The probable

explanation is that the mild steel behaves in a ductile manner, as did the perspex bends, and suffers severe erosion at small angles of impingement. However, when the "pocket" has been formed the impingement angle has increased to between 80° and 90° and the increase in resistance to erosion is now partly due to the plastic deformation of the mild steel, which is no longer suffering the cutting-action associated with low impingement angles. Also, the pocket now contains a dynamic layer of powder which protects the bend from the direct impact of particles - this layer changes its identity continuously.

A conventional bend design used to avoid plant shut-down due to bend wear is to reinforce the outside of the bend with a mild-steel channel backing filled with a suitable concrete. Plate 16⁹¹ is a radiograph of such a bend and it clearly shows a primary wear pocket developing in precisely the same manner as for the perspex bend-tests.

Some proprietary bends utilize the "pocket" to minimise wear in that the bends contain a shaped recess in which material collects and the material which follows impinges on the collected material rather than on the material of the bend. These bends are generally of very small radius and cause a high pressure loss, thus reducing the efficiency of material transfer.

8.5 Conclusions

The erosion resistance of different materials changes as the angle of impingement changes. When the particles are harder than the bend material, rapid erosion of the bend occurs at low angles of impingement - 15° to 30° . The rate of wear at this primary wear point decreases as the impact angle

increases, until no measurable further increase in erosion occurs for impact angles between 80° and 90° . The change in flow pattern induced by the developed pocket can result in erosion of the inside surface over an area of 30° to 60° bend angle, the peak wear occurring at approximately 40° to 45° . A secondary wear zone gradually develops on the outside surface and the peak wear occurs at a bend angle of about 75° . This secondary wear point can exceed the magnitude of the primary wear point.

The deflecting flow phenomenon illustrates the necessity for choosing the bend geometry, defined by D/d_p , with caution. If D/d_p was excessive, for example, a radius of curvature of 20 ft for a 4 in. bore pipe, that is $D/d_p = 120$, then the air-solid flow would be deflected many times as it passed around the bend and so prediction of the wear points would become impossible. The accurate prediction of major wear points for relatively long-radius bends is important for the economic protection of such bends with replaceable backing-pieces and so on. Thus, remembering that sharp-bends and elbows produce large pressure-drops, then a compromise is the obvious solution when handling abrasive materials. Prediction of wear points is complicated by air velocity and solid-to-air ratio, however, for a bend of geometry approximating to $D/d_p = 20$, it is feasible to deduce a narrow range of bend angle within which severe wear will occur.

The analysis of the experimental data yielded the following equations:-

(i) for a normal dilute-phase conveying system:-

$$w \propto \frac{(W_p/W_f)^{1.36}}{v^{1.25}}$$

(ii) for a very dilute-phase conveying system:-

$$w \propto \frac{1}{(W_p/W_f)^{1.36} \times v^{1.25}} \cdot$$

These equations refer to the erosion at the primary wear point only and for 90° bends in a vertical-to-horizontal orientation - they are also restricted by the other limitations imposed by the experimental apparatus. However, when many more powders and bends have been investigated it should be possible to obtain a general equation which defines the powder as well as the flow conditions. The analysis emphasises that the solids-to-air ratio must be considered, in addition to velocity, when evaluating bend erosion. This theory is confirmed by Mehring⁹⁰ who states that records from numerous industrial plants indicate that the rate of wear is dependent upon material-to-air ratio and upon velocity - the wear decreasing with increased material-to-air ratio in accordance with the equations derived here.

The author is currently negotiating with the National Research Development Corporation for the development of an erosion resistant bend, which consists mainly of brittle material with a ductile or resilient material in appropriate positions.

Table 8.1

Flow Conditions and Mean Wear Rates for the Four Bends

Bend number	1	2	3	4
Mean wear rate lb/in	11,400	910	12,400	128,000
Air velocity ft/s	280	330	290	96
W_p/W_f lb/lb	3.3	0.5	3.8	3.3

Table 8.2

Powder Properties

Powder sample	New Powder	Sample taken at end of tests on bend 1	Sample taken at end of tests on bend 3	Sample taken at end of tests on bend 4
Mean particle diameter, microns	60	60	55	50
Particle shape	Fig. 8	Fig. 9	Fig. 10	Fig. 11
"Poured" angle of repose, degrees	33	36	36	30
"Drained" angle of repose, degrees	36	65	65	55
Degree of cohesiveness	3	29	29	25
Minimum bulk density, lb/ft ³	103	103	106	132
Maximum bulk density, lb/ft ³	121	123	129	144

8.6 Suggestions for Further Work

The industrial implications alone justify an extensive programme of research into the erosion of bends being implemented. It is suggested that a rig should be designed solely for bend wear tests and which would be capable of almost continuous operation on a 24 hour basis. As a result, measurable depths of wear will be obtained quickly and the necessarily repetitive nature of such experiments relieved of a certain amount of tediousness. It would be of little value to pursue a programme of accelerated wear tests, effected by using very high particle velocities, and it is recommended that particle velocities, phase densities, particle and bend materials only be selected after a survey of industrial practice. A useful course of study, based upon 90 degree bends only, would necessitate variation of the following system parameters:-

- (i) The solid particles: varied in terms of hardness, strength, particle shape and size; these being some of the more important physical properties.
- (ii) The bend material: varied in terms of ductility, brittleness and resilience.
- (iii) Bend geometry: varied in terms of the ratio of the radius of curvature to the radius of the pipe; preferably using pipes of circular cross-section and at least two inches diameter.
- (iv) Bend orientation: the lead-in pipes must be accurately aligned and be varied to have horizontal-to-horizontal, horizontal-to-vertical, and vertical-to-horizontal situations.

Typical measurements and observations to be recorded

are:-

- (a) Solids-to-air ratio, W_p/W_f : if possible this should be varied from very dilute phase to dense phase, a most interesting range would be $100 > W_p/W_f > 0.5$.
- (b) Particle velocity: this can be satisfactorily replaced by the superficial air velocity for very fine particles in a dilute-phase system. In a dense phase suspension or with coarse particles the problem of particle velocity evaluation becomes more complex.
- (c) Angle of particle impingement.
- (d) Depth of wear at several stations around the bend.
- (e) Flow pattern for the different flow conditions and the effect of an eroded surface upon flow behaviour.
- (f) Temperature of the bend material near to important impact points.
- (g) Pressure drop around the bends and the effect of erosion, particularly for the case of a reinforced bend in which a wear pocket has developed, upon the magnitude of the pressure differential.
- (h) Determination of the particle size and shape at frequent intervals; particularly important if the solids have to be re-circulated. It would be advantageous for at least part of the investigation to use powder on a once-through basis.

It is evident that some of the above suggestions

require visual observation of the two-phase flow, however, bends manufactured from mild steel, linatex (a resilient material), basalt and so on must be tested. The use of radiographic techniques to determine wear patterns and depths of wear would thus be necessary.

The aim of such an investigation would be to produce an all-embracing equation which would enable bend wear rate to be predicted. An essential requirement would be to examine the laboratory investigations by carrying-out a series of carefully planned erosion experiments in an industrial environment.

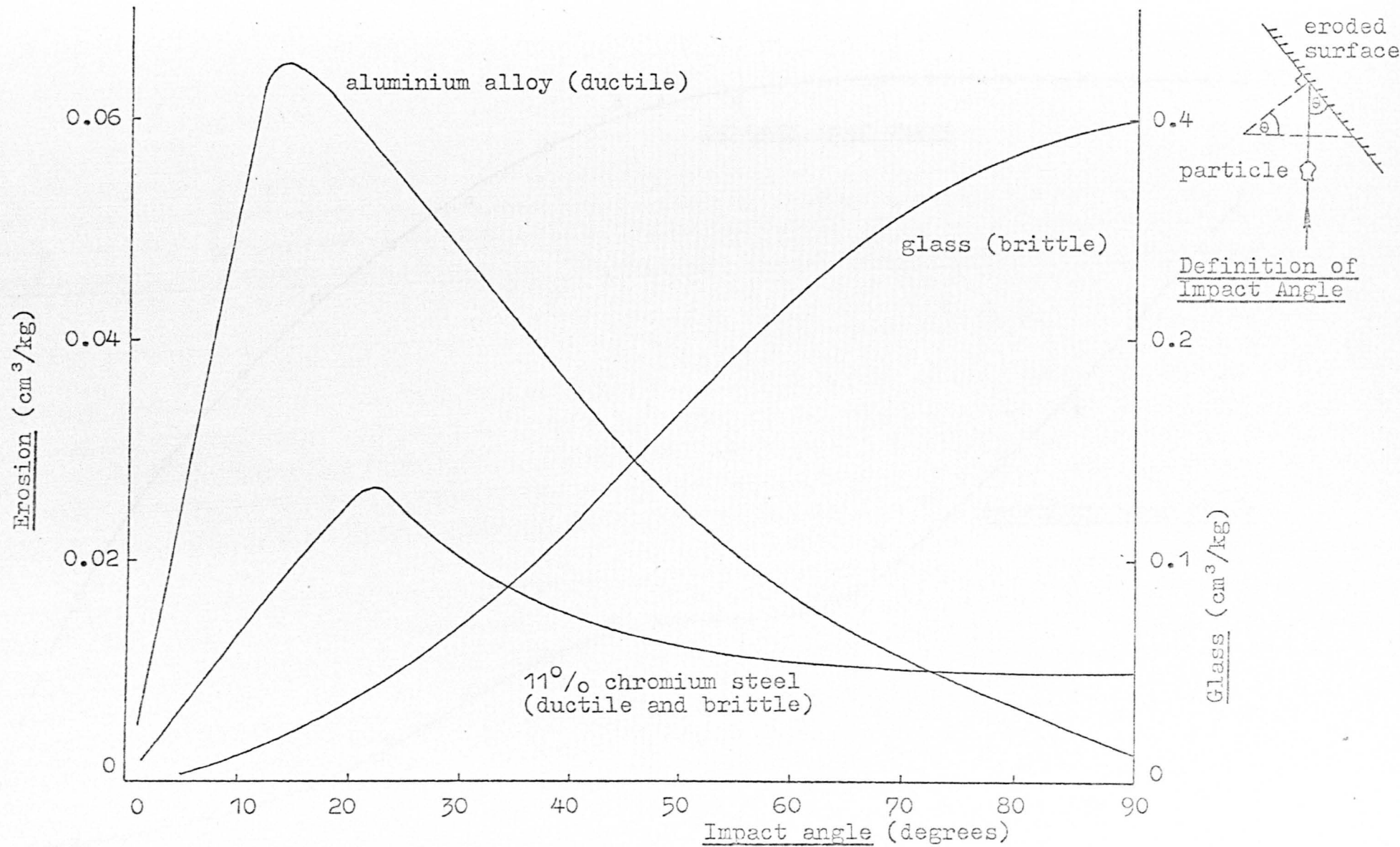


Fig. 8.1 Variation of Volume Removal with Incidence Angle for Various Ductile and Brittle Materials.

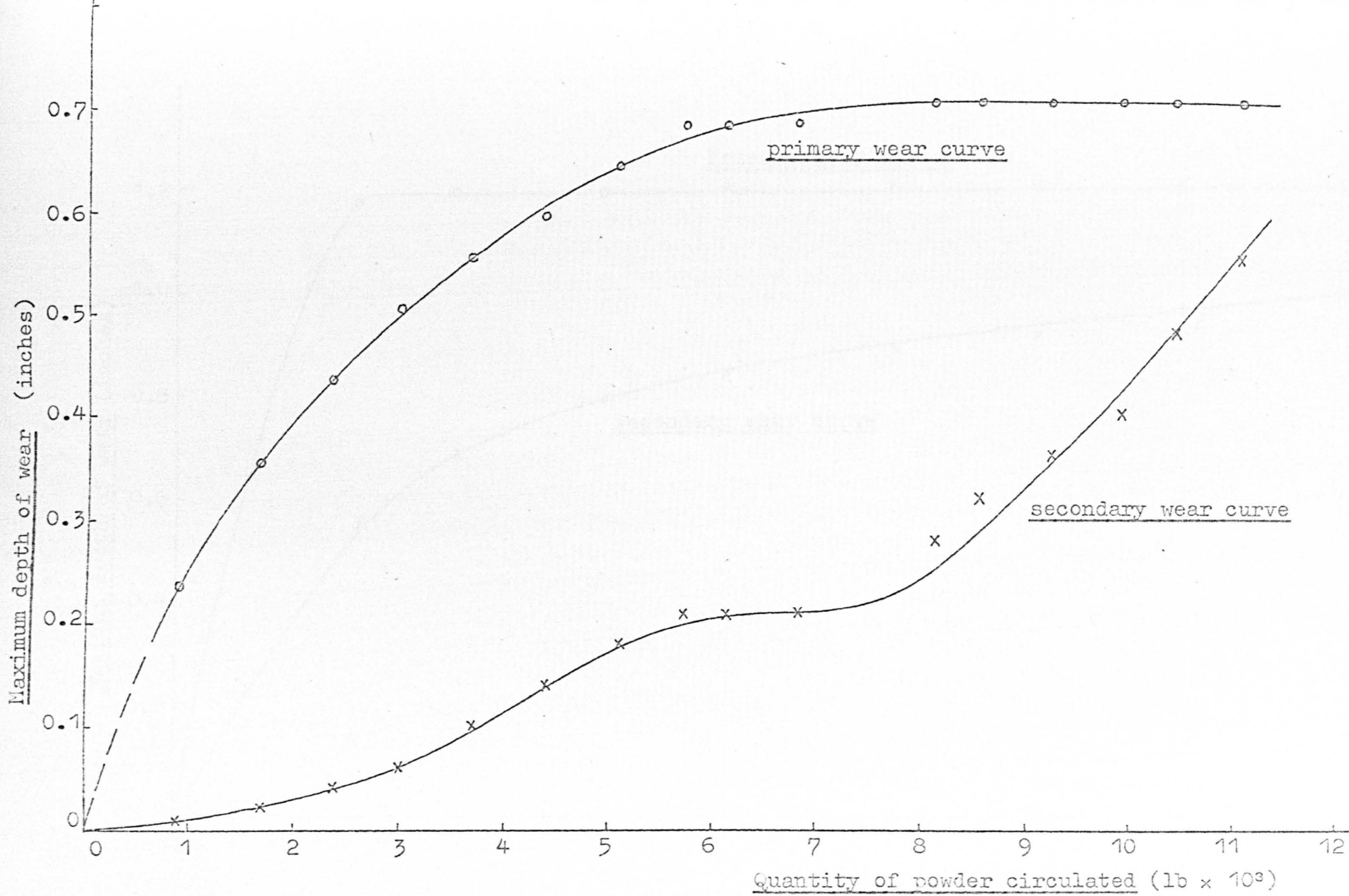


Fig. 8.3 Rate of Wear at the Primary and Secondary Wear Points for Bend 1.

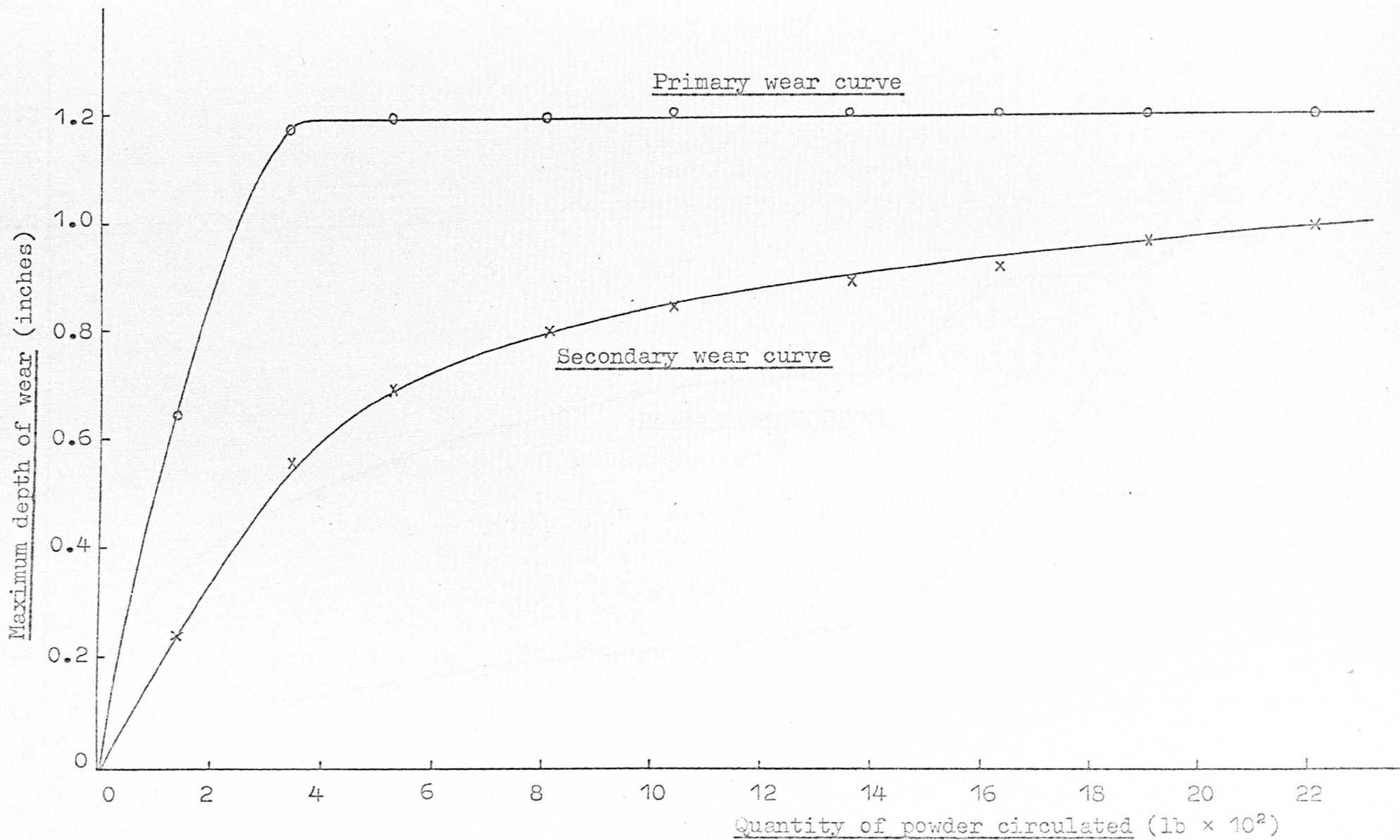


Fig. 8.4 Rate of Wear at the Primary and Secondary Wear Points for Bend 2.

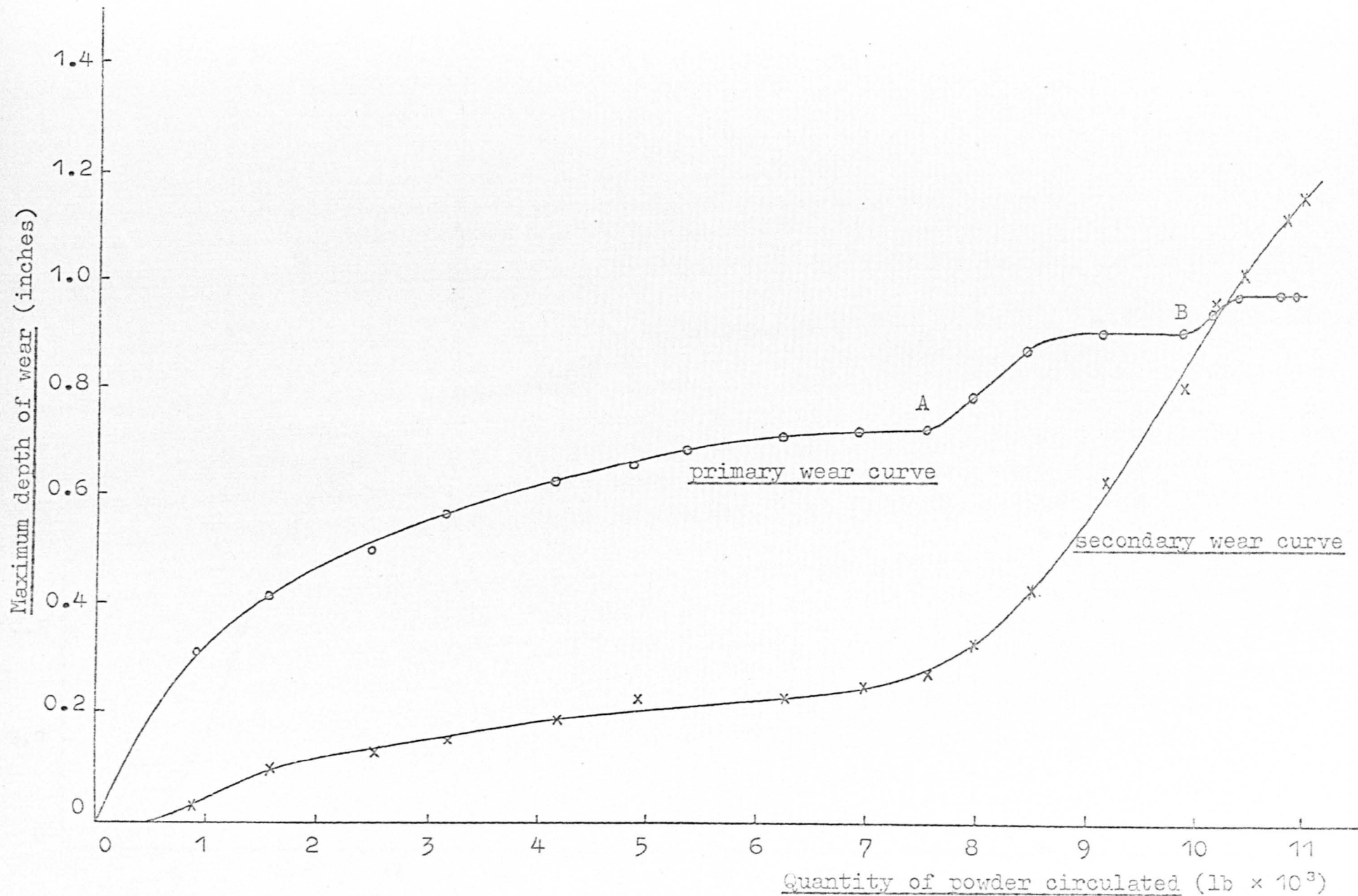


Fig. 8.5 Rate of Wear at the Primary and Secondary Wear Points for Bend 3.

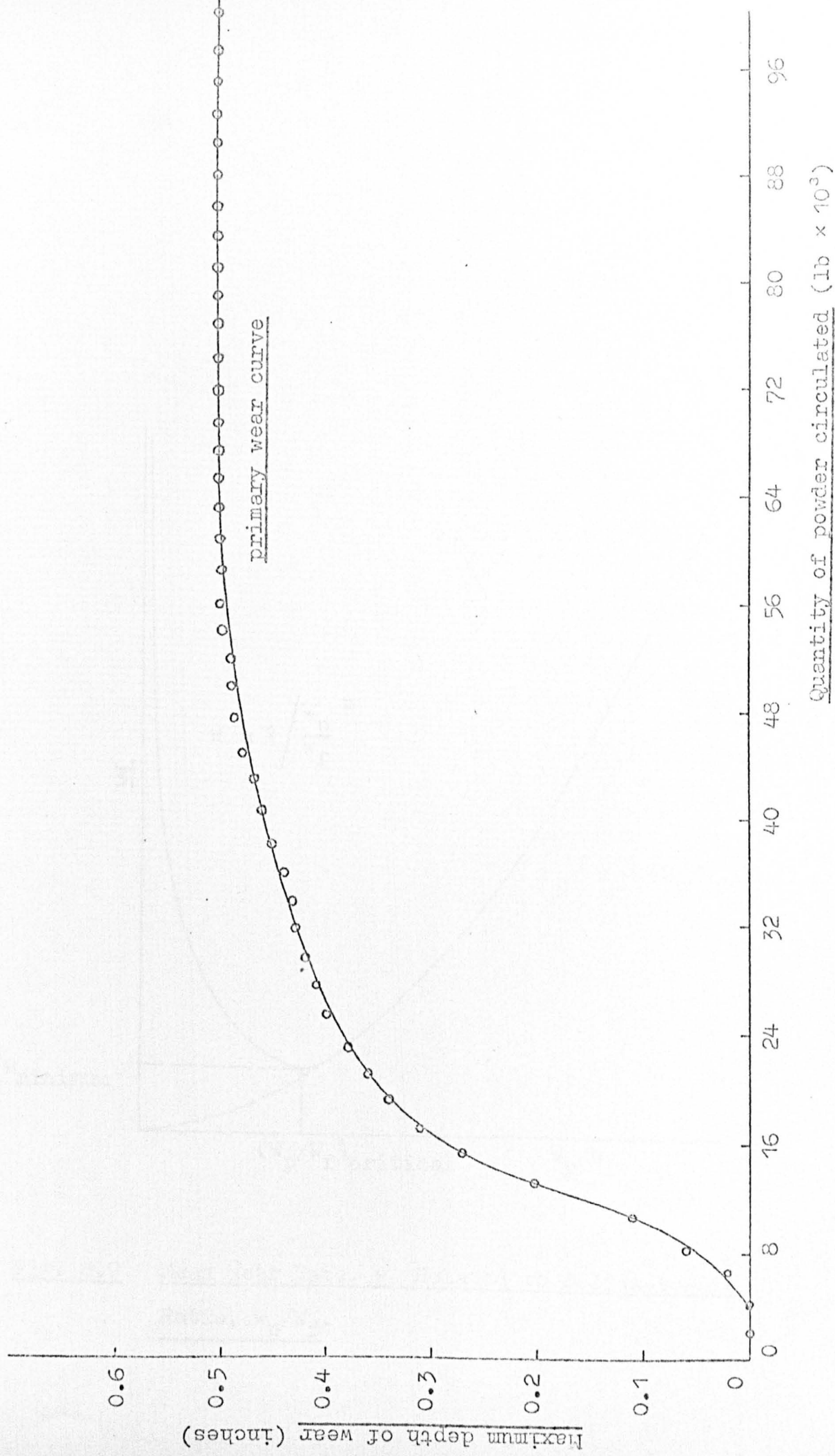


Fig. 8.6 Rate of Wear at the Primary Wear Point for Bend 4.

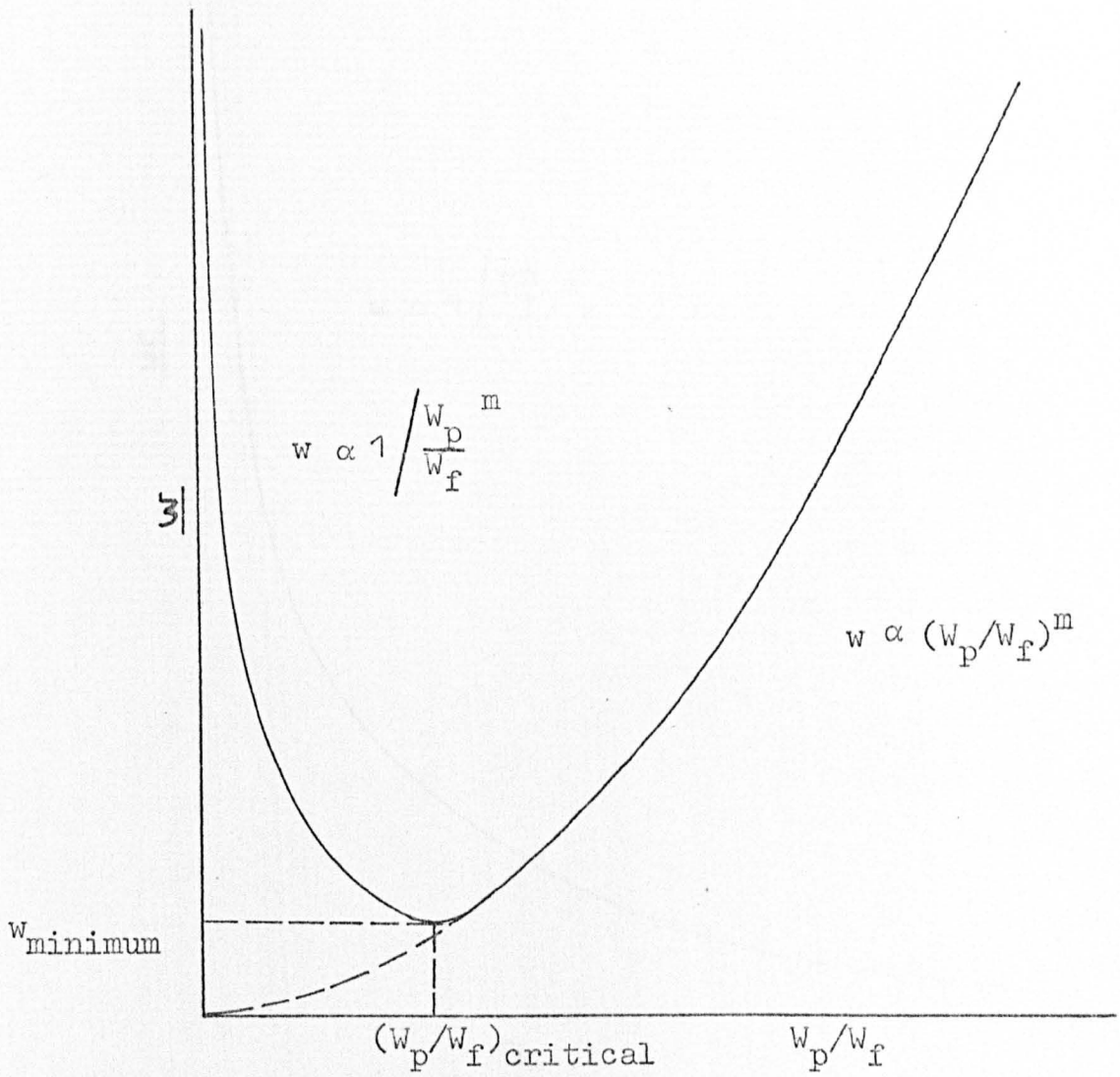


Fig. 8.7 Mean Wear Rate, w , Related to Solids-to-Air Ratio, W_p/W_f .

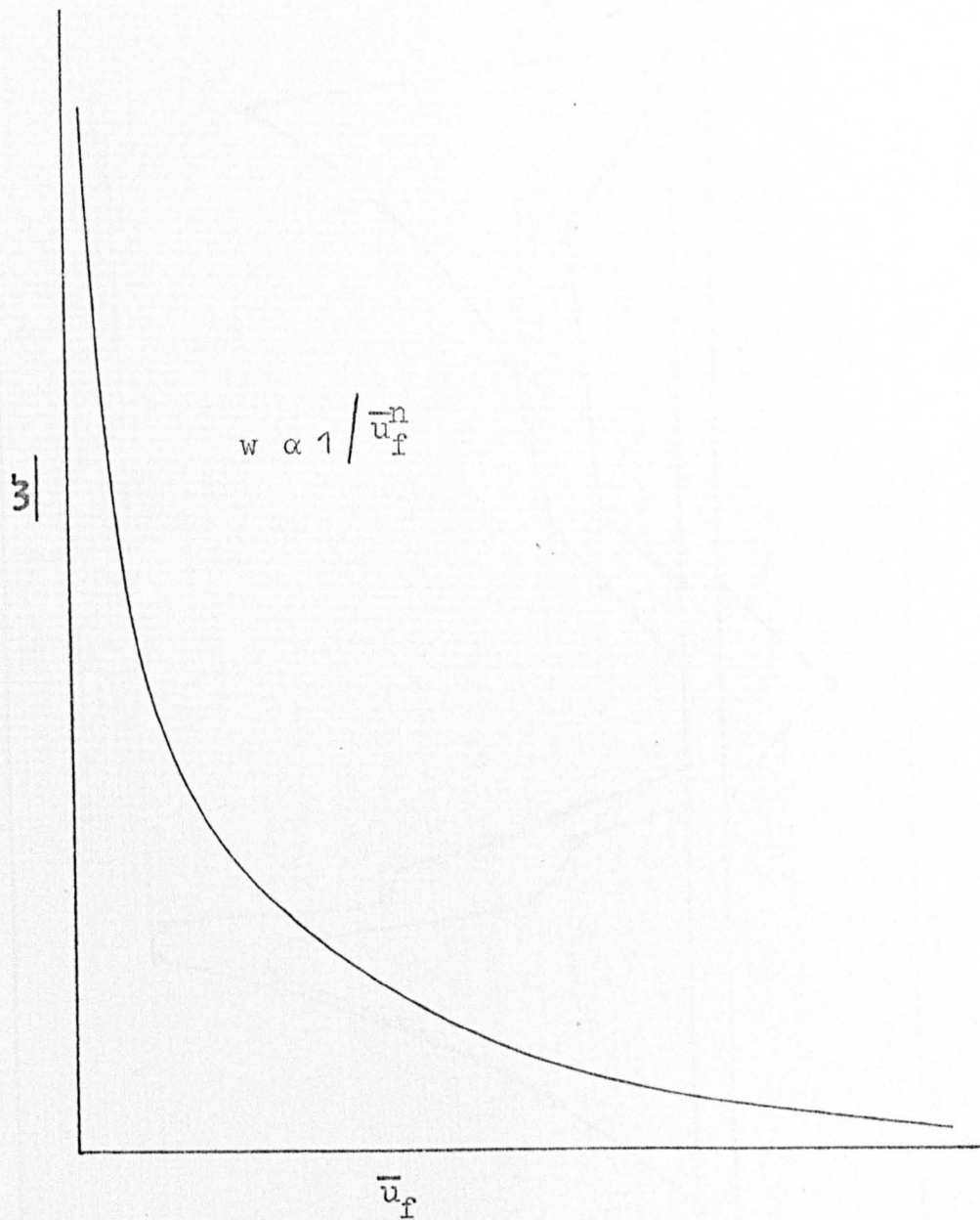


Fig. 8.8 Mean Wear Rate, w , Related to Conveying Air Velocity, \bar{u}_f .

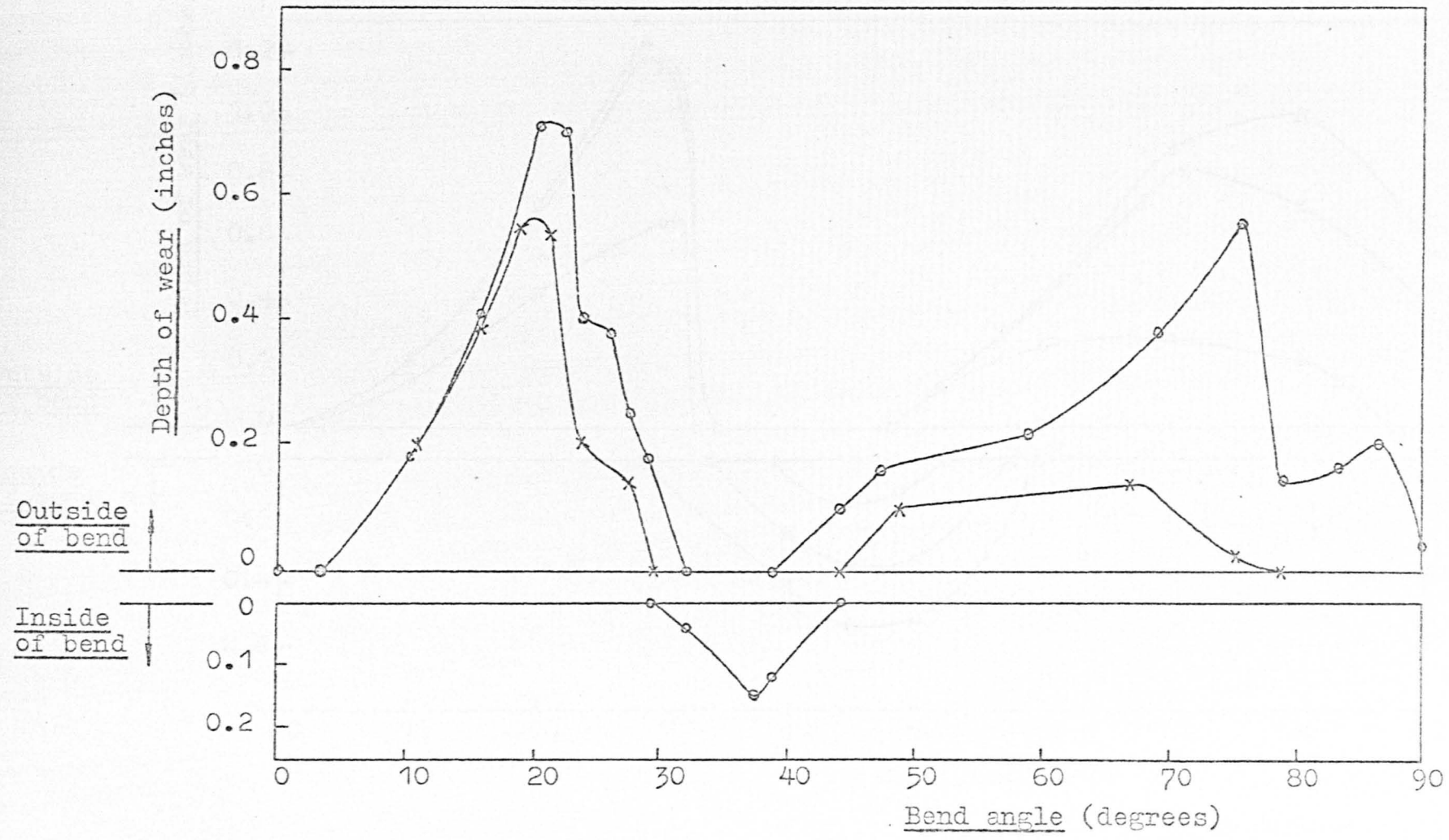


Fig. 8.9 Wear Development for Bend 1.

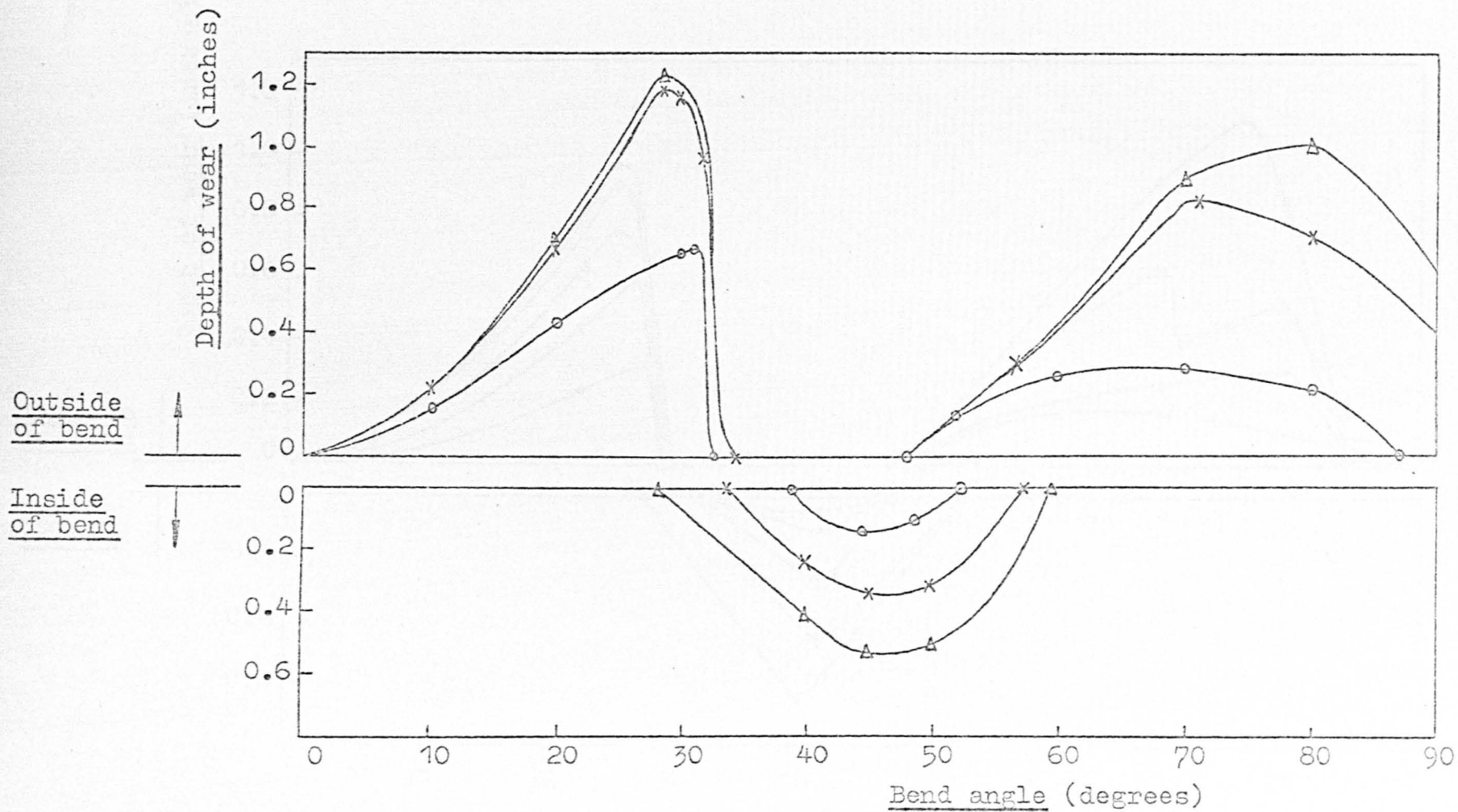


Fig. 8.10 Wear Development for Bend 2.

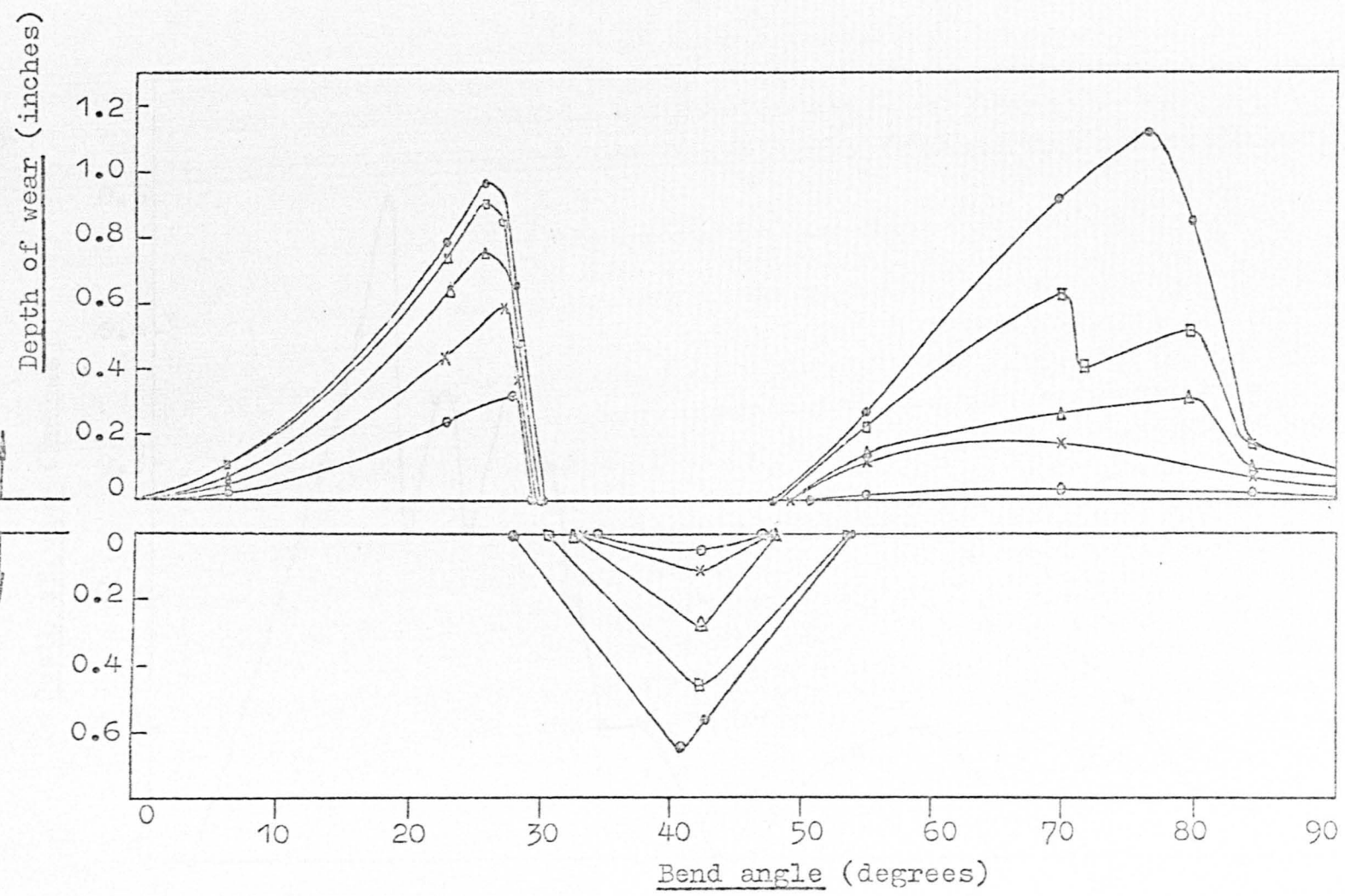


Fig. 8.11 Wear Development for Bend 3.

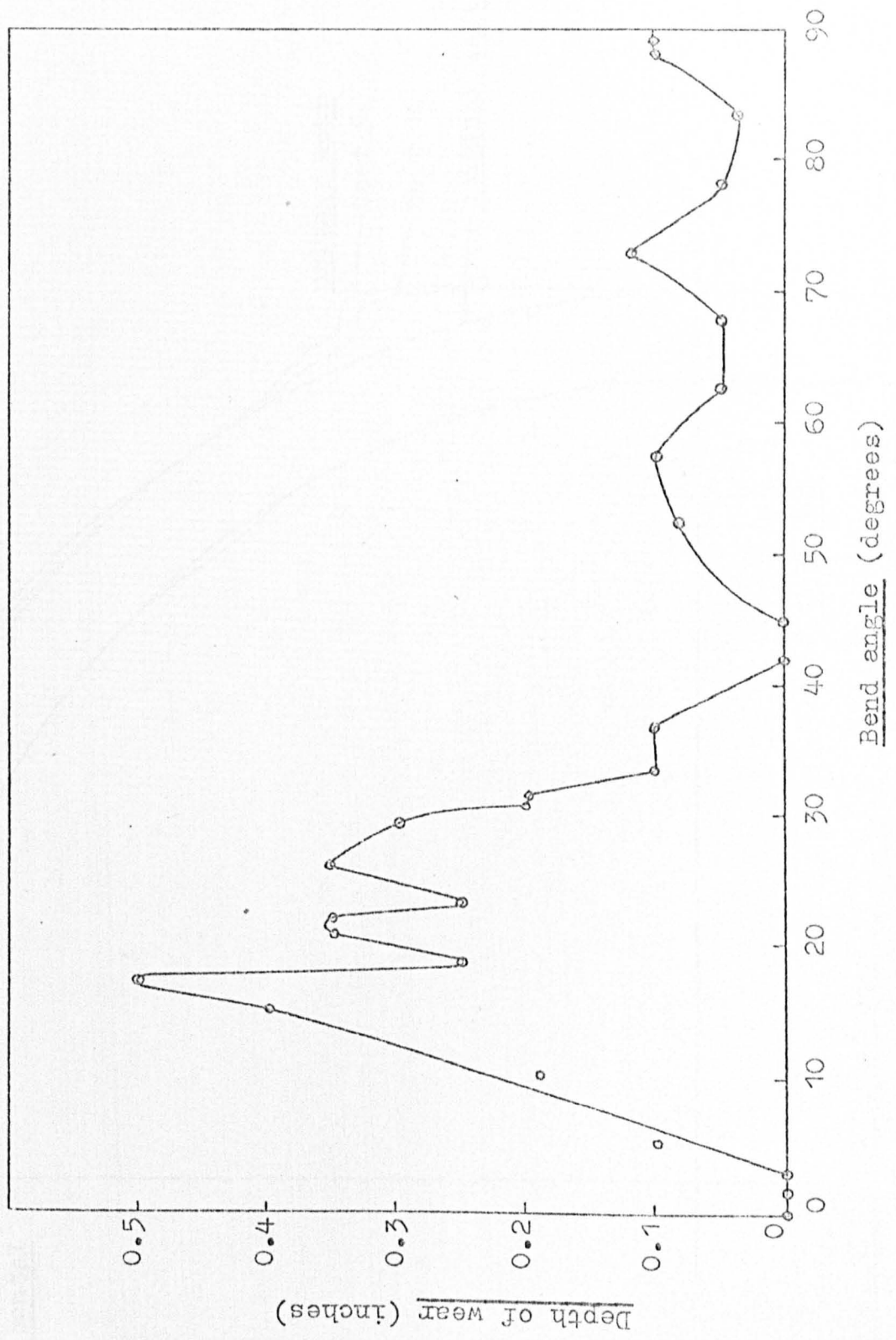


Fig. 8.12 Wear development for bend 4.

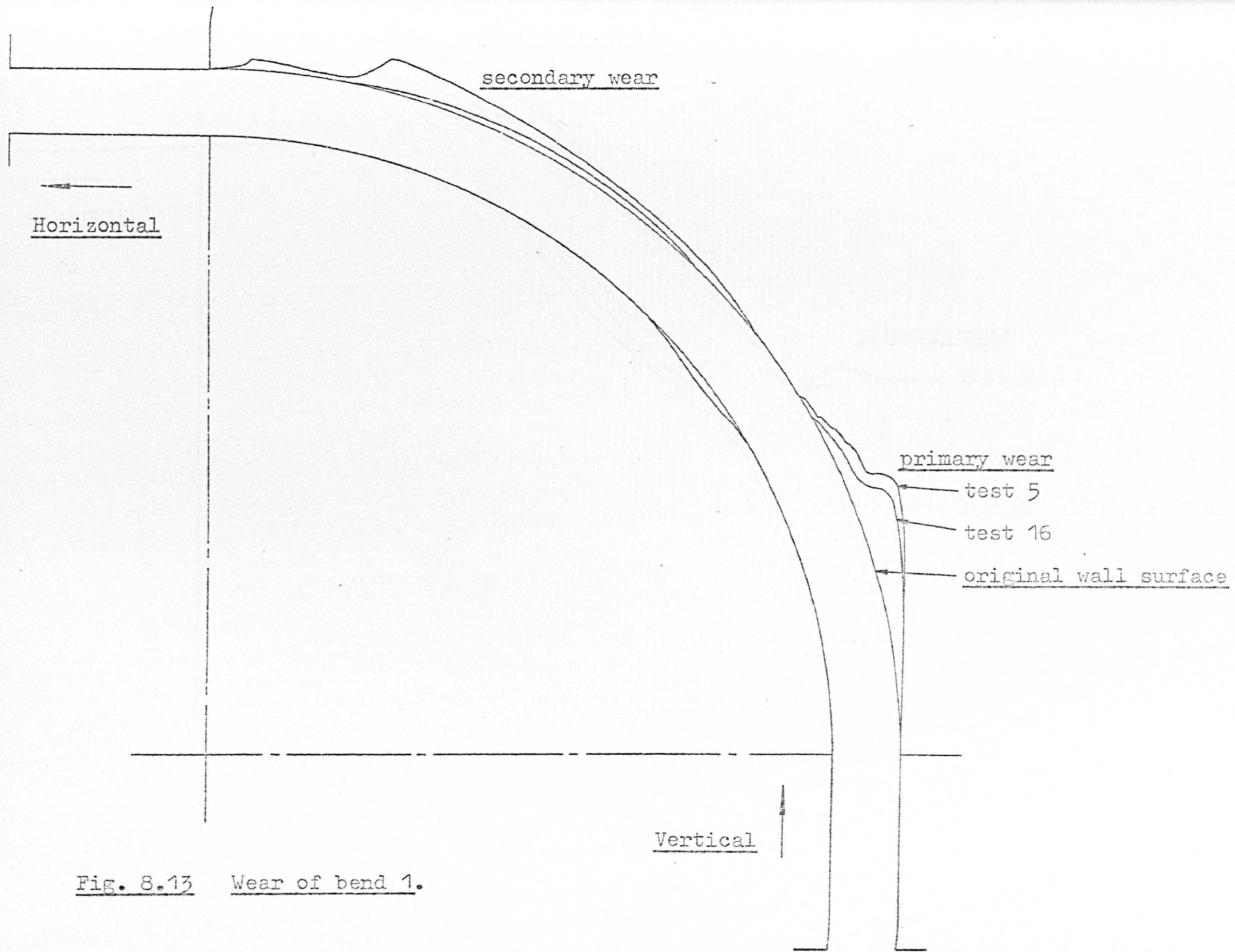


Fig. 8.13 Wear of bend 1.

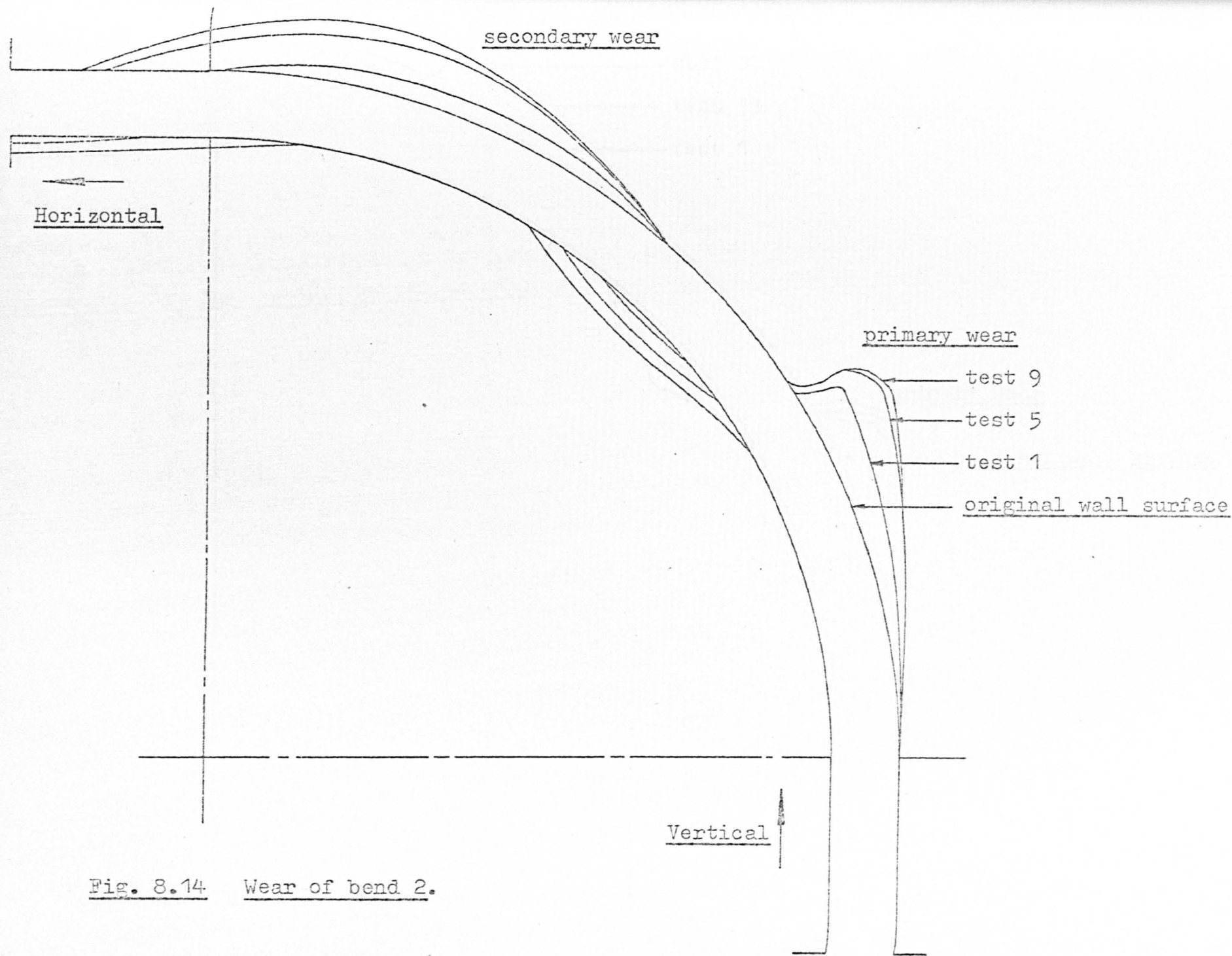


Fig. 8.14 Wear of bend 2.

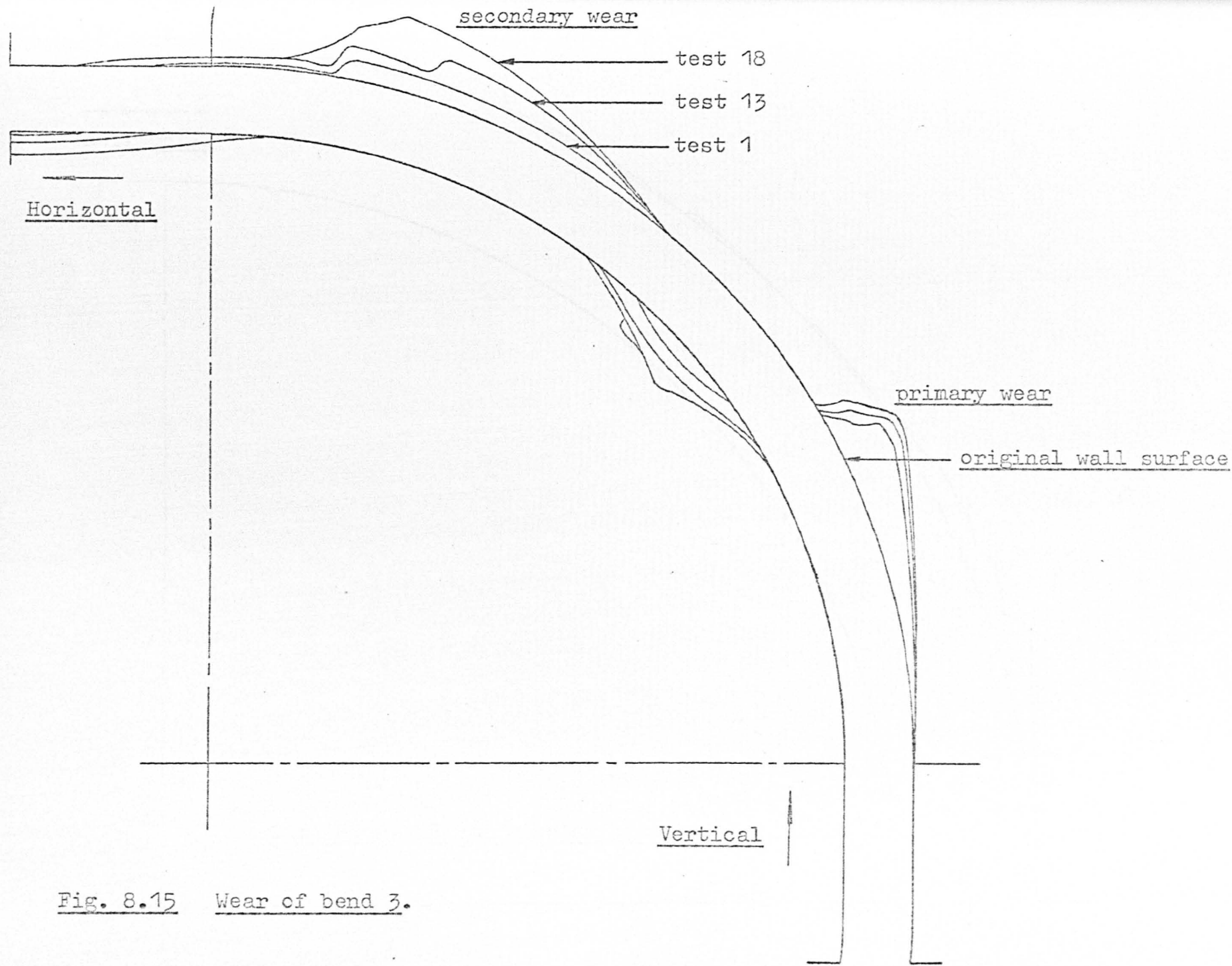


Fig. 8.15 Wear of bend 3.

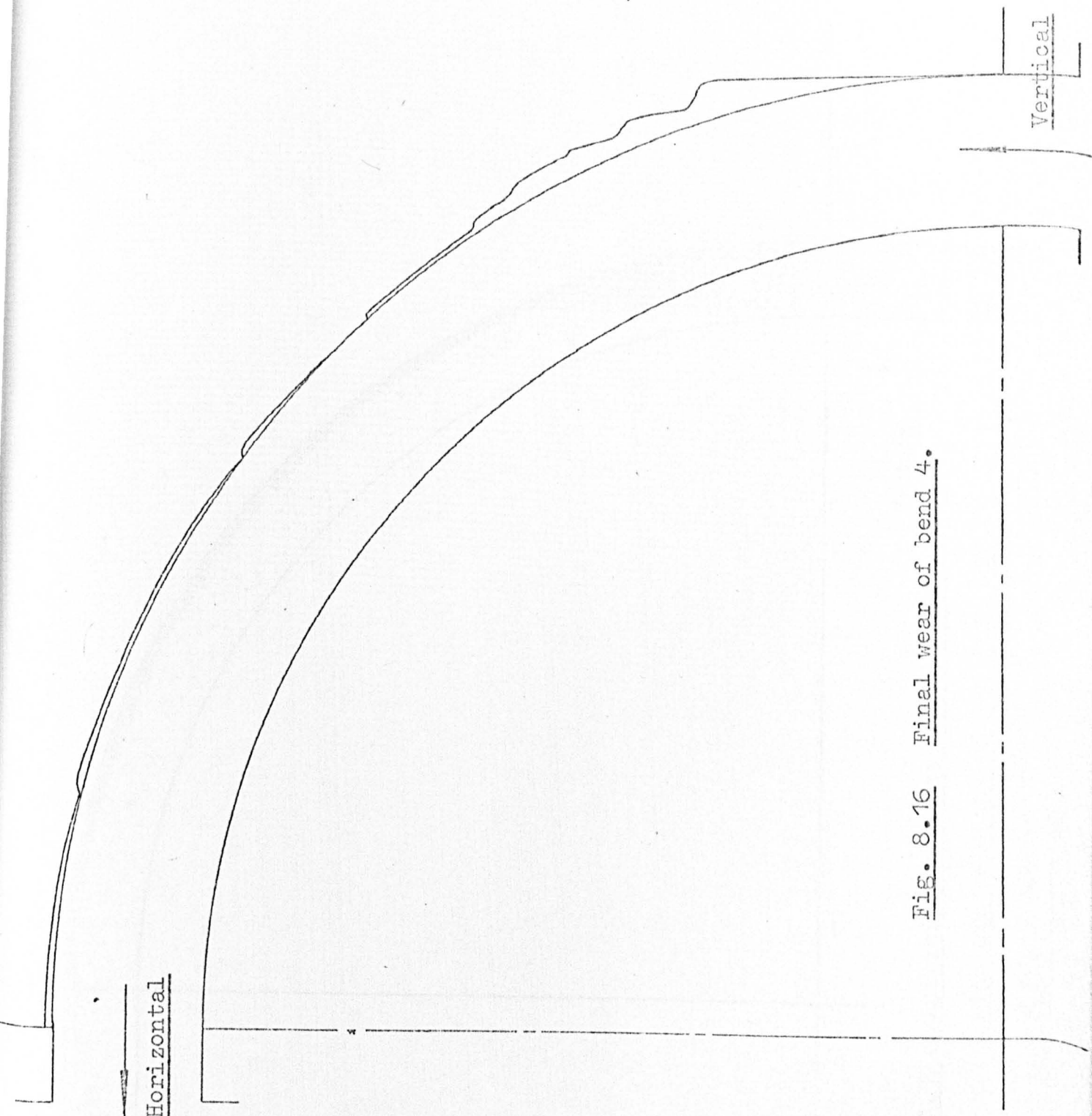


Fig. 8.16 Final wear of bend 4.

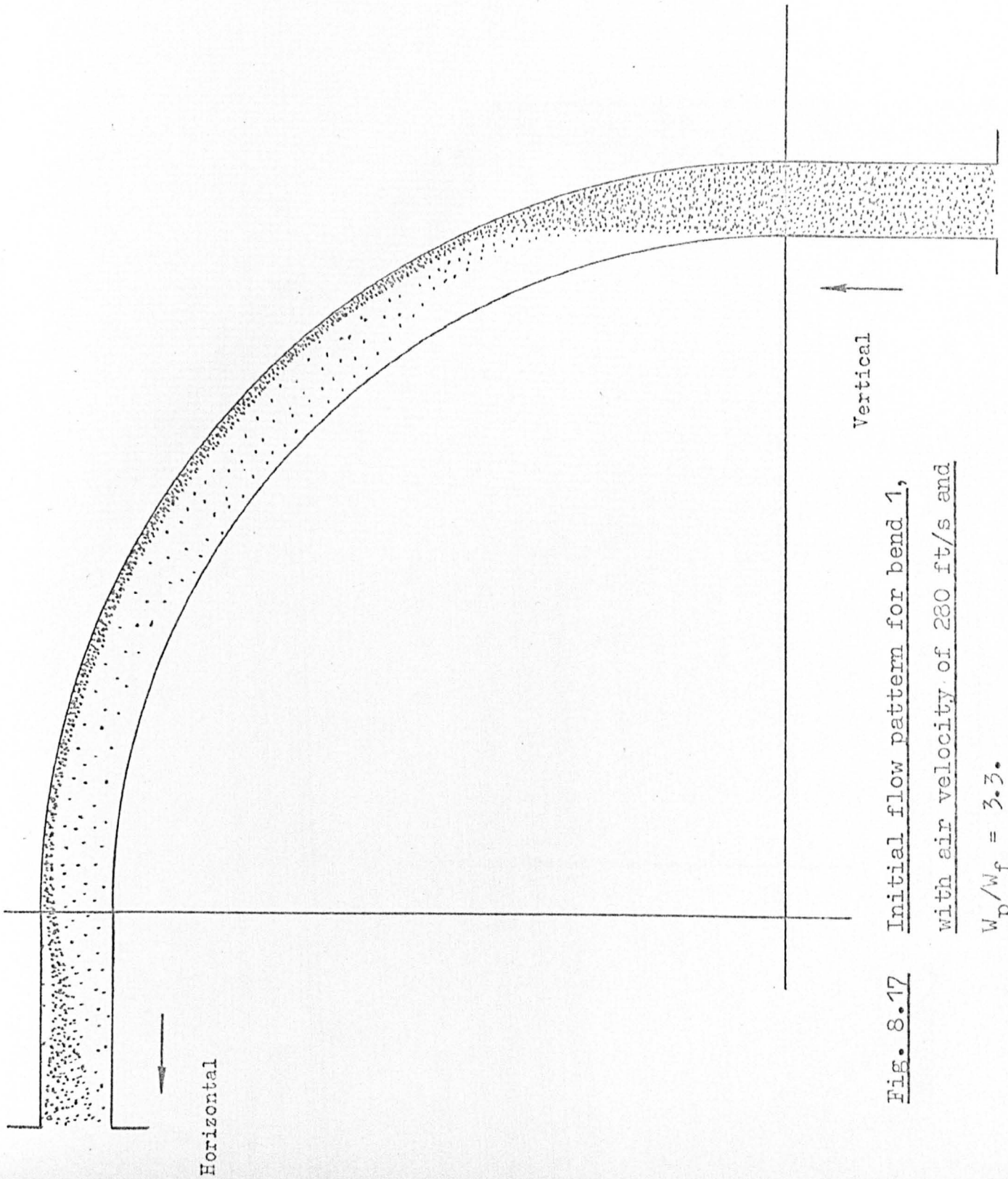


Fig. 8.17 Initial flow pattern for bend 1,
with air velocity of 280 ft/s and
 $\frac{W_p}{W_f} = 3.3.$

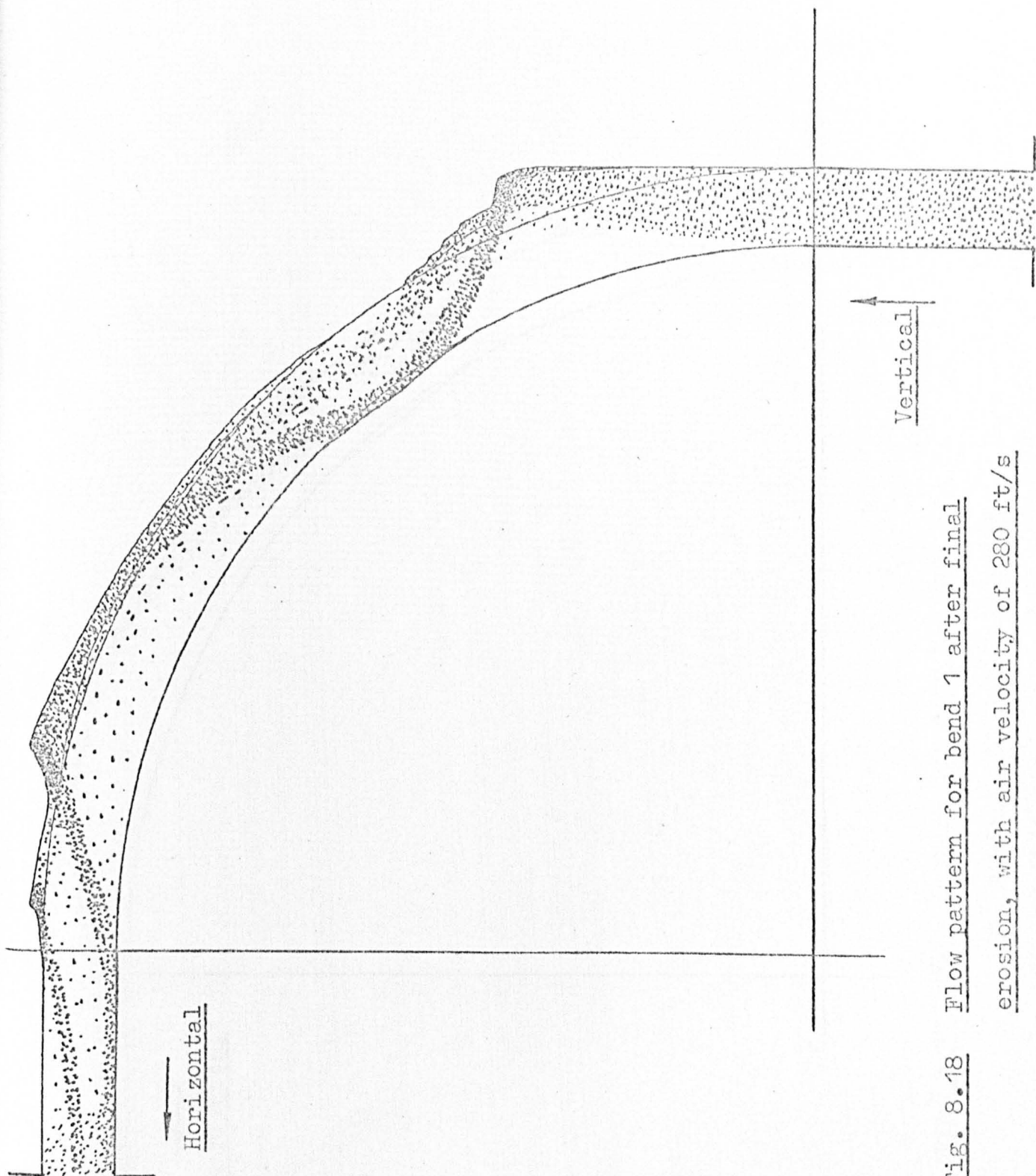


Fig. 8.18 Flow pattern for bend 1 after final
erosion, with air velocity of 280 ft/s
and $w_p/w_f = 3.3$.

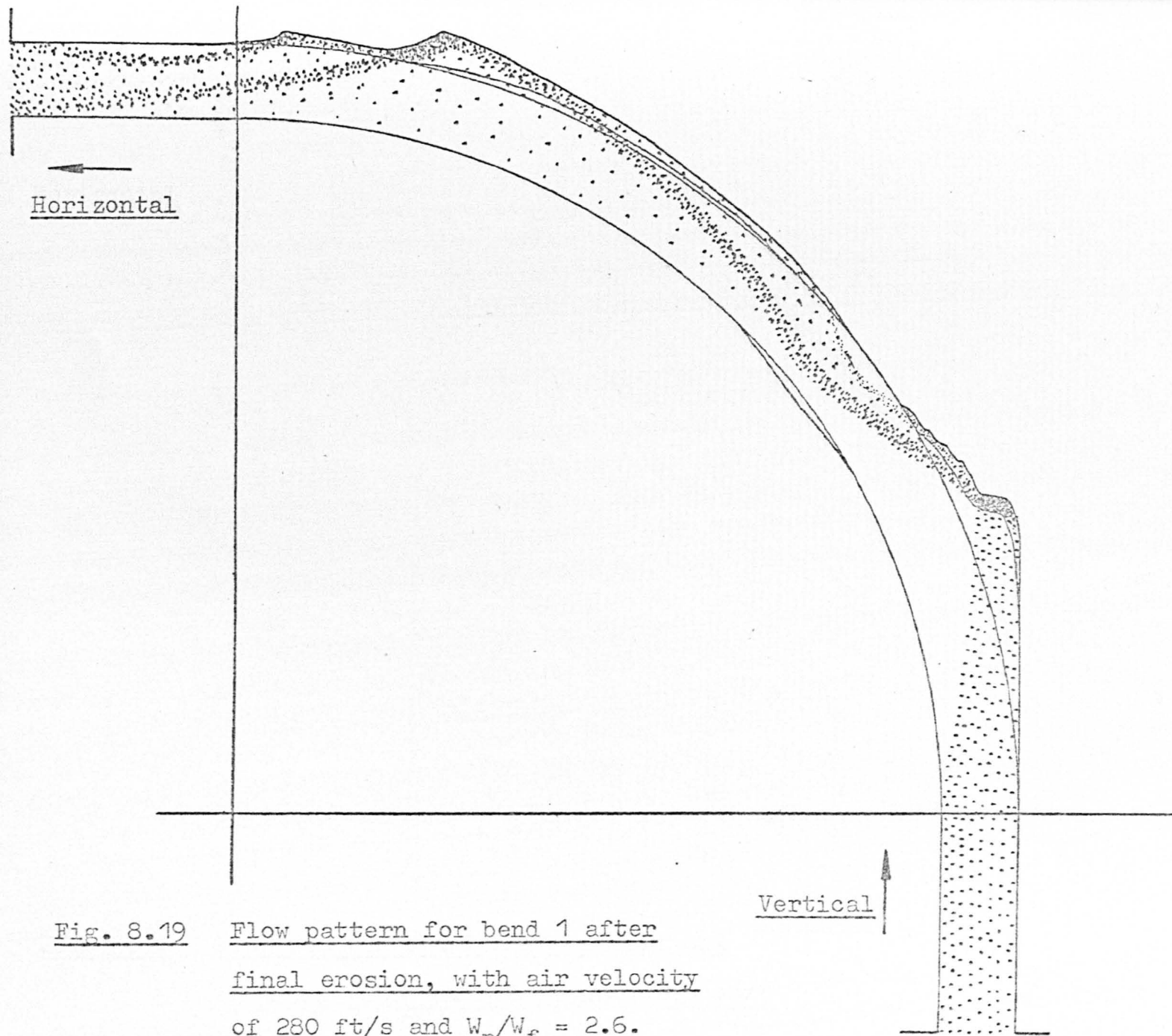
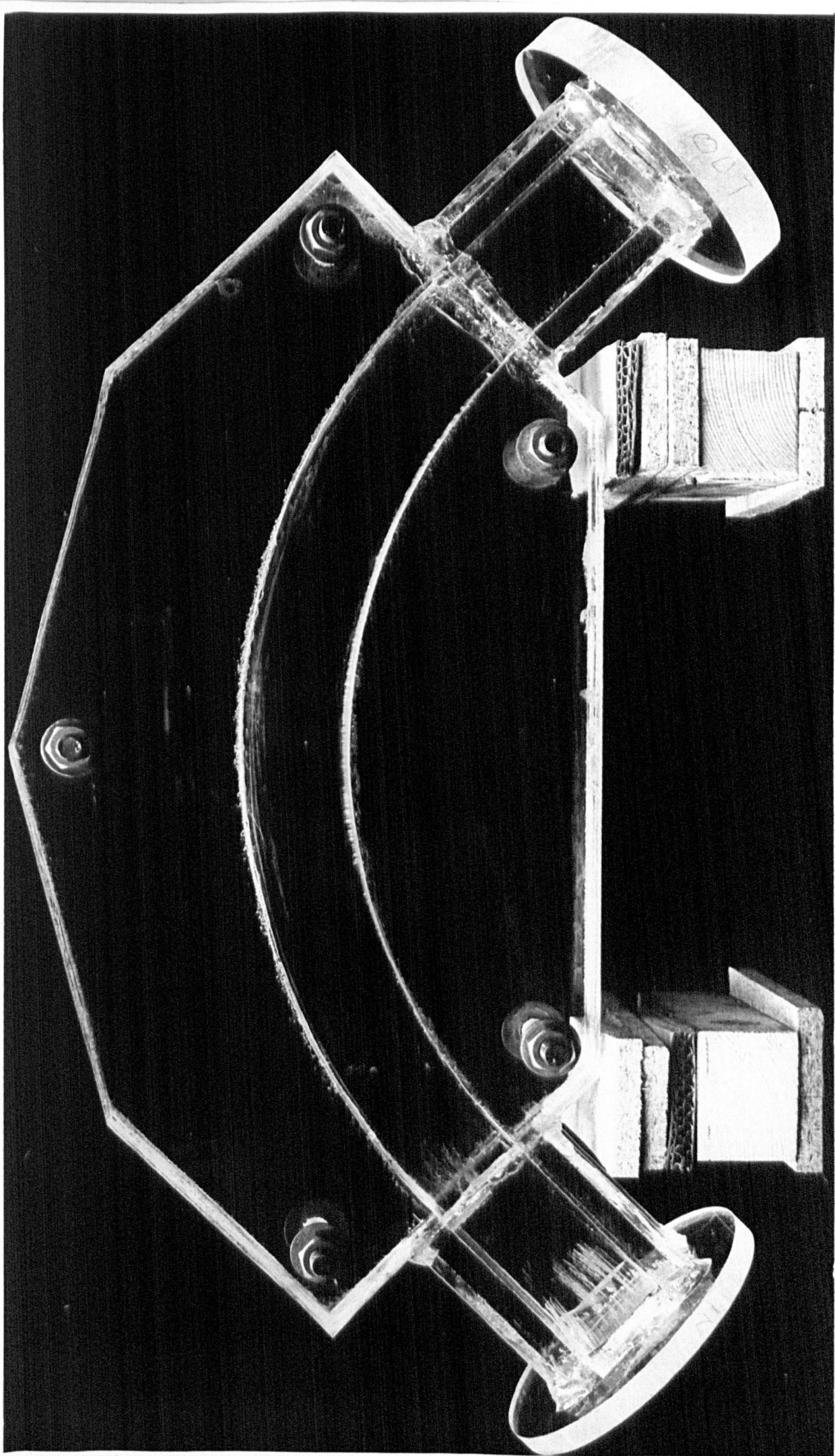


Fig. 8.19 Flow pattern for bend 1 after
final erosion, with air velocity
of 280 ft/s and $W_p/W_f = 2.6$.

Plate 8 : 2" - 90° Bend.



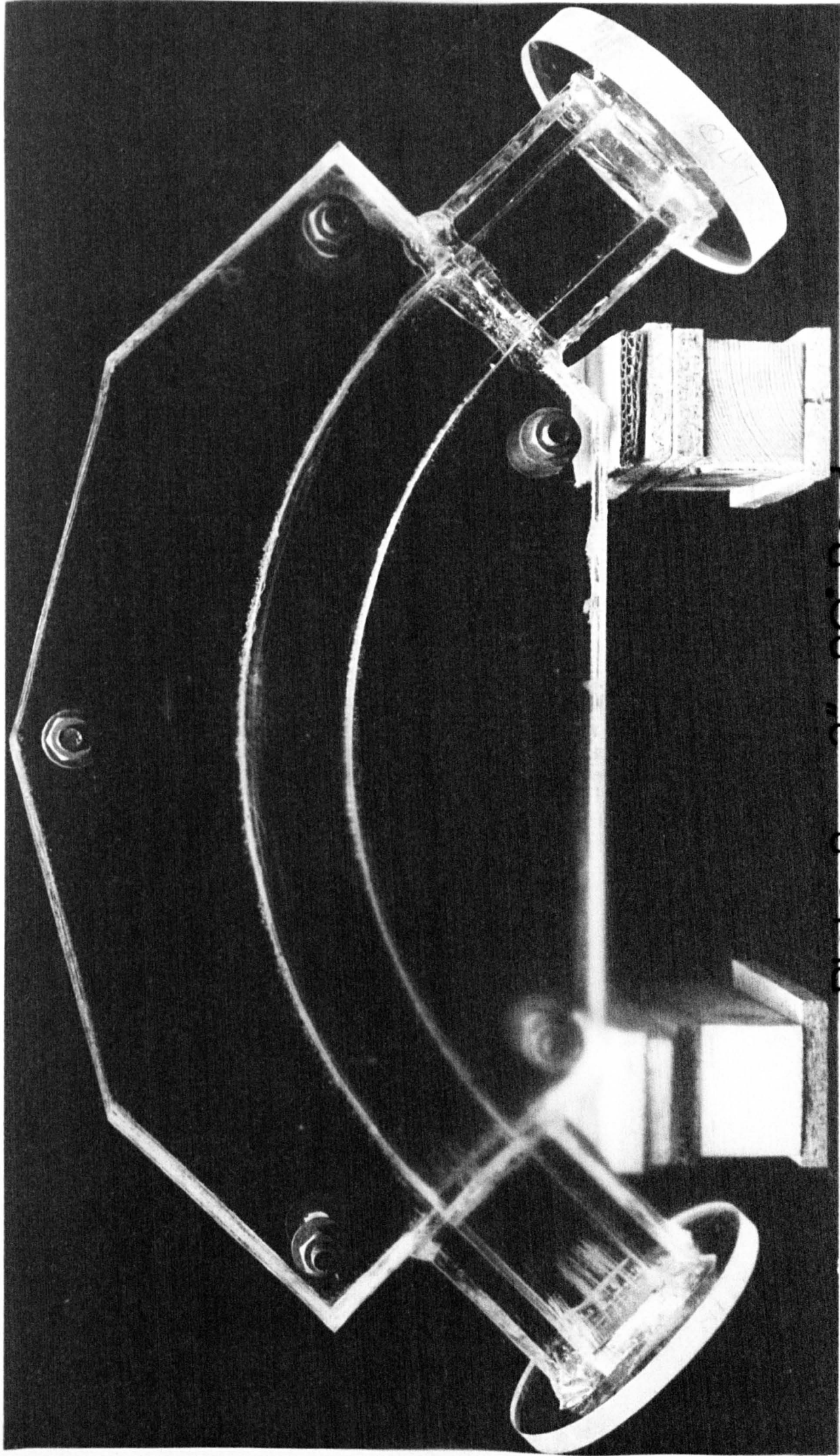
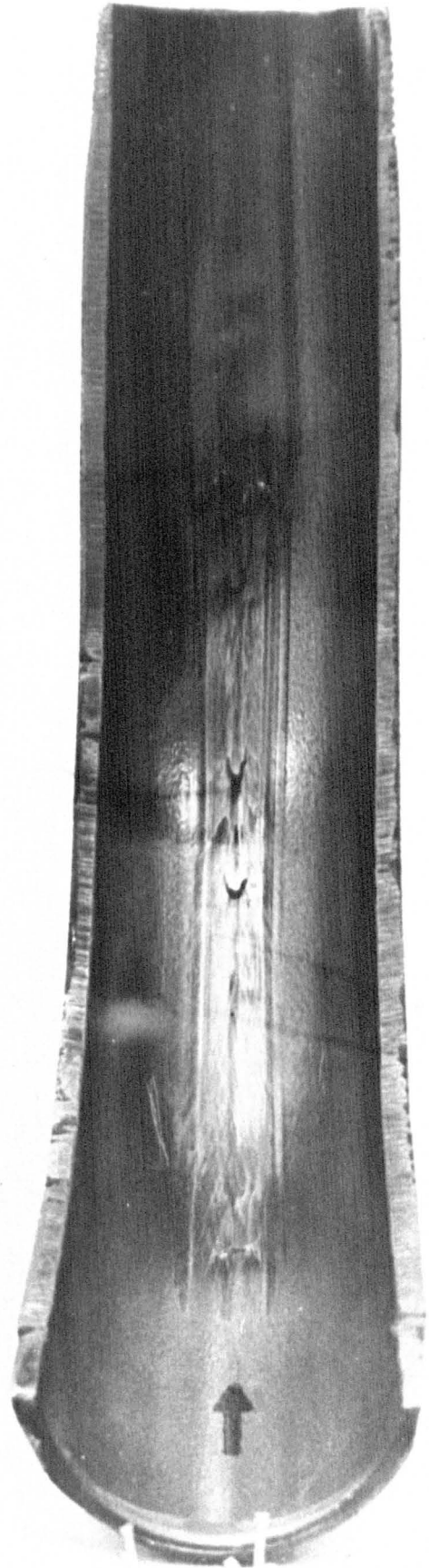
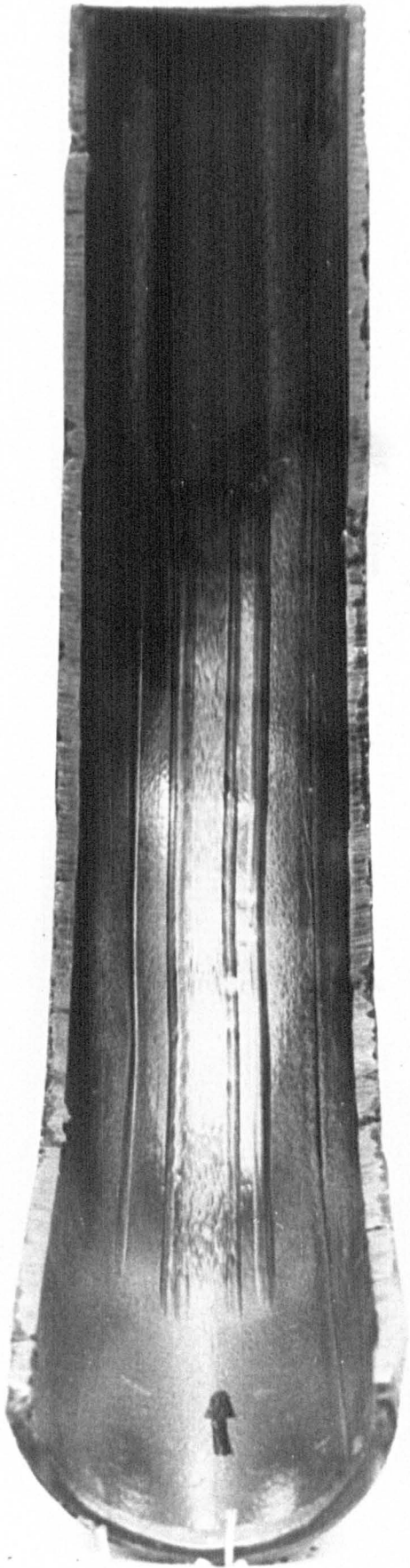


Plate 8: 2" - 90° Bend.

Plate 9: Progressive Wear.



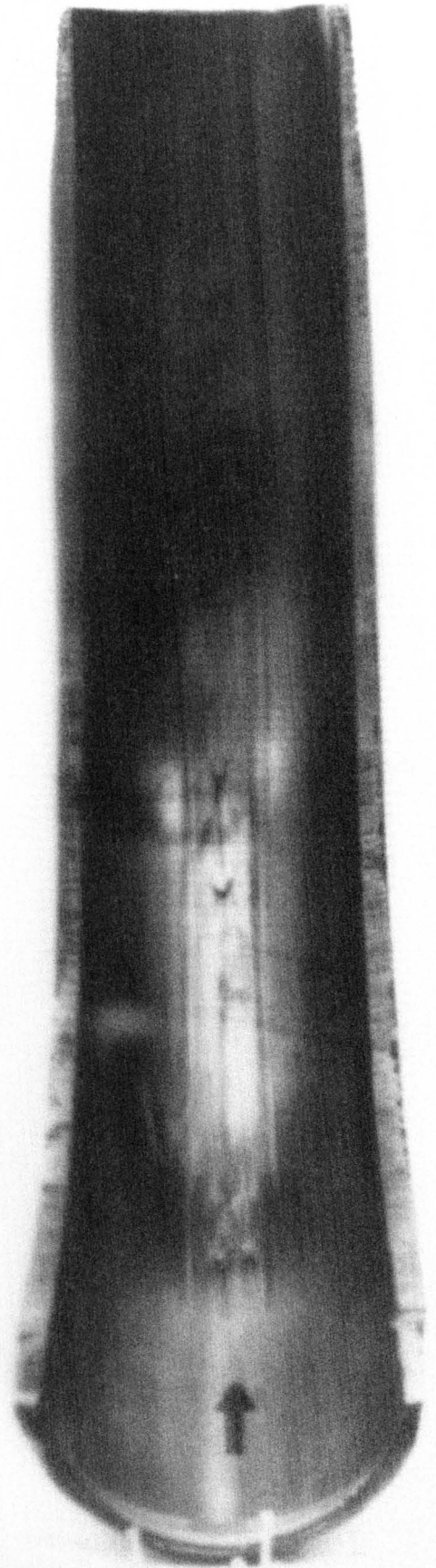
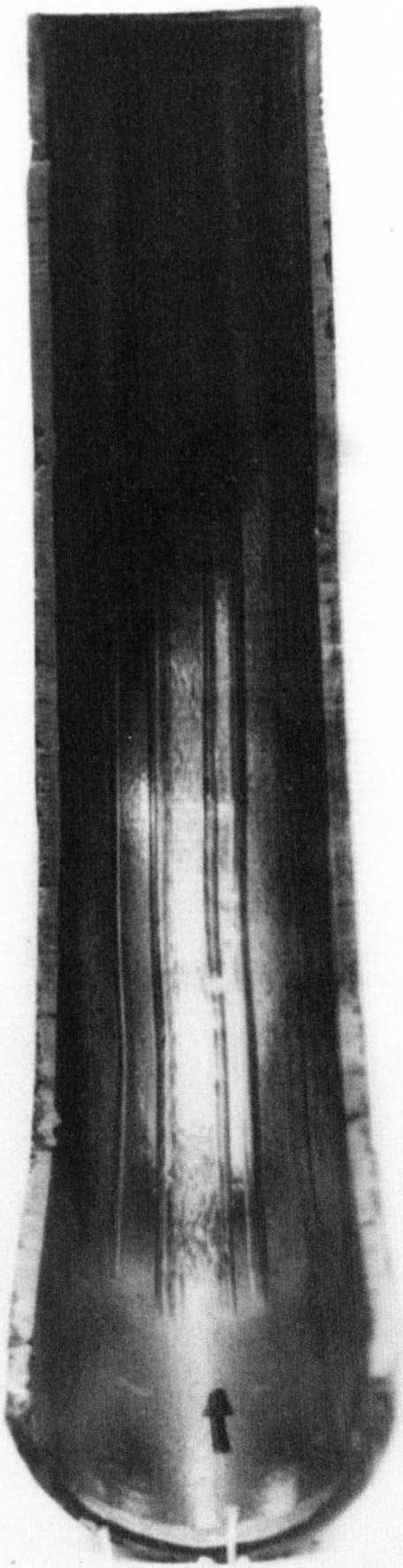


Plate 9: Progressive Wear.

Plate 10.

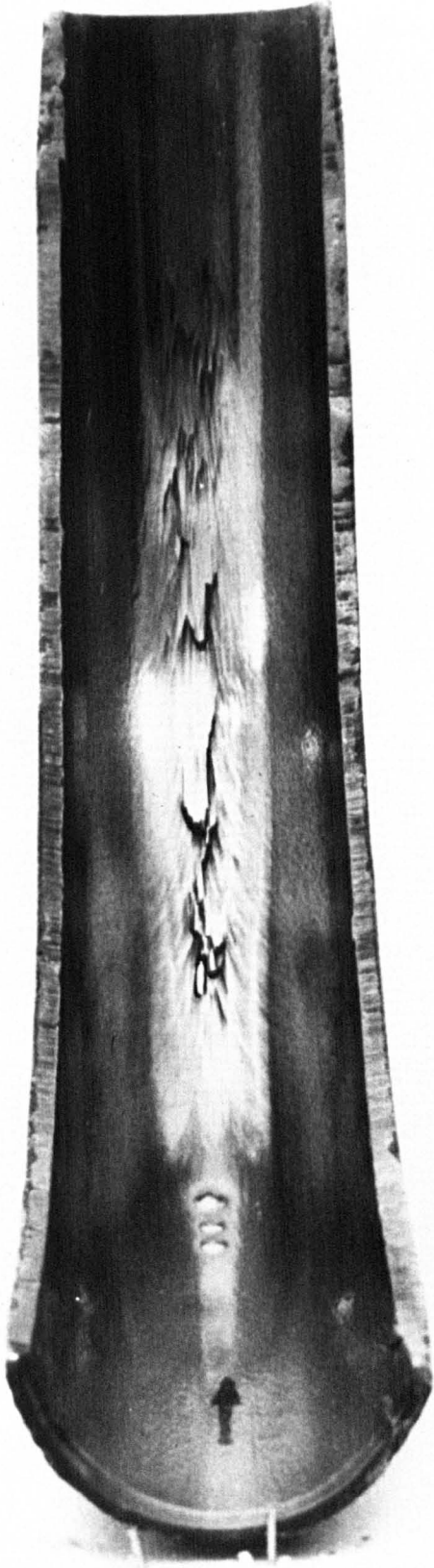
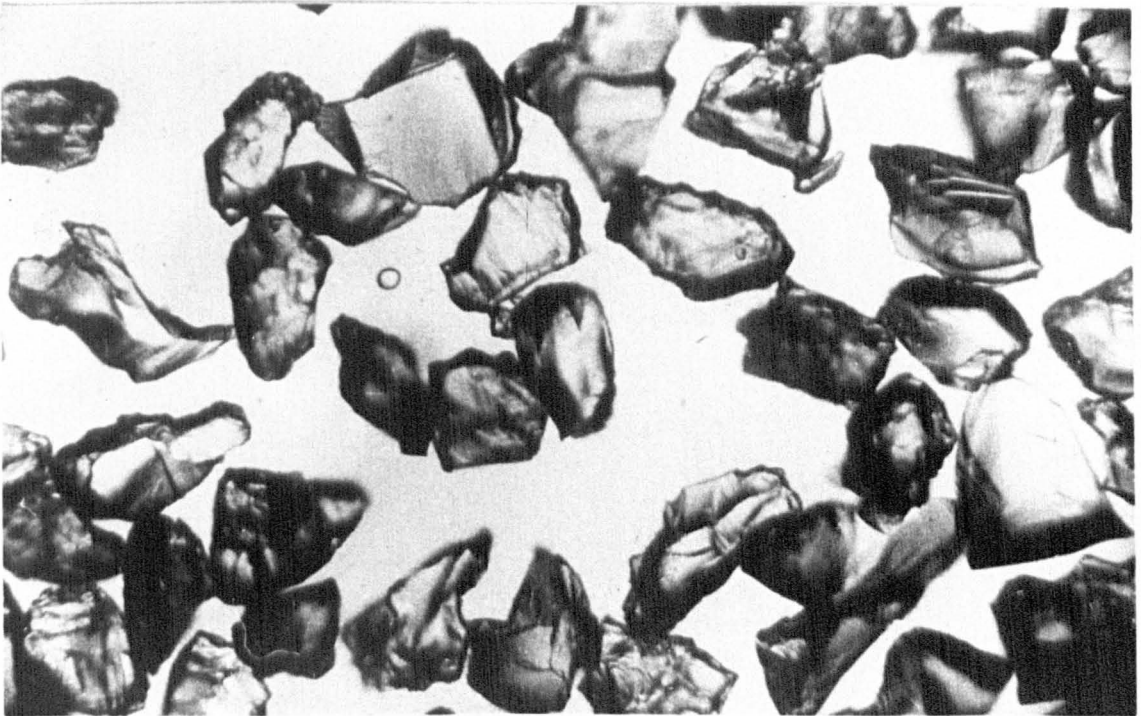
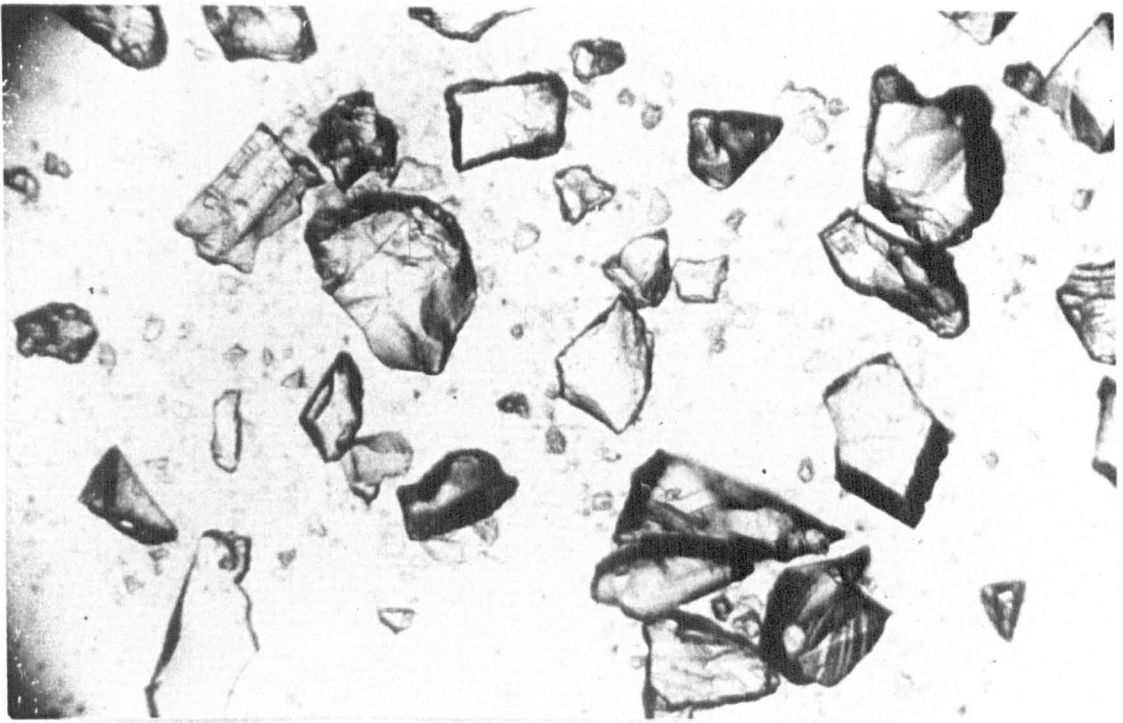


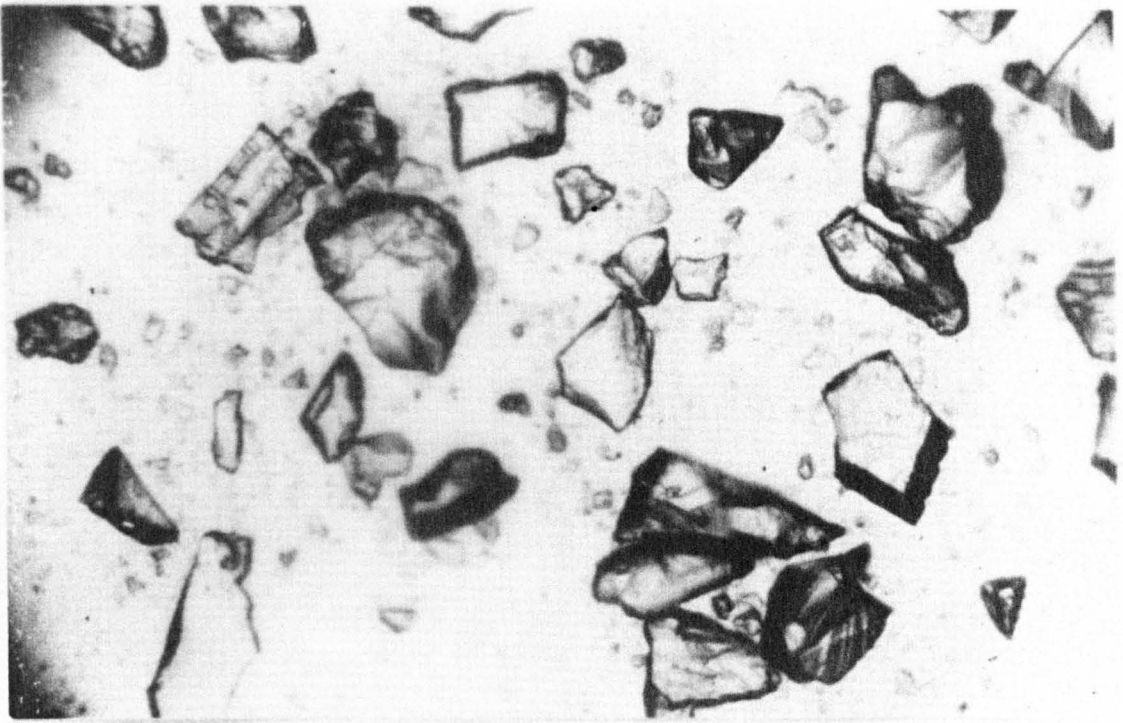


Plate 10.

240 mesh: after bend | tests.

Plate II: new alumina.





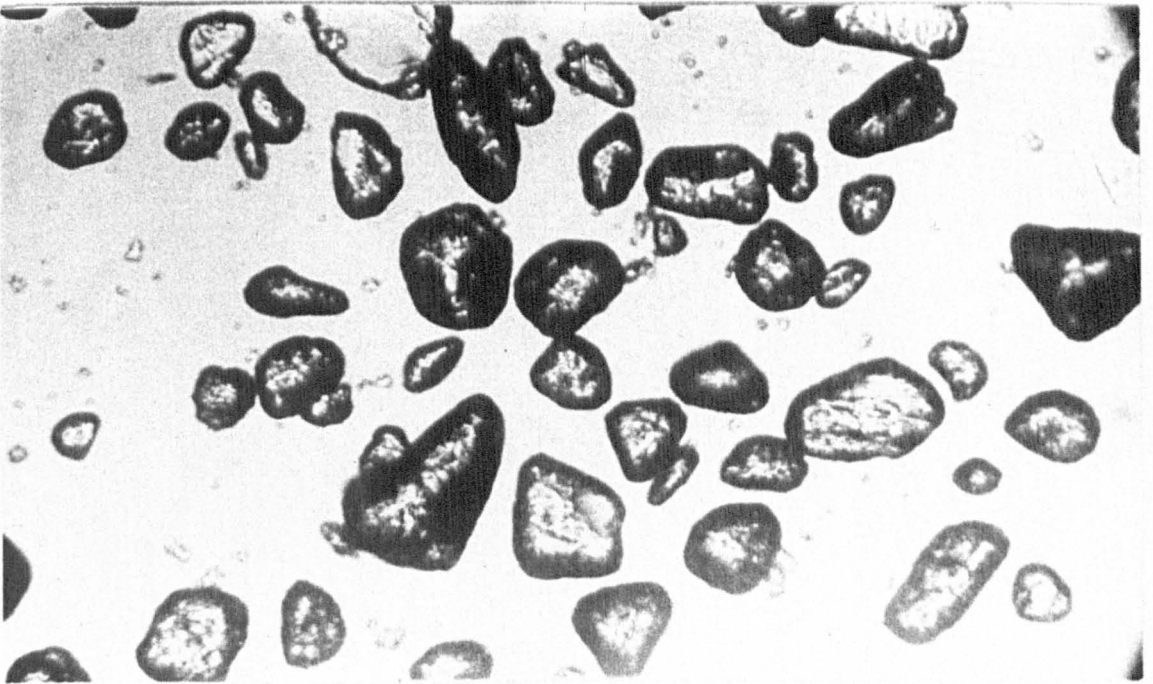
240 mesh: after bend I tests.

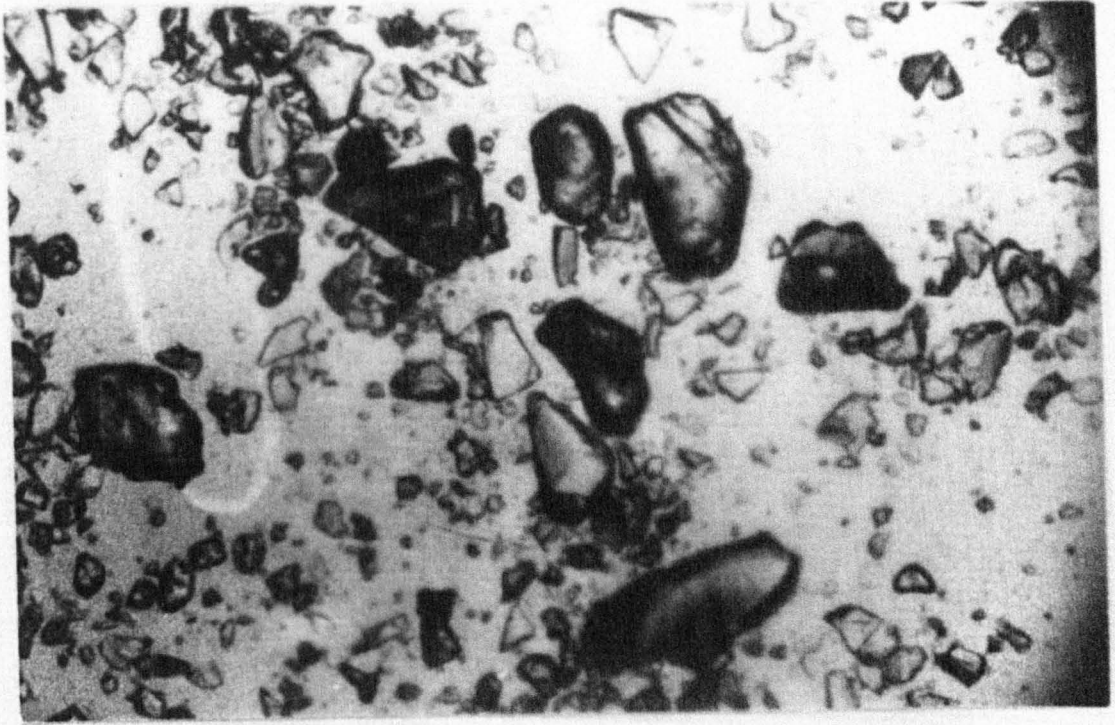


Plate II: new alumina.

240 mesh: after bend 3 tests.

Plate 12: ultimate particle shape.



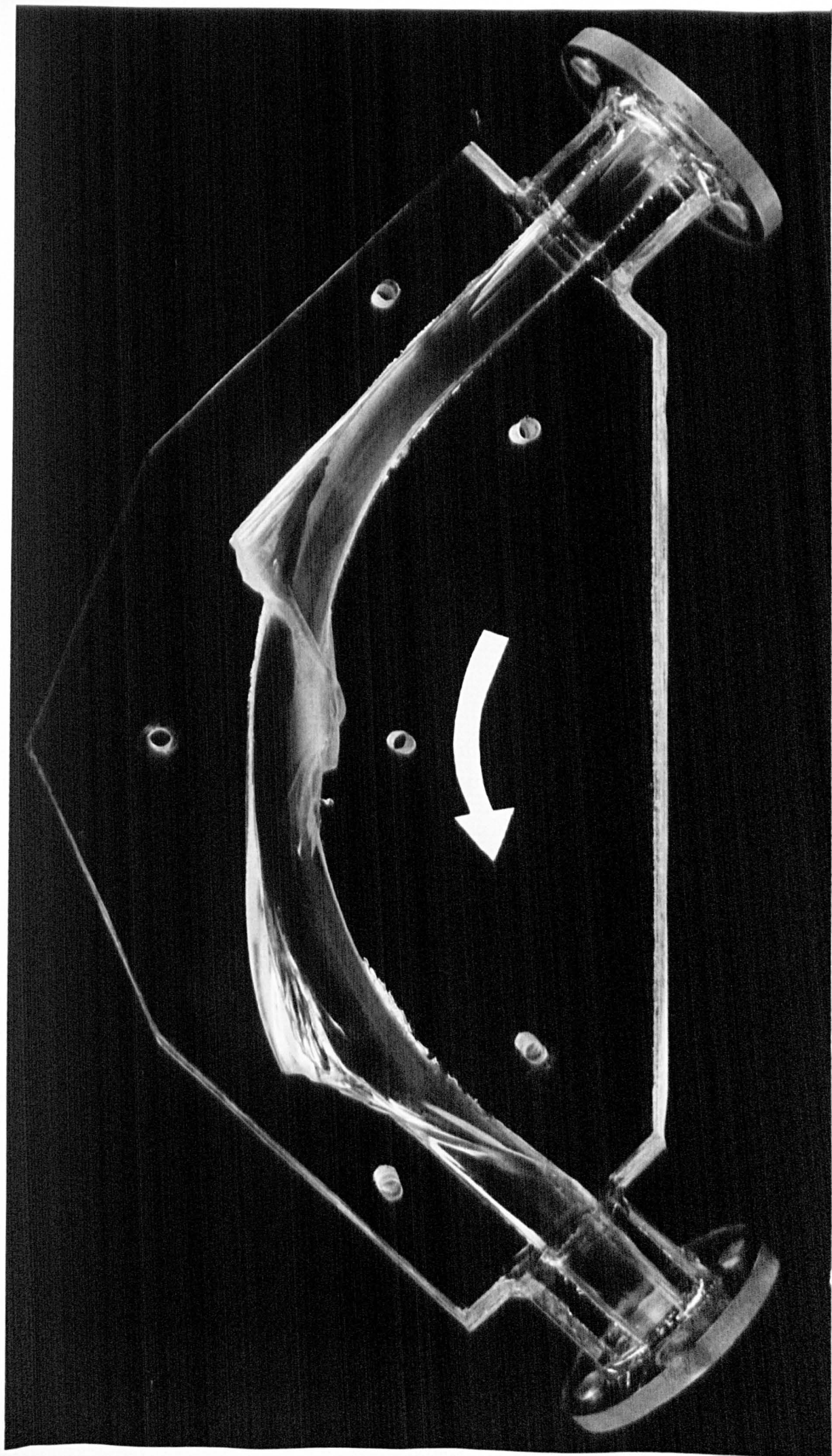


240 mesh: after bend 3 tests.



Plate 12: ultimate particle shape.

Plate 13: Bend 2.



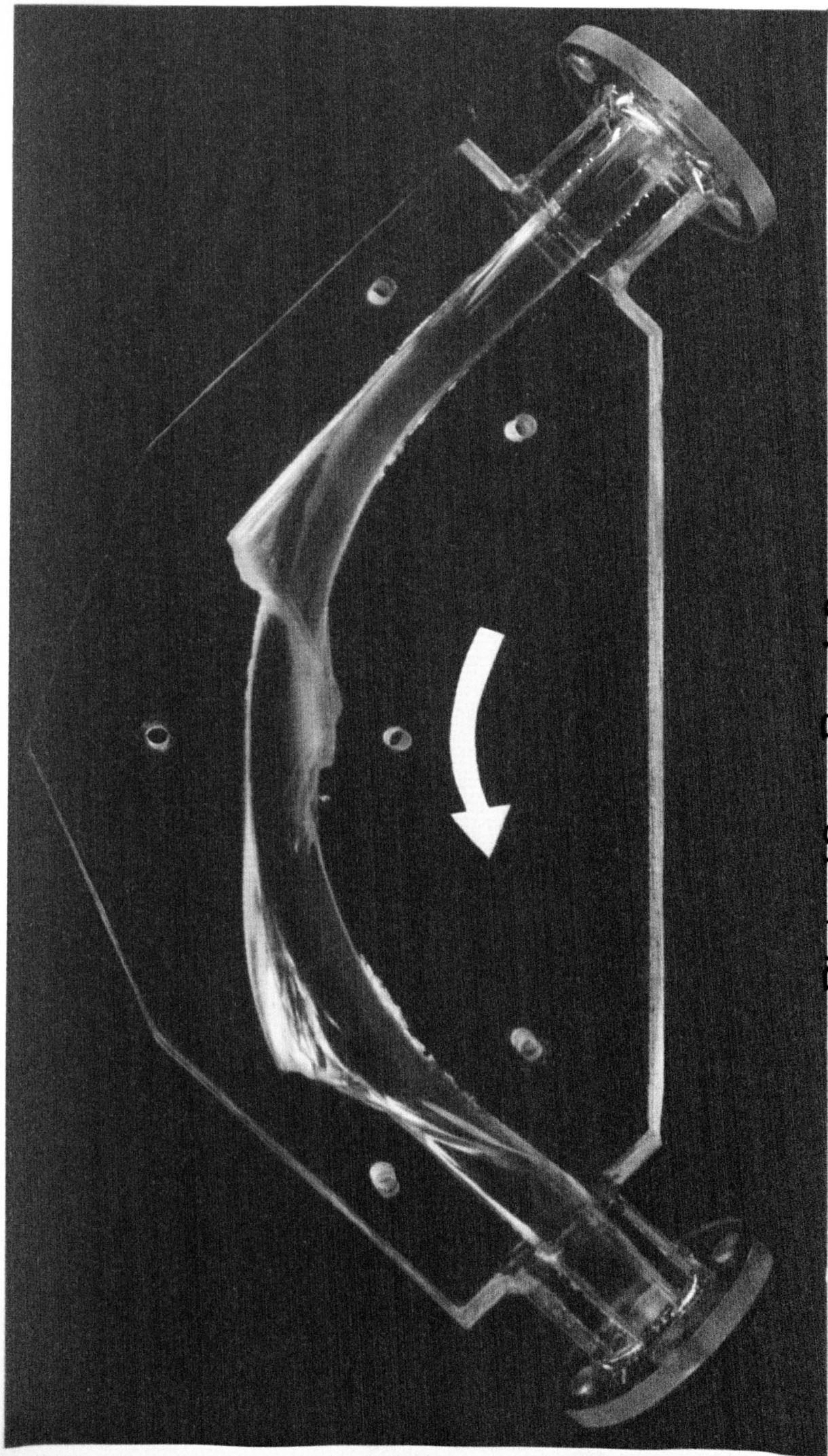
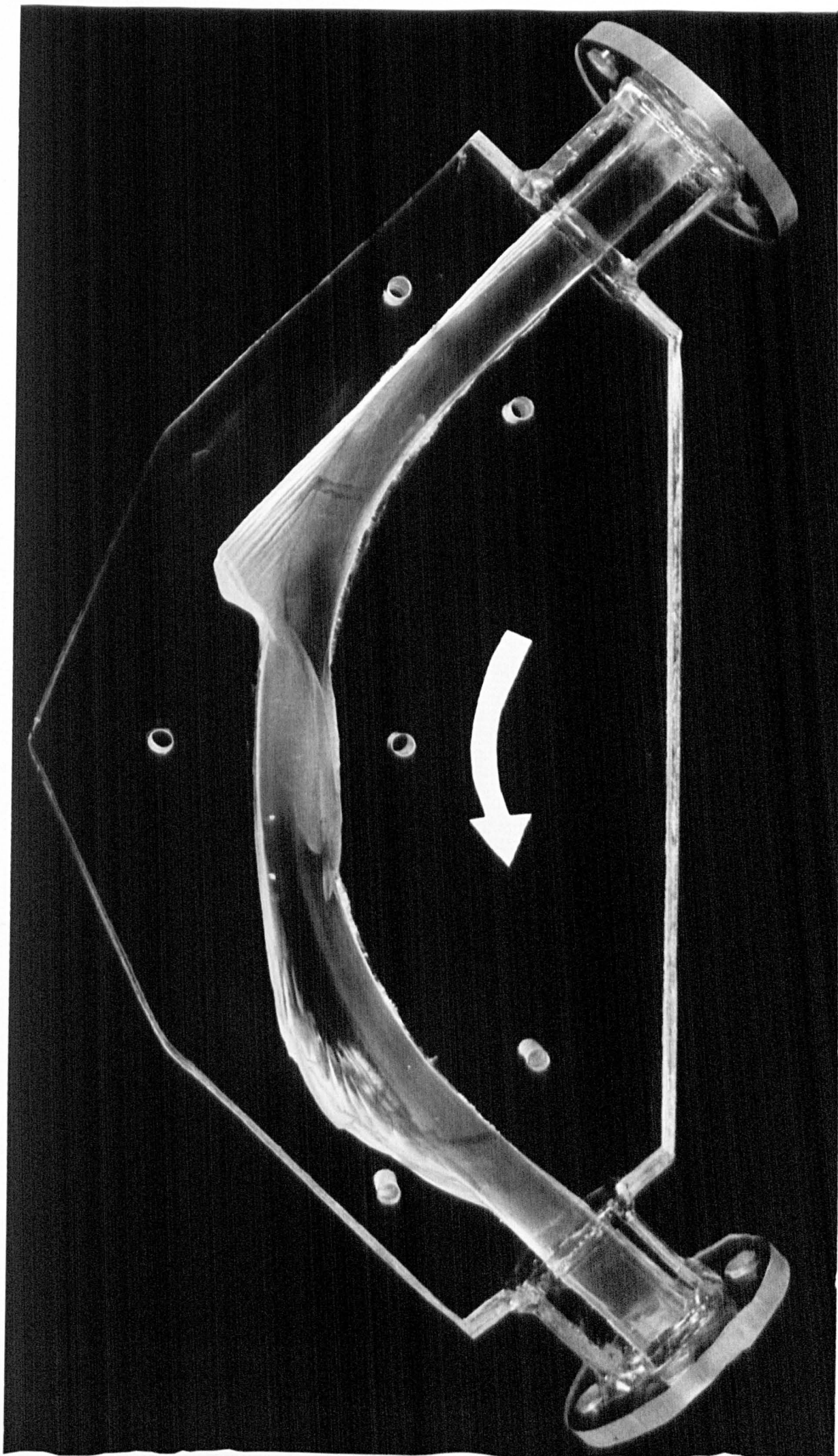


Plate 13: Bend 2.

Plate 14: Bend 3.



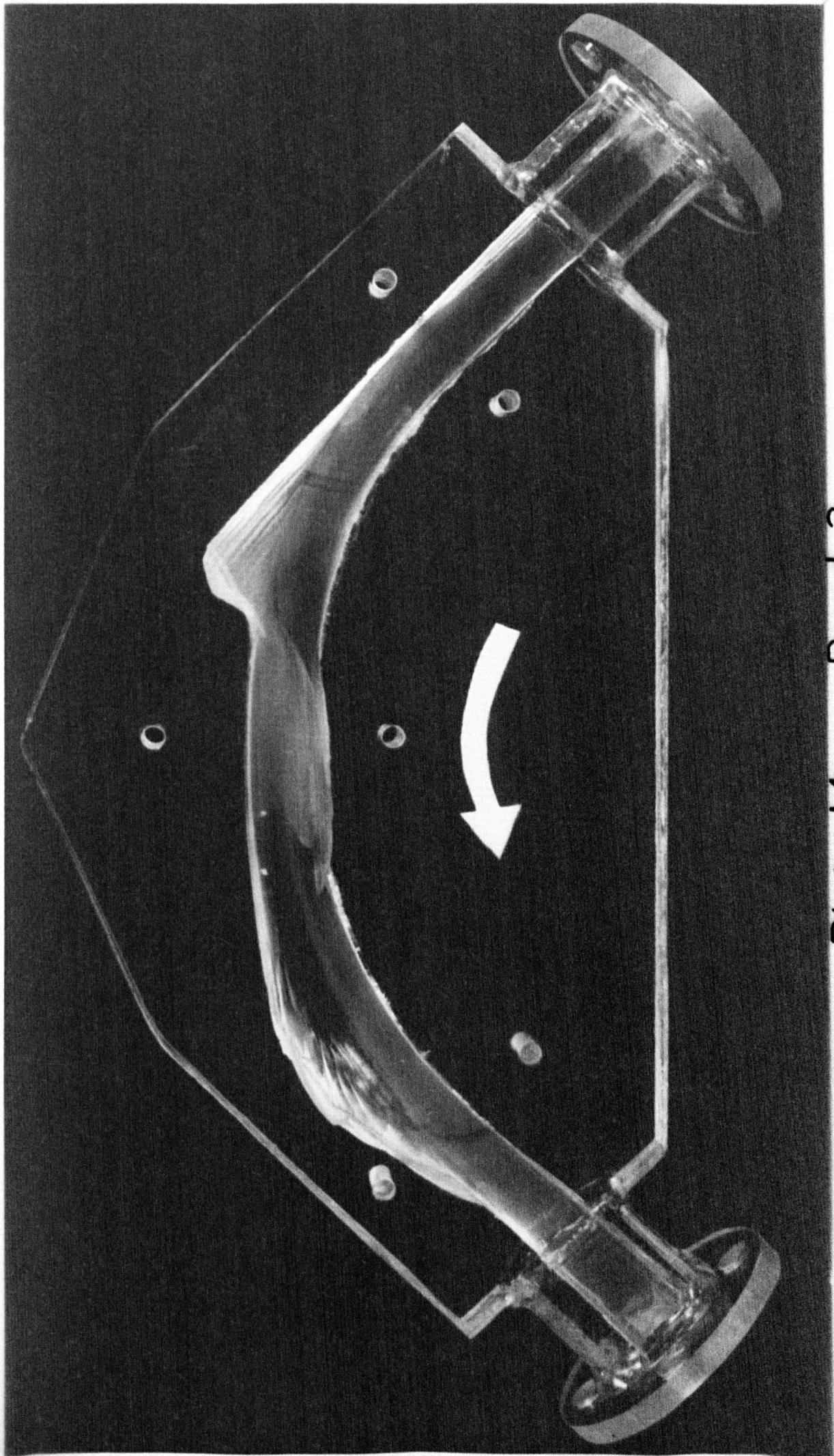
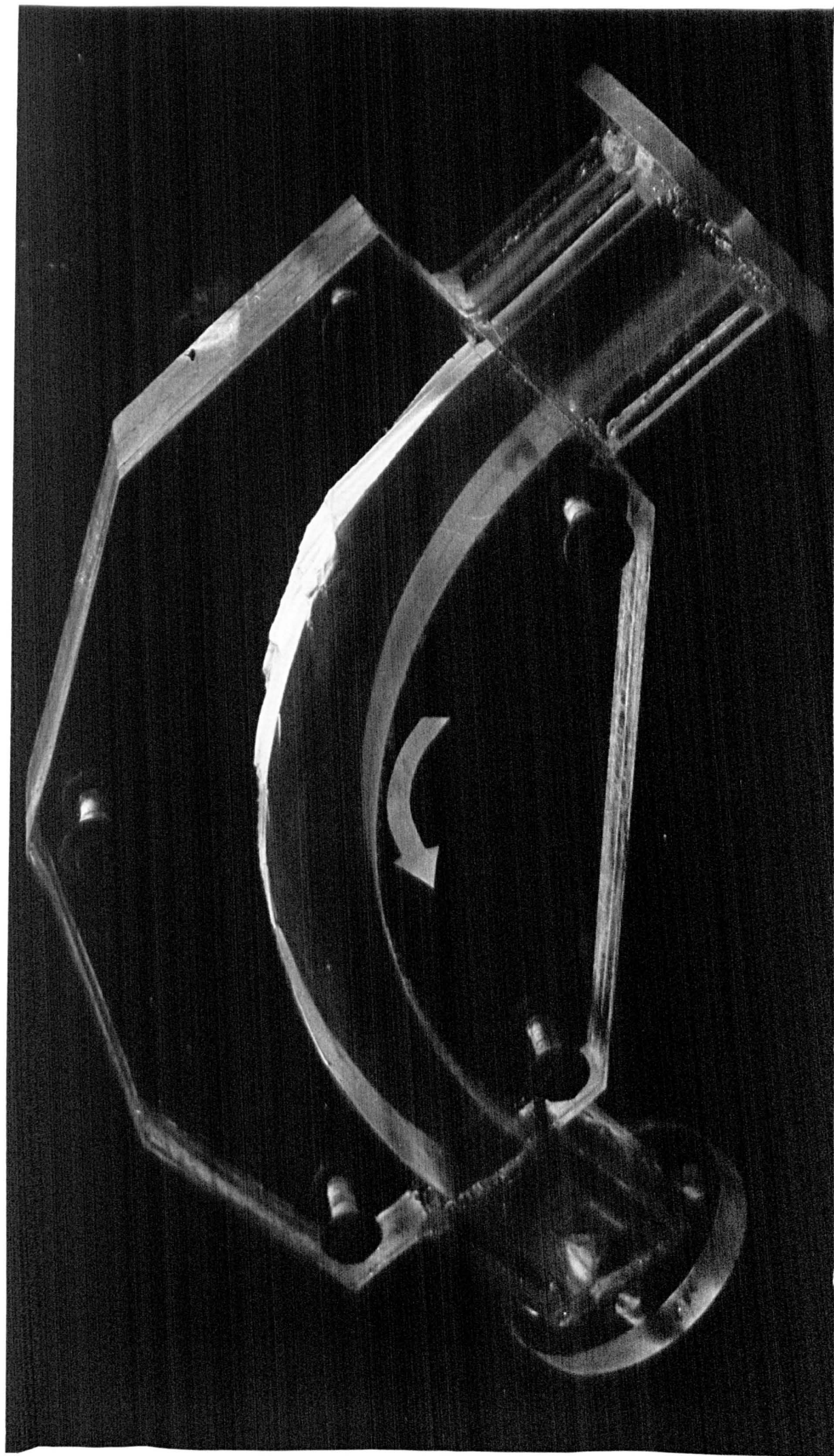


Plate 14: Bend 3.

Plate 15: Bend 4.



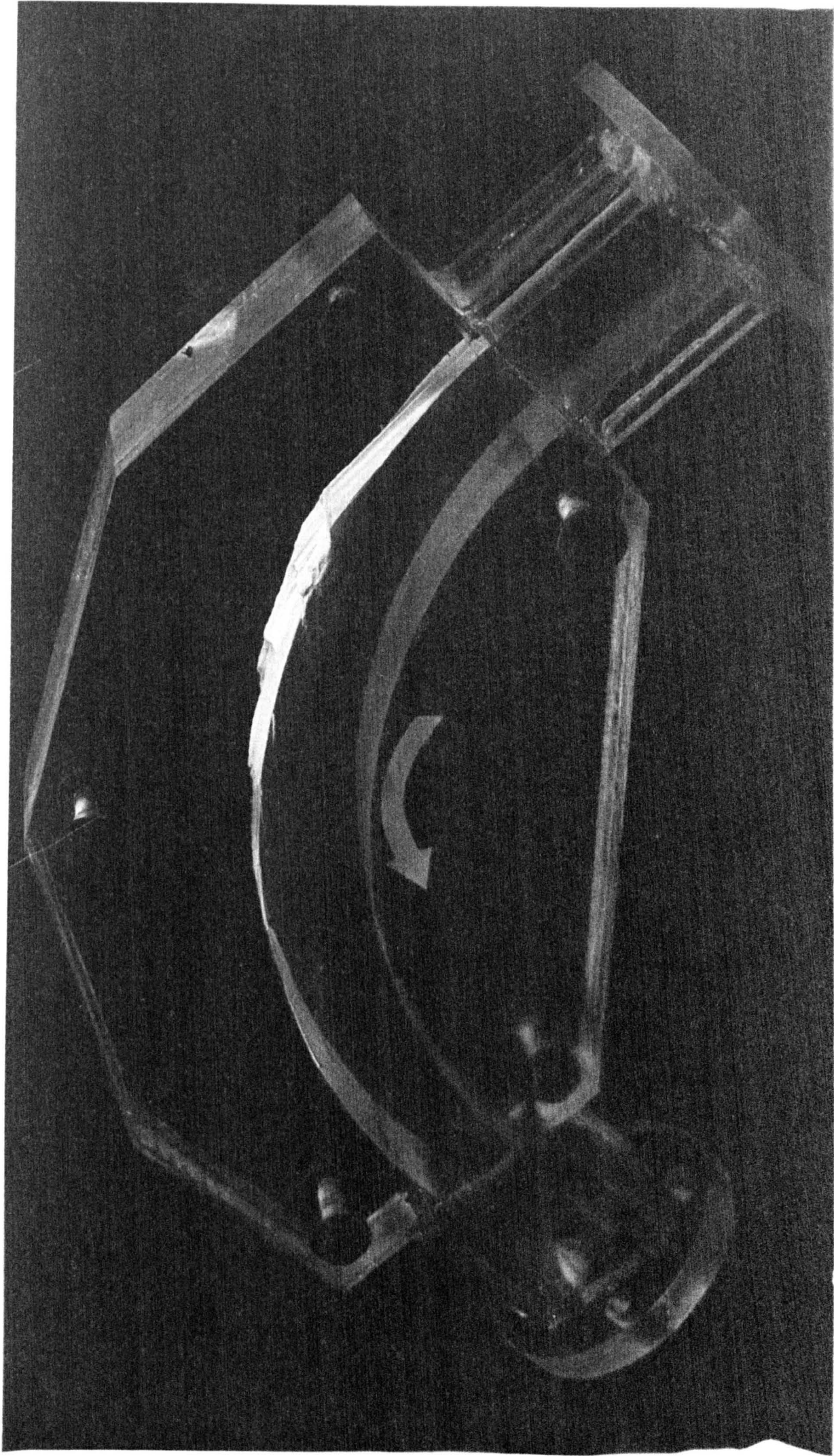
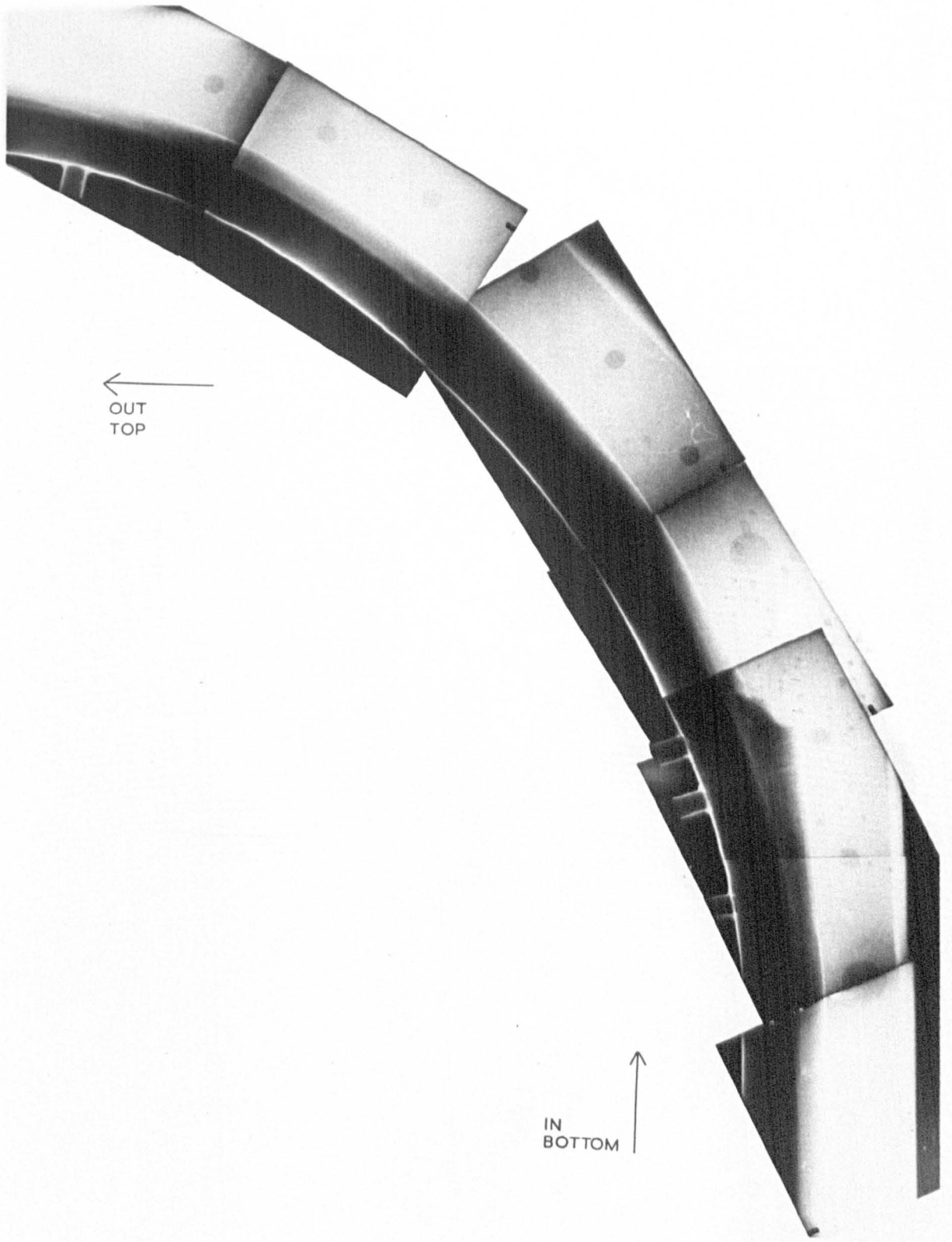


Plate 15: Bend 4.

Plate 16: Radiograph, 4" Bend.



←
OUT
TOP

↑
IN
BOTTOM

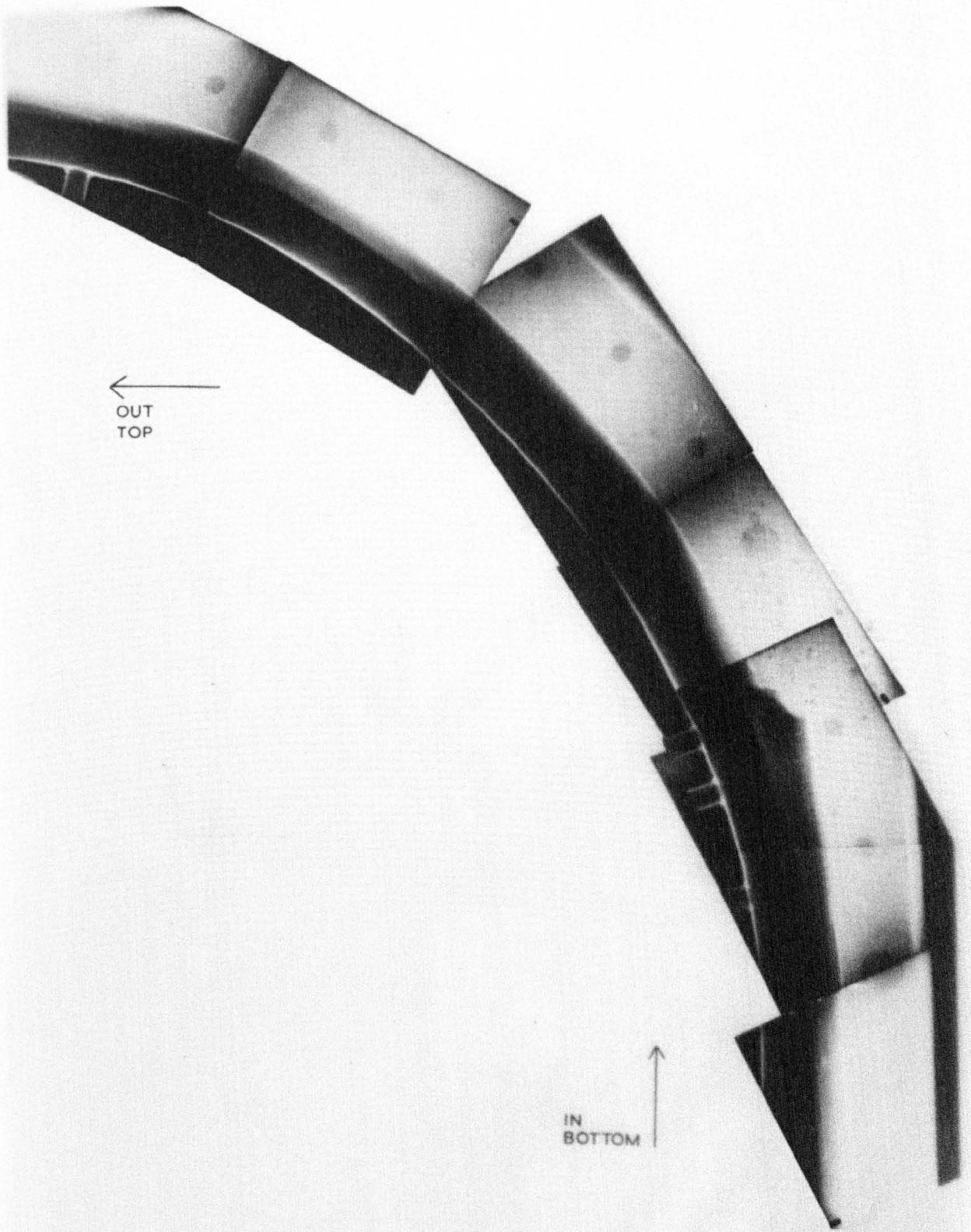
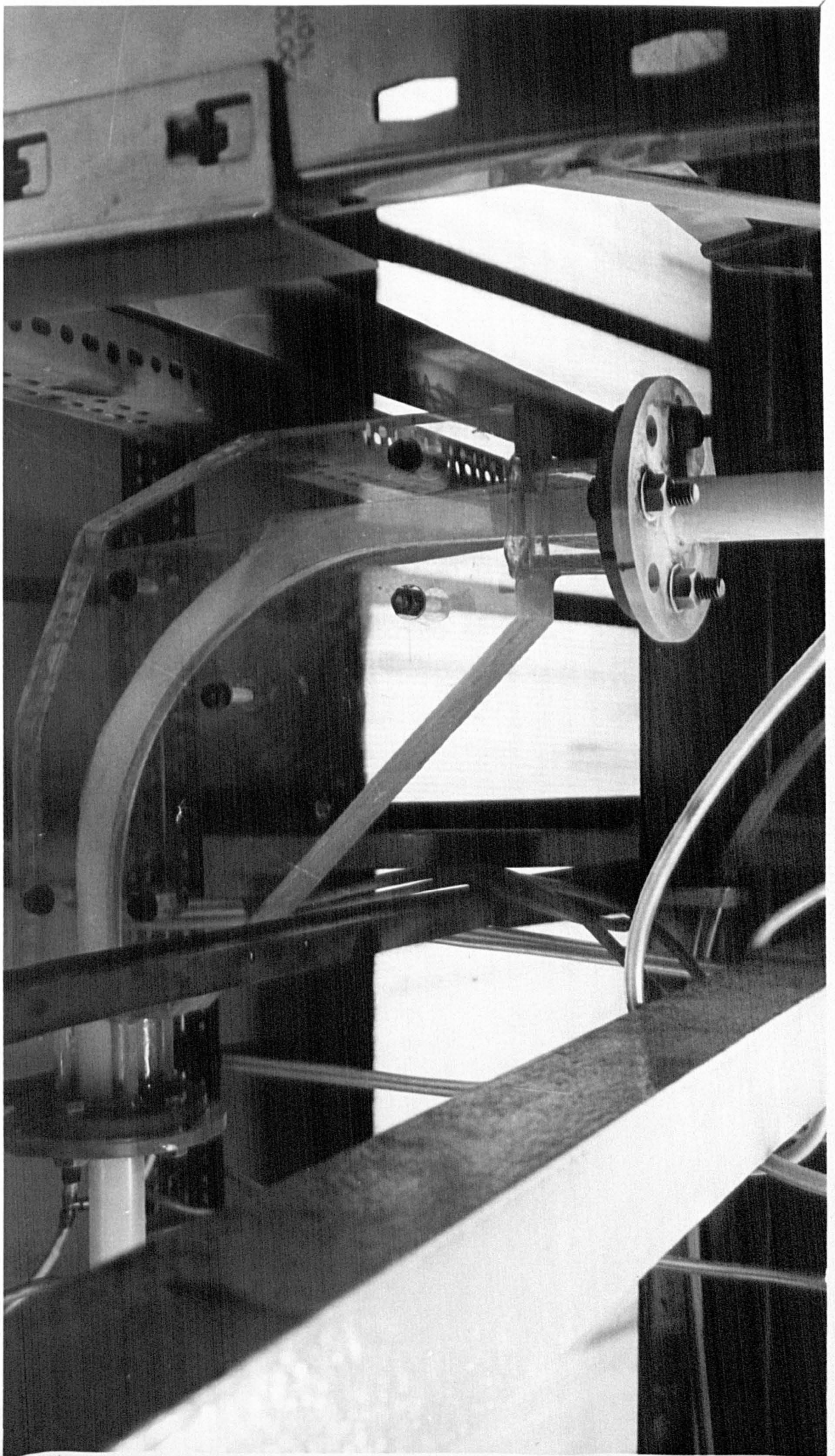


Plate 16: Radiograph, 4" Bend.

Plate 17: Wear Tests Rig.



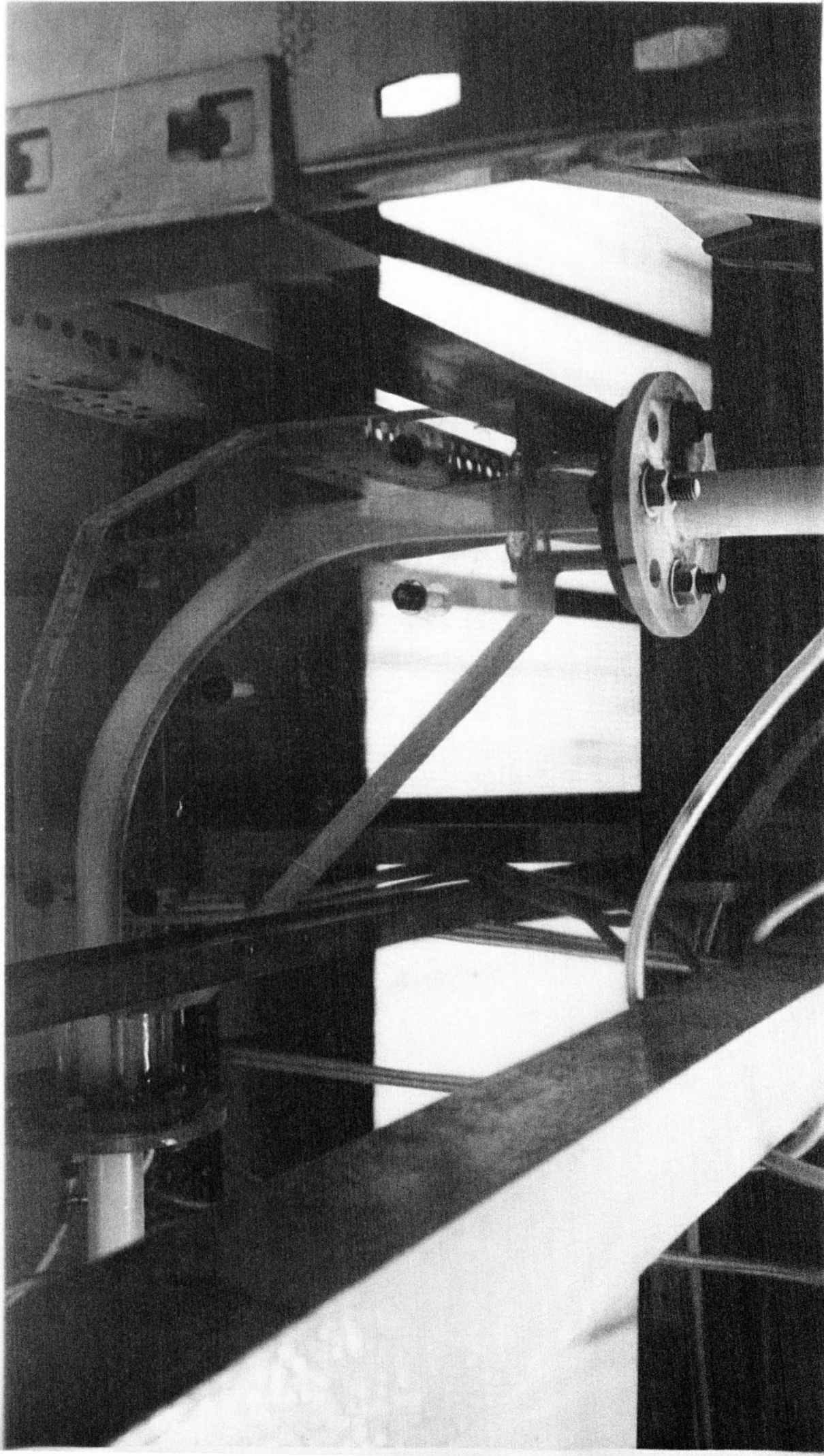


Plate 17: Wear Tests Rig.

CHAPTER 9

CONCLUSIONS

These final conclusions are intended to be general and for more specific deductions the reader is referred to sections 5.6, 6.6, 7.6 and 8.5 in which observations are advanced concerning investigations related to the particular chapter.

It may be concluded that a useful test rig has been developed for two-phase gas-solid circulation which has the advantage of versatility in the extent of projected investigations. This flexibility was demonstrated during the present work by the diversity of studies into different sized particles flowing through vertical and horizontal pipes, and around bends of varying geometry, in addition to an examination of the mechanism of bend erosion by impinging abrasive particles. The long-term usefulness of the equipment is well illustrated by the recent minor adaptations which have provided the facility for a comprehensive programme of work relating to the heat transfer characteristics of flowing gas-solid suspensions.

The suppression of turbulence by very fine particles was evident from many of the experimental results, this phenomenon being particularly stressed in that part of the work concerned with flow through vertical pipes. The investigations reported for suspension flow through the horizontal duct immediately following a 90° bend indicated the importance of location of static pressure tapings, on account of the influence of the bend resulting in a deviating flow in the downstream straight section. The proximity of "choking" in vertical ducts, with particles descending up to four feet before being arrested and subsequently re-conveyed, and "saltation" in horizontal ducts, with the fast-moving particles above the slowly moving bed of

deposited material continually disturbing the upper layer of the bed, were observed visually through the transparent test-sections.

The pressure loss experiments for different bends revealed deviating flow with fine particles as well as large particles, and the unusual pressure distribution within the bend was satisfactorily explained by noting the dynamic pressure contribution to the static pressure reading, which resulted from impingement of the solid particles on the bend wall. The results suggested that a valuable correlation procedure for gas-solid flow in bends may exist in the functional relationship between a related coefficient of resistance, $\psi_{bs}/\theta \cdot \beta^2$, and an extended Reynolds' number, R_e/β^2 .

The final series of experiments were concerned with bend erosion and they provided an explanation of the mechanism of bend erosion which should have some industrial potential. The tests facilitated the prediction of major wear points and analysis of the experimental data yielded an equation which expressed wear rate in terms of the superficial air velocity and, for the first time, the phase density as defined by W_p/W_f .

The vast number of experimental results have been too great to allow an exhaustive treatise to be presented in this thesis. It has been mentioned previously that these further results will subsequently be submitted for publication elsewhere.

The project has stimulated the author to propose several further studies in the general field of pneumatic transportation, these suggestions appear in sections 5.7, 6.7, 7.7 and 8.6.

The computer programs used in this work are included for reference. Section A.1.1 refers to the pitot-tube traverse calculations discussed in Chapter 4 (section 4.3.3). The program in section A.1.2 evaluates all the basic flow parameters, dimensionless groups and pressure differentials required for the present study. The programming was carried out on an Elliot 803 computer which has a relatively small storage capacity and it was not possible to run the entire program in one sequence. This difficulty was resolved by selecting part of the program to evaluate the basic flow data and pressure drops, whilst another combination of program tapes ascertained the required dimensionless parameters.

Section A.1.3 contains the pre-data information which provides the essential flexibility necessary for efficient operation of a lengthy computer program.

PITOT TRAVERSE'

BEGIN

INTEGER DATE,TEST,I,J,K,II,JJ,KK,DIA,L,LL,SPACE,
RAD,M,MM,N,NN,N2

REAL R,AP,RT,MV,TEMP,P1R,P1L,HZ,
P1OR,P1OL,P109,P109Z,PA,P10,ROE,VEL,MU,RE,ENOTS,A,B,C,D,E,X'

REAL ARRAY H(1:50),V(1:50),RD(1:50),RO(1:50),ML(1:50),T(1:50)'

SWITCH S:=S1,S2'

PROCEDURE XSPACE(M)'

INTEGER M'

BEGIN

IF M=5*SPACE THEN

BEGIN

PRINTCCL??'

SPACE:=SPACE+1'

END SPACE'

END XSPACE'

S1:SPACE:=1'

READ TEST,DATE,DIA,AP,RT,ENOTS,P1L,P1R,P109Z,P109,X,HZ'

PA:=(13.6*AP+(P1L-P1R)/2.54)*5.192'

R:=96.0'

P10:=P1OL-P1OR'

P109:=(P109-P109Z)*0.2304'

NN:=DIA/0.1+1

N2:=NN/2+0.5

PRINT CCL8?DATEES3??,SAMELINE,DATE,

CCL?TEST NO?,SAMELINE,ES5??,DIGITS(3),TEST,

CCL?PIPE DIA ?,SAMELINE,DIGITS(2),DIA,

SAMELINE,&.INCHES?,

CCL?ATMOS PRESSES3??,SAMELINE,ALIGNED(2,2),AP,SAMELINE,&IN HG?;

CCL?ROOM TEMPES4??,ALIGNED(2,1),SAMELINE,RT,

SAMELINE,&DEG C?'

FOR I:=1 STEP 1 UNTIL NN-1 DO

· BEGIN
READ ML(I)'

IF DIA=2 THEN T(1):=273.9+24.2*(-0.65+0.925*ML(1))+RT'
IF DIA=3 THEN T(1):=273.9+24.2*(-0.55+ML(1))+RT'

RO(I):=PA/(R*T(I))'
END ML'

TEMP:=0'

FOR I:=1 STEP 1 UNTIL NN-1 DO

· BEGIN

READ H(I)'

H(I):=H(I)-HZ'

TEMP:=TEMP+T(I)'

V(I):=SQRT(ABS(4020*X*H(I)/RO(I)))'

RD(I):=DIA/2-0.1*(I-1)'

· END READ

V(NN):=V(1)'

RD(NN):=-DIA/2'

RO(NN):=RO(NN-1)'

T(NN):=T(NN-1)'

TEMP:=TEMP/(NN-1)'

A:=B:=C:=D:=0'

FOR I:=2 STEP 1 UNTIL N2 DO

· BEGIN

A:=A+RD(I)*V(I)'

C:=C+RO(I)*RD(I)*V(I)'

· END AC

A:=A+RD(1)*V(1)*0.2/2+(RD(1)*V(1)+RD(2)*V(2))*0.8/2-RD(2)*V(2)/2'

C:=C+RO(1)*RD(1)*V(1)*0.2/2+(RO(1)*RD(1)*V(1)+RO(2)*RD(2)*V(2))*0.8/2
-RO(2)*RD(2)*V(2)/2

FOR I:=N2 STEP 1 UNTIL NN-1 DO

·BEGIN
B:=B+RD(1)*V(1)
D:=D+RO(1)*RD(1)*V(1)
END·BD

B:= B+RD(NN)*V(NN)*0.2/2+RD(NN)*V(NN)*0.8/2+RD(NN-1)*V(NN-1)*(-0.1)

D:=D+RO(NN)*RD(NN)*V(NN)*0.5-0.1*RO(NN-1)*RD(NN-1)*V(NN-1)

ROE:=(C-D)*14.4/(1.61*DIA*DIA*(A-B))

MU:=(7.46+0.018*(TEMP-300))*0.0001

RE:=5*ROE*(A-B)*DIA/(22.5*MU)

E:=3.142*DIA*DIA/4

PRINT EEL2?ENOTSES8??, SAMELINE, ALIGNED(2,2), ENOTS,
EEL?AV DENSITYES5??, SAMELINE, ALIGNED(0,4), ROE, ELB/CU FT?,
EEL?VISCOSITYES6??, SAMELINE, ALIGNED(0,6), MU,
EEL?REYNOLDS NO?, SAMELINE, ALIGNED(6,0), RE,
EEL?ORIFICE PDES3??, SAMELINE, ALIGNED(2,2), P109, EIN. WATER?,
EEL?AV VELOCITYES??, SAMELINE, ALIGNED(3,1), (A-B)/(2*E), EFT/S?,
EEL?VEL ABS7??, SAMELINE, ALIGNED(3,1), A/E, EFT/S?,
EEL?VEL BES7??, SAMELINE, ALIGNED(3,1), -B/E, EFT/S?,
EEL?MASS FLOW ?, SAMELINE, ALIGNED(4,3), (C-D)/460.0, ELB/S?,
EEL?MF A ?, SAMELINE, ALIGNED(4,3), C/230.0, ELB/S?,
EEL?MF B ?, SAMELINE, ALIGNED(4,3), -D/230.0, ELB/S?

PRINT EEL3?

RAD VEL VEL*RAD TEMP ROE?

FOR I:=1 STEP 1 UNTIL NN DO

·BEGIN
PRINT ALIGNED(1,1), RD(1), SAMELINE, ALIGNED(5,1), V(1), ALIGNED(5,2),
V(1)*RD(1), ALIGNED(7,1), T(1), ALIGNED(2,4), RO(1)
XSPACE(1)
END PRINT
GOTO S1
END

MASONVENABLES PNEUCURVE A'

BEGIN

INTEGER DATE,TEST,POWDER,I,J,K,II,JJ,KK,DIA,L,LL,SPACE,
RAD,M,MM,N,NN,U,V,W,POW,WW,WX,WY,IA,IB,IC'

REAL R,AP,RT,P1,P1Z,P2,P2Z,P3,P3Z,P4,P4Z,P14,MV,T,P1R,P1L,
P1OR,P1OL,P109,P109Z,PA,P10,MS,MA,MAF,MAO,MR,KOPP,ROE,VEL,VELF,VELO,
MU,RE,ENOTS,FR,SLOPE1,SLOPE2,SLOPE3,A,B,C,D,E,PGS,PACC,PD,LAMDA,
ROES,PT,PO,DIAS,ES,ESW,FN,A1,A2,A3,A4,A5,A6,A7,B1,B2,B3,B4,B5,B6,B7'

READ IA,IB,IC'

BEGIN

INTEGER ARRAY WZ(1:12)'

REAL ARRAY PN(1:IA),X(1:IB,1:IC),MAV(1:2,1:15),ORIF(1:15),
PRD(1:12,1:15),AIR(1:15)'

PROCEDURE XSPACE(LINES,TRIGGER)'

INTEGER LINES,TRIGGER'

BEGIN

IF TRIGGER=LINES*SPACE THEN

BEGIN

PRINT EEL??'

SPACE:=SPACE+1'

END SPACE'

END XSPACE'

PROCEDURE XYPRINT(X,M,N)'

INTEGER M,N'

REAL ARRAY X'

BEGIN

PRINT EEL3??'

FOR J:=M STEP 1 UNTIL N DO

PRINT ALIGNED(3,2),SAMELINE,X(30,J)'

PRINT EEL2??'

SPACE:=1'

FOR I:=12 STEP 1 UNTIL 29 DO

BEGIN

PRINT EEL??'

FOR J:=M STEP 1 UNTIL N DO

PRINT ALIGNED(2,3),SAMELINE,X(I,J)/X(54,J)'

XSPACE(3,I-11)'

END 29'

PRINT EEL??'

SPACE:=1'

FOR I:=31 STEP 1 UNTIL 48 DO

BEGIN

PRINT EEL??'

FOR J:=M STEP 1 UNTIL N DO

PRINT ALIGNED(2,3),SAMELINE,X(I,J)/X(54,J)'

XSPACE(3,I-30)'

END 48'

END XYPRINT'

```

PROCEDURE XPRINT(X,M,N)
INTEGER M,N
REAL ARRAY X
  BEGIN
PRINT '???'
FOR J:=M STEP 1 UNTIL N DO
PRINT ALIGNED(3,2),SAMELINE,X(30,J)
PRINT '???'
SPACE:=1
FOR I:=12 STEP 1 UNTIL 29 DO
  BEGIN
PRINT '???'
FOR J:=M STEP 1 UNTIL N DO
PRINT ALIGNED(3,2),SAMELINE,X(1,J)
XSPACE(3;1-11)
END 29
PRINT '???'
SPACE:=1
FOR I:=31 STEP 1 UNTIL 48 DO
  BEGIN
PRINT '???'
FOR J:=M STEP 1 UNTIL N DO
PRINT ALIGNED(3,2),SAMELINE,X(1,J)
XSPACE(3;1-30)
END 48
END XPRINT

```

```

PROCEDURE RDCURVES(X,Y,M,N)
REAL ARRAY X,Y
INTEGER M,N
  BEGIN
INTEGER I,J
FOR I:=1 STEP 1 UNTIL N DO
  BEGIN
READ X(I)
FOR J:=1 STEP 1 UNTIL M DO
READ Y(J,I)
END
END RDCURVES

```

```

PROCEDURE INPOLCURVES(X,Y,M,N,XX,YY)'
REAL ARRAY X,Y'
INTEGER M,N'
REAL XX,YY'
  BEGIN
  INTEGER I'
  FOR I:=1 STEP 1 UNTIL N-1 DO
  IF X(I) LESSEQ XX AND X(I+1) GR XX THEN
  YY:= Y(M,I)+(Y(M,I+1)-Y(M,I))*(XX-X(I))/(X(I+1)-X(I))'
  END INPOLCURVES'

  BEGIN
  REAL POW240,POW320,POW500,DYP,LENY,LENC,LENH,IPSV,IPSH,IPSC'
  SWITCH S:=S1,S2,S3,S4,S5,S6,S7,S8,S9,S10,S11,S12,S13,S14,S15,
  S16,S17,S18'
  RDCURVES(ORIF,MAV,2,15)'
  READ WX,W'
  FOR I:=1 STEP 1 UNTIL WX DO
  READ WZ(I)'
  RDCURVES(AIR,PRD,WX,3)'
  S10:READ POW240,POW320,POW500'
  S1:READ TEST,DATE,DIA'
  IF TEST LESS 100 THEN
  READ AP,RT,POWDER'
  IF TEST GR 100 THEN
  READ RT,AP,POWDER'
  SPACE:=1'
  K:=1'
  PRINT SEL8?DATE&S3??,SAMELINE,DATE,
  &L?TEST NO?,SAMELINE,&ES5??,DIGITS(3),TEST,
  &L?PIPE DIA ?;SAMELINE,DIGITS(2),DIA,
  SAMELINE,& INCHES?,
  &L?POWDER MESH?,DIGITS(4),SAMELINE,POWDER,
  &L?ATMOS PRES&S3??,SAMELINE,ALIGNED(2,2),AP,SAMELINE,& IN HG?,
  &L?ROOM TEMP&S4??,ALIGNED(2,1);SAMELINE,RT,
  SAMELINE,&DEG C?'

```

IF TEST LESS 100 THEN

· BEGIN

RAD:=0'

JJ:=1'

FOR J:=1 STEP 1 UNTIL 30 DO

FOR I:=1 STEP 1 UNTIL 18 DO

·BEGIN

READ PN(JJ)'

IF I NOTEQ 1 THEN GOTO S3'

KK:=CHECKR(PN(JJ))'

IF KK=19191 THEN N:=J-1 ELSE GOTO S3'

GOTO S2'

S3: JJ:=JJ+1'

END READ'

END TEST LESS 100'

IF TEST GR 100 THEN

· BEGIN

READ RAD,LAMDA'

PRINT

CEL?RADIUS?, SAMELINE, CES6??, DIGITS(3), RAD, & INCHES?,

CEL?LAMDA?, SAMELINE, CES7??, ALIGNED(3,0), LAMDA'

JJ:=1'

FOR J:=1 STEP 1 UNTIL 20 DO

FOR I:=1 STEP 1 UNTIL 48 DO

·BEGIN

READ PN(JJ)'

IF I NOTEQ 1 THEN GOTO S5'

KK:=PN(JJ)'

IF KK=19191 THEN N:=J-2 ELSE GOTO S5'

GOTO S2'

S5: JJ:=JJ+1'

END READ'

END TEST GR 100'

```

S2:FOR J:= 1 STEP 1 UNTIL N DO
  BEGIN
  IF TEST LESSEQ 20 THEN
    BEGIN
    JJ:=18*(J-1)'
    X(1,J):=MS:=PN(JJ+1)'
    X(30,J):=KOPP:=PN(JJ+2)'
    P1Z:=PN(JJ+4)'
    P1:=PN(JJ+5)'
    P2Z:=PN(JJ+6)'
    P2:=PN(JJ+7)'
    P3Z:=PN(JJ+8)'
    P3:=PN(JJ+9)'
    P4Z:=PN(JJ+10)'
    P4:=PN(JJ+11)'
    P1L:=PN(JJ+12)'
    P1R:=PN(JJ+13)'
    P10L:=PN(JJ+14)'
    P10R:=PN(JJ+15)'
    P109Z:=PN(JJ+16)'
    P109:=PN(JJ+17)'
    MV:=PN(JJ+18)'

```

```

GOTO S7'
  END 0 20'

```

```

IF TEST LESS 100 THEN
  BEGIN
  X(1,J):=MS:=PN(J)'
  P1Z:=PN(N*3+J)'
  P1:=PN(N*4+J)'
  X(30,J):=KOPP:=PN(N+J)'
  P2Z:=PN(N*5+J)'
  P2:=PN(N*6+J)'
  P3Z:=PN(N*7+J)'
  P3:=PN(N*8+J)'
  P4Z:=PN(N*9+J)'
  P4:=PN(N*10+J)'
  P1L:=PN(N*11+J)'
  P1R:=PN(N*12+J)'
  P10L:=PN(N*13+J)'
  P10R:=PN(N*14+J)'
  P109Z:=PN(N*15+J)'
  P109:=PN(N*16+J)'
  MV:=PN(N*17+J)'
  GOTO S7'
  END 21 99'
GOTO S4'

```

S7:

```

  IF DIA=1 THEN BEGIN
    MV:=-0.845+0.91*MV'
    SLOPE1:=SLOPE2:=1'
    L:=4'
    X(11,J):= PD:=ABS(P1+P2-P1Z-P2Z)*SLOPE1'
  END 1'

```

IF DIA=2 THEN BEGIN
MV:=-0.425+0.925*MV'

L:=4'

IF TEST LESS 7 THEN BEGIN

SLOPE1:=0.0875*2.54'

SLOPE2:=0.1398*2.54'

SLOPE3:=0.0604*2.54'

X(11,J):=PD:=(P1-P1Z)*SLOPE1+(P2-P2Z)*SLOPE3'

END TEST6'

IF TEST GR 6 THEN BEGIN

SLOPE1:=0.0875*2.54'

SLOPE2:=0.210*2.54'

X(11,J):=PD:=(P1+P2-P1Z-P2Z)*SLOPE1'

END TEST7'

END 2'

IF DIA=3 THEN BEGIN

MV:=-0.55+MV'

SLOPE1:=0.0328*2.54'

SLOPE2:=0.0604*2.54'

L:=2'

X(11,J):= PD:=(P1-P1Z)*SLOPE1'

END 3'

GOTO S6'

S4: IF TEST GR 100 THEN
BEGIN

KK:=29+J'

X(1,J):=MS:=PN(KK+1)'

X(30,J):=KOPP:=PN(KK+2)'

P1Z:=PN(12)'

P1:=PN(KK+12)'

P2Z:=PN(13)'

P2:=PN(KK+13)'

P3Z:=PN(14)'

P3:=PN(KK+14)'

P1L:=PN(KK+8)'

P1R:=PN(KK+9)'

P1OL:=PN(KK+6)'

P1OR:=PN(KK+7)'

P1O9Z:=PN(KK+4)'

P1O9:=PN(KK+5)'

MV:=PN(KK+10)'

FOR I:=1 STEP 1 UNTIL WX DO

IF WZ(1)=DIA+RAD THEN WW:=1'

MV:=-PRD(WW,1)+PRD(WW,2)*MV'

SLOPE1:=2.54*PRD(WW,3)'

IF DIA=3 THEN L:=2 ELSE L:=4'

IF DIA=3 THEN PD:=ABS(P2-P2Z-P3+P3Z)*SLOPE1

ELSE PD:=ABS(P1-P1Z-P3+P3Z)*SLOPE1'

X(11,J):=PD'

GOTO S6'

END TEST GR 100'

S6: IF TEST LESSEQ 62 THEN A:=0.787'
 IF TEST GREQ 63 THEN A:=0.2305'
 IF TEST GREQ 201 THEN A:=0.2493'
 IF TEST GREQ 250 THEN A:=0.1645'

POW:=POWDER/10-1'
 IF POW=-1 THEN DIAS :=1000000'
 IF POW=240 THEN DIAS:=POW240'
 IF POW=320 THEN DIAS:=POW320'
 IF POW=500 THEN DIAS:=POW500'

ROES:=3.94*62.3'

P109:=(P109-P109Z)*A'
 INPOLCURVES(ORIF,MAV,1,15,P109,MAO)'

X(50,J):=MA:=MAO'
 PA:=(13.6*AP+(P1L-P1R)/2.54)*5.192'
 IF TEST GREQ 250 THEN PA:=(AP+P1L+P1R)*13.6*5.192'
 IF TEST GREQ 257 THEN PA:=(AP+P1L-P1R)*13.6*5.192'

X(58,J):=PA'
 T:=273.9+24.2*MV+RT'
 R:=96.0'

X(2,J):=ROE:=PA/(R*T)'
 X(3,J):=MU:=(7.46+0.018*(T-300))*0.0001'
 VELO:=576*MA/(3.142*DIA*DIA*ROE)'

X(49,J):=VEL:=VELO'
 X(4,J):=VELF:=(9.552*((DIA)**(5/7))*((PD)**(4/7)))/((ROE**((3/7))
 *(MU**((1/7)))*(L**((4/7))))'

P10:=P10L-P10R'
 X(5,J):=RE:=5*ROE*VEL*DIA/MU'
 X(6,J):=MAF:=60*ROE*VELF*DIA*DIA*3.142/576'

X(7,J):=MR:=MS/(MA*60)'
 X(8,J):=PGS:=2.54*L*ROE*(1+MR)/5.192'
 X(9,J):=PACC:=2.54*410.4*MA*MA*PD*(1+MR)/((DIA**4)*PA*ROE)'

FN:=0.0008+0.055/(RE**0.237)'
 X(53,J):=PO:=3.404*3600*MA*MA*L*FN/(ROE*DIA**5)'

X(10,J):=FR:=12*VEL*VEL/(DIA*32.2)'
 X(51,J):=PT:=PD-(PACC+PGS)'
 X(52,J):=ES:=ROE*DIA*DIA/(ROES*DIAS*DIAS*RE)'

IF TEST LESS 100 THEN GOTO S8'

FOR I:=12 STEP 1 UNTIL 29 DO
 X(I,J):=(PN(J*29+1)-PN(I))*SLOPE1'
 FOR I:=31 STEP 1 UNTIL 48 DO
 X(I,J):=(PN((N+1)*29+19*J+1-29)-PN((N+1)*29+1-29))*SLOPE1'
 S8:
 END CALC'

IF W GREQ 2 THEN GOTO S10'

PRINTEEL2??'

PRINTE

KOPP ROE MU VELO RE FR MA MS MR ES ESW
@+1 @+3 @+5?'

FOR J:=1 STEP 1 UNTIL N DO
BEGIN

PRINT

ALIGNED(3,0),X(30,J),SAMELINE,

ALIGNED(0,3),X(2,J)*10,

ALIGNED(0,3),X(3,J)*1000,

ALIGNED(3,1),X(49,J),

ALIGNED(6,0),X(5,J), SAMELINE,

ALIGNED(5,0),X(10,J),

ALIGNED(2,2),X(50,J)*60,

ALIGNED(2,2),X(1,J),

ALIGNED(1,2),X(7,J),

ALIGNED(0,5),X(52,J),

ALIGNED(0,6),X(52,J)*(100000)/(X(5,J))'

XSPACE(5,J)

END PRINT 1'

IF W=0 THEN 100 THEN GOTO S7'

BEGIN

PRINT EEL2? THEN PRINT(1,1,N) ELSE

KOPP PD PGS P.ACC PT PO F/FO (-) -1 MAO MAF VELF?'

IF DIA=1 THEN U:=2 ELSE U:=1'

IF DIA=1 THEN V:=2 ELSE V:=3'

SPACE:=1'

FOR J:=1 STEP 1 UNTIL N DO

BEGIN

PRINT

ALIGNED(3,0),X(30,J),SAMELINE,

ALIGNED(U,V),X(11,J),

ALIGNED(U-1,V+1),X(8,J),

ALIGNED(U,V+1),X(9,J),

ALIGNED(U,V),X(51,J),

ALIGNED(U,V),X(53,J),

ALIGNED(2,2),X(51,J)/X(53,J),

ALIGNED(3,2),X(51,J)/X(53,J)-1,

ALIGNED(2,2),X(50,J)*60,

ALIGNED(2,2),X(6,J),

ALIGNED(3,1),X(4,J)'

XSPACE(5,J)'

END PRINT 2'

END U=0'

```
IF W=1 THEN  
  BEGIN
```

```
PRINT E&L2?
```

```
KOPP PD PGS P.ACC PT PO F/FO ()-1?
```

```
IF DIA=1 THEN U:=2 ELSE U:=1'
```

```
IF DIA=1 THEN V:=2 ELSE V:=3'
```

```
SPACE:=1'
```

```
FOR J:=1 STEP 1 UNTIL N DO  
  BEGIN
```

```
  PRINT
```

```
  ALIGNED(3,0),X(30,J),SAMELINE,
```

```
  ALIGNED(U,V),X(11,J),
```

```
  ALIGNED(U-1,V+1),X(8,J),
```

```
  ALIGNED(U,V+1),X(9,J),
```

```
  ALIGNED(U,V),X(51,J),
```

```
  ALIGNED(U,V),X(53,J),
```

```
  ALIGNED(2,2),X(51,J)/X(53,J),
```

```
  ALIGNED(3,2),X(51,J)/X(53,J)-1'
```

```
  XSPACE(5,J)'
```

```
  END PRINT 2'
```

```
  END U=1'
```

```
IF TEST LESS 100 THEN GOTO S9'
```

```
IF N LESS 9 THEN XPRINT(X,1,N) ELSE
```

```
  BEGIN
```

```
  XPRINT(X,1,8)'
```

```
  PRINT E&L3??'
```

```
  XPRINT(X,9,N)'
```

```
  END X GR 8'
```

```
S9:GOTO S1'
```

S10:

FOR J:=1 STEP 1 UNTIL N DO

BEGIN

A1:=X(12,J)

A2:=X(15,J)

A3:=X(16,J)

A4:=X(17,J)

A5:=X(27,J)

A6:=X(28,J)

A7:=X(29,J)

KK:=DIA+RAD

IF KK=33 THEN

BEGIN

A2:=X(18,J)

A3:=X(19,J)

A4:=X(20,J)

A5:=X(31,J)

A6:=X(32,J)

A7:=X(33,J)

END KK=33

```
X(12,J):=X(13,J)-A1'  
X(13,J):=X(14,J)-A1'  
X(14,J):=-A1'  
X(15,J):=X(15,J)-A1'  
X(16,J):=X(16,J)-A1'  
X(17,J):=X(17,J)-A1'
```

```
X(18,J):=X(18,J)-A2'  
X(19,J):=X(19,J)-A3'  
X(20,J):=X(20,J)-A4'  
X(21,J):=X(21,J)-A2'  
X(22,J):=X(22,J)-A3'  
X(23,J):=X(23,J)-A4'
```

```
X(24,J):=X(24,J)-A2'  
X(25,J):=X(25,J)-A3'  
X(26,J):=X(26,J)-A4'  
X(27,J):=X(27,J)-A2'  
X(28,J):=X(28,J)-A3'  
X(29,J):=X(29,J)-A4'
```

```
X(31,J):=X(31,J)-A5'  
X(32,J):=X(32,J)-A6'  
X(33,J):=X(33,J)-A7'  
X(34,J):=X(34,J)-A5'  
X(35,J):=X(35,J)-A6'  
X(36,J):=X(36,J)-A7'
```

```
X(37,J):=X(37,J)-A5'
```

```
X(38,J):=X(38,J)-A6'  
X(39,J):=X(39,J)-A7'  
X(40,J):=X(40,J)-A5'  
X(41,J):=X(41,J)-A6'  
X(42,J):=X(42,J)-A7'
```

```
X(43,J):=X(43,J)-A5'  
X(44,J):=X(44,J)-A6'  
X(45,J):=X(45,J)-A7'  
X(46,J):=X(46,J)-A5'  
X(47,J):=X(47,J)-A6'  
X(48,J):=X(48,J)-A7'
```

```
IF KK=33 THEN  
  BEGIN  
  X(31,J):=X(31,J)-A2'  
  X(32,J):=X(32,J)-A3'  
  X(33,J):=X(33,J)-A4'  
  END KK=33 TWICE
```

```
END  
GOTO S12'
```

S12:

FOR I:=1 STEP 1 UNTIL WX DO
IF WZ(1)=DIA+RAD THEN WW:=1'

LENV:=PRD(WW,4)'
LENC:=PRD(WW,5)'
LENH:=PRD(WW,6)'

FOR J:=1 STEP 1 UNTIL N DO
BEGIN

PD:=X(27,J)'

ROE:=X(2,J)'

MR:=X(7,J)'

VEL:=X(49,J)'

MA:=X(50,J)'

PA:=X(58,J)'

X(8,J):=PGS:=2.54* $\text{RAD} \cdot \text{ROE} \cdot (1+\text{MR}) / (5.192 \cdot 12)$ '

X(54,J):=DYP:= $\text{ROE} \cdot \text{VEL} \cdot \text{VEL} / 132$ '

X(9,J):=PACC:= $2.54 \cdot 410.4 \cdot \text{MA} \cdot \text{MA} \cdot \text{PD} \cdot (1+\text{MR}) / ((\text{DIA} \cdot 4) \cdot \text{PA} \cdot \text{ROE})$ '

X(51,J):=PT:= $\text{PD} - (\text{PACC} + \text{PGS})$ '

X(58,J):= $3.404 \cdot 300 \cdot \text{MA} \cdot \text{MA} \cdot \text{LENC} \cdot \text{FN} / (\text{ROE} \cdot \text{DIA} \cdot 5)$ '

PD:=X(46,J)'

X(55,J):=PGS:=0'

X(56,J):=PACC:= $2.54 \cdot 410.4 \cdot \text{MA} \cdot \text{MA} \cdot \text{PD} \cdot (1+\text{MR}) / ((\text{DIA} \cdot 4) \cdot \text{PA} \cdot \text{ROE})$ '

X(57,J):=PT:= $\text{PD} - (\text{PACC} + \text{PGS})$ '

X(59,J):= $\text{X}(58, \text{J}) \cdot \text{LENH} / \text{LENC}$ '

FOR I1:=12 STEP 1 UNTIL 29 DO
PN((J-1)*36+I1-11):=X(I1,J)/DYP'

FOR I1:=31 STEP 1 UNTIL 48 DO
PN((J-1)*36+I1-12):=X(I1,J)/DYP'

PN(600+(J-1)*3+1):=IPSV:= $\text{PN}((\text{J}-1) \cdot 36+4) \cdot \text{DIA} / \text{LENV}$ '

PN(600+(J-1)*3+2):=IPSC:= $\text{PN}((\text{J}-1) \cdot 36+16) \cdot \text{DIA} / \text{LENC}$ '

PN(600+(J-1)*3+3):=IPSH:= $\text{PN}((\text{J}-1) \cdot 36+34) \cdot \text{DIA} / \text{LENH}$ '

END CALCS CAND H'

PRINT ££L2?
CURVE PARAMETERS

KOPP PD PGS P.ACC PT PO F/FO ()-1 DYP?

IF DIA=1 THEN U:=3 ELSE U:=1'
IF DIA=1 THEN V:=1 ELSE V:=3'
SPACE:=1'

FOR J:=1 STEP 1 UNTIL N DO
BEGIN

PRINT
ALIGNED(3,0),X(30,J),SAMELINE,
ALIGNED(U,V),X(27,J),
ALIGNED(U-1,V+1),X(8,J),
ALIGNED(U,V+1),X(9,J),
ALIGNED(U,V),X(51,J),
ALIGNED(U,V),X(58,J),
ALIGNED(2,2),X(51,J)/X(58,J),
ALIGNED(3,2),X(51,J)/X(58,J)-1,
ALIGNED(3,3),X(54,J)'

XSPACE(5,J)'
END PRINT 2'

PRINT ££L2?
HORIZONTAL PARAMETERS

KOPP PD PGS P.ACC PT PO F/FO ()-1?

IF DIA=1 THEN U:=3 ELSE U:=1'
IF DIA=1 THEN V:=1 ELSE V:=3'
SPACE:=1'

FOR J:=1 STEP 1 UNTIL N DO
BEGIN

PRINT
ALIGNED(3,0),X(30,J),SAMELINE,
ALIGNED(U,V),X(46,J),
ALIGNED(U-1,V+1),X(55,J),
ALIGNED(U,V+1),X(56,J),
ALIGNED(U,V),X(57,J),
ALIGNED(U,V),X(59,J),
ALIGNED(2,2),X(57,J)/X(59,J),
ALIGNED(3,2),X(57,J)/X(59,J)-1'

XSPACE(5,J)'
END PRINT 2'

PRINT EEL2?
RESISTANCE NUMBERS

KOPP IPSV IPSC IPSH IV/MR IC/MR IH/MR ERE RRN?
SPACE:=1'
FOR J:=1 STEP 1 UNTIL N DO
BEGIN
KK:=600+(J-1)*3'
PRINT
ALIGNED(3,0),X(30,J),SAMELINE,
ALIGNED(1,4),PN(KK+1),
ALIGNED(1,4),PN(KK+2),
ALIGNED(1,4),PN(KK+3),
ALIGNED(2,5),PN(KK+1)/X(7,J),
ALIGNED(2,5),PN(KK+2)/X(7,J),
ALIGNED(2,5),PN(KK+3)/X(7,J),
ALIGNED(3,1),X(5,J)*DIA*DIA/(4*PI*PI),
ALIGNED(0,5),PN(KK+2)*2/(3.1416*SQRT(2*PI/DIA))'
XSPACE(5,J)
END PRINT IPS'

IF W=3 THEN GOTO S13'
IF N LESS 9 THEN XPRINT(X,1,N) ELSE
BEGIN
XPRINT(X,1,8)'
PRINT EEL3??'
XPRINT(X,9,N)'
END X GR 8'

IF W=4 THEN GOTO S13'
IF N LESS 9 THEN XYPRINT(X,1,N) ELSE
BEGIN
XYPRINT(X,1,8)'
PRINT EEL3??'
XYPRINT(X,9,N)'
END XYN GR8'

S13:
GOTO S1'
END 3'
END 2'
END 1'

Computer Results Print-out Explanation

To facilitate presentation of computerised data the following abbreviations were used:-

- (i) KOPP this represents the hand-wheel setting on the variable speed screwfeeder drive and is used as an identifier for all results, in addition to enabling the solids flowrate to be established from the appropriate calibration curve.
- (ii) ROE test-section air density in lb/ft^3 .
- (iii) MU test-section air dynamic viscosity in lb/ft min. a + 3 means times 10^{-3} .
- (iv) VELO test-section air velocity in ft/s .
- (v) RE duct Reynolds' number.
- (vi) FR duct Froude number.
- (vii) MA air mass flowrate in lb/min .
- (viii) MS solids mass flowrate in lb/min .
- (ix) MR solids-to-air ratio, W_p/W_f .
- (x) ES eddy scale ratio, $\rho_f D^2 / \rho_p d_p^2 R_e$.
- (xi) ESW eddy scale ratio at wall, ES/R_e .
- (xii) PD measured pressure drop in $\text{cm H}_2\text{O}$.
- (xiii) PGS pressure drop due to supporting solids in $\text{cm H}_2\text{O}$.
- (xiv) P.ACC pressure drop due to acceleration of suspension in $\text{cm H}_2\text{O}$.
- (xv) PT pressure drop due to composite fluid friction in $\text{cm H}_2\text{O}$.
- (xvi) PO calculated pressure drop due to air only flowing in $\text{cm H}_2\text{O}$.
- (xvii) F/FO ratio of friction factor of suspension to that for air only.

(xviii) () -- 1 ratio of solids friction factor to that for air only.

(xix) IPSV, IPSC,
IPSH resistance numbers for vertical, curved and horizontal test-sections respectively.

(xx) ERE extended Reynolds' number, R_e/β^2 .

(xxi) RRN related resistance number, $\psi_{bS}/\theta.\beta^{\frac{1}{2}}$.

(xxii) Powder mesh . '0' means air only flowing;

2407 means 240 mesh powder and large screwfeeder;

2408 means 240 mesh powder and medium screwfeeder;

and similarly for the 320 and 500 mesh powders, the fourth digit merely indicates the size of screwflight used.

Pressure drop across orifice plate, (in H ₂ O)	Mass flowrate of air, (lb/s)	Superficial air velocity in three inch pipe, (ft/s)
0.5	0.042	12.3
1.0	0.077	22.5
1.5	0.104	30.0
2.0	0.121	35.5
2.5	0.135	40.0
3.0	0.149	43.8
3.5	0.162	47.6
4.0	0.175	51.2
4.5	0.187	54.4
5.0	0.200	57.5
5.5	0.212	60.1
6.0	0.223	62.6
6.5	0.234	65.0
7.0	0.244	68.6

Test section identification (dia. + rad. of curv.)	Temperature Calibration		Manometer slope	Length parameters (in)		
	intercept	gradient		Vertical duct	Bend	Horizontal pipe
1	0	0	0	0	0	0
2	0	0	0	0	0	0
3	0	0	0	0	0	0
12	0.623	0.890	0.309	71.80	31.40	40.20
21	0.610	0.900	0.309	73.30	28.22	40.00
33	0.650	0.880	0.309	61.50	47.10	28.00
22	0.650	0.925	0.707	69.63	31.40	40.06
14	0.584	0.800	0.707	77.80	18.84	41.25
11	0.752	0.775	4.412	81.19	15.70	42.50

0.002087; 0.001181; 0.000512: mean particle diameter in inches for the 240, 320 and 500 mesh powders respectively.

APPENDIX A.2.

PERFORMANCE OF A CALIBRATED SCREW-FEEDER

P.J.Walton⁺, B.Sc., P.A.Arundel⁺, B.Sc., J.S.Mason^{*}, B.Sc., C.Eng.,
H.Haque⁸, Ph.D., R.G. Boothroyd⁺, Ph.D., C.Eng.

Note : This paper was presented by J.S. Mason at a conference entitled "Bunker Extraction Gear", organised by The Institution of Mechanical Engineers, (19th October 1971).

Abstract

Performance data is reported on the behaviour of a variable-speed screw-feeder outlet from a small bunker using various solid materials. Different sizes of powdered alumina, zinc and zinc/glass-fibre mixture were discharged at uniform flow-rates: four screw-flights being used to give a 1000:1 range of mass flow. The main problems encountered were rat-holing and arching, which was very severe with the zinc/glass-fibre mixture. Many methods were tried in an attempt to offset these effects. Criteria for determining the effectiveness (η) of screw-feeder delivery rates are discussed. A new theory for a more accurate prediction of the volumetric feed rate is developed.

+ Department of Mechanical Engineering, University of
Birmingham.

* Liverpool Polytechnic.

8 Pakistan Atomic Energy Commission.

Introduction

The feeder which is illustrated in Fig. 1 was used to deliver a calibrated uniform feed of several different powders into fluidising units. Essentially the same design and size of feeder was used by all the authors, except that in some earlier studies a screw-rejection shaft seal⁽¹⁾ was used instead of the "Monoflon" packed seal which is illustrated. Because the research was not concerned specifically with screw-feeders, no power consumption measurements were taken. Nevertheless, it was vitally important that the delivery rate from the feeder was accurately known and reproducible. Consequently, this aspect was studied in some detail. The predicted delivery rate of a screw-feeder is probably of more interest than the predicted power consumption since the drive-motor size is likely to be dictated by occasional 'nipping' characteristics of powder in the conveyor and not by normal friction losses.

The feeder was protected from overload by shear-couplings and pains were taken to ensure that 'nipping' and serious attrition of recirculated powder did not occur. It was concluded that a choke/flight clearance equal to the screw blade thickness (t) was sufficient to avoid attrition difficulties. By using different diameter screw-flights the feeder delivered a continuously variable solids flow-rate in the range 1000:1 (e.g. 0.2 - 220 lb zinc dust/minute). Each screw had a constant pitch (P) and diameter (D_0) so that the powder entrainment took place within approximately the first pitch length of the screw as illustrated in Fig. 2 leaving most of the powder in the bunker 'dead'. There was a strong tendency for rat-holing with the smallest ($D_0 = 0.625$ ") screw.

In practice this was of no consequence as the rat-hole was filled in by the intermittent re-charging of the bunker from an automatic gate lock⁽²⁾. The timing of each phase of the gate lock operation was adjustable for this and other purposes. It may well be a debatable matter as to whether the constant pitch and diameter screw is really necessary for the most accurate and uniform feed control.

Factors affecting feeder flow

So many variables can affect the flow rate of solids that a comprehensive study of each parameter is hardly feasible. The following classification of relevant parameters is suggested:-

a) Geometrical.

- 1) Flight size ($D_0 = 2R_0$).
- 2) $R_c/R_0 = K$, (ratio of core shaft radius/flight radius).
- 3) Screw pitch/diameter P/D_0 ratio.
- 4) Speed of rotation.

b) Powder.

- 1) Forces (i.e. gravity) which cause particles to fill the flight in the 'live' part of the bunker.
- 2) Density change of entrained solids.
- 3) Friction of entrained powder on flight, on core shaft and on surrounding solids.
- 4) The arching pressure packing characteristics of the surrounding powder. This determines the stresses which cause the screw to entrain the powder. Further down the screw these stresses act on the moving core and influence its helical motion and hence propulsion.

At present there is no really satisfactory theory to predict the flow rate of a screw-conveyor running full and the

difficulty with fine cohesive powders is even more acute. Significant internal shearing of the powder is likely to occur so that present analyses^(3,4) which only assume shear at powder/flight and surrounding powder interfaces only give an approximate picture of the solids motion. In particular the 'degree of fill' of a uniform pitch diameter screw is determined almost entirely within the first two pitch segments as is illustrated in Fig. 2. The flights further downstream where the powder is 'dead' have no effect on the volumetric throughput. The motion of filling is highly complex with considerable spill-over of powder at segment A Fig. 2.

The bulk density of powder is probably reduced considerably by this 'loosening up' motion at A to allow easy dilation of the powder and facilitate shearing within the segments B further downstream. It seems that the ease with which so many powders can be screw-conveyed must result from this lowering of the solids bulk density at A. It seems therefore that the degree of fill of the flights in a feeder is determined by the stress-shear relationships of a very loosely packed powder. Thus the usual static shear cell tests⁽⁵⁾ are probably of little relevance to this situation.

The dead powder at C usually plays little part in the motion. Hence the choke tube D merely prevents 'carry-over' of the surrounding powder due to the shearing stress from the powder moving in the screw helix. The powder in the bed at E is only restrained from moving with the powder in the screw by stresses which are little higher than those of the tensile strength of the powder. In short the choke merely prevents intermittent breakaway of the powder at the edge of the bunker and thus promotes uniform discharge. It also

eliminates any flooding tendencies of the powder.

Despite these complexities an attempt will be made to examine comparatively the volumetric flow rate in feeders of similar geometry but different size. For comparison purposes the concept of volumetric flow effectiveness of a conveyor must be developed.

Volumetric flow effectiveness - selection of a suitable criterion

In assessing the expected ideal flow-rate from a screw-conveyor it is reasonable to use the 'no internal shear' theories of Bates⁽³⁾ and Metcalf⁽⁴⁾ although an examination of displacement vector diagrams over the full range of values of θ (Fig. 3) shows that some internal shear is very likely to take place in most cases. It is assumed that the packing characteristics of a conveyor running full are sufficient for shear and pressure forces acting on the powder to be uniform round the screw periphery. Additionally, the speed of the screw is insufficient for centrifugal forces to be relevant.

The vector diagram of particle motion is shown in (Fig. 3). Considering the situation of the flight tip the vector V_a is found to be in an equilibrium position where the resultant OA of the normal and frictional forces from the flight balances the shear drag force from the external powder. As this drag acts along the line of motion of the powder, while the direction of OA is fixed, any deviation of the motion from the line will produce a restoring force to maintain the equilibrium. If internal shear is assumed the drag force will be transmitted through the powder so that the much simplified (Fig. 3) is suitable for arbitrary radius r .

From (Fig. 3).

- 1) The powder motion is 2-dimensional only (i.e. there can be no radial displacement).
- 2) The axial velocity vector V_L varies with the radius.

In addition,

$$\tan \theta = \frac{r}{R_0} \cdot \tan \phi_0 \text{ from the screw geometry.}$$

Thus, the powder at r follows a helical motion at angle $(\theta + \phi)$ with respect to the conveyor axis.

The conveyor effectiveness can be defined as

$$\eta = \frac{\text{Actual volumetric discharge rate of powder}}{\text{Maximum theoretical flow rate of powder}} \cdot$$

It is assumed in this expression that the screw action at A in Fig. 3 produces only a small fractional change in density of the powder although this may be sufficient for a vast change in its dilation and shear properties.

The selection of a maximum theoretical flow rate seems an uncertain issue. A rather stringent specification is based on the swept volume and assumes that the powder could be conveyed with no helical motion. Clearly this is impossible without exceptionally high friction at the outer edge of the conveyed plug of solids and some special mechanism to restrain shear in the azimuthal direction.

In this case:-

$$\eta_1 = \frac{\text{Volume of powder delivered/revolution of screw}}{2\pi^2 R_0^3 (1 - k^2) \tan \phi_0} \quad (1)$$

Essentially this is the loading factor used by Metcalf⁽⁴⁾ and Carleton et al⁽⁶⁾. A more reasonable theoretical flow model would include the helical motion associated with an ideal smooth flight, $\phi = 0$. In this case, powder motion would be directly perpendicular to the flight

surface at any radius r , so that

$$\eta_2 = \frac{\text{Volume of powder delivered/revolution of screw}}{\pi^2 R_o^3 (1 - k^2) \sin 2\theta_o} \quad (2)$$

However, even in this case helical motion only results from the surface pressure forces of a perfectly smooth flight whereas stress at the shearing powder interface at R_o resists rotation of the powder. In this case, internal shear strain takes place and the axial displacement is greater at R_o than at R_c . One method to produce a model of no internal shear and account for some of the azimuthal drag is to introduce the lag and lead terms used by Bates⁽³⁾. Thus the axial displacement will be less than predicted at R_o and more at R_c and at some radius R_m will be equal to that predicted by the vector diagram. Bates considered this to be

$$R_m = R_o \left(\frac{1 + k^2}{2} \right)^{\frac{1}{2}}$$

Thus, still assuming that the friction angle $\phi = 0$

$$\eta_3 = \frac{\text{Volume of powder delivered/revolution}}{\pi^2 R_o^3 (1 - k^2) \left(\frac{1 + k^2}{2} \right)^{\frac{1}{2}} \sin 2\theta_m} \quad (3)$$

$$\theta_m = \tan^{-1} \frac{P}{\pi D_o \left(\frac{1 + k^2}{2} \right)^{\frac{1}{2}}} = \tan^{-1} \left(\frac{P}{2\pi R_m} \right)$$

Bates suggested that in a real (i.e. non-ideal conveyor) at θ_m the true axial displacement would be found at angle $(\theta + \phi)$. Whence,

$$\eta_4 = \frac{\text{Volume of powder delivered/revolution}}{2\pi R_o^3 \left(\frac{1 + k^2}{2} \right)^{\frac{1}{2}} \tan \theta_m \cdot \cos \theta_m \cdot \cos(\theta_m + \phi) \pi (1 - k^2) / \cos \phi} \quad (4)$$

This theory can be extended by considering the forces acting on a small section of material, but then the problem can only be solved by making rather doubtful assumptions.

However, a solution may be obtained by averaging the axial velocity over a cross-section of the dust in an axial plane. This theory allows for internal and azimuthal shear, the latter being necessary for any nett axial motion of the solids. Furthermore, for an advance to be possible the total azimuthal shear force must be less than the total flight face friction forces, (otherwise the device will eventually seize solid). As shown by the diagrams of Bates, omitting the loss and gain adjustments, the axial displacement at R_c is less than at R_o - consequently there is a tendency for compaction to occur towards R_c and for voids to be created. These will be filled by powder nearer to R_o which is prevented from moving radially by the surrounding material. Thus, there is a nett balancing out of the axial advancement between R_o and R_c , i.e. a cyclic motion within the flight. Instantaneously the axial advancement of powder is given by V_L in (Fig. 3). Thus a radial profile of V_L can easily be constructed and a mean value V_L calculated. From (Fig. 3):-

$$P = 2\pi r \tan \theta, \quad V_s = 2\pi r$$

$$x = V_L \cot \theta = V_s - V_t$$

$$\frac{V_L}{2\pi r - x} = \cot (\theta + \phi).$$

Hence
$$V_L = \frac{2\pi r}{(\cot \theta + \tan (\theta + \phi))} .$$

Therefore, the mean value is given by,

$$R_c \int^{R_o} 2\pi r \, dr \, V_L = \pi R_o^2 (1 - k^2) \bar{V}_L$$

= Predicted volume delivered (V).

The solution of this equation gives,

$$\text{Volume } V = \frac{P^3}{2\pi} \left[\frac{1}{2} \cot^2 \theta + \log_e \sin \theta - \tan \phi \cdot \cot(\theta + \phi) \right]_{\theta_c}^{\theta_o}$$

and

$$\eta_5 = \frac{\text{Actual volumetric discharge/revolution}}{V} \quad (5)$$

In each of these expressions (equations 1 to 5) the measured effectiveness η can quite justifiably be multiplied by a factor $(1 - t/p)^{-1}$, where t is the blade thickness (assumed constant). This allows for in-operative space occupied by the screw. The effect of this factor is shown as η_{5t} in Fig. 4, Table 2. As can be seen in (Fig. 4) the numerical difference between equations 1, 2 and 3 is not very great ($\phi = 0$), but if ϕ takes a reasonable value considerable changes in η are noted. (Curves $\eta_4, \eta_5, \eta_{5t}$). From two separate friction experiments with zinc dust on a metal surface a range of ϕ ($24^\circ < \phi < 30^\circ$) was found; an average $\phi = 27^\circ$ being taken.

Fig. 5 shows typical examples of calibration curves. With fresh uncirculated powder the delivery rate was always less, the effect being more marked with finer and hence more cohesive powders. This was attributed to dampness, loss of fines (in this particular study) and smoothing of rough particles (again a characteristic of this particular study only). Prolonged exposure of the powder to the packed static state also, no doubt, acted to the same effect. After only a short period of re-circulation (3-4 cycles), the powder delivery rate was accurately reproducible in all cases. The 320 mesh powder gave similar results in between the 240 and 500 mesh results shown in Fig. 5.

Powder Density

One of the most uncertain factors in assessing η is the lack of knowledge of density of the powder within the screw-flight. Low density in the screw-flight is desirable to allow dilation, easy shear and hence low energy conveying with minimal degradation. Damp powders have a lower density than dry ones as cohesion inhibits consolidation. The low value of η (see Fig. 5) with damp new powder can to a large extent be explained by low density. Table 1 Appendix 2 shows examples of tests with alumina.

The value ρ_2 was used in calculating η_1 as it was felt that light tapping was appropriate to the entrainment of solids in the screw. Because one can only measure the mass flow from a feeder, the uncertainty in ρ throws considerable doubt on the true volumetric flow. There is no doubt that the higher delivery rate of recirculated powder can be accounted for entirely by its greater bulk density.

In fact, the evidence in this work was that different powders did not seem to exhibit radically different values of η for the typical P/D_0 values of approximately unity which are commonly used.

On plotting the data against the various parameters involved it seems that η depends on screw diameter (D_0) to the greatest extent as shown in Fig. 6 although one might also suppose that there appears to be a tendency for η to fall with increase in (R_c/R_0) as shown in Fig. 4. Decrease in (P/D_0) always increases η but reduces nett throughput.

Flow of very cohesive powder

With adequate breaking of the arching tendencies (which are described in the next section) the 1" feeder gave

essentially the same calibration with both zinc (curve A) and zinc/fibre mixture (curve C, Fig. 7) up to about 90 rpm above which speed the fibre/mixture delivery rate fell well below the linear relationship (shown as dotted line).

The zinc/fibre mixture: 62 parts of (5 - 40 μ) diameter zinc particles to 1 part glass-fibre by weight. Fibres were 5×10^{-4} in. diameter \times 0.25" length. Before mixing the powder/fibre volume ratio is 4:1. The departure from linearity of the powder alone was less marked. The conveying efficiency of the 2" screw with fibre (curve D) was substantially less than that (curve B) for powder flowing alone. One might speculate that either (or more likely both) of the following factors were responsible.

- 1) The presence of fibres tends to inhibit consolidation of solids when the screw is filling so giving less dense solids delivery. This would be expected to affect both screws however.
- 2) Fibres at the periphery of the screw may tend to draw a larger swept volume of solids into the screw than might be anticipated from the value R_0 . The fibre/powder mixture has a much higher tensile strength when compacted than powder alone although its shear strength is not likely to increase in the same proportion. The fall in conveying velocity from the linear relationship at higher shaft speeds is to be expected as gravitational forces become insufficient to carry the powder into the feeder to fill it fully.

Reliability of Flow

The smallest ($D_0 = 0.625$ ") feeder could be bent easily

by impact of falling solids. Accurate alignment of the parts of the feeder was found to be most important to minimise attrition and premature shaft seal failure. Particularly bad alignment can even cause seizure (as can non-uniform pitching) and this may indeed be a measure of powder consolidation within the flights. A choke length of one pitch diameter was sufficient to ensure uniform discharge. The pressure drop (0.5 to 5 cm H₂O) across the choke section depended on the feed rate and volume replacement via the balance air pipe (Fig. 1). The zinc powder tended to flood across the largest flights even when the plant was shut down.

The zinc/fibre mixture gave by far the greatest handling difficulty due to its exceptionally cohesive nature, (its angle of repose was effectively 90°). Compaction of the fibre occurred at E shown cross-hatched in (Fig. 2). The compacted deposit consisted of an abnormally high fraction of fibre indicating that segregation had occurred. The problem was eased considerably by the fluidising pad F which increased the dilation of the sheared mixture. Arching in the bunker was an even more difficult problem with this material. Several types of arch-breaker were tried with limited success. One type used flexible springs attached to a 70° oscillating cross-shaft as a means to minimise arch-breaker powder consumption. The idea behind the use of springs is that their effective volume changes with bending and this might have allowed dilation of the powder in the arch. Unfortunately, the arch accommodated itself to the movement of the springs. In addition it seems that the oscillatory motion of the springs was far too slow for this method to be effective. Substitution of 8 × 5/16" diameter rods instead of the

springs was successful in breaking the arch. It is felt however that more elegant methods could have been used to overcome this problem.

Conclusions

- 1) A constant velocity method of calculating the volumetric flow rate gives an improved prediction of effectiveness (η_5).
- 2) The measured effectiveness increases with increasing D_o and decreasing (P/D_o) .
- 3) A decrease in effectiveness occurs if the packed density of the solid decreases due to the presence of fibrous material or dampness.
- 4) Fibrous material can also upset the filling of the screw-feeder at high speeds causing a further reduction in ' η '.
- 5) With reference to powders only, it was found in this work that the nature of the material conveyed had only a marginal effect on ' η '.
- 6) Arching of the flow causes uneven solids transfer. This difficulty was tackled but with only limited success.
- 7) Reliability of the feeding test equipment is critically dependent on the manufacture of the screw-flight and the alignment of the screw-feeder assembly.

APPENDIX 1

References

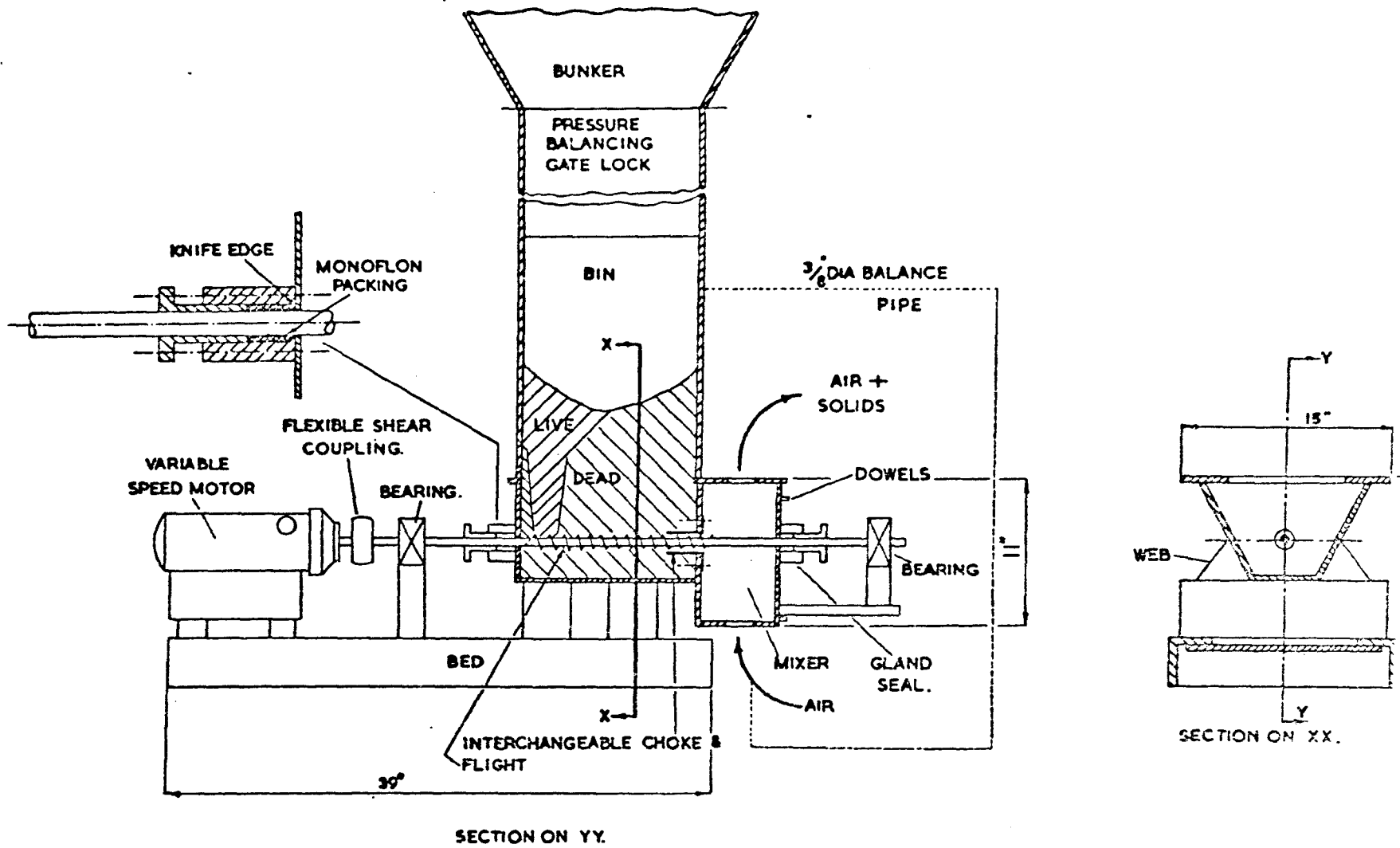
- 1 R.G. Boothroyd and A.S. Goldberg. Brit. Chem. Eng. 1970, 15, 68.
- 2 P.J. Walton, L.N. Gammon and R.G. Boothroyd. Paper presented at Int. Powder Technology and Bulk Solids Conf. Harrogate, 12-14th May 1971.
- 3 L. Bates. Trans. ASME (J. Eng. In.), 1969, 91B, 295.
- 4 J.R. Metcalfe. Proc. I. Mech. E. 1965-66, 180, Part 1, 131.
- 5 R.L. Brown and J.C. Richards. Principles of Powder Mechanics, 1970, Pergamon: Oxford.
- 6 Carleton, A.J., Miles, J.E.P. and Valentin, F.H.H. Trans. ASME (J. Eng. Ind.) 1969, 91B, 329.

APPENDIX 2

Table 1 Static Bed Properties of Alumina

Mesh	Circulation History	ρ_1	ρ_2	ρ_3	ρ_4	Angle of repose
320	Test 71	1.91	2.03	2.18	2.22	35°
320	New Powder	1.64	1.79	1.96	2.06	39°
500	Test 110	1.68	1.76	1.89	1.96	40°
500	New Powder	1.40	1.48	1.64	1.85	49°

The conditions for the densities were ρ_1 - minimum bulk density (no tapping) ρ_2 - after 3 tappings, ρ_3 - after 10 tappings and ρ_4 - the maximum observed bulk density after tapping to constant volume.



SCREW FEEDER.

FIG. 1

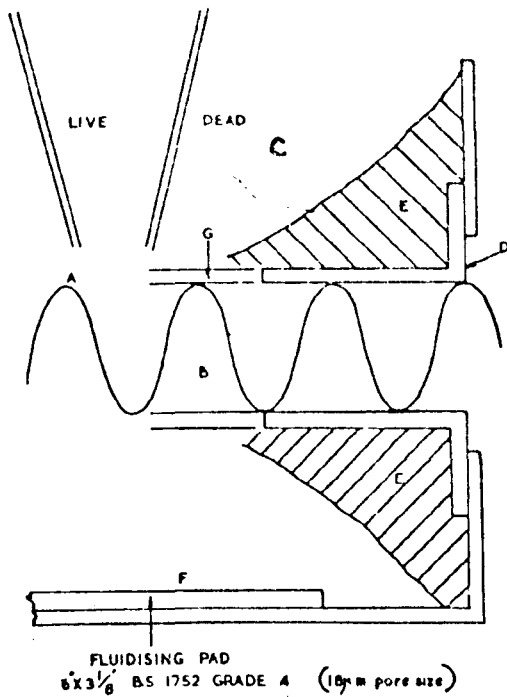


FIG. 2 FEATURES OF SOLIDS FLOW.

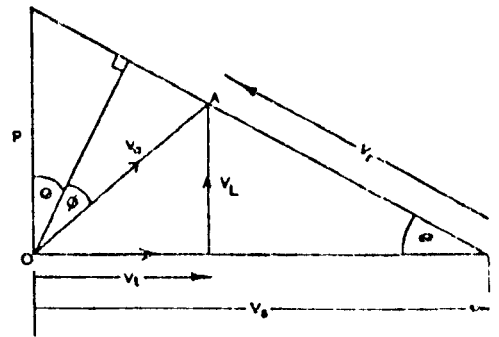


FIG. 3 VELOCITY AND DISPLACEMENT OF POWDER IN SCREW-FLUIDER

TABLE 2. DETAILS OF FLIGHTS AND POWDERS.

Symbol numbers appear on figures.

SYMBOL NUMBER	MATERIAL	ADDITIONAL INFORMATION	D_c	D_o	P	t	P/D_o	Choke: Bore in
1	Zinc		0.37	0.62	0.50	0.06	0.80	0.58
2	Zinc		0.50	1.00	1.18	0.12	1.25	-
3	Zinc		0.62	1.50	1.25	0.09	0.82	-
4	Zinc		0.62	2.50	1.87	0.12	0.75	2.70
5	Zinc		-	2.00	2.00	-	1.00	-
6	Alumina		0.62	2.50	1.87	0.12	0.75	2.70
7	Alumina	240 mesh,	0.62	1.69	1.31	0.12	0.77	1.70
8	Alumina	500 mesh,	0.62	1.69	1.31	0.12	0.77	1.70
9	Alumina	240 mesh, new damp and unpolished,	0.62	1.69	1.31	0.12	0.77	1.70
10	Alumina	240 mesh, circulated up to test 6,	0.62	1.69	1.31	0.12	0.77	1.70
11	Alumina	240 mesh, circulated up to test 71,	0.62	1.69	1.31	0.12	0.77	1.70
12	Alumina	500 mesh, new damp uncirculated,	0.62	1.69	1.31	0.12	0.77	1.70
13	Alumina	500 mesh, circulated up to test 34,	0.62	1.69	1.31	0.12	0.77	1.70
14	Alumina	500 mesh, circulated up to test 88	0.62	1.69	1.31	0.12	0.77	1.70
15	Alumina	320 mesh,	0.62	1.50	1.00	0.12	0.66	1.70
16	Alumina	500 mesh,	0.62	1.50	1.00	0.12	0.66	1.70
17	Alumina	320 mesh,	0.62	1.69	1.31	0.12	0.77	1.70
18	Alumina	240 and 320 mesh.	0.62	2.50	1.81	0.12	0.72	1.70
19	Zinc		0.50	1.00	1.00	-	1.00	-
20	zinc/fibre		0.50	1.00	1.00	-	1.00	-
21	zinc/fibre		0.62	2.00	2.00	-	1.00	-

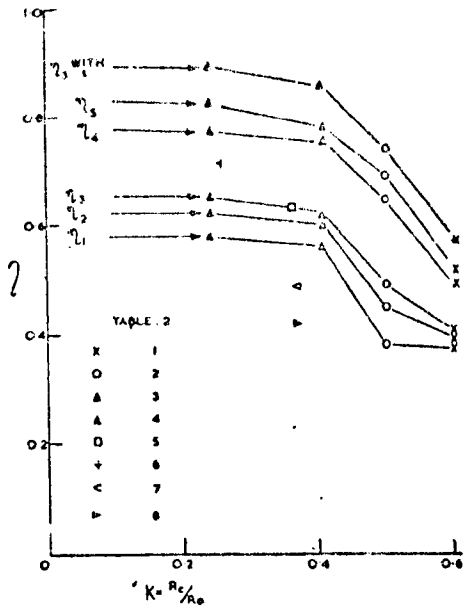


FIG 4 VARIOUS CALCULATIONS OF EFFECTIVENESS.

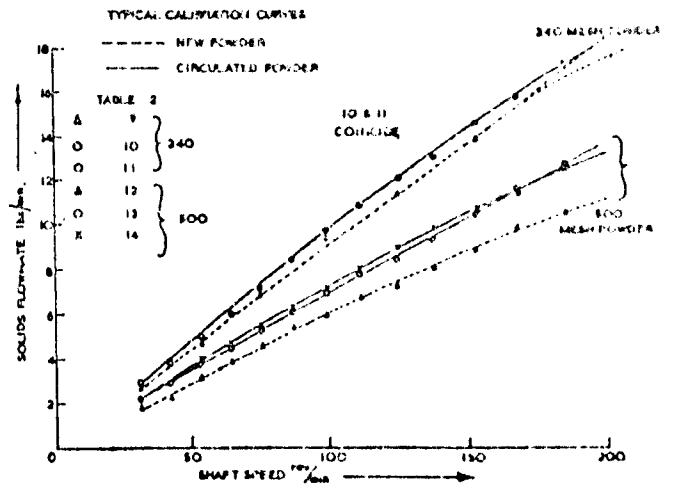


FIG 5 CALIBRATION OF ALUMINA.

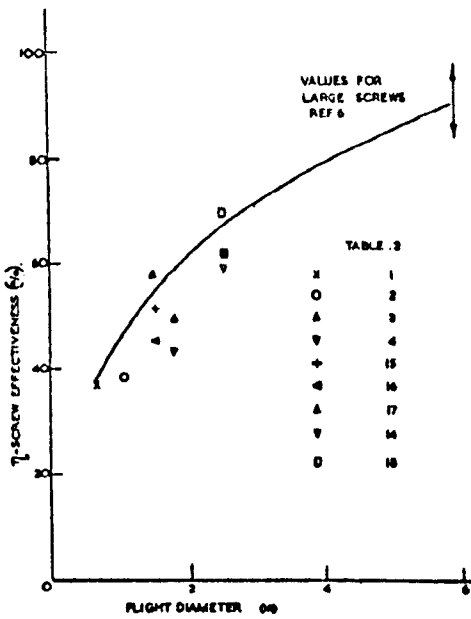


FIG 6 INFLUENCE OF SCREW DIAMETER ON EFFECTIVENESS.

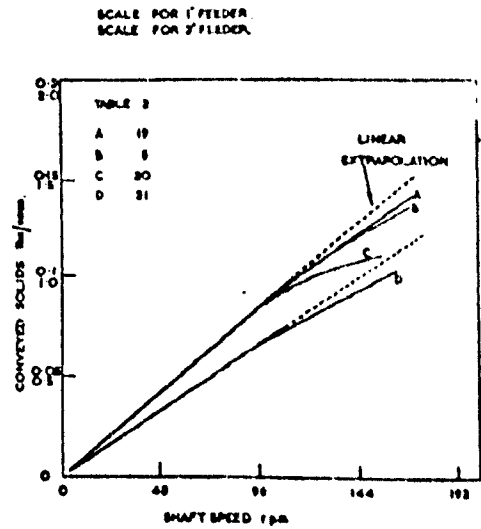


FIG 7 CALIBRATION OF ZINC AND ZINC FIBRES.

APPENDIX A.3.

Appendix A.3.

A.3.1 Perspex Hoppers

The purpose of this section is to warn future investigators of the problems associated with using perspex hoppers in a powder handling system which requires the hoppers to be frequently pressurised to about 8 lbf/in² gauge.

The bunkers identified as (R), (S) and (T) in Fig. 3.2 were manufactured in perspex at the commencement of the present investigation. The author selected transparent bunkers for the obvious advantages of immediate visual evidence of screw-feeder powder starvation, rat-holing, "bridging" across the hopper outlets, and continuous knowledge of the whereabouts of the charge of powder. It was initially felt that the very fine 500 mesh alumina particles may cause flow problems within the hoppers, and the smooth surface finish of perspex was an added advantage. The arrangement of the perspex hoppers can be seen by reference to plate 7.

The first few months of commissioning the test rig was almost entirely devoted to sealing the hoppers from air leakages. The powder flowed through the hoppers quite beautifully and the system was most impressive. Eventually the equipment was rendered air-tight, after many bottles of perspex cement, and the apparatus available for the first quantitative series of tests. The first test was absolutely catastrophic in that the centre hopper (S) fractured completely in the conical section just above the lower pinch valve. The three perspex hoppers were immediately dismantled and replaced with mild steel bunkers which have proved quite successful. The perspex hoppers have been repaired and a new project investigating the

flow of powders through hoppers is currently being formulated.

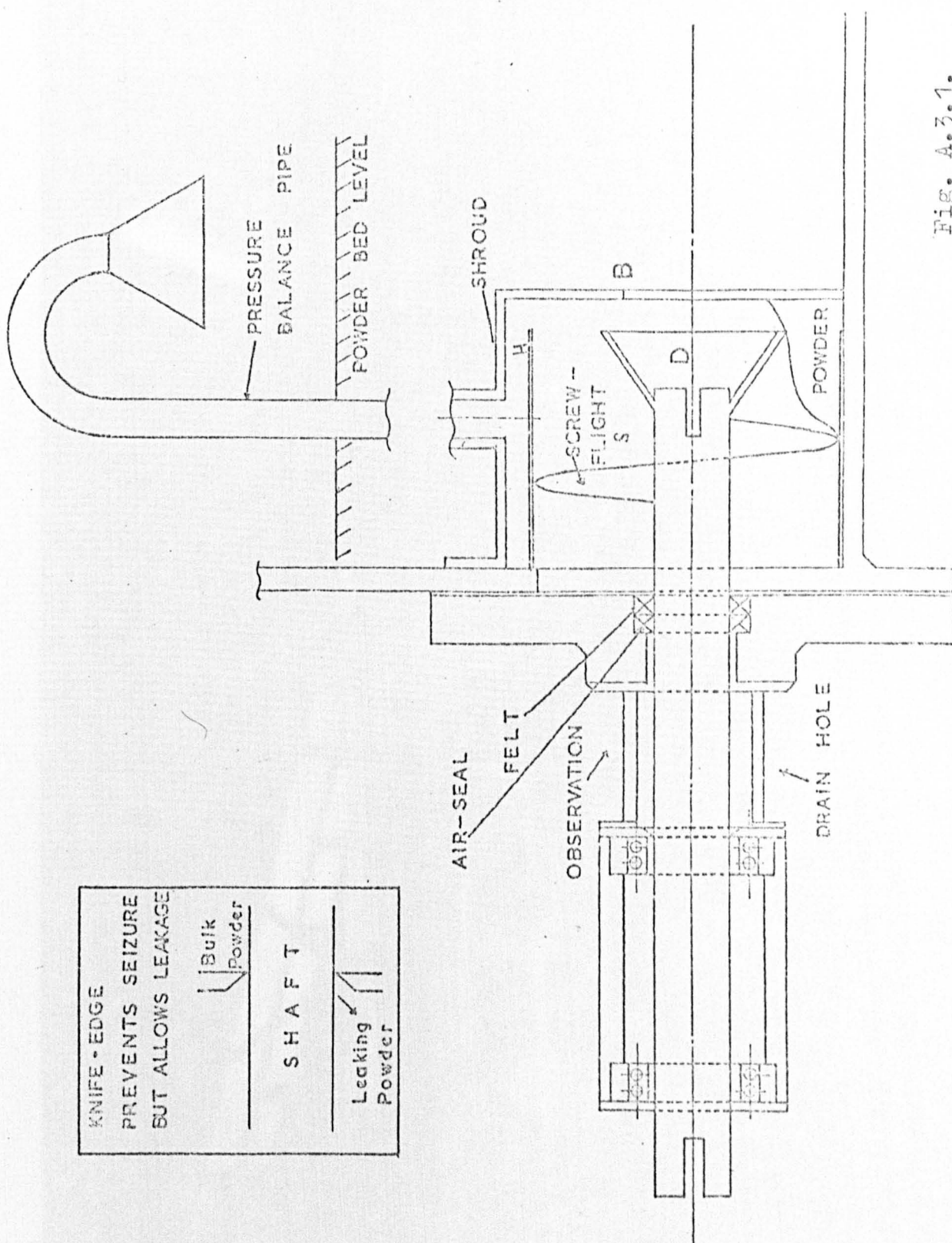
A.3.2 Bearing and Seal Assembly

It can be seen by reference to Figs. 3.2 and A.3.1 that the bearing at the drive end of the screw-feeder must support a shaft which penetrates a pressurised solids supply bunker. The design problem was to provide a bearing capable of accommodating an end thrust which also incorporates a suitable seal for the rotating drive shaft, thus preventing powder leaking from the supply bunker. Ingress of the abrasive particles into bearings and seal caused severe wear which accentuated the problem of leakage prevention.

The final design was similar to that shown in Fig. A.3.1, which consists of an outrigger type of bearing with a bulkhead and drain hole to protect the ball-bearings in the event of failure of the seal. The assembly in its final form dispensed with the pressure balance pipe and the shroud in the form illustrated. The shroud was replaced by an integral housing, (H) in Fig. A.3.1, which provided a clearance of about 0.05 inch between the housing and the dust-rejection screw-flight (S). This housing shrouded the immersed part of the drive shaft from the powder bed and the large screw-flight (S) prevented the bulk of the powder from penetrating to the ring of felt seals. The problem was now reduced to that of restraining air-borne dust from entering the bearing. It was hoped that the felt seals fitting tightly to the drive shaft would suffice, however, the seals certainly proved an adequate absorber of dust but gradually became impregnated with consequent loss of effectiveness. A further "line of defence" was the provision of an air seal comprising of two rubber 'O' rings which gripped the drive shaft and were

displaced by a small bush having four milled slots. Relatively high pressure air could be admitted to the shaft via the milled-slots, the air seal being mounted externally to the solids seal. The knife-edge retaining plates for the felt seals proved most effective in preventing seizure of the shaft by compacted powder. The unit operated successfully for six months without application of the air seal. Very slight leakage of powder from the drain hole was the first indication of seal failure. Dismantling the assembly showed that the felt seals had become impregnated as expected, but the major cause of leakage appeared to be the excessive wear of the mild steel primary drive shaft beneath the 'O' rings, which had suffered considerable damage. A new shaft was manufactured from much harder steel (E.N.100) and the 'O' rings and felt seals were re-newed. This assembly functioned well for almost two years and leakage problems did not occur until the bend erosion tests were almost complete. The unit has recently been slightly modified to incorporate "Monoflon" packed seal, as reported in appendix A.2., instead of the felt seals, and trouble-free operation is expected.

The screw insert guide (D) proved most useful in simplifying the task of connecting a screw-flight to the tongue and socket torque transmission arrangement at the end of the drive shaft, access to the screw-feeder housing being through the outlet end of the feeder. This design allowed easy interchangeability of screw-flights.



KNIFE - EDGE
 PREVENTS SEIZURE
 BUT ALLOWS LEAKAGE

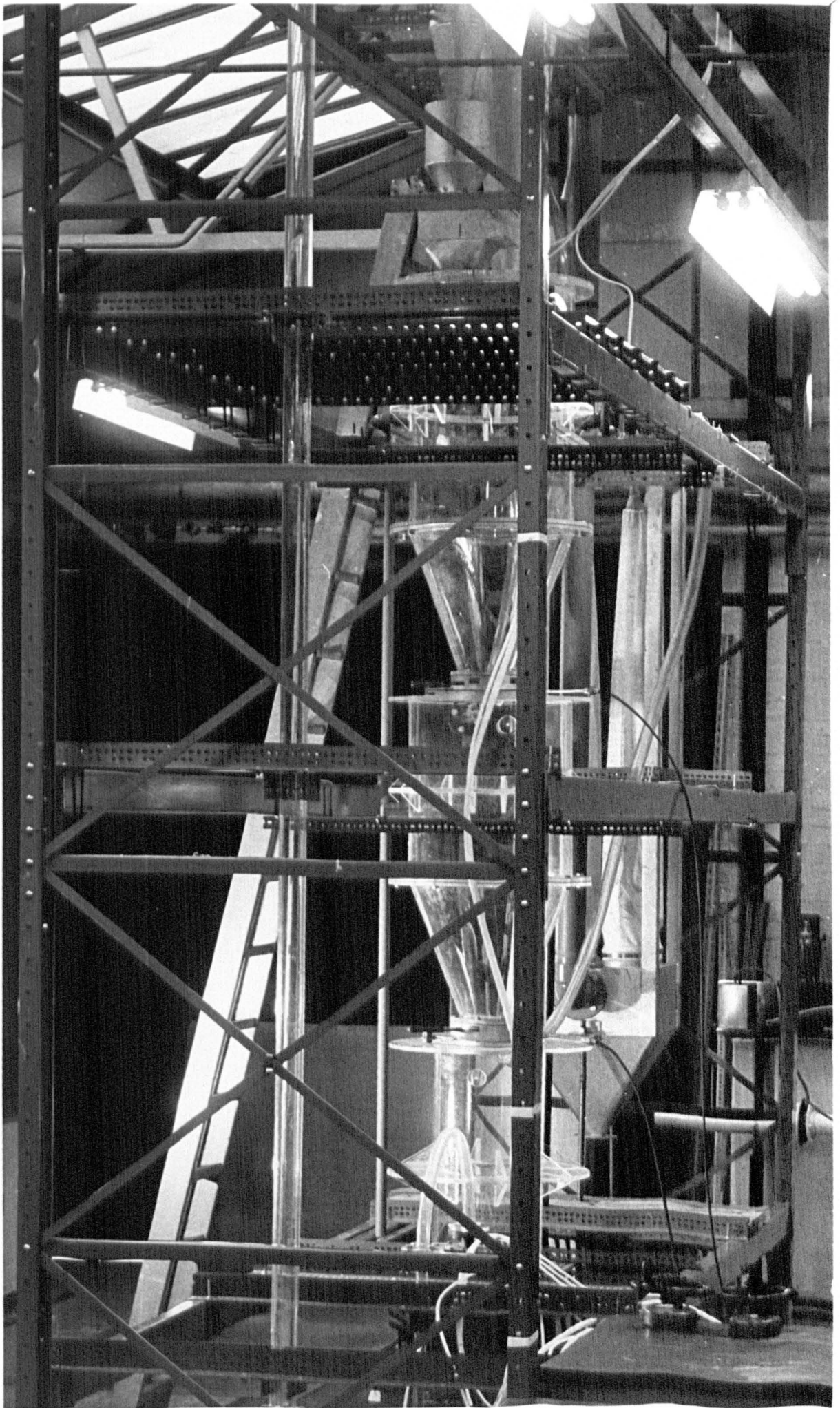
Bulk Powder

S H A F T

Leaking Powder

Fig. A.3.1.

Plate 7: Perspex Rig.



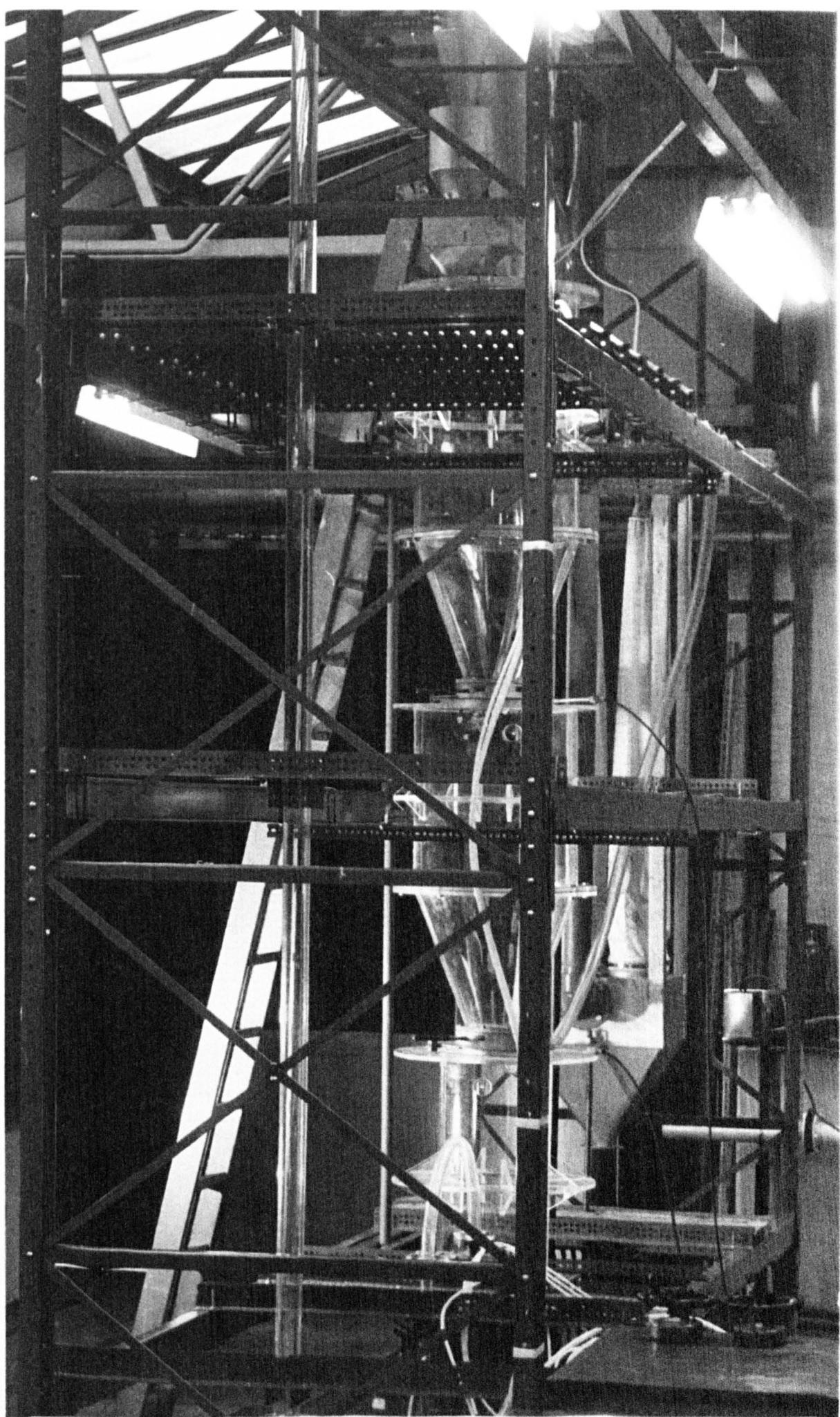


Plate 7: Perspex Rig.

APPENDIX A.4.

CHINA CLAY INVESTIGATION

A.4.1 Introduction

The main objective of the present research investigation was to produce information on the transportation of particulate matter which would be of some value to industry. The author was very conscious that although three particle sizes of alumina were conveyed only one type of powder had been used. Consequently, when approached by a firm to examine the conveyability of china clay, the author readily accepted. The results of this brief investigation are included here as evidence of the author's awareness and interest in the whole field of powder handling.

A.4.2 Experimental Procedure and Apparatus

The non-abrasive properties of china clay and the necessity of observing visually the flowability of the clay along horizontal ducts and around bends required some modifications to the apparatus. The part of the suspension flow loop identified by (L) in Fig. 3.2 was originally two inch mild steel ducting, this was replaced by fairly rigid 2.5 inch bore clear P.V.C. tubing, and the part identified by (N) substituted by a two inch diameter perspex bend having a radius of curvature of 24 inches.

The method of plant operation was similar to that described in section 3.4 and the measurements taken are evident from Table A.4.1.

A.4.3 Powder Property Determinations

It has been mentioned previously that the first requirement of any pneumatic conveying investigation is an understanding of the physical properties of the material to be transported.

A brief summary of the data acquired is as follows:-

(i) Sample A : the Lee Moor Grade B china clay was delivered in one cwt. bags and a representative sample obtained using a "cone and quartering" technique. Analysis of this sample provided the following information:-

(a) Moisture content for several samples varied between 8.5% and 9.1% by weight.

(b) Bulk density: poured value 63 lb/ft³,
final tamped value ... 71 lb/ft³.

(c) Particle size spectrum: 55% finer than 2 microns,
8% larger than 10 microns.

(ii) Sample B : this was obtained after transporting sample A around the test rig seven times; the china clay having achieved its ultimate physical nature. Analysis of this sample yielded the following:-

(a) Moisture content for several samples varied between 0.0% and 0.8% by weight.

(b) Bulk density: poured value 21 lb/ft³,
final tamped value ... 31 lb/ft³.

(c) Particle size spectrum: 100% finer than 2 microns.

The maximum air temperature at inlet to the mixing unit was 42°C and this caused the large reduction in moisture content. The solid particles soon achieved a particle size distribution below 2 microns and the china clay in this form was highly cohesive and agglomerated easily. The reduction in bulk density was quite dramatic and has far-reaching effects in hopper design.

A.4.4 Test Results Summary

Table A.4.1

	Sample A			Sample B			
Superficial air velocity, (ft/s)	128	103	66	133	106	76	69
Pressure drop/ft in vertical duct, (in H ₂ O)	0.70	0.55	0.20	0.50	0.40	0.25	0.20
Pressure drop/ft in horizontal duct, (in H ₂ O)	1.85	1.25	0.50	0.50	0.45	0.35	0.35
Pressure drop around 24 in radius bend, (in H ₂ O)	3.20	2.50	0.90	1.60	1.20	1.00	1.00
Pressure drop/ft for bend, (in H ₂ O)	1.10	0.80	0.30	0.53	0.40	0.33	0.33
Screw-feeder delivery, (lb/min)	28	28	28	4.5	4.5	4.5	4.5
Solids loading lb solid/lb air	2.4	3.0	4.7	0.30	0.46	0.64	0.72

Thus, as the conveying air velocity reduced to just below 70 ft/s, the pressure drop in all cases diminished until the values for samples A and B were virtually the same, despite the quantity of A circulated being six times the quantity of B. As a result, a system designed with the pressure drops for the ultrafine clay as a basis is recommended.

A.4.5 Scaling-Up

It was required to calculate the total pressure drop for a four inch diameter conveying line consisting of 110 ft horizontal pipe, 50 ft vertical pipe and four 4 ft radius bends. The firm accepted that to scale-up from the test rig's

two inch system to a four inch system incorporating far longer runs of ducting was not feasible, but they requested an order of magnitude for the overall pressure drop.

The air velocity in the 4 inch system was assumed to be 4,000 ft/min (approximately 67 ft/s), and by applying a very simplified Fanning-type equation to the pressure differentials in two and four inch systems, a conversion factor of 0.4, for the pressure drop in a 4 inch duct, was obtained. Thus, for an air velocity of 4,000 ft/min in a 4 inch conveying line the following pressure drops can be expected:-

	Solids flowrate (lb/min)	Pressure drop/ft in vertical duct, (in H ₂ O)	Pressure drop/ft in horizontal duct, (in H ₂ O)	Pressure drop/ft for bend, (in H ₂ O)
Sample A	28.0	0.08	0.10	0.12
Sample B	4.5	0.08	0.12	0.13

The above pressure drops are based upon a 2 ft radius bend in a 2 inch system being equivalent to a 4 ft radius bend in a 4 inch system, and the horizontal pressure drop being a maximum since the china clay was accelerating. So, the total pressure drop when conveying 4.5 lb/min of very fine china clay through 4 inch diameter pipes at an air velocity of 4,000 ft/min is given by:-

(a) 110 ft horizontal duct:- $\Delta p = 110 \times 0.12 = 13.2$
in H₂O;

(b) 50 ft vertical duct:- $\Delta p = 50 \times 0.08 = 4.0$ in H₂O;

(c) 4 - 4 ft radius bends:- $\Delta p = 4 \times 6.28 \times 0.13 = 3.3$
in H₂O.

Hence, total pressure drop = 20.5 in H₂O. The pressure drop through a suitable dust extraction system would be about 8 in H₂O, giving a total system pressure drop around 1 lbf/in². Allowing for a substantial increase in pressure drop for a proportionate increase in the solids flow rate, a compressor rated at 10 lbf/in² gauge delivery pressure and 600 ft³/min of free air delivered should be adequate.

A.4.6 Conveyability of China Clay

The screw-feeder delivered the new clay (sample A) quite satisfactorily and this clay was easily transported around the test rig. There was no evidence of "packing-up" on bends at air velocities above 4,000 ft/min. The feeder delivered only 4.5 lb/min of the very fine clay (sample B) for the same speed of rotation that delivered 28 lb/min of sample A clay. Examination of the screw-flight at the end of the tests revealed that a one-eighth inch thick layer of clay had compacted around the flight, which also showed signs of corrosion due to the moisture originally present in the clay. However, after the clay had become entrained in the conveying air no difficulty in transporting the gas-solid mixture was experienced. At the lower air velocities a fine deposit of particles built-up on the pipe-wall, but this did not impair the ability to pneumatically convey the fine clay. In fact, the air flow was frequently stopped momentarily and the clay was allowed to block the pipe system; immediate increase in the air velocity always proved successful in re-conveying the settled material. Finally, purging the system with air proved adequate for cleaning the transport lines of deposited fines.

There was no evidence of wear on the perspex bend and, as expected, it can be assumed that erosion of bends due to

abrasion by china clay particles will not occur.

A.4.7 Flowability of China Clay through Storage Hoppers

The mild steel cylindrical storage hoppers (S and R in Fig. 3.2) are 18 inches diameter with a conical discharge, 70 degrees to the horizontal, having a 6 inch diameter outlet. The clay in its "processed" form would not flow through the hoppers and arched across the outlet in "text-book" manner. The sample A clay flowed much more easily but lengthy residence time in the hopper aggravated the problem.

The moisture content of the clay was very evident in that the inside surfaces of the hoppers suffered almost immediate corrosion, indicating that lining of the hopper walls is necessary to avoid contamination of the product.

Unreliable discharge from hoppers is a definite hazard and the problem of extracting the china clay depends largely upon the following characteristics:-

- (i) Variation in moisture content.
- (ii) Changes in bulk density.
- (iii) Particle size distribution.
- (iv) Method of depositing material into hopper.
- (v) Presence of foreign material.

These parameters change with time and with handling and so a successful scheme for handling this material will depend upon a detailed knowledge of this continually varying product.

The moisture content of the clay requires that mild steel hoppers be lined with rubber or epoxy resin, they may also need to be lagged to avoid condensation problems. The hopper lining should be selected to have the additional advantage of promoting slip along the hopper walls, fibre-

glass has good slip values and would also obviate ferrous contamination of the clay.

Allowing for the above desirable design features and providing sufficient ullage space to ensure that adequate volume exists for complete separation of material from the airstream, the following dimensions indicate the capacity required for a receiving hopper to hold 50 tons of china clay (quantity quoted by firm):-

- (a) Fibreglass hopper; smooth, repairable, corrosion - resistant and relatively cheap.
- (b) Straight cylindrical section 12 ft dia. × 35 ft high having a 15° coned top and 14 ft deep coned bottom with a 70° angle to the horizontal. Volumetric capacity of 4,600 to 4,700 ft³ and weight of empty hopper approximately 6 to 7 tons. This hopper would hold 50 tons of material having a bulk density of 30 lb/ft³, allowing a 20% ullage, this rather high allowance provides for some variation in the bulk density.
- (c) Overall vertical height would be 50 ft.

A.4.8 Alternative Ways of Hopper Discharge

It is evident that china clay is not free-flowing and some means of facilitating discharge is recommended:-

- (i) The "Sonoforce" technique of sonic activation should be successful in facilitating the flow of china clay. Unfortunately, the noise generated by these activators is likely to be greater than 90 decibels, and so this factor alone may be sufficient reason to preclude the application of "Sonoforce".

- (ii) The Simons bin activator appears eminently suitable for ensuring discharge at a controlled rate. It could easily be fitted to the fibreglass hopper discussed above and would reduce the overall vertical height.
- (iii) Aeration pads may be used provided the china clay does fluidise and not merely aerate, the latter phenomenon occasionally assists the flow by agitating the material, however, it may cause "rat-holing". It is quite feasible that fluidisation would be successful in facilitating hopper discharge, in which case it is recommended that the fluidising air is only applied during extraction. Excessive aeration reduces the bulk density of the material and may result in uncontrollable discharge.

A.4.9 Air Filtration

A conventional cyclone is generally not satisfactory below 5 to 10 microns, unless agglomeration has occurred. Thus, the bulk of the china clay would not be extracted by a cyclone collector and a fabric filter is recommended. The usual design basis of 5 ft³/min of conveying air per ft² of filter cloth indicates that a filter cloth area of about 120 ft² would suffice. The D.C.E. "Dalamatic" venting unit with terylene pads and high pressure reverse jet cleaning is recommended.

A.4.10 Material Entrainment

A rotary air lock should be satisfactory for handling new clay from the main silo. However, intermediate hoppers will be required to discharge finer clay of greatly reduced bulk density, so adequate venting of the exhaust air becomes

necessary to avoid this air preventing material from flowing into the pockets.

If the powder handling plant uses a pressure vessel system incorporating slide valves, these valves will ultimately seize due to the clay becoming compacted in the slides. As a result, a sophisticated slide valve would be required to overcome problems of compaction and leakage of powder if the material is aerated.

The china clay could undoubtedly be conveyed in dense-phase by means of a high pressure transfer technique such as the "fluidised powder pump". A typical unit would deliver clay having a bulk density of 20 lb/ft³ at a rate up to 100 ton/h. This would be a batch system, an average batch being 2 tons, operating at a pressure of 40 to 50 lbf/in².

A.4.11 Conclusions

A successful bulk powder handling plant for china clay must be based upon understanding the continually varying product which is being conveyed.

Pneumatic conveying of china clay is a viable proposition, the minimum safe conveying velocity being 3500 to 4000 ft/min. Caution must be exercised in hopper design on account of the variation in bulk density during handling, the cohesive arching of the "processed" material, and possible corrosion due to the moisture content of the clay.

APPENDIX A.5.

ADDITIONAL GRAPHICAL RESULTS

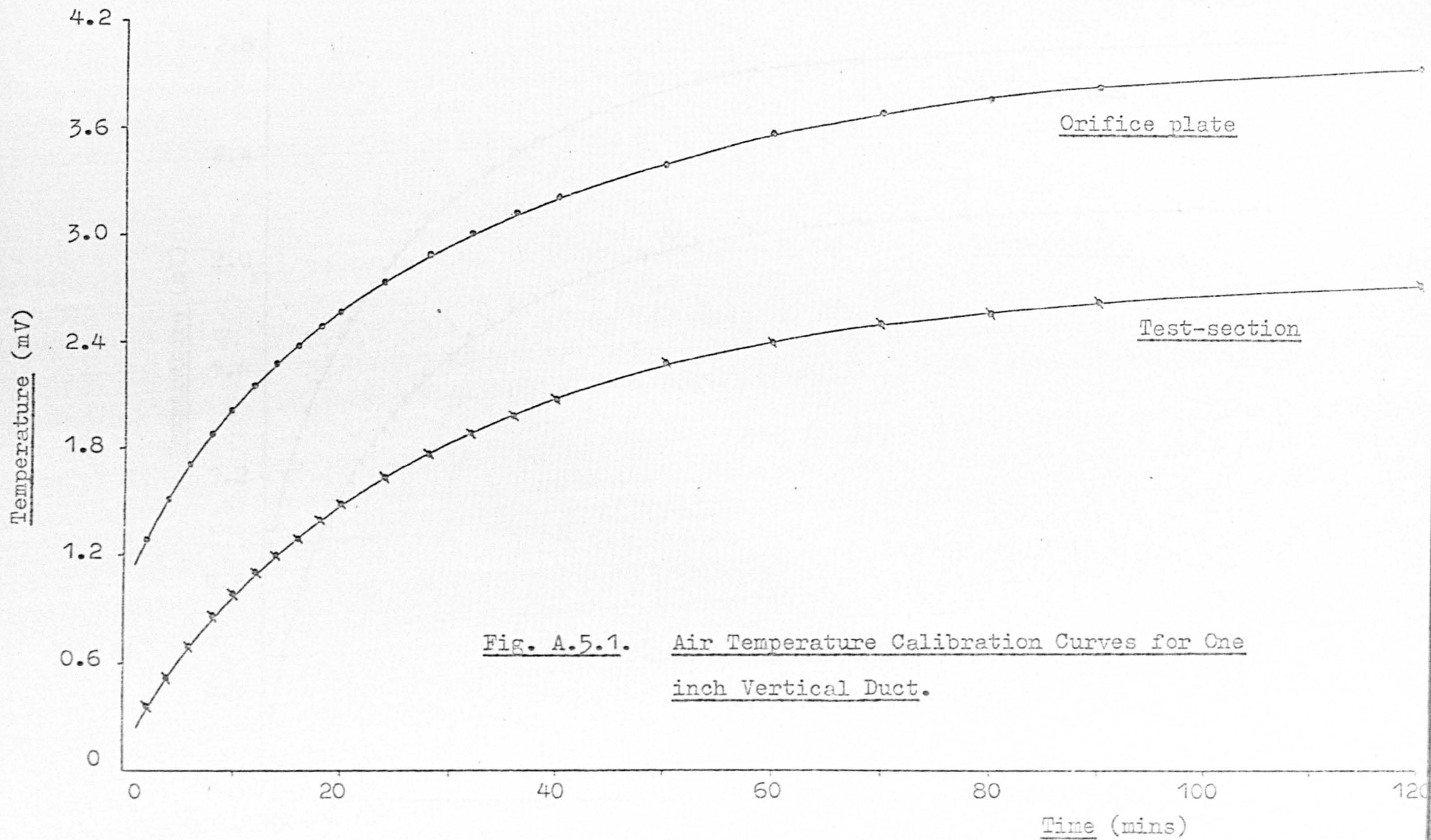


Fig. A.5.1. Air Temperature Calibration Curves for One
inch Vertical Duct.

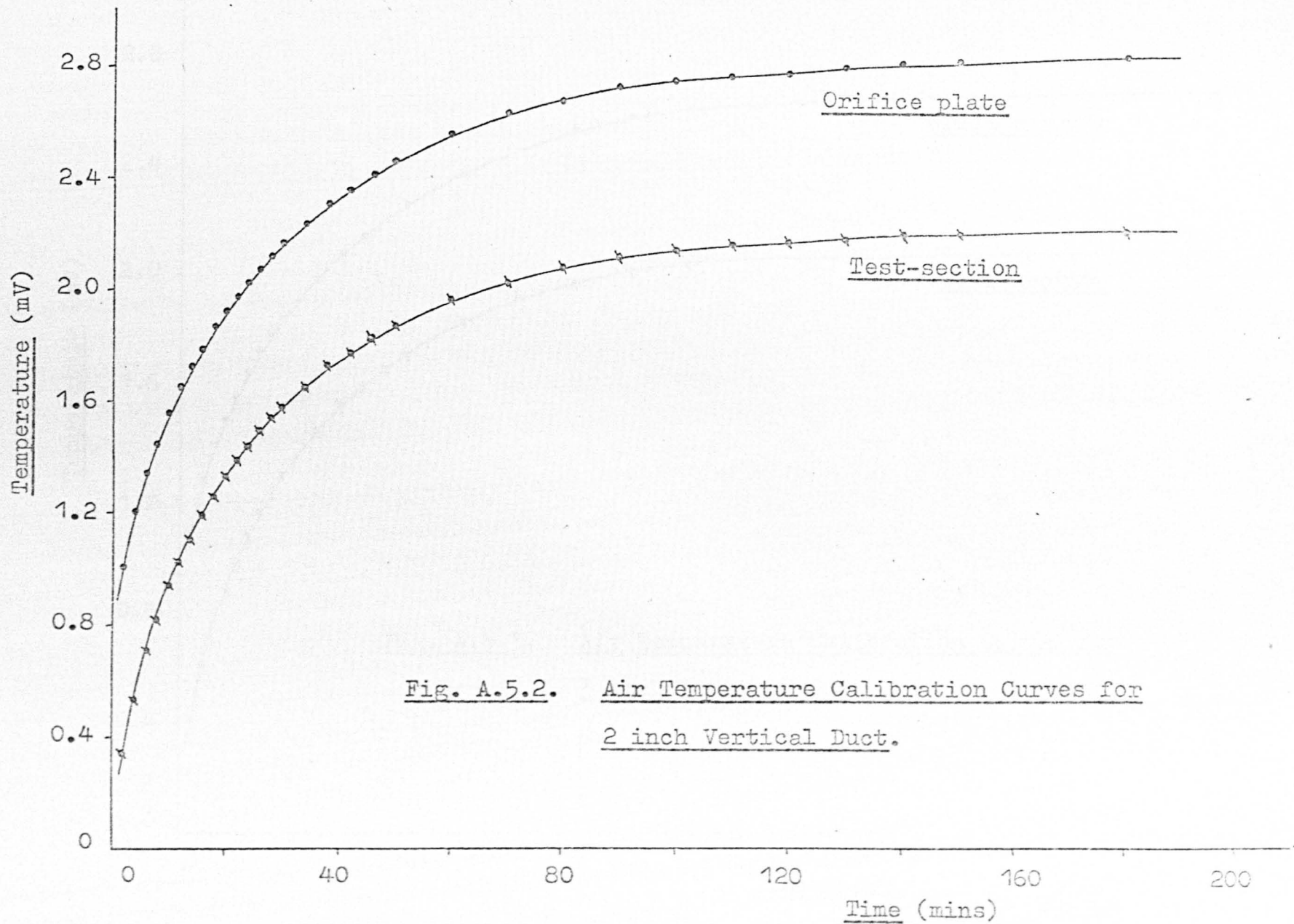


Fig. A.5.2. Air Temperature Calibration Curves for
2 inch Vertical Duct.

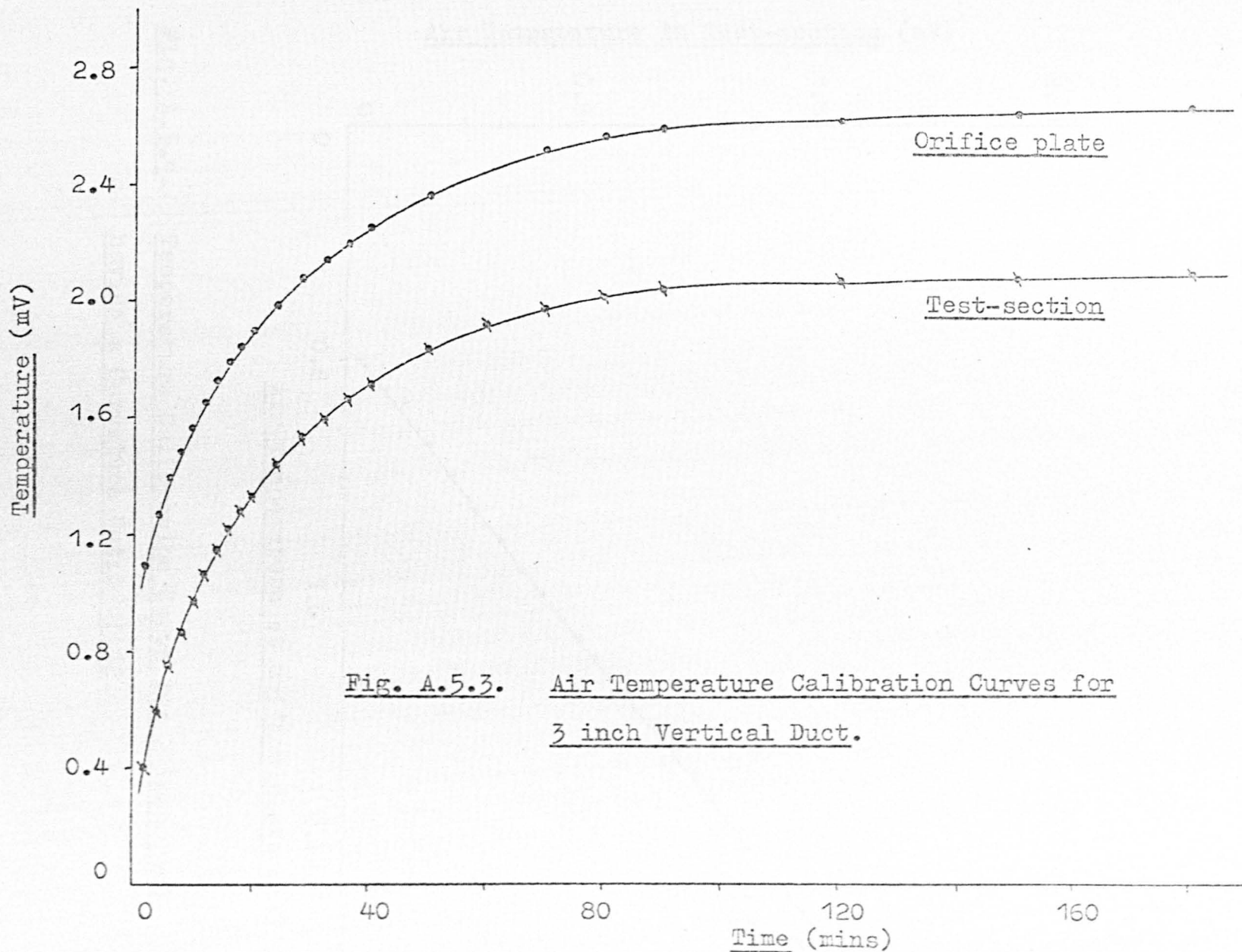


Fig. A.5.3. Air Temperature Calibration Curves for
3 inch Vertical Duct.

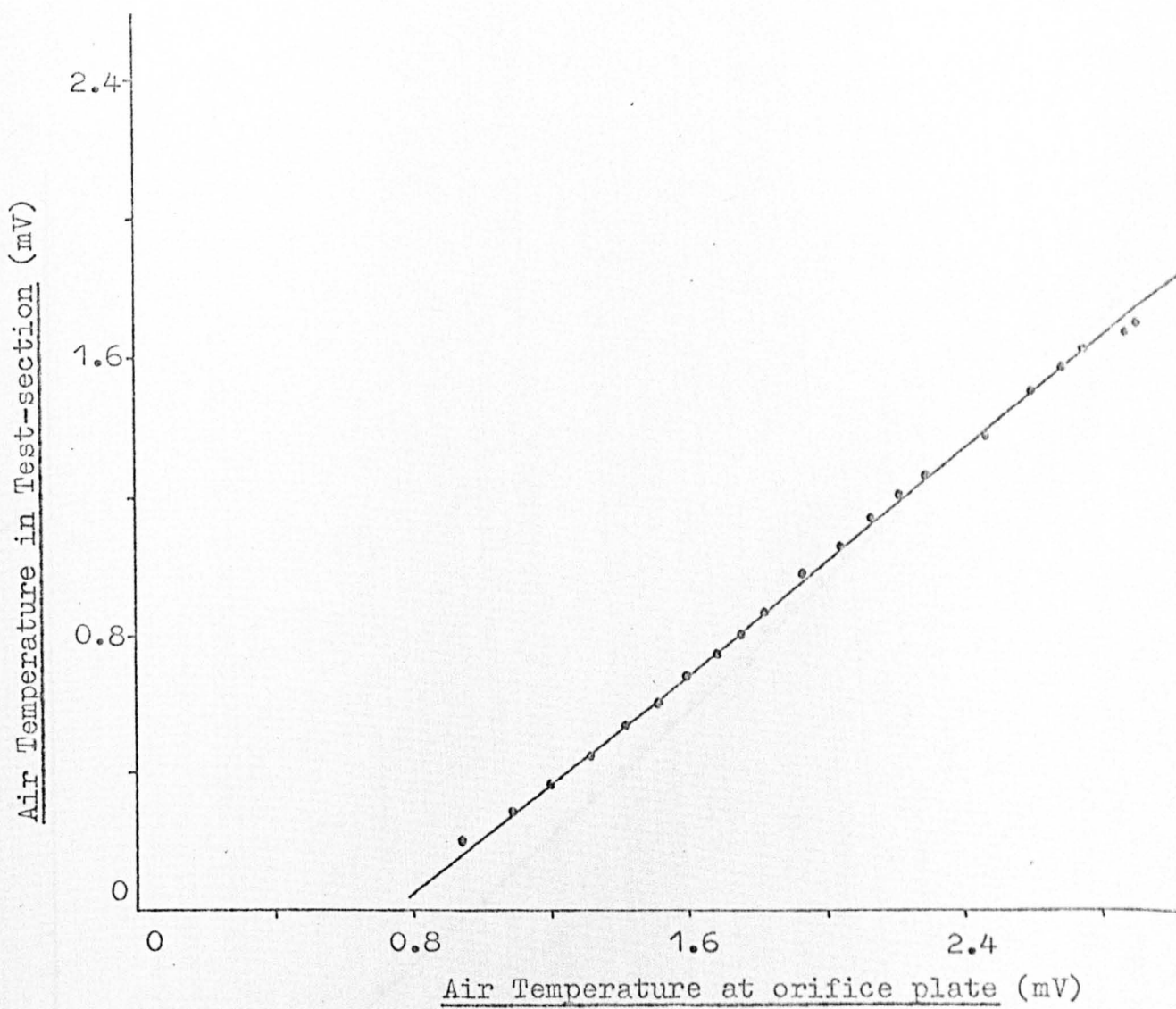


Fig. A.5.4. Temperature Calibration Curve for 2 inch Bend
having a Curvature Ratio of 12.

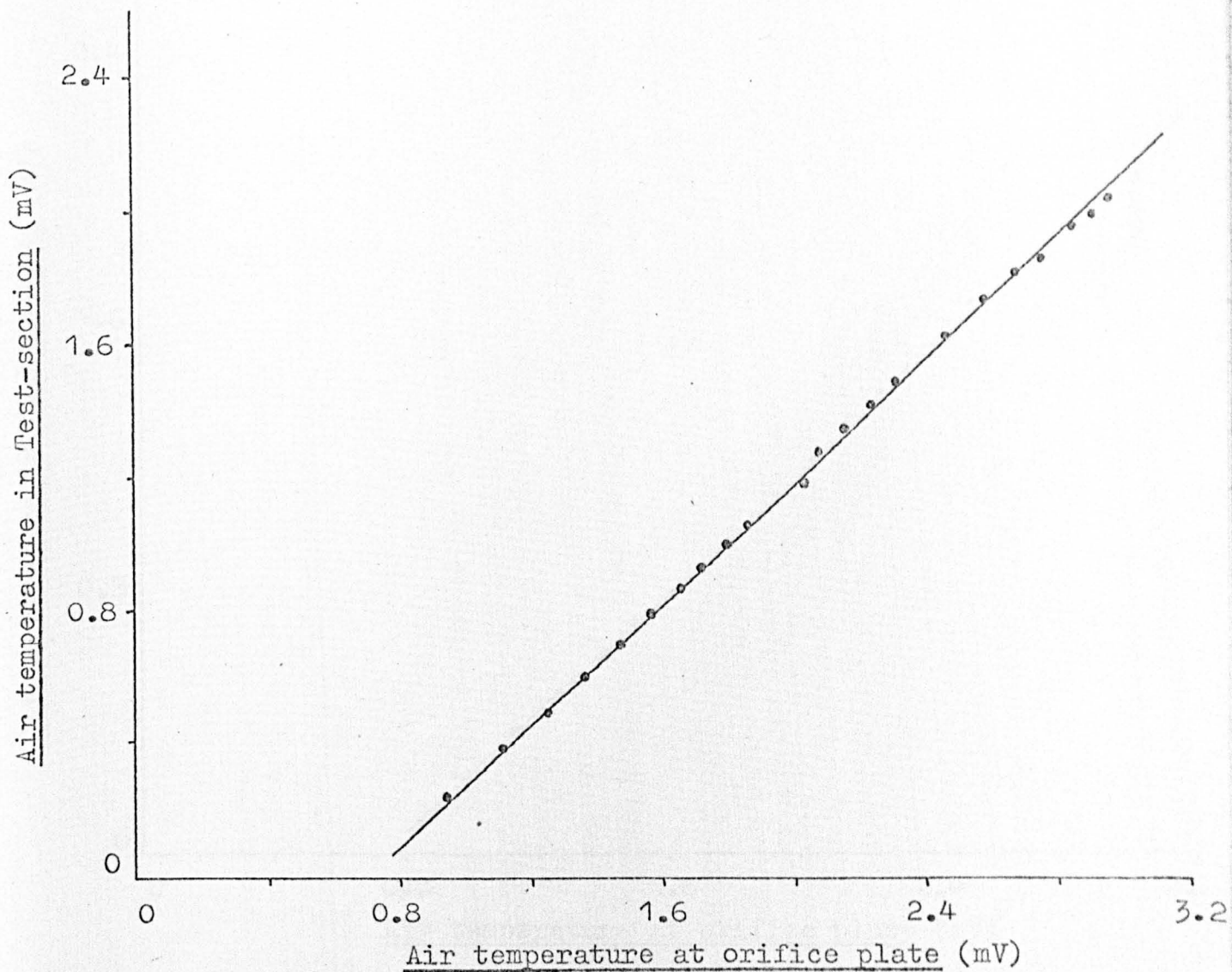


Fig. A.5.5. Temperature Calibration Curve for 2 inch Bend having a Curvature Ratio of 20.

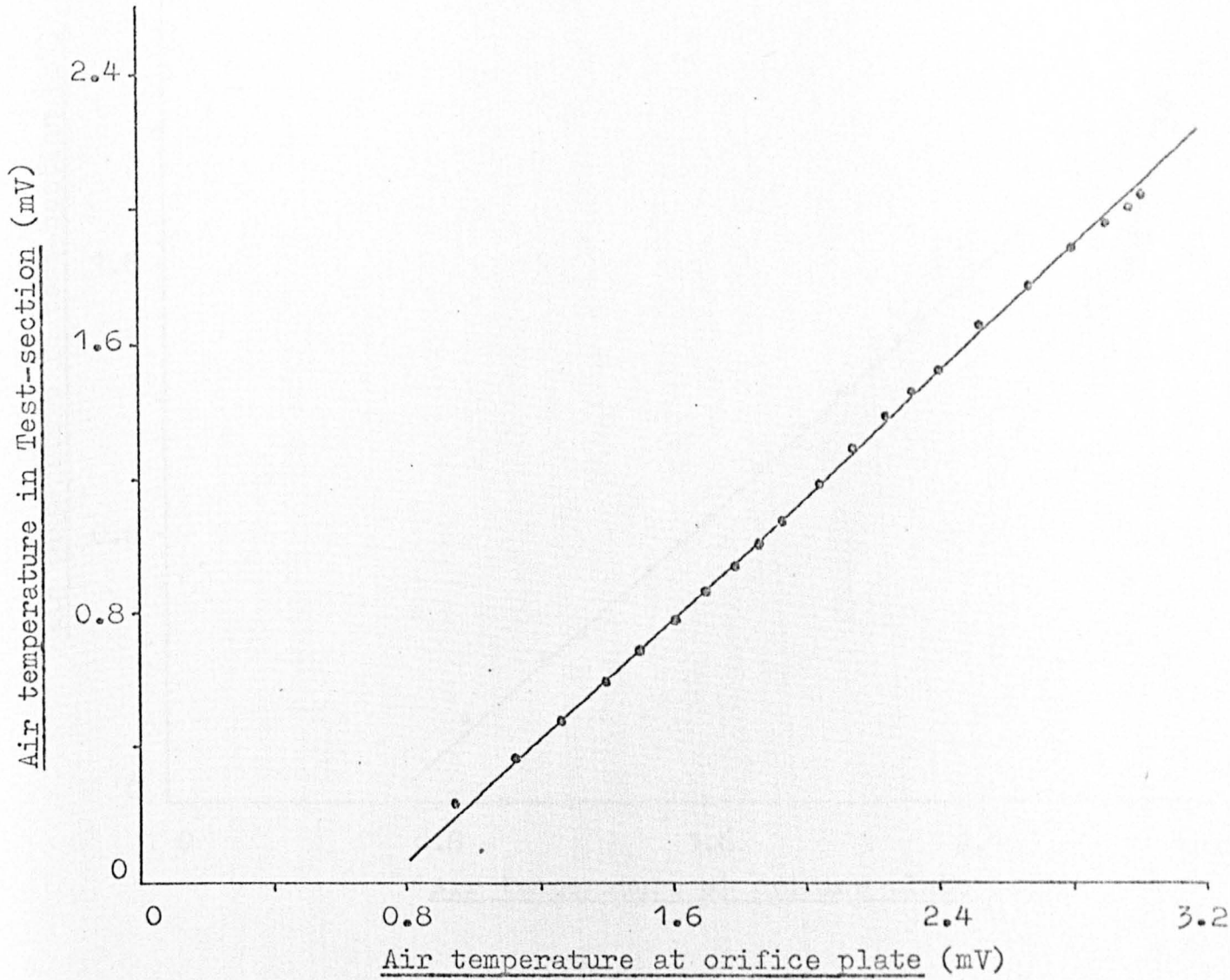


Fig. A.5.6. Temperature Calibration Curve for 3 inch Bend
having a Curvature Ratio of 13.3.

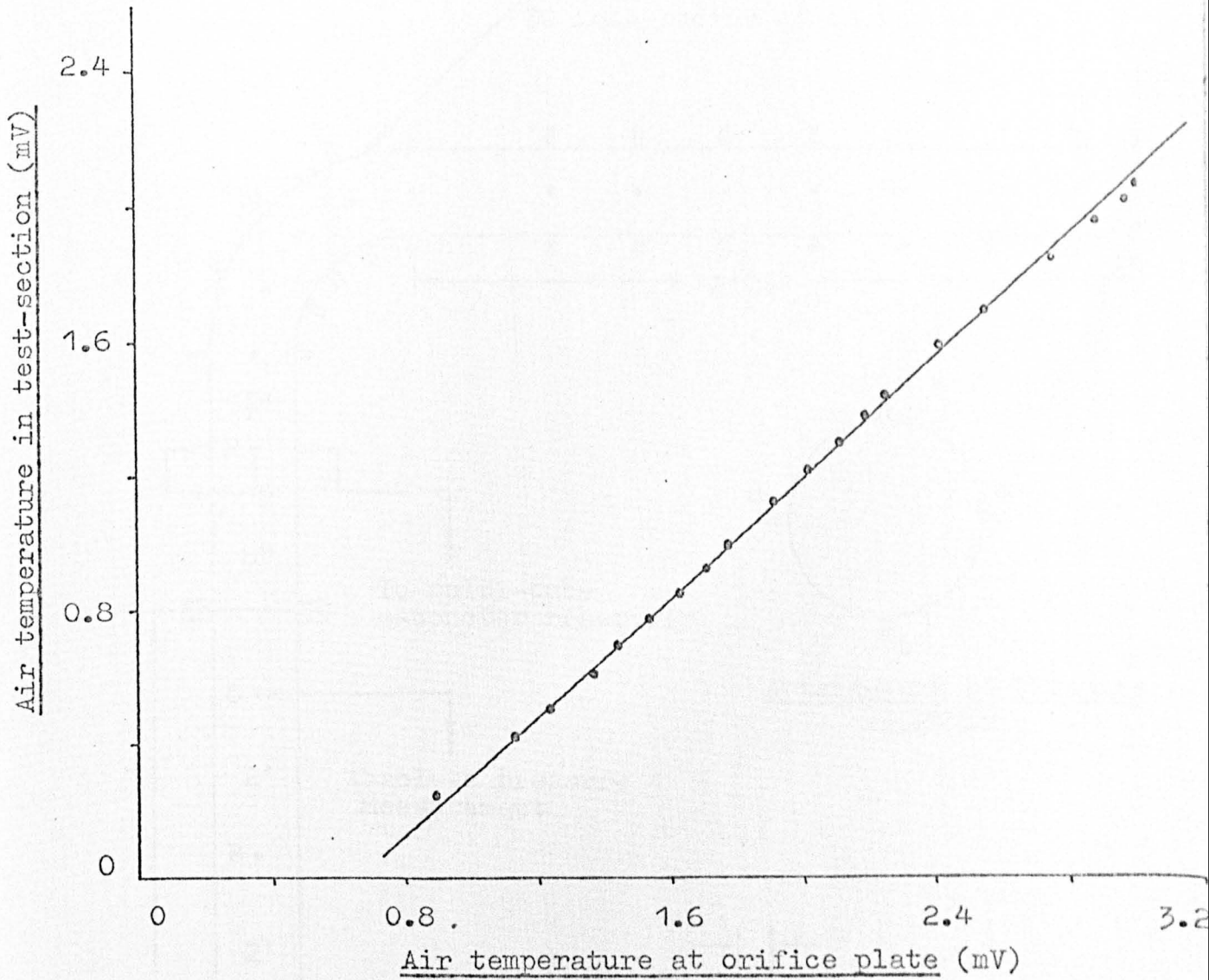


Fig. A.5.7. Temperature Calibration Curve for 3 inch Bend
having a Curvature Ratio of 20.

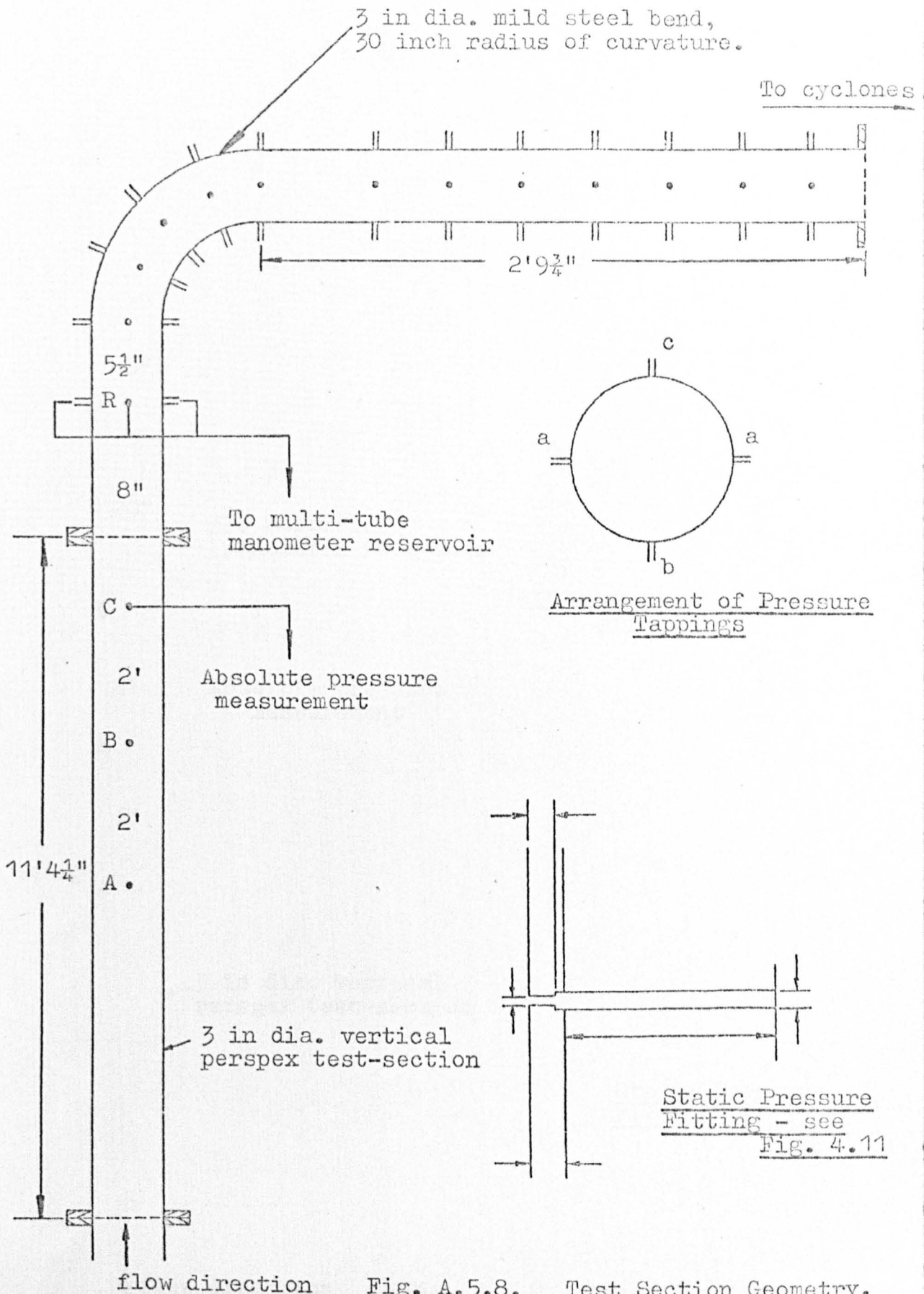


Fig. A.5.8. Test Section Geometry.

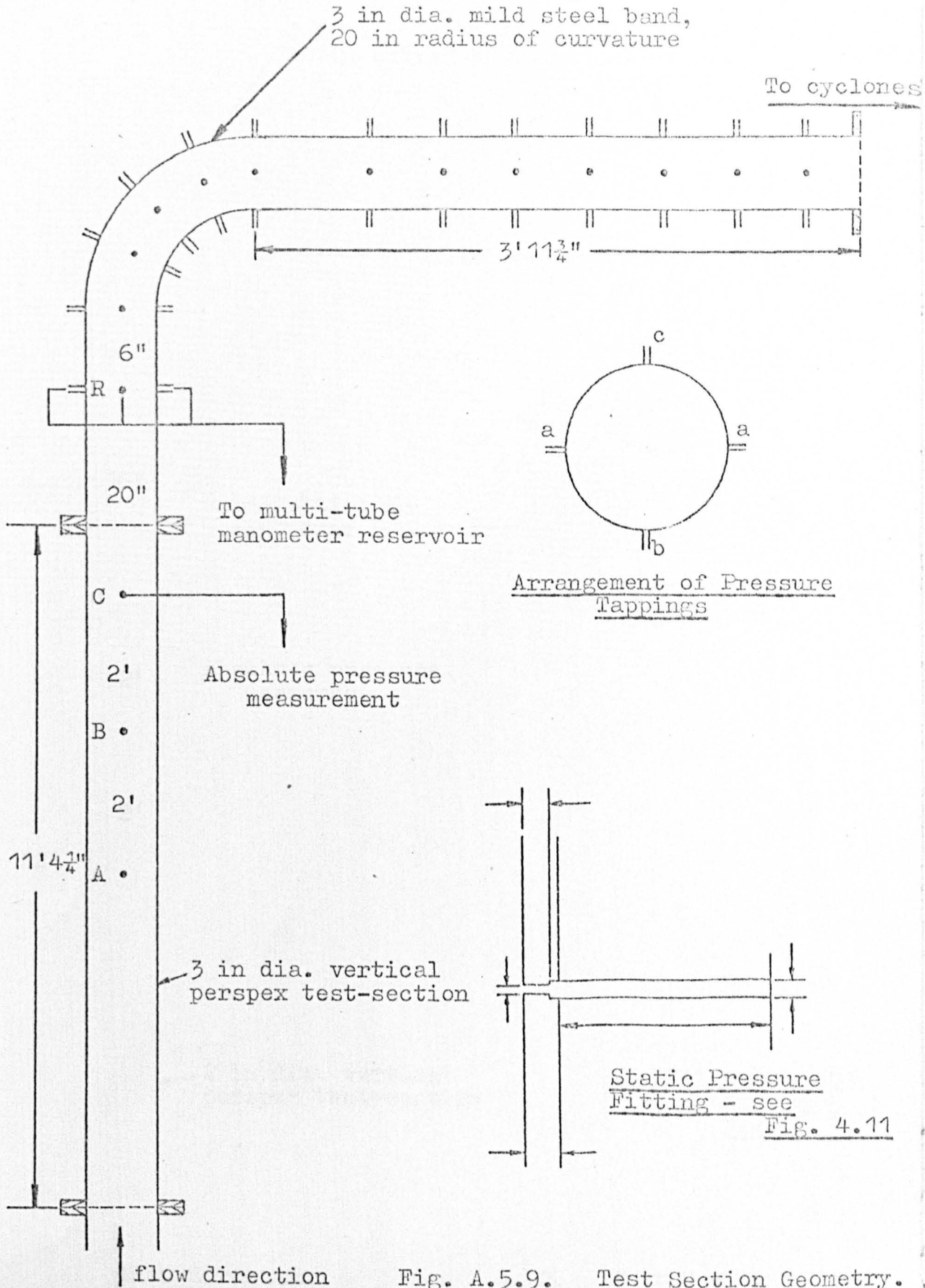


Fig. A.5.9. Test Section Geometry.

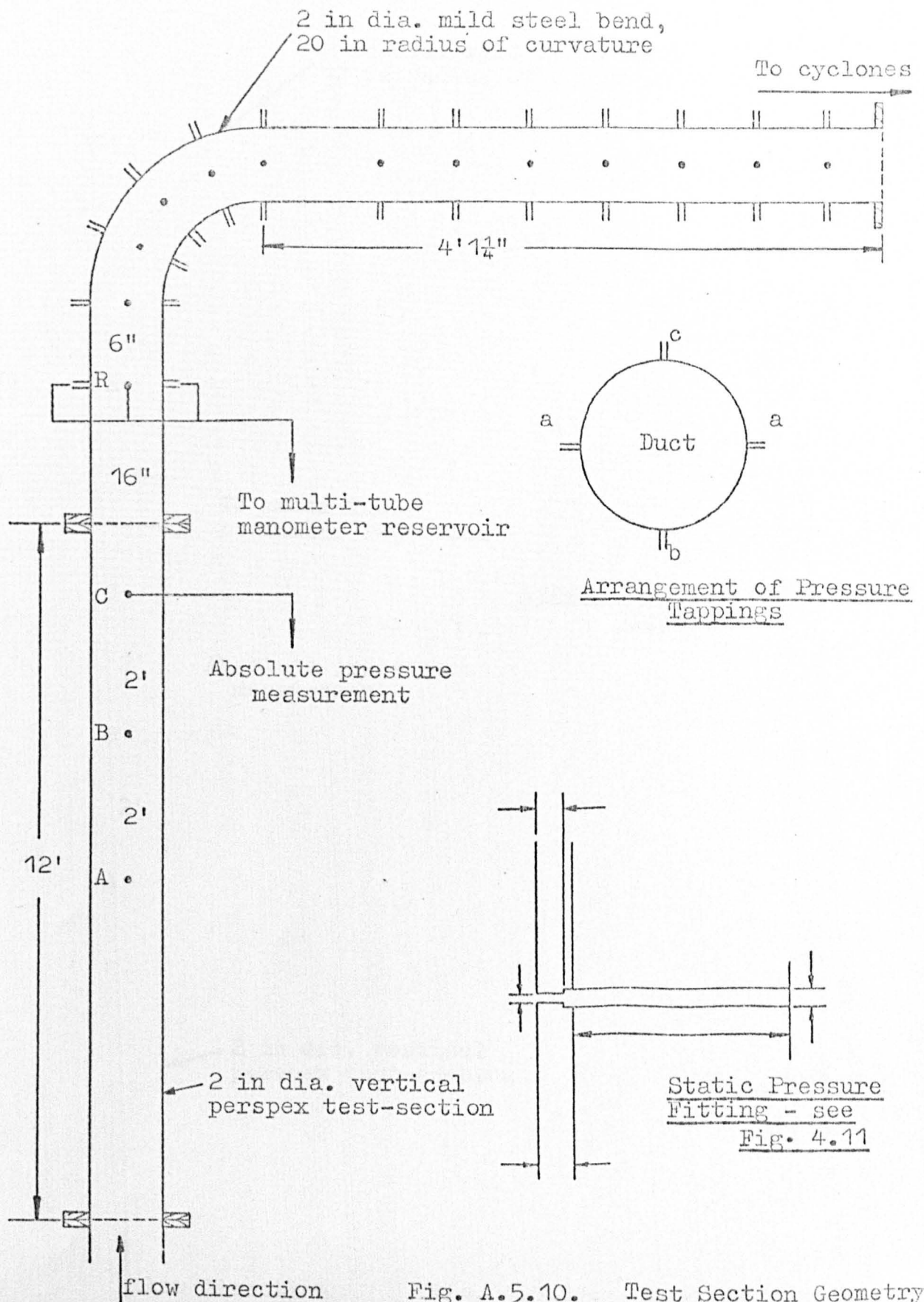


Fig. A.5.10. Test Section Geometry..

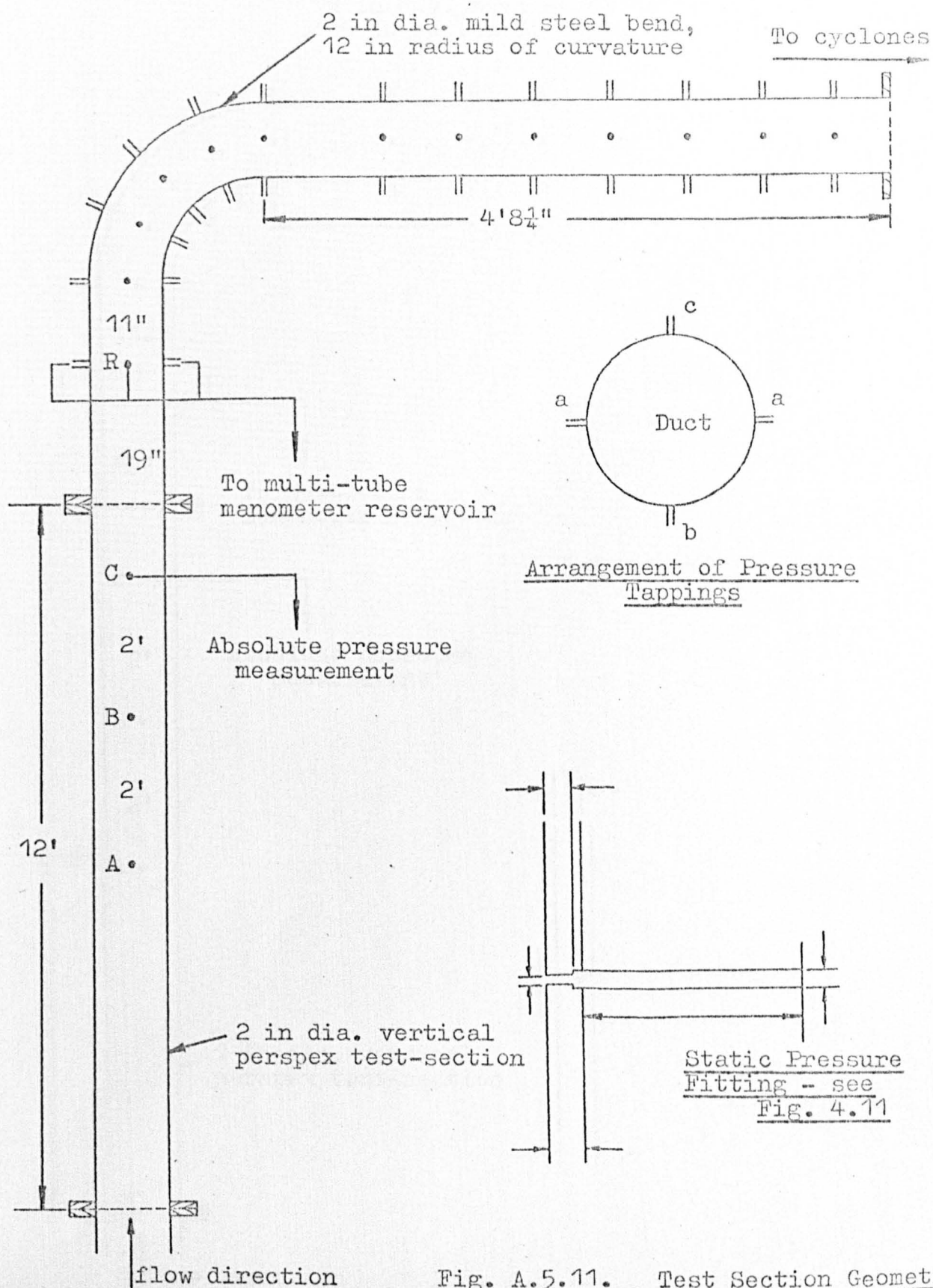


Fig. A.5.11. Test Section Geometry.

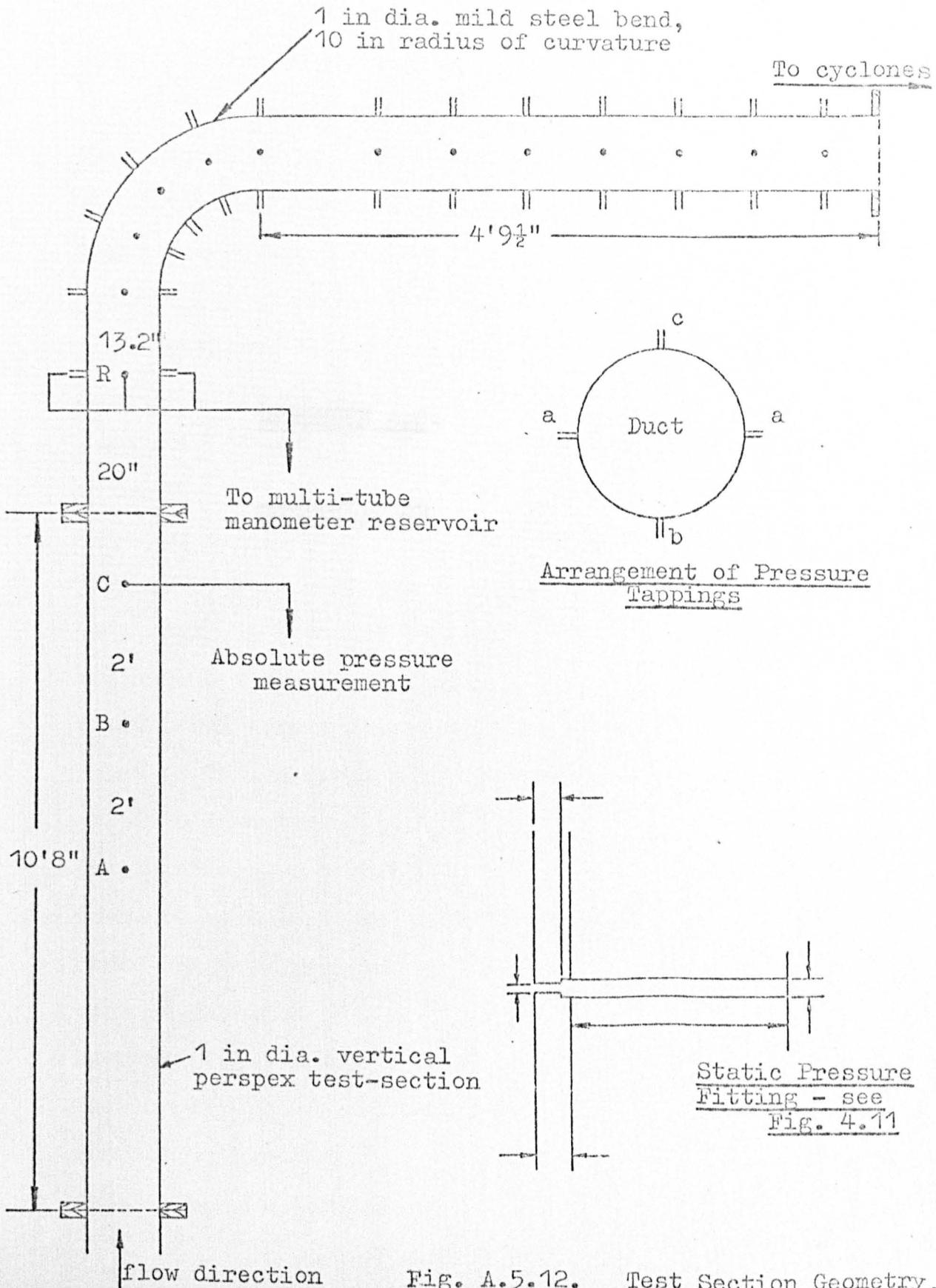


Fig. A.5.12. Test Section Geometry.

APPENDIX A.6.

NOMENCLATURE

Appendix A.6. Nomenclature

A	cross sectional area of pipe
D	duct diameter
D_c	bend curvature diameter
F_r	Froude number of the gas flow, \bar{u}_f^2/gD
L	length of test section
M	Mach number of the gas stream
P_A	absolute fluid pressure in test section
P_S	fluid stagnation pressure
R	perfect gas constant
R_e	duct Reynolds' number, $\rho_f \bar{u}_f D/\mu$
T	absolute temperature of fluid
T_f	absolute temperature of carrier fluid in test section
U	velocity
\bar{u}_f	mean gas velocity in duct
$(u_f)_r$	gas velocity at a radius r of the duct
\bar{u}_p	mean particle velocity in duct
\dot{V}_f	volumetric flowrate of fluid
W_f	fluid total mass flowrate in test section
W_p	solid particles total mass flowrate in test section
d_p	particle diameter
g	acceleration due to gravity
h_o	pressure head loss due to fluid friction
k	pipe surface roughness
m	mass of particle
q	electric charge on a particle
r	radial distance from pipe centre
t_a	ambient temperature
x	axial distance along duct

β	curvature ratio, D_c/D
γ	ratio of specific heats
λ_0	pipe friction factor for gas flowing alone
λ_p	solids friction factor
λ_s	gas-solid suspension friction factor
θ	bend angle
ϕ	"some function of"
μ	absolute fluid viscosity
ρ_f	fluid density
ρ_p	particle density
ρ_w	density of water
τ	wall shear stress in duct
ΔP_{af}	pressure differential due to acceleration of carrier fluid
ΔP_{ap}	pressure differential due to acceleration of solid particles
ΔP_{Ff}	pressure drop due to friction by gas in the gas-solid suspension
ΔP_{Fp}	pressure drop due to solids friction
ΔP_{Fs}	pressure drop due to friction by both solids and gas
ΔP_m	total measured pressure differential
ΔP_0	pressure drop due to air flowing alone
ΔP_T	total pressure drop
$\Delta P_{\rho f}$	hydrostatic pressure differential due to fluid phase
$\Delta P_{\rho p}$	hydrostatic pressure differential due to solids phase
ΔP_{Vb}	proportional pressure loss in vertical duct induced by downstream bend
ψ	coefficient of resistance
ψ_{hf}	coefficient of resistance for horizontal duct with fluid only flowing
ψ_{hp}	resistance number for horizontal duct and solid particles
ψ_{hs}	resistance number for horizontal duct and gas-solid suspension

ψ_{vf}	vertical pipe resistance number with fluid only
ψ_{vp}	vertical pipe resistance number with solids only
ψ_{vs}	vertical pipe resistance number for suspension
ψ_{bf}	bend resistance number with fluid only
ψ_{bp}	bend resistance number with solids only
ψ_{bs}	bend resistance number for suspension

Suffixes

a	ambient
ds	dispersed solids
f	carrier fluid or gas phase
F	friction
o	refers to flow of gas alone
p	refers to a particle or particles
s	refers to the gas-solid suspension
1	refers to inlet of test section where measurements taken
2	refers to outlet of test section where measurements

The above symbols have the same meaning throughout the entire text, with the exception of the previously published work in section 5.8 which contains its own nomenclature.

It has occasionally been found more convenient, in short single digressions, to define the symbols in the nearby text.

APPENDIX A.7.

REFERENCES

- 1 Boothroyd, R.G. "Pressure Drop in Duct Flow of Gaseous Suspensions of Fine Particles", Trans. Instn. Chem. Engrs., 44, T306, (1966).
- 2 Jones, J.H., Braun, W.G., Daubert, T.E., and Allendorf, H.D. "Estimation of Pressure Drop for Vertical Pneumatic Transport of Solids", A.I.Ch.E.Jl., 13, No. 3, p.608, (1967).
- 3 Mason, J.S. and Boothroyd, R.G. "Comparison of Friction Factors in Pneumatically-Conveyed Suspensions using Different-Sized Particles in Pipes of Varying Size", Pneumotransport 1, B.H.R.A. Conference, Cambridge, (Sept. 1971).
- 4 Mehta, N.C., Smith, J.M., and Comings, E.W. "Pressure Drop in Air-Solid Flow Systems", Ind. Eng. Chem., 49, No. 6, p.986, (June 1957).
- 5 Duckworth, R.A., and Kakka, R.S. "The Influence of Particle Size on the Frictional Pressure Drop caused by the Flow of a Solid-Gas Suspension in a Pipe", Pneumotransport 1, B.H.R.A. Conference, Cambridge, (Sept. 1971).
- 6 Gasterstadt, J. Zeitschrift des VDI, 68, No. 24, (June 1924).
- 7 Farbar, L. "Flow Characteristics of Solid-Gas Mixtures", Ind. Eng. Chem., 41, p.1148, (1949).
- 8 Vogt, E.G., and White, R.R. "Friction in the Flow of Suspensions", Ind. Eng. Chem., 49, p.1731, (1948).
- 9 Barth, W. "Strömungsvorgänge beim Transport von Festteilchen und Flüssigkeitsteilchen in Gasen", Chemie-Ing.-Techn., 30, No. 3, p.171, (1958).

- 10 Papai, L. "Examination of the Starting Section in Pneumatic Grain Conveying", Acta Technica, 14, p.95, (1955).
- 11 Hariu, O.H., and Molstad, M.C. "Pressure Drop in Vertical Tubes in Transport of Solids by Gases", Ind. Eng. Chem., 41, p.1148, (1949).
- 12 Segler, G. "Untersuchungen an Körnergebläsen und Grundlagen für ihre Berechnung", Mannheim 1934. Selbstverlag.
- 13 Doig, I.D., and Roper, G.H. "Air Velocity Profiles in the Presence of Cocurrently Transported Particles", I. and E.C. Fundamentals, 6, No.2, (May 1967).
- 14 Torobin, L.B., and Gauvin, W.H. "Fundamental Aspects of Solids-Gas Flow", Can.J. Chem. Eng., 37, p.129, (1959); 37, p.167, (1959); 37, p.224, (1959); 38, p.142, (1960); 38, p.182, (1960); 39, p.113, (1961).
- 15 Cramp, W.J. J. Roy. Soc. Arts, 69, p.283, (1920/21).
- 16 Cramp, W.J. Prac. Chem. Eng., 7, p.67, (1925).
- 17 Cramp, W.J., and Priestley, A. The Engineer, 137, p.34, 64, 89, (1924).
- 18 Belden, D.H., and Kassel, L.S. "Pressure Drop Encountered in Conveying Particles of Large Diameter in Vertical Transfer Lines", Ind. Eng. Chem., 41, p.1174, (1949).
- 19 Korn, A.H. "How Solids Flow in Pneumatic Handling Systems", Chem. Eng., 57, p.108, (March 1950).

- 20 Barth, W. "Physikalische und wirtschaftliche Probleme des Transportes von Festteilchen in Flüssigkeiten und Gasen", Chemie-Ing.-Techn., 32, No. 3, p.164, (1960).
- 21 Hitchcock, J.A., and Jones, C. "The Pneumatic Conveying of Spheres through Straight Pipes", Brit. J. Appl. Phys., 9, p.218, (1958).
- 22 Stemerding, S. "The Pneumatic Transport of Cracking Catalyst in Vertical Risers", J. Eng. Sc., 17, pp.599-608, (1962).
- 23 Hinkle, B.L., Ph.D. Thesis, Georgia Inst. Technol. (1953).
- 24 Bannister, H. "Theory and Design of Pneumatic Transport Systems", C.P.E., p.241, (July 1959).
- 25 Clark, R.H., Charles, D.E., Richardson, J.F., and Newitt, D.M. "Pneumatic Conveying, Part 1: The Pressure Drop during Horizontal Conveyance", Trans. Inst. Chem. Engrs., 30, (4), pp.209-222, (1952).
- 26 Coulson, J.M., Richardson, J.F. "Chemical Engineering", Vol. 2, pp.873-875, Pergamon Press, London (1955).
- 27 van der Lingen, T.W., and Koppe, R. "Moving Granular Materials by Air Line", Engineering, p.349, (Sept. 1963).
- 28 Uematsu, T., Morikawa, Y., Cho, K., Morikuni, I., Asada, Y., and Yamamoto, H. "Pneumatische Förderung in lotrechter Rohrleitung", Bulletin of JSME, 8, (31), pp.367-375, (1965).
- 29 Boothroyd, R.G. "Duct Flow of Gaseous Suspensions of Fine Particles", Ph.D. Thesis, Birmingham, (1967).

- 30 Boothroyd, R.G. "Similarity in Gas-Borne Flowing Particulate Suspensions", Paper presented at the Materials Handling Conference, Boston, Mass., A.S.M.E. Paper No. 68 - MH 11, (20th-23rd Oct. 1968).
- 31 Boothroyd, R.G. "Turbulence Characteristics of the Gaseous Phase in Duct Flow of a Suspension of Fine Particles", Trans. Instn. Chem. Engrs., 45, T297, (1967).
- 32 Boothroyd, R.G. "Flowing Gas-Solids Suspensions", Chapman and Hall, London, (1971).
- 33 McCarthy, H.E., and Olson, J.H. "Turbulent Flow of Gas-Solids Suspensions", Ind. Eng. Chem. Fundamentals, 7, (3), p.471, (Aug. 1968).
- 34 Duckworth, R.A., and Rose, H.E. "The Fluid Transport of Powdered Materials in Pipelines", Inst. Chem. Engrs., Symposium Series No. 27, pp.53-64, (1968).
- 35 Duckworth, R.A., and Rose, H.E. "Transport of Solid Particles in Liquids and Gases", The Engineer, 227, 5903, pp.392-396, (14 March, 1969). The Engineer, 227, 5904, pp.430-433, (21 March, 1969). The Engineer, 227, 5905, pp.478-483, (28 March, 1969).
- 36 Boyce, M.P., and Blick, E.F. "Fluid Flow Phenomena in Dusty Air", J. Basic Engr., A.S.M.E., Paper No. 69 - WA/FE - 24, p.2, (1969).
- 37 Chandok, S.S., and Pei, D.C.T. "Particle Dynamics in Solids-Gas Flow in a Vertical Pipe", Pneumotransport I, B.H.R.A. Conference, Cambridge, (Sept. 1971).

- 38 Zenz, F.A. "Two-Phase Fluid-Solid Flow", Ind. Eng. Chem., 41, p.2801, (1949).
- 39 Zenz, F.A. "Minimum Velocity for Catalyst Flow", Petroleum Refiner, 36, (6), p.13, (1957).
- 40 Zenz, F.A. "Nine Variables in Catalyst Flow", Petroleum Refiner, 36, (7), p.23, (1957).
- 41 Zenz, F.A. and Othmer, D.F. "Fluidisation and Fluid-Particle Systems", Reinhold Pub. Corp., N.Y., (1960).
- 42 Doig, I.D., and Roper, G.H. "The Minimum Gas Rate for Dilute Phase Solids Transportation in a Gas Stream", Aust. Chem. Engr., 4, (1), p.9, (1963).
- 43 Stannard, B. "A Theoretical Analysis of Pneumatic Conveying", Trans. Instn. Chem. Engrs., 39, p.21, (1961).
- 44 Kovacs, L. "Some Similarity Criteria of Pneumatic Conveying", Pneumotransport I, B.H.R.A. Conference, Cambridge, (Sept. 1971).
- 45 Chand, P. "Response of Particles under Pneumatic Conveyance", Pneumotransport I, B.H.R.A. Conference, Cambridge, (Sept. 1971).
- 46 Hinze, J.O. "Momentum and Mechanical-Energy Balance Equations for a Flowing Homogeneous Suspension with Slip between the Phases", Appl. Sci. Res., Sect. A, 11, pp.33-46, (1962).
- 47 Leung, L.S., Wiles, R.J., and Nicklin, D.J. "On the Design of Vertical Pneumatic Conveying Systems", Pneumotransport I, B.H.R.A., Cambridge, (1971).

- 48 Schuchart, P. "Resistance Laws for the Hydraulic and Pneumatic Transport of Solid Materials in Horizontal Straight Pipes", Chemie-Ing.-Tech., 23, pp.1251-1259, (1969). (In German).
- 49 Schuchart, P. "Resistance Laws in Pneumatic Transport in Pipe Bends", Chemie-Ing.-Tech., 21/22, pp.1060-1067, (1968). (In German).
- 50 Goto, K., and Iinoya, K. "Pressure Drops of a Steady Solids-Gas Two-Phase Flow", Kagaku Kogaku, 27, pp.12-17, (1963).
- 51 Welschhof, G. "Pneumatic Conveying at High Particle Concentrations", V.D.I.-Forschungsheft, 492, (1962).
- 52 Rausch, W. "Investigation of the Pneumatic Transport of Solid Flows", Fordern u. Heben, 12, pp.968-976, (1966). (In German).
- 53 Pinkus, O. "Pressure Drops in the Pneumatic Conveyance of Solids", J. Appl. Mech., 19, (4), pp.425-431, (Dec. 1952).
- 54 Depew, C.A. "Heat Transfer to Flowing Gas-Solids Mixtures in a Vertical Duct", Ph.D. Thesis, (Rept. No. U.C.R.L.-9280), Univ. of California, Berkeley, (1957).
- 55 Soo, S.L., and Trezek, G.J. "Turbulent Pipe Flow of Magnesia Particles in Air", Ind. Eng. Chem. Fundl., 5, (3), pp.388-392, (August 1966).
- 56 Boothroyd, R.G. and Walton, P.J. "Fully Developed Turbulent Boundary Layer Flow of a Fine Solid-Particle Gaseous Suspension", Nature (Physical Science), (1971).

- 57 Pietsch, W.B. "Adhesion and Agglomeration of Solids during Storage, Flow and Handling - a survey", Trans. A.S.M.E. Paper No. 68 MH-21.
- 58 Kada, H., and Hanratty, T.J. "Effect of Solids on Turbulence in a Fluid", A.I.Ch.E.Jl., 6, p.624, (1960).
- 59 Dallavalle, J.M., Orr, C., and Hinkle, B.L. "The Aggregation of Aerosols", Brit. J. Appl. Phys., 5, (3), S.198, (1954).
- 60 Marble, F.E. "Mechanism of Particle Collision in the One-Dimensional Dynamics of Gas-Particle Mixtures", Phys. of Fluids, 7, (8), p.1270, (1964).
- 61 Richardson, J.F., and McLeman, M. "Pneumatic Conveying - part II", Trans. Instn. Chem. Engrs., 38, p.257, (1960).
- 62 Soo, S.L., Trezek, G.J., Dimick, R.C., and Hohnstreiter, G.F. "Concentration and Mass Flow Distribution in Gas-Solid Suspensions", Ind. Eng. Chem. Fund., 3, (2), p.98, (1964).
- 63 Soo, S.L. "Effect of Electrification on the Dynamics of a Particulate System", Ind. Eng. Chem. Fund., 3, (1), p.75, (1964).
- 64 Montgomery, D.J. "Static Electrification of Solids", Solid State Phys., 9, p.139, (1959).
- 65 Shaw, P.E. Nature, 118, p.659, (1926).
- Shaw, P.E., and Jex, C.S. Proc. Phys. Soc., 39, p.449, (1927). Proc. Roy. Soc., 111A, p.339, (1926). Proc. Roy. Soc., 118A, p.97, (1928). Proc. Roy. Soc., 118A, p.108, (1928).
- Shaw, P.E. Proc. Roy. Soc. 122A, p.49, (1929).

- 66 Townsend, A.A. "The Structure of Turbulent Shear Flow", C.U.P., (1956).
- 67 Bakhmeteff, B.A. "Mechanics of Turbulent Flow", Princeton, N.J., (1936).
- 68 Pai, S.I. "On Turbulent Flow in a Circular Pipe", J. Franklin Inst., 256, p.337, (1953).
- 69 Sabersky, R.H., and Acosta, A.J. "Fluid Flow", Macmillan, N.Y., (1964).
- 70 Schlichting, H. "Boundary Layer Theory", 4th Edition, McGraw-Hill, New York, (1960).
- 71 Laufer, J. "The Structure of Turbulence in Fully Developed Pipe Flow", N.A.C.A., Report 1174, (1954).
- 72 Baw, P.S., and Peskin, R.L. "Density Profiles in Gas-Solid Suspension Flow", A.I.A.A.Jl., 5, p.815, (1967).
- 73 Goldberg, A.S., and Boothroyd, R.G. "Measurements in Flowing Gas-Solids Suspensions Part I", Brit. Chem. Eng., 14, (12), p.1705, (Dec. 1969).
- 74 Boothroyd, R.G. and Goldberg, A.S. "Measurements in Flowing Gas-Solids Suspensions Part II", Brit. Chem. Eng., 15, (3), p.357, (March 1970).
- 75 Arundel, P.A. "Instrumentation for Measurements in Dense Vertically Flowing Suspensions of Fine Zinc Particles", Ph.D. Thesis, Birmingham, (1971).
- 76 Peskin, R.L., and Briller, R. Tech. Rpt. No. 109-ME-F NYO 2930-7, Rutgers Univ., New Brunswick, N.J.
- 77 Dean, R.C. (Ed.) "Aerodynamic Measurements", Gas Turbine Laboratory, M.I.T., (1963).

- 78 Schlichting, H. "Boundary Layer Theory", 4th Edition, McGraw-Hill, New York, p.562, (1960).
- 79 Fischer, J. Chem. Eng., 65, p.114, (1958).
- 80 Richards, J.C. (Ed.) "The Storage and Recovery of Particulate Solids", I. Chem. E., London, (1966).
- 81 Finnie, I. "Erosion of Surfaces by Solid Particles", Wear, 3, 87, (1960).
- 82 Finnie, I. "Erosion by Solid Particles in a Fluid Stream", Symposium on Erosion and Cavitation, A.S.T.M.S.T.P., 307, 70, (1962).
- 83 Finnie, I., Wolak, J. and Kabil, Y. "Erosion of Metals by Solid Particles", J. Materials, 2, 682, (1967).
- 84 Tilly, G.P. "Erosion caused by Airborne Particles", Wear, 14, 63, (1969).
- 85 Bitter, J.G.A. "A Study of Erosion Phenomena Part 1", Wear, 6, 5, (1963).
- 86 Bitter, J.G.A. "A Study of Erosion Phenomena Part 2", Wear, 6, 169, (1963).
- 87 Neilson, J.H., and Gilchrist, A. "Erosion by a Stream of Solid Particles", Wear, 11, 111 (1968).
- 88 Boothroyd, R.G. "Erosion Problems in Industrial Plant", Short Course on Industrial Powder Handling Technology, University of Birmingham, (1971).
- 89 Wen, C.Y., and Simons, H.P. "Flow Characteristics in Horizontal Fluidised Solids Transport", A.I. Ch.E.Jl., 5, No. 2, p.263, (1958).

- 90 Mehring, R.F. "Pneumatic Conveying Hazards", Powder Handling and Storage Symposium, Powder Advisory Centre, (1971).
- 91 Doran, T.E. "Personal communication", Pilkington Brothers Research and Development Laboratories, Lathom, (1971).
- 92 Patterson, R.C. "Pulverized-Coal Transport through Pipes", Trans. A.S.M.E., Jl. Engr. Power, Paper No. 58-SA-24, p.43, (1958).
- 93 Uematu, V.T., and Morikawa, Y. "Die experimentelle Untersuchung über die Teilchenbewegung und über die Geschwindigkeitsverteilung der Förderluft in einer pneumatischen Förderleitung", Bull. J.S.M.E., 4, No.15, p.525, (1961).
- 94 Zenz, F.A. "Conveyability of Materials of Mixed Particle Size", Ind.Eng. Chem. Fundls., 3, No.1, p.65, (1964).
- 95 Bagnold, R.A. "The Physics of Blown Sand and Desert Dunes", Methuen, London, (1941).
- 96 Hjulstrom, F. Bull. Geol, Inst., Upsala, 25, (1936).
- 97 Jordan, D.W. Brit. J. Appl. Phys., 5, Suppl 3, S.194-8, (1954).
- 98 Trezek, G.J., and France, D.M. "Axial Pressure Correlation for Accelerating Particulate Pipe Flow", Ind.Eng. Chem. Fundls., 7, p.247, (May 1968).
- 99 Doig, I.D., and Roper, G.H. "Energy Requirements in Pneumatic Conveying, Aust. Chem. Engr., pp.9-23, (Feb. 1963).

- 100 Jotaki, T., and Tomita, Y. "Solids Velocities and Pressure Drops in a Horizontal Pneumatic Conveying System", Pneumotransport 1, B.H.R.A. Conference, Cambridge, (Sept. 1971).
- 101 Ikemori, K., and Munakata, H. "On the Velocity of Solids and the Pressure Losses in the Pneumatic Transport of Grains by Pipelines", Pneumotransport 1, B.H.R.A. Conference, Cambridge, (Sept. 1971).
- 102 Ito, H. "Pressure Losses in Smooth Pipe Bends", Trans. A.S.M.E., Jl. Bas. Engr., Paper No. 59-Hyd-4, pp.1-10, (1959).
- 103 Schuchart, P. "Pneumatic Conveying", C.P.E., pp.76-80, (May 1970).
- 104 Young, H.T. "Design and Application of Closed Loop Pneumatic Conveyor Systems", A.S.M.E., Paper No.61-BSH-6.
- 105 Fischer, J. "Practical Pneumatic Conveyor Design", Chem. Eng., 65, No. 11, p.114, (1958).
- 106 Fischer, J. "Pneumatic Transport in the Integration of Processing Systems", Chem. Eng. Progress, 59, No. 5, pp.64-68, (May, 1963).
- 107 Michell, S.J. "Designing a Pneumatic Conveyor", Brit. Chem. Eng., pp.356-358, (July, 1957).
- 108 Westervelt, R.P. "Planning and Maintaining Pneumatic Conveyor Systems", Plant Engr., (Nov. 1966).
- 109 Gluck, S.E. "Design Tips for Pneumatic Conveyers", Hydrocarbon Processing, 47, No. 10, pp.88-95, (Oct. 1968).

- 110 "Pneumatic Handling of Powdered Materials", E.E.U.A. Handbook No. 15, Constable and Co., (1963).
- 111 Tills, J.W. "An Introduction to Pneumatic Conveying with Particular Reference to Granular Sugar", Pneumotransport 1, B.H.R.A. Conference, Cambridge, (Sept. 1971).
- 112 Jepson, G., Poll, A., and Smith, W. "Heat Transfer in a Gas-Solid Line", Trans. Instn. Chem. Eng., 41, p.207, (1963).
- 113 Schluderberg, D.C., Whitelaw, R.L., and Carlson, R.W. "Gaseous Suspensions - A New Reactor Coolant", Nucleonics, pp.67-76, (Aug. 1961).
- 114 Cooper, W.F. "The Practical Estimation of Electrostatic Hazards", Brit. J. Appl. Phys., 4, Suppl. 2, S71, (1953).
- 115 Rose, H.E. "Dust Explosion Hazards", Brit. Chem. Eng., 15, No. 3, p.371, (1970).
- 116 Henry, P.S.H. "Survey of Generation and Dissipation of Static Electricity", Brit. J. Appl. Phys., 4, Suppl. 2, S.6, (1953).
- 117 Mühle, J. Unpublished research. The Chair for Thermodynamik und Verfahrenstechnik der TU Berlin.
- 118 White, C.M. "Streamline Flow through Curved Pipes", Proc. Roy. Soc. A.123, pp.645-663, (1929).
- 119 Hawthorne, W.R. "Secondary Circulation in Fluid Flow", Proc. Roy. Soc., A 206, pp. 374-387, (1951).
- 120 Martin, M.E., and Deverson, E.C. "The Effect of Bend Outlet Conditions on the Pressure Losses in Bent Circular Pipes", A.R.C. Technical Report C.P. No. 505, (1960).

- 121 Horlock, J.H. "Some Experiments on the Secondary Flow in Pipe Bends", Pro. Roy. Soc. A 234, p.335, (1955).
- 122 McConalogue, D.J., and Srivastava, R.S. "Motion of a Fluid in a Curved Tube", Pro. Roy. Soc. A 307, pp.37-53, (1968).
- 123 Ito, H. "Friction Factors for Turbulent Flow in Curved Pipes", Trans. A.S.M.E., Jl. Bas. Engr., pp.123-132, (June 1959).
- 124 Weidner, G. Forsch. Ing.-Wes., 21, No. 5, p.145, (1955).
- 125 Uematu, T., and Morikawa, Y. "Pressure Losses in the Bend of a Horizontal Conveyor for Granular Materials", Bull. J.S.M.E., 4, No. 15, pp.531-538, (1961).
- 126 Haag, A. "Velocity Losses in Pneumatic Conveyor Pipe Bends", Brit. Chem. Eng., 12, No. 1, (Jan. 1967).
- 127 Morikawa, Y. "Pressure Drop and Particle Movement in Bends of Pneumatic Transport Lines at Low Material Loads", Grndl. Landtechn., 16, No. 2, pp. 65-69, (1966).
- 128 Jung, R. "Die Strömungsverluste in 90°-Umlenkungen beim Pneumatischen Staubtransport", Brennst.-Wärme-Kraft, 19, No. 9, pp.430-435, (1967).
- 129 Kriegel, E. "Pressure Loss and Wear in Pipe Bends during Pneumatic Conveying", Verfahrens Technik, 4, No. 8, pp.333-339, (Aug. 1970).

"Calculation of Pressure-Drop in Horizontal and Vertical Bends Inserted in Pneumatic Conveying Pipes", Pneumotransport 1, B.H.R.A. Conference, Cambridge, (Sept. 1971).

APPENDIX A.8.

PLATE CAPTIONS AND KEYS

Appendix A.8. Plate Captions and Keys

Plates 1 and 2 : General views of the gas-solids flow ring.

Key to plates 1 and 2, and Figs. 3.2 and 3.3:-

- A Compressor air inlet
- B Sliding vane compressor
- C Relief valve
- D Saunder's 3 inch air-operated diaphragm valve
- E Orifice plate
- F Saunder's 3 inch manually operated valve
- G Reducing section
- H Air-solids mixing unit
- J 1 inch diameter air bleed-off line
- K 3, 1 inch air-operated Saunder's diaphragm valves
- L 2 inch diameter mild steel ducting from mixing unit to test section
- M Perspex duct approach section to test section
- N Mild steel return duct to air filtering plant
- P Primary cyclone
- Q Secondary cyclone
- R Main hopper in mild steel
- S Pressure hopper in mild steel
- T Solids supply bunker in mild steel
- U Screw-feeder
- V Bearing and seal assembly
- W Variable speed drive, 0 - 180 rev/min
- X Fabric filter bags
- Y Dusty air, 3 inch plastic pipe

- Plates 3 and 4 : Other features of equipment obscured in plates 1 and 2.
- Plate 5 : High pressure nitrogen purging system for cleaning manometer lines.
- Plate 6 : Typical set of multi-tube manometer readings photographed during a test run.
- Plate 7 : Initial arrangement of rig with perspex hoppers.
- Plate 8 : 2 inch square-section bend prior to wear tests.
- Plate 9 : Progressing wear pattern of 2 inch diameter, 9 inch radius, standard mild steel bend.
- Plate 10 : The standard bend worn through and also typical "pocketing" of a similar bend previously reinforced.
- Plate 11 : Particle shape for 240 mesh alumina powder when new and after erosion tests on bend 1.
- Plate 12 : Particle shape for 240 mesh alumina powder after erosion tests on bend 3 and after tests on bend 4.
- Plate 13 : Final erosion pattern of bend 2.

- Plate 14 : Final erosion pattern of bend 3.
- Plate 15 : Erosion of bend 4.
- Plate 16 : Radiograph of 4 inch bore pipe fitted with a channel wear-back filled with concrete.
- Plate 17 : Perspex bend installed in test rig.

APPENDIX A.9.

SUPPLEMENTARY LIST OF FIGURE CAPTIONS

Some figures have insufficiently detailed captions and a more complete description is provided here.

Figs. 3.2 and 3.3 See Plate Captions (Appendix A.8.) for key to plates 1 and 2.

Fig. 4.9 • refers to pitot traverse from pipe centre to wall.
 ◦ refers to pitot traverse from wall to pipe centre.

Fig. 4.10 ◦ refers to pitot-tube derived results as on pre-data tape.
 • refers to Fanning friction factor calculation assuming constant fluid density and viscosity.
 Δ refers to actual results from test C3, using pressure drop calculation.

Figs. 4.13 and 4.14 ◦ experimental results.
 • theoretical values.

Fig. 4.15 • calibration before test 1.
 ◦ calibration after test 230.
 240 mesh, medium screwflight.

Fig. 4.16

- test 16 calibration.
- test 264 calibration.
320 mesh, medium screwflight.

Fig. 4.17

- test 16 calibration.
- test 88 calibration.
500 mesh, medium screwflight.

Fig. 4.18

- test 1 calibration, 240 mesh.
- test 16 calibration, 320 mesh.
- test 88 calibration, 500 mesh.
Medium screwflight.

Fig. 4.19

- test 6 calibration.
- test 183 calibration.
240 mesh, large screwflight.

Fig. 4.20

- test 9 calibration.
- test 46 calibration
- test 173 calibration.
320 mesh, large screwflight.

Fig. 4.21

- test 163 calibration.
- test 206 calibration.
500 mesh, large screwflight.

Fig. 4.22

- test 183 calibration, 240 mesh.
- test 173 calibration, 320 mesh.
- test 163 calibration, 500 mesh.

Fig. 4.24

- new 240 mesh powder.
- △ after test 1.
- test 79.
- ▣ test 128.

Fig. 4.25

- new 320 mesh powder.
- △ test 16.
- ▣ test 46.

Fig. 4.26

- new 500 mesh powder.
- △ test 17.
- test 34.
- ▣ test 110.

Fig. 5.1

- $W_p/W_f = 0.2$ to 0.5 , 240 mesh.
- $W_p/W_f = 0.5$ to 0.8 , 240 mesh.
- ▣ $W_p/W_f = 0.8$ to 1.4 , 240 mesh.
- × $W_p/W_f = 1.4$ to 2.0 , 240 mesh.
- ▽ $W_p/W_f = 2.0$ to 3.0 , 240 mesh.
- + $W_p/W_f = 3.0$ to 4.0 , 240 mesh.
- $W_p/W_f = 4.0$ to 5.0 , 240 mesh.
- ✎ $W_p/W_f = 0.2$ to 0.5 , 500 mesh.
- ✎ $W_p/W_f = 0.5$ to 0.8 , 500 mesh.
- ✎ $W_p/W_f = 0.8$ to 1.4 , 500 mesh.
- ✎ $W_p/W_f = 1.4$ to 2.0 , 500 mesh.
- ✎ $W_p/W_f = 2.0$ to 3.0 , 500 mesh.
- ▲ Air only.

Fig. 5.2

- x Air only.
- $W_p/W_f = 0.2$ to 0.5 , 500 mesh.
- $W_p/W_f = 0.2$ to 0.5 , 240 mesh.
- ♠ $W_p/W_f = 0.5$ to 0.8 , 500 mesh.
- ♠ $W_p/W_f = 0.5$ to 0.8 , 240 mesh.
- ▼ $W_p/W_f = 1.1$ to 1.5 , 500 mesh.
- ▼ $W_p/W_f = 1.1$ to 1.5 , 240 mesh.
- ⋈ $W_p/W_f = 2.0$ to 3.0 , 500 mesh.
- ⋈ $W_p/W_f = 2.0$ to 3.0 , 240 mesh.

Fig. 5.3

- x Air only.
- $W_p/W_f = 0.2$ to 0.5 , 500 mesh.
- $W_p/W_f = 0.2$ to 0.5 , 240 mesh.
- ◻ $W_p/W_f = 0.9$ to 1.1 , 500 mesh.
- ◻ $W_p/W_f = 0.9$ to 1.1 , 240 mesh.
- ▼ $W_p/W_f = 2.5$ to 3.0 , 240 mesh.
- ⋈ $W_p/W_f = 4.0$ to 5.0 , 500 mesh.
- ⋈ $W_p/W_f = 4.0$ to 5.0 , 240 mesh.

Fig. 5.4

- $W_f = 7.0$ lb/min.
 - ♠ $W_f = 7.8$ lb/min.
 - ▼ $W_f = 8.04$ lb/min.
 - ▼ $W_f = 8.4$ lb/min.
 - + $W_f = 8.7$ lb/min.
- All 240 mesh.

Fig. 5.5

- $W_f = 6.5$ lb/min.
 - ✎ $W_f = 6.8$ lb/min.
 - ✎ $W_f = 7.4$ lb/min.
 - △ $W_f = 7.7$ lb/min.
 - x $W_f = 9.2$ lb/min.
- All 500 mesh.

Fig. 5.6

- △ $W_f = 6$ to 8 lb/min.
 - $W_f = 8$ to 10 lb/min.
 - $W_f = 10$ to 12 lb/min.
- All 240 mesh.

Fig. 5.7

- △ $W_f = 6$ to 8 lb/min.
 - $W_f = 8$ to 10 lb/min.
 - $W_f = 10$ to 12 lb/min.
- All 320 mesh.

Fig. 5.8

- △ $W_f = 5$ to 7 lb/min.
 - x $W_f = 7$ to 8 lb/min.
 - $W_f = 8$ to 9 lb/min.
 - $W_f = 9$ to 10 lb/min.
 - $W_f = 10$ to 12 lb/min.
- All 500 mesh.

Fig. 5.9

- 240 mesh.
 - ✎ 320 mesh.
 - 500 mesh.
- All with $W_f = 7.0$ to 9.5 lb/min.

Fig. 5.10

- $W_p/W_f = 0.5$ to 1.5 , 500 mesh.
- $W_p/W_f = 0.5$ to 1.5 , 240 mesh.
- ✱ $W_p/W_f = 2.0$ to 6.0 , 500 mesh.
- ✱ $W_p/W_f = 2.0$ to 6.0 , 240 mesh.

Fig. 5.11

- x Air only.
- ▲ $W_p/W_f = 0.7$ to 1.0 , 500 mesh.
- △ $W_p/W_f = 0.7$ to 1.0 , 240 mesh.
- $W_p/W_f = 1.6$ to 2.0 , 500 mesh.
- $W_p/W_f = 1.6$ to 2.0 , 240 mesh.
- ✱ $W_p/W_f = 2.0$ to 6.0 , 500 mesh.
- ✱ $W_p/W_f = 2.0$ to 6.0 , 240 mesh.

Fig. 5.12

- x Air only.
- ▲ $W_p/W_f = 0.7$, 500 mesh.
- △ $W_p/W_f = 0.7$, 320 mesh.
- $W_p/W_f = 1.7$, 500 mesh.
- $W_p/W_f = 1.7$, 320 mesh.
- ✱ $W_p/W_f = 3.2$, 500 mesh.
- ✱ $W_p/W_f = 3.2$, 320 mesh.

Fig. 5.13

- △ $W_p/W_f = 0.8$ to 1.5 .
 - $W_p/W_f = 1.5$ to 2.5 .
 - ✱ $W_p/W_f = 2.5$ to 3.5 .
- All 320 mesh.

Fig. 5.14

- $W_p/W_f = 0.8$ to 1.5 .
 - $W_p/W_f = 1.5$ to 2.5 .
 - $W_p/W_f = 2.5$ to 3.5 .
- All 500 mesh.

Fig. 5.15

- $W_p/W_f = 1.0.$
 - $W_p/W_f = 2.0.$
 - x $W_p/W_f = 4.0.$
- All 500 mesh.

Fig. 5.16

- $R_e = 14 \times 10^4$ to $18.4 \times 10^4.$
 - $R_e = 6 \times 10^4$ to $10 \times 10^4.$
- Both 500 mesh.

Fig. 5.17

- $R_e = 9.5 \times 10^4$ to $11.0 \times 10^4.$
- 500 mesh.

Fig. 5.18

- 320 mesh, R_e varying.

Fig. 5.19

- $W_p/W_f = 0.2$ to $0.5.$
 - $W_p/W_f = 0.5$ to $1.0.$
 - $W_p/W_f = 1.0$ to $1.5.$
 - $W_p/W_f = 1.5$ to $2.0.$
 - ▲ $W_p/W_f = 2.0$ to $3.0.$
 - △ $W_p/W_f = 3.0$ to $4.0.$
 - x $W_p/W_f = 4.0$ to $5.0.$
- All 320 mesh.

Fig. 5.20

- 500 mesh, W_p/W_f and R_e varying.

Fig. 6.1

- x Air only.
 - $W_p/W_f = 0.3$ to $0.4.$
 - ▲ $W_p/W_f = 1.0$ to $1.5.$
 - $W_p/W_f = 2.0$ to $4.0.$
- All 500 mesh.

Fig. 6.2

- ⊗ $W_p/W_f = 0.6$ to 0.7 .
 - Δ $W_p/W_f = 1.0$ to 1.5 .
 - ∅ $W_p/W_f = 2.0$ to 2.5 .
 - ⋈ $W_p/W_f = 2.5$ to 3.5 .
 - $W_p/W_f = 3.5$ to 4.5 .
 - $W_p/W_f = 4.5$ to 5.5 .
- All 320 mesh.

Fig. 6.3

- x Air only.
 - $W_p/W_f = 0.3$ to 0.4 .
 - $W_p/W_f = 0.6$ to 0.7 .
 - ▲ $W_p/W_f = 1.0$ to 1.5 .
 - ⋈ $W_p/W_f = 1.5$ to 2.0 .
 - ▼ $W_p/W_f = 2.5$ to 3.5 .
 - $W_p/W_f = 3.5$ to 4.5 .
- All 500 mesh.

Fig. 6.4

- $W_p/W_f = 0.3$ to 0.4 .
- $W_p/W_f = 0.6$ to 0.7 .
- Δ $W_p/W_f = 1.0$ to 1.5 .
- ⋈ $W_p/W_f = 1.5$ to 2.0 .
- ▼ $W_p/W_f = 2.5$ to 3.5 .
- $W_p/W_f = 3.5$ to 4.5 .

Fig. 6.5

- x Air only.
 - $W_p/W_f = 0.3$ to 0.5 .
 - $W_p/W_f = 0.6$ to 0.8 .
 - ▲ $W_p/W_f = 1.0$ to 1.5 .
 - Δ $W_p/W_f = 1.5$ to 2.0 .
 - ⋈ $W_p/W_f = 2.0$ to 3.5 .
- All 500 mesh.

Fig. 6.6

- $W_p/W_f = 0.3$ to 0.5 .
 - $W_p/W_f = 0.6$ to 0.8 .
 - ▲ $W_p/W_f = 1.0$ to 1.5 .
 - ✎ $W_p/W_f = 2.0$ to 3.5 .
- All 320 mesh.

Fig. 6.7

- ✎ $W_f = 2.5$ to 3.5 lb/min.
 - $W_f = 3.5$ to 5.0 lb/min.
 - △ $W_f = 5.0$ to 6.5 lb/min.
 - ▲ $W_f = 6.5$ to 8.0 lb/min.
- All 320 mesh.

Fig. 6.8

- $W_f = 4$ to 5 lb/min.
 - △ $W_f = 5$ to 6.5 lb/min.
 - ▲ $W_f = 6.5$ to 8 lb/min.
 - ✎ $W_f = 8$ to 10 lb/min.
 - ✎ $W_f = 10$ to 12 lb/min.
- All 500 mesh.

Fig. 6.9

- ▲ $W_f = 6.5$ to 8 lb/min.
 - ✎ $W_f = 8$ to 10 lb/min.
 - $W_f = 10$ to 12 lb/min.
- All 320 mesh.

Fig. 6.10

- △ $W_f = 8$ to 9 lb/min.
 - ▲ $W_f = 9$ to 10 lb/min.
 - $W_f = 10$ to 12 lb/min.
- All 500 mesh.

Fig. 6.11

- $W_f = 7$ to 8 lb/min.
 - ▲ $W_f = 8$ to 10 lb/min.
 - $W_f = 10$ to 12 lb/min.
- All 320 mesh.

Fig. 6.12

- ▲ $R_e = 6 \times 10^4$ to 9×10^4 .
 - ♠ $R_e = 11 \times 10^4$ to 14×10^4 .
 - $R_e = 15 \times 10^4$ to 19×10^4 .
- All 500 mesh.

Fig. 6.13

- ▲ $R_e = 4 \times 10^4$ to 6×10^4 .
 - $R_e = 6 \times 10^4$ to 7×10^4 .
 - ♠ $R_e = 7 \times 10^4$ to 8×10^4 .
 - ♠ $R_e = 8 \times 10^4$ to 9×10^4 .
 - $R_e = 9 \times 10^4$ to 11×10^4 .
- All 500 mesh.

Fig. 6.14

- ▲ $R_e = 4.0 \times 10^4$ to 5.5×10^4 .
 - ♠ $R_e = 5.6 \times 10^4$ to 6.4×10^4 .
 - $R_e = 6.5 \times 10^4$ to 7.6×10^4 .
- All 500 mesh.

Fig. 6.15

- ▲ $R_e = 4.0 \times 10^4$ to 5.5×10^4 .
 - $R_e = 5.6 \times 10^4$ to 6.4×10^4 .
 - $R_e = 6.5 \times 10^4$ to 7.6×10^4 .
- All 240 mesh.

Fig. 6.16

- $W_p/W_f = 0.2$ to 0.4 .
 - $W_p/W_f = 0.6$ to 0.8 .
 - ✎ $W_p/W_f = 1.0$ to 1.3 .
 - ✎ $W_p/W_f = 1.5$ to 2.0 .
 - ▲ $W_p/W_f = 2.3$ to 3.5 .
- All 500 mesh.

Fig. 6.17

- x Air only.
 - $W_p/W_f = 0.2$ to 0.4 .
 - $W_p/W_f = 0.6$ to 0.8 .
 - ✎ $W_p/W_f = 1.0$ to 1.3 .
- All 500 mesh.

Fig. 6.18

- $W_p/W_f = 0.2$ to 0.4 .
 - $W_p/W_f = 0.6$ to 0.8 .
 - ✎ $W_p/W_f = 1.0$ to 1.3 .
 - ✎ $W_p/W_f = 1.5$ to 2.0 .
- All 240 mesh.

Fig. 6.19

- x Air only.
 - $W_p/W_f = 0.2$ to 0.4 .
 - $W_p/W_f = 0.6$ to 0.8 .
 - ✎ $W_p/W_f = 1.0$ to 1.3 .
 - ▲ $W_p/W_f = 2.5$ to 3.5 .
- All 500 mesh.

Fig. 6.20

- $W_p/W_f = 0.2$ to 0.4 .
 - $W_p/W_f = 0.6$ to 0.8 .
 - ✎ $W_p/W_f = 1.0$ to 1.3 .
 - ▲ $W_p/W_f = 2.5$ to 3.5 .
- All 500 mesh.

Fig. 6.21 to 6.27

- Centre or "a" pressure tappings.
- ▲ Bottom or "b" pressure tappings.
- Top or "c" pressure tappings.

Fig. 6.21

$$W_p = 10.2 \text{ lb/min.}$$

$$W_p/W_f = 1.32.$$

500 mesh.

Fig. 6.22

$$W_p = 36.5 \text{ lb/min.}$$

$$W_p/W_f = 5.00.$$

500 mesh.

Fig. 6.23

————— $W_p = 2.05 \text{ lb/min, } W_p/W_f = 0.18.$

----- $W_p = 6.65 \text{ lb/min, } W_p/W_f = 0.61.$

----- $W_p = 12.2 \text{ lb/min, } W_p/W_f = 1.19.$

All 500 mesh.

Fig. 6.24

————— $W_p = 10.0 \text{ lb/min, } W_p/W_f = 0.96.$

----- $W_p = 30.0 \text{ lb/min, } W_p/W_f = 3.32.$

Both 500 mesh.

Fig. 6.25

————— $W_p = 3.0 \text{ lb/min, } W_p/W_f = 0.26.$

500 mesh.

----- $W_p = 2.95 \text{ lb/min, } W_p/W_f = 0.26.$

240 mesh.

Fig. 6.26

————— $W_p = 10.4 \text{ lb/min, } W_p/W_f = 1.33.$

240 mesh.

----- $W_p = 34.5 \text{ lb/min, } W_p/W_f = 4.02.$

500 mesh.

Fig. 6.27

————— $W_p = 1.8 \text{ lb/min}, W_p/W_f = 0.16.$
- - - - - $W_p = 4.8 \text{ lb/min}, W_p/W_f = 0.44.$
- - - - - $W_p = 36.5 \text{ lb/min}, W_p/W_f = 3.97.$
All 500 mesh.

Fig. 7.1

• $R_e = 10.98 \times 10^4; W_p/W_f = 0.24.$
◦ $R_e = 9.68 \times 10^4; W_p/W_f = 1.07.$
✱ $R_e = 6.20 \times 10^4; W_p/W_f = 3.28.$
All 500 mesh.

Fig. 7.2

Δ $R_e = 11.9 \times 10^4; W_p/W_f = 0.18.$
◻ $R_e = 10.1 \times 10^4; W_p/W_f = 0.70.$
• $R_e = 9.5 \times 10^4; W_p/W_f = 1.19.$
All 500 mesh.

Figs. 7.3 to 7.8
and Fig. 7.22

• Centre or "a" pressure tapplings.
▲ Bottom or "b" pressure tapplings.
◻ Top or "c" pressure tapplings.

Fig. 7.3

————— $R_e = 10.98 \times 10^4, W_p/W_f = 0.24.$
- - - - - $R_e = 9.68 \times 10^4, W_p/W_f = 1.07.$
Both 500 mesh.

Fig. 7.4

R_e range 10.2×10^4 to $11.2 \times 10^4.$
 W_p/W_f range 0.18 to 0.61.
500 mesh.

Fig. 7.5

————— $R_e = 7.13 \times 10^4, W_p/W_f = 0.26.$
- - - - - $R_e = 6.67 \times 10^4, W_p/W_f = 1.05.$
Both 240 mesh.

Fig. 7.6

$R_e = 15.92 \times 10^4$, $W_p/W_f = 0.32$.
320 mesh.

Fig. 7.7

$R_e = 9.33 \times 10^4$, $W_p/W_f = 1.57$.
320 mesh.

Fig. 7.8

$R_e = 9.36 \times 10^4$, $W_p/W_f = 4.44$.
320 mesh.

Fig. 7.9

- $R_e = 10 \times 10^4$ to 11.2×10^4 .
 - ◌ $R_e = 8 \times 10^4$ to 9×10^4 .
 - ◌ $R_e = 7 \times 10^4$ to 8×10^4 .
 - ◌ $R_e = 6 \times 10^4$ to 7×10^4 .
 - ◌ $R_e = 5 \times 10^4$ to 6×10^4 .
- All 500 mesh.
- x ψ_{bp} for solid particles only.

Fig. 7.10

- $R_e = 10 \times 10^4$ to 11×10^4 .
 - ◌ $R_e = 9 \times 10^4$ to 10×10^4 .
 - ◌ $R_e = 8 \times 10^4$ to 9×10^4 .
 - ◌ $R_e = 7 \times 10^4$ to 8×10^4 .
- All 240 mesh.
- x ψ_{bp} for solid particles only.

Fig. 7.11

- x $R_e = 3 \times 10^4$ to 4×10^4 .
 - ◌ $R_e = 4 \times 10^4$ to 4.6×10^4 .
 - ◌ $R_e = 5.2 \times 10^4$ to 5.8×10^4 .
 - ◌ $R_e = 5.8 \times 10^4$ to 6.4×10^4 .
 - ◌ $R_e = 6.4 \times 10^4$ to 7.0×10^4 .
- All 500 mesh.

Fig. 7.12

- ♣ $R_e = 4 \times 10^4$ to 4.6×10^4 .
 - ♠ $R_e = 5.2 \times 10^4$ to 5.8×10^4 .
 - ♠ $R_e = 5.8 \times 10^4$ to 6.4×10^4 .
 - $R_e = 6.4 \times 10^4$ to 7.0×10^4 .
- All 240 mesh.

Fig. 7.13

- ♠ $R_e = 6 \times 10^4$ to 8×10^4 .
 - ♣ $R_e = 8 \times 10^4$ to 10×10^4 .
 - ♣ $R_e = 10 \times 10^4$ to 12×10^4 .
 - $R_e = 12 \times 10^4$ to 14×10^4 .
 - $R_e = 14 \times 10^4$ to 16×10^4 .
- All 320 mesh.

Fig. 7.14

- ♠ $R_e = 6 \times 10^4$ to 7.5×10^4 .
 - $R_e = 8.5 \times 10^4$ to 11.2×10^4 .
- Both 500 mesh.

Fig. 7.15

- ♣ Test 260, $R_e = 9.21 \times 10^4$ to 15.92×10^4 .
 - Test 262, $R_e = 7.19 \times 10^4$ to 12.51×10^4 .
- Both 320 mesh.

Fig. 7.16

- × Air only.
 - $W_p/W_f = 0.2$ to 0.4 .
 - $W_p/W_f = 0.6$ to 0.8 .
 - ♣ $W_p/W_f = 1.0$ to 1.5 .
- All 240 mesh.

Fig. 7.17

- Test 207, $R_e = 11.19 \times 10^4$ to 9.47×10^4 , $W_p/W_f = 0.18$ to 1.19 .
 - ✎ Test 210, $R_e = 8.48 \times 10^4$ to 7.05×10^4 , $W_p/W_f = 0.23$ to 1.61 .
- Both 500 mesh.

Fig. 7.18

- Air only.
 - $W_p/W_f = 0.2$ to 0.35 .
 - △ $W_p/W_f = 0.5$ to 0.65 .
 - ✎ $W_p/W_f = 0.9$ to 1.1 .
 - x $W_p/W_f = 1.4$ to 1.6 .
- All 500 mesh.

Fig. 7.19

- $W_p/W_f = 0.2$ to 0.3 .
 - $W_p/W_f = 0.6$ to 0.7 .
 - ✎ $W_p/W_f = 0.9$ to 1.1 .
- All 500 mesh.

Fig. 7.20

- $W_p/W_f = 0.3$ to 0.5 .
 - $W_p/W_f = 0.9$ to 1.2 .
 - ✎ $W_p/W_f = 1.6$ to 1.9 .
 - ✎ $W_p/W_f = 2.3$ to 2.7 .
 - ✎ $W_p/W_f = 3.0$ to 3.5 .
 - x $W_p/W_f = 4.0$ to 5.0 .
- All 320 mesh.

Fig. 7.21

- Test 260, $R_e = 9.21 \times 10^4$ to 15.92×10^4 , $W_p/W_f = 0.32$ to 3.11 .
 - Test 261(a), $R_e = 5.99 \times 10^4$ to 8.97×10^4 , $W_p/W_f = 0.58$ to 2.98 .
 - ✎ Test 261(b), $R_e = 3.22 \times 10^4$ to 5.54×10^4 , $W_p/W_f = 0.92$ to 3.47 .
- All 320 mesh.

Fig. 8.9

- × Test 5.
- Test 16.

Fig. 8.10

- Test 1.
- × Test 5.
- Δ Test 9.

Fig. 8.11

- Test 1.
- × Test 5.
- Δ Test 10.
- ◻ Test 13.
- Test 18.

Fig. 8.12

- Test 46.